ISSN 0386-5878
Technical Memorandum
of PWRI No. 3480

PROCEEDINGS OF THE FOURTH U.S.-JAPAN WORKSHOP ON EARTHQUAKE PROTECTIVE SYSTEMS FOR BRIDGES

DECEMBER 9 AND 10, 1996

EARTHQUAKE ENGINEERING DIVISION
EARTHQUAKE DISASTER PREVENTION RESEARCH CENTER
PUBLIC WORKS RESEARCH INSTITUTE
MINISTRY OF CONSTRUCTION

1, Asahi, Tsukuba-shi, Ibaraki-ken 305 Japan

Copyright © (1996) by P. W. R. I.

All rights reserved. No part of this book may be reproduced by any means, nor transmitted, nor translated into a machine language without the written permission of the Director General of P. W. R. I.

この報告書は，土木研究所長の承認を得て刊行したものである。したがって，本報告書の全部又は一部の転載，複製は，土木研究所長の文書による承認を得ずしてこれを行ってはならない。

ISSN 0386-5878
Technical Memorandum
of PWRI No.3480

PROCEEDINGS OF THE FOURTH U.S.-JAPAN WORKSHOP ON EARTHQUAKE PROTECTIVE SYSTEMS FOR BRIDGES

by

**Shigeki Unjoh, Toru Terayama,
Yukio Adachi, Jun-ichi Hoshikuma,
Kazuhiro Nagaya, Michio Ohsumi and Takashi Sato**

Synopsis:

The proceedings document the results of the Fourth U.S.-Japan Workshop on Earthquake Protective Systems for Bridges which was held at Osaka, Japan, on December 9 and 10, 1996, under the auspices of the Panel on Wind and Seismic Effects, UJNR. The Workshop was organized by the Task Committee G "Structural Control and Intelligent Material Systems" (U.S. side chairperson: Dr. S. C. Liu, NSF, Japan side chairperson: Dr. S. Unjoh, PWRI) in cooperation with the Task Committee J "Wind and Earthquake Engineering for Transportation Systems" (U.S. side chairman: Mr. J. D. Cooper, FHWA, Japan side chairman: Mr. Y. Fujishiro, PWRI) of the Panel.

Key words: Bridge Earthquake Protective Systems, Bridge Menshin, Seismic Isolation, High Damping, Rubber Bearing, UJNR

FOREWARD

The proceedings include the results of the Fourth U.S.-Japan Workshop on Earthquake Protective Systems for Bridges which was held at Osaka, Japan, on December 9 and 10, 1996 under the auspices of the UJNR Panel on Wind and Seismic Effects. The workshop was organized by the Task Committee G "Structural Control and Intelligent Material Systems" (Japan-side chair : Dr. Shigeki Unjoh, Head of Earthquake Engineering Division, Earthquake Disaster Prevention Research Center, Public Works Research Institute, U.S.-side chair : Dr. S. C. Liu, Program Director, Earthquake Hazards Mitigation Program, National Science Foundation) in cooperation with the Task Committee J "Wind and Earthquake Engineering for Transportation Systems" (Japan-side chair : Mr. Yasuyuki Fujishiro, Director of Structure and Bridge Department, Public Works Research Institute, U.S.-side chair : Mr. James D. Cooper, Chief of Structures Division, Turner-Fairbank Highway Research Center, Federal Highway Administration) of the Panel. The workshop was jointly coordinated by Dr. Shigeki Unjoh and Dr. Ian G. Buckle, Deputy Director of the National Center for Earthquake Engineering Research (NCEER). The staff of the Earthquake Engineering Division of PWRI, consisting of Messrs. Toru Terayama, Yukio Adachi, Jun-ichi Hoshikuma, Kazuhiro Nagaya, Michio Ohsumi and Takashi Sato arranged the workshop on behalf of the Japan side. The U.S.-side steering committee for this workshop, consisting of Dr. Ian G. Buckle and Mr. Ian M. Friedland of NCEER, Dr. Frieder Seible of University of California, San Diego and Dr. Gregory L. Fenves of University of California, Berkeley, organized the workshop on behalf of the U.S.-side participants. The U.S.-side financial support was provided by the National Science Foundation and the Federal Highway Administration.

The aims of the workshop were: (1) to bring together experts from both countries to exchange technical information on current research and practical efforts being made in the area of earthquake protective systems for bridges, and (2) to identify future needs and opportunities between the two countries for cooperative research.

A broad range of technical topics were presented at the workshop. These included:

- Testing of Seismic Isolation Hardware
- Seismic Isolation Design
- Design Applications
- Dynamic Characteristics of Seismically-Isolated Bridges
- Active and Hybrid Control for Bridges
- High Damping Systems for Long Span Bridges

The workshop was attended by 20 U.S. and 66 Japanese participants. In total, 20 papers were presented ; 12 papers from Japan, 8 papers from the United States. The proceedings includes (1) all technical papers in the order in which they were presented during the workshop, (2) resolutions that were unanimously approved by the participants during the closing session of the workshop, and (3) the workshop program and the list of participants.

We wish to express our profound gratitude and sincere appreciation to all participants in the workshop for supporting the workshop by active presentations and discussions. In particular, we would like to thank Dr. K. Kawashima, Dr. H. Otsuka, Dr. I. G. Buckle and Dr. H.S. Lew for leading the discussions.

Grateful thanks are also extended to the Japan side members. Sincere appreciation goes to the members of the Joint Research Program between PWRI and 19 private companies on Seismic Isolation for Long-Span Bridges. Special appreciation also goes to the Kinki Construction Bureau of the Ministry of Construction, Hanshin Expressway Public Corporation, Metropolitan Expressway Public Corporation, Trans-Tokyo Bay Highway Corporation, Bridgestone Corporation for the generous cooperation in the workshop and during the study tour. We also would like to thank the assisting staff members, Messrs. M. Takahashi, K. Murai and K. Tasaki of PWRI, for the smooth progress of the schedule.

Shigeki UNJOH,
Toru TERAYAMA,
Yukio ADACHI,
Jun-ichi HOSHIKUMA,
Kazuhiro NAGAYA,
Michio OHSUMI, and
Takashi SATO
Earthquake Engineering Division
Earthquake Disaster Prevention Research Center
Public Works Research Institute

February, 1997





保 存 用

TABLE OF CONTENTS

PAPERS

Session 1: State of the Art

(Co-Chairs: S. Unjoh, G. Fenves)

"Menshin Design of Highway Bridges" 3
by K. Kawashima, S. Unjoh
Presented by: Kazuhiko Kawashima

"Update on the Proposed AASHTO Guide Specification for Seismic Isolation Design" 23
by R. Lacalle
Presented by: Roberto Lacalle

Session 2: Passive/Hybrid Protective Systems

(Co-Chairs: H. Iemura, A. Kiremidjian)

"Development of High Damping Systems for Long Span Bridges" 37
by S. Unjoh, H. Otsuka, Y. Goto, I. Shimoda, Y. Maehara, T. Takeda
Presented by: Shigeki Unjoh

"Development of High Damping Devices for Long Span Bridges and the Design Method" 51
by S. Unjoh, Y. Goto, I. Shimoda, Y. Maehara
Presented by: Yozo Goto

"Aging Studies of High-Damping Rubber and Lead-Rubber Seismic Isolators" 75
by P. Clark, J. Kelly, I. Aiken
Presented by: Peter Clark

"Development of Super High Damping Rubber Damper for the Seismic Response Control of Long Span Bridges" 91
by K. Goda, S. Suzuki, Y. Suitsu, S. Unjoh H.Otsuka, K. Nagaya
Presented by: Kengo Goda

Session 3: Hybrid/Semi-active Systems and Smart Materials

(Co-Chairs: A. Igarashi, A. Itani)

"Modeling of a Variable Damper and its Application" 105
by T. Sato, M. Sato, S. Tanaka, K. Toki
Presented by: Tadanobu Sato

"Seismic Response Control of PC Cable-Stayed Bridge under Construction by Active Mass Damper" 115
by M. Tsunomoto, H. Otsuka, S. Unjoh, K. Nagaya
Presented by: Meguru Tsunomoto

"Thermo-visco-elasto-plastic Modeling of Elastomeric and Lead-Rubber Bridge Bearings" 131
by J. Mander, D-K Kim, S. Chen
Presented by: John Mander

Session 4: Experimental and Field Observations 1
(Co-Chairs: T. Sato, S. Arzoumanidis)

"Analysis of Seismic Response of Yama-age Bridge" 149
by S. Unjoh
Presented by: Shigeki Unjoh

"Seismic Isolation and Energy Dissipation Technologies: a Test and Evaluation Program for Highway Bridge Applications" 165
by K. Almand
Presented by: Kathleen Almand

"The Restoring Force Characteristics of LRB under the Influence of Variable Axial Loads and Rotational deformation" 181
by H. Iemura, A. Igarashi, Y, Chen, H. Nakajima
Presented by: Akira Igarashi

"Field Testing of a Four-span Seismically Isolated Bridge" 195
by A. Gilani, S. Mahin, G. Fenves, J. Chavez, I.Aiken
Presented by: Gregory Fenves

"Enhancement of Lateral Seismic Load Distribution in Continuous Girder Bridges : Test of Stiffening and Damping Components of a New Device" 209
by W. Tanzo, J. Hernandez Jr., H. Mutsuyoshi, A. Tsuzuki
Presented by: J. Hernandez Jr.

Session 5: Experimental and Field Observations 2
(Co-Chairs: M. Abe, A. Elgamal)

"Design of the 19-Span Continuous Rigid Frame Bridge with Seismic Isolator" 225
by H. Hayashi, S. Kawakita
Presented by: Shiro Kawakita

"Testing of Protective Systems and Hardware for Bridge Applications" 243
by A. Whittaker, I. Aiken, P. Clark, G. Fenves, N. Makris, S. Mahin
Presented by: Andrew Whittaker

"The Analysis of Seismic Response of the Bridge with Menshin Bearings during the Hyogo-ken Nanbu Earthquake" 259
by T. Naganuma, Y. Horie, H. Kobayashi, N. Sasaki
Presented by: Toshihiko Naganuma

Session 6: **Methods/Issues and Applications**

(Co-Chairs: H. Otsuka, A. Taylor)

"Use of Visco-Elastic Dampers to Suppress Seismic Vibration of Bridges" 269
by M. Shinozuka, J-M Kim, R. Purasinghe
Presented by: Masanobu Shinozuka

"Effectiveness of Unseating Prevention Devices with Energy Dissipation" 285
by K. Kawashima, M. Yabe
Presented by: Masaaki Yabe

"Seismic Protection of Bridges with Fluid Dampers and the Issue of Viscous Heating" 309
by N. Makris, S. McMahon
Presented by: Nicos Makris

RESOLUTIONS 327

(Co-Chairs: S. Unjoh, I. Buckle)

APPENDICES

WORKSHOP PROGRAMS 331
PARTICIPANTS 341

Session 1

State of the Art

(Co-Chairs: S. Unjoh, G. Fenves)

"Menshin Design of Highway Bridges"
by K. Kawashima, S. Unjoh
Presented by: Kazuhiko. Kawashima

"Update on the Proposed AASHTO Guide Specification for Seismic Isolation Design"
by R. Lacalle
Presented by: Roberto Lacalle

MENSHIN DESIGN OF HIGHWAY BRIDGES

Kazuhiko Kawashima[1] and Shigeki Unjoh[2]

1) Professor, Department of Civil Engineering, Tokyo Institute of Technology, O-okayama, Meguroku, Tokyo, 152, Japan
2) Head, Earthquake Engineering Division, Public Works Research Institute, Ministry of Construction, Tsukuba Science City, Ibaraki-ken, 305, Japan

ABSTRACT

This paper describes the menshin design (seismic isolation) of highway bridges in Japan. The menshin design has been extensively used in design of highway bridges since the 1995 Hyogo-ken Nanbu earthquake. It was included in the new "Part V Seismic Design" of the "Design Specifications of Highway Bridges" in 1996. This paper describes the outline of the menshin design method as well as a background of the introduction of the menshin design into the new code.

KEY WORDS Seismic isolation, menshin design, highway bridges, seismic design

INTRODUCTION

Various technical developments have been conducted for long time to reduce bridge response during an earthquake[1)2)10)12)23)25)]. A first attempt in Japan was the use of viscous dampers which were installed between a deck and piers. Viscous dampers were often adopted in 1970s, but because temperature effect was predominant at those days, they were used as the damper stoppers. Other type of devices such as SU-damper, PC cable spring, tapered plate-spring and link have been effectively adopted for bridges from short and medium span to long span bridges[10)].

The seismic isolation has been incorporated since late 1980s in highway bridges in Japan. Various analyses have been conducted for the effectiveness of the seismic isolation. The first design manual was issued in a form of the "Guidelines for Base Isolation Design of Highway Bridges" in 1989 as a final accomplishment of a 3-year research program[10)]. It has been recognized through such studies that the elongation of natural period causes various disadvantage in an application to the highway bridges.

One of the most significant problems is the large clearance required between a deck and an abutment or between two adjacent decks so that the deck can move with an amount of design displacement of isolators and dampers. This could be in the range of 300- 600 mm during the

Hyogo-ken Nanbu type earthquakes, whereas the clearance is generally about 50 - 100 mm in the conventional design. The large clearance at expansion joints increases noise and vibration pollution, and increases maintenance due to heavy traffic. Although the knock-off abutment was studied through experiments and analysis, it was found not easy to shear-off the upper part of an abutment in the back-fill side because of a resistance of pavement and back-fills[4]. Anchor bolts required, against heavy traffic load, to tie down the upper part of the knock-off abutment to the lower part is also problem for smooth shear-off.

From such reasons, it is preferable not to increase natural period for aiming to decrease the seismic force, but to put an emphasis on an increase of energy dissipation and a distribution of lateral force of a deck to as many substructures as possible. It may be effective to adjust natural period of a bridge so as to avoid the resonance with ground motion.

Such design concept was more clearly formulated as "menshin design" in a 3-year joint research program between the Public Works Research Institute and 28 companies from 1989 to 1992. From a study for favorable application of the seismic isolation, it was found that the menshin design is effective to construct super-multi-span continuous bridges with deck length over 1 km[3]. Also studied was an application of the menshin design for the seismic retrofit of existing bridges. Use of isolators and dampers was found effective to connect existing simply supported bridges so that they behave as a continuous bridge against traffic loads[28]. In the program, not only the menshin design method but also various devices such as high damping laminated rubber bearings[26], sliding friction bearings[6], unseating prevention devices[22], and a finger expansion joint movable not only in longitudinal direction but in transverse direction[22] were developed. Requirements for menshin devices in static and dynamic behavior and approving test procedures were also proposed[13][14]. Including those technical developments, the "Manual for Menshin Design of Highway Bridges" was issued by the Public Works Research Institute in 1992[11][24].

Based on the Guidelines and the Menshin Manual, a pilot program to construct several menshin bridges was initiated in 1989 in the Ministry of Construction. A working group was formulated in the Ministry of Construction to supervise the design and construction. Miyagawa bridge, three-span continuos plate girder bridge with a deck length of 105 m, was completed in 1992 as the first menshin bridge in the program[19].

During the steady increase of implementation of the menshin design, Hyogo-ken Nanbu earthquake occurred in January 1995 to cause destructive damage to various structures. Highway bridges also suffered destructive damage. Importance to increase ductility of structural components and redundancy of bridges was strongly recognized from the damage[16][20]. When the "Guide Specifications for Reconstruction and Repair of Highway Bridges which Suffered Damage

due to the Hyogo-ken Nanbu Earthquake" was issued by the Ministry of Construction on February 27, 1995[21], it was described in the Guide Specifications that the menshin design should be more actively used to mitigate shocks and reduce lateral force by increasing energy dissipation. It was suggested in the Guide Specifications that the Menshin Manual should be referred to in design of the menshin bridges. It was also recommended in the Guide Specifications that the laminated rubber bearings, in particular menshin bearings should be more used in stead of steel bearings vulnerable to seismic disturbance. It had been recognized for long time that laminated rubber bearings are superior to steel bearings from maintenance and corrosion point of view. Lead rubber bearings (LRBs) and high damping rubber bearings (HDRs) were suggested in the Guide Specifications.

Subsequently in May 1995, it was decided by the Ministry of Construction that the Guide Specifications should be referred to in seismic design of all new bridges and seismic retrofit of existing bridges in the country as an emergency measure until the Design Specifications of Highway Bridges was revised. Based on such a background, LRB and HDR have been increasingly used since the Hyogo-ken Nanbu earthquake. Not only in the menshin bridges but also in the bridges where tall laminated rubber bearings are required to distribute the lateral force of a superstructure to substructures, LRB and HDR have been used. Although statistical data are not available at this moment, majority of highway bridges use the laminated rubber bearings, LRB and HDR.

The "Design Specifications of Highway Bridges" was revised in November 1996[7]. There were various major revisions. The first was the introduction of thorough check of lateral capacity for all structural components in which seismic effect is predominant. Although the lateral capacity had been checked since 1990 (1990 Design Specifications), it was not mandatory, and had been used only for reinforced concrete piers. Furthermore, because it was not a design method but a "check," it had been effective only to increase the sections and reinforcements, if required, which were designed by the Seismic Coefficient Method. In the 1996 Specifications, the "check of lateral capacity" was upgraded to a seismic design method called as "Lateral Capacity Method," which has the equal importance with the Seismic Coefficient Method. It has been used for not only reinforced concrete piers but all structural components where seismic effect is predominant. The second was the introduction of the ground motions induced during the Hyogo-ken Nanbu earthquake as a Type-II design force. The third was the introduction of menshin design. Main part of the Menshin Manual was included in the 1996 Specifications as Chapter 8 in the "Part V Seismic Design."

This paper introduces the menshin design which was included in the new "Part V Seismic Design" of the "1996 Design Specifications of Highway Bridges."

SEISMIC PERFORMANCE LEVEL

Table 1 shows a classification of the seismic performance levels and design methods. The bridges are categorized into two groups depending on their importance; standard bridges (Type-A bridges) and important bridges (Type-B bridges). Seismic performance levels depends on the importance of bridges. For moderate ground motions induced by earthquakes with high probability to occur, both A and B bridges should behave in an elastic manner without any essential structural damage. For extreme ground motions induced by earthquakes with low probability to occur, the Type-A bridges should prevent critical failure, while the Type-B bridges should perform with limited damage.

In the Lateral Capacity Method, two types of ground motions must be considered. The first is the ground motions which could be induced by plate boundary earthquakes with magnitude of about 8 at a distance of about 50 Km from the faults. Ground motions which developed at Tokyo during the 1923 Kanto earthquake are a typical target of this type of ground motions. The second is the ground motions developed by earthquakes with magnitude of about 7-7.2 at very short distances. Obviously the ground motions developed at Kobe during the Hyogo-ken Nanbu earthquake are typical target of this type of ground motions. The first and the second ground motions are called as Type-I and Type-II ground motions, respectively. The recurrence time of the Type-II ground motion is much longer that that of the Type-I ground motion.

Table 1 Seismic Performance Levels

<table>
<tr><th rowspan="2" colspan="2">Type of Design Ground Motions</th><th colspan="2">Importance</th><th colspan="2">Design Methods</th></tr>
<tr><th>Type-A Bridges (Standard Bridges)</th><th>Type-B Bridges (Important Bridges)</th><th>Equivalent Static Lateral Force Methods</th><th>Dynamic Analysis</th></tr>
<tr><td colspan="2">Ground Motions with High Probability to Occur</td><td colspan="2">Prevent damage</td><td>Seismic Coefficient Method</td><td rowspan="3">Step by Step Analysis or Response Spectrum Analysis</td></tr>
<tr><td rowspan="2">Ground Motions with Low Probability to Occur</td><td>Type-I (Plate-Boundary Earthquakes)</td><td rowspan="2">Prevent Critical Failure</td><td rowspan="2">Limited Damage</td><td rowspan="2">Lateral Capacity Method</td></tr>
<tr><td>Type-II (Inland Earthquakes)</td></tr>
</table>

Lateral force coefficient k_{hc} in the Lateral Capacity Method is given as

$$k_{hc} = c_Z \cdot k_{hc0} \quad (1)$$

in which c_Z = modification coefficient for zone, and is 0.7, 0.85 and 1.0 depending on zone, and k_{hc0} = standard modification coefficient. Table 2 and Fig. 1 show the standard lateral force coefficients k_{hc0} for the Type-I and the Type-II ground motions. The Type-I ground motions have been used since 1990 (1990 Specifications), while the Type-II ground motions were newly introduced in the 1996 Specifications. It should be noted here that the k_{hc0} at stiff site (Group I) has been always assumed smaller than the k_{hc0} at moderate (Group II) and soft soil (Group III) sites in the Type-I ground motions as well as the seismic coefficients used for the Seismic Coefficient Method. The Type-I ground motions were essentially estimated from an attenuation equation for response spectra[8]. Although the response spectral accelerations at short natural period are generally larger at stiff sites that at soft soil sites, the tendency has not been explicitly included in the past. This is because damage has been more developed at soft sites than at stiff sites. To consider this fact, the design force at stiff sites has been always assumed smaller than that at soft sites even at short natural period. However without such a traditional consideration, the Type II ground motions were determined by simply taking envelops of response accelerations of major strong motions recorded at Kobe during the Hyogo-ken Nanbu earthquake. It was considered appropriate to set realistic ground motions.

The acceleration response spectral intensity at short natural period is higher in the Type-II ground motions than in the Type-I ground motions. However, the duration of extreme accelerations is much longer in the Type-I ground motions than the Type-II ground motions. The duration was only 8-10 seconds in the strong motions recorded at Kobe during the Hyogo-ken Nanbu earthquake. As will be described later, such a difference of the duration is taken into account to evaluate the ductility factor of a pier.

Table 2 Lateral Force Coefficient k_{hc0} in the Lateral Capacity Method

(a) Type-I Ground Motions

Soil Condition	Lateral Force Coefficient k_{hc0}		
Group I (stiff)	$k_{hc0}=0.7$ for $T \leqq 1.4$		$k_{hc0}=0.876T^{-2/3}$ for $1.4<T$
Group II (moderate)	$k_{hc0}=1.51T^{1/3} \geqq 0.7$ for $T<0.18$	$k_{hc0}=0.85$ for $0.18 \leqq T \leqq 1.6$	$k_{hc0}=1.16T^{-2/3}$ for $1.6<T$
Group III (soft)	$k_{hc0}=1.51T^{1/3} \geqq 0.7$ for $T<0.29$	$k_{hc0}=1.0$ for $0.29 \leqq T \leqq 2.0$	$k_{hc0}=1.59T^{-2/3}$ for $2.0<T$

(b) Type-II Ground d Motions

Soil Condition	Lateral Force Coefficient k_{hc0}		
Group I (stiff)	$k_{hc0}=4.46T^{2/3}$ for $T<0.3$	$k_{hc0}=2.0$ for $0.3 \leqq T \leqq 0.7$	$k_{hc0}=1.24T^{-4/3}$ for $0.7<T$
Group II (moderate)	$k_{hc0}=3.22T^{2/3}$ for $T<0.4$	$k_{hc0}=1.75$ for $0.4 \leqq T \leqq 1.2$	$k_{hc0}=2.23T^{-4/3}$ for $1.2<T$
Group III (soft)	$k_{hc0}=2.38T^{2/3}$ for $T<0.5$	$k_{hc0}=1.50$ for $0.5 \leqq T \leqq 1.5$	$k_{hc0}=2.57T^{-4/3}$ for $1.5<T$

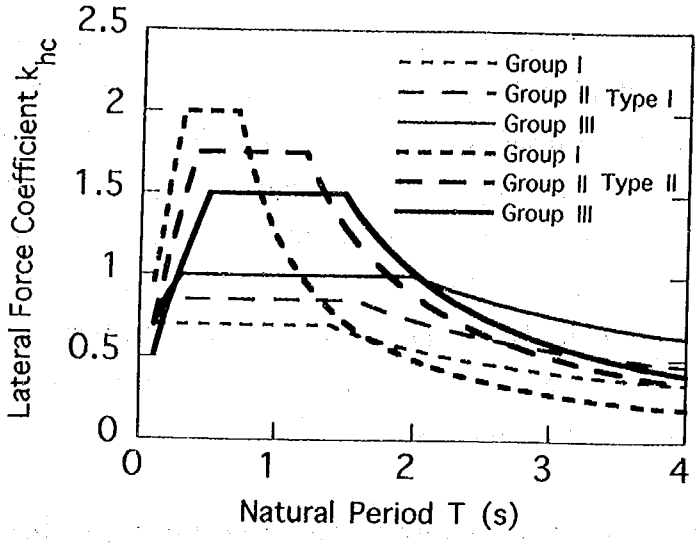


Fig. 1 Type I and Type II Ground Motions for the Lateral Capacity Method

BASIC PRINCIPLE OF MENSHIN DESIGN

Implementation of the menshin bridges should be carefully decided, from not only seismic performance but function for traffic and maintenance point of view, based on the advantage and disadvantage of increasing natural period. The menshin design should not be adopted at the following conditions;

(a) sites vulnerable to lose bearing capacity due to the soil liquefaction and the lateral spreading
(b) bridges supported by flexible columns
(c) soft soil sites where potential resonance with surrounding soils could be developed by increasing the fundamental natural period
(d) bridges with uplift force at bearings

It is suggested that the design should be made with an emphasis on an increase of energy dissipating capability and a distribution of lateral force to as many substructures as possible. To concentrate the hysteretic deformation at not piers but bearings, the fundamental natural period of a menshin

bridge should be about 2 times or longer than the fundamental natural period of the same bridge supported by the conventional bearings. It should be noted that an elongation of natural period aiming to decrease the lateral force should not be attempted.

Simple devices stable against extreme earthquakes have to be used. The bearings have to be anchored to a deck and substructures with bolts, and should be replaceable. The clearance has to be provided between a deck and substructures or between two adjacent decks.

MENSHIN DESIGN AND DESIGN FORCE

Idealization

In the menshin design, the bridges are first designed by the standard equivalent linear static design method. Then seismic safety of the static design is precisely evaluated by a dynamic response analysis. Menshin devices are generally idealized by a set of equivalent linear springs in the equivalent static analyses while they are idealized by either the equivalent linear springs or nonlinear hysteretic springs in the dynamic response analysis. Equivalent stiffness and equivalent damping ratio of isolator and dampers are the key parameters in the equivalent linear analysis.

In the equivalent static analysis, natural period T of a menshin bridge is evaluated following the standard procedure as

$$T = 2.01\sqrt{\delta} \tag{2}$$

$$\delta = \frac{\sum w_i \cdot u_i^2}{\sum w_i \cdot u_i} \tag{3}$$

in which w_i = dead weight per unit length of a bridge at i-th point and u_i = lateral displacement developed at i-th point by subjecting to a lateral force equivalent to the dead weight in a desired direction.

Modal damping ratio of a menshin bridge h for the fundamental mode is computed as[15]

$$h = \frac{\sum K_{Bi} \cdot u_{Bi}^2 \cdot \left\{ h_{Bi} + \frac{h_{Pi} \cdot K_{Bi}}{K_{Pi}} + \frac{h_{Fui} \cdot K_{Bi}}{K_{Fui}} + \frac{h_{F\theta i} \cdot K_{Bi} \cdot H^2}{K_{F\theta i}} \right\}}{\sum K_{Bi} \cdot u_{Bi}^2 \cdot \left\{ 1 + \frac{K_{Bi}}{K_{Pi}} + \frac{K_{Bi}}{K_{Fui}} + \frac{K_{Bi} \cdot H^2}{K_{F\theta i}} \right\}} \tag{4}$$

in which h_{Bi} = damping ratio of i-th damper, h_{Pi} = damping ratio of i-th pier or abutment, h_{Fui} = damping ratio of i-th foundation associated with translational displacement, $h_{F\theta i}$ = damping ratio of i-th foundation associated with rotational displacement, K_{Pi} = equivalent stiffness of i-th pier or abutment, K_{Fui} = translational stiffness of i-th foundation, $K_{F\theta i}$ = rotational stiffness of i-th

foundation, u_{Bi}= design displacement of i-th menshin device, and H= distance from a bottom of pier to a gravity center of a deck.

A bridge may be divided into several sub-structures in which energy dissipating mechanism can be assumed essentially the same. If one can specify a damping ratio of each sub-structure for a given mode shape, the modal damping ratio for i-th mode may be evaluated as

$$h_i = \frac{\sum \phi_{ij}{}^T \cdot h_{ij} \cdot k_j \cdot \phi_{ij}}{\Phi_i{}^T \cdot K \cdot \Phi_i} \tag{5}$$

in which h_{ij} = damping ratio of j-th substructure in i-th mode, ϕ_{ij}=mode vector of j-th substructure in i-th mode, k_j = stiffness matrix of j-th substructure, K= stiffness matrix of a bridge, and Φ_i= mode vector of a bridge in i-th mode, and is given as

$$\Phi_i{}^T = \left\{\phi_{i1}{}^T,\ \phi_{i2}{}^T,\ \cdots\cdots,\ \phi_{in}{}^T\right\} \tag{6}$$

Table 3 shows recommended damping ratios for major structural components.

Table 3 Recommended Damping Ratios for Major Structural Components in a Menshin Bridge

Structural Components	Elastic Response		Nonlinear Response	
	Steel	Concrete	Steel	Concrete
Deck	0.02-0.03	0.03-0.05	0.02-0.03	0.03-0.05
Rubber Bearings	0.02		0.02	
Menshin Bearings	Equivalent damping ratio by Eq. (26)		Equivalent damping ratio by Eq.(26)	
Substructures	0.03-0.05	0.05-0.1	0.1-0.2	0.12-0.2
Foundations	0.1-0.3		0.2-0.4	

Design Force

Menshin bridges are designed by both the Seismic Coefficient Method and the Lateral Capacity Method. In the Seismic Coefficient Method, a lateral force coefficient ranging from 0.2 to 0.3 has been used based on the allowable stress design approach.

In the Lateral Capacity Method, the equivalent lateral force coefficient k_{hem} in the menshin design is evaluated as

$$k_{hem} = \frac{k_{hcm}}{\sqrt{2\mu_m - 1}} \tag{7}$$

$$k_{hcm} = c_E \cdot k_{hc} \tag{8}$$

in which k_{hcm} = lateral force coefficient in menshin design, μ_m = allowable ductility factor of a pier, c_E = modification coefficient for energy dissipating capability (refer to Table 4), and k_{hc} = lateral force coefficient by Eq. (1).

Because the k_{hc} is the lateral force coefficient for a bridge supported by the conventional bearings, Eq. (8) means that the lateral force in the menshin design can be reduced, as large as 30 %, by the modification coefficient c_E depending on the modal damping ratio of a bridge.

Table 4 Modification Coefficient for Energy Dissipation Capability

Damping Ratio for 1st Mode h	Coefficient c_E
h<0.1	1.0
0.1≦h<0.12	0.9
0.12≦h<0.15	0.8
h≧0.15	0.7

It is important to note here that the allowable ductility factor μ_m in Eq. (7) depends on the type of ground motions and that μ_m is smaller than the allowable ductility factor μ_a in the conventional design evaluated as

$$\mu_a = 1 + \frac{\delta_u - \delta_y}{\alpha \cdot \delta_y} \tag{9}$$

in which α = safety factor, δ_y = yield displacement of a pier, and δ_u = ultimate displacement of a pier. In Eq. (9), the ultimate displacement δ_u is evaluated as

$$\delta_u = \delta_y + (\phi_u - \phi_y)(h - L_p/2)L_p \tag{10}$$

in which ϕ_y = yield curvature of a pier at bottom, ϕ_u = ultimate curvature of a pier at bottom, h = height of a pier, and L_p = plastic hinge length of a pier. The plastic hinge length is given as

$$L_p = 0.2h - 0.1D \qquad (0.1D \le L_p \le 0.5D) \tag{11}$$

in which D is a width or a diameter of a pier.

The yield curvature ϕ_y and ultimate curvature ϕ_u in Eq. (10) are evaluated assuming a stress-strain relation of reinforcements and concrete as shown in Fig. 2. The stress σ_c - strain ε_c relation of concrete is assumed as[5)]

$$\sigma_c = \begin{cases} E_c\varepsilon_c\left\{1 - \frac{1}{n}\left(\frac{\varepsilon_c}{\varepsilon_{cc}}\right)^{n-1}\right\} & (0 \le \varepsilon_c \le \varepsilon_{cc}) \\ \sigma_{cc} - E_{des}(\varepsilon_c - \varepsilon_{cc}) & (\varepsilon_{cc} \le \varepsilon_c \le \varepsilon_{cu}) \end{cases} \tag{12}$$

$$n = \frac{E_c\varepsilon_{cc}}{E_c\varepsilon_{cc} - \sigma_{cc}} \tag{13}$$

in which σ_{cc}= strength of confined concrete, E_c= elastic modulus of concrete, ε_{cc}= strain at maximum strength, and E_{des}= gradient at descending branch. In Eq. (12), σ_{cc}, ε_{cc} and E_{des} are determined as

$$\sigma_{cc} = \sigma_{ck} + 3.8\alpha\rho_s\sigma_{sy} \tag{14}$$

$$\varepsilon_{cc} = 0.002 + 0.033\beta\frac{\rho_s\sigma_{sy}}{\sigma_{ck}} \tag{15}$$

$$E_{des} = 11.2\frac{\sigma_{ck}^2}{\rho_s\sigma_{sy}} \tag{16}$$

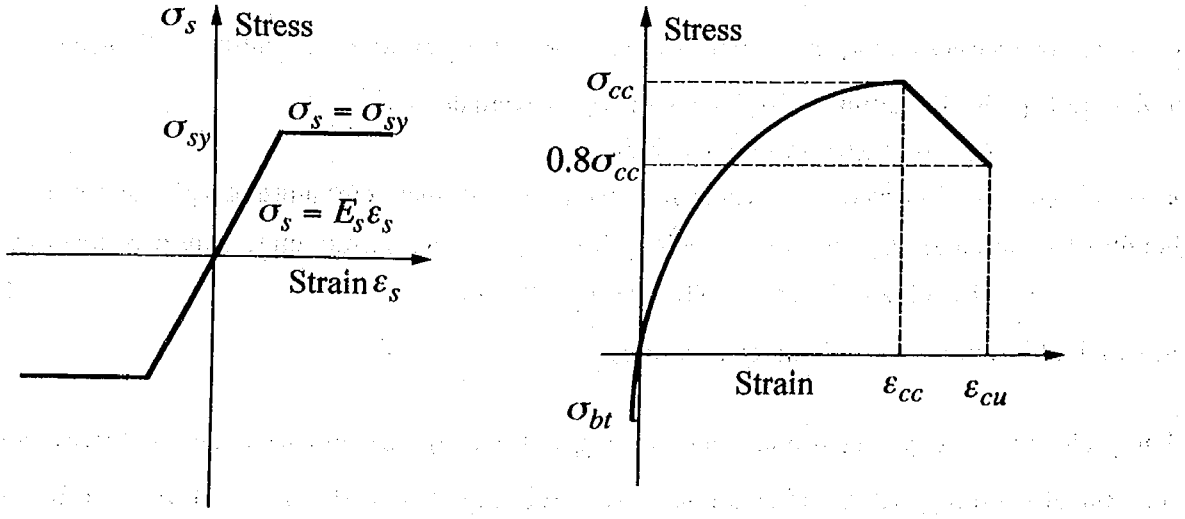
in which σ_{ck}= design strength of concrete, σ_{sy}= yield strength of reinforcements, α and β= coefficients depending on shape of a pier (α=1.0 and β=1.0 for a circular pier, and α=0.2 and β=0.4 for a rectangular pier), and ρ_s= tie reinforcement ratio defined as

$$\rho_s = \frac{4A_h}{s \cdot d} \tag{17}$$

in which A_h= area of tie reinforcements, s= space of tie reinforcements, and d= effective with of tie reinforcements.

The ultimate curvature ϕ_u is defined as a curvature when concrete strain at longitudinal reinforcing bars in compression reaches an ultimate strain ε_{cu} defined as

$$\varepsilon_{cu} = \begin{cases} \varepsilon_{cc} & \text{for Type I ground motions} \\ \varepsilon_{cc} + \dfrac{0.2\sigma_{cc}}{E_{des}} & \text{for Type II ground motions} \end{cases} \tag{18}$$



(a) Steel (b) Concrete

Fig. 2 Stress and Strain Relation of Confined Concrete and Reinforcing Bars

It is important to note here that the ultimate strain ε_{cu} depends on the types of ground motions; the ε_{cu} for the Type-II ground motions is larger than that for the Type-I ground motions. Based on a loading test, it is known that a certain level of failure in a pier such as a sudden decrease of

lateral capacity occurs at smaller lateral displacement in a pier subjected to a loading hysteresis with more number of load reversals[9)27)]. To reflect such a fact, it was decided that the ultimate strain ε_{cu} should be evaluated by Eq. (18), depending on the type of ground motions. Thus, the allowable ductility factor μ_a depends on the type of ground motions; the μ_a is larger in a pier subjected to the Type-II ground motions than a pier subjected to the Type-I ground motions.

It should be noted that the safety factor α in Eq. (9) also depends on the type of bridges as well as the type of ground motions as shown in Table 5. This is to preserve higher seismic safety in the important bridges, and to take account of the difference of recurrent time between the Type-I and the Type-II ground motions.

Table 5 Safety Factor α in Eq. (9)

Type of Bridges	Type-I Ground Motions	Type-II Ground Motions
Type-B	3.0	1.5
Type-A	2.4	1.2

On the other hand, in the menshin design, the allowable ductility factor of a pier μ_m in Eq. (7) is evaluated by

$$\mu_m = 1 + \frac{\delta_u - \delta_y}{\alpha_m \cdot \delta_y} \tag{19}$$

in which α_m is a safety factor used in menshin design, and is given as

$$\alpha_m = 2\alpha \tag{20}$$

Eq. (20) means that the allowable ductility factor in the menshin design μ_m should be smaller than the allowable ductility factor μ_a by Eq. (9) in the conventional design. The purpose to use smaller allowable ductility factor in the menshin design is to make the nonlinear hysteretic behavior of a pier at the plastic hinge zone as small as possible.

Dynamic Response Analysis

Dynamic response analysis is required in the menshin design to verify seismic safety of the static design. In dynamic response analysis, ground motions which are spectral fitted to the following response spectra are used;

$$S_I = c_Z \cdot c_D \cdot S_{I0} \tag{21}$$

$$S_{II} = c_Z \cdot c_D \cdot S_{II0} \tag{22}$$

in which S_I= acceleration response spectrum for Type-I ground motions, S_{II}= acceleration response spectrum for Type-II ground motions, S_{I0}= standard acceleration response spectrum

for Type-I ground motions, S_{II0} = standard acceleration response spectrum for Type-II ground motions, c_Z = modification coefficient for zone (refer to Eq. (1)), and c_D = modification coefficient for damping ratio given as

$$c_D = \frac{1.5}{40h+1} + 0.5 \tag{23}$$

Table 6 Standard Acceleration Response Spectra

(a) Type-I Response Spectra S_{I0}

Soil Condition	Response Acceleration S_{I0} (gal=cm/sec^2)		
Group I	$S_{I0}=700$ for $T_i \leqq 1.4$	$S_{I0}=980/T_i$ for $T_i > 1.4$	
Group II	$S_{I0}=1{,}505T_i^{1/3}$ for $T_i < 0.18$	$S_{I0}=850$ for $0.18 \leqq T_i \leqq 1.6$	$S_{I0}=1{,}360/T_i$ for $T_i > 1.6$
Group III	$S_{I0}=1{,}511T_i^{1/3}$ for $T_i < 0.29$	$S_{I0}=1{,}000$ for $0.29 \leqq T_i \leqq 2.0$	$S_{I0}=2{,}000/T_i$ for $T_i > 2.0$

(b) Type-II Response Spectra S_{II0}

Soil Condition	Response Acceleration S_{II0} (gal=cm/sec^2)		
Group I	$S_{II0}=4{,}463T_i^{2/3}$ for $T_i \leqq 0.3$	$S_{II0}=2{,}000$ for $0.3 \leqq T_i \leqq 0.7$	$S_{II0}=1{,}104T_i^{5/3}$ for $T_i > 0.7$
Group II	$S_{II0}=3{,}224T_i^{2/3}$ for $T_i < 0.4$	$S_{II0}=1{,}750$ for $0.4 \leqq T_i \leqq 1.2$	$S_{II0}=2{,}371T_i^{5/3}$ for $T_i > 1.2$
Group III	$S_{II0}=2{,}381T_i^{2/3}$ for $T_i < 0.5$	$S_{II0}=1{,}500$ for $0.5 \leqq T_i \leqq 1.5$	$S_{II0}=2{,}948T_i^{5/3}$ for $T_i > 1.5$

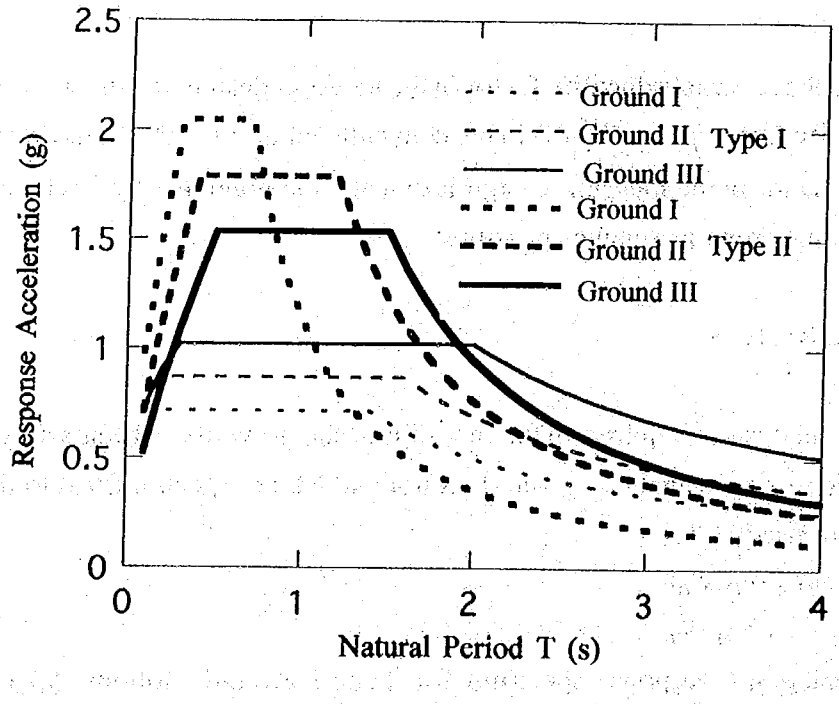


Fig. 3 Response Acceleration Spectra (h=0.05) for Type I and Type II Ground Motions

Table 6 and Fig. 3 show the standard acceleration response spectra (damping ratio h=0.05) for the Type-I and Type-II ground motions.

It is recommended to use at least three ground motions per analysis, and take an average, considering the validity of the analysis, to evaluate the response.

DESIGN OF DEVICES

The bearings are classified into two groups. The first is the bearings which resist the seismic force of Eq. (7). The second is the bearings which resist the seismic force considered in the Seismic Coefficient Method. The first and the second bearings are called as the Type-B bearings and the Type-A bearings, respectively. Seismic performance of the Type-B bearings is, of course, much higher than the Type-A bearings. In the Type-A bearings, a displacement limiting device, which will be described later, has to be co-installed in both longitudinal and transverse directions, while it is not required in the Type-B bearings. Because of the importance of bearings as one of the main structural components, the Type-B bearings should be used in the menshin bridges.

Isolators and dampers must be designed for a desired design displacement u_B. The design displacement u_B is evaluated as

$$u_B = \frac{k_{hem} \cdot W_u}{K_B} \tag{24}$$

in which k_{hem}= equivalent lateral force coefficient by Eq. (7), K_B= equivalent stiffness, and W_u= dead weight of a superstructure. It should be noted that because the equivalent lateral force coefficient k_{hem} depends on the type of ground motions, the design displacement u_B also depends on it.

The equivalent stiffness K_B and equivalent damping ratio h_B of a device are evaluated as

$$K_B = \frac{F(u_{Be}) - F(-u_{Be})}{2u_{Be}} \tag{25}$$

$$h_B = \frac{\Delta W}{2\pi W} \tag{26}$$

$$u_{Be} = c_B \cdot u_B \tag{27}$$

in which $F(u)$= restoring force of a device at a displacement u, u_{Be}= effective design displacement, ΔW= energy dissipated per cycle, W= elastic strain energy, and c_B= coefficient to evaluate effective displacement (=0.7).

In design of devices, the following requirements have to be satisfied:

1) The displacement computed by Eq. (24) should be within ±10% from the assumed design displacement u_B, and the equivalent damping ratio evaluated by Eq. (26) should not be less that the equivalent damping ratio assumed in design.

2) Shear strain induced in a laminated rubber bearing γ subjected to a lateral force equivalent to the equivalent lateral force coefficient k_{hem} by Eq. (7) are evaluated as

$$\gamma = \frac{u_B}{\sum_{i=1}^{n} t_{ei}} \tag{28}$$

in which u_B= design displacement of a rubber bearing by Eq. (24), t_{ei} = thickness of i-th rubber, and n= number of layers of rubber. The shear strain by Eq. (28) should be less than 250 %.

3) Local shear strain should be less than the rupture strain divided by a safety factor of 1.2. Recommended rupture strains are presented in Table 7.

Table 7 Recommended Rupture Strain of Rubber

Type of Rubbers	Shear Modulus (N/mm^2)	Rupture Strain (%)
Natural Rubbers	80	500
	100	500
	120	400
Chloroplane Rubbers	80	400
	100	400

4) The devices have to be designed and fabricated so that scatter of the equivalent stiffness K_B and the equivalent damping ratio h_B be within ±10% of the design values.

5) The devices have to be stable against at least 50 and 15 load reversals, for the Type-I and Type-II ground motions, respectively, with the design displacement by Eq. (24) under a vertical force equivalent to the dead weight of a superstructure.

6) Tangential stiffness of a device should be positive at any displacement within the design displacement. This is to prevent a possible shake-down of the devices in one side, when they are subjected to large cyclic load reversals.

7) A deck should return to the rest position even after it is subjected to an large earthquake. The residual displacement u_{BR} developed in a device after it is smoothly released from a deformed displacement equivalent to the design displacement by Eq. (24) should be less than 10% of the design displacement.

8) The equivalent stiffness and the equivalent damping ratio of a device shall be stable against a change of load condition and natural environment such as the temperature change.

UNSEATING PREVENTION SYSTEMS

Unseating prevention measures are required for the highway bridges. Because of the unique structural response of the menshin bridges, some additional measures are required. The measures required for the highway bridges are as:

1) The unseating prevention systems have to be so designed that unseating of a superstructure from their supports can be prevented even if unpredictable failures of the structural members occur.
2) The unseating prevention systems are consisted of providing enough seat length, a falling-down prevention device, a displacement limiting device, and a settlement prevention device.
3) Against longitudinal response, enough seat length must be provided and a falling-down prevention device must be installed at the ends of a superstructures, if the Type-B bearings are used. On the other hand, if the Type-A bearings are used, a displacement limiting device has to be further installed at not only the ends of a superstructure but each intermediate support in a continuous bridge.
4) Against transverse response, a displacement limiting device is requested at each support, if the Type-A bearings are used, while it is not required in the Type-B bearings, except in skewed bridges, curved bridges, bridges supported by columns with narrow crest, bridges supported by few bearings per piers, and bridges constructed at the sites vulnerable to lateral spreading associated with soil liquefaction.

The seat length S_E is evaluated as

$$S_E = u_R + u_G \geq S_{EM} \tag{29}$$

$$S_{EM} = 70 + 0.5l \tag{30}$$

$$u_G = 100 \cdot \varepsilon_G \cdot L \tag{31}$$

in which u_R= relative displacement (cm) developed between a superstructure and a substructure subjected to a seismic force equivalent to the equivalent lateral force coefficient k_{hem} by Eq. (7), u_G= relative displacement of ground along the bridge axis, S_{EM}= minimum seat length (cm), ε_G= ground strain induced during an earthquake along the bridge axis, and is 0.0025, 0.00375, and 0.005 for Group I, II and III sites, respectively, L= distance which contributes to the relative displacement of ground (m), and l = span length (m). If two adjacent decks are supported by a pier, the lager span length should be l in evaluating the seat length.

In addition to the above requirements, the following measures should be adopted in the menshin design.

1) To prevent collisions between a deck and an abutment or between two adjacent decks, enough clearance must be provided. The clearance between those structural components S_B shall be evaluated as

$$S_B = \begin{cases} u_B + L_A & \text{between a deck and an abutment} \\ c_B \cdot u_B + L_A & \text{between two adjacent decks} \end{cases} \quad (32)$$

in which u_B= design displacement of menshin devices (cm) by Eq. (24), L_A = redundancy of a clearance (generally ± 1.5cm), and c_B = modification coefficient for clearance (refer to Table 8). The modification coefficient c_B was determined based on an analysis of the relative displacement response spectra[17]. It depends on a difference of natural periods $\Delta T = T_2 - T_1$ ($T_1 \geq T_2$), in which T_1 and T_2 represent the natural period of the two adjacent bridge systems.

Table 8 Modification Coefficient for Clearance c_B

$\Delta T / T_1$	c_B
$0 \leqq \Delta T / T_1 < 0.1$	1
$0.1 \leqq \Delta T / T_1 < 0.8$	$\sqrt{2}$
$0.8 \leqq \Delta T / T_1 \leqq 1.0$	1

The clearance at an expansion joint L_E is evaluated as

$$L_E = u_B + L_A \quad (33)$$

in which u_B= design displacement of menshin devices (cm) by Eq. (24), and L_A = redundancy of a clearance (generally ± 1.5cm).

CONCLUDING REMARKS

The menshin design has been adopted extensively throughout the country since the Hyogo-ken Nanbu earthquake. It obviously extended the freedom of design and construction of the bridges, in particular the bridges with multiple-span continuous bridges with a deck length over 0.5km. However, it should be noted that seismic performance of the menshin bridges against an extreme earthquake has not yet fully verified. For example, what is the most appropriate clearance between a deck and an abutment or between two adjacent decks, and what is the effect of hysteretic behavior of piers at the plastic hinge on the total response of bridges requires more analysis. More accumulation of analysis and experience is a key for future technical development of the menshin design and seismic isolation.

ACKNOWLEDGMENTS

Drafting of the revised version of the "Part V Seismic Design" of the "Design Specifications of Highway Bridges" was conducted at the "Special Sub-committee for Seismic Countermeasures for Highway Bridges" and was approved by the Bridge Committee, Japan Road Association. The first and second authors of this paper served as chairman and an executive member in the Special Sub-committee.

REFERENCES

1) Billings, I.J. and Kirkcaldie, D.K.: Base Isolation of Bridges in New Zealand, Proc. New Zealand-Japan Workshop on Base Isolation of Highway Bridges, Wellington, New Zealand, 1987.

2) Buckle, I. G. and Mayes, R. L.: Seismic Isolation- History, Application and Performance- A World View, Earthquake Spectra, Vol. 6, No. 2, 1990

3) Goto, Y., Tokunaga, M., Yoshimura, T. and Sintaku, M.: Seismic Response of Multi-span Continuous Bridge with Length of 1 km, Proc. 1st US-Japan Workshop on Earthquake Protective Systems of Bridges, February 1992, Buffalo, NY, USA, Technical Report NCEER 92-0004, National Center for Earthquake Engineering Research, State University of New York at Buffalo

4) Goto, Y., Kikuchi, T., Kimishima, T., Matsuo, F., Ozaki, D. and Tsukamoto, A.: Development of Expansion Joint, Stoppers and Knock-off Abutment for Menshin Design, Proc. 2nd US-Japan Workshop on Earthquake Protective Systems of Bridges, Technical Memorandum, No. 3196, Public Works Research Institute, 1992

5) Hoshikuma, J., Kawashima, K., and Nagaya, K.: A Stress-Strain Model for Reinforced Concrete Bridge Piers Confined by Hoop Reinforcement, Proc. Japan Society of Civil Engineers, No. 520/V-28, pp. 1-11, 1995

6) Iguchi, T.: Development of Sliding Friction Damper, Proc. 1st US-Japan Workshop on Earthquake Protective Systems of Bridges, February 1992, Buffalo, NY, USA, Technical Report NCEER 92-0004, National Center for Earthquake Engineering Research, State University of New York at Buffalo

7) Japan Road Association: Design Specifications of Highway Bridges, Part I Commonn Part, Part II Steel Bridges, Part III Concrete Bridges, Part IV Foundations, and Part V Seismic Design, 1996

8) Kawashima, K., Aizawa, K. and Takahashi, K.: Attenuation of Peak Ground Motions and Absolute Acceleration Response Spectra, Report of PWRI, Vol. 166, Public Works Research Institute, 1985

9) Kawashima, K. and Koyama, T.: Effect of Number of Loading Cycles on Dynamic Characteristics of Reinforced Concrete Bridge Pier Columns, Structural Engineering/ Earthquake Engineering, Vol. 5, No. 1, pp. 183-191, Japan Society of Civil Engineers, 1988

10) Kawashima, K., Hasegawa, K. and Nagashima, H. : A Perspective of Menshin Design for Highway Bridges in Japan, Proc. 1st US-Japan Workshop on Earthquake Protective Systems of Bridges, February 1992, Buffalo, NY, USA, Technical Report NCEER 92-0004, pp. 3-26, National Center for Earthquake Engineering Research, State University of New York at Buffalo

11) Kawashima, K. : Manual for Menshin Design of Highway Bridges, Proc. 2nd US-Japan Workshop on Earthquake Protective Systems of Bridges, Tsukuba, Japan, PWRI Technical Memorandum No. 3196, pp. 195-219, Public Works Research Institute, Japan

12) Kawashima, K. : Menshin Design of Highway Bridges in Japan, Proc. 3rd US-Japan Workshop on Earthquake Protective Systems of Bridges, January 1994, Berkeley, CA, USA, Technical Report NCEER 94-0009, pp.1.3-1.31, National Center for Earthquake Engineering Research, State University of New York at Buffalo

13) Kawashima, K., Hasegawa, K., Nagashma, H., Makiguchi, Y. and Suizu, Y. : Certificate Test of Menshin Devices, Proc. 1st US-Japan Workshop on Earthquake Protective Systems of Bridges, February 1992, Buffalo, NY, USA, Technical Report NCEER 92-0004, pp. 205-212, National Center for Earthquake Engineering Research, State University of New York at Buffalo

14) Kawashima, K., Makiguchi, Y., Suizu, Y. and Endo, K. : Approving Test Procedure for Menshin Devices, Proc. 2nd US-Japan Workshop on Earthquake Protective Systems of Bridges, Tsukuba, Japan, PWRI Technical Memorandum No. 3196, pp. 3-20, Public Works Research Institute, Japan

15) Kawashima, K., Nagashima, H. and Iwasaki, H.: Evaluation of Modal Damping Ratio of Bridges Based on Strain Energy Proportional Method, Proc. 9th US-Japan Bridge Workshop, Technical Memorandum, Public Works Research Institute, Tsukuba, Japan, 1993

16) Kawashima, K.: Impact of Hanshin/Awaji Earthquake on Seismic Design and Seismic Strengthening of Highway Bridges, Report No. TIT/EERG 95-2, Tokyo Institute of Technology., 1995

17) Kawashima, K. and Sato, H.: Relative Displacement Response Spectrum and Its Application, Proc. 11th World Conference on Earthquake Engineering, Acapulco, Mexico, 1996

18) Kimishima, T., Harada, H. and Ozaki, D.: Development of a Finger Joint Movable in Horizontal Directions for Menshin Bridges, Proc. 1st US-Japan Workshop on Earthquake Protective Systems of Bridges, February 1992, Buffalo, NY, USA, Technical Report NCEER 92-0004, National Center for Earthquake Engineering Research, State University of New York at Buffalo

19) Matsuo, Y. and Hara, K.: Design and Construction of Miyagawa Bridge, Proc. 1st US-Japan Workshop on Earthquake Protective Systems of Bridges, February 1992, Buffalo, NY, USA, Technical Report NCEER 92-0004, National Center for Earthquake Engineering Research, State University of New York at Buffalo

20) Ministry of Construction: Report on the Damage of Highway Bridges by the Hyogo-ken Nanbu Earthquake, Committee for Investigation on the Damage of Highway Bridges Caused by the Hyogo-ken Nanbu Earthquake, 1995

21) Ministry of Construction: Guide Specifications for Reconstruction and Repair of Highway Bridges Which Suffered Damage due to the Hyogo-ken Nanbu Earthquake, 1995

22) Ozaki, D. and Matsumoto, F.: Development of Falling-off Prevention Devices for Menshin Bridges, Proc. 1st US-Japan Workshop on Earthquake Protective Systems of Bridges, February 1992, Buffalo, NY, USA, Technical Report NCEER 92-0004, National Center for Earthquake Engineering Research, State University of New York at Buffalo

23) Priestley, N., Seible, F. and Calvi, M.: Seismic Design and Seismic Retrofit of Bridges, John Wiley and Sons, 1996

24) Public Works Research Center: Menshin Manual of Highway Bridges, English version is available by Sugita, H. and Mahin, S.: Manual for Menshin Design of Highway Bridges: Ministry of Construction, Japan, Report No. UCB/EERC 94-10, Earthquake Engineering Research Center, University of California, Berkeley, 1994

25) Skinner, Robinson, McVerry: Introduction to Seismic Isolation, John Wiley and Sons, 1993

26) Suizu. Y. and Sudo, C. (Part 1), Kawashima, K., Koshitoge, M., Endo, K., Yamada, C., and Nishimoto, T. (Part 2), and Nishikawa, I., Kato, M., Ito, M., and Muramatsu, Y. (Part 3): Development of High Damping Rubber Bearings for Menshin Design, Proc. 1st US-Japan Workshop on Earthquake Protective Systems of Bridges, February 1992, Buffalo, NY, USA, Technical Report NCEER 92-0004, National Center for Earthquake Engineering Research, State University of New York at Buffalo

27) Takemura, H. and Kawashima, K.: Effect of Number of Load Reversal on Ductility and Dynamic Strength of Reinforced Concrete Piers, Report No. TIT/EERG 96-5, Tokyo Institute of Technology, 1996

28) Yamaguchi, M., Makiguchi, Y. and Kawasaki, I.: Application of Menshin Design to Seismic Retrofit of Bridges by Connecting Slabs of Adjacent Girders, Proc. 1st US-Japan Workshop on Earthquake Protective Systems of Bridges, February 1992, Buffalo, NY, USA, Technical Report NCEER 92-0004, National Center for Earthquake Engineering Research, State University of New York at Buffalo

UPDATE ON THE PROPOSED AASHTO GUIDE SPECIFICATION FOR SEISMIC ISOLATION DESIGN

Roberto Lacalle, P. E.
California Department of Transportation
Sacramento, California

ABSTRACT

In 1990 the AASHTO Subcommittee on Bridges and Structures adopted a Guide Specification for Seismic Isolation Design (AASHTO 1991). The adoption of these guide specifications presented a major step forward in the acceptance and use of isolation bearings in the United States, especially elastomeric based systems. In the five years since the adoption of the Guidelines, there has been significant progress in the development and understanding of new isolation bearing technologies that are not elastomeric based. To update the guide specification and fully utilize the potential of the new systems, the AASHTO T-3 Seismic Design Committee chaired by Mr. James E. Roberts of California was charged with assisting in the development of a comprehensive technical guide specification for seismic isolation design. To eliminate biases and develop a truly comprehensive specification, the T-3 Committee assembled a task group to accomplish this goal. This paper covers the proposed major revisions and additions to the current 1991 Guide Specification.

INTRODUCTION

Since the adoption of the 1991 Guide Specification for Seismic Isolation Design by AASHTO, significant progress has been made in the understanding and development of new isolation bearing technologies that are not elastomeric based. To fully utilize the potential of the new systems, the AASHTO T-3 Seismic Design Committee chaired by Mr. James E. Roberts of California assembled a task group to develop a comprehensive technical guide specification for seismic isolation design. The Task Group consists of three state engineers: James E. Roberts from California (chairman; working chairman is Roberto Lacalle), Myint M. Lwin from Washington and Ralph E. Anderson from Illinois; three professors: Dr. John F. Stanton from University of Washington, Dr. Michael C. Constantinou from University of Buffalo, SUNY, and Dr. James M. Kelly/Dr. Ian Aiken from University of California at Berkeley; three industry representatives: Dr. Ronald L. Mayes of Dynamic Isolation Systems, Dr. Victor A. Zayas of Earthquake Protective Systems and Paul Bradford of R. J. Watson; and one Federal Highway representative: Dr. Hamid Ghasemi.

The approach the Task Group took to develop the guide specification was to update and expand the current 1991 AASHTO Guide Specification for Seismic Isolation Design rather than develop an entirely new document.

THE PROPOSED GUIDE SPECIFICATION FOR SEISMIC ISOLATION DESIGN

The proposed Guide Specifications are written as supplemental to the AASHTO Standard Specifications for Highway Bridges, 15th Edition (Interim 1995), Division I-A: Seismic Design.

Specifically the guideline contains:

- Fundamental requirements for seismic isolation design;
- Required tests of isolation systems;
- Lambda factor methodology;
- Elastomeric bearing design and construction;
- Sliding bearing design and construction; and
- A section for other systems not specifically covered.

The proposed Guide Specifications are intended for systems that isolate in the horizontal plane only, i.e., the system is assumed to be essentially rigid in the vertical direction. In addition, the Guide Specifications are currently intended for passive isolation systems only.

SIGNIFICANT CHANGES

Response Modification Factor (R)

The response modification factor for all substructures was taken as half of those given in Table 3 of the AASHTO Standard Specifications (Division I-A: Seismic Design), but not less than 1.5.

Response Modification Factor (R)

SUBSTRUCTURE	R	PROPOSED R
Wall-Type Pier	2	1.5
Reinforced Concrete Pile Bents		
a. Vertical Piles Only	3	1.5
b. One or more Batter Piles	2	1.5
Single Columns	3	1.5
Steel or Composite Steel and Concrete Pile Bents		
a. Vertical Piles Only	5	2.5
b. One or more Batter Piles	3	1.5
Multiple Column Bent	5	2.5

The 1991 Guide Specification allowed use of lower R-Factors when a lower ductility demand on the substructure was desired. The proposed guide specification requires the use of lower R-Factors to reduce substructure damage and to ensure proper performance of the isolation system. It is important to note that upon yielding of the pier, the bearing stops deforming. That is, deformation takes place only in the pier (Constantinou, 1996).

Analysis Procedures

The analysis procedures were updated to reflect the AASHTO Standard Specifications for Highway Bridges, 15th Edition (Interim 1995), Division I-A: Seismic Design. That is:

Procedure 1: Uniform Load Method

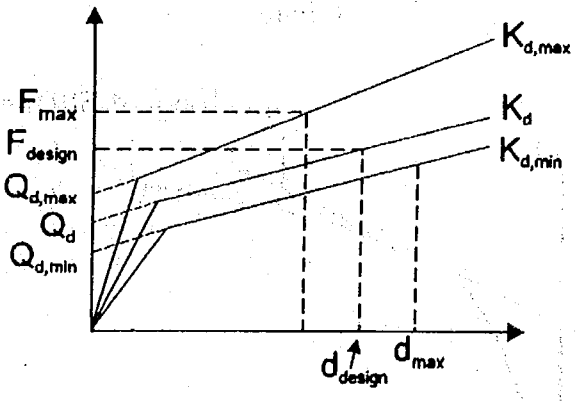
Procedure 2: Single Mode Spectral Method

Procedure 3: Multimode Spectral Method

Procedure 4: Time-History Method

The analysis of the bridge shall be performed using the design properties of the isolation system. To simplify nonlinear behavior of the isolator unit, a bilinear simplification may be used (Figure 1). The analysis shall be repeated using upper bound properties ($Q_{d,max}$, $K_{d,max}$) in one analysis and lower bound properties ($Q_{d,min}$, $K_{d,min}$) in another analysis. The purpose of this upper- and lower-bound analysis is to determine the maximum forces on the substructure elements and the maximum displacements of the isolation system.

Figure 1



An upper and lower bound analysis is not required if the displacements using the displacement equation and the elastic seismic response coefficient do not vary from the design values by more than ±15 percent when the maximum and minimum values are used. For these simplified calculations, B values corresponding to more than 30 percent damping can be used to establish the ±15 percent limits.

Displacement equation

$$d = \frac{250AST_e}{B} \text{ (mm)}$$

$$d = \frac{10AST_e}{B} \text{ (inches)}$$

- Elastic seismic response coefficient $C_S = \frac{AS_I}{T_e B}$

where: A = Acceleration coefficient

B = Damping coefficient

S = Dimensional site coefficient for isolation design for the given soil profile

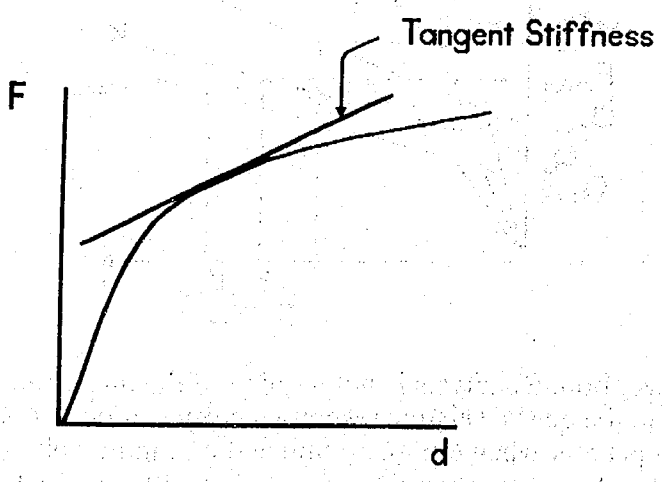
T_e = Period of vibration (seconds)

Lateral Restoring Force

The proposed specification requires that the isolation system be configured to produce a lateral restoring force such that the period corresponding to the tangent stiffness of the force deflection curve (Figure 2) of the isolation system up to the design displacement shall always be less than six seconds. Nonlinear analysis is required for periods greater than four seconds. The rational behind the change is that the existing criteria (lateral force at the design displacement is at least 0.025W greater than the lateral force at 50 percent of the design displacement) is too restrictive in lower acceleration regions and too liberal in higher acceleration regions. Hence, an isolator in a high seismic region such as California was required to have only a fraction of the restoring force required in another portion of the country. Systems without sufficient restoring force are not allowed.

The purpose of the lateral restoring force requirement is to prevent cumulative displacements, to accommodate isolator installation imperfections, such as out of level, and to prevent negative stiffness due to column rotations.

Figure 2



Required Tests of Isolation Systems

All isolation systems shall verify seismic performance by correlating shake table test results with analytically predicted responses prior to consideration for use.

The characteristics of the isolation system that are used in design shall be verified by tests. As a minimum, the following tests shall be conducted:

- Lateral load tests in accordance with tests prescribed in the NIST Report, CERF Report or HITEC Report.
- Shaking table tests at a scale of no less than 1/4 full scale.

Prototype Tests

(1) Thermal – Three fully reversed cycles of loads at a lateral displacement corresponding to the maximum thermal displacement.

This test verifies the lateral force exerted by the isolation system at the maximum thermal displacement.

(2) Wind and Braking – Twenty fully reversed cycles between limits of plus or minus the maximum load at a duration not less than 40 seconds. After the cyclic testing, the maximum load shall be held for one minute.

This test verifies the resistance of the isolation system under service load conditions.

(3) Seismic – Three fully reversed cylces of loading at each of the following multiples of the Design Displacement: 1.0, 0.25, 0.50, 0.75, 1.0 and 1.25 in the sequence shown.

This test verifies the dynamic response of the isolation system for various displacements.

(4) Seismic – $(15\ S_i)/B$ cycles not to exceed 25 but not less than 10 fully reversed cycles of loading at 1.0 times the Design Displacement. The test shall be started from a displacement equal to the Service Displacement.

This test verifies the survivability of the isolator after a major earthquake.

(5) Wind and Braking – The wind and braking test (test No. 2) is repeated to verify service load performance after a seismic event.

(6) Performance Verification – Three fully reversed cycles of loading at the Design Displacement.

This test verifies the performance of the bearing after the sequence of tests has been completed.

If the isolators are for low temperature areas, then the performance verification test must be repeated at temperatures of -7, -15, -21 or -26 degrees Celsius (20, 5, -5 or -15 degrees Fahrenheit) for temperature zones A, B, C, and D respectively.

The test temperature represents 75 percent of the difference between the base temperature and the extreme temperature in Table 14.3.2 of the AASHTO Standard Specification (Division I).

System Adequacy

The performance of the prototype specimens shall be assessed as adequate if the following conditions are satisfied:

- The force-deflection plots, excluding the viscous damping component, of all tests specified in the prototype tests have a positive incremental force carrying capacity consistent with the lateral force restoring requirements. The purpose of this requirement is to ensure that the hysteretic elements of the system are stable.
- The effective stiffness of any individual cycle shall not differ by more than plus or minus 10 percent of the effective stiffness average over all three cycles.
- There is no greater than a 20 percent change in effective stiffness between the first cycle and any subsequent cycle of each test specimen for the seismic displacement tests.

Stability Verification

The vertical load carrying elements of the isolation system shall be demonstrated to be stable under one fully reversed cycle at a specified displacement under a combined vertical load of:

Maximum Vertical Load	Minimum Vertical Load
$1.2\ D + LL_S + 0.35\ AD + OT$	$0.9\ D - (0.35\ AD + OT)$

where: D = Dead Load

A = Horizontal peak ground acceleration

OT = Overturning

LL_S = Seismic live load

The seismic live load is a percentage of the total live load considered applicable for design by the Engineer of Record. Typically live load is not considered in Load Group VII of the AASHTO Standard Specifications (Division I). However, since isolated structures are generally much more flexible, additional mass from the live load may need to be considered.

Wear and Fatigue Tests

Wear and or fatigue tests shall be conducted to quantify the wear or fatigue occurring over a minimum displacement of 1.6 km (1 mile). The test shall be performed at the design contact pressure and rotation at room temperature. The test speed (rate of application) shall not be less than 63.5 mm/minute (2.5 inches/minute). If the isolators are for low temperature areas, then 10 percent of the test shall be performed at temperatures of -7, -15, -21, -26 degrees Celsius (20, 5, -5, or -15 degrees Fahrenheit) for temperature zones A, B, C, and D respectively.

In lieu of the low temperature test criteria, a 4.8 km (3 mile) test may be performed when approved by the Engineer of Record.

Nominal Properties of the Isolation System

The minimum and maximum effective stiffness of the isolation system shall be established by cyclic tests covered in the specification. The design properties that affect the effective stiffness (K_{max} and K_{min}) shall be determined from K_d and Q_d and modified by the appropriate lambda (λ) factors to account for the effects of temperature, aging, scragging, velocity and variability of materials, as follows:

$$K_{d,max} = K_d \times \lambda_{max}$$

$$K_{d,min} = K_d \times \lambda_{min}$$

$$Q_{d,max} = Q_d \times \lambda_{max}$$

$$Q_{d,min} = Q_d \times \lambda_{min}$$

Similarly, the equivalent viscous damping ratio (β) shall be modified by the appropriate lambda factors as follows:

$$\beta_{max} = \beta \times \lambda_{max}$$

$$\beta_{min} = \beta \times \lambda_{min}$$

Lambda (λ) Methodology

The lambda methodology presented in the proposed specification is largely based on research and data accumulated by Professor Constantinou of SUNY. The approach is entirely new to the specification and it represents one of the more significant changes made.

The procedure provides a rational and systematic tool for dealing with variables such as: temperature, aging, frequency, velocity, travel, contamination and scragging, all of which directly or indirectly affect the design and performance of the isolation bearing. Naturally, all lambda values do not apply to all the various systems. For instance, frequency lambdas are relevant to devices with viscoelastic behavior (elastomeric bearings) and velocity lambdas are relevant to sliding systems.

Minimum and maximum lambda values will be determined by selecting the appropriate adjustment factors as follows:

$$\lambda_{min} = \lambda_{min,t} \times \lambda_{min,a} \times \lambda_{min,f} \times \lambda_{min,v} \times \lambda_{min,tr} \times \lambda_{min,c}$$

$$\lambda_{max} = \lambda_{max,t} \times \lambda_{max,a} \times \lambda_{max,f} \times \lambda_{max,v} \times \lambda_{max,tr} \times \lambda_{max,c}$$

where:

λ_t = Factors to account for temperature

λ_a = Factors to account for aging (including corrosion)

λ_f = Factors to account for effect of frequency

$$\lambda_f = \frac{G \text{ at frequency equal to inverse of } T_e}{G \text{ at frequency of testing}}$$

λ_v = Factors to account for effect of velocity

$$\lambda_v = \frac{\mu \text{ at relevant velocity}}{\mu \text{ at velocity of testing}}$$

λ_{tr} = Factors to account for effects of travel (wear)

λ_c = Factors to account for effects of contamination (in sliding systems)

λ_{scrag} = Factors to account for the effects of scragging a bearing (elastomeric systems)

Lambda adjustment factors are applied to λ factors to account for the probability of occurrence. The following adjustment factors shall apply to all λ factors except λ_v and λ_f.

1.0 for critical bridges

0.75 for essential bridges

0.66 for all other bridges

The adjustment factor shall apply to the portion of a λ that deviates from unity.

Example:

$\lambda_{max,c}$ = 1.2 without adjustment factor

$\lambda_{max,c}$ = $1 + (1.2 - 1)\ 0.75 = 1.15$ for adjustment factor of 0.75

$\lambda_{min,tr}$ = 0.9 without adjustment factor

$\lambda_{min,tr}$ = $1 - (1 - 0.9)\ 0.75 = 0.925$ for adjustment factor of 0.75

ELASTOMERIC BEARING DESIGN AND CONSTRUCTION

The elastomeric bearing sections were found adequate by the Task Group and remain largely unchanged in the proposed specifications.

SLIDING BEARINGS

The proposed specification has two new sections which cover sliding bearing design and construction. The new sections cover bearings that utilize PTFE and stainless steel as well as other sliding interfaces.

The PTFE section was modeled after the existing AASHTO LRFD Code. Service load design coefficients of friction for PTFE sliding surfaces were taken from NCHRP Report No. 10-20A, final report. Service coefficients of friction for other sliding surfaces will be established by testing and adjusted by the appropriate lambda values in accordance with the document. Seismic

coefficients of friction will be determined from the area under the force displacement loops of three cycles divided by the total travel distance.

Service contact stresses for PTFE are the same as those specified by the AASHTO LRFD Code, however, they may be exceeded when demonstrated by tests on full size bearings and the wear test requirements are satisfied. Service contact stresses for other sliding surfaces will be determined by testing full size bearings and qualified by the wear test.

The allowable seismic contact stresses for PTFE were determined by increasing service contact stresses 70 percent.

OTHER ISOLATION SYSTEMS

The final section of the proposed guide specification covers all other isolation systems that contain a flexible element, restoring force capacity and energy dissipation capacity and were not covered in the previous sections of the document.

Acceptance of the system shall be based on satisfying the requirements set forth in the system characterization tests, design, fabrication, installation, inspection, maintenance, prototype testing, and quality control testing sections.

System Characterization Tests

The characteristics of the isolation system that are used in design shall be verified by tests. As a minimum, the following tests shall be conducted:

- Lateral load tests in accordance with tests prescribed in the NIST Report, CERF Report or HITEC Report.
- Shaking table tests at a scale no less than 1/4 full scale.
- Tests to investigate the variations in system properties and their effects on response. At a minimum, the effects on temperature, rate-dependency, prior loading (including wear), and environmental effects shall be investigated. Values for λ_{min} and λ_{max} shall be developed from these tests.
- In addition to the foregoing test data, information from previous field experience in other applications may be used to demonstrate the system characteristics.

Design Procedure

A complete, rational, design procedure for the isolation system shall be provided to the Engineer prior to the start of the prototype testing. This procedure shall include:

- The bases for the selection of the limiting material stresses, deformations or other critical response quantities.
- The method for predicting the cyclic load deformation relationship of the system.
- The method for predicting the stability limit of the system.

At least one design example shall be submitted with the design procedure, including the calculations for obtaining the maximum force response and maximum displacement response.

Fabrication, Installation, Inspection and Maintenance Requirements

All special requirements for fabrication, installation, inspection and maintenance shall be submitted, in writing, to the Engineer prior to the start of prototype testing. As a minimum, these shall include:

- Materials to be used and the specifications that they must satisfy.
- Any special material testing requirements.
- Fabrication sequence and procedures.
- Fabrication tolerances and surface finish requirements.
- Any special handling requirements.
- Installation procedures and tolerances.
- Maintenance requirements, including a schedule for replacement of any components, for the lifetime of the system.

Prototype Testing

Prototype testing shall be conducted for each job in order to demonstrate that the design achieves the performance requirements set out in the job specifications. Insofar as possible, the tests shall conform to those defined in the prototype section of the document. The Engineer may, at his discretion, require additional tests to verify particular characteristics of the system.

Quality Control Testing

Quality control testing shall be conducted on every bearing. Test requirements and acceptance requirements shall be established by the Engineer.

SUMMARY

An updated and expanded AASHTO Guide Specification for Seismic Isolation Design is under development by the T-3 Task Group. The Task Group, under the authority of the AASHTO T-3 Seismic Design Committee, has updated the existing 1991 AASHTO Guide Specification for Seismic Isolation Design to reflect changes in the AASHTO Standard Specifications for Highway Bridges and expanded it to reflect the development of new isolation bearing technologies.

To date, the Proposed Guide Specification for Seismic Isolation Design is still under revision by the T-3 Task Group. The Proposed Guide Specification has not been approved by the T-3 Seismic Design Committee nor has it been reviewed by the AASHTO Subcommittee on Bridges and Structures. It is anticipated that the proposed specification will be ready for ballot next June 1997 for the annual AASHTO meeting in Jackson, Wyoming.

ACKNOWLEDGEMENTS

The proposed "Guide Specification for Seismic Isolation Design" was developed on a fast track schedule thanks to the hard work and efforts of the T-3 Task Group. The Author thanks the T-3 Task Group: James E. Roberts, Myint M. Lwin, Ralph E. Anderson, Dr. John F. Stanton, Dr. Michael C. Constantinou, Dr. James M. Kelly, Dr. Ian Aiken, Dr. Ronald L. Mayes, Dr. Victor A. Zayas, Paul Bradford, and Dr. Hamid Ghasemi for their dedication. The Author also thanks Li-Hong Sheng and Judi L. Wong for their assistance.

REFERENCES

1. *AASHTO (1991), Guide Specifications for Seismic Isolation Design,* American Association of State Highway and Transportation Officials (AASHTO).

2. Draft (9/96), *Guide Specification for Seismic Isolation Design,* Roberts J.E., Lacalle R., Sheng L.H., Stanton J.F., Constantinou M.C., Kelly J.M., Aiken I., Mayes R.L., Zayas V.A., Bradford P., Ghasemi H., Lwin M.M., Anderson R.E.

Session 2

Passive/Hybrid Protective Systems

(Co-Chairs: H. Iemura, A. Kiremidjian)

"Development of High Damping Systems for Long Span Bridges"
by S. Unjoh, H. Otsuka, Y. Goto, I. Shimoda, Y. Maehara, T. Takeda
Presented by: Shigeki. Unjoh

"Development of High Damping Devices for Long Span Bridges and the Design Method"
by S. Unjoh, Y. Goto, I. Shimoda, Y. Maehara
Presented by: Yozo Goto

"Aging Studies of High-Damping Rubber and Lead-Rubber Seismic Isolators"
by P. Clark, J. Kelly, I. Aiken
Presented by: Peter Clark

"Development of Super High Damping Rubber Damper for the Seismic Response Control of Long Span Bridges"
by K. Goda, S. Suzuki, Y. Suitsu, S. Unjoh, H.Otsuka, K. Nagaya
Presented by: Kengo Goda

DEVELOPMENT OF HIGH DAMPING SYSTEMS FOR LONG SPAN BRIDGES

Shigeki UNJOH [1], Hisanori OTSUKA [2], Yozo GOTO [3]
Ikuo SHIMODA [4], Yasuo MAEHARA [5] and Tetsuo TAKEDA [6]

1) Head, Earthquake Engineering Division, Earthquake Disaster Prevention Research Center, Public Works Research Institute, Ministry of Construction
2) Professor, Department of Civil Engineering, Kyushu University
3) General Manager, Civil Engineering Department, Technical Research Institute, Obayashi Corporation
4) Director, Development Section, Oiles Corporation
5) Director, Earthquake Research and Development Department, Yachiyo Engineering Co., Ltd
6) Vice Director, Civil Engineering Department, Kajima Institute of Construction Technology

ABSTRACT

A long-span bridge is a relatively flexible structure and have generally smaller damping characteristics. Since the damping characteristics significantly affects the earthquake response of the superstructure, therefore, to augment the damping characteristics is expected to effectively reduce the section forces and displacement response which are critical in the rational and economical design of the bridge. Three years research program on the "Development of Seismic Isolation Design using High damping Materials for Long-Span Bridges" was conducted by the Public Works Research Institute, jointly with the Public Works Research Center and 19 private firms from 1993 to 1995[1,2]. This paper presents the outline of the joint research program and the development of new seismic response control devices to increase the damping characteristics for long-span bridges.

1. INTRODUCTION

Long-span bridges have generally smaller damping characteristics. The longer span bridge has generally the smaller damping ratio, and the vibration of superstructures is

easy to be developed by environmental external forces such as wind and earthquakes, etc. The damping characteristics of long–span bridges are significantly affect the seismic response of superstructures and the force transmitted to substructures from superstructures. Therefore, it is expected to reduce the section force and displacement response which are critical in the design by increasing the damping characteristics of the superstructure.

Technology to increase damping characteristics of long–span bridges has been recently developed, that is the seismic response control technology using passive, active and hybrid control devices. Seismic isolation design (Menshin design) has been adopted for the short and mid–span general bridges[3]. For the general bridges, the damping augmentation is made by seismic isolation bearings. However, for long–span bridges, damping augmentation devices which are applicable not only for bearing but girder and substructures are expected to be developed using new materials and new structural concept. Fig.1 shows the illustration of the development of high damping systems for long–span bridges.

Three years joint research program on the "Development of Seismic Isolation Design using High damping Materials for Long–Span Bridges" was conducted by the Public Works Research Institute, jointly with the Public Works Research Center and 19 private firms from 1993 to 1995. The objectives of the program was to develop new high damping systems using high damping materials and new structural concept which are applicable for the long–span bridges. This paper presents the outline of the joint research program and the development of new seismic response control devices to increase the damping characteristics for long–span bridges. Nineteen private firms consist of material makers of steel and rubber,. bridge makers, general contractors, and design consulting companies.

2. JOINT RESEARCH PROGRAM

Firstly, the damping characteristics of long–span bridges were studied. Based on the experimental studies of the actual bridge vibration tests using eccentric–mass–shakers, it is know that the damping ratio obtained is generally smaller than about 0.01. Therefore, it is of great importance issue to augment the damping characteristics and to reduce section forces which are critical in the design is expected to be effectively performed.

Based on this objectives, the following three subjects was selected in the joint research program.

(1) R&D on High Damping Devices using New Materials and New Structures
   1) Development of new high damping materials applicable for long-span bridges
   2) Development of durable and stable system for long term use as 50 years
   3) Development of small effect for non-seismic situation of bridges
(2) R&D on Design Methods for High Damping Systems
   1) Evaluation methods of damping characteristics of bridges with high damping systems
   2) Selection methods for the location of high damping systems
   3) Design methods of high damping systems and bridge
(3) Applicability Study of High Damping Systems
   1) Seismic response control of bridge under construction
   2) Applicability of high damping systems for cable-stayed bridge, suspension bridge, high pier bridge, and substructure

3. DAMPING CHARACTERISTICS OF LONG-SPAN BRIDGE

Damping characteristics is one of the most important factor for the evaluation of the dynamic behavior of the bridges. For the purpose of studying the damping characteristics of actual long-span bridge bridges, the dynamic vibration testes data using eccentric-mass-shaker were investigated[4].

Table 1 shows the long-span suspension bridges studied where the vibration testes using eccentric-mass-shaker were made after the completion of bridges in Japan. There are some more bridges where the tests were made in the world, but the tests were made by using ambient vibration testing methods. Therefore, in this study analyses was limited to the tested data using the eccentric-mass-shaker. In Table 1, the longest bridge is ① Minami-Bisan-Seto Bridge on Honshu-Shikoku Bridge with center span length of 1,100m, the shortest one is ⑩ Omine Bridge with center span length of 120m. ① Minai-Bisan-Seto bridge and ② Onaruto bridge have double deck with highway and railway. ⑪ Rainbow bridge has double deck with highway and new transportation system. The others has single deck.

In the seismic design, the vibration in the longitudinal and transverse directions is important. Since the past experimental data are originally t o study the stability against wind, the data is in the vertical and torsional directions.

3.1 Natural Frequency

Fig.2 shows the relation between the center span length and the fundamental natural frequency based on the tested data. In the figure, statistical linear equation obtained

from the data were shown and the statistical equations for the cable–stayed bridges were also shown[5]. It should be noted that since the statistical equation for the cable–stayed bridges were obtained from the data with the center span length less than 400m, therefore, span range over 400m is estimation of the out of data range. The natural frequency is smaller for the bridge with longer span length. Statistical equations for the suspension bridges and cable–stayed bridges are almost the same in the vertical vibrations. However, the gradient of the statistical equation for the torsional vibration of the suspension bridges is smaller than that of the cable–stayed bridges. It means that the torsional stiffness for cable–stayed bridges is much larger than that of suspension bridges.

Although the number of data is not enough, good agreement was obtained between the tested data and the statistical equation. The statistical linear equation was obtained as

Vertical Vibration

$$f_1^{BV} = 30.1\, L^{-0.772} \quad (r=0.978)$$

Torsional Vibration

$$f_1^{T} = 246\, L^{-0.070} \quad (r=0.978) \qquad (1)$$

where

f_1^{BV} : fundamental natural frequency (Hz) for vertical vibration
f_1^{T} : fundamental natural frequency (Hz) for torsional vibration
L : center span length (m)
r : correlative coefficient

3.2 Damping Characteristics

Fig.3 shows the relation between the center span length and the averaged damping ratio. The averaged damping ratio means the averaged data of the damping ratios which were obtained for the several modes. In the figure, the statistical equation and the equation of the cable–stayed bridges were also shown. The damping ratio is ranging form 0.002 to 0.034 and large scatter was found in the relation between the damping ratio and the center span length.

Although the number of data is not enough, the statistical linear equation was obtained as similar to that for the natural frequency.

Vertical Vibration

$$h^{BV} = 0.237\, L^{-0.645} \quad (r=0.812)$$

Torsional Vibration

$$h^{T} = 0.082\, L^{-0.307} \quad (r=0.396) \qquad (2)$$

where

h^{BV} : averaged damping ratio for vertical vibration
h^{T} : averaged damping ratio for torsional vibration

L : center span length (m)
r : correlative coefficient

Based on the tested data, it is found that the damping ratio for longer span bridges is smaller. Although the statistical equation was obtained using the data ranging to 1,100m, the damping ratio for the long-span bridge with center span length of 2,000m is estimated as about 0.002 and 0.004 in the vertical and torsional vibrations, respectively.

4. NEW DAMPING AUGMENTATION DEVICES DEVELOPED

The new development through the three years research project are shown in Table 2. These are summarized as follows.

(1) R&D on High Damping Devices using New Materials and New Structures
Ten kinds of high damping devices in total were developed. Table 3 shows the outline of new high damping devices developed. Developed devices were tested and the design equations were also developed. Shaking table tests using a cable-stayed bridge model with high damping devices developed were also made for the verification of the effectiveness of the high damping systems developed.

(2) R&D on Design Methods for High Damping Systems
In th design of long-span bridge with high damping systems, it is important to evaluate the damping characteristics of the bridge based on the energy absorption capability. In this study, the evaluation methods of damping characteristics of the bridges in consideration with the nonlinear hysteresis force displacement relation. To efficiently expect the appropriate damping effect for the bridge structure, the high damping devices have to be appropriately arranged on the bridge. The arranging methods and a simple model for the investigation of the arranging the devices were developed for cable-stayed bridge and high pier bridge.

(3) Application of High Damping Systems
High damping systems are effective to reduce the earthquake response of the long-span bridges through the study of the applicability of the high damping systems for the several long-span bridges. Since there are several bridge types for the long span bridges, the appropriate design methods are required for the design of bridge with high damping devices. In this study, th design methods for controlling the vibration of the bridge under construction, applicability to high pier bridge, cable-stayed bridge, and suspension bridges were studied.

5. CONCLUSIONS

The high damping systems applicable for the long span bridges were developed through the joint research program. The applicability of high damping devices developed for the long span bridges were also studied. Based on this study, the following conclusion were made.

(1) Based on the data of bridges where the dynamic vibration tests were made, the damping characteristics is smaller for longer span bridges. Although the statistical equation was obtained based on the data ranging to 1,100m, the damping ratio for the long-span bridge with center span length of 2,000m is estimated as about 0.002 and 0.004 in the vertical and torsional vibrations, respectively.

(2) Ten kinds of high damping devices in total were developed. Developed devices were tested and the design equations were also developed. Shaking table tests using a cable-stayed bridge model with high damping systems were also made for the verification of the effectiveness of high damping systems developed.

(3) High damping systems are effective to reduce the earthquake response of the long-span bridge through the study of the applicability of the high damping systems for the bridges.

ACKNOWLEDGEMENTS

This study were made through the joint research. The authors appreciate the all participants to the joint research program for their eager work to develop the high damping devices.

REFERENCES

1) Public Works Research Institute, Public Works Research Center and 19 Private Firms : Research Report on the Development of High Damping Systems for Long Span Bridges (No.1 – No.3), Joint Research Report of PWRI, No. 101, 127, 151, (1994.3, 1995.3, 1996.3)
2) Otsuka, H., Unjoh, S., Nagaya, K., and Sato, T. : Application of Seismic Control Design Using High Damping Materials for Long Span Bridges, Bridge and Foundation Engineering, 96–8, 1996–8
3) Public Works Research Institute : Development of Menshin Design of Highway Bridges, October, 1992, Technical Note of PWRI, Vol.60
4) Kawashima, K., Otsuka, H., Unjoh, S., and Mukai, H., : The Damping Characteristics and Seismic Response Characteristics of Long Span Bridge Based on the Vibration Test Data., Civil Engineering Journal, Vol.37, No.3, 1195.3
5) Public Works Research Institute : Research on the Seismic Design of Cable–Stayed Bridge (Vol.1), Technical Memorandum of PWRI, Vol.2388, 1986

Table 1 Suspension Bridge in Japan Where the Vibration Tests Were Made

Bridge Name	Construction Year	Structure	Span Length(m)
① Minami–Bisan –Seto	1988	3–span continuous Truss Girder (Double)	264+1,100+264
② Onaruto	1985	3–span, 2–hinge Truss Girder (Double)	320+864+312
③ Oshima	1988	1–span Box Girder	140+560+140
④ Kanmon	1973	3–span, 2–hinge Truss Girder	178+712+178
⑤ Wakato	1962	3–span, 2–hinge Truss Girder	89+367+89
⑥ Hakogase	1967	3–span, 2–hinge Truss Girder	30+206+30
⑦ Kamiyoshino	1971	1–span Truss Girder	32.6+250.8+32.6
⑧ Konohana	1989	3–span, Mono–Cable Box Girder	120+300+120
⑨ Sonohara	1969	1–span Truss Girder	136
⑩ Omine	1970	1–span Truss Girder	120
⑪ Rainbow	1993	3–span, 2–hinge Truss Girder (Double)	114+570+114

Table 2 Development of Three Year Joint Research Program

R&D Issue	Summary of Developed Technology
High Damping Devices	(1) Ten kinds of new high damping devices were developed. 1) Rotational Lead Extrusion Damper 2) Bending Damper using Low Yield Point Steel 3) Canti-Lever Damper using Low Yield Point Steel 4) Super Rubber Damper 5) Super High Damping Rubber Bearing 6) 3-Dimensional Composite Material 7) Friction Pavement 8) Powerful TMD 9) Damper at the Girder end 10) TLD (2) Experimental Study of High Damping Devices Developed (3) Proposal of Design Equations for High Damping Devices (4) Verification Tests by Shake Table Tests of Model Bridge
Design Methods	(1) Estimation Methods of Damping Ratio of Total Bridge based on the Energy Absorption Consideration (2) Efficient Arranging Methods of High Damping Devices
Application	(1) Seismic Response Control of Bridge under Construction 1) Control Devices using AMD and Variable Stiffness Damper 2) Verification Tests by Shake Table Tests of Model Bridge (2) Seismic Isolation of Foundation 1) Seismic Isolation Design of Large Rigid Foundation using isolation and mass-damper concepts 2) Isolation Foundation for Cable-Stayed Bridge (3) Application to High Pier Bridge Damper at girder ends, slab isolation, application of TMD and AMD (4) Application to Cable-Stayed Bridge Damper, TLD, Cylindrical High Damping Rubber Damper, 3-D Composite Material Damper (5) Application to Suspension Bridge Cable Damper

Table 3(1) High Damping Devices Developed for Long Span Bridge

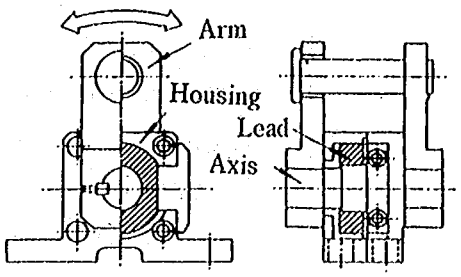
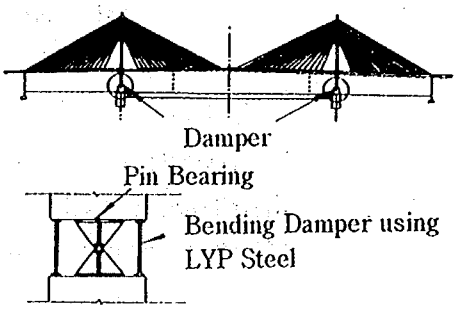
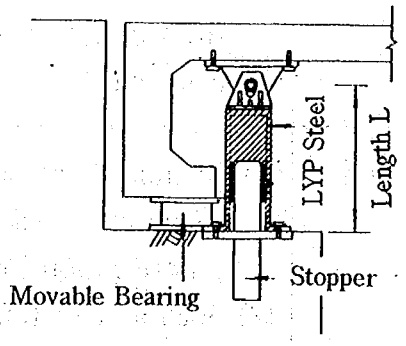
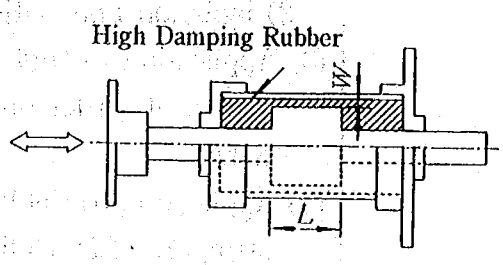
Devices	Energy Absorption	Illustration
Rotational Lead Extrusion Damper	Energy absorption by plastic deformation of lead (cylinder type and rotation type)	
Bending Damper using Low Yield Point Steel	Energy absorption by plastic deformation of low yield point steel (at the bottom of cable-stayed bridge)	
Canti-Lever Damper using Low Yield Point Steel	Energy absorption by plastic deformation of low yield point steel (canti-lever type)	
Super Rubber Damper	Energy absorption by deformation of high damping rubber (shear type and flow type)	(Flow Type Damper) 
Super High Damping Rubber Bearing	Damping characteristics is larger than usual high damping rubber bearings (equivalent damping ratio is larger than 20%)	

Table 3(2) High Damping Devices Developed for Long Span Bridge

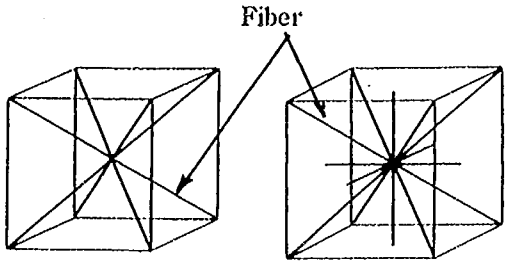
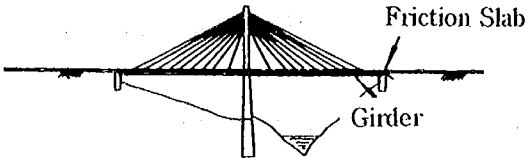
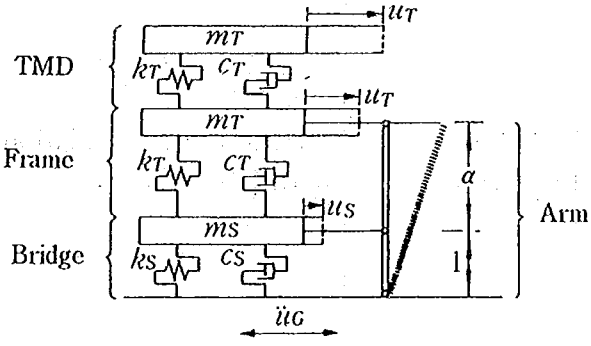
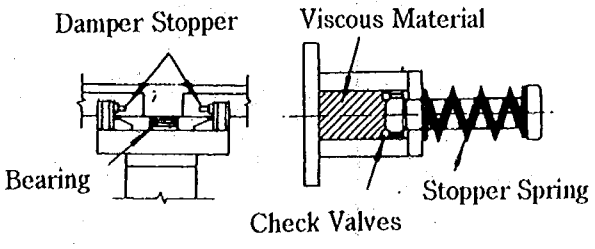
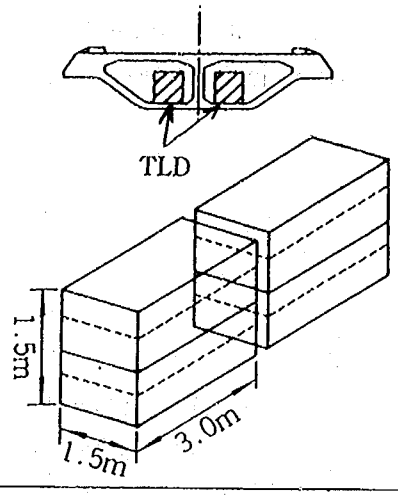
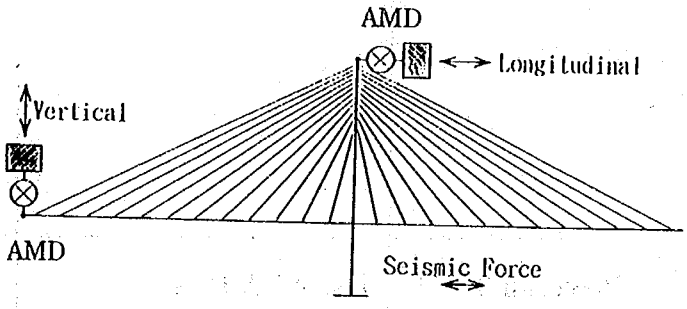
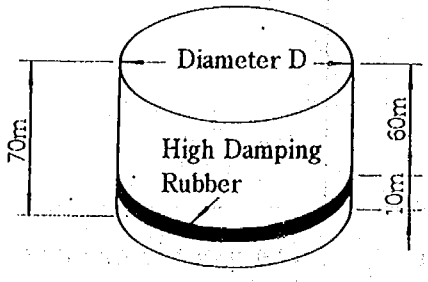
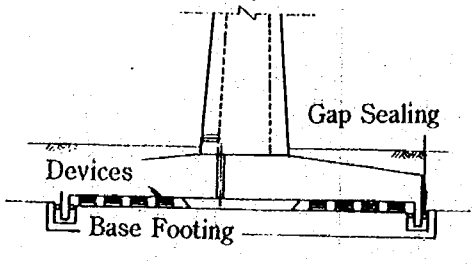
Devices	Energy Absorption	Illustration
3–Dimensional Composite Material	Composite Material with grass fiber reinforced plastic and epoxy resin	(Structure of Fiber) 
Friction Pavement	Energy absorption by friction between slab and bridge girder	(Application to Cable–Stayed Bridge) 
Powerful TMD	Usual TMD is strengthened by arm action	
Damper at Girder end	Dampers is installed at girder ends	

Table 3(3) High Damping Devices Developed for Long Span Bridge

Devices	Energy Absorption	Illustration
TLD	Energy absorption by liquid sloshing vibration	(TLD is installed in the girder box) 
Control of Bridge under Construction by AMD	AMD to increase the seismic safety of bridges under construction	
Isolation Foundation	Large scale foundation with isolation	(Rigid Foundation)  (Foundation of Cable-Stayed Bridge) 

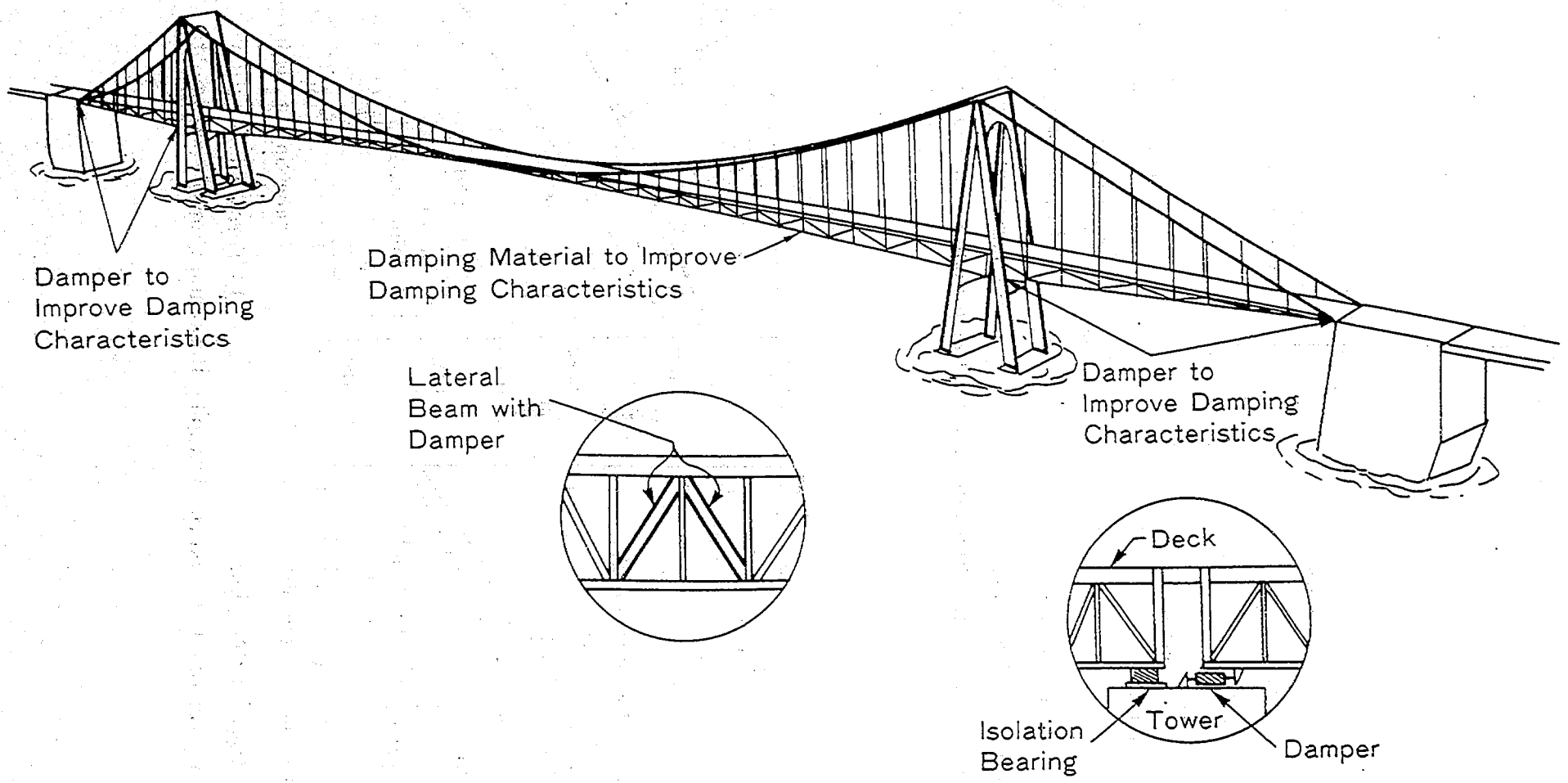
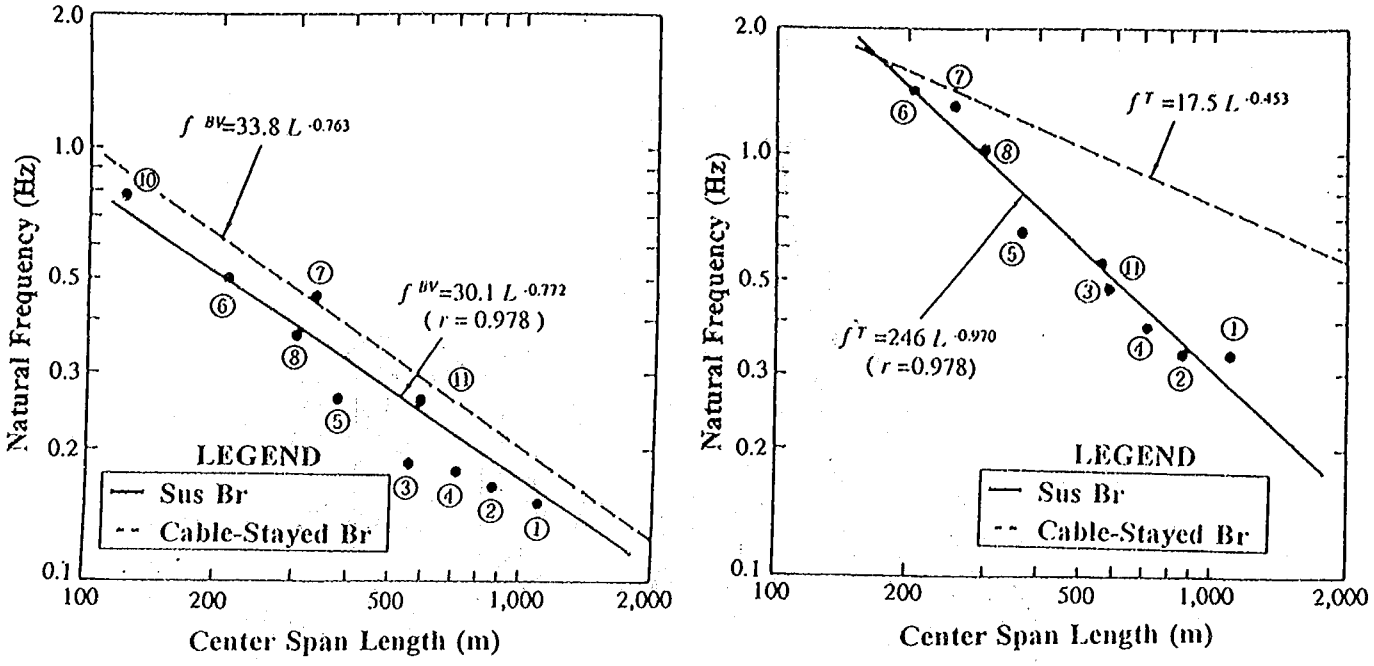
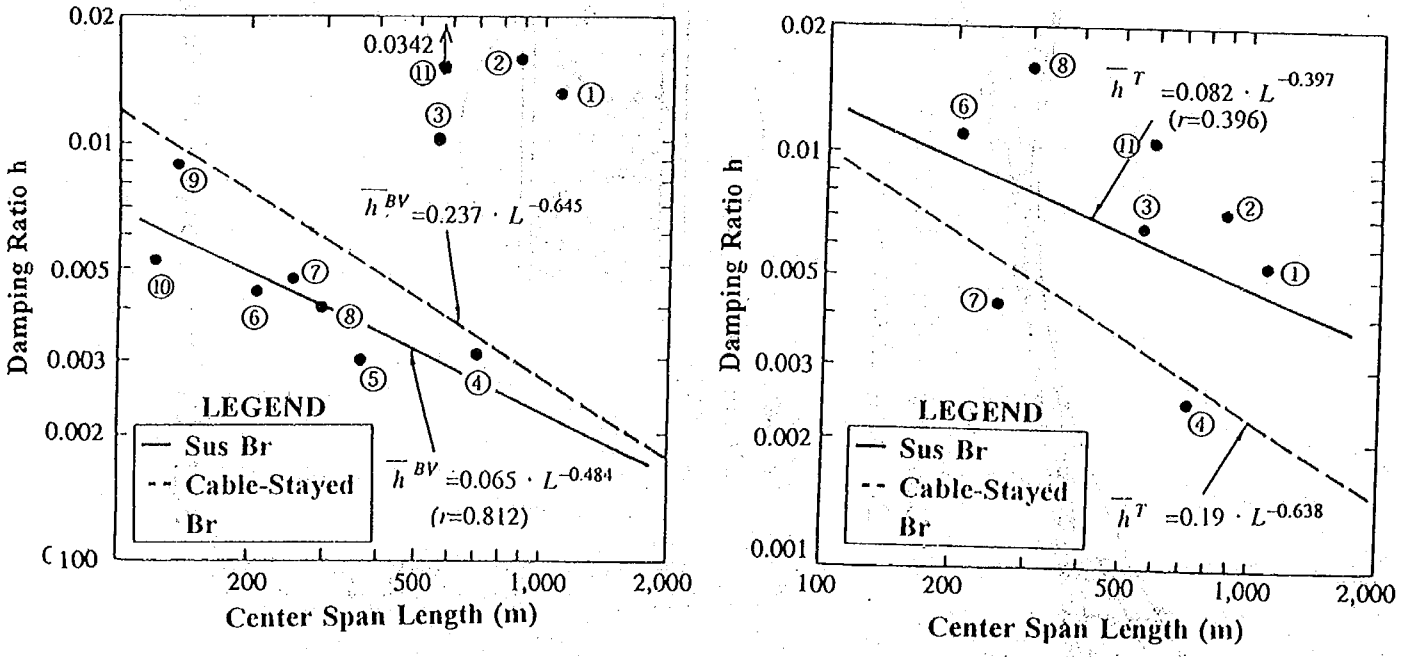


Fig.1 Illustration of High Damping Systems for Long-Span Bridges



(a) Vertical Vibration (b) Torsional Vibration

Fig.2 Relation between the Fundamental Natural Frequency and Center span Length



(a) Vertical Vibration (b) Torsional Vibration

Fig.3 Relation between the Damping Ratio and Center span Length

DEVELOPMENT OF HIGH DAMPING DEVICES FOR LONG SPAN BRIDGES AND THE DESIGN METHOD

Shigeki Unjoh[1], Yozo Goto[2], Ikuo Simoda[3], and Yasuo Machara[4]

1)Head, Earthquake Engineering Division, Public Works Research Institute, Ministry of Construction, Tsukuba Science City, Ibaragi, Japan
2)General Manager, Civil Engineering Department, Technical Research Institute,Obayashi Corporation, Kiyose-shi, Tokyo, Japan
3)General Manager, Development Section, Structural Equipment Division, Oiles Corporation, Fujisawa-shi Kanagawa, Japan
4)General Manager, Second Engineering Division, Yatiyo Engineering Corporation Meguro-ku, Tokyo, Japan

ABSTRACT

Cable stayed bridges and other long span bridges are low damping structures, and there is a possibility that earthquake response could be effectively decreased by the appropriate installation of devices that improve levels of damping. A joint research project was set up by the Public Works Research Institute of the Ministry of Construction, the Public Works Research Center and 19 companies from private sector to develop high-damping devices and design methods that utilize them. This report introduces some of the devices developed and the design methods.

INTRODUCTION

Damping levels for long span bridges generally become lower the longer the span of the bridges are, and this easily leads the bridges vibrate. In long span bridges, damping has great effect on the earthquake response of the super structures and the section force passed through to the foundations, and the section of structural members could be efficiently decreased by improving the damping, leading to the expectation of more economic designs.

In order to improve damping in long span bridges, it is necessary to develop damping devices and vibration control devices suitable for long span bridges. It is also necessary to establish a method of design with high-damping as the objective. For this purpose, a joint research project was set up between 1993 and 1995 by the Public Works Research Institute of the Ministry of Construction, the Public Works Research Center and 19 companies from private sector.

This joint research project was divided into three separate fields,(1) development of high damping devices with the use of new materials and new mechanisms, (2) the development of design methods that utilize the devices, and (3) the applications of the design methods to long span bridges. This paper will report on the five types of high damping devices developed in (1) and a certain point of the design method developed in (2).

DEVELOPMENT OF HIGH DAMPING DEVICES

Lead Extrusion Damper (Oiles Corporation was in charge.)

1) Structural Aspect

As lead possesses a re-crystallization property, the material durability is good and it is confirmed that its characteristics against repeated excitation when placed in a housing are stable. A lead extrusion damper (LED) for lead poured into a cylinder type housing has already been developed in New Zealand (Fig. 1), and a rotation type LED for small capacity has been developed in Japan. This joint research project, therefore, developed a rotation type LED as large as possible for application with long span bridges. Fig. 2 indicates the prototype of the large-scale rotation type LED with a capacity of 35tf. Horizontal movement is converted across to the shaft's rotary movement with the use of an arm, and the protrusion attached to the rotation shaft molds the lead within the housing.

2) Result of Performance Tests

A representative hysteresis curve is indicated in Fig. 3. Backlash was monitored in two locations of the curve. The backlash with a load close to zero was created by the arm and rod pin, and the backlash with a load close to 20tf was caused by the gap between the lead and the rotation shaft protrusion. This gap can be reduced by increasing the pressure on the lead poured into the housing.

Fig. 4 shows the relationship between displacement and resistance, and Fig. 5 shows the effect of the exciting frequency on the relationship between displacement and absorbed energy. Resistance increases in accordance with increased displacement, but the rate of increase gradually decreases.

This tendency is the same as the characteristics held by lead during shearing deformation and it is assumed that resistance is generated in rotation type models also through shearing. The area of hysteresis loop indicated that a tendency for the absorbed energy it to increase accordance with increased displacement existed.

As a remarkable difference in the frequency was not recognized with these diagrams, the velocity dependency was assumed to be minimal.

The temperature of the lead increased and the resistance fluctuated when the number of times a repeated load was placed on it was increased. A repeated load was placed on a small device with a capacity of 1.5tf three-hundred times, and the results of the relationship between temperature rises and resistance is indicated in Fig. 6. Although the temperature rose from 30 degrees to 70 degrees, the amount of fluctuation in the resistance remained at approximately 20%

3) Conclusions

Rotation type LEDs possess the following features;

① The ability to absorb energy existed from a comparatively small displacement.

② Amplitude dependency was observed in resistance and absorbed energy.

③ Frequency dependency in resistance and absorbed energy was minimal.

④ Repetition led to increases in temperature, but the effects on performance were relatively small.

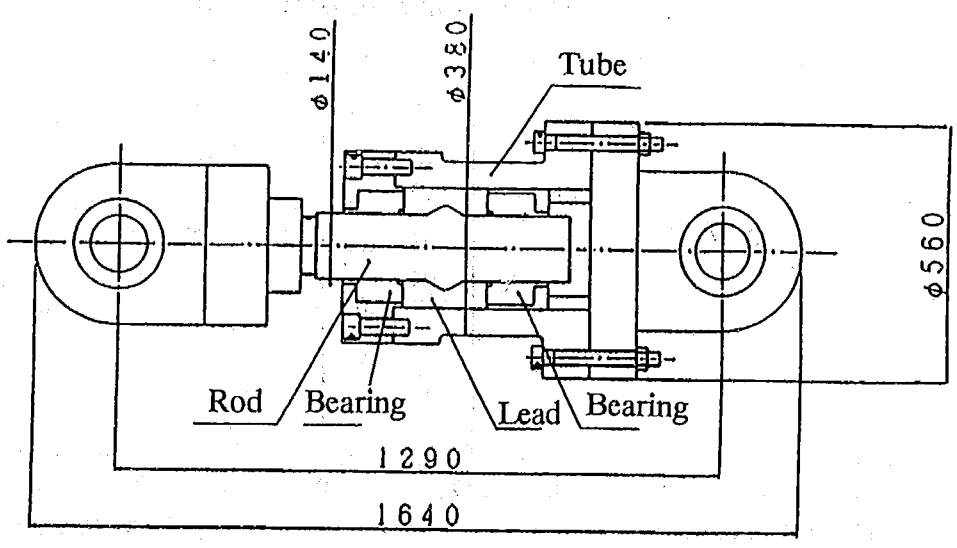


Figure 1 Cylinder Type LED

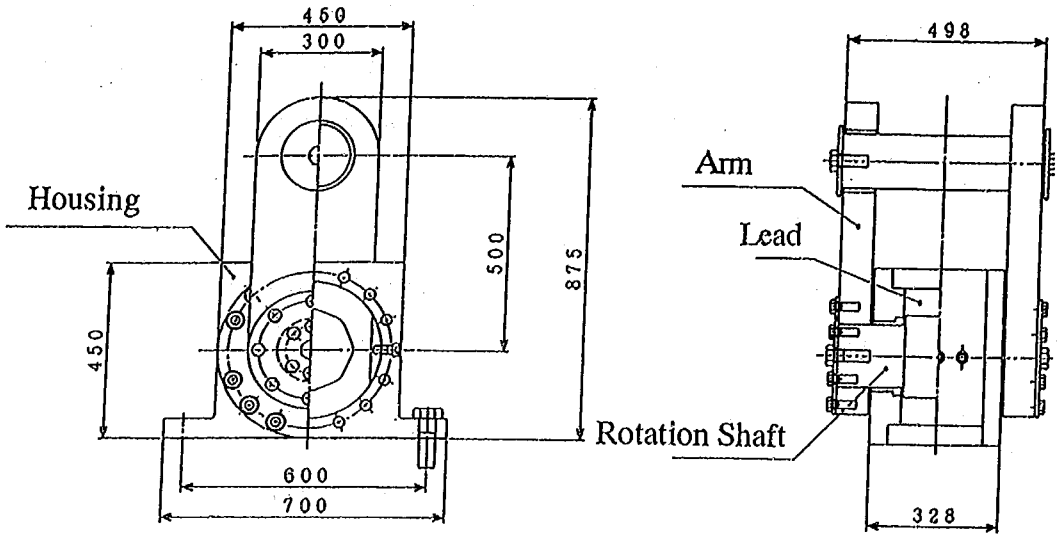


Figure 2 Rotation Type LED (Capacity : 35tf)

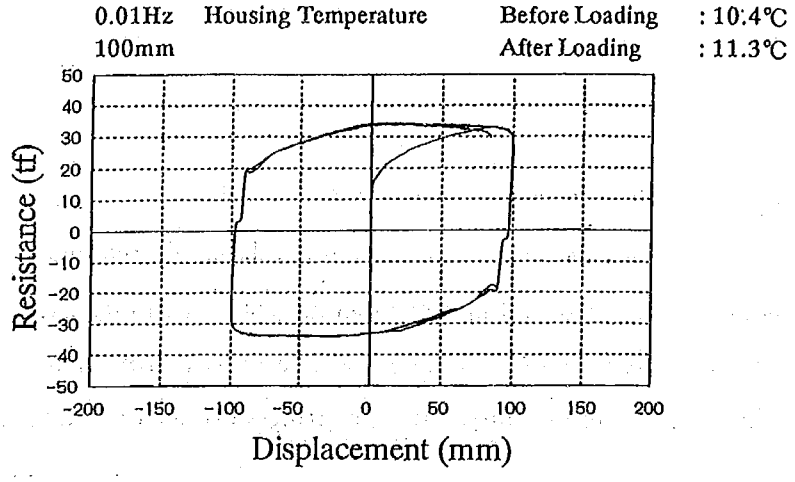


Figure 3 Hysteresis Curve (0.01Hz, 100mm)

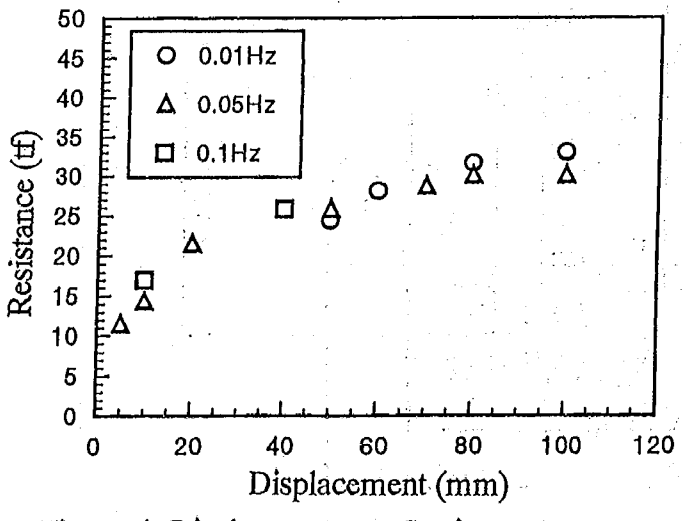


Figure 4 Displacement vs. Resistance

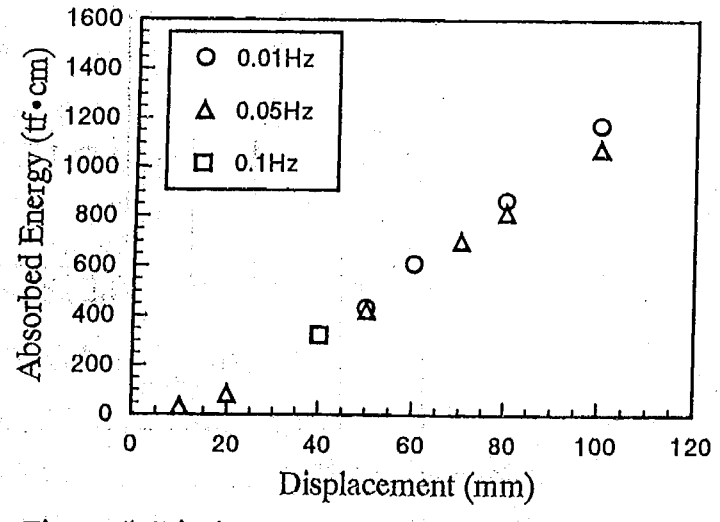


Figure 5 Displacement vs. Absorbed Energy

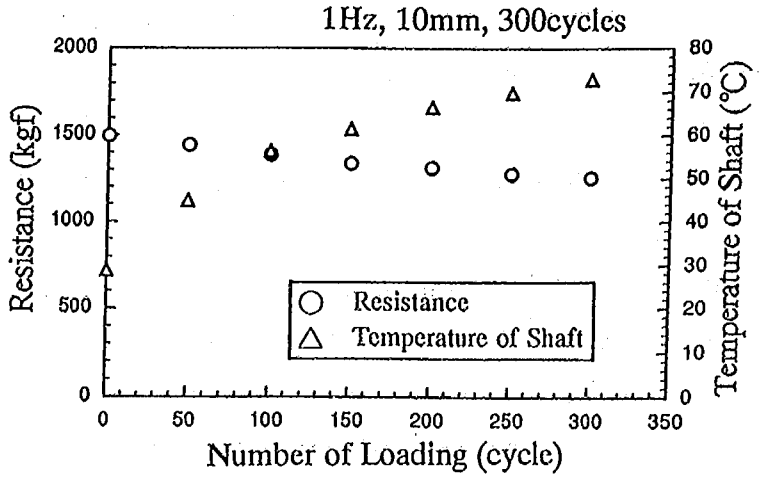


Figure 6 Temperature Rise and Resistance Drop due to Repeated Load

Very Low Yield Point Steel Damper
(Takenaka Civil Engineering & Construction CO., LTD. was in charge.)

1) Structural Aspect

As the very low yield point steel (BT-LYP100) is a material that does not display a clear yield point, it has excellent hysteresis energy absorption capacities. A cantilever beam-type damper was therefore developed with the use of very low yield point steel assuming that it could be placed between the main girder and main tower of cable stayed bridges, and between the girder and pier, or girder and abutment of high pier long span bridges.

An outline diagram of the damper is provided in Fig. 7. Stoppers were used in combination with the objective of widening the plastic zone of the cantilever.

2) Result of Performance Tests

Fig. 8 provides an outline diagram of a dynamic loading frame and the test device with a two stages gap included between the very low yield point steel's cantilever and the stopper.

A representative hysteresis curve is indicated in Fig. 9. The cantilever came into contact with the lower stopper with +/-5mm of displacement amplitude and even came into contact with the upper stopper with +/-10mm of displacement amplitude. Significant changes appeared in the stiffness of

the damper through the contact, but the changes were not sharp. It was also confirmed that the hysteresis curve was not affected by loading speed.

Fig. 10 and Fig. 11 show the relationship between equivalent damping constants, equivalent stiffness (secant stiffness) and displacement amplitude extracted from the hysteresis curve. Although sufficient damping for analytical estimate was not attained owing to a certain amount of play in the area where the test device was attached, the damping constant maintained an almost stable value through the effects of the stoppers even when the displacement amplitude was increased. The amount of reduction in equivalent stiffness was relatively low.

3) Conclusions

① By combining a multi-stage stopper with the cantilever beam type damper with the use of very low yield point steel, it was possible to make a damper that was comparatively unaffected by displacement amplitude and loading speed.

② The non-linear finite element analysis predicted the damper's hysteresis curve.

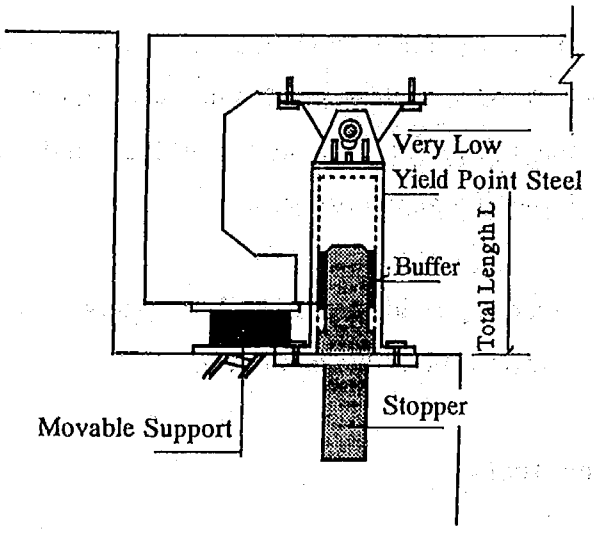


Figure 7 Outline Diagram of Cantilever Damper

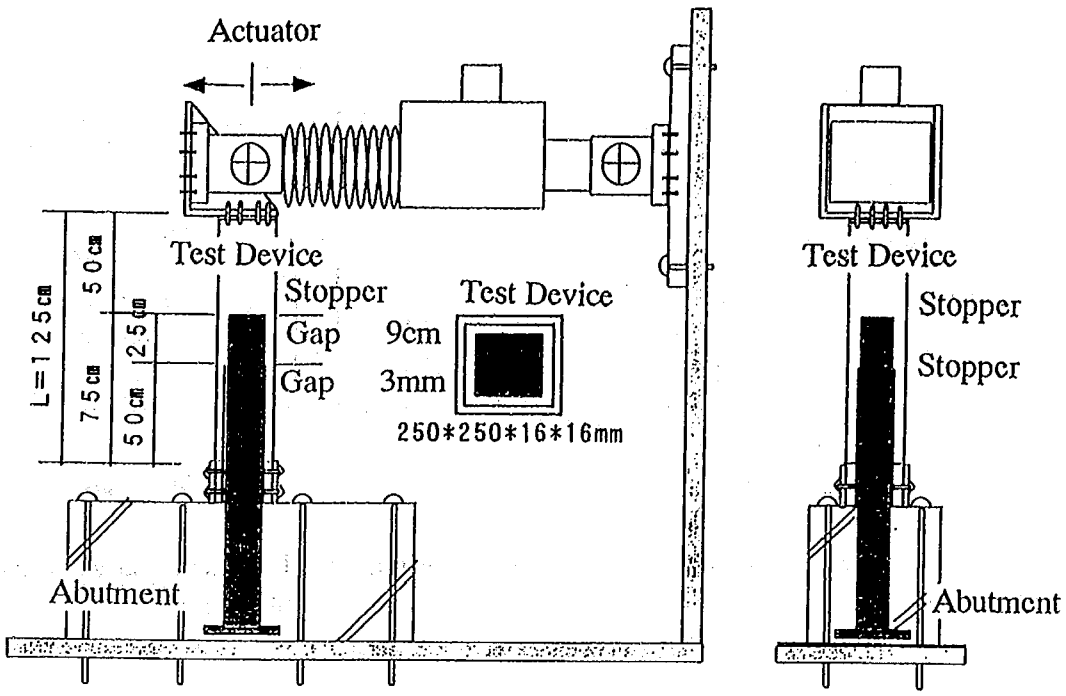
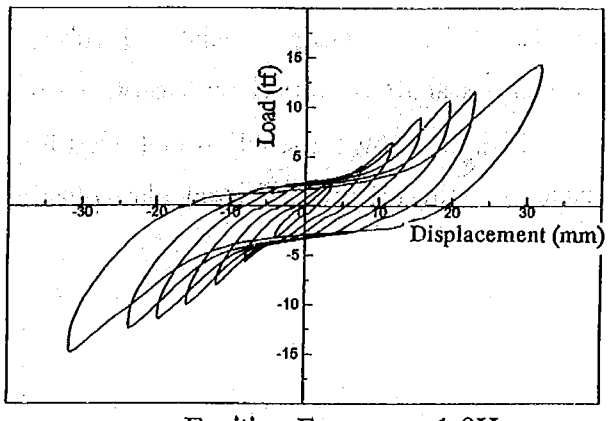
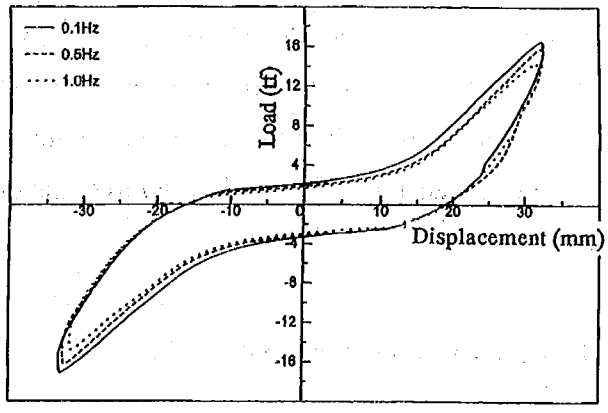


Figure 8 Dynamic Loading Frame



Exciting Frequency 1.0Hz



Displacement Amplitude ±30mm

Figure 9 Hysteresis Curve

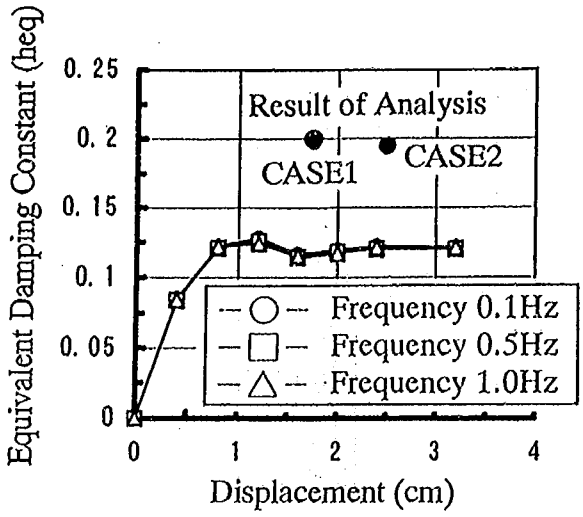


Figure 10 Displacement vs. Equivalent Damping

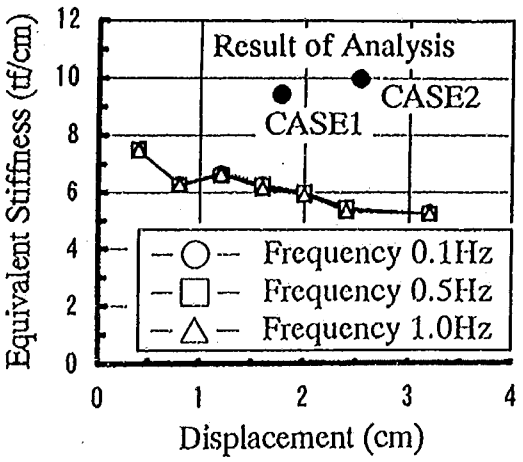


Figure 11 Displacement vs. Equivalent Stiffness

Highly Plastic Rubber Damper (Bridgestone Corporation was in charge.)

1) Structural Aspect

A flow resistance type damper was developed by this research project with high plasticity rubber. An outline diagram of the device is displayed in Fig. 12. The structure consists of rubber (unvulcanized fluid rubber) poured into a sealed housing and a shaft equipped with protrusions that create the plastic flow of the rubber to absorb energy. Fig. 12 shows a small model used for the performance test. The rubber poured inside possesses certain features of ideal elast-plastic material.

2) Result of Performance Tests

A representative hysteresis curve for load displacement relations is indicated in Fig. 13. The curves were almost square for all amplitudes, and resistance increased as the amplitude and frequency became larger. Fig. 14 shows the relationship between displacement speed and resistance. Resistance were in proportion to 0.28 powers of velocity.

Fig. 15 indicates the characteristics obtained when a constant displacement amplitude was subjected to continuously and repeatedly. The temperature rose by approximately 20 degrees of centigrade for every one-hundred repeat on 50cm amplitude. The rate of decrease for the

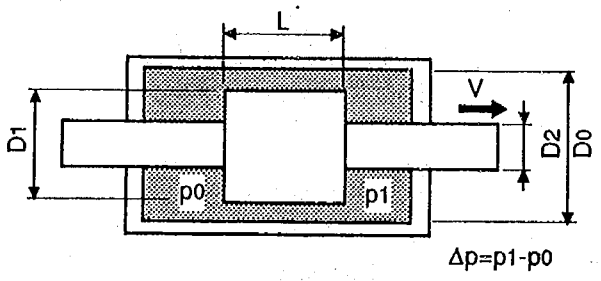
resistance at this point was approximately 30%, but the hysteresis curve had little change and remained stable.

3) Design Method

If the poured rubber is asumed to be non-Newtonian viscous fluid and the shear stress and differential pressure within the housing is to be proportional, it is possible to express the resistance F_D of the damper with equation (1) and equation (2).

$$F_D = \frac{C'\pi D_0 D_1 L}{D_0 - D_1} V^n \tag{1}$$

$$C' = C\left\{\frac{4(D_0 + D_1)}{(D_0 - D_1)^2}\right\}^n \tag{2}$$



In this case, V: velocity, C: material constant and n: material constant becomes 0.28, $D_1 >> D_2$.

4) Conclusions

① The resistance of dampers made with high plasticity rubber was in proportion to approximately 0.28 powers of velocity.

② Comparatively stable characteristics were indicated for repeated loading.

③ The resistance to which the dampers are subject can be evaluated with equation (1) and equation (2).

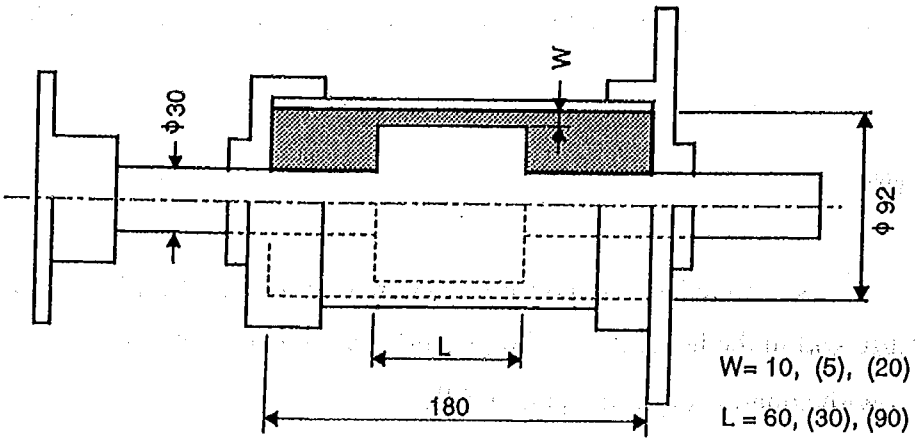


Figure 12 High Plastic Rubber Damper

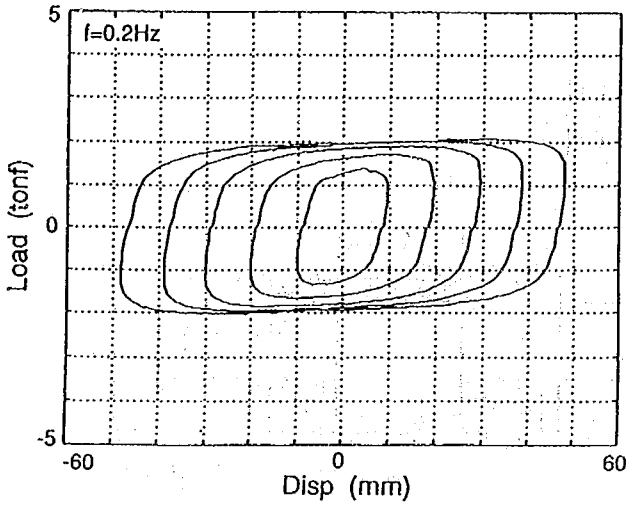


Figure 13 Hysteresis Curve (W=1cm, L=6cm)

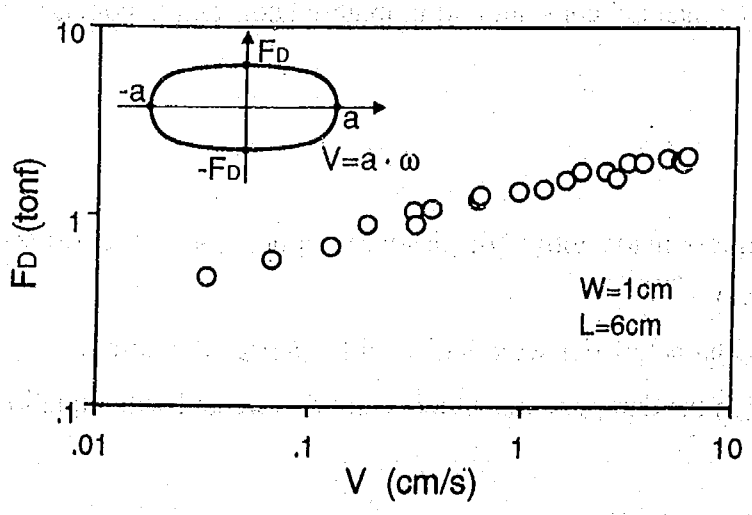


Figure 14 Velocity vs. Resistance (W=1cm, L=6cm)

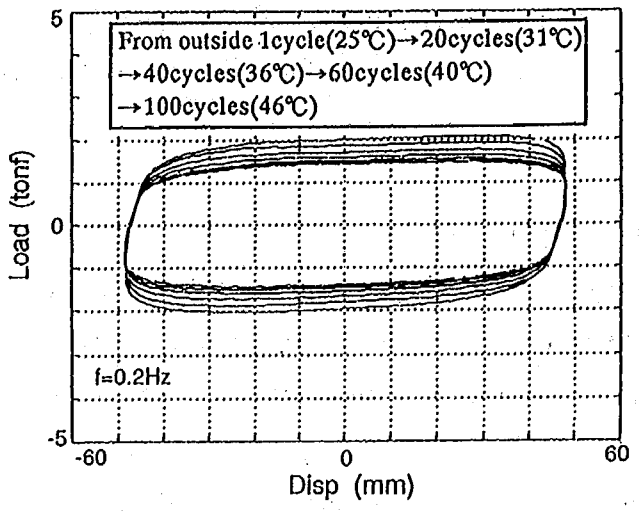


Figure 15 Hysteresis Curve taking Number of Times of Repeated Load as Parameter

Very High Damping Rubber Bearing
(The Yokohama Rubber Company was in charge.)

1) Structural Aspect

Very high damping rubber has been developed with an equivalent viscous damping constant of approximately 15% and is currently being used as Menshin bearings for normal bridges, but this joint research developed a rubber with even higher damping capabilities. An investigation into the installation of dampers made with this rubber at the connection points of suspension bridges and cable stayed bridges was also carried out.

Fig. 16 shows the structure outline of a device that utilizes the developed rubber. By permitting the upward and downward displacement and using comparatively soft springs for the horizontal relative displacement, the manifestation of a large damping effect can be expected.

2) Performance Tests

A high rigidity type and low rigidity type of very high damping rubber were developed having approximately 20% of equivalent damping constant as an object.

The characteristic change when repeated displacement was enforced at a test temperature of

between -10 degrees and 40 degrees of centigrade with a frequency of 0.2Hz, and a shear strain ratio of +/-100% is shown in Fig. 17. Damping remained stable whereas the rigidity was observed to change.

Characteristic changes when displacement was enforced in a series with a test temperature of 2 degrees and a frequency of 0.2Hz are shown in Figs. 18-19. Ten cycles of displacement was applied for each of four stages between a shear strain ratio of 25% and 150% in the first series, and the average value from between cycle 4 and cycle 10 amongst the ten cycles is shown. The second series shows the data acquired by repeating the same test after all cycles had ended for the first series. The loading history effect and the shear strain effect were found slightly in the shear rigidity. The high rigidity type showed a tendency for the equivalent damping constant to decrease in accordance with increases in shear strain.

Fig. 20 shows the effects of loading velocity. The shear strain showed a tendency to increase slightly as the frequency became higher, but fluctuations in the equivalent damping constant were minimal.

3) Conclusions

① A shear type damping device made of very high damping rubber was proposed under the intention that it would be installed at the contact point of the upper and lower structures of long span bridges, and two types of device using very high damping rubber were developed.

② The developed dampers were affected by temperature and the rigidity was affected by the loading history, shear strain and loading velocity. But, it was confirmed that these values were within the boundaries of practical use.

③ Confirmation of long-term durability was not evaluated and will be the subject of a later inquiry.

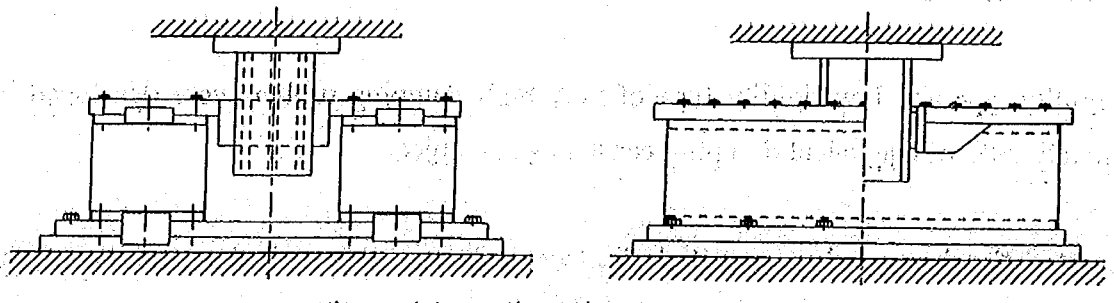
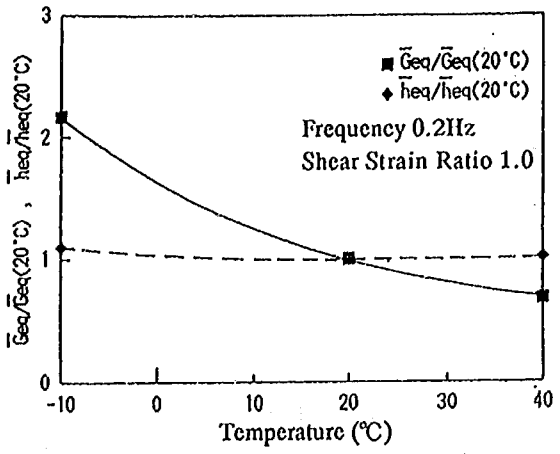
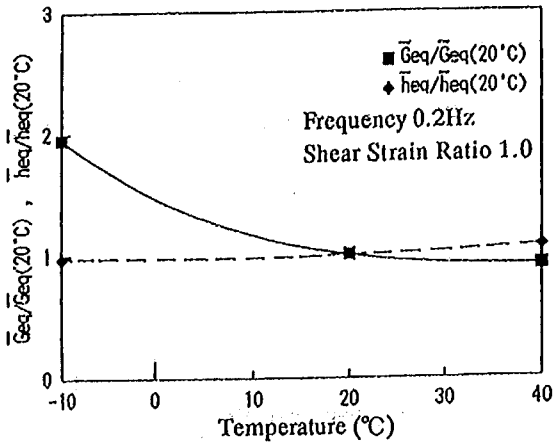


Figure 16 Outline Diagram of Damper

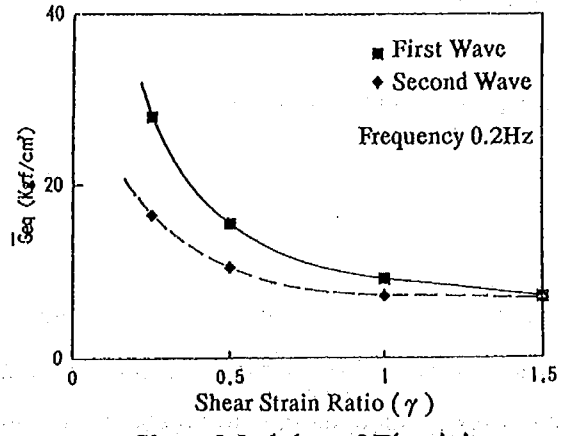


High Rigidity & High Damping Rubber

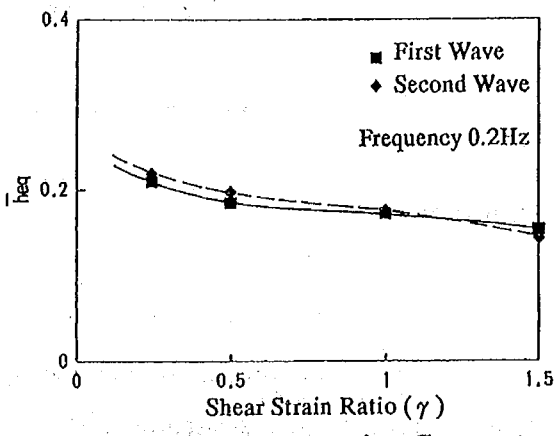


Low Rigidity & High Damping Rubber

Figure 17 Effect of Temperature

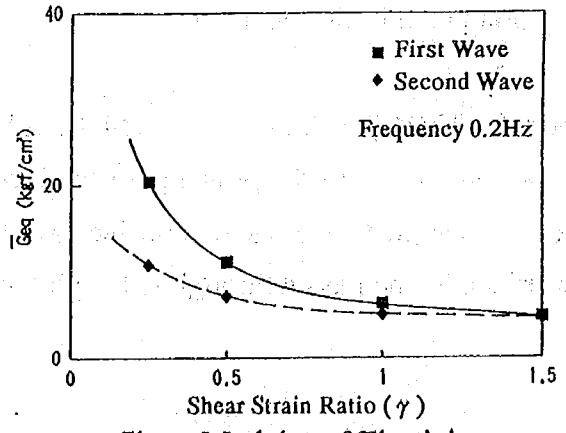


Shear Modules of Elasticity

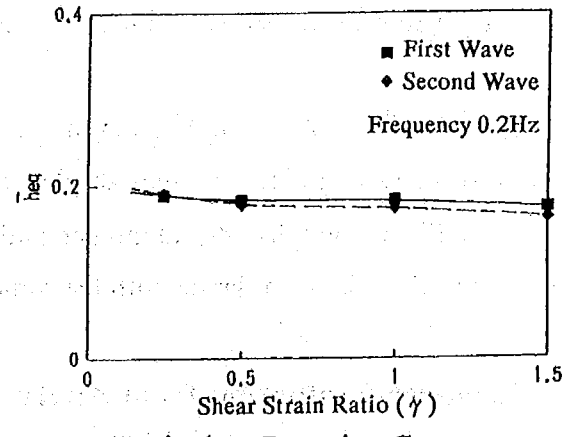


Equivalent Damping Constant

Figure 18 Effect of Amplitude (High Rigidity High Damping Rubber)

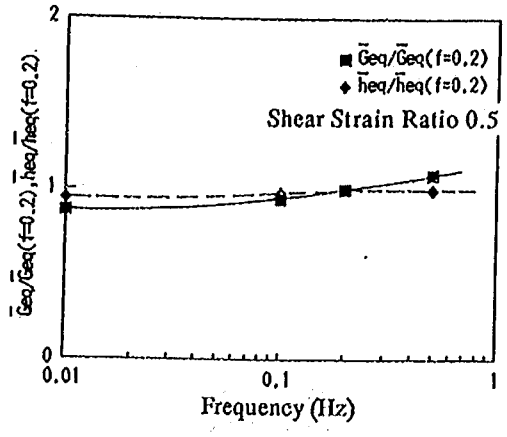


Shear Modules of Elasticity

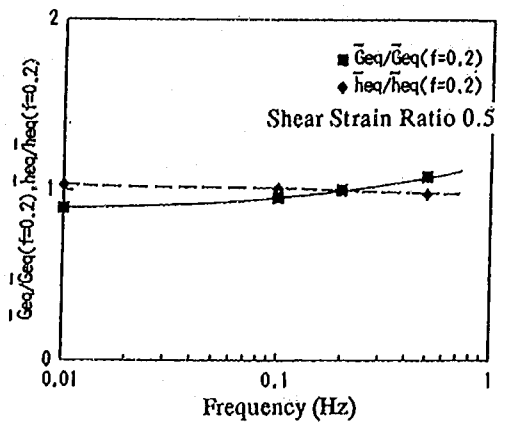


Equivalent Damping Constant

Figure 19 Effect of Amplitude (Low Rigidity High Damping Rubber)



Frequency Dependency
(High Rigidity & High Damping Rubber)



Frequency Dependency
(Low Rigidity & High Damping Rubber)

Figure 20 Effect of Loading Velocity

Powerful TMD (Lever-Amplified TMD, Kumagai-gumi CO.,LTD. was in charge.)

1) Structural Aspect

TMDs have accumulated many results as vibration control devices. But, although they are effective against external forces, such as the steady vibrations caused by wind, etc., they have not so effective reduction against strong unsteady external forces, such as earthquakes, particularly against maximum peak response. On the other hand, the bridge girders are connected to the abutments at each end of the bridge. Then, this joint research developed a damper with increased TMD vibration control forces by taking some of the reaction in the bridge abutment.

Fig. 21 shows a dynamic conceptual outline of the Powerful TMD (Lever-Amplified TMD). It has a function to increase girder response displacement in accordance with the principle of the levers that act as a fixed point for the abutment and passes it through to the TMD, and increase the reaction of the TMD in accordance with the same lever principle and pass it through to the girder.

2) Performance Evaluation from Analysis

The equation of motion for the model in Fig. 21 can be stated with equation (3) if the girder and TMD are simplified to be two degrees of freedom system.

$$\begin{bmatrix} m_S & 0 \\ 0 & m_T \end{bmatrix}\begin{bmatrix} \ddot{u}_S \\ \ddot{u}_T \end{bmatrix}+\begin{bmatrix} c_S+r_L{}^2c_T & -r_Lc_T \\ -r_Lc_T & c_T \end{bmatrix}\begin{bmatrix} \dot{u}_S \\ \dot{u}_T \end{bmatrix} + \begin{bmatrix} k_S+r_L{}^2k_T & -r_Lk_T \\ -r_Lk_T & k_T \end{bmatrix}\begin{bmatrix} u_S \\ u_T \end{bmatrix} = -\begin{bmatrix} m_S & 0 \\ 0 & m_T \end{bmatrix}\begin{bmatrix} 1 \\ 1 \end{bmatrix}\ddot{u}_G \tag{3}$$

Here, the characters S, T and G represent the girder, the TMD and the foundation respectively. r_L is the lever ratio.

Also, the optimums tuning condition and optimum damping condition were applied in equation (4) and equation (5).

$$\nu_{opt} = \frac{1}{1+r_L{}^2\mu} \tag{4}$$

$$h_{opt} = \sqrt{\frac{3r_L{}^2\mu}{8\{1+r_L{}^2\mu\}}} \tag{5}$$

Here, ν_{opt} represents the optimum frequency ratio in the target mode for vibration control for the TMD and girder, h_{opt} represents the TMD's optimum damping constant, and μ represents the mass ratio of the TMD weight and the girder.

In addition to this, the damping constant observed when the two degrees of freedom system composed of the TMD and girders are converted across to an equivalent single degree of freedom system for the girder only was applied in the following equation.

$$h_{eff} = c_h \cdot h_{eff\,0} = c_h \cdot \frac{h_T r_L{}^2 \mu\nu}{\left(\nu^2-1\right)^2+\left(2h_T\nu\right)^2} \tag{6}$$

Here, C_h is an unsteadiness coefficient of seismic waves and a factor of approximately 0.7 is applicable in accordance with ν being the natural frequency ratio of the TMD and the girder.

In order to confirm the effectiveness of the Powerful TMD (Lever Amplified TMD), earthquake response analysis was performed on the four-spans high pier pre-stressed concrete moment frame bridge indicated in Fig. 22 with a multiple masses model. Table 1 shows the main modes of bridge axial direction. As the effective mass ration of the first mode is a large 0.85, the TMD was designed with the vibration control mode as the first mode. The response trace when μ=0.03 and r_L=4 are shown in Fig. 23. It was found from the acceleration trace that the first mode response is restrained. The response displacement rate in Fig. 23 shows that although the first wave showed movement similar to no vibration control half way though, the subsequent displacement was restrained. Reaction for the pier was the same, and the reactions on the abutment reach approximately 300tf.

3) Conclusions

① A TMD with increased vibration control effect was developed based on TMDs with the use of reaction from the abutment. The formulation of the dynamic model gave the optimum tuning method and effective damping evaluation method.

② Comparisons were made with existing TMDs by analyzing earthquake response, and higher level of vibration control effectiveness was obtained.

③ The required stroke of the mass of this TMD and the abutment reaction are greatly affected by input earthquake motion.

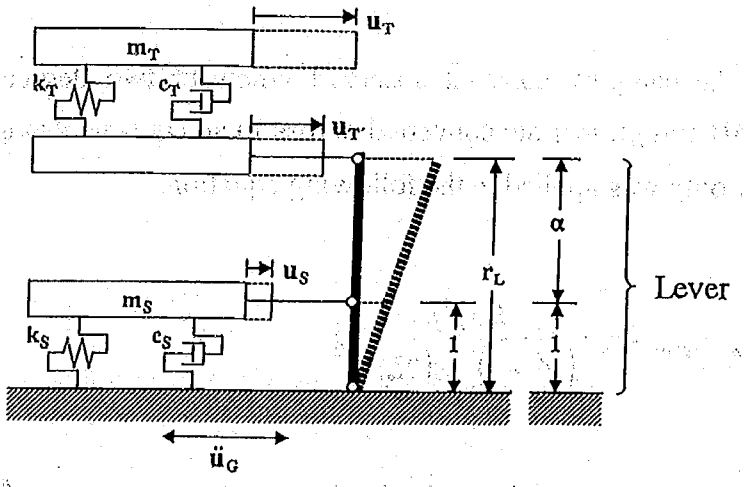


Figure 21 Conceptual Outline of Powerful TMD (Lever-Amplified TMD)

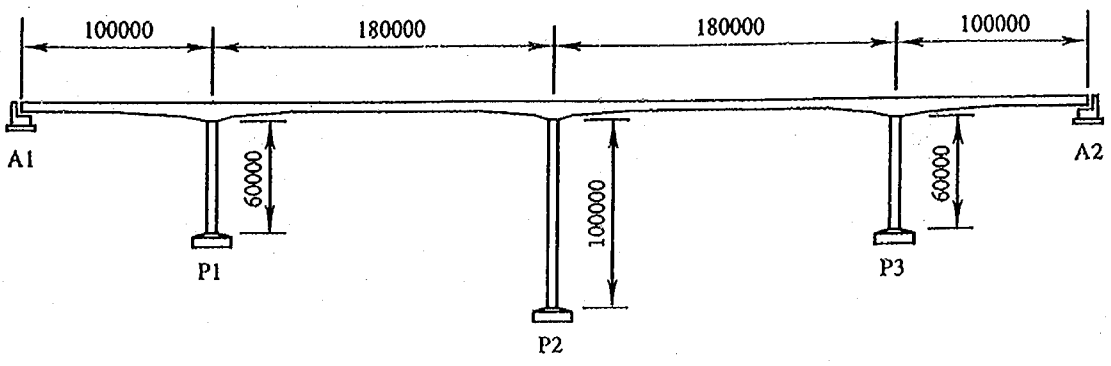


Figure 22 Model Bridge

Table 1 Main Modes of Vibration (Axial Direction)

Mode i	Natural Period T_i (sec)	Excitation Coefficient β_{xi}	Effective Mass m_{xi} (tf•s²/m)	Effective Mass Ratio $m_{xi}/\Sigma m_{xi}$
1	3.223	1.037	2180.6	0.846
2	1.657	0.343	48.1	0.019
3	0.732	0.404	78.4	0.030
4	0.608	0.178	9.7	0.004
5	0.457	-0.082	3.8	0.001
6	0.282	-0.269	48.2	0.019
7	0.241	0.121	5.8	0.002
8	0.236	0.235	41.1	0.016
9	0.188	0.111	12.2	0.005
10	0.180	-0.164	8.3	0.003
All Mode			2490.8	1.000

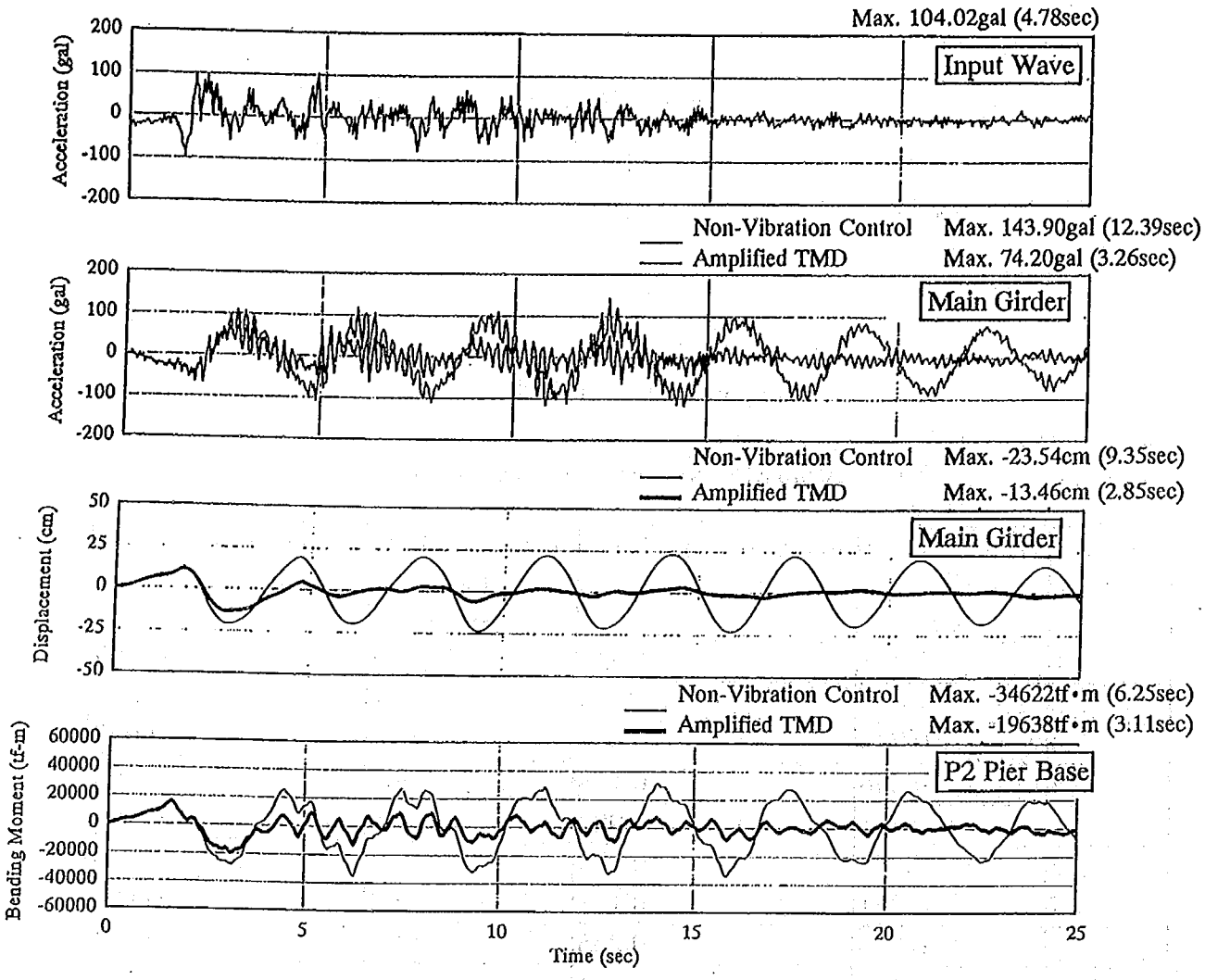


Figure 23 Response Trace

DEVELOPMENT OF OPTIMUM ARRANGEMENT OF DAMPERS

Objectives

In order to improve the earthquake resistance of cable stayed bridges, suspension bridges and other long span bridges, it is necessary for the dampers and other devices to be created on a huge scale. It is therefore desirable to develop a method that increases effectiveness at minimal costs. This joint research investigated the methods of arranging devices that attain required damping effects while being subject to minimal damping capacity.

Fundamental Points Related to the Optimum Arrangement of Dampers

There are examples of research into the optimum arrangement of dampens in the fields of building construction and machinery. By referring to the design method of the active vibration control optimum arrangement in high-rise buildings by Kobori, etc., the optimum arrangement index method (Ref. 2) by F. Y. Cheng, etc., and the research carried out into machine engineering by Sato (Ref. 3), the following multiple degrees of freedom system's optimum damping arrangement for bridges were summarized as follows:

① In the case of dampers subject to damping effects at the points such as TMD, installation was carried out in the web position of the vibration mode.
② In the case of relative displacement detection type dampers, installation was carried out between the mode's web and node.
③ In the case of strain detection type dampers, installation was carried out in the position where the maximum strain occurred.
④ A common factor for all types is the necessity to perform installation at the largest vibration mode for the excitation coefficient and response spectrum values against seismic motion.

Case Study (Kaihatsu Consultant Corporation and Takenaka Civil Engineering & Construction CO., LTD. were in charge.)

A case study was carried out into the optimum arrangement of dampers on cable stayed bridges.

The only realistic location for the arrangement of dampers on cable stayed bridges is between the main tower and girder, and between the girder at both ends and the abutments. Consequently, a fundamental investigation was carried out with the 3 masses model shown in Fig. 24. A damping effect of 1% on the entire structures was assumed for when no dampers were attached in the following analysis, and non-linearity was considered by the equivalent linearization method when the damper model was a bi-linear type (set as u_Y=1cm and $K_2=K_1/6$).

1) In the case when dampers are attached to the middle supports. (Between the base of the main tower and the main girders)

The result of analysis with the response spectrum using the three masses model is indicated in Fig. 25 for the damper's first stiffness along the lateral axis. Almost the same result was obtained when this was compared with the results of the model being created in further detail, which provided evidence as to the validity of the three masses model. It was also found that an optimum value for the damper exists when attention was turned to the moment of the base of the pier.

2) In the case where viscous dampers were attached to the end support and hysteresis dampers to the middle support.

Although hysteresis dampers are relatively easy to maintain, they are not suitable for installation on end supports as they have the first stiffness. On the other hand, most viscous dampers require maintenance owing to their mechanical configuration, but they have the advantage of easily absorbing thermal expansion and deformation caused by creep and dry shrinkage. Utilizing the advantages of these two types of dampers in cable stayed bridges, it was concluded that the ideal situation would be to install viscous dampers in the end supports and hysteresis dampers in the middle supports.

Considering two types of yield strength for hysteresis dampers, q=10,000tf and q=1,000tf, the maximum girder displacement was calculated when the viscosity of viscous dampers was changed from c=5,000 to 40,000tf*sec/m. The sensitivity of the maximum bending moment on the base of the main tower and the maximum bending moment on the base of the pier were also analyzed. The results of this are shown in Figs. 26 to 28. The following points were pointed out from these results:

① It was found from Fig. 26 that the bending moment of the base of the main tower was increase two-fold when the hysteresis dampers were not used in combination.

② It was found from Fig. 27 that the maximum response displacement on girders was larger in comparison to other cases when hysteresis dampers with a yield strength of 10,000tf were used. This was thought to be the result of change in the vibration characteristics of the entire structure when the yield strength was excessive.

③ It was found from this model that a reduction effect on the maximum displacement of girders and each maximum section force was conspicuous when the yield strength of the hysteresis damper was 1,000tf and the viscosity of the viscous damper was 10tf*sec/m.

④ The bending moment on the base of the main tower had a tendency to increase when c=25,000tf*sec/m or more, but the moment on the main pier showed a tendency to become lower. This is thought to be the result of excessive confiing effect on the edge of the girders caused by the viscous dampers leading to a shift in the model's vibration characteristics.

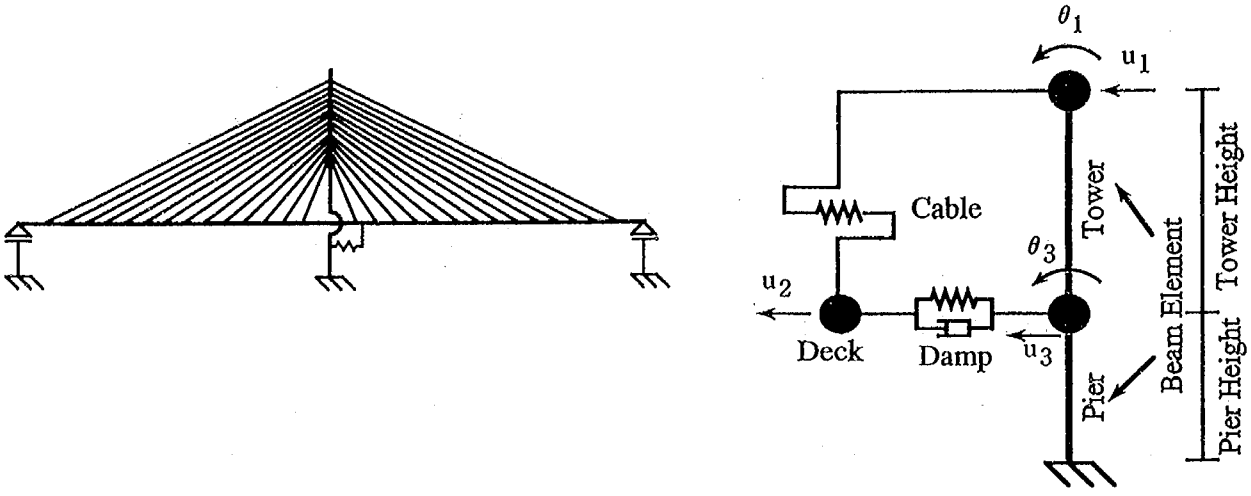


Figure 24 Simplified Cable Stay Bridge Model

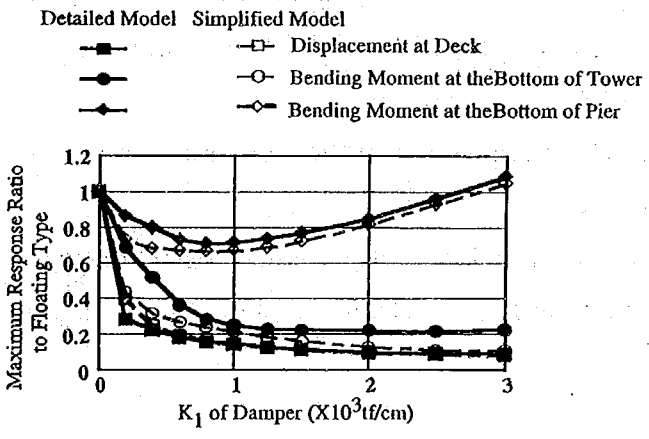


Figure 25 Ratio of Response vs. K_1 (First Rigidity)

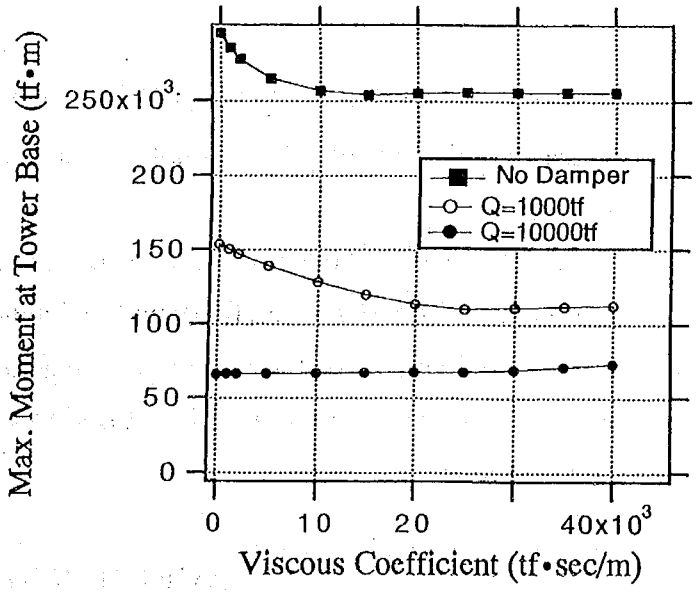


Figure 26 Bending Moment of Main Tower vs. Damping Coefficien

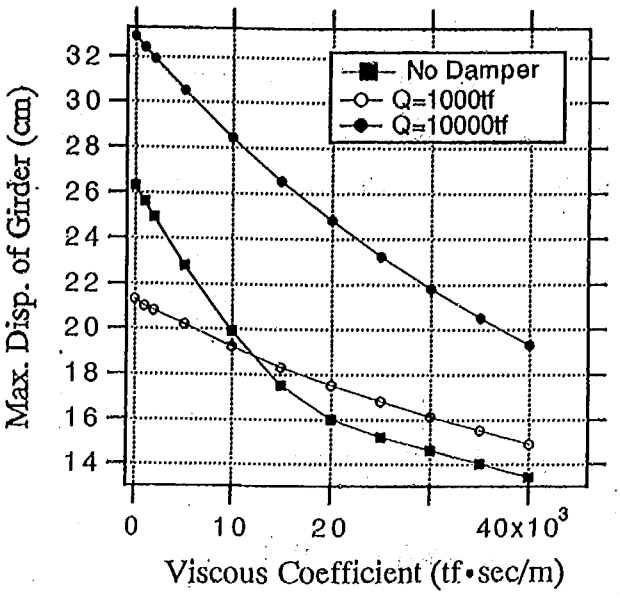


Figure 27 Max. Disp. of Girder vs. Damping Coefficient

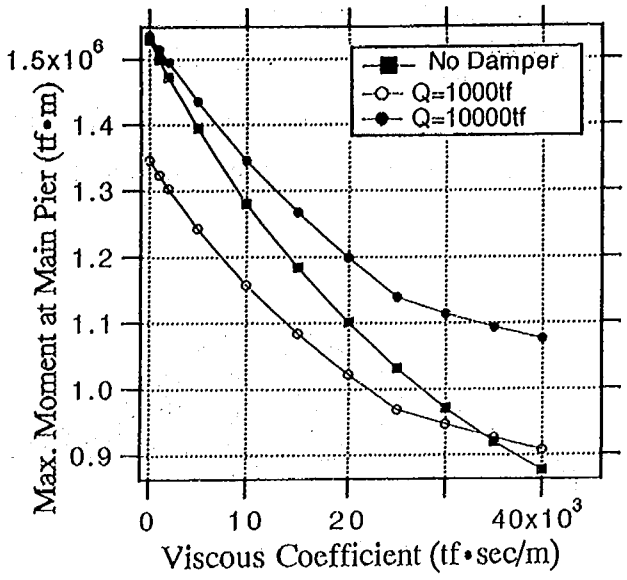


Figure 28 Bending Moment of Pier vs. Damping Coefficient

CONCLUSIONS

(1) A wide varieties of dampers were developed to make the best use of the characteristics of each of materials, and a devices that could be applied to attaining high damping effects on long span bridges were developed. Devices not introduced within this report have also been proposed for actual use.

(2) Amongst the dampers developed, there is a necessity to implement further research into scale-up procedures, long-term durability and maintenance.

(3) A basic requirement for the optimum arrangement of the relative displacement detection type dampers is to insert the dampers in a location within the largest relative amplitude in the main response mode.

ACKNOWLEDGMENTS

This report refers to the achievements made by the Joint Research on Development of the Menshin Technology for Long Span Bridges using High Damping Material consisting of the Public Works Research Institute of the Ministry of Construction, the Public Works Research Center and 19 companies in the private sector. We would like to extend our gratitude to Professor Kawashima of the Tokyo Institute of Technology and Professor Otsuka of Kyushu University to not only took

part in the joint research, but also provided guidance.

REFERENSES

1) Public Works Research Institute of the Ministry of Construction, the Public Works Research Center and 19 companies in the private sector. Report on Joint Research on Development of the Menshin Technology for Long Span Bridges using High Damping Material (Part 1), (Part 2), (Part 3), Report on Joint Research Projects by the Public Works Research Institute: 1994, 1995, 1996 (in Japanese).

2) Takuji Kobori, others: Study on Structural Performance Variable Type Vibration Control System for Multistory Building, Proceedings of the Active Vibration Control Symposium, March 1992 (in Japanese).

3) Kazunori Seto: Vibration Control of Multi-degrees of Freedom System, Dynamics Handbook, October 1993 (in Japanese).

AGING STUDIES OF HIGH-DAMPING RUBBER AND LEAD-RUBBER SEISMIC ISOLATORS

Peter W. Clark, James M. Kelly, Ian D. Aiken
Earthquake Engineering Research Center
University of California at Berkeley
Berkeley, California

ABSTRACT

Tests have been performed recently on three pairs of full-size elastomeric bearings originally manufactured and tested in 1983 in conjunction with the design and construction of the first seismically-isolated building in the United States. Four of these bearings are high-damping rubber (HDR): one pair was removed from underneath the building and subjected to the original production and prototype test programs; the other pair had been kept in storage since the original prototype test program and was retested under the same conditions. The other two bearings were lead-rubber isolators, and these were retested according to their original prototype test program. The results from the HDR production bearings indicate relatively small changes in the elastomer moduli, depending on the shear strain amplitude, but changes in the moduli up to about 20 percent were observed in the pair of prototype bearings. This may be the result of changes in the manufacturing process between the time the prototypes were completed and the production run was initiated. In contrast, preliminary results from the LRB bearings indicate negligible changes in the long-term stiffness properties, although digitization and analysis of the original prototype loops is still underway. The energy dissipation characteristics of both types of bearings were essentially unchanged. These initial results provide confidence that the long-term mechanical characteristics of elastomeric isolators will not differ substantially from those assumed in the design.

INTRODUCTION

Because seismic isolation is a relatively new technology, there is concern in the engineering profession regarding the long-term performance of the devices used. This concern exists for all types of systems: stiffness variations may be caused in elastomeric-based bearings such as high-damping rubber (HDR) or lead-rubber bearings (LRB) due to changes in the elastomer matrix; friction-based systems may exhibit variations in the break-away coefficient of friction as a result of long-term contact between dissimilar materials; external mechanical damping devices used in hybrid systems may require inspection or maintenance to ensure proper operation over the life of a structure. At this time, there is relatively little experimental data available on the long-term mechanical characteristics of the majority of isolation and energy dissipation devices in use or being proposed for use.

This paper focuses on a series of retests of elastomeric isolators which were originally manufactured and tested in conjunction with the construction of the first seismically isolated building in the United States — the Foothill Communities Law and Justice Center. The building was designed in the early 1980's, and construction was completed in 1985. During the design phase, two different isolation systems were considered — one using HDR bearings and one using LRB

isolators. Four prototype bearings of each type were constructed and tested in 1983; the HDR system was eventually selected for installation in the building.

Two pairs of prototype bearings from each system have been retested recently using the original prototype test program. In addition, two HDR bearings were removed from the building and subjected to both the original quality-control test program and the prototype test program. In total, this retest program provides data on the long-term properties of three different pairs of elastomeric bearings — two pairs of HDR bearings and one pair of LRB bearings.

Description of Building and HDR Isolation System

The Foothill Communities Law and Justice Center (FCLJC) is a five-story plus basement braced steel frame supported on 98 HDR bearings. The building is located within 21 km (13.5 miles) of the San Andreas Fault and less than 3.5 km (2 miles) from the Sierra Madre fault zone in Rancho Cucamonga, California, and is owned by the County of San Bernardino. The combination of the extreme seismic hazard at the site and the importance of the structure to the County's post-earthquake response and recovery led to the selection of seismic isolation as the most cost-effective means of ensuring the functionality of the FCLJC in the wake of a major earthquake. A thorough summary of the design and analysis of the building is provided in [1]. Since the time of its completion, the building has been the subject of several research investigations and has withstood several moderate earthquakes without damage.

The isolation system installed in the FCLJC incorporates eight different bearing designs and four different high damping rubber compounds. Each bearing has an outer diameter of 0.76 m (30 in.) and a shim diameter of 0.61 m (24 in.); several different combinations of shim/rubber thicknesses allow a range of axial loads to be accommodated. To verify the adequacy of both the final design and the manufacturing procedures prior to construction of the production bearings, four prototype HDR bearings were built by Oil States Industries (now the Structural Bearings Division of Furon), Athens, Texas, and were tested at the Earthquake Engineering Research Center (EERC) of the University of California at Berkeley in July, 1983. The results of these tests are detailed in [22]. After the HDR system was selected for use in the building, the production bearings were manufactured and tested between September and November, 1983. Installation occurred in spring of 1984. All of the production bearings were manufactured at the Oil States Industries plant in Athens, Texas, and were tested at their plant in Arlington, Texas.

The prototype and production manufacturing and testing sequence described above was instituted in part because the use of seismic isolation for the FCLJC represented the first application of this innovative technology. For the same reason, a long-term maintenance program was established that specified that production bearings be removed from the building and tested ten years after installation. Two of the original four HDR prototypes have been stored at the EERC while the other two prototype HDR bearings, one of which was cut in half for inspection, are on permanent display at the building. In 1992, as part of a Department of Energy sponsored research program, one of the prototype HDR isolators was again subjected to the original prototype test program in the EERC single-bearing test machine. The results of that test program, while not fully conclusive, indicated no significant change in the properties of the single prototype bearing [3].

The ten-year anniversary of the completion of the building in the summer of 1995 initiated the retesting program for the two production HDR bearings. These bearings were removed from the building on August 5 and 6, 1995. Two prototype isolators of the same design and compound that had been in storage at EERC (one of which had been tested in 1992 as described above) were installed under the building while the original bearings were being tested. After the retests of the production bearings, they were replaced under the building, and the prototype bearings were retested.

All of the bearings — both the prototype and production — that were made available for retesting were originally classified as "type A" isolators and use an elastomer compound referred to as 243-65. This design has a total height of rubber of 0.304 m (11.97 in.) and a layer shape factor of 9.5. The nominal design axial load is 1535 kN (345 kips); in the building these bearings support a range of axial loads. The bearings are connected to the foundation and superstructure via dowel pins, instead of the bolted connection which is more commonly used today. The maximum anticipated displacement of the corner bearings, calculated based on the maximum credible earthqake defined for the site at the time of the design, is 0.381 m (15 in.). There is a gap between the perimeter of the building and the exterior retaining wall of 0.41 m (16 in.).

Description of LRB Isolation System

In parallel with the design of the HDR isolation system for the FCLJC, several LRB designs were developed. The LRB isolation system selected for the design validation (prototype) phase used four different bearing sizes with lead cores included in a number of bearings. These bearings were manufactured by Oil States Industries in Athens, Texas. The outer diameter of all of the isolators was 0.76 m (30 in.) with a total height of rubber of 0.257 m (10.12 in.). The displacement for the testing evaluation was also 0.257 m (10.12 in.), corresponding to a shear strain of 100%. The lead core diameter chosen was 0.14 m (5.5 in.), and the layer shape factor was 13.6. According to the limited test results reported in [1], the elastomer used was not strictly linear; the effective modulus decreases as a function of shear strain to a value of approximately 0.966 MPa (140 psi) at 75 percent strain. The LRB bearings use the same doweled connection detail as the HDR bearings.

The energy dissipation characteristics of the LRB isolators designed for the FCLJC depend strongly on the applied axial load because of the importance of confinement on the behavior of the lead core. The design axial load was 2000 kN (450 kips), but tests were performed at loads ranging from 445 kN (100 kips) to 3560 kN (800 kips). As described below, substantial variations (up to 50%) were observed in the energy dissipated as the axial load was varied.

STIFFNESS VARIABILITY OF RUBBER COMPONENTS

The desire for retesting arises from several concerns over the long-term variability in the mechanical properties of natural rubber components. Modern rubbers are typically compounded with chemical additives designed to minimize deterioration of the polymer matrix due to exposure to oxygen, and particularly ozone. One laboratory procedure intended to measure the degree to which rubber components may degrade involves accelerated aging small samples through exposure to elevated temperatures. While this method invariably leads to ozone cracking that extends

through the sample, it is unlikely that such a mechanism could develop in a bulk rubber component such as a seismic isolation bearing. This assertion has been confirmed by two separate studies of a rubber block cut from the edge of a bridge bearing which had been in service for 100 years [4,5]. Although the original rubber had not incorporated any chemical antioxidants at the time of manufacture, these investigations found that while the rubber had deteriorated substantially at the surface, at depths of greater than 3.8-6.4 mm (0.15-0.25 in.), the sample exhibited acceptable hardness measurements, cross-linking density, and elongation to break. The long-term stability of a chemically-protected bulk component would be expected to be better as any degradation of the outer surface serves to protect the inner material. Additional information about the effects of bulk on the aging of natural rubbers is given in [6].

An unrelated effect which has the potential to affect the long-term stiffness of a bulk rubber component is age hardening. This phenomenon occurs when free sulfur vulcanizates that did not react during the original vulcanization of a component slowly form cross-links within the rubber matrix over time. The rate of age hardening depends on the completeness of the initial vulcanization and the temperature of the rubber; dense concentrations of free vulcanizates and higher temperatures accelerate the formation of additional cross-links. It is unclear what effect bulk volume has on the rate of age hardening, but examination of at least one bridge bearing after 20 years in service showed a negligible change in stiffness characteristics from the original specification [7,8].

Complicating the effects of age hardening in high-damping rubber seismic isolation bearings is the possibility of damage to cross-links and rubber-filler bonds during initial testing, that then heal if the bearing is left unstrained. High-damping rubbers incorporate filler particles (carbon black or other oils or resins) that serve to increase the modulus and damping of the finished elastomer. However, upon shearing a rubber sample, some of the bonds between the fillers and the rubber matrix are broken, leading to a decreased modulus if the shear is applied again within a short time. Although the sample will generally heal (the rate of healing is a function of temperature), it will likely never achieve the initial stiffness because not all of the bonds will re-form. Although the terminology is not universal, the phenomenon of strain softening (and subsequent recovery) is commonly known as Mullins' effect [9], and the permanent stiffness loss is referred to as scragging. Both Mullins' effect and scragging are strain-dependent processes, i.e. the extent of softening at a given strain increases as the maximum strain imposed on the material is increased.

ORIGINAL TEST RESULTS

HDR Bearings — Prototype Tests

The prototype testing program defined for both the HDR and LRB bearings represented the first evaluation of full-size seismic isolation bearings in the United States. The loading apparatus specially designed and constructed for this program was configured to test four bearings simultaneously. The advantage of this configuration was that the shear loads were self-equilibrating within the test fixture, and a single vertical loading ram could apply the axial load without having to withstand moments generated in the isolators. The disadvantage of this system lies in the fact that only the averaged force-displacement behavior of the four bearings could be measured, so no

results for individual bearings loaded in shear are available.

The prototype test program was designed to establish the behavior of the isolators under a wide range of axial loads and shear strains. All of the tests consisted of a single half-cycle of displacement; the rate of loading used in the 1983 tests is not known. For shear strains of 2, 3, 5, 10, and 20 percent, tests were performed at axial loads of 445, 1110, and 1778 kN (100, 250, and 400 kips). At shear strains of 40, 60, and 80 percent, tests were performed with axial loads of 1110 and 1778 kN (250 and 400 kips). At shear strains of 100, 109, and 116 percent, a single half-cycle at an axial load of 1778 kN was performed. Finally, at the maximum design displacement of 0.38 m (15 in.), an axial load of 2590 kN (582 kips) was used. The intent of the increased axial load in this final test was to simulate large overturning moments which were anticipated in the building under the design earthquake. There were no failures observed in any of the prototype bearings, which was confirmed by cutting one of the bearings in half after the tests for a detailed examination.

Complete results from the original prototype test program are provided in [2]. A variety of bearing mechanical properties are presented in this report, but the details of their calculation are not thoroughly documented. For example, horizontal effective stiffnesses are presented that apparently are intended to represent the peak-to-peak stiffness of a fully-reversed hysteresis cycle, even though all of the tests consisted of half cycles. These effective stiffnesses actually appear to have been calculated based on the slope between the peak shear force (at maximum displacement) to the negative force as the bearing returns to zero displacement. Equivalent viscous damping values are also reported for the half-cycle loops in the original test report; it is unclear how these were calculated.

Although no digital data were recorded during the prototype tests, the original *X-Y* plots have been retained. To allow consistent comparisons to be made between the original prototype results and those from the retests, the original *X-Y* plots have been digitized by hand. These digitized loops then were analyzed using origin-to-peak effective stiffness calculations to give the shear test results presented here.The most important result to note is that the prototype stiffnesses at 40 and 60 percent shear strain were somewhat lower than the stiffnesses derived from the production tests at 50 percent shear strain (described below). This implies that there may have been a change in the manufacturing procedures subsequent to the completion of the prototype test program, leading to stiffer bearings in the production phase.

HDR Bearings — Production Tests

The successful performance of the prototype isolators provided confidence such that the scope of the production test program could be narrowed substantially while still ensuring that the individual bearings were of sufficient quality to be installed in the building. Only five tests were performed on each production bearing, and no digital data acquisition was in place; therefore, the amount of data available for each bearing is limited. The test set-up allowed two bearings to be tested at once. Separate displacement transducers were used to measure vertical displacements during the compression tests (two transducers for each bearing), allowing separate compression stiffnesses to be calculated. Under combined compression and shear loading, a single displacement and force were recorded for the pair of bearings, leading to an averaged horizontal stiffness.

No data was recorded during the first two scragging tests, nor was data recorded during the final compression test in which a visual inspection was performed. The compression loads were applied by hand, and there is no record of the precise loading history. The rate of shear loading is also unknown but was probably less than 0.25 m/minute (10 in./minute).

The two bearings that were removed from the building, numbers A2 and A5, were not tested together in the original production test program. Bearing A2 was tested with bearing A4, and bearing A5 was tested with bearing A17. Although individual compression stiffnesses are available for each bearing, the configuration of the shear testing set-up prevented individual shear stiffnesses from being calculated. Therefore, only the averaged stiffnesses of bearing sets A2-A4 and A5-A17 are available.

With regard to the compression test results, presented in the top portion of Table 1, it can seen that the stiffnesses of bearings A2, A4, and A5 are reasonably close, while bearing A17 is considerably softer (approximately 15 percent less than the mean of the other three bearings). The original test report indicates that bearing A17 had the lowest vertical stiffness of the 22 type-A bearings made from the 243-65 rubber compound. While such a significant deviation from the mean might be attributed to an unreliable test, multiple tests of bearings A2 and A17 gave virtually equal compression stiffness results.

Measured Stiffness [MN/m (kips/in.)]	Bearing Number			
	A4	A2	A5	A17
K_V original	589 (3362)	548 (3126)	602 (3436)	491 (2802)
K_V original (2nd run)	—	553 (3157)	—	498 (2840)
K_V 1995	—	538 (3072)	572 (3265)	—
K_H at 2% strain — original	12.3 (70)		11.4 (65)	
K_H at 2% strain — 1995	—	8.7 (49.9)		—
K_H at 10% strain — original	4.9 (28)		4.6 (26)	
K_H at 10% strain — 1995	—	3.5 (19.7)		—
K_H at 25% strain — original	2.8 (16)		2.5 (14)	
K_H at 25% strain — 1995	—	2.2 (12.4)		—
K_H at 50% strain — original	1.7 (9.8)		1.7 (9.5)	
K_H at 50% strain — 1995	—	1.6 (9.4)		—

All vertical stiffnesses computed based on peak-to-peak dial gage displacements in the load range from 0.6 to 1.5P_{DES}, where P_{DES} = 1533 kN (345 kips).

Table 1. Measured Bearing Properties in Production Tests

The production shear test results are also shown in Table 1, expressed as effective stiffness values at shear strains of 2, 10, 25, and 50 percent. The method of calculation of these stiffnesses was not detailed in the original report [1], but it appears they are based on the secant from zero load and displacement to the measured load at the specified strain level. It is useful to compare these values with the averages observed for the complete set of type-A production bearings manufactured with the 243-65 compound, in which there were 22 bearings and 11 averaged values (because the bearings were tested in pairs). At shear strains amplitudes of 2, 10, 25, and 50 percent, the mean stiffnesses were 10.2, 4.31, 2.54, 1.65 MN/m (58.2, 24.6, 14.5, and 9.4 kip/in.), respectively, with standard deviations of 1.23, 0.57, 0.26, 0.098 MN/m (7.0, 3.25, 1.48, and 0.56 kip/in.), respectively. This implies that the A2-A4 pair is within one standard deviation of the mean over all amplitudes, but the A5-A17 bearing pair is actually outside of this bound at every shear strain level but 50 percent. Coupled with the fact that bearing A17 had the lowest compression stiffness of all of the type-A bearings tested, the implication is that bearing A5 is much stiffer than most of the other type-A bearings. This should be kept in mind when interpreting the long-term shear test results.

LRB Bearings

Four prototype LRB bearings were constructed and tested at EERC at approximately the same time as the tests on the HDR system (July 1983). The test program was very similar to that employed for the HDR bearings, with the exception that a wider range of axial loads were examined (up to 3555 kN [800 kips]) due to the variation in the energy dissipation characteristics of these bearings as a function of axial load. Also, the maximum shear strain in these tests was limited to 100 percent, corresponding to a displacement of 0.257 m (10.12 in.). Less detailed results are available from these tests as compared to the HDR prototype tests; only a very brief summary is presented in [1]. However, the original *X-Y* plots were saved, and digitization of these by hand has been initiated recently. At this time, only the first test to each strain level has been digitized for the purposes of the comparisons presented below, but this work is ongoing and additional results will be published at a later date.

RETESTS OF HDR BEARINGS

Prototype Shear Test Results

The prototype bearings were retested in February 1996 at EERC in a test machine typically configured to test four large bearings simultaneously. For the retests of the pair of prototype bearings, this machine was temporarily modified by inserting two "dummy" bearings in one portion of the machine and locking them in place by means of a rigid beam. This left only one side of the machine free to displace, allowing a single pair of bearings to be tested. In this configuration, the test machine is capable of producing displacements of ±0.406 m (±16 in.) and shear forces of approximately 667 kN (150 kips) per bearing. The peak axial load which can be delivered to the bearing pair is approximately 3336 kN (750 kips).

In general the retests of the HDR prototype bearings exhibited significantly larger stiffness values than had been seen in the original prototype tests, and this was observed over the entire range of shear strains. However, when the results from these bearings are compared with the shear

stiffnesses of the production bearings when subjected to the prototype test sequence (see below), the 1996 stiffness values for the prototype bearings are nearly equal to those for the production bearings. This implies that the original production bearings were substantially stiffer than the original prototype bearings, and the explanation for this discrepancy is not clear. One possibility is that the manufacturing process was changed slightly after the prototype bearings were constructed, leading to a different curing relationship and therefore different elastomer characteristics.

Figure 1 shows an example of the variations in the effective stiffness of the prototype bearings (and the production bearings) at a shear strain of 100 percent. While the force-displacement relationships from the tests performed in 1995 and 1996 (on the production and prototype bearings, respectively) are nearly identical, the digitized loop from the prototype tests in 1983 peaks at a force approximately 20 percent lower. This trend was observed in all of the tests above approximately 50 percent shear strain (as seen in Figure 2). It is very important to note that this trend is not apparent below 50 percent shear strain because of strain-softening in the production bearings — the production shear test to 50 percent was run on these bearings immediately before the prototype sequence was performed.

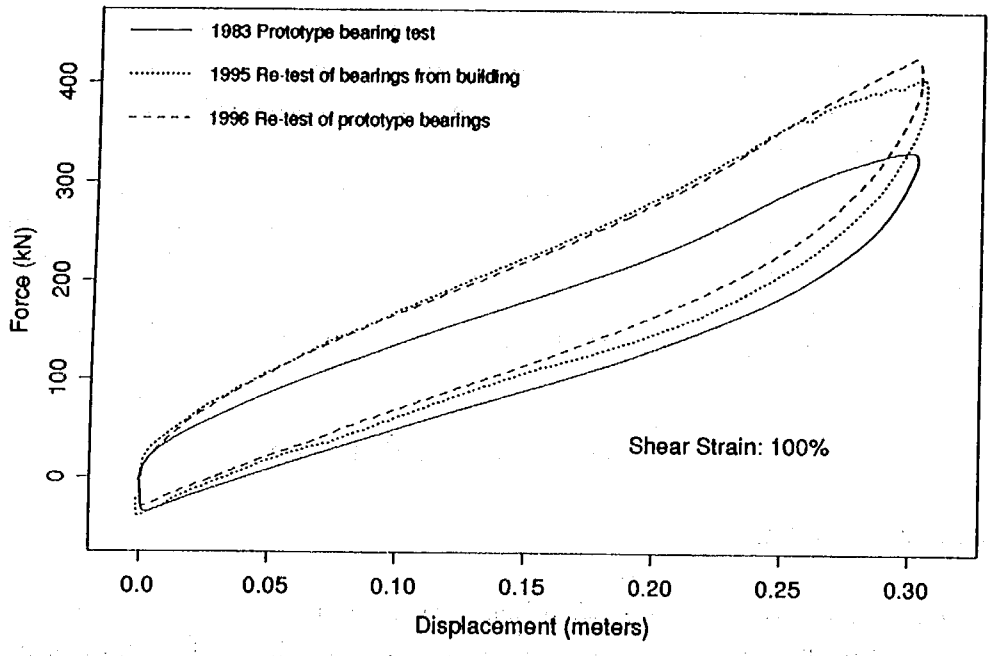


Figure 1. Comparison of Force-Displacement Loops from HDR Isolators

Production Compression Test Results

The retests on the production bearings were performed on August 31, 1995. To allow direct comparisons to be made with the original production test data, the two bearings were subjected first to the production test sequence, followed by the prototype test sequence and two large-displacement tests. All of the tests were performed in a test machine at the Structural Bearings Division of Furon, in Athens, Texas. This test machine is capable of combined compression and shear testing of seismic isolation bearings under axial loads up to 26,688 kN (6000 kips) and shear loads

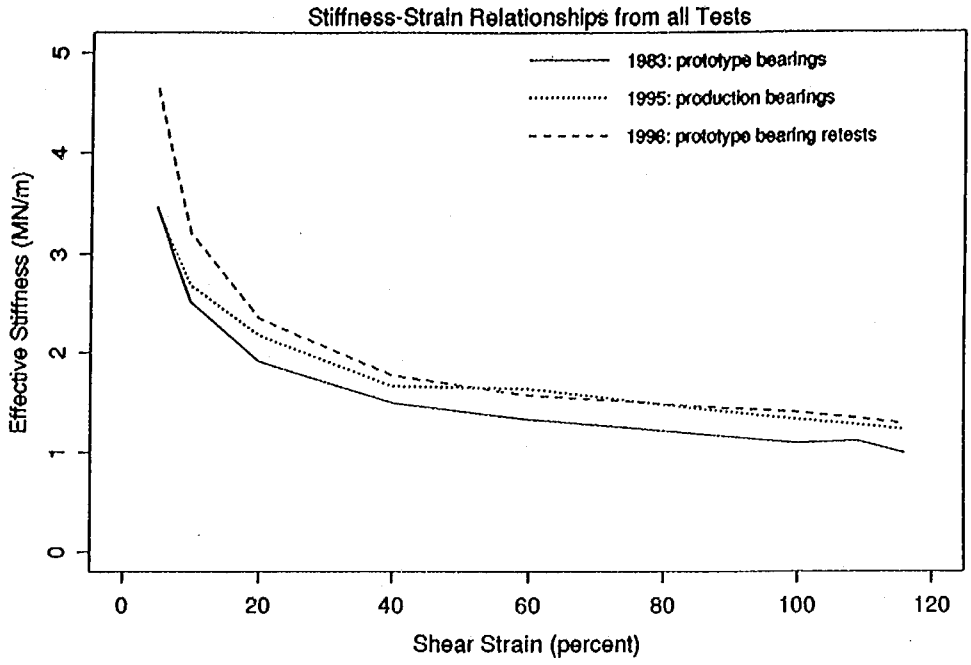


Figure 2. Variation in Effective Stiffness for All HDR Isolators

up to 4448 kN (1000 kips). The maximum stroke of the test machine is 0.610 m (±24 in.), and the maximum horizontal velocity is approximately 0.406 m/minute (16 in./minute).

The results of the compression tests on the production bearings are valuable because they represent the only basis on which the long-term performance of individual isolators from the FCLJC can be evaluated. Because no data was recorded during the original scragging tests (in which the bearings were loaded first to $0.75P_{des}$ and then $1.0P_{des}$), no useful comparisons can be made from these tests. However, the digital data recorded during the first retest of bearing A5 (corresponding to the original scragging test) does indicate some temporary displacement offset after the first cycle. It is likely that this behavior is a result of the bearing deforming to fit properly in the test machine.

In evaluating the compression tests, the displacement data for axial loads less than $0.4P_{des}$ was deemed unreliable, and it is felt that the most reliable vertical stiffness is that calculated over the load range from 0.6 to $1.5P_{des}$. The results, and comparisons with the original production compression stiffnesses, are shown in Table 1. It is clear that there is very little difference in the compression stiffnesses of the bearings during the retests as compared with the original data. In fact, the bearings are slightly softer by up to 4 percent. This is in contrast to the stiffening which would be expected if these bearings had age hardened.

Production Shear Tests

As noted before, the 1983 production tests measured the average stiffness of pairs of bearings at discrete displacements, and the A2-A5 bearing pair was not tested together originally. Although this arrangement prevents direct comparisons with the original tests, a general trend can be revealed by evaluating the shear test results in tandem with the compression test results.

Because the production shear test was only a single half-cycle of displacement to 50 percent shear strain, the original effective stiffnesses were determined from force values that were manually read at the target displacements during the cycle to 50 percent. In the production retest, the entire curve was traced, and the forces (and therefore the effective stiffnesses) at the target displacements were determined from the digital data. Figure 3 shows the recorded force-displacement curve superimposed on the force-displacement curve derived from the original production tests. At strains below 50 percent the retest data is actually softer than the original result, contrary what would be expected if the bearings had age hardened. Combined with the previous observation that bearing A5 was one of the stiffest of the original set, this result implies that there has been very little change in stiffness of the production bearings over the 12 years since their manufacture and testing.

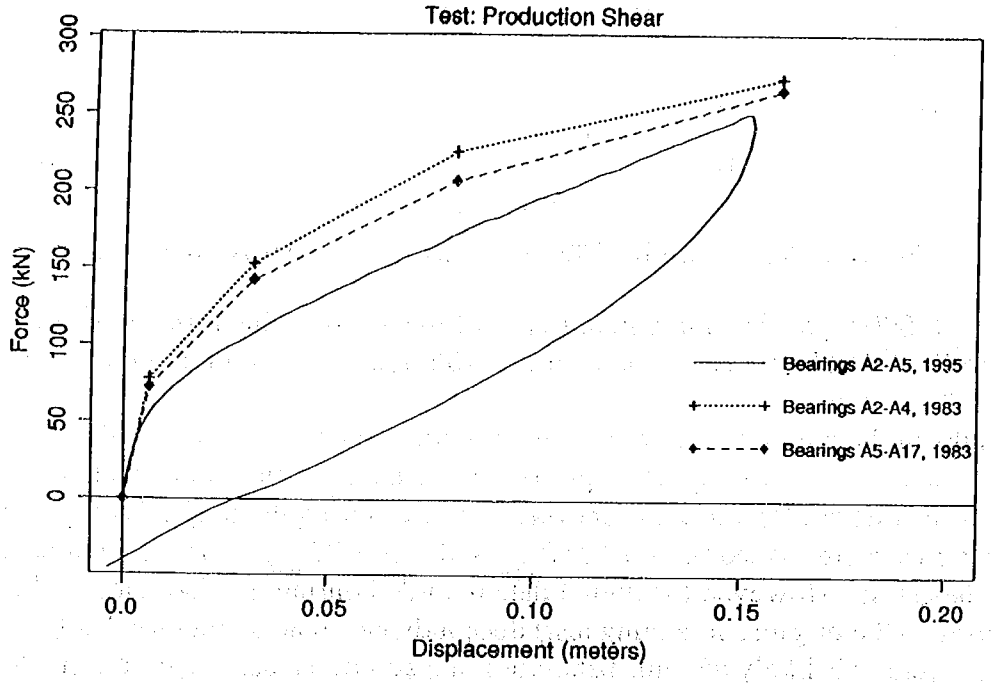


Figure 3. Comparison of Original Data (Derived) and Retest Data from HDR Production Bearings

Finally, it is interesting to examine the cyclic large-displacement tests which were performed at the end of both the prototype and production retests (Figure 4). In this test the bearings were displaced to 0.406 m (16 in.), representing the limit of the seismic gap around the FCLJC. Both the production bearings and the prototype bearings exhibit approximately equal (peak-to-peak) effective stiffnesses, but the unloading portions of the curves are quite different. This implies that there may be something unique about the two test machines used which influenced the results, however the difference is not immediately clear. It should be noted that there was no damage to the production bearings during this large-displacement retest, and they were eventually reinstalled underneath the building. However, one of the prototype bearings experienced debonding between the exterior cover layer and the outer surface of its bottom endplate. It is doubtful that this influenced the force-displacement behavior of the bearing since the primary damage was to the cover rubber.

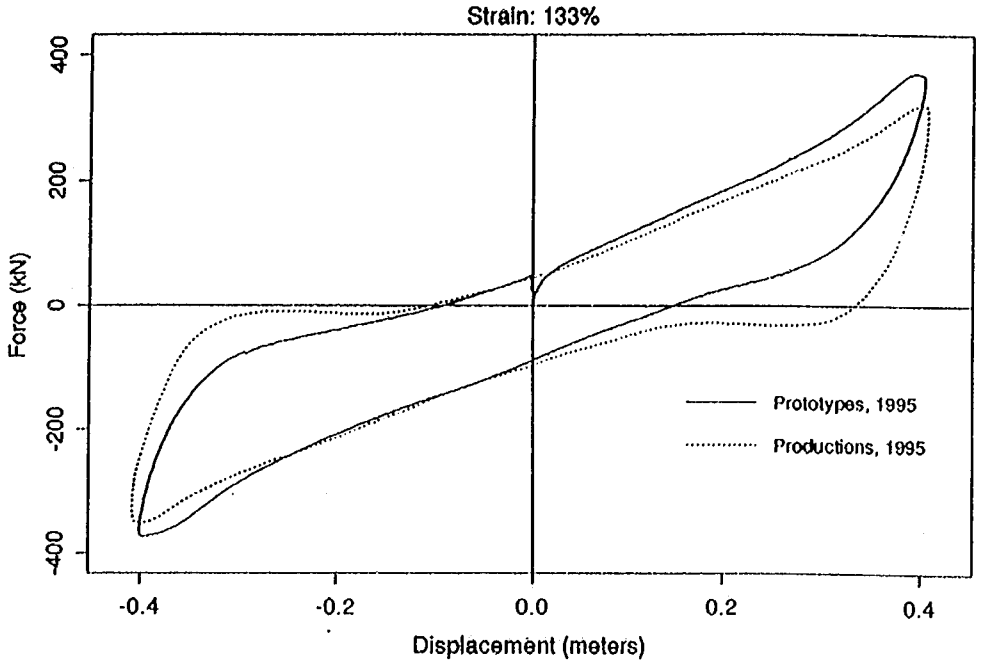


Figure 4. Large-Displacement Behavior of Retested HDR Bearings

RETESTS OF LRB BEARINGS

In general, the measured force-displacement curves from the retests of the LRB bearings were similar to the original tests, although the retest to 100 percent shear strain under an axial load of 445 kN (100 kips) exhibited roll-out instability, perhaps due to insufficient confinement of the bearing and the configuration of the test machine. Such behavior was not observed in the original tests of the LRB prototype bearings. The remainder of the tests showed full loops with a similar dependence on axial load as was observed in the original test program. In fact, for LRB isolators of this shape factor and similar connection details (doweled rather than bolted), it is likely the case that the mechanical properties will exhibit substantially greater dependence on axial load than on any aging effects.

Figure 5 presents the variation in effective stiffness of the LRB isolators from the original prototype tests and the 1996 retests. In this case the first cycle at each strain level is plotted, and the axial load is 445 kN (100 kips), with the exception of the data point at 100 percent shear strain in which the axial load was 890 kN (200 kips). Figure 6 shows a similar plot for the energy dissipated per cycle, or equivalently, the area contained within the force-displacement loop. Again aging has virtually no influence on the long-term energy dissipation characteristics of the bearing, attesting to the material stability of the lead core. Finally, Figure 7 shows a test in which three fully-reversed displacement cycles to 100 percent shear strain were carried out. The hysteretic behavior in this test appears to be very stable, and no damage was apparent in the bearing. As mentioned above, the original tests are still being digitized, and additional comparisons between the behavior of the LRB isolator in the retests and the complete original prototype test program will be made in the near future.

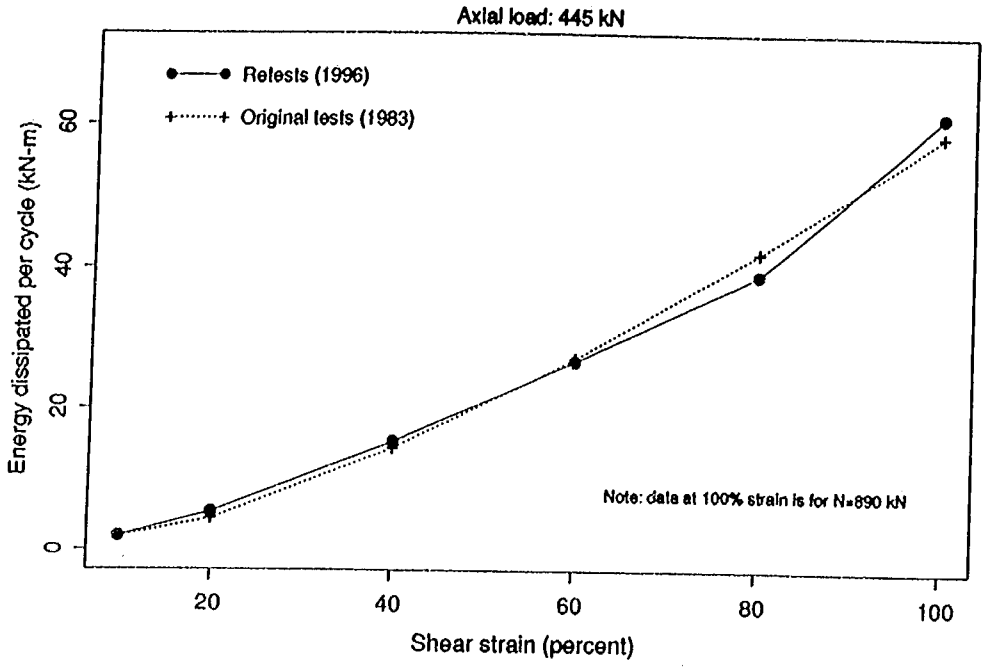


Figure 5. Comparison of Effective Stiffnesses of LRB Prototype Bearings

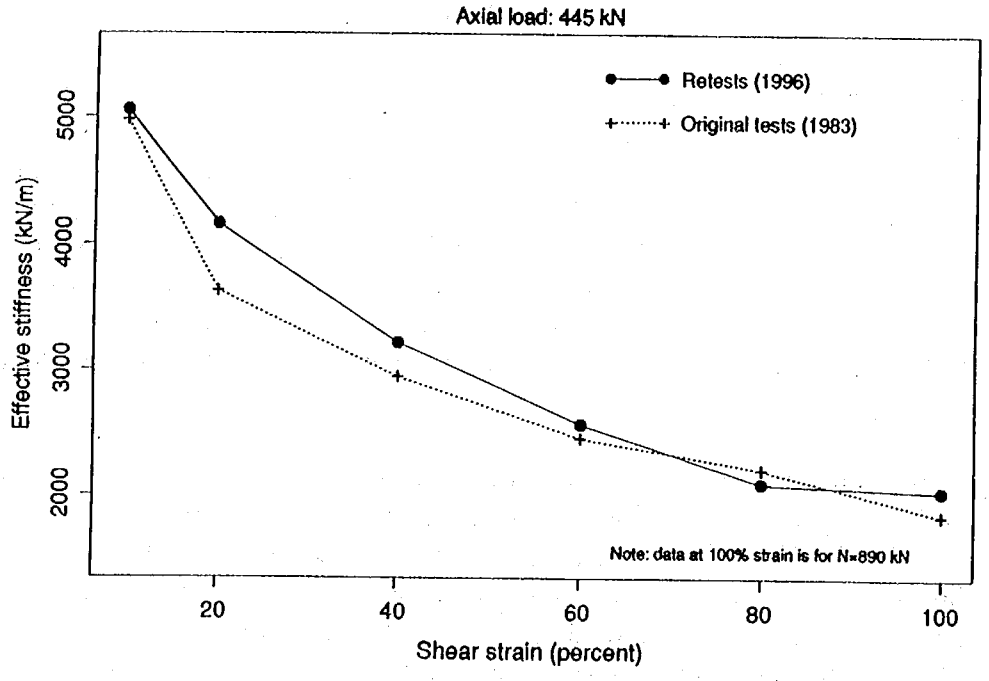


Figure 6. Comparisons of Energy Dissipation of LRB Prototype Bearings

SUMMARY AND CONCLUSIONS

This report has presented the results of a series of retests of HDR and LRB seismic isolation bearings from the Foothill Communities Law and Justice Center more than ten years after their manufacture. Both prototype and production bearings were subjected to test programs similar to those originally conducted in 1983, and all of the bearings exhibited stable hysteretic behavior

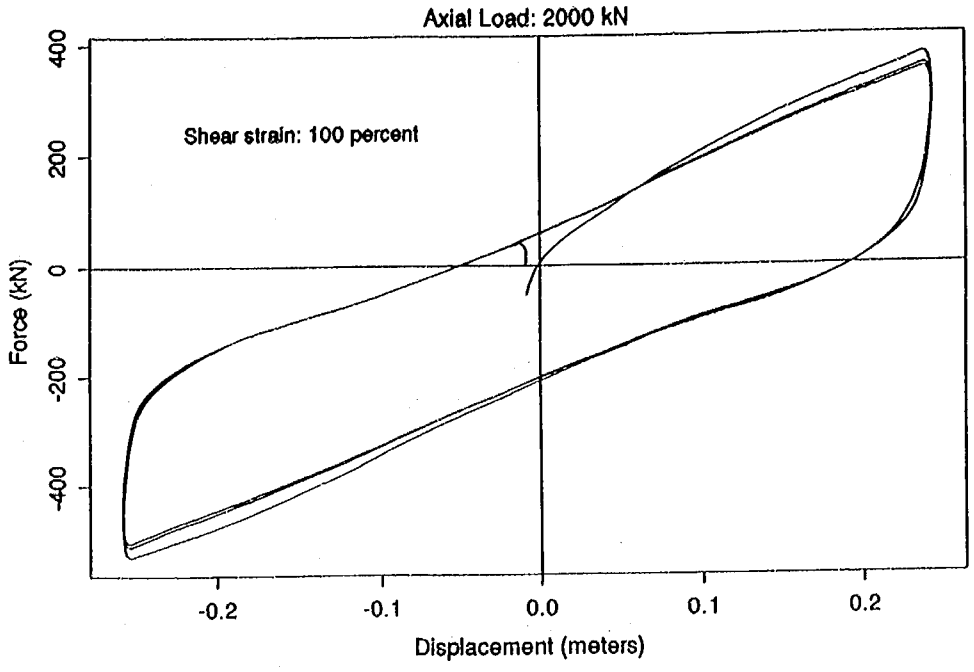


Figure 7. Large-Displacement Behavior of LRB Prototype Bearings

with relatively minor variations in mechanical characteristics from those determined in the original tests. In particular, the compression and shear stiffnesses of the production HDR bearings, which were removed from the building in the summer of 1995, changed less than 5% from their original values after being in the building for more than ten years. Preliminary results from the LRB isolators indicate negligible changes.

Beyond the fundamental chemical reactions which may influence the long-term modulus of a rubber compound, several other sources of stiffness variability and uncertainty may have influenced the results presented here, for example the influence of sustained axial load, effects of loading rate, the relatively small sample size (in the case of the production bearings, only two out of 98 bearings were tested), variations within the sets of prototype bearings (in the case of the HDR and LRB prototypes, results from only two bearings of the original sets of four are available), varying calibration and configuration of test machines, etc. With regard to the HDR bearings, the differences between the results from the production bearings and those from the prototype bearings may have been caused by the adoption of a different manufacturing process after the prototype phase. The fact that the production bearings do not appear to have stiffened implies that they were cured almost completely at the completion of the manufacturing process; the age hardening of the prototype bearings could be a result of an incomplete initial cure. Only future tests of these bearings will be able to confirm this explanation.

Finally, it should be noted that minor stiffness variations in individual bearings (or even in the complete isolation system) will not lead to dramatic differences in the dynamic response of an isolated structure from that which is assumed in its design for several reasons. First, the test results presented here indicate that a variation in stiffness on the order of 20 percent may be possible, depending on the incompleteness of the original cure, among other things. This is of a similar magnitude with the uncertainty associated with the total mass of a building, and is probably sig-

nificantly less than the uncertainty associated with ground motion characteristics at a particular site. On top of this, the change in period is proportional to the square root of the change in stiffness so that relatively large stiffness variations are required to alter the period, and earthquake acceleration response spectra for soils such as those at the FCLJC site exhibit little variation as the period is increased beyond about 1.5 seconds. This implies that even if the period changes appreciably, the change in the base shear coefficient will be minor, although the corresponding change in the bearing displacement should be evaluated.

As the number of projects incorporating seismic isolation systems continues to increase, it is certain that the data concerning long-term mechanical characteristics will also increase. The difficulty in interpreting some of the results in this study indicates the importance of thorough testing and documentation of test procedures and results to ensure that data obtained in the future can be compared directly with original information.

ACKNOWLEDGEMENTS

The retests of the HDR bearings from the FCLJC were performed with funding from the Federal Highways Administration through the National Center for Earthquake Engineering Research. The removal and replacement of the bearings from the building was paid for by the County of San Bernardino, California. Assistance from John Giblin and Ken Taylor from the County is gratefully acknowledged. The HDR production bearing retests were donated by the Structural Bearings Division of Furon in Athens, Texas. The efforts of the staff at Furon, and in particular Robert Meyers and Steve Bennett, is greatly appreciated. The HDR prototype retests were performed at EERC, where the assistance of Wesley Neighbor is sincerely acknowledged. Advice on the original test program for the HDR bearings from Dr. Alexander Tarics was also extremely useful, as was access to the original data provided by Rodney Holland.

The retests of the LRB bearings were funded by the California Department of Transportation as part of the Coordinated Protective Systems Research Project between Caltrans and EERC. Preliminary evaluations of the original data and assistance in preparing this paper from Colman Cronin is acknowledged. The ongoing support of Caltrans is greatly appreciated.

REFERENCES

[1.] Tarics, A.G., D. Way, and J.M. Kelly, (1984), "The implementation of base isolation for the Foothill Communities Law and Justice Center," *A Report to the National Science Foundation and the County of San Bernardino*, Reid and Tarics Associates, San Francisco, California, November.

[2.] Kelly, J.M., and M. Celebi, (1984), "Verification testing of prototype bearings for a base isolated building," *Report No. UCB/SESM-84/01*, Department of Civil Engineering, University of California at Berkeley, March.

[3.] Gluekler, E.L., (1993), "Status of reactor seismic isolation technology development in the USA and summary of IAEA specialists meeting," *International Post-SMiRT Conference Seminar on Isolation, Energy Dissipation, and Control of Vibration of Structures*, Capri,

Italy, August 23-25.

[4.] Stevenson, A., (1985), "Longevity of natural rubber in structural bearings," *Plastics and Rubber Processing*, Vol. 5, No. 3.

[5.] Yamazaki, N., H. Nakauchi, and M. Miyazaki, (1992), "Durability of rubber isolators — characterization of a 100 years used rubber bearing," *Proceedings of the International Workshop on Recent Developments in Base-Isolation Techniques for Buildings*, Tokyo, Japan, April.

[6.] Roberts, A.D. ed., (1988) *Natural Rubber Science and Technology*, Oxford University Press, New York.

[7.] Price, A.R., and M.A. Fenn, (1983), "Removal and testing of elastomeric bridge bearings," *TRRL Supplementary Report 812*, Transport and Road Research Laboratory, Department of Transport, United Kingdom.

[8.] Stevenson, A. and A.R. Price, (1986), "A case study of elastomeric bridge bearings after 20 years service," *Proceedings of the Second World Congress on Joint, Sealing, and Bearing Systems for Concrete Structures*, Vol. 1, American Concrete Institute SP94, Austin, Texas.

[9.] Mullins, L., (1969), "Softening of rubber by deformation," *Rubber Chemistry and Technology*, Vol. 42, No. 1, February.

DEVELOPMENT OF SUPER HIGH DAMPING RUBBER DAMPER FOF THE SEISMIC RESPONSE CONTROL OF LONG SPAN BRIDGES

by

Kengo GODA [1], Shigenobu SUZUKI [1], Yoji SUIZU [2],
Shigeki UNJO [3], Hisanori OTSUKA [4], Kazuhiro NAGAYA [5]

1. Engineer ; Seismic Isolation Technology and Vibration Control Department, Bridgestone Co. Ltd.
2. General manager ; Seismic Isolation Technology and Vibration Control Department, Bridgestone Co. Ltd.
3. Head ; Earthquake Engineering Division, Earthquake Disaster Prevention Department, Public Works Research Institute, Ministry of Construction
4. Professor, Department of Civil Engineering Kyushu University
5. Research Engineer ;Earthquake Engineering Division, Earthquake Disaster Prevention Department, Public Works Research Institute, Ministry of Construction

ABSTRACT

In the long span bridge such as the cable stayed bridge and suspension bridge, it is an important subject that the vibration caused by the earthquake and wind is reduced. Due to the long inherent period and small damping capacity, the long span bridge has generally such a character that the vibration easily occures and does not readily go down. For the long span bridge like this, in order to increase the damping capacity and to elevate the durability, the purpose of this study is that the super high damping rubber damper of the shearing type as the high damping device should be developed. By performing the shaking table test of the bridge model supposing the long span bridge, an effectiveness of the super high damping rubber damper of the shearing type has been investigated. Along with it, because the reproducibility in the analysis of experimental results could be verified, by executing the simulation analysis of the bilinear modeling of the hysteresis character in the load and displacement of the super high damping damper, the results will now be reported here.

Key Words: Super High Damping Rubber Damper, Long Span Bridge, Cable-Stayed Bridge, Shaking Table Test, Dynamic Response Analysis

INTRODUCTION

The long span bridge including the suspension bridge and cable stayed bridge is the flexible structure with a long inherent period, and it is known that it has in general the structure with the small damping capacity by which the vibration does not readily reduce once it vibrates. Whereas an influence affected by the wind, generally speaking, becomes predominant, there are some cases when an influence caused by the earthquake becomes predominant if the damping capacity is small. In such a case, it is thought to be held good that the response in case of the earthquake should be effectively reduced by elevating the damping capacity of the superstructure of the long span bridge.[1) 2) 3)]

The purpose of this study is that the super high damping rubber damper (the damper utilizing the rubber material with a higher damping capacity than that of the rubber material used for the usual high damping rubber) of shearing type should be developed as the high damping device for the long span bridge. Hereupon, in order to investigate an effectiveness of the super damping rubber damper, by manufacturing the model bridge (the cable stayed bridge) modeling the long span bridge, the experiment on the shaking table and the dynamic response analysis have been carried out.[1)]

OUTLINE OF SHAKING TABLE TEST

Model of Bridge and Super High Damping Rubber Damper of Shearing Type

The model of the long span bridge used for the experiment is shown in Fig. 1. The model is made supposing the cable stayed bridge (the complete system), and H-steel or I-steel is used for the main girder, main tower, pier and substructure, and the PC steel wire is used for the cable members. The length of the main girder is 7.2m, and the height of the main tower is 2.5m, and furthermore so as to adjust the weight to the law of similarity, the weight is added on to the main girder, main tower and pier. Moreover, the model bridge was modeled the real bridge with an inherent period in a degree of 5 second, and the spatial scale was made to be 1/56, and the time scale was made to be 1/5. In addition, when the shaking table is moving, in order to prevent the generation of the torsional vibration and flexural oscillation (vertical motion) of the main girder, by stretching the wire diagonally in the vertical direction to the vibration direction of bridge axis from the edge of main girder (4 locations), the movement direction of the main girder was confined so that only the horizontal vibration (direction of bridge axis) could occur.

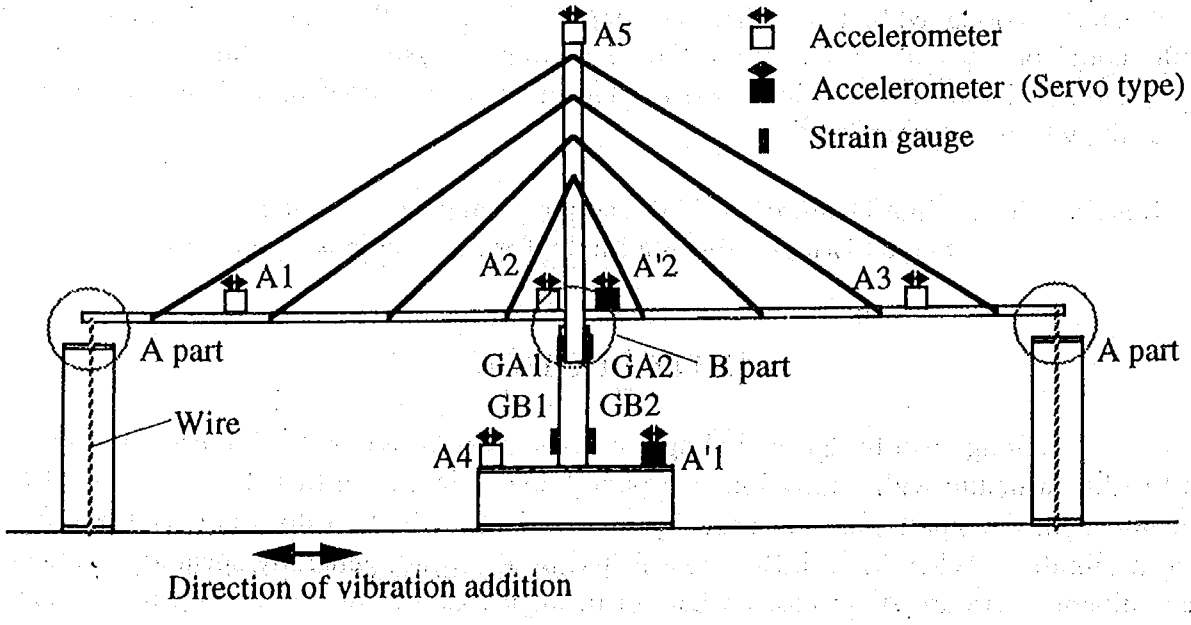
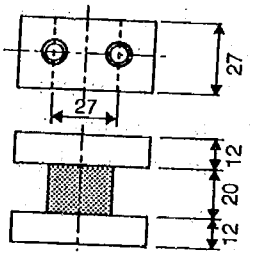
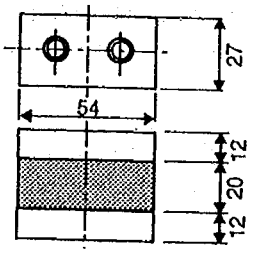


Fig. 1 Model of long span bridge ; Locationof measurement and damper installation

The damper used for the experiment has been made to be a monolithic construction by doing the vulcanized adhesion of the high damping rubber of SBR (styrene-butadiene-rubber) series called the super high damping rubber damper as shown in Table 1 with the steel. In contrast to that the equivalent damping ratio of the high damping lamination rubber used for the usual seismic isolation device is about a degree of 15% (the loss factor tan δ = apporoximately 0.3), the equivalent damping ratio of the super high damping rubber used in this experiment is about a degree of 30% (the loss factor tan δ = apporoximately 0.6), and accordingly it is the material with a very large damping capacity in a wide amplitude range (shear strain domain). The other distinctive characteristics of the super high damping rubber damper will be shown below. ① It has a dependency on amplitude and shows the character being close to the hysteresis damping of the elasto-plastic type. ② Its dependency on velocity is relatively small. However, although a difference is observed between in case of the earthquake and in case of the low velocity when the girder extends/contracts at an ordinary temperature, an influence affected by it on the substructure is small because the rigidity decreases in case of the low velocity. ③ The dependency on the temperature is relatively small.

Table 1 Type of damper used for each Shaking Table Test

Case of experiment	Installation location of damper	Shape and Size of damper
Case 1	without damper	-
Case 2	Damper of shearing type Installation location: A part in Fig. 1 Amount: each 1 set, 2 set in total	
Case 3	Damper of shearing type Installation location: B part in Fig. 1 Amount: 1 set	

Method of Shaking Table Test

The experiment has been carried out in 3 cases as shown in Table 1: Namely the case when the damper is not installed (case 1), the case when the damper is installed between the edge of main girder and pier (case 2), and the case when the damper is installed between the central main girder and pier (case 3). Considering the law of similarity, kind of ground and scale of earthquake, as the input seismic wave to the shaking table, each 4 levels for each case, namely 12 cases of the shaking table test have been executed in total: Namely the seismic wave for the Class I Ground Seismic Coefficient Method Level 46 Gal (Ground I Seismic Coefficient Method Level), the seismic wave for the Class I Ground Bearing Capacity Method Level 160 Gal (Ground I Bearing Capacity Method Level), the seismic wave for the Class III Ground Seismic Coefficient Method Level 62 Gal (Ground III Seismic Coefficient Method Level), and the seismic wave for the Class III Ground Bearing Capacity Method Level 200 Gal (Ground III Bearing Capacity Method Level).

As for the measurement, as shown in Fig. 1, the horizontal acceleration in the shaking table, main tower and main girder, and the bending strain on basal part of the main tower and the pier have been measured. In addition, for the purpose of measuring the relative displacement of the main girder, the accelerometer of the servo type was installed on the shaking table and main girder.

Furthermore, so as to obtain the data of the principal vibration mode, the sampling time of data was set at 100 Hz.

RESULTS OF SHAKING TABLE TEST

Time Hysteresis Response Waveform

The acceleration of input wave, the time hysteresis response waveform of the response acceleration in the main girder and main tower, the response displacement of main girder, and the response bending strain on the basal part of main girder and on the basal part of pier, when the seismic wave of Class I Ground Bearing Capacity Method Level (it is called Ground I Bearing Capacity Method Level in the following) is input, are shown in Fig 2. In the same manner, the time hysteresis response waveform when the seismic wave of the Class III Ground Bearing Capacity Level (it is called Ground III Bearing Capacity Method Level in the following) is input, is shown in Fig 3.

Concerning to the case when Ground I Bearing Capacity Method Level is input, the response of each kind in case 1 and case 2 will be compared in Fig 2. Whereas the response acceleration of the main girder has in both cases the waveform in which the high order vibration modes are piled up on the first order vibration mode, the first order inherent vibration only for the most part responds after the input of seismic wave has finished.

In case 2 as compared with case 1, while the response does not reduce during inputting the seismic wave, it can be confirmed that the first order inherent vibration reduces quickly after finishing the seismic wave input. In both cases, the response waveform of main tower had the waveform in which the high order vibration modes accumulated in complexity beside the first order vibration mode, and in case 2 when the damper was installed, the decrease of response was hardly observed. In addition in both cases, as for the response displacement of the main girder, the first order vibration is prominent, and in case 2 when the damper is installed, it can be confirmed that the inherent vibration reduces rapidly after finishing the seismic wave input, and that the maximum response value (the absolute value) goes down. Although the first order vibration is predominant also for the bending strain response in the basal part of main tower and basal part of pier, the response in the basal part of main tower has the waveform in which the second order and the third order vibration modes exist. In case 2 as compared with case 1, as same as in case of the response displacement of the main girder, also as for the response bending strain on basal part of the main tower and pier, it can be confirmed that the inherent vibration reduces quickly after finishing the seismic wave input and that the maximum response value (the absolute value) goes down.

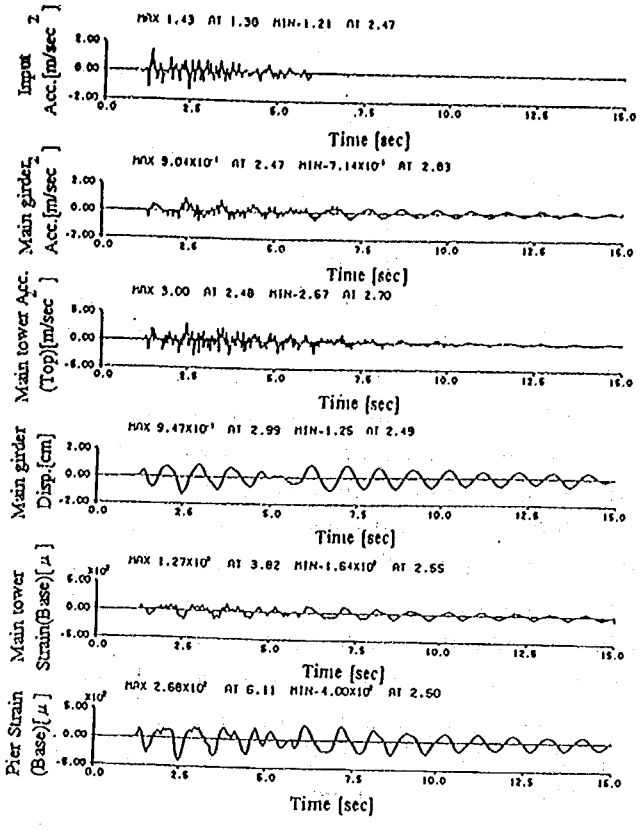
In addition, also in comparison with each kind of response in case 1 and case 2 when Ground III Bearing Capacity Method Level is input, whereas there is the same tendency as the case of Ground I Bearing Capacity Method Level, the effect of seismic response control is a little to some extent on the whole, when comparing with the case of Ground I Bearing Capacity Method Level.

The summary of the first order inherent frequency and the equivalent damping ratio in each case is sown in Table 2. Although there is scarcely the damping capacity in the model itself, by installing the damper, it can be understood that the damping of some 0.16 in case 2 and some 0.12 in case 3 is added. Hereupon, the inherent frequency was obtained from the input seismic wave and the transmissibility of response acceleration of main girder, and the equivalent damping ratio was gained by the half-power method from the transfer function.

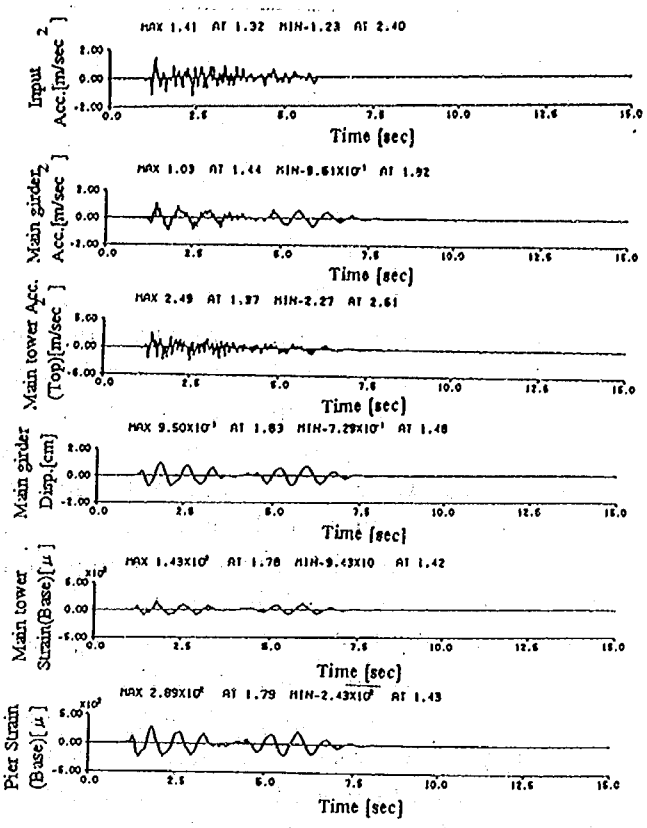
In the experiment, because the damping capacity was too big for the bridge, the inherent period changed from a degree of 1 second to a degree of 0.6 second. However it is hopefully thought that the damper with an appropriate capacity, by which the vibration system will not be changed, is installed.

Table 2 First order inherent frequency and damping ratio of each case of experiment

Case of experiment	Inherent period (sec) (real size bridge)	Equivalent damping Ratio
Case 1	0.91 ~ 1.00 (4.55 ~ 5.00)	0.02 ~ 0.03
Case 2	0.63 ~ 0.77 (3.15 ~ 3.85)	0.18 ~ 0.20
Case 3	0.67 ~ 0.83 (3.35 ~ 4.15)	0.12 ~ 0.16

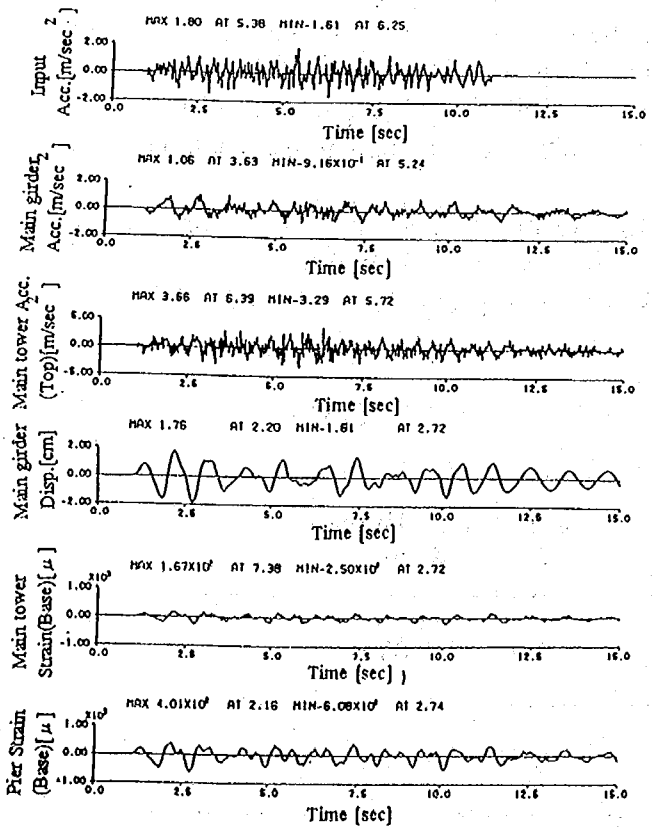


Case 1 (without damper)

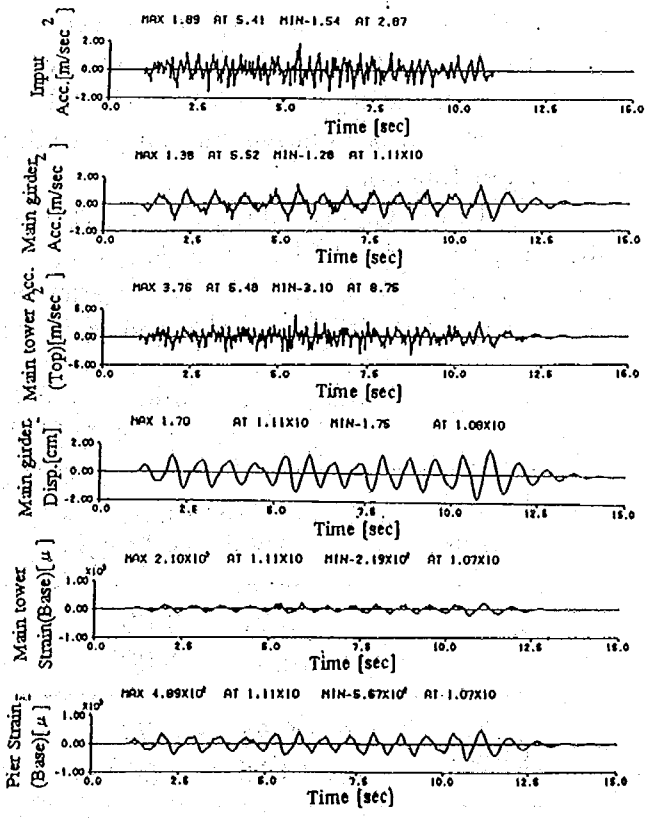


Case 2 (with damper)

Fig. 2 Class I Ground Bearing Capacity Method Level



Case 1 (without damper)



Case 2 (with damper)

Fig. 3 Class III Ground Bearing Capacity Method Level

Maximum Response Acceleration

As for the case when the seismic wave of the class I Ground Seismic Coefficient Method Level (it is called Ground I Seismic Coefficint Method Level in the following) is input, the maximum response value (the absolute value) of each of the input seismic wave acceleration, the main girder response acceleration and the main tower response acceleration are shown in Fig. 4. Similarly, the case when Ground I Bearing Capacity Method Level is input is shown in Fig. 5, and the maximum response value when the seismic wave of the Class III Ground Seismic Coefficient Method Level (it is called the Ground III Seismic Coefficient Method Level in the following) is input, is shown in Fig. 6, and the case of Ground III Bearing Capacity Method Level is shown in Fig. 7. According to them, although there is no amplification tendency being common to every case, the main girder response acceleration and the main tower response acceleration scarcely go down. As one of its factors, it is pointed up that high order vibration modes being piled up on the first order vibration mode do not reduce.

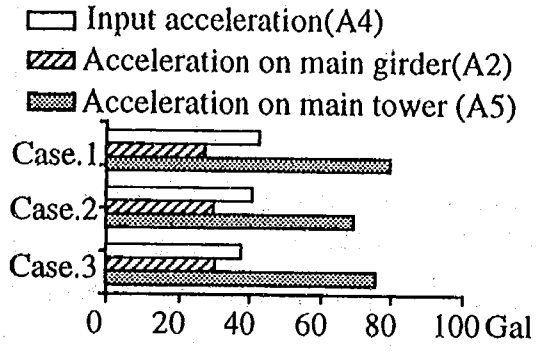


Fig. 4 Maximum response acceleration when I class ground 46 Gal is input

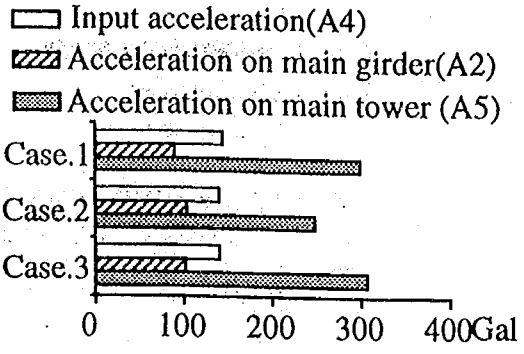


Fig. 5 Maximum response acceleration when I class ground 160 Gal is input

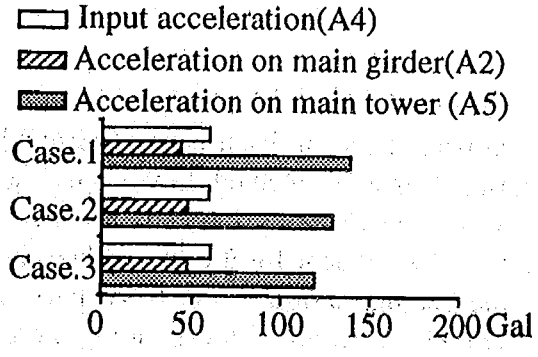


Fig. 6 Maximum response acceleration when III class ground 62 Gal is input

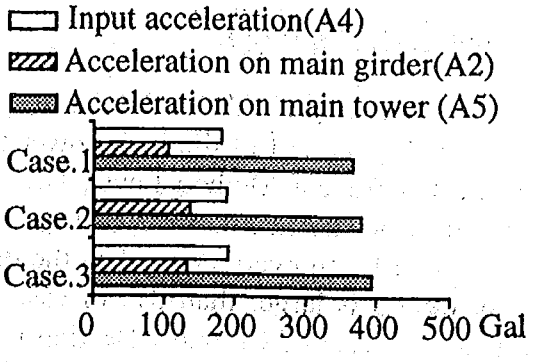


Fig. 7 Maximum response acceleration when III class ground 200 Gal is input

Maximum Response Displacement

The maximum response value (the absolute value) of the main girder response displacement of Ground I Seismic Coefficient Method Level, Ground I Bearing Cpacity Method Level, Ground III Seismic Coefficient Method Level and Ground III Bearing Capacity Method Level is shown in Fig. 8. In every case when the damper is installed, the maximum value of the main girder displacement reduces in common. As compared with case 1, it is 0.63 ~ 0.97 in case 2, and 0.52 ~ 0.73 in case 3, and consequently by installing the damper, it can be said that the maximum relative displacement of the main girder can be reduced.

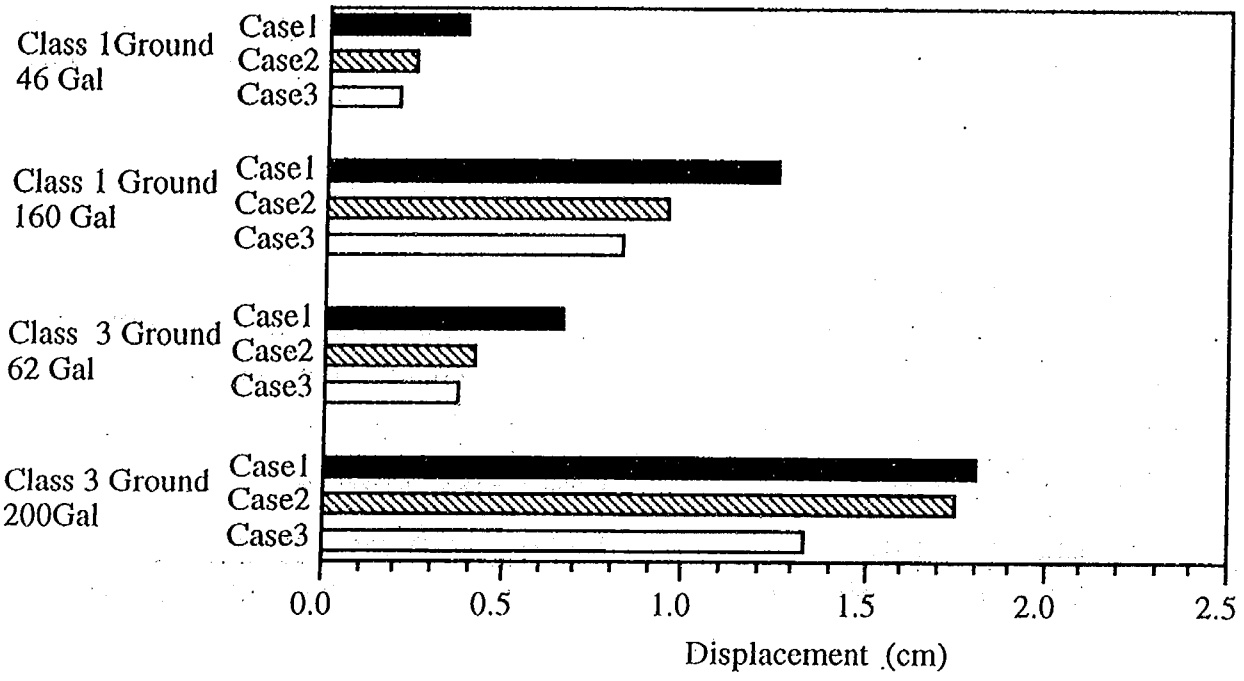


Fig. 8 Maximum response displacement by each class of ground and by each case (Shaking table test)

Maximum Bending Strain

The change in the maximum response value (the absolute value) of the bending strain from the top part of the main tower to the basal part of pier in each case of Ground I Seismic Coefficient Method Level, Ground I Bearing Capacity Method Level, Ground III Seismic Coefficient Method Level and Ground III Bearing Capacity Level is shown in Fig. 9 - Fig. 12. In every case when the damper is installed, except for the case when the value of case 3 is larger than that of case 1 as for the bending strain in the basal part of main tower in case of Ground I Bearing Capacity Method Level, all of the bending strain of case 2 and case 3 are smaller compared with those of case 1. In the basal part of pier, as compared with case 1, the bending strain is 0.56 ~ 0.93 in case 2, and 0.57 ~ 0.79 in case 3. It is thought that the bending strain of the member profile in the basal part of pier in case of earthquake can be reduced by the effect of damper.

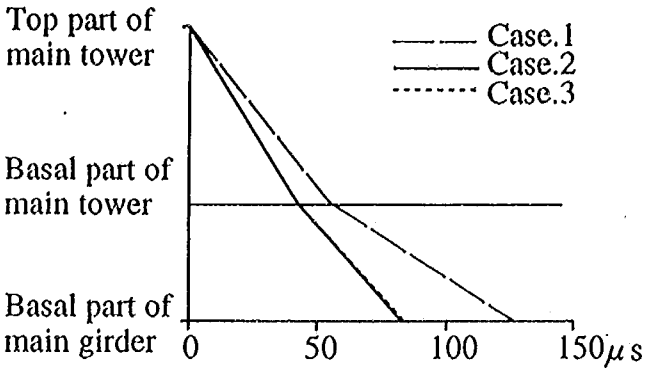


Fig. 9 Maximum bending strain when class I ground 46 Gal is input

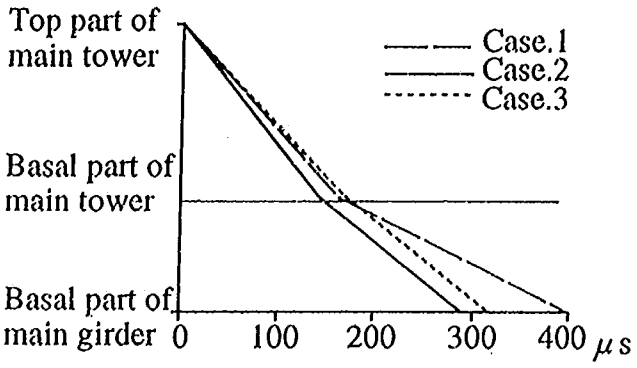


Fig. 10 Maximum bending strain when class I ground 160 Gal is input

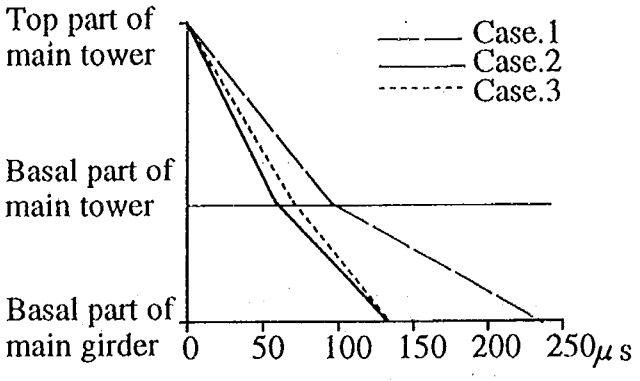


Fig. 11 Maximum bending strain when class III ground 62 Gal is input

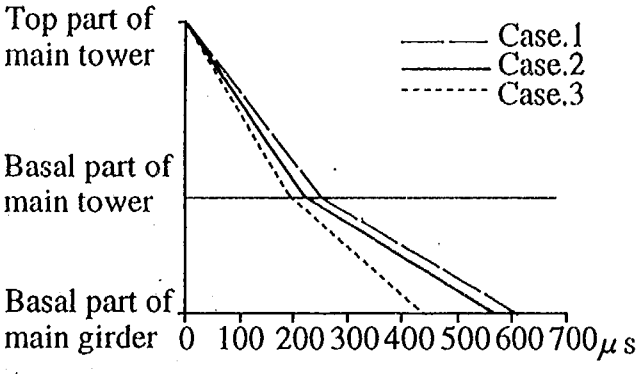


Fig. 12 Maximum bending strain when class III ground 200 Gal is input

ANALYTICAL RESULTS

Method of Analysis

In the analysis, the bridge model was modeled by the elements of mass and beam system shown in Fig 13, and subsequently the hysteresis characteristics of load and displacement based on the elemental loading test experiment were modeled by the bilinear model shown in Fig. 14. The damper modeled in each case of shaking table test is arranged at A part and B part shown in Fig. 13.

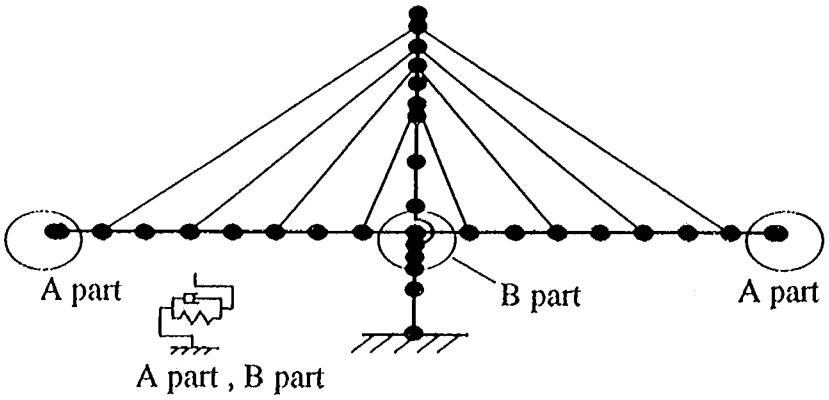


Fig. 13 Analytical model of model bridge

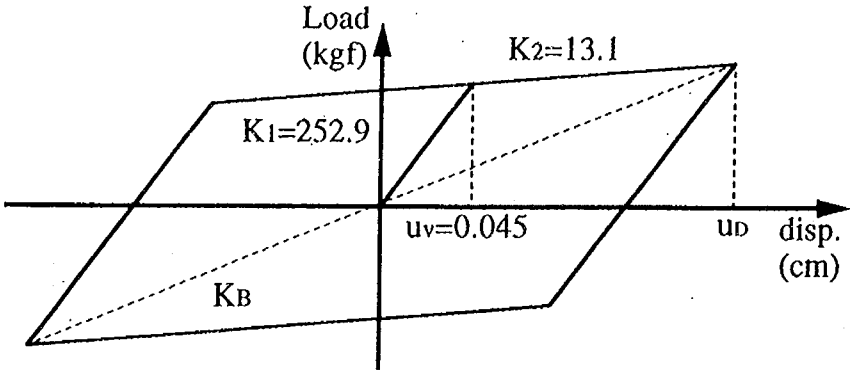
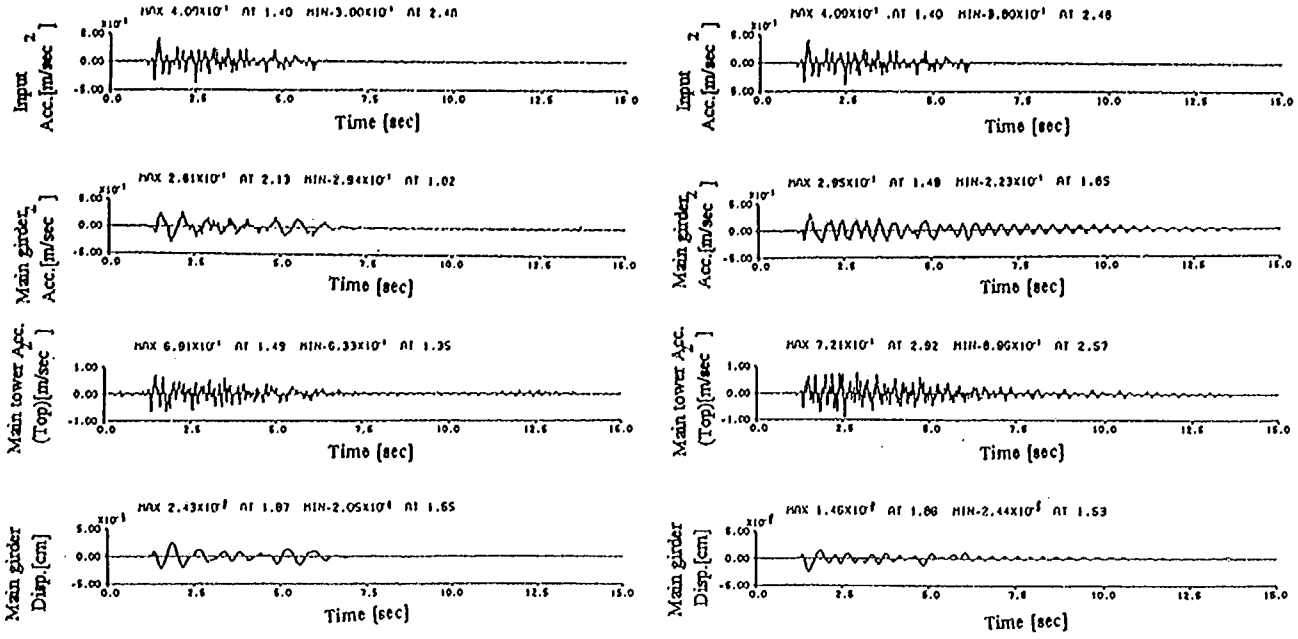


Fig. 14 Bilinear model of super high damping rubber damper (case 2)

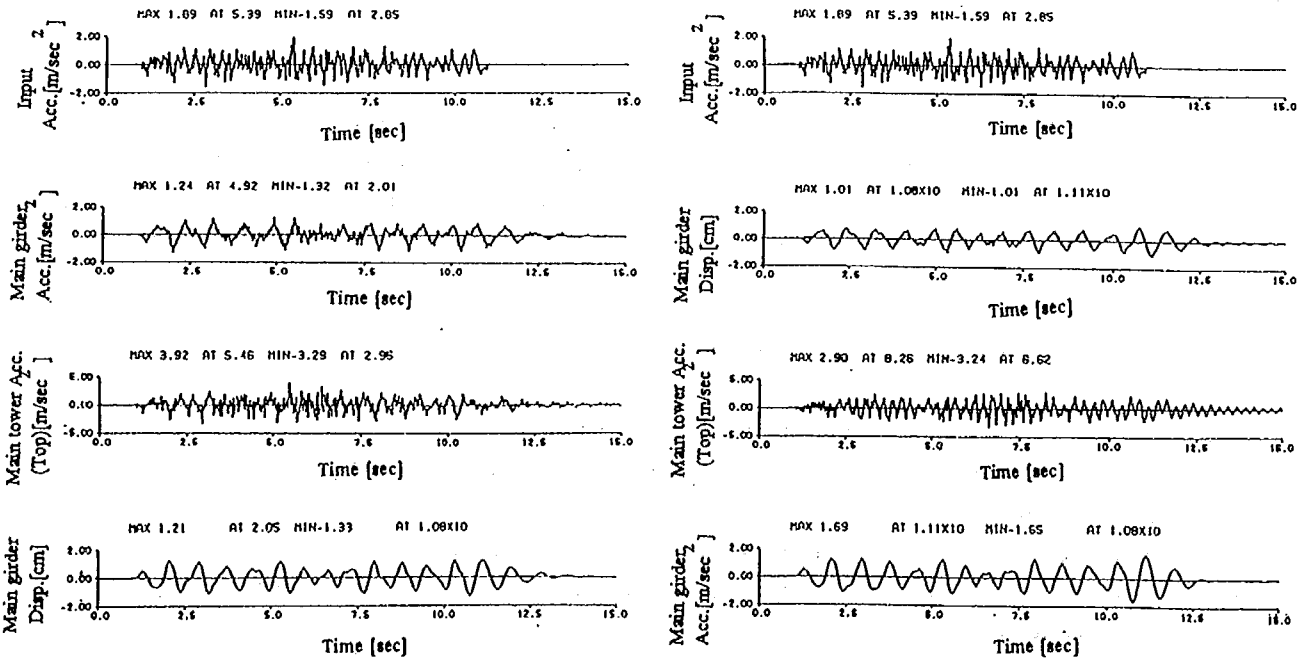
Comparison of Analytical Results with Shaking Table Test Results

The comparison between the experimental results and the analytical results of time hysteresis response waveform of the input acceleration, the response acceleration of main girder, response acceleration of main tower and the response displacement of main girder when the seismic wave of Ground I Seismic Coefficient Method Level and Ground III Bearing Capacity Level are input, is shown in Fig. 15 and Fig. 16. As for case 2 of Ground I Seismic Coefficint Method Level, in the analysis, although the reduction of the response acceleration in the main girder and main tower, on which the high order vibration modes influence beside the first order mode, is not observed, the response displacement in the main girder, in which the first order inherent frequency is prominent, rapidly goes down after finishing the seismic wave input, and consequently it is in the same tendency as the results of shaking table test. As compared with the results of shaking table test, whereas the response acceleration in the main girder and main tower is somewhat different due to the influence of the high order vibration mode, as for the displacement of the main girder, in which the first order inherent frequency is predominant, the maximum response value, inherent period and so forth result in a relatively good agreement. The roughly same thing can be said also in other cases including Ground III Bearing Capacity Method Level, and moreover the effectiveness of damper was confirmed by the analysis, and the results shaking table test could be, for the most part, reproduced.



Case 2 (Shaking table test) Case 2 (Analysis)

Fig.15 Class I Ground Seismic Coefficient Method Level



Case 3 (Shaking table test) Case 3 (Analysis)

Fig. 16 Class III Ground Bearing Capacity Method Level

SUMMARY

For the purpose of examining the effectiveness of the super high damping rubber damper of shearing type for the long span bridge, in this report, the shaking table test in case when the super high damping rubber damper is installed for the model of the long span bridge, and its dynamic response analysis have been carried out. The gist is summarized in the following:

(1) The bending moment in the basal part of pier and in the basal part of main tower could be reduced by installing the damper.

(2) The relative displacement of main girder could be reduced by installing the damper.

(3) Because the damper was so arranged that it displayed the seismic isolation effect against the first order vibration mode, the acceleration in the main girder and in the top part of main tower, where the high order vibration modes were piled up on the first order vibration mode, was scarcely reduced.

(4) Also in the dynamic response analysis, the damping capacity of the damper could be confirmed, and in addition to it, by doing the bilinear modeling of the hysteresis characteristics in the load and displacement of the damper of shearing type, the results of shaking table test could be roughly exactly reproduced.

In this shaking table test, because the damper capacity was too big, the inherent period of the bridge model changed and therefor the vibration system made a change. Based on it, it is planned from now on that the damping capacity of damper will be confirmed by the dynamic response analysis changing the rigidity and damping of damper.

APPENDIX

This study has been executed in "Joint Study on Seismic Isolation Technology of Long Span Bridge using High Damping Material" jointly done by the Public Works Research Institute of the Ministry of Construction, the Foundation of Civil Engineering Research Center and 19 private companies.

REFERENCES

(1) Public Works Research Institute, Ministry of Construction:
Report of Joint Study on Seismic Isolation Technology of Long Span Bridge using High Damping Material (No. 1), Mar., 1994

(2) Public Works Research Institute, Ministry of Construction:
Report of Joint Study on Seismic Isolation Technology of Long Span Bridge using High Damping Material (No. 2), Mar., 1995

(3) Public Works Research Institute, Ministry of Construction:
Report of Joint Study on Seismic Isolation Technology of Long Span Bridge using High Damping Material (No. 3), Mar., 1996

(4) Kengo Goda, Shigenobu Suzuki, Yoji Suizu, Shigeki Unjo, Hisatetsu Otsuka, Kazuhiro Nagaya: Shaking Table Test of Model of Long Span Bridge using Super High Damping Rubber Damper and its Analysis, 51st annual technical lecture meeting, Academy of Civil Engineering, I-B, pp. 126-127, Sept., 1996

Session 3

Hybrid/Semi-active Systems and Smart Materials

(Co-Chairs: A. Igarashi, A. Itani)

"Modeling of a Variable Damper and its Application"
by T. Sato, M. Sato, S. Tanaka, K. Toki
Presented by: Tadanobu Sato

"Seismic Response Control of PC Cable-Stayed Bridge under Construction by Active Mass Damper"
by M. Tsunomoto, H. Otsuka, S. Unjoh, K. Nagaya
Presented by: Meguru Tsunomoto

"Thermo-visco-elasto-plastic Modeling of Elastomeric and Lead-Rubber Bridge Bearings"
by J. Mander, D-K Kim, S. Chen
Presented by: John Mander

MODELING OF A VARIBLE DAMPER AND ITS APPLICATION

Tadanobu SATO
Disaster Prevention Research Institute, Kyoto University, Gokasho,Uji Kyoto 611 Japan

Makoto SATO
Chubu Electric Power Co. Lmd., Shinmach, Higashiku Nagoya 461-91 Japan

Satoru TANAKA and Kenzo TOKI
School of Civil Engineering, Kyoto University, Yoshida, Sakyouku 606-01 Japan

SUMMARY

A small-size variable damper without external accumulator was developed. A series of calibration tests have been conducted to develop a mechanical model of variable damper which gives the relationship among damping force, velocity of piston and valve opening ratio. The control algorithm to generate damper force is derived from mechanical model of the observed damper characteristics. The feature of the algorithm to determine the valve opening ratio is very simple without feedback mechanism, which is determined directly from measured piston velocity and the targeted damping force. The efficiency of developed control system were proved by producing various types of hysteric relationship between damping force and piston displacement.

INTRODUCTION

Active control systems for seismic-excited civil engineering structures have been developed to the degree where practical implementations have been made in a number of buildings[1]. The active structural vibration control mechanisms are classified into full active and semi-active types. The full active type such as the active mass damper not only requires large control force, it could also be detrimental if the control system happened to malfunction. Semi-active type represented by a semi-active damper is an attractive in the control of the dynamic response of structure system because it requires very small energy to control the system. Different types of semi-active dampers have been proposed ranging from simple electrorhorogical dampers[2] to hydraulic dampers with mechanically controlled orificing.[3,4]Semi-active dampers combine passive structural control[5] with the benefits of active structural control[6] to produce optimal, yet stable and reliable damper systems.

In this paper we present the design and dynamic behavior of hydraulic damper to develop a mechanical model of the variable damper. The device developed here is an adjustable hydraulic damper equipped with a flow control valve composed of a linear motor and valve opening level feedback system.

OUTLINE OF THE DEVELOPED VARIABLE DAMPER

The design plan and cross-sectional view of developed variable damper are shown in **Figure 1** and **2**. The damper is designed to generate the maximum damping force of 600kgf and maximum relative displacement of damper piston to be ±10 cm. A servo valve is installed at the center of the by-pass steel pipe which connecting the right and left cylinder cells. The servo valve is composed of the spool valve with the stroke of 0.5mm which is controlled by a linear force motor. The essential specification of the variable damper is given in **Table 1**.

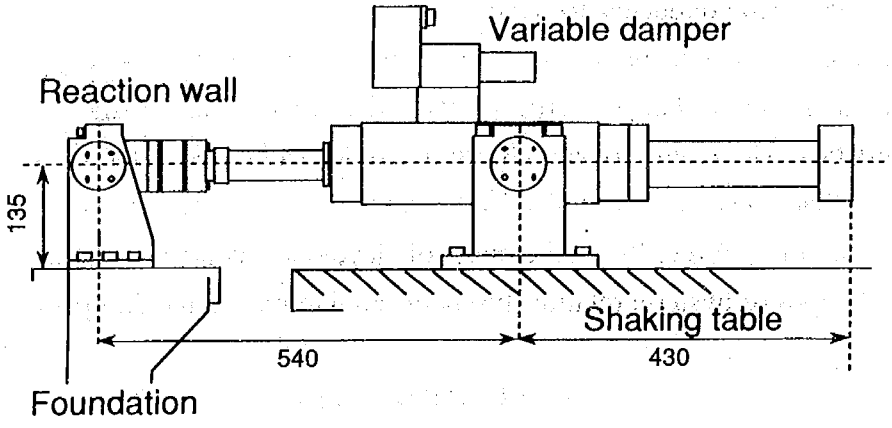


Figure 1. Small-sized model of variable damper

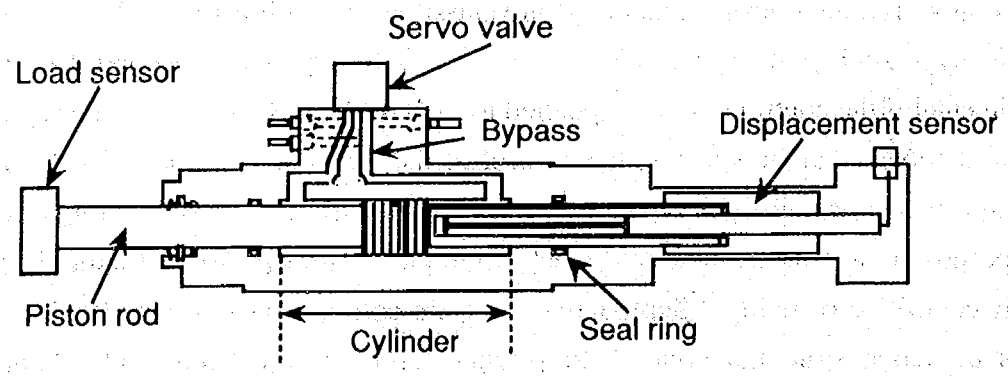


Figure 2. Small-sized model of variable damper (cross section)

Table 1. Specification of variable damper

Main part		
diameter of cylinder		4.20 cm
diameter of piston rod		3.50 cm
pressure area of piston		4.23 cm^2
piston stroke		±10.00 cm
volume of oil	cylinder	89.00 cm^3
	bypass pipe(left)	7.46 cm^3
	bypass pipe(right)	12.48 cm^3
weight of variable damper		57.10 kg

Valve part	
value of k in eq.(4) $\left(\frac{\text{pressure drop}}{(\text{vorume of oil flow})^2}\right)$	1.26 kg/cm^7

DYNAMIC LOADING TEST OF THE DEVELOPED VARIABLE DAMPER

To obtain basic characteristics of the variable damper the piston of variable damper is sinusoidally excited under the condition that the valve opening ratio is kept at a constant value.The generated damping force and the piston velocity as well as displacement are measured. The variable damper is set up on the shaking table as shown in **Figure 1** and one end of piston rod is anchored at the reaction wall. The shaking table is sinusoidally excited with several combination of amplitudes and frequencies. For each case several valve opening ratios are set from the full open condition to the level of maximum damping force being 400kgf. Several examples of hysterics loops obtained during experiments are shown in **Figure 3**. As can be seen the dynamic characteristics of developed variable damper differ from the pure viscous damper of which hysteresis loop is an ellipse. The deference becomes large for the case of the large displacement

amplitude of piston rod and the small valve opening ratio. The time when maximum damping force generated is delayed from that of maximum velocity of piston rod attained. This means that there is a time delay between the velocity of piston and the oil flow rate at the valve.

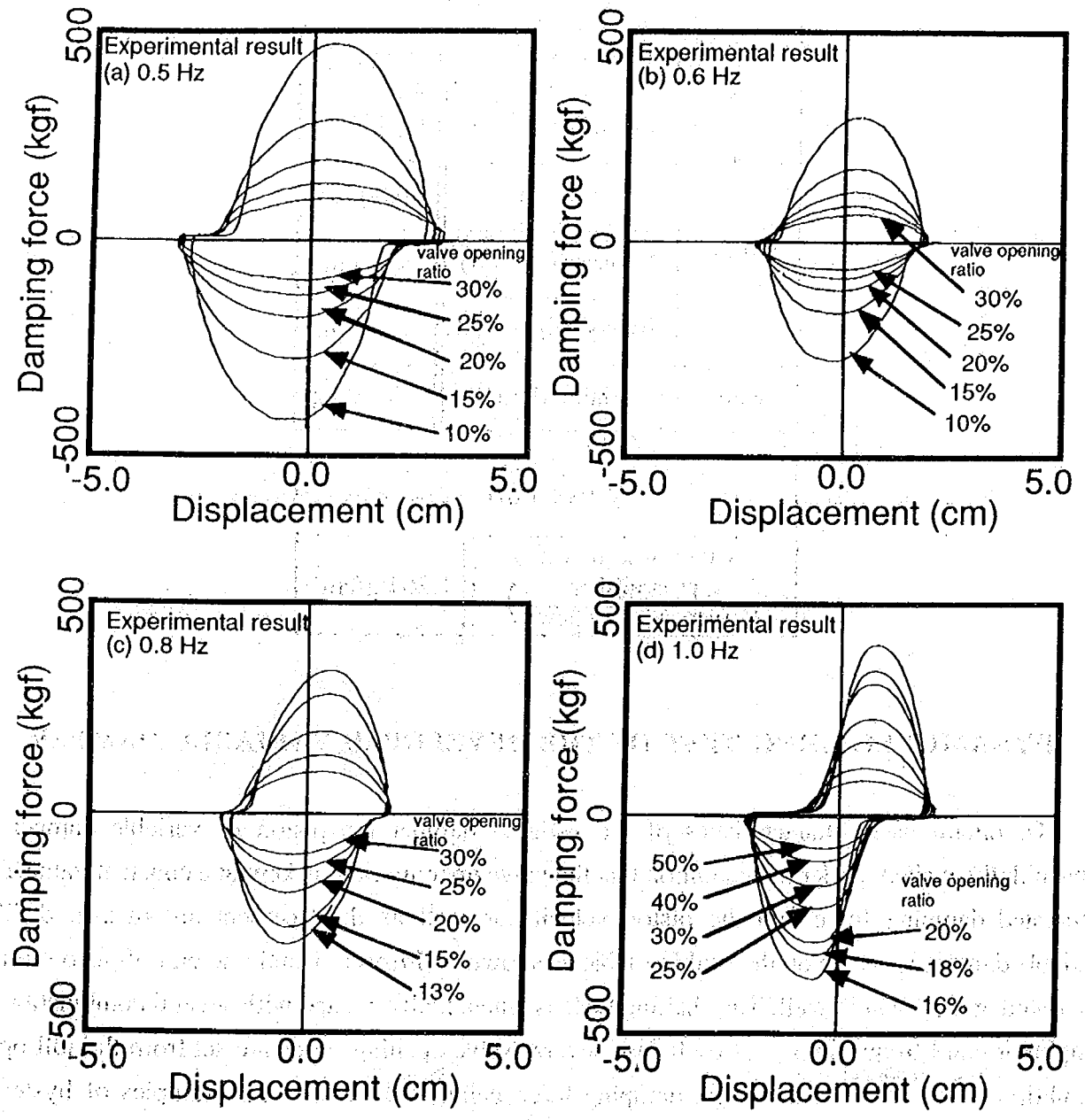


Figure 3. Hysteresis loops of damping force

MODELING OF VARIABLE DAMPER

The damper force, F, is assumed to be expressed by

$$F = A(P_2 - P_1) + F_{fr} \tag{1}$$

in which A is the area of cross section of piston, P_1 and P_2 oil pressure of right and left cylinders, F_{fr} the friction force between the piston and cylinder. Neglecting the pressure loss in the bypass pipe the pressure drop at the valve, ΔP, is given by the pressure difference between right and left chambers.

$$\Delta P = P_2 - P_1 \tag{2}$$

The volumetric oil flow rate through the bypass pipe Q is determined by the continuity equation

$$Q = A\dot{x} \tag{3}$$

in which A is the area of piston cross section, $\dot{x}$ the velocity of piston.

The relation between the maximum volumetric oil flow rate and the pressure drop is designed to satisfy the following relation

$$Q_m = \sqrt{\frac{\Delta P}{k}} \tag{4}$$

in which k is a constant determined by the servo valve characteristic as given in **Table 1**. Because the loss factor of valve is depend on the valve opening ratio $\delta\,(0 \le \delta \le 1)$ the volumetric oil flow rate can be expressed as follow:

$$Q = \beta\delta Q_m = \beta\delta\sqrt{\frac{\Delta P}{k}} \tag{5}$$

in which β is a correction coefficient expressed as a nonlinear function of δ . Eliminating Q using Eqs.(3) and (5) we can get

$$\Delta P = k\left(\frac{A\dot{x}}{\beta\delta}\right)^2 \tag{6}$$

Substituting Eq.(6) into Eq.(1) the relation between the damper force and the piston velocity is given as a function of the valve opening ratio

$$F = k\frac{A^3\dot{x}^2}{\beta^2\delta^2} + F_{fr} \tag{7}$$

The value of F_{fr} in this equation and the relationship between the unknown coefficient β and the valve opening ratio δ are determine by the inverse analysis using experimental data shown in **Figure 3**. The identified value of F_{fr} is about 5.6 kgf for each case of experiments. The relation between β and δ is in **Figure 4** and the maximum volumetric flow rate vs. δ is in **Figure 5**. Form these figures we confirm the assumption that the correction coefficient β is only dependent on the valve opening ratio and independent on the volumetric oil flow rate. The regression equation expressing relation between β and δ is

$$\beta = \begin{cases} 1.00 & (\delta \geq 0.4) \\ -7.63\times(\delta - 0.4)^3 + 1.00 & (\delta < 0.4) \end{cases} \tag{8}$$

This relation is expressed by the full line in **Figure 4**.

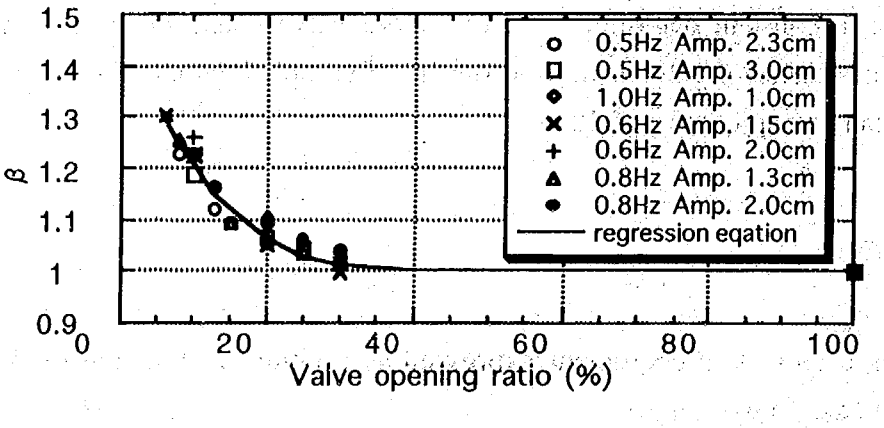


Figure 4. Relation of between valve opening ratio and value of β

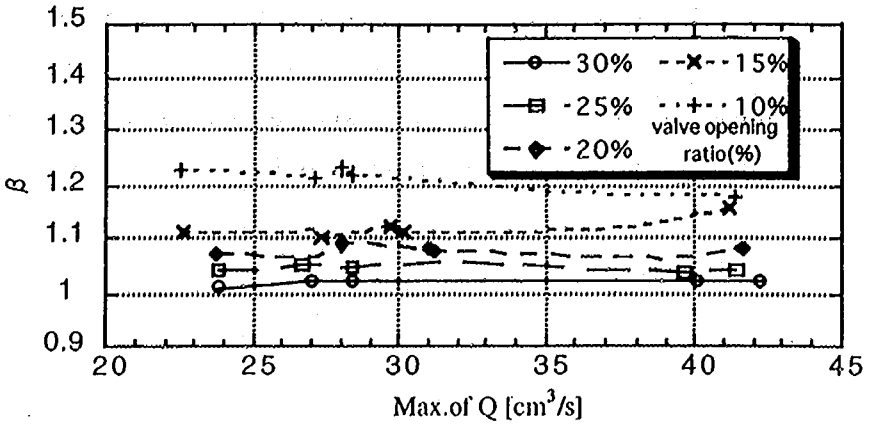


Figure 5. Relation of between maximum oil flow rate and value of β

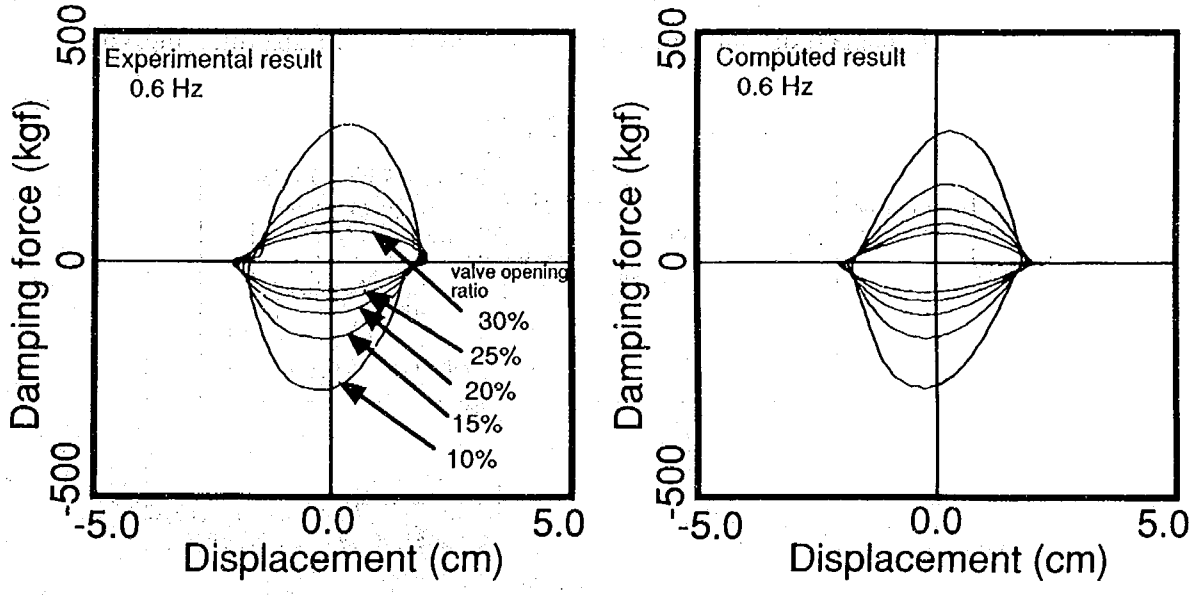


Figure 6. Comparison between experimental result and computed result

To simulate a hysterics loop for a constant valve opening ratio the average time delay of 0.03sec between the time at the maximum damping force being generated and the time at maximum piston velocity being attained is obtained from experimental data. Theoretically simulated hysteresis loops are compared with experimental results for the case that the frequency of harmonic piston displacement is 0.6Hz (**Figure 6**). The result show that the developed model of the variable damper possesses good performance ability.

THE CONTROL SYSTEM OF VARIABLE DAMPER

The system to control the valve opening ratio is shown in **Figure 7**. To control the valve opening ratio δ we use the following equation derived from Eq.(7)

$$\delta = \left|\frac{\dot{x}}{\beta(\delta)}\right| \sqrt{\frac{kA^3}{|F_T - F_{fr}|}} \tag{9}$$

in which F_T is the target damper force. Because the value of β in Eq.(9) is a function of δ the iterative calculation is necessary to determine the value of δ within the digital time interval, 0.01sec, to control the valve opening ratio in this experiment. The convergence of valve of δ is guaranteed by using a high speed digital signal processor (DSP) within this time interval.

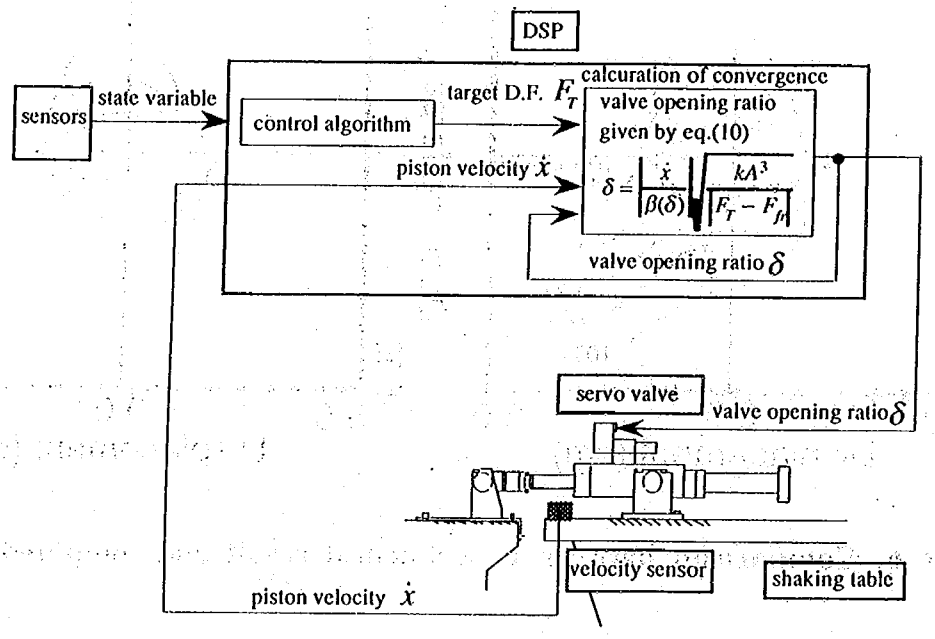


Figure 7. Control system for valve opening ratio

To demonstrate capability of the developed system to control the variable damper it is placed on the shaking table and one side of the piston end is anchored on the foundation as shown in **Figure 7**. The shaking table is moved by sinusoidal signal being controlled to generate the displacement amplitude of 2 cm and frequency of 0.5Hz. The valve opening ratio is then controlled to produce an arbitrary hysteresis loop. The first example is an elliptic hysteresis loop

which can only be generated by a pure viscous damper. The time history of valve opening ratio and hysteresis loop is shown in **Figure 8**. The second example is a friction type hysteresis loop as shown in **Figure 9**. The broken lines in both figures are target values. Although small disturbance can be seen when the movement of piston direction is reversed the over all response of the variable damper shows good agreement with target values.

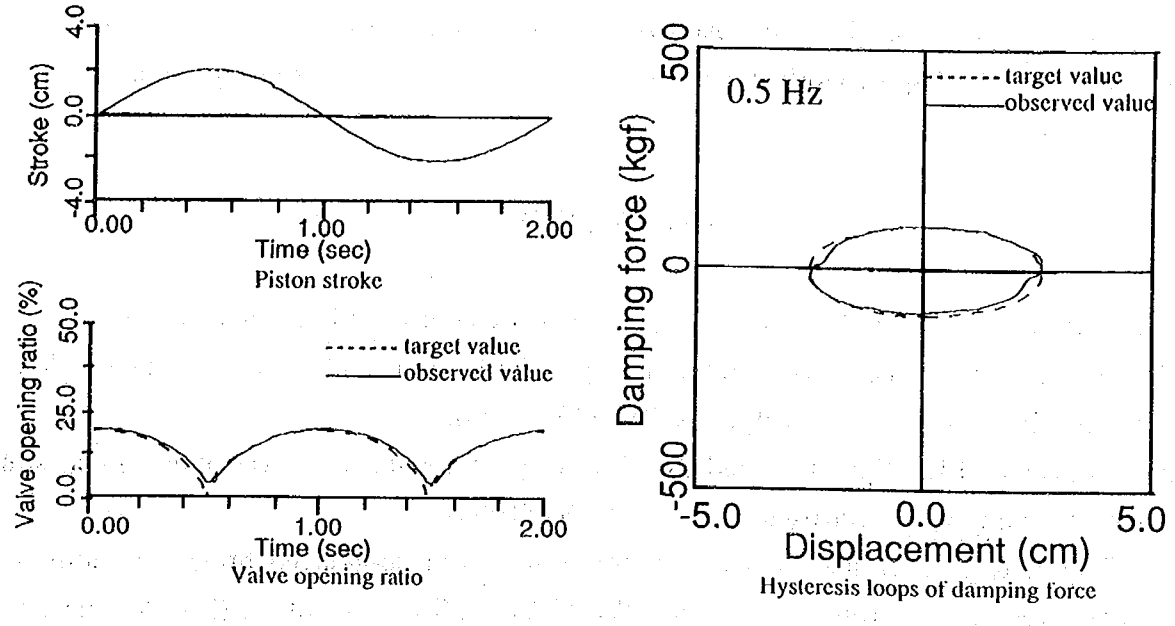


Figure 8. Simulation of a damper with constant damping coefficient

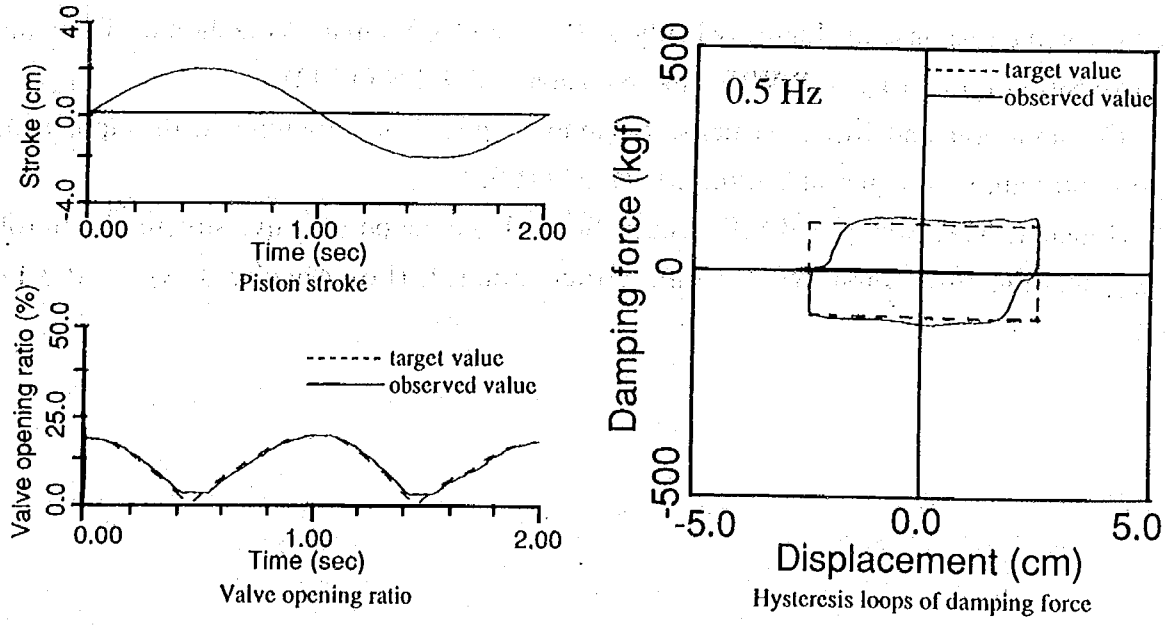


Figure 9. Simulation of a friction damper

CONCLUSION

An adjustable hydraulic damper was developed and its performance was studied through the dynamic loading tests. The mechanical model of the variable damper was derived to construct the control system of the developed variable damper. The derived relation between the damping force and the valve opening ratio was implemented into a micro-computer composed of the high speed digital signal processor which is the main part of the control system. The developed control system of the variable damper worked well to demonstrate wide capability for generating arbitrary hysteresis loops.

REFERENCES

1. T.T. Soong, and A.M.Reinhorn, Case studies of active control and implementation issue, ATC 17-1, Seminar on Seismic Isolation, Energy dissipation and Active control, Applied Technology Council, Redwood City, CA,701-713 (1993).
2. N.G. Stevens, J.L. Sproston and R. Stanway, Experimental evaluation of a simple electroviscus damper, J.Electrostatics, 15, 275-283 (1984)
3. W.N. Patten, R.L. Sack and Q. He, Suppression of vehicle-induced bridge vibration via a semiactive structural controller, Proc. First World Conf. Struct. Control, (Los Angelse, CA), 1, FA1-30-FA1-38 (1994).
4. K. Kawashima, S. Unjho, H. Iida and H. Mukai, Effectiveness of the variable damper for reducing seismic response of highway bridges, Proc. 2nd US-Japan Workshop on Earthquake Protective System for Bridges, PWRI, Tukuba, Japan, 479-494 (1992).
5. M.C. Constantinou and M.D. Symans, Seismic response of structures with supplemental damping, Structural Design Tall Build., 20, 77-92 (1993).
6. G.W. Housner, T.T. Soong and S.F. Masri, Second generation of active structural control in civil engineering, Proc. First World Conf. Struct. Control, (Los Angelse, CA), 1, P-3-P-31 (1994).

SEISMIC RESPONSE CONTROL OF PC CABLE-STAYED BRIDGE UNDER CONSTRUCTION BY ACTIVE MASS DAMPER

Meguru TSUNOMOTO [1], Hisanori OTSUKA [2], Shigeki UNJOH [3] and Kazuhiro NAGAYA [4]

1) Senior Research Engineer, Technical Division, Oriental Construction Co., Ltd., Tokyo, Japan
2) Professor, Department of Civil Engineering, Kyushu University, Fukuoka, Japan
3) Head, Earthquake Engineering Division, Public Works Research Institute, Ministry of Construction, Tsukuba, Japan
4) Research Engineer, ditto

ABSTRACT

This research aims to improve the stability of PC cable-stayed bridges during the construction by the cantilever erection method. Effectiveness of the seismic response control system using Active Mass Damper (AMD) is analytically and experimentally studied. It is found that by operating AMD which is attached at the end of girder in vertical direction, the section force developed at the tower bottom was reduced by 20-40%.

INTRODUCTION

The cantilever erection method is often used for the construction of long-span prestressed concrete (PC) cable-stayed bridges. The method is suitable for the construction of long-span cable-stayed bridges because the structural characteristics of the bridge is effectively used by the method and it is not restricted by the condition under the girder. The bridge under construction, however, is a relatively unstable structure supported only by a single tower. There are some cases, therefore, where special attention is required to safeguard against the dynamic external forces such as earthquake and wind loads.

When designing a bridge under-construction, half of the value of the design seismic forces is usually adopted as the design earthquake force. In that case, section forces developed at the pier bottom are roughly equal to those of the completed bridge. Consequently, if the earthquake response of the completed bridge has been reduced by the use of the damper[1], the earthquake design force may become critical for the design of the members. Because movable sections are temporarily fixed during the construction, seismic response control or seismic isolation systems that will be adopted after the completion of the construction are usually difficult to apply for the bridge during the construction. On the other hand, it is possible that an efficient seismic response control system can be applied for

the bridge under construction because of a relatively small number of restrictions for the control system, such as compactness, durability and maintenanceablity, etc. There is a need, therefore, to develop special seismic control systems suitable for use during construction.

In this study, a bridge subjected to earthquake ground motion in the longitudinal direction was chosen. The seismic response characteristics during cantilever construction were investigated, which is necessary for such purposes as the determination of the location of the control system. For the purpose of response control, an active mass damper (AMD) system was employed[2], and the effectiveness of AMD was studied through simulation analysis. The results thus obtained were verified through the shake table tests using a scaled bridge model.

BRIDGE MODEL STUDIED AND EARTHQUAKE GROUND MOTION

Bridge Model Studied

In this study, 3–span continuous PC cable–stayed bridge with a central span length of 400 m is adopted. A floating type girder support system and fan shape cable arrangement is assumed. Fig. 1 shows a general view of the idealized bridge.

The cantilever erection method is illustrated in Fig. 2. It was assumed that the girder–pier connection would be fixed during the erection. As the weights of erection equipment, 1.37 MN of a traveller at each end of the girder and 0.78 MN of a crane at the top of the

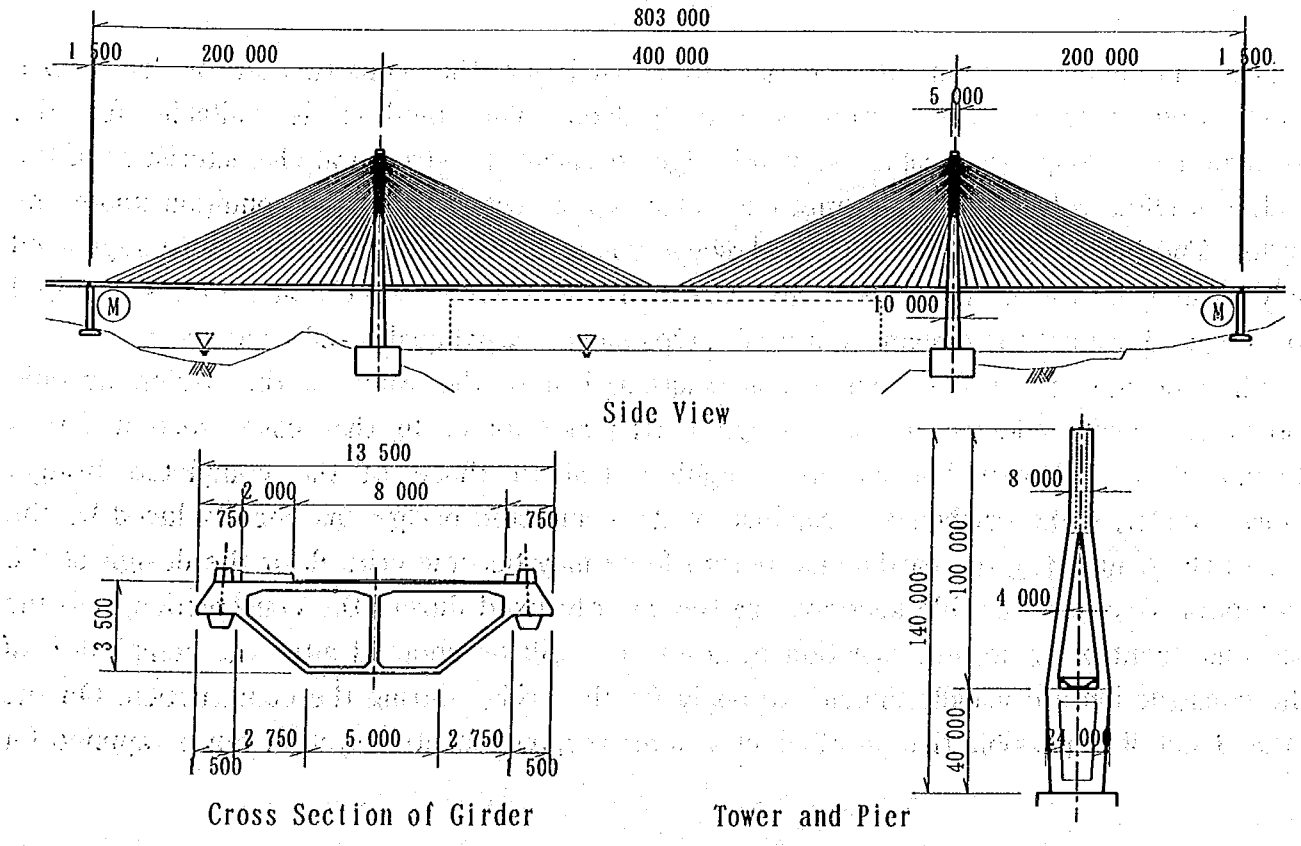


Fig. 1 General View of PC Cable–Stayed Bridge Studied

tower were taken into consideration. The total weight becomes 359 MN when the girder is fully extended. In the dynamic analysis, the damping ratio of 1.0% was assumed for the bridge model[3].

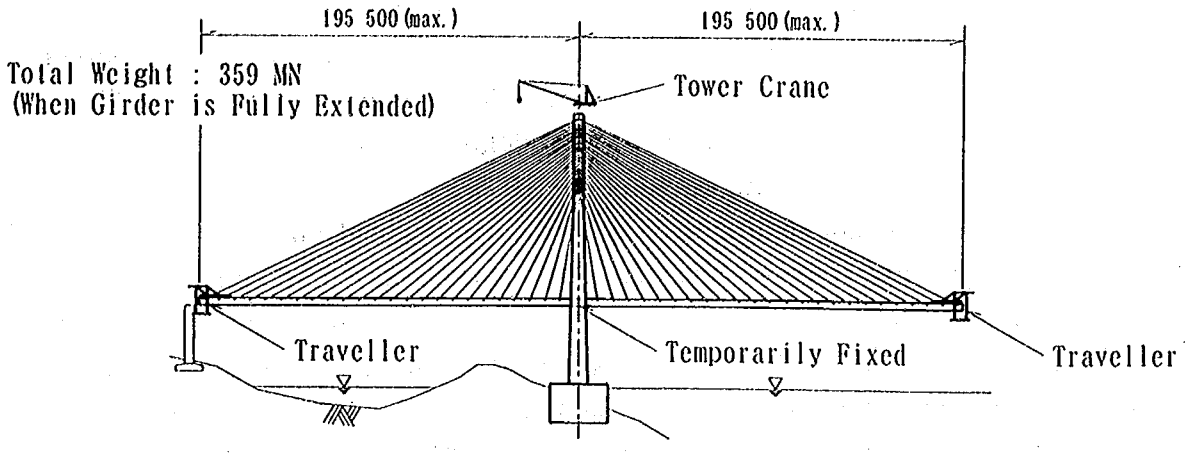
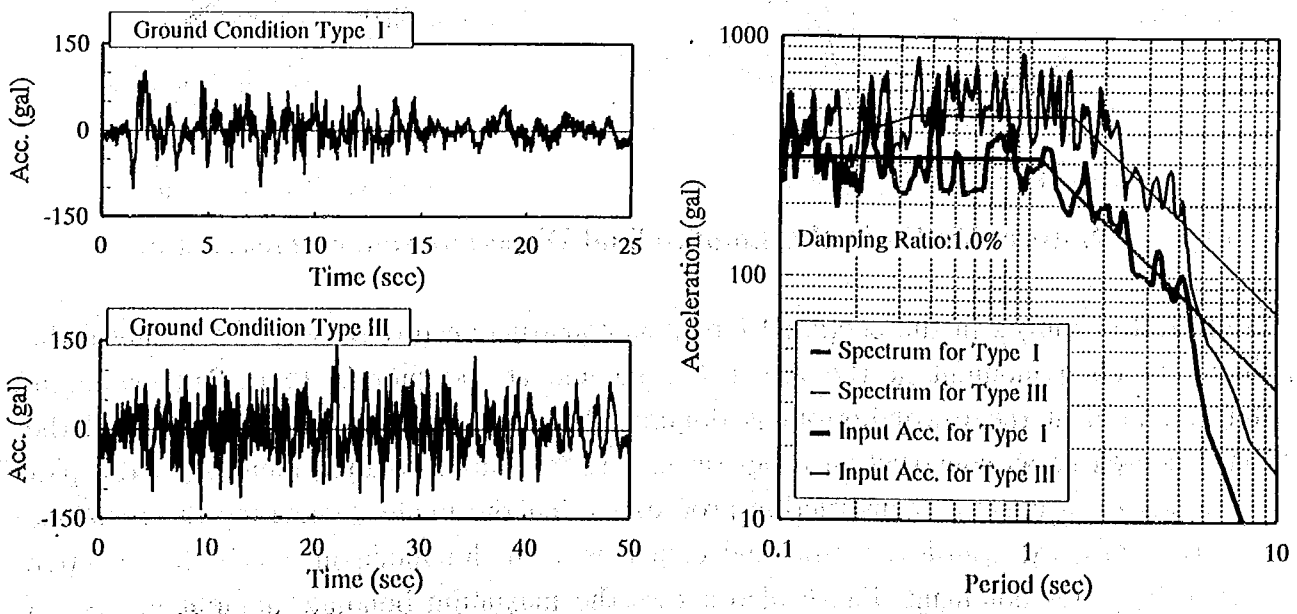


Fig. 2 Construction by Cantilever Erection Method

Earthquake Ground Motion

The acceleration response spectra and standard input accelerations specified in the Design Specifications for Highway Bridges in Japan were adopted for the analyses and the experiments[4]. For the evaluation of seismic response characteristics and the applicability of AMD during construction, 1/2 times the amplitude of the response spectrum and that of the standard input acceleration for the ground condition Type I were used as an input acceleration. In the standard input acceleration for the ground condition Type I and III were also used for the shake table tests. Fig. 3 shows the earthquake ground motion used for the analyses and the experiments.



(a) Standard Input Accelerations (b) Response Spectra

Fig. 3 Earthquake Ground Motion Used for the Analyses and the Experiments

SEISMIC RESPONSE CHARACTERISTICS OF BRIDGE UNDER CONSTRUCTION

To investigate the natural vibration and seismic response characteristics of the bridge under construction, the dynamic analyses using the response spectrum method were conducted. The extended length of girder was changed as a parameter. The ratio of extended girder length to full extension was defined here as a cantilever ratio. the cantilever ratios was assumed in the range of 25–100%.

Fig. 4 shows the dominant natural modes in the longitudinal direction for the cantilever ratios of 50 and 100%. Fig. 5 shows changes in the natural period and effective mass ratio of each mode with the cantilever ratio. The natural period became longer as the cantilever ratio increased, but the rate of the increase was lower in higher modes. At cantilever ratios of around 25%, the effective mass ratio was dominated in the 1st and 3rd modes; at around 50%, in the 2nd mode; and at 75% and above, in the 3rd mode. Thus, the dominant modes shifted with the construction progress.

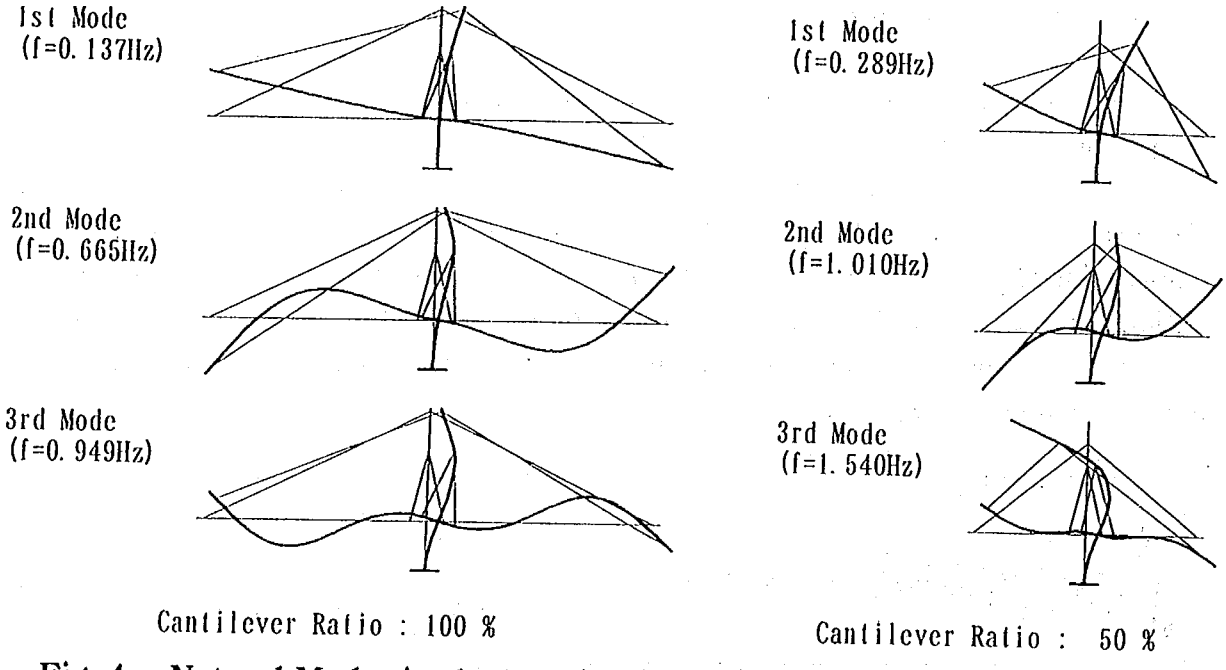
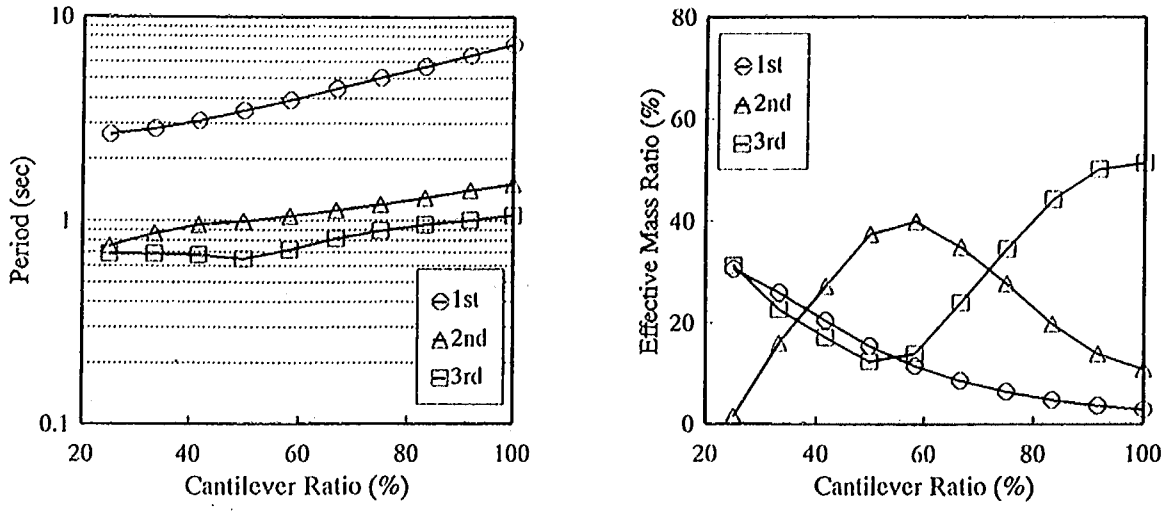


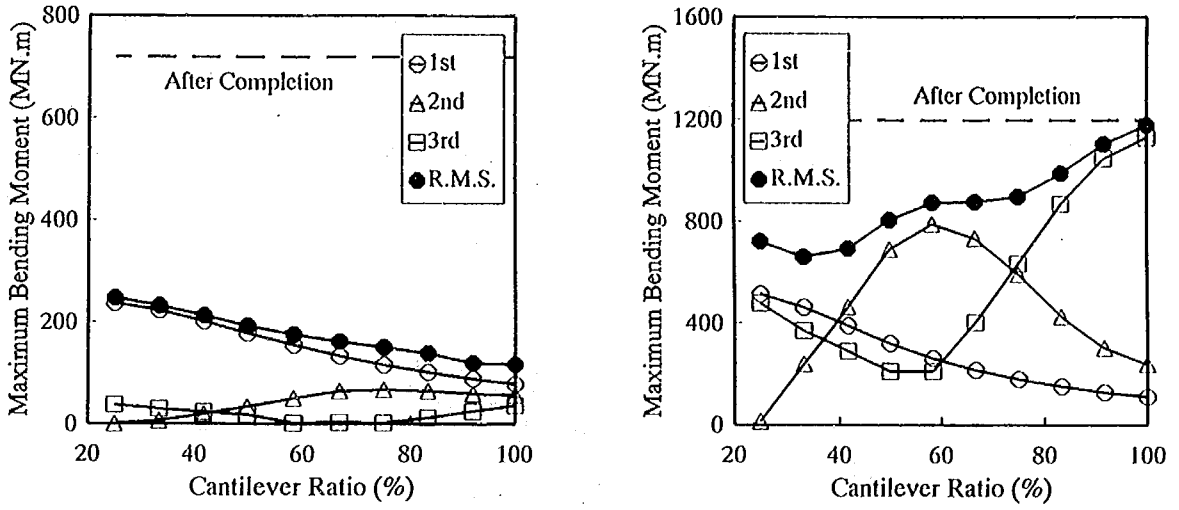
Fig. 4 Natural Modes in the Longitudinal Direction under Construction

To illustrate changes in the sectional forces as construction progresses, Fig. 6 shows the maximum bending moment at the tower bottom and at the pier bottom. The maximum bending moment at the tower bottom is dominated by response of the 1st mode, and the response decreases as construction progresses. The maximum bending moment at the pier bottom tends to increase as construction progresses, but the mode dominating the response value varies with the cantilever ratio and coincides with the mode in which the effective mass ratio becomes dominant. Fig. 6 also shows the maximum bending moment in case of the completed bridge. The maximum bending moment at the pier bottom at the cantilever ratio of 100% is roughly equal to that for the completed bridge.



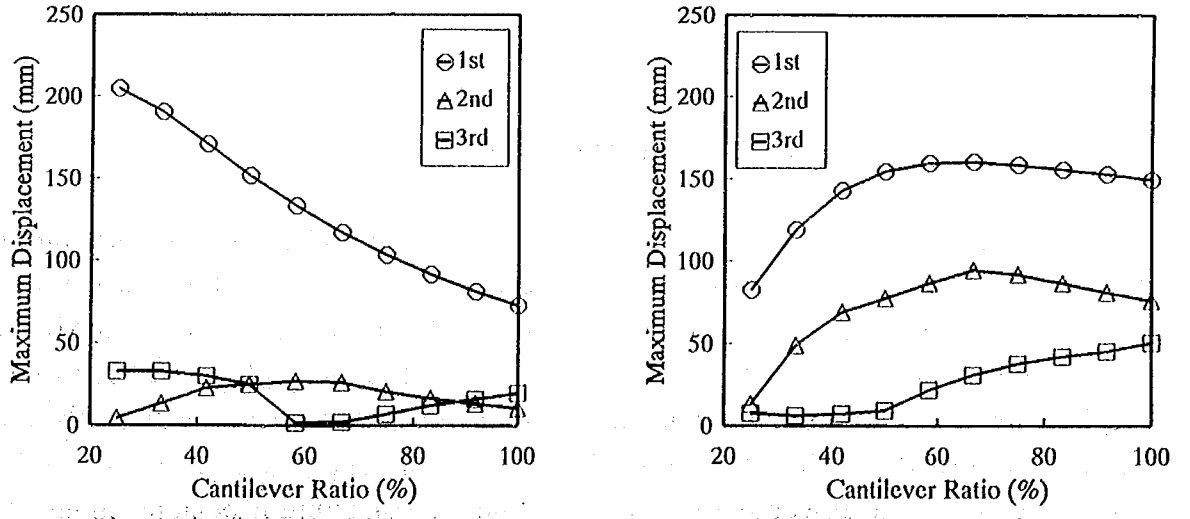
(a) Natural Period (b) Effective Mass Ratio

Fig. 5 Natural Vibration Characteristics under Construction



(a) Section Force at Tower Bottom (b) Section Force at Pier Bottom

Fig. 6 Section Forces under Construction



(a) Longitudinal Disp. at Tower Top (b) Vertical Disp. at Girder End

Fig. 7 Response Displacements under Construction

To illustrate changes in response displacement as construction progresses, Fig. 7 shows the maximum value of longitudinal displacement at the tower top and vertical displacement at the end of the girder in each modes. At cantilever ratio of 50% and less, the longitudinal displacement at the tower top tends to be larger than the vertical displacement at the girder end. At cantilever ratio of more than 50%, however, the vertical displacement at the girder end becomes greater. This indicates that installing a response control system at the girder end to work for the vertical direction is more effective than installing it at the tower top for the longitudinal direction.

STUDY ON EFFECTIVENESS OF AMD

The Active Mass Damper system (AMD) was selected as a mean of seismic response control during bridge construction[5]. In the study, attention was given to the fully extended state of girder. As shown in Fig. 8, the case where the AMD operates in the longitudinal direction at the tower top and the case where it operates in the vertical direction at the girder end were considered. The AMD was controlled by the direct velocity feedback (DVFB) method, in which control forces were calculated from velocity response at the location of the AMD. The control gain was adjusted so that the maximum control force became around 3.5 MN (about 1% of the total weight of the bridge). Control was provided for the 3rd modes which vibration dominating sectional forces at the pier bottom, and all modes.

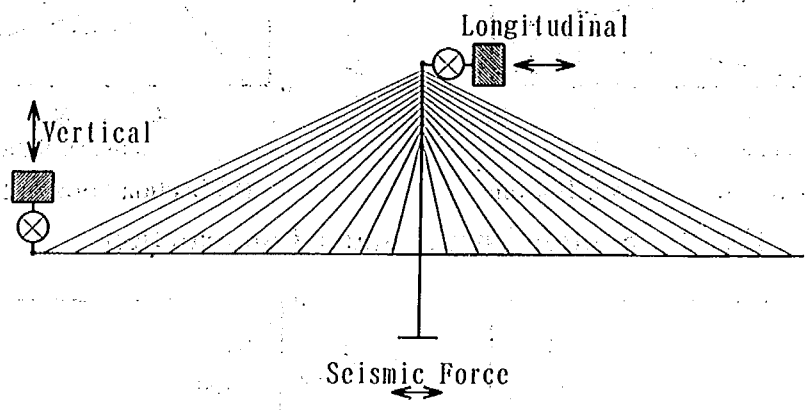


Fig. 8 Location of AMD

Figs. 9 and 10 show bending moments at the tower bottom and at the pier bottom and control forces by the AMD in the case where an AMD was installed at the tower top and the case where an AMD was installed at the girder end. In the case where the AMD was installed at the tower top, the maximum bending moment at the pier bottom was reduced by about 15%, but the maximum bending moment at the tower bottom was reduced only about 5%. In the case where the AMD was installed at the girder end, the response control for the bending moment at the tower bottom was low, but the maximum bending moment at the pier bottom was reduced by 35%. This indicates that installing the AMD at the girder end is more effective in controlling seismic response than installing it at the tower top.

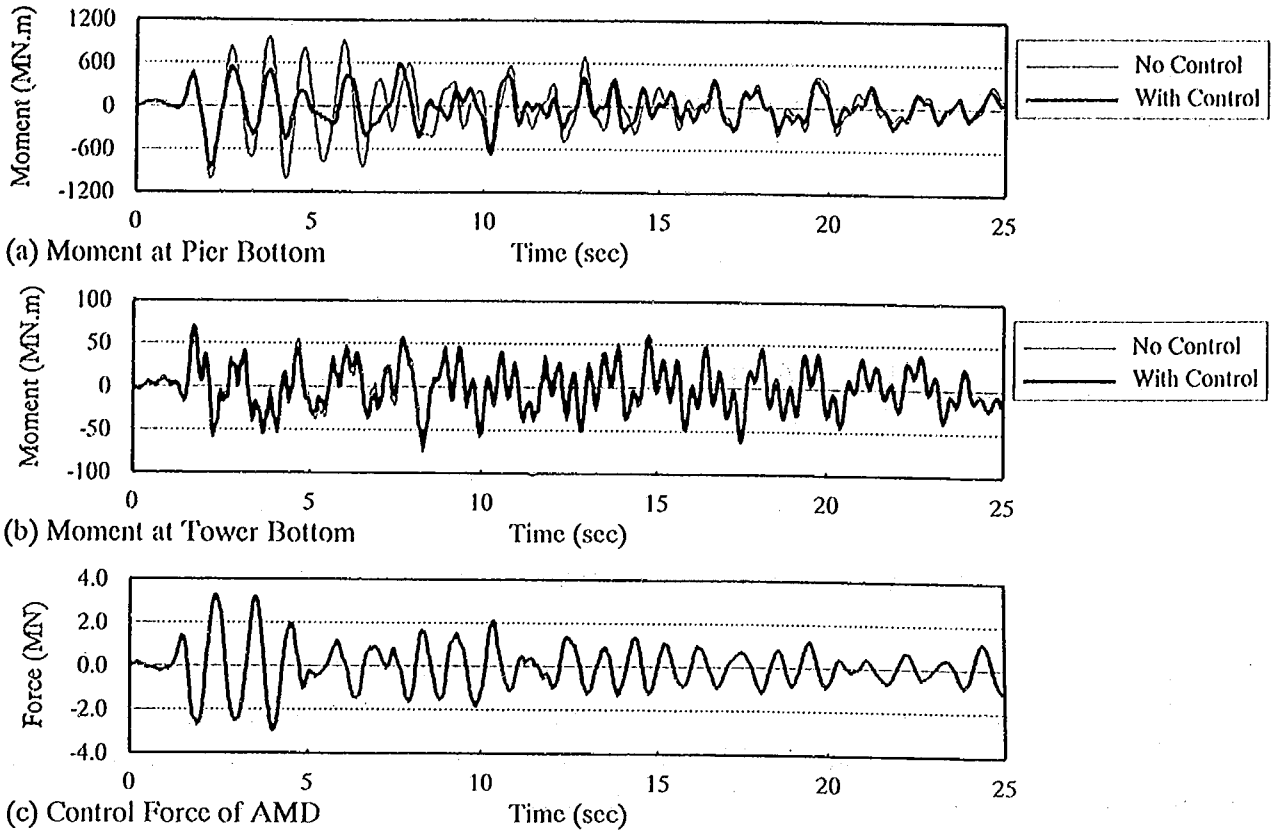


Fig. 9 AMD at Tower Top (Control for 3rd Mode)

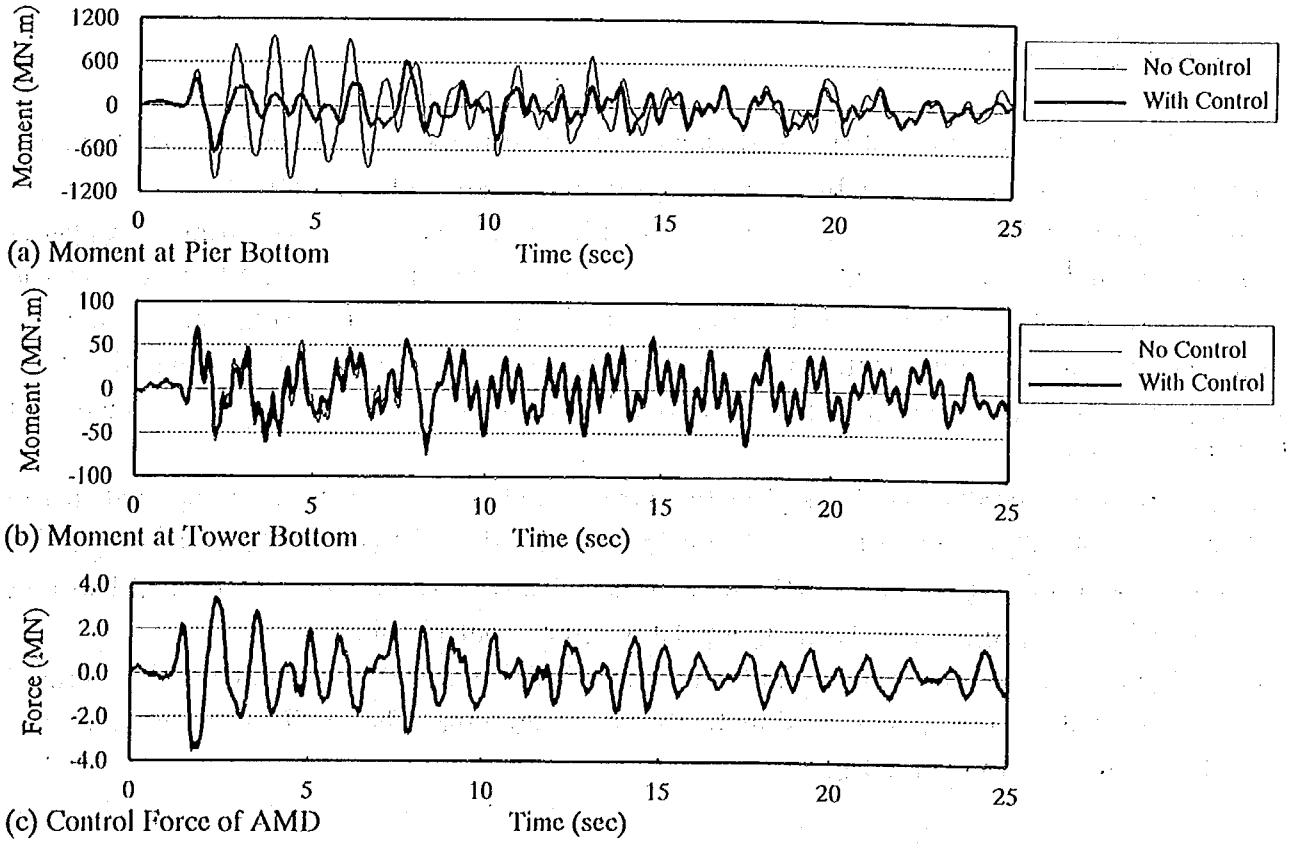
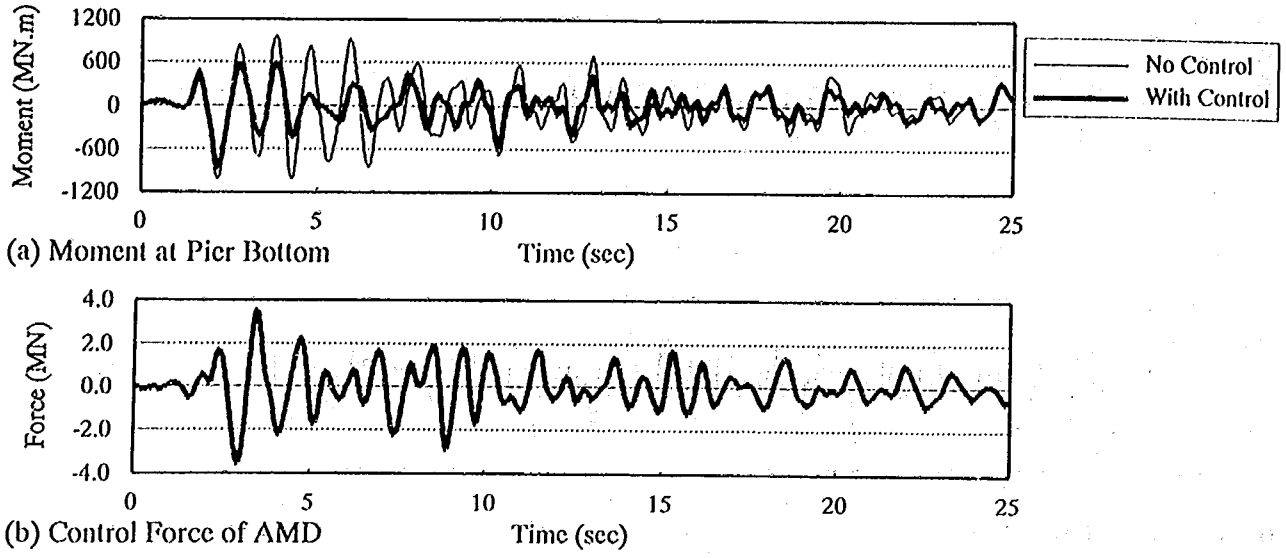


Fig.10 AMD at Girder End (Control for 3rd Mode)



(a) Moment at Pier Bottom

(b) Control Force of AMD

Fig.11 AMD at Girder End (Control for All Mode)

Fig. 11 shows the result of the analysis of the case where all modes were controlled with the AMD installed at the girder end. The results indicate that when all modes are controlled, most of energy is consumed by lower–modes. The response control in reducing the bending moment at the pier bottom is less effective.

MODEL RESPONSE CONTROL TESTS USING AMD

Outline of the Tests

To verify the performance of the AMD for the seismic response control of a bridge under construction, a series of shake table tests was conducted using a bridge model.

The bridge model was designed to model the fully extended state of the bridge. A spatial scale of 1:56 and a temporal scale of 1:10 were assumed. The length of the bridge model is 7.2 m and the total weight is 34.3 kN. Fig. 12 and Photo. 1 show the bridge model and the setup for the shake table tests. The number of cables was reduced so that the near similarity to the natural vibration characteristics be maintained. Fig. 13 shows the modes of the bridge model.

The AMD was installed at the end of the girder, and control forces were applied in the vertical direction. The control forces were calculated by the DVFB method by the response velocities measured, where the AMD was installed. Table 1 shows the test cases. The test parameters were the input acceleration, input level, and control gain.

Fig. 14 shows the AMD used in the tests. The AMD has a 490 N mass which is operated in the vertical direction and a maximum stroke of 80 mm. The AMD can generate the control force up to 150 N at 1 Hz.

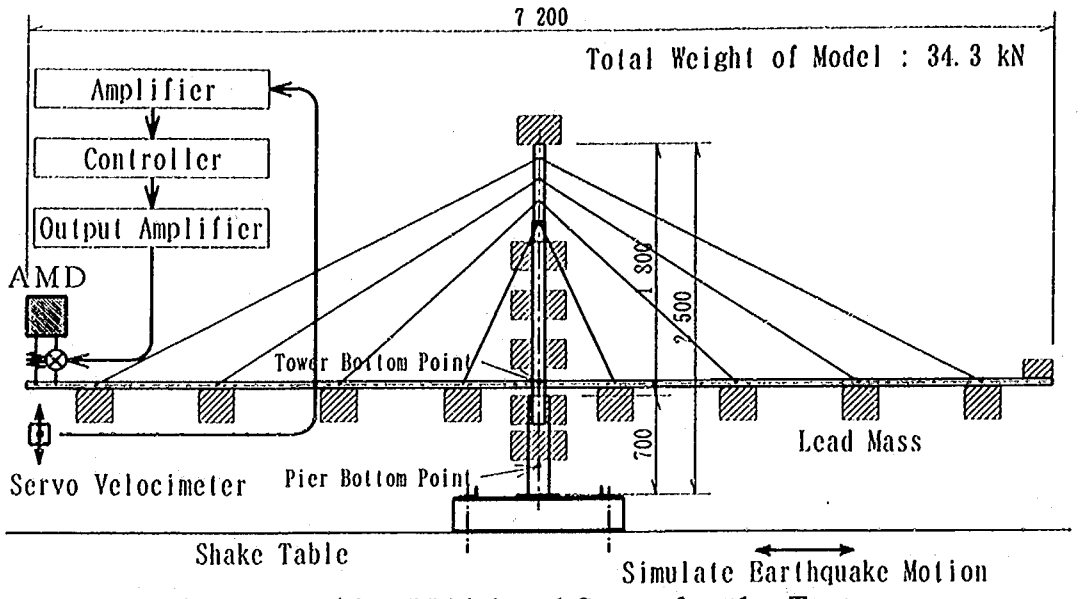


Fig.12 Bridge Model and Setup for the Tests

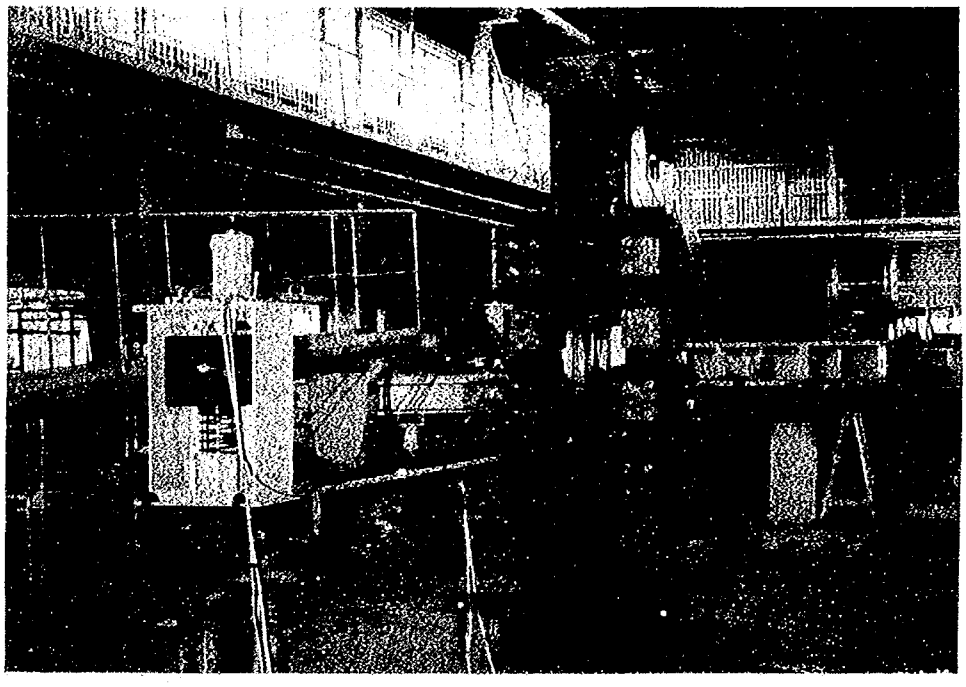
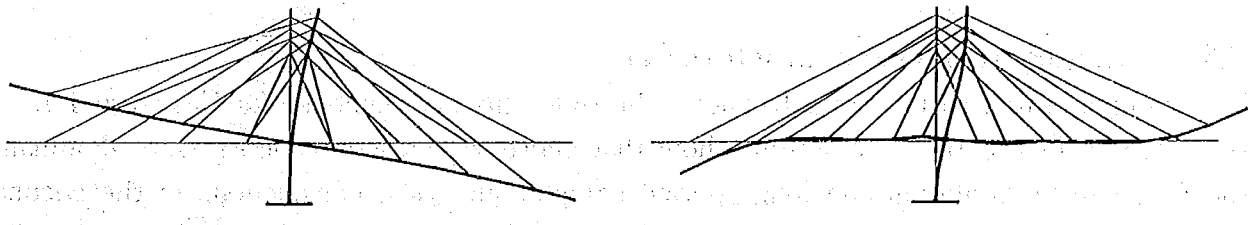


Photo. 1 Model Response Control Tests



1st Mode (Analysis : 1.03 Hz)
(Experiment : 1.00 Hz)

2nd Mode (Analysis : 5.54 Hz)
(Experiment : 5.58 Hz)

Fig.13 Natural Modes of the Bridge Model

Table 1 Test Cases

Input Acceleration	Max. Acc. (gal)	Case	Control Gain			
			No	100	200	500
Ground Condition Type I 1/2 Time Scale	50	1	○	○	○	○
	100	2	○	○	○	–
	150	3	○	○	○	–
Ground Condition Type III 1/2 Time Scale	50	4	○	○	○	○
	100	5	○	○	○	–
Ground Condition Type I 1/10 Time Scale	200	6	○	–	○	○
Ground Condition Type III 1/10 Time Scale	150	7	○	–	○	○
Damping Ratio of 1st Mode (%)			1.1	2.5	3.7	4.6

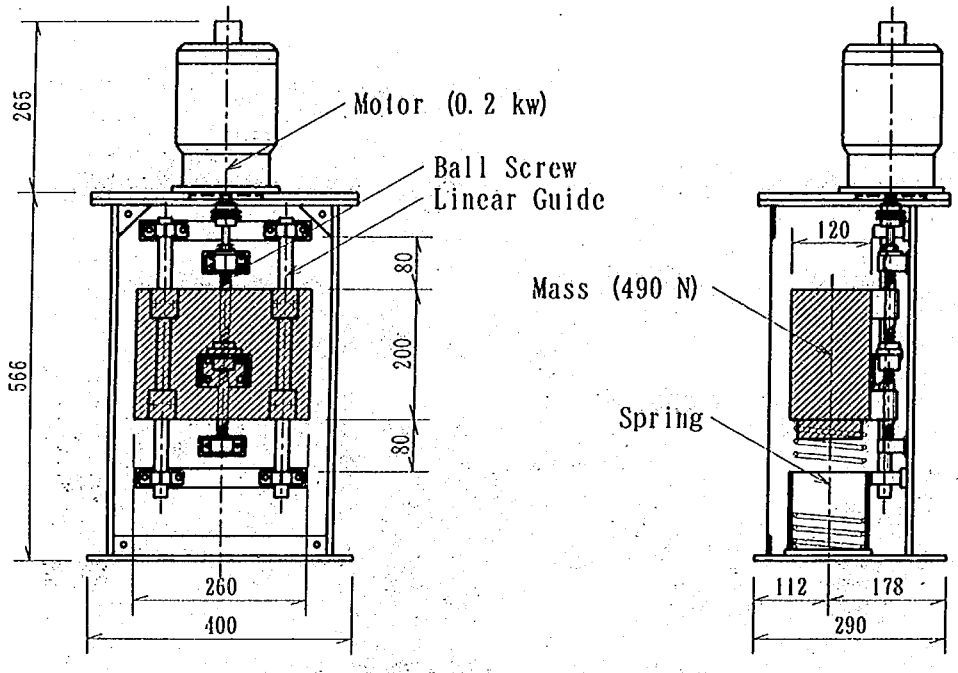


Fig.14 AMD Used in the Test

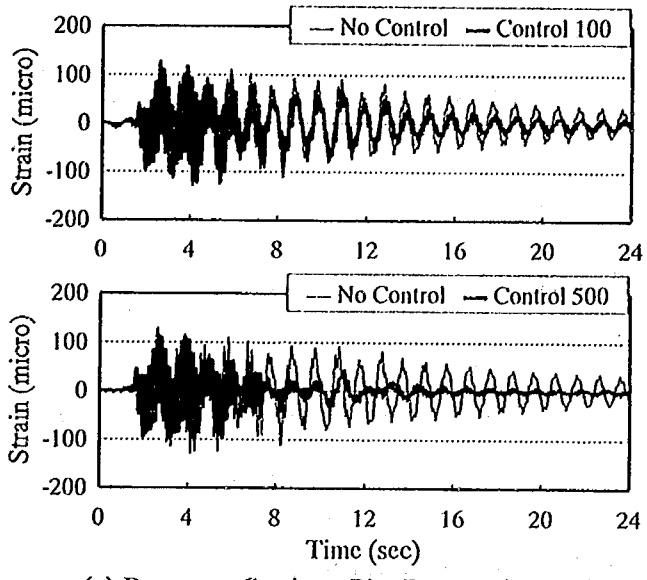
Test Results

(1) Time–history response characteristics

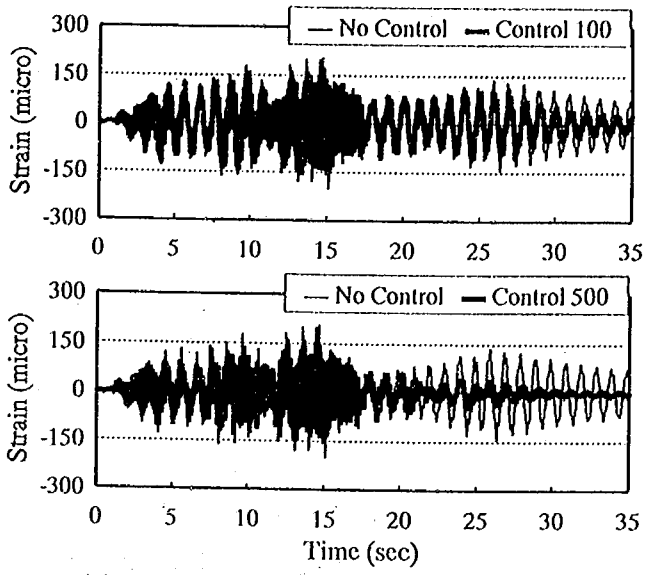
As examples of test results, Fig. 15 shows the time–history response for Case 1 and 4.

Response strains at the pier bottom show that short–period components were dominant in the first half of excitation and long–period components were conspicuous in the second half. When seismic response was controlled, little decrease in amplitude was observed while short–period components were dominant. As long–period components became dominant, however, the response was effectively controlled, and the effectiveness was much remarkable when the gain was larger.

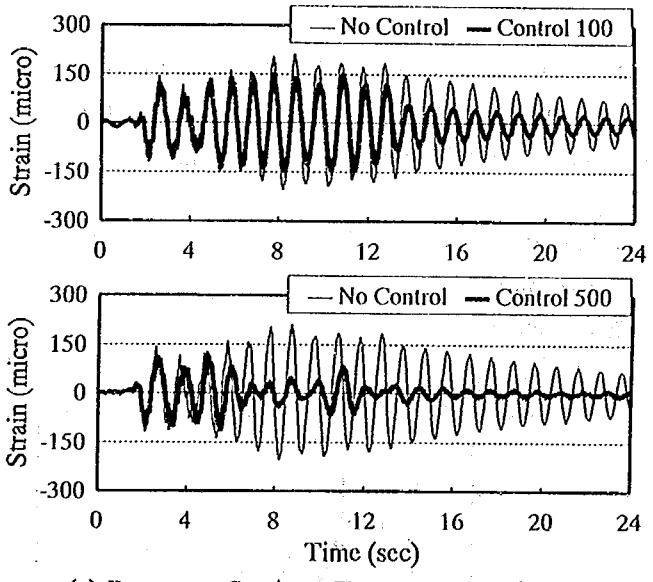
Response strains at the tower bottom were dominated by components within a certain range of periods. When seismic response was controlled, early response did not effectively control. But higher gains tended to result in the reductions.



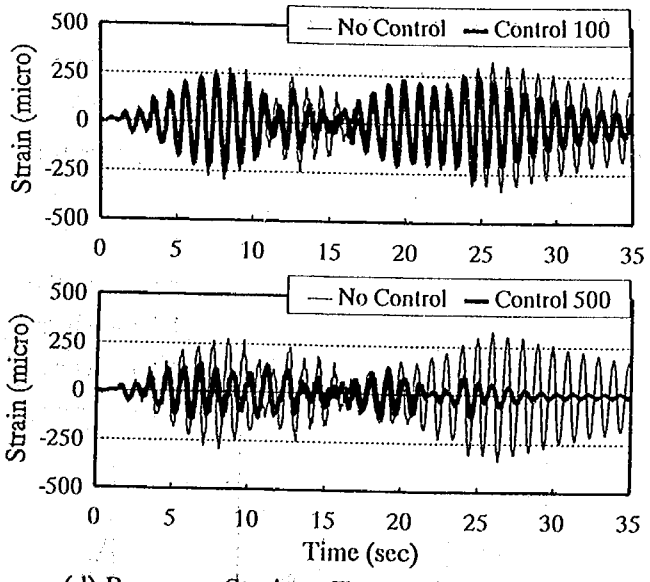
(a) Response Strain at Pier Bottom (Case 1)



(b) Response Strain at Pier Bottom (Case 4)



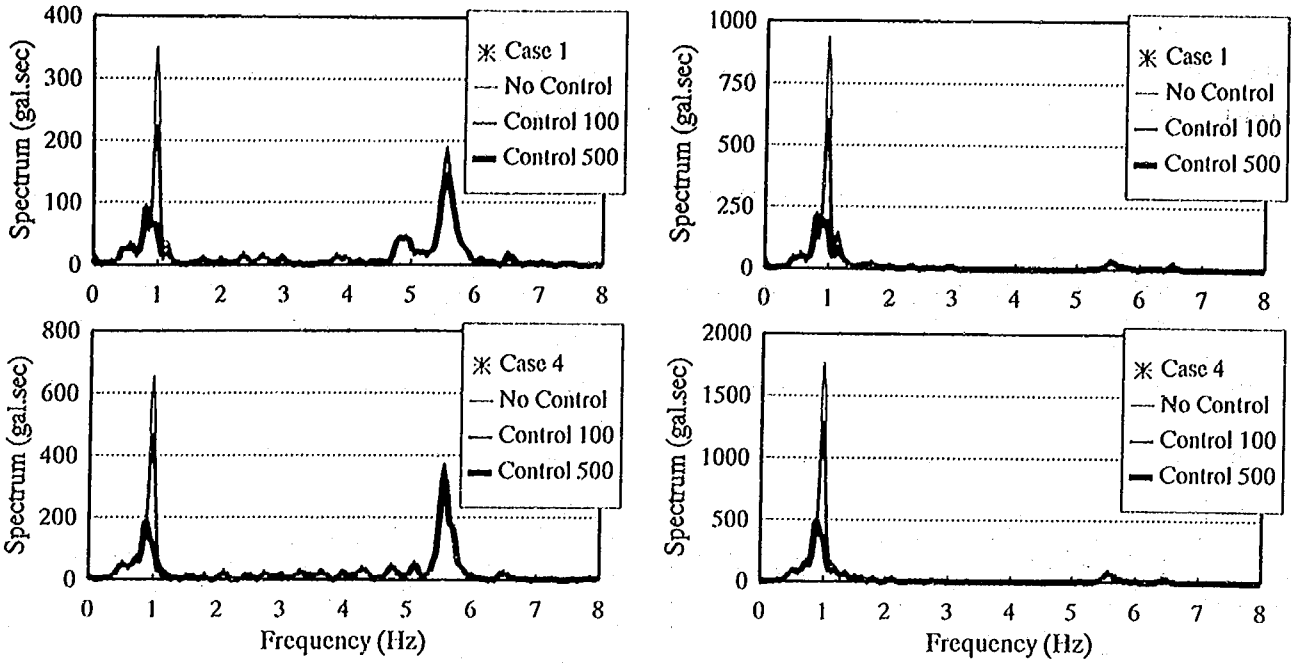
(c) Response Strain at Tower Bottom (Case 1)



(d) Response Strain at Tower Bottom (Case 4)

Fig.15 Time History Responses

Fig. 16 shows Fourier spectra for the response strains at the pier bottom and at the tower bottom. The spectra for the pier bottom show two dominant frequencies. The 1st mode clearly show the effect of response control, while the spectra for 2nd mode are not reduced. This is partly due to the use of the DVFB method for the control. Another reason is thought to be that, as indicated by the rocking phenomenon of the AMD, the AMD could not follow the 2nd mode. Judging from the fact that the spectra for the tower bottom are dominated by only 1st mode, that is why the effect of response control at the tower bottom was greater than at the pier bottom.

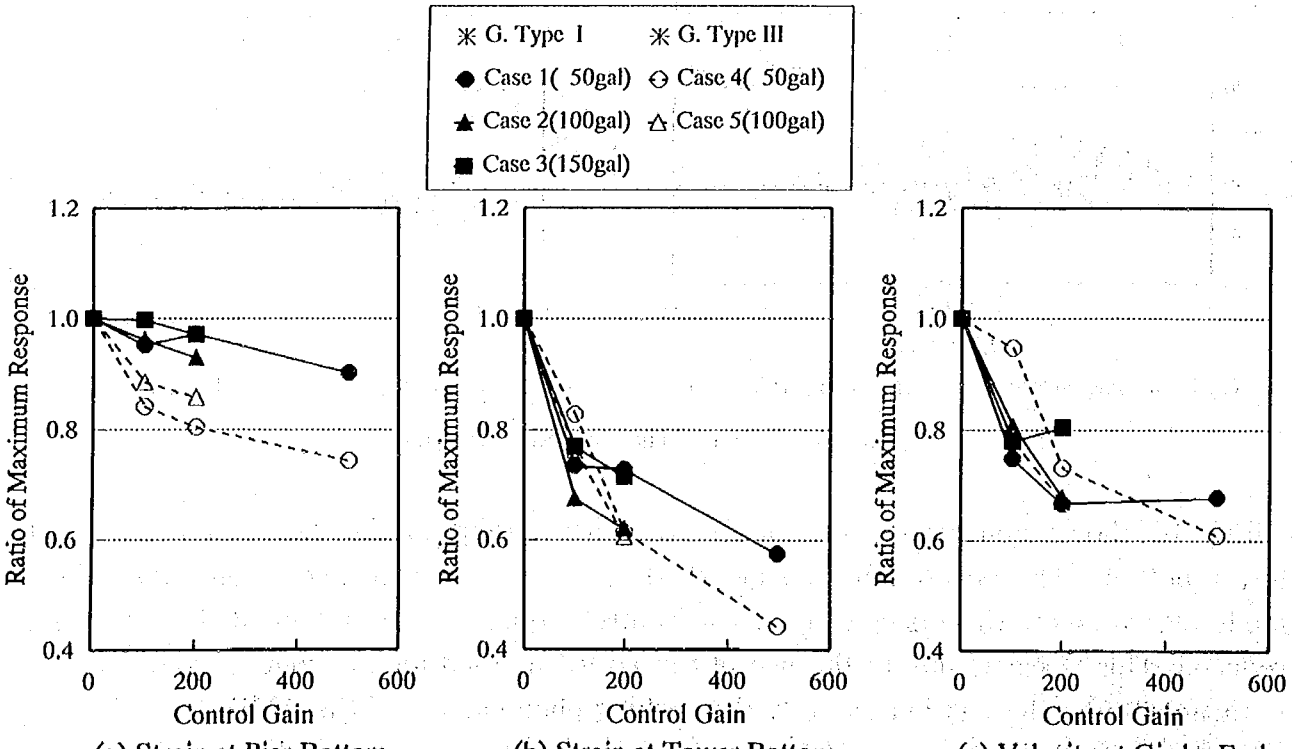


(a) Response Strain at Pier Bottom (b) Response Strain at Tower Bottom

Fig.16 Fourier Spectra of Response Strains

(2) Maximum response

Figs. 17 and 18 show the ratios of the maximum values of controlled response to those of uncontrolled response. Fig. 17 shows the test case where a 1/2 time scale was used for the input acceleration, and Fig. 18 shows the test case where a 1/10 time scale was used.



(a) Strain at Pier Bottom (b) Strain at Tower Bottom (c) Velocity at Girder End

Fig.17 Ratio of Maximum Response (1/2 Time Scale)

In the test case where the 1/2 time scale was used for the input acceleration, decreases in the maximum response strain at the pier bottom were 5–10% for the ground motion of ground condition Type I and 15–25% for the ground motion of ground condition Type III, while decreases in the maximum response strain at the tower bottom were 20–40%. The reason for these differences is that although the response strains at the tower bottom are dominated by the 1st mode to which can be effectively controlled, at the pier bottom are dominated not only by the 1st mode but also the 2nd mode to which the response control system is less effective. The response velocity at the girder end was reduced by 20–40%.

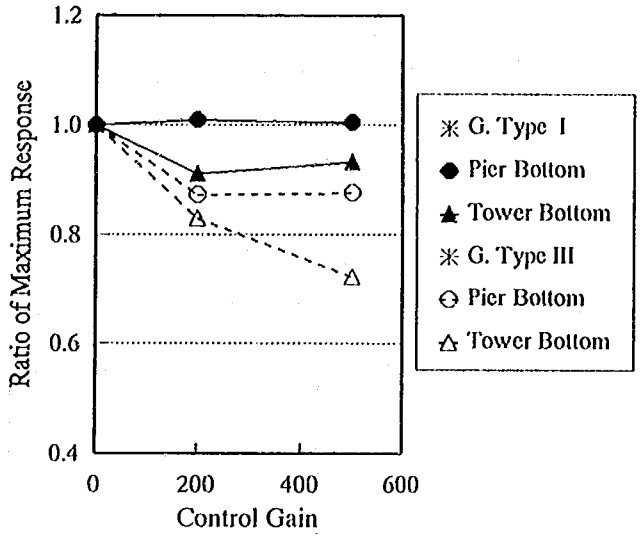


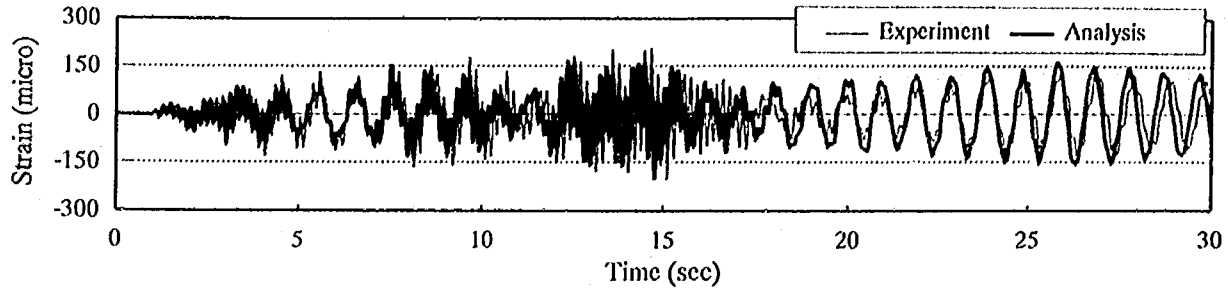
Fig.18 Ratio of Maximum Response (1/10 Time Scale)

In the test case where the 1/10 time scale was used for the input acceleration, the excitation time was only about 2.5 seconds and 5.0 seconds for the ground motion of ground condition Type I and III, respectively. Since the frequency components of input accelerations corresponding to the 1st mode were small, response control was less effective. It is noted, however, that the maximum response at the tower bottom was nevertheless reduced by about 10% for the ground motion of ground condition Type I and about 20% for the ground motion of ground condition Type III.

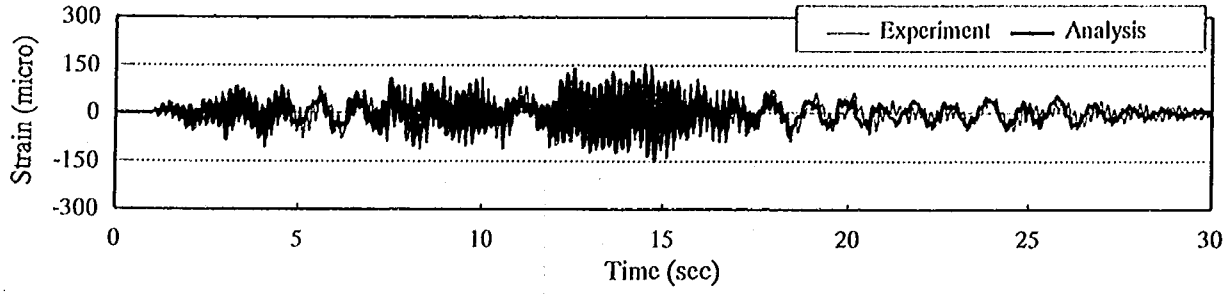
Simulation Analysis

As an example of a simulation analysis of the shake table test, Fig. 19 shows the response strains at the pier bottom in Case 4. In the analysis, a record accelerations obtained on the shake table was used as an input accelerations. The measured damping ratio, a measured value of 1.1% obtained from the bridge model was used. The results of the simulation analysis closely approximate the characteristics of the observed response strains by the analysis method used.

Fig. 20 shows calculated and measured values of the ratio of the maximum response with and without control. Measured and calculated values show good agreement.

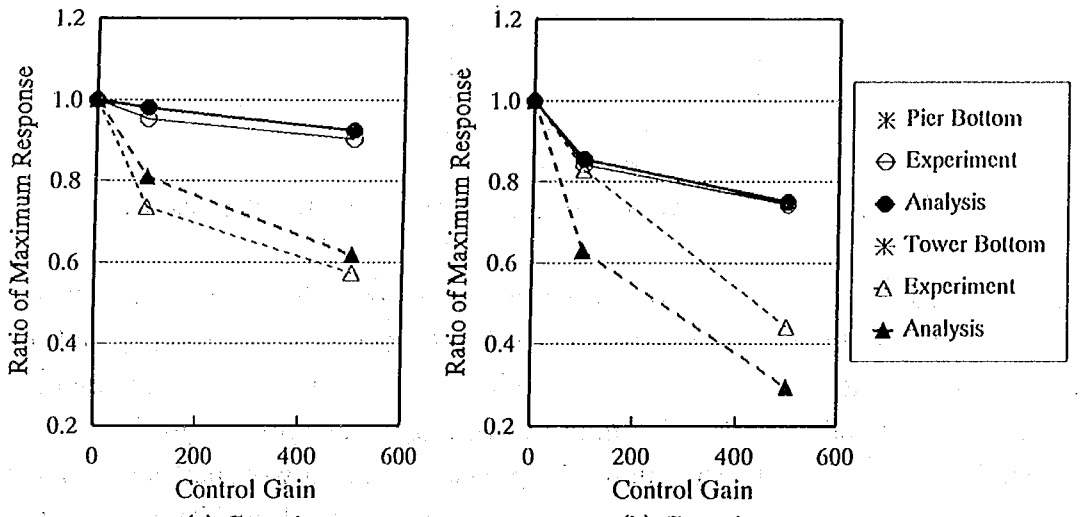


(a) No Control



(b) Control 500

Fig.19 Simulation Analysis (at Pier Bottom, Case 4)



(a) Case 1 (b) Case 4

Fig.20 Calculated Ratio of Maximum Response

CONCLUSIONS

Usefulness of the AMD as a seismic response control system for a PC cable-stayed bridge under construction was evaluated analytically and experimentally. The following conclusions are made:

(a) As the cantilever construction progresses, the dominant natural mode of the effective mass ratio shifts from the 1st to the 3rd mode. Section forces at the pier bottom are due primarily to the mode of which the effective mass ratio is dominant.

(c) Since AMD changes natural vibration characteristics, it makes an effective seismic response control system for use during bridge construction. According to a simulation

analysis, installing an AMD at the girder end of the bridge is more effective in controlling seismic response than installing an AMD at the tower top.

(c) In the shake table tests using a bridge model, the AMD reduced response by 5–25% at the pier bottom and by 20–40% at the tower bottom.

(d) The results of the simulation analysis reproduced the test results with high accuracy.

Thus, applicability of AMD has been studied generally. There are some issues, however, yet to be addressed in order to use practically, including: control theory which makes effective seismic response control possible[6], mechanism and reliability of practical systems to be installed on real bridges, and behavior in response to seismic forces exceeding design forces.

ACKNOWLEDGEMENT

This study was intended to explore one of the themes of a joint research program on "Development of earthquake protective technologies for long–span bridges with high–damping systems" by the Public Works Research Institute, Public Works Research Center, and 19 private–companies. The authors would like to thank Dr. Goto and Mr. Higuchi of Obayashi Corp. and all other participants for support. The authors are also grateful to Dr. Okabayashi of Nagasaki Univ., and Dr. Shimoda and Mr. Mochimaru of Oiles Corp. who provided advice in connection with the AMD.

REFERENCES

[1] Public Works Research Institute et al. : Report of Joint Research Program on Development of Earthquake Protective Technologies for Long–Span Bridge with High–Damping Systems, Part 1, Reports of PWRI, No.101, 1994., Part 2, Reports of PWRI, No.127, 1995., Part 3, Reports of PWRI, No.151, 1996.

[2] Subcommittee on Vibration Control : Vibration Control of structures, Proc. of Colloquium on Control of Structures, Part A, JSCE, 1991.

[3] Kawashima, K., Unjoh, S. and Tsunomoto, M. : Estimation of Damping Ratio of Cable–Stayed Bridges for Seismic Design, Journal of Structural Engineering, ASCE, Vol.119, No.4, pp.1015–1031, 1993.

[4] Japan Road Association : Specifications for Highway Bridges, Part V Seismic Design, 1994.

[5] Tsunomoto, M., Higuchi, S. and Goto, Y. : Seismic Characteristics and Vibration Control of PC Cable–Stayed Bridge under Construction, Proc. of the First Japan–Italy Workshop on Seismic Design of Bridges, pp.439–456, 1995.

[6] Okabayashi, T., Komatsu, M. and Tsunomoto, M. : Active Vibration Control of the Prestressed Concrete Stress Ribbon Bridge Using by H∞ Control Theory, Reports of the Faculty of Engineering Nagasaki University, Vol.24, No.43, pp.249–257, 1994.

THERMO-VISCO-ELASTO-PLASTIC MODELING OF ELASTOMERIC AND LEAD-RUBBER BRIDGE BEARINGS

J. B. Mander, D-K Kim, and S. S. Chen

Department of Civil Engineering
State University of New York at Buffalo

ABSTRACT

Elastomeric and lead-rubber bearings may exhibit significant stiffening due to cold temperature effects as well as some velocity dependency (strain rate effect). Both of these attributes that affect non-linear behavior must be accounted for when accurately modeling bearing behavior, thus a thermo-visco-elasto-plastic model is proposed to account for cold temperature and strain rate effects in both rubber and lead. The results of an experimental investigation where the bearings are tested under lateral cyclic loading with constant axial load are presented. A non-linear system identification least squares procedure is developed to determine material properties of rubber and lead. It is demonstrated that the proposed thermo-visco-elasto-plastic analytical model is able to simulate well the reversed cyclic loading behavior of elastomeric and lead-rubber bearings. An analytical study is conducted on a bridge structure where seismic force and displacement demands are compared at normal temperatures ($+20°C$) with the expected performance at cold temperatures ($-30°C$). For elastomeric bearings, results of the analytical study show that due to improved hysteretic damping effects at cold temperatures, force demands do not increase and displacements slightly reduce. For lead-rubber bearings, cold temperatures stiffen and strengthen the lead so there is about a 30% increase in force demand but a corresponding reduction in displacement demand.

INTRODUCTION

Consideration of the dynamic properties of rubber is important in the design of bridge bearings for use in vibration and seismic isolation. It is essential for the designer to have a knowledge of how these properties vary with temperature and frequency (strain rate).

Although the seismic performance of seismic isolation bearings has been extensively investigated, the in-service performance of such bearings under cold climatic conditions, such as in northern North America, is not well understood. In spite of the increased stiffness of elastomers at low temperatures, designers usually calculate the forces transmitted by the bearings using the stiffness derived from laboratory tests (commonly about $+20°C$). However, it has been recommended that the increase in stiffness due to low temperature crystallization of elastomeric bearings should be allowed for in design (Stanton et al., 1982). Since the horizontal force transmitted by the superstructure to the substructure is a function of the elastomer's shear modulus, the extent of the stiffening must be known (Stanton et al., 1991).

Furthermore, because natural rubber is a visco-elastic material and bearing formulations contain carbon black, its shear moduli are dependent on frequency. Frequency (or strain rate) dependency has a significant influence on the elastic modulus of rubber. Dynamic tests

produce a higher shear modulus and Young's modulus than quasi-static tests, and to account for this some design specifications require that the shear modulus be doubled when computing stress and strain due to dynamic load (Stanton et al., 1982).

In this paper a thermo-visco-elasto-plastic model is proposed to account for cold temperature and strain rate effects. Shear moduli, yield stress, and some material dependent coefficients are the parameters needed to describe the model. If these parameters are identified from the experimental results of bearing systems, the model they describe should simulate the real system. Therefore, experimental laboratory studies were conducted to explore the effects of low temperature and strain rate on both elastomeric and lead-rubber bridge bearings. To obtain the parameters for the proposed analytical model a numerical non-linear optimization scheme was employed.

The thermo-visco-elasto-plastic model has been applied to a bridge problem to investigate the effects of variable thermal effects on the seismic response. Force and displacement demands are compared at normal temperatures ($+20°C$) with the expected performance at cold temperatures ($-30°C$).

A THERMO-VISCO-ELASTO-PLASTIC MATERIAL MODEL

The overall shear force F of the proposed thermo-visco-elasto-plastic model for the lead-rubber bearing takes the following form:

$$F = F_r + F_L = \tau_r A_r + \tau_L A_L \tag{1}$$

in which F_r and F_L are shear forces applied to rubber and confined lead, respectively and A_r and A_L are rubber area and lead area, respectively.

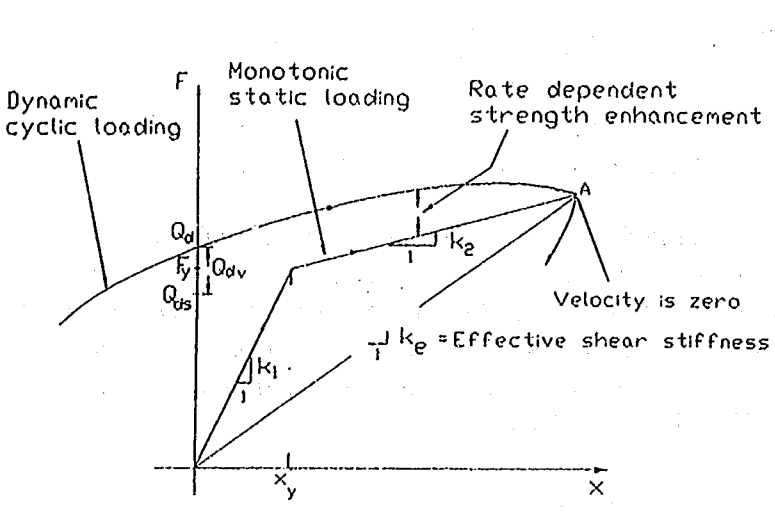
The shear displacement x can be obtained from the following equation when the controlled shear strain γ is in terms of total rubber height h_r:

$$x = \gamma h_r \tag{2}$$

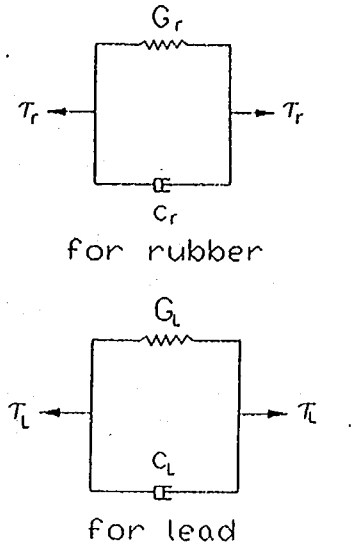
Fig. 1 presents a thermo-visco-elasto-plastic constitutive model of the Kelvin type for modeling both the elastomer (natural rubber has been considered herein, but neoprene is also valid) and the confined lead core. Fig. 1(a) shows a general force-displacement diagram for the monotonic static contribution (independent of velocity) and cyclic dynamic contribution (velocity dependency or strain rate effects) of bearing behavior. In this figure Q_d is dynamic shear force at zero displacement which is composed of a static part Q_{ds} and dynamic part Q_{dv} (strength enhancement due to strain rate effect) as follows:

$$Q_d = Q_{ds} + Q_{dv} \tag{3}$$

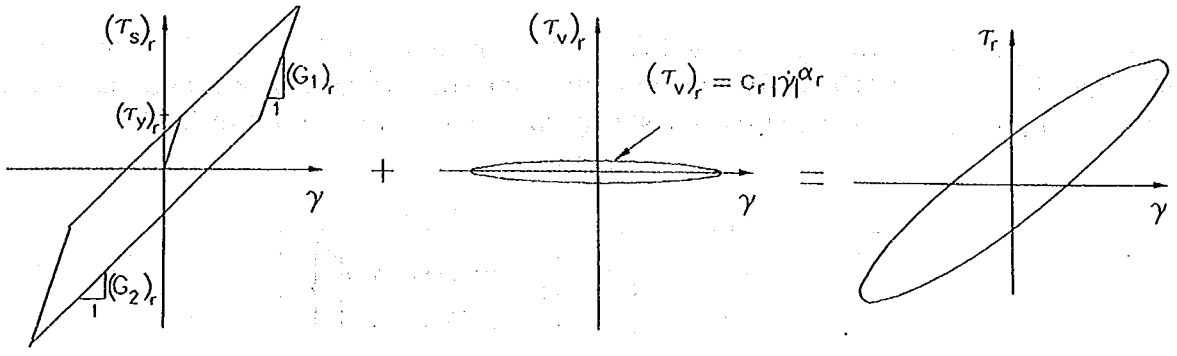
in which



(a) Force-Displacement Diagram



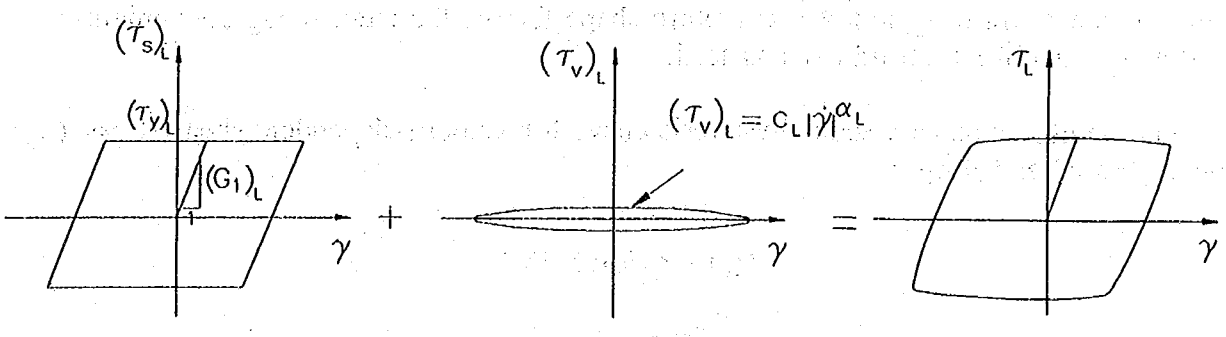
(b) Kelvin Model



(c) Static Part for Rubber

(d) Dynamic Part for Rubber

(e) Overall Behavior for Rubber



(f) Static Part for Lead

(g) Dynamic Part for Lead

(h) Overall Behavior for Lead

Fig. 1 Thermo-Visco-Elasto-Plastic Model for Elastomeric and Lead-Rubber Bearings

$$Q_{ds} = F_y - k_2 x_y = F_y(1-q) \tag{4}$$

in which F_y = yield shear force of bearing, x_y = yield shear displacement of bearing, $q = k_2/k_1$, k_1 = initial stiffness of bearing, and k_2 = post-yield stiffness of the bearing.

The static contribution can be accounted for by a bilinear hysteresis rule and the dynamic contribution can be accounted for by a nonlinear viscosity rule. Fig. 1(b) shows a quasi-visco elasto-plastic Kelvin model in which the parallel static spring and dynamic dashpot exhibit non-linear behavior. The total rubber/elastomer or lead shear stress (τ) in the bearing can be calculated as the sum of the spring shear stress (τ_s) and velocity dependent (viscous) shear stress (τ_v) which are shown in Fig. 1(c) and 1(d), respectively:

$$\tau_r = (\tau_s) + (\tau_v) \tag{5}$$

in which (τ_s) is a function of temperature and shear strain, and (τ_v) is a function of temperature and velocity; note here the subscripts s and v stand for spring and velocity, respectively.

The four-parameter model proposed first by Menegotto and Pinto (1973) and used by Pekcan, Mander and Chen (1995) for modeling visco-elastic spring dampers may be used to define an elasto-plastic hysteresis curve for spring shear stress (τ_s) as follows:

$$\tau_r = \tau_0 + (G_1)(\gamma - \gamma_0)\left[q + \frac{1-q}{\left\{1 + \left|\frac{(G_1)(\gamma-\gamma_0)}{(\tau_y)-\tau_0}\right|^R\right\}^{\frac{1}{R}}}\right] \tag{6}$$

in which γ = bearing shear strain under consideration, γ_0 = bearing shear strain at the beginning of unloading or reloading, (G_1) = initial shear modulus, $q = (G_1)/(G_2)$ where (G_2) = post yield shear modulus, (τ_y) = yield shear stress, τ_0 = bearing shear stress corresponding to shear strain γ_0 and R = curvature shape factor, the latter being conveniently adopted as $R = 2.0$ for both rubber and lead.

The nonlinear quasi-viscous hysteresis curve for velocity-dependent shear stress (τ_v) can be expressed as follows:

$$(\tau_v) = c\, sign(\dot{\gamma})\, |\dot{\gamma}|^{\alpha} \tag{7}$$

in which c = material constant, $\dot{\gamma}$ = strain rate, and α = positive real exponent.

Thus for elastomeric as well as lead-rubber bearings, the proposed stress-strain model for both the rubber and lead materials takes the following form:

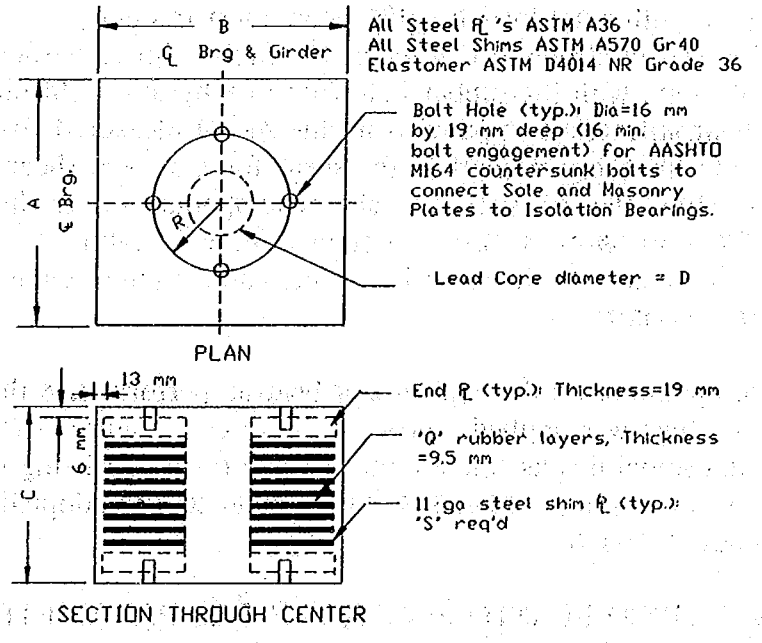
$$\tau = \tau_0 + (G_1)(\gamma - \gamma_0)\left[q + \frac{1-q}{\sqrt{1 + \left|\frac{(G_1)(\gamma - \gamma_0)}{(\tau_y) - \tau_0}\right|^2}}\right] + c\,sign(\dot{\gamma})\,|\dot{\gamma}|^{\alpha} \tag{8}$$

where the parameters (G_1), q, (τ_y), c and α are material specific and must be identified from experiments.

When modeling lead (Fig. 1(b)), it is well known that its behavior is elasto-perfectly-plastic (Skinner et al., 1993), thus for lead it will be assumed that $q = 0$, and that lead may also behave quasi-visco/elasto-plastically in accordance with equation (8).

EXPERIMENTAL INVESTIGATION

The experimental apparatus that was previously developed by the authors for testing steel bridge bearings was used for this investigation of seismic isolation bearing behavior. This test setup was designed to emulate the boundary conditions of a SOG bridge deck and stiff concrete substructure. The rig enabled the testing of bearing systems under combined axial (gravity) load and reversed cyclic longitudinal (thermal/braking/seismic) or transverse (seismic/centrifugal/wind) loadings. The bearings tested as part of the experimental investigation were prototypes used for seismically retrofitting the Southbound Rte 400 highway bridge crossing Cazenovia Creek, near East Aurora, New York. The dimensions of elastomeric and lead-rubber base isolation bearings used in this study are presented in Fig. 2. The elastomer was identified as *ASTM D4014 NR Grade 36* and the hardness of elastomer is *ASTM D2240: 55 ± 5 shore A points*.



Dimension \ Type	Elastomeric Bearing	Lead-Rubber Bearing
A	330 mm	279 mm
B	330 mm	279 mm
C	225 mm	175 mm
D	-	63.5 mm
Q	14	10
R	114 mm	76 mm
S	13	9

Fig. 2 Dimensions of the Bridge Bearings Tested in this Study.

The bearings were tested under quasi-dynamic reversed cyclic lateral loads at increasing displacement amplitudes under constant axial load of 356 *kN* and 90 *kN* for laminated and lead-rubber bearings, respectively. This level of axial load was equal to the average tributary superstructure dead load at the pier and abutment seats of the prototype Rte. 400 bridge. The vertical load was applied in "force control" by a hydraulic actuator whereas the horizontal load was applied by "displacement control" of a 1100 *kN* servo control hydraulic actuator. The applied loads were measured by analog load cells connected in series with the actuators. Displacements of the top and bottom bearing were measured with sonic transducers. The overall bearing displacements are the top mounting plate displacements with respect to the base-bolting plate.

Experimental Observations

Low temperatures induce crystallization and thermal stiffening. Both effects cause a significant increase in stiffness of the elastomer. To investigate the effect of temperature on elastomeric seismic isolation bearing performance, the specimen with the steel mounting plate attached was placed in a freezer and the temperature lowered to $-60°C$. It should be noted that full-size bridge bearings have significant mass, and 8 to 12 hours may be required for the low temperature to fully penetrate the bearing (Stanton, 1982). For the present studies, the specimen was kept in the freezer for at least three days to ensure that the low temperature fully penetrated the entire bearing. To keep track of the temperature change, two thermocouples were used; one was attached just beneath the surface of the rubber, the other was inserted well inside the bearing. The cold bearing together with mounting plates was removed from the freezer and quickly installed in the test rig, insulated with polystyrene and immediately tested.

A combination of semi irregular and regular sine wave form consisting of maximum shear strain amplitude 50% was adopted with axial load $P = 356$ *kN* and test frequency $f = 0.1$ *Hz*. As the temperature of the bearing drops to low levels the rubber "glass-hardens" and as a result there is significant stiffening with the rubber behaving in a hysteretic fashion. The shear stiffness is the effective shear stiffness (computed from the secant measured from peak to peak in the hysteresis loop) and the shear strength is the shear force at zero shear displacement. Elastomeric bearings exhibit thermal stiffening at low temperatures. In this study for rubber with a hardness of 50 ± 10 *Shore A Points*, a significant temperature sensitivity was observed — about 200% and 600% increase in stiffness and strength when the temperature was lowered from $+20°C$ to $-48°C$.

To investigate the effect of temperature on the lead-rubber bearing performance the same procedure as for elastomeric bearings was applied. From the cold temperature ($-32°C$) to the room temperature ($+20°C$) a sinusoidal displacement control wave form consisting of two reversed cycles at each rubber strain amplitude 25%, 50%, 75% and 100% was adopted with axial load $P = 90$ *kN* and test frequency $f = 0.1$ *Hz*.

IDENTIFICATION OF THERMO-VISCO-ELASTO-PLASTIC MODEL PARAMETERS

The system identification procedure for the appropriate bearing parameters was carried out on the elastomeric and lead-rubber bearings shown in Fig. 2. To obtain the parameters for

each test, a standard spreadsheet based quasi-Newton non-linear optimization scheme was employed. The optimum parameters are defined as minimum in the sum of square of the errors in forces between the experimental results and the proposed analytical model.

Parameter Identification for Elastomeric Bearings

This identification procedure has been carried out on the elastomeric bearing systems which were tested previously. All tests were initially analyzed blindly and it was found that curvature shape factor R and constant α changed only a little. Thus for all subsequent identification of test results $R = 2.0$ and for rubber $\alpha_r = 0.5$ were adopted.

For rubber, the initial and post yield shear moduli $(G_1)_r$ and $(G_2)_r$, yield shear stress $(\tau_y)_r$, and material constant c_r are temperature dependent and can be expressed in terms of exponential functions:

$$\frac{(G_1)_r}{(G_1)_{r\,20}} = \exp\left[\frac{20-T}{66.4}\right]^5; \quad \frac{(G_1)_r}{(G_1)_{r\,20}} = \exp\left[\frac{20-T}{76.7}\right]^5; \quad \frac{(\tau_y)_r}{(\tau_y)_{r\,20}} = \exp\left[\frac{20-T}{79.2}\right]^5; \quad \frac{c_r}{c_{r\,20}} = \exp\left[\frac{20-T}{52.7}\right]^3 \tag{9}$$

in which T = temperature in degrees Celsius, and at room temperature $(T = 20^\circ C)$ the following values for the parameters were obtained from the system identification analysis:

$$(G_1)_{r\,20} = 1.33\,MPa; \quad (G_2)_{r\,20} = 1.00\,MPa; \quad (\tau_y)_{r\,20} = 0.215\,MPa; \quad c_{r\,20} = 0.04\,MPa$$

The actual experimental responses and the computed model responses based on the identified values using equation (9) are compared in Fig. 3 for an experimental shear strain amplitude of 50%. Good agreement between the model and the experimental observations is evident.

Parameter Identification for Lead-Rubber Bearings

The parameters previously identified for the rubber alone were used as a basis for assessing the contribution of lead in lead-rubber bearings. Therefore, the identification procedure was carried out only on the lead which is confined by rubber. Using $R = 2.0$ as before, identification of test results revealed that constant $\alpha_L = 0.25$ gave the best fit to the experimental results.

The material properties for lead, namely the initial shear modulus $(G_1)_L$, yield shear stress $(\tau_y)_L$, and the material constant c_L are temperature dependent and can also be expressed in terms of exponential functions:

$$\frac{(G_1)_L}{(G_1)_{L\,20}} = \exp\left[\frac{20-T}{161}\right]; \quad \frac{(\tau_y)_L}{(\tau_y)_{L\,20}} = \exp\left[\frac{20-T}{71.3}\right]; \quad \frac{c_L}{C_{L\,20}} = 1 \tag{10}$$

where at room temperature the following parameters were identified:

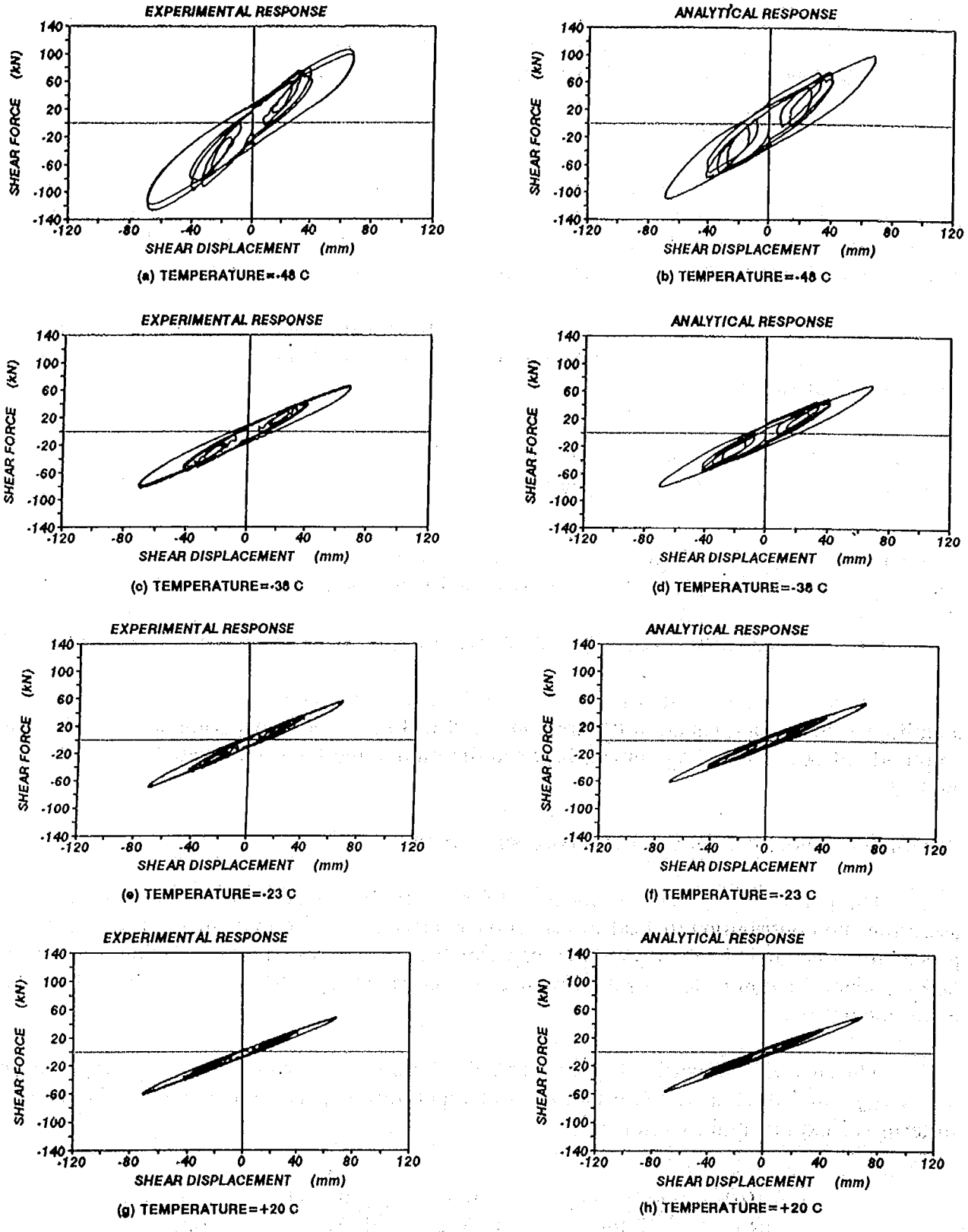


Fig. 3. **Experimental Results of Laminated Rubber Bearings Tested at Different Temperatures Compared with Force-Displacement Predictions Made by the Proposed Thermo-Visco-Elasto-Plastic Model.**

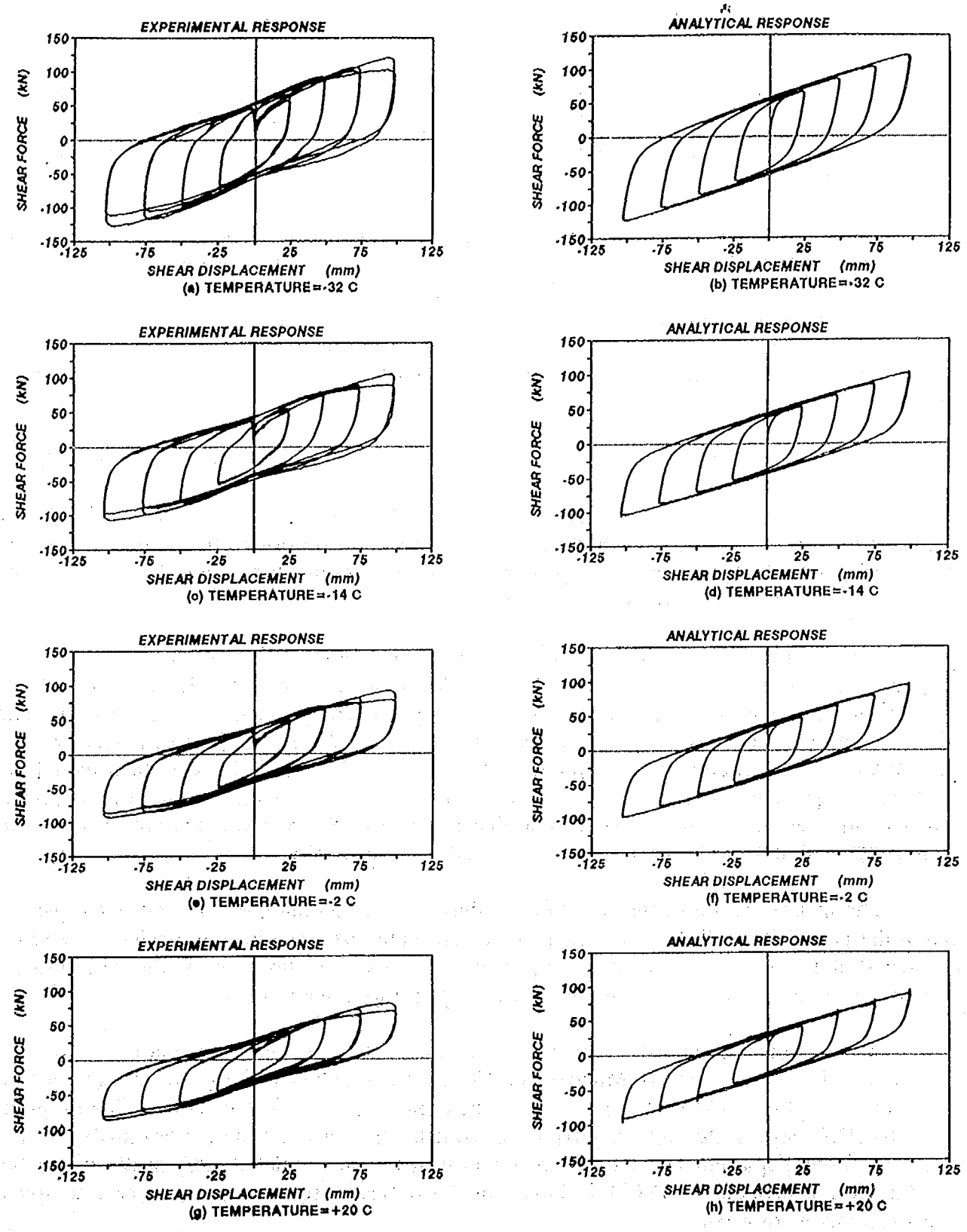


Fig. 4. **Experimental Results of Lead-Rubber Bearings Tested at Different Temperatures Compared with Force-Displacement Predictions Made by the Proposed Thermo-Visco-Elasto-Plastic Model.**

$$(G_1)_{L\,20} = 336\ MPa\ ; \quad (\tau_y)_{L\,20} = 6.16\ MPa\ ; \quad c_{L\,20} = 2.46\,MPa$$

The actual experimental response and the computed model responses based on the identified values (equations (9) and (10)) are compared in Fig. 4 for the sine wave displacement control. Again, good agreement between the analytical model and the experimentally observed results is apparent.

It should also be noted that the analytical model was tested on other types of elastomeric and lead-rubber bearings found in the literature. For example, test results provided by Skinner et al. (1993) were compared with the model predictions and good agreement between theory and experiment was obtained—without adjusting the parameters in the model. It is thus considered that the model is adequately validated and able to be applied in a predictive sense with a degree of confidence in its reliability. Such an application is described in what follows.

ANALYTICAL STUDY OF SEISMIC RESPONSE OF BRIDGES IN COLD CLIMATES

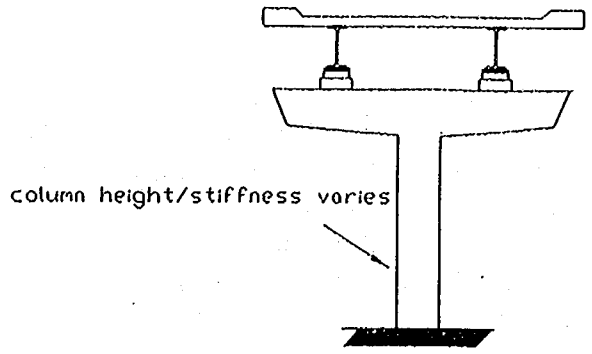
An analytical study was undertaken with the objective of examining the effect of cold temperatures on the seismic force and displacement demands on bridge bearings of either the elastomeric or lead-rubber type when placed in a bridge system, that system having different dynamic properties (natural periods of vibration).

Fig. 5 shows a single span portion of a two-girder bridge with two bearings at each support. This simplified structure was chosen to keep the analysis tractable and is based on a similar configuration of the Rte. 400 bridges recently studied by Wendichansky (1996). The width, length and thickness of concrete deck used are $4.6\,m$, $25.3\,m$ and $0.23\,m$, respectively. Two $W36{\times}150$ steel girders were adopted as shown in Fig. 5a, while the analytical model of the bridge is presented in Fig. 5b. To focus on the non-linear seismic demand of each type of bearing, only bearing elements exhibit non-linear behavior. Seismic weights ($W = 356 \times 4 = 424\,kN$) of $W/4$, $W/2$ and $W/4$ are lumped at joints 1, 2 and 3, respectively.

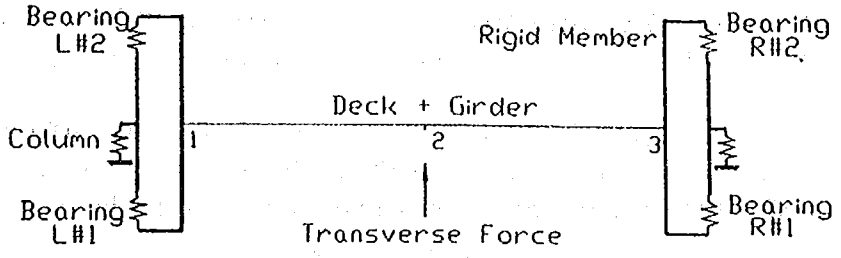
The natural period of the structure is adjusted by changing the stiffness of the piers. When the period is small the structure may be considered as a single span bridge seated on near-rigid abutments, whereas when the period is long the structure may be thought of as a one span (lollipop) portion of a "long" multiple span bridge with tall piers.

As mentioned previously, the response of rubber bearings is somewhat strain rate dependent. Recently, Pekcan, Mander and Chen (1995) included this strain rate effect to the link element in the DRAIN-2DX program. Therefore, this modified version of the program DRAIN-2DX was selected for the purpose of conducting inelastic time history analyses. The observed force-displacement relationships for bearings were simulated analytically using the combination of elements in DRAIN-2DX. An elasto-plastic truss element and two nonlinear link elements were used.

Several assumptions were made to reduce a complicated problem to a relatively simple problem. The analytical model was developed based on the following assumptions:



(a) SIMPLIFIED BRIDGE STRUCTURE



Plan View

(b) COMPUTATIONAL IDEALIZATION

Fig. 5. Configuration of Idealized Bridge for Analytical Study

(i) All inelastic behavior is assumed to be concentrated in the bearing elements.

(ii) Both mass proportional and stiffness proportional damping where the damping is approximately 5% of the critical damping for the first two modes is used.

(iii) All the analyses were performed with variable numerical integration time-steps ranging from 0.01 sec to 0.0001 sec.

(iv) Ground accelerations considered only the transverse horizontal component. (5) For comparative studies the properties of bearings at room temperature ($+20°C$) and cold temperature ($-30°C$) were adopted. Figs 3 and 4 respectively show the analytical model predictions compared with the experimental response for the elastomeric and lead-rubber bearings at temperatures ranging from the standard $+20°C$ down to $-48°C$. Because of the variable amplitudes these results including strain rate effect.

Nonlinear dynamic analysEs of the prototype bridge were performed using four ground acceleration records: El Centro NS ($PGA = 0.35g$); Pacoima Dam S74W ($PGA = 1.08g$); Northridge, Sylmar Hospital Parking Lot N-S ($PGA = 0.6g$); and Kobe, Kobe Station ($PGA = 0.83g$).

Results from Analytical Study

Fig. 6 shows the temperature dependence of maximum forces and displacements over the natural period range of the bridge seated on elastomeric bearings. Due to the flexibility of elastomeric bearing alone the natural period of bridge seated on rigid piers or abutments is T_1 = 1.22 and 1.09 sec at +20°C and at -30°C, respectively. It is observed that the maximum bearing force increments are negligible presumably due to smaller bearing displacement at cold temperature.Moreover, due to the added hysteretic damping that is inherent at cold temperatures the displacement demands are reduced by typically 15%.

Fig. 7 shows the temperature dependence of lead-rubber bearings and its effect on the maximum forces and displacements at each bridge natural period. Note that the natural period of the bridge is lower than the elastomeric bearing case because of the stiffness contribution of the lead. The natural period of bridge seated on rigid piers or abutments is T_1 = 0.391 and 0.341 sec at +20°C and at -30°C, respectively. It is observed that the maximum bearing forces slightly increase whereas the displacements decrease at cold temperatures.

Such an increase in force demand due to the low temperature effects on the lead-rubber bearing should be allowed for in the design of the bridge substructure. In general, the expression for the structural safety requirement may be written in the well-known LRFD form:

$$\phi R_n \geq \Sigma \gamma_i Q_i \qquad (12)$$

where ϕ = strength reduction factor, R_n = nominal resistance, γ_i = overload factors and Q_i = various load effects. In cold regions, when the winter temperature is about -30°C, the design load factor γ = 1.3 may be selected for substructure design under lead-rubber bearings. Design displacements are reduced by a similar amount.

CONCLUSIONS

Based on the present study, the following conclusions can be drawn:

1. At extremely cold temperatures, rubber "glass-hardens" and as a result laminated elastomeric bearings that may be used for seating bridge girders behave in a significantly non-linear fashion. About 200% and 600% increase in stiffness k_e and strength Q_d was observed in tests when the temperature was lowered from +20°C to -48°C.

2. Cold temperatures affect the performance of the lead-rubber seismic isolation bearing. Over the range of temperatures (+20°C to -32°C) elastic stiffness k_1, post-yield stiffness k_2, and strength Q_d varied by some 80%, 40% and 80%, respectively.

3. The hysteresis performance of elastomeric seismic isolation bearings may be characterized by a temperature dependent non-linear Kelvin model—that is a combination of a bi-linear static spring and velocity dependent nonlinear viscous dashpot.

4. The hysteresis loops of lead-rubber bearings may be obtained by adding the effects of confined lead to the model of the elastomeric bearing. The effects of confined lead can be

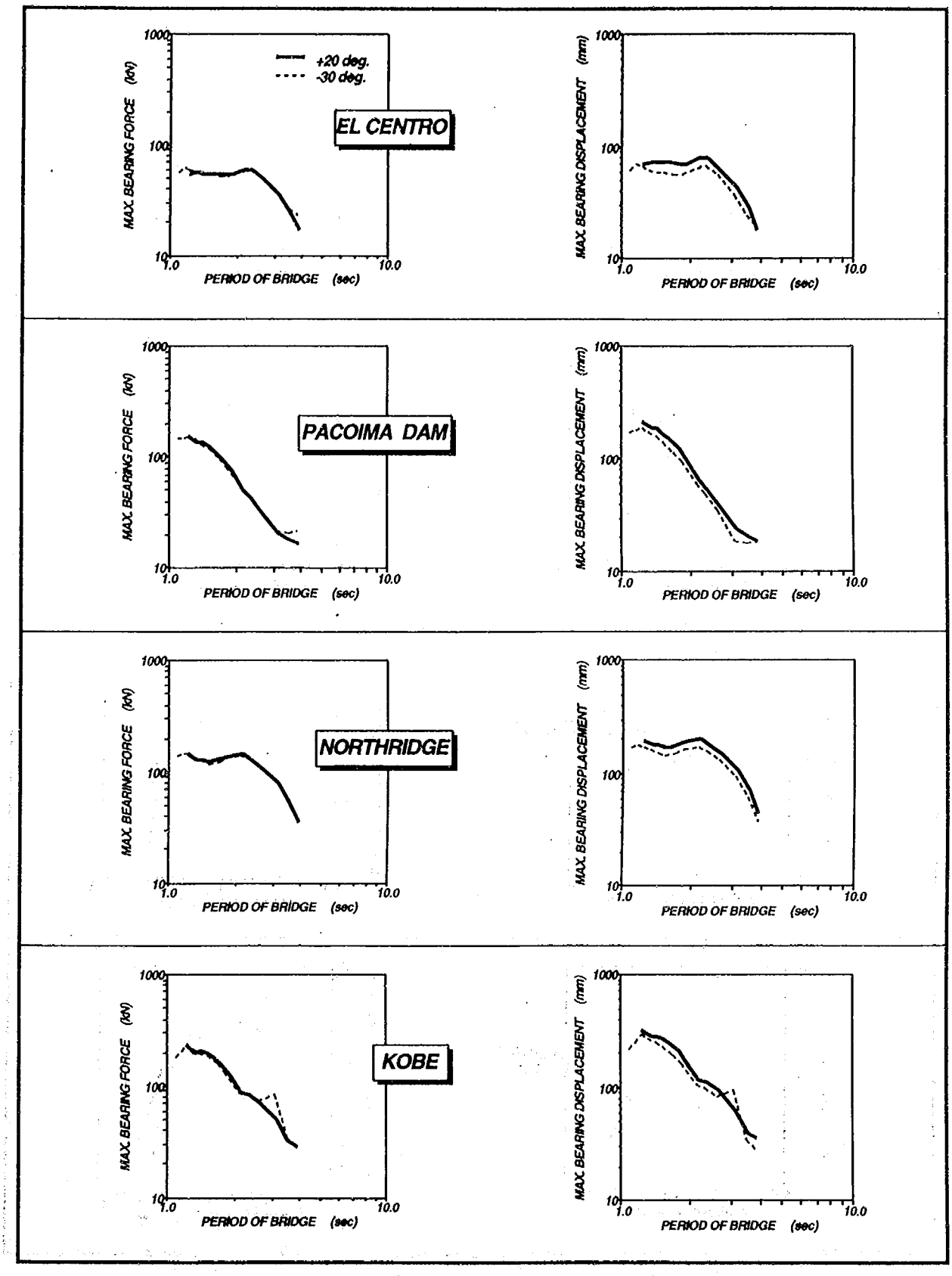


Fig. 6 Force and Displacement Demands on Elastomeric (Laminated Rubber) Bridge Bearings at Normal and Cold Temperatures

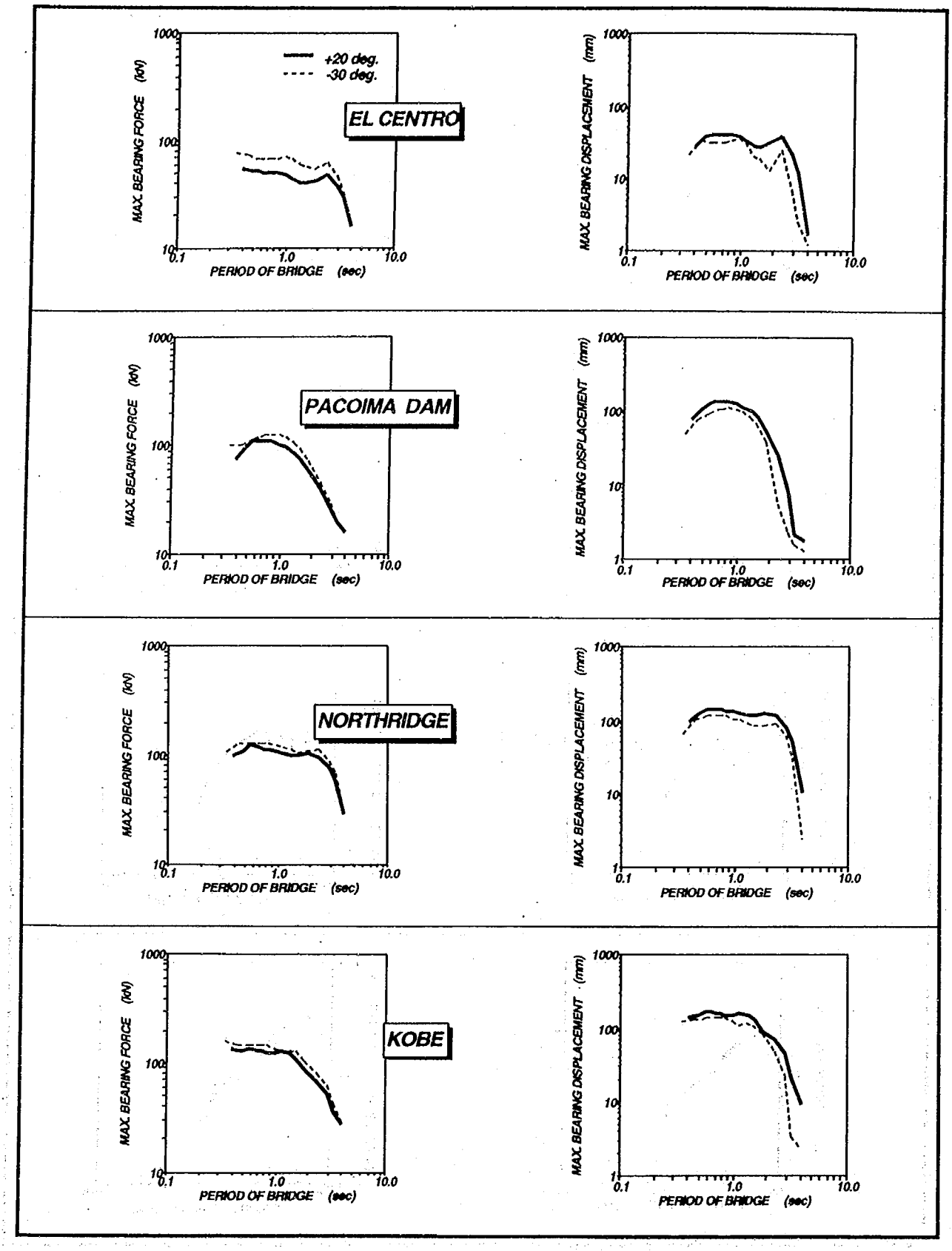


Fig. 7 Force and Displacement Demands on Lead-Rubber Bearings at Normal and Cold Temperatures

expressed by using additional bi-linear spring (perfect elasto-plastic spring) and another strain rate dependent nonlinear viscous dashpot. The presence of the lead core provides considerable energy absorbing capacity.

5. At cold temperatures (-30°C for this study) the *increment* in maximum bearing forces is negligible for bridges with elastomeric bearings. This is due to correspondingly smaller bearing displacement demands resulting from additional hysteretic damping that arises in the elastomer at cold temperatures.

6. For bridges with lead-rubber bearings there is a consistent increase of bearing force demand of some 30% for cold temperature response (-30°C). This force increase must be accounted for in the substructure design.

ACKNOWLEDGEMENTS

Financial support is gratefully acknowledged from the National Center for Earthquake Engineering Research through a contract with the Federal Highway Administration on Seismic Vulnerability of Existing Highway Construction (FHWA Contract DTFH61-92-C-00106). Dynamic Isolation Systems, Inc. provided a pair of lead-rubber and ordinary laminated elastomeric bearings for testing.

REFERENCES

Menegotto, M., and Pinto, P.E. (1973), "Method of Analysis for Cyclically Loaded Reinforced Concrete Plane Frames Including Changes in Geometry and Non-Elastic Behavior of elements Under Combined Normal Forces and Beaning" IABSE Symposium on the Resistance and Ultimate Deformability of Structures Acted on by Well-Defined Repeated Loads, Lisbon.

Pekcan, G., Mander, J.B., and Chen, S.S. (1995), "Experimental Performance and Analytical Study of a Non-Ductile Reinforced Concrete Frame structures Retrofitted with Elastomeric Spring Dampers," Technical Report NCEER-95-0010, National Center for Earthquake Engineering Research, State University of New York at Buffalo.

Skinner, R.I., Robinson, W.H., and McVerry, G.H. (1993), An Introduction to Seismic Isolation, John Wiley & Sons, 354 pp.

Stanton, J.F. and Roeder, C.W. (1982), "Elastomeric Bearings Design, Construction, and Materials," National Cooperative Highway Research Program, Report 248, Transportation Research Board, National Research Council, Washington, D.C.

Stanton, J.F., Purkiss, C. and Roeder C.W. (1991), "Development of Bridge Bearing Provisions for Recommended AASHTO LRFD Bridge Specification," Third World Congress on Joint Sealing and Bearing Systems for Concrete Structures, Volume 2-Bearings and Isolators, Toronto, Ontario, Canada, pp. 736-762.

Wendichansky, D.A., (1996)," Experimental Investigation of the Dynamic Response of Two Bridges Before and After Retrofitting with Elastomeric Bearings," Ph.D. Dissertation, Department of Civil Engineering, State University of New York at Buffalo.

Session 4

Experimental and Field Observations 1

(Co-Chairs: T. Sato, S. Arzoumanidis)

"Analysis of Seismic Response of Yama-age-Bridge"
by S. Unjoh
Presented by: Shigeki Unjoh

"Seismic Isolation and Energy Dissipation Technologies: a Test and Evaluation Program for Highway Bridge Applications"
by K. Almand
Presented by: Kathleen Almand

"The Restoring Force Characteristics of LRB under the Influence of Variable Axial Loads and Rotational deformation"
by H. Iemura, A. Igarashi, Y, Chen, H. Nakajima
Presented by: Akira Igarashi

"Field Testing of a Four-span Seismically Isolated Bridge"
by A.Gilani, S. Mahin, G. Fenves, J. Chavez, I. Aiken
Presented by: Gregory Fenves

"Enhancement of Lateral Seismic Load Distribution in Continuous Girder Bridges: Test of Stiffening and Damping Components of a New Device"
by W. Tanzo, J. Hernandez Jr., H. Mutsuyoshi, A. Tsuzuki
Presented by: J. Hernandez Jr.

ANALYSIS OF THE SEISMIC RESPONSE OF YAMA-AGE BRIDGE

Shigeki UNJOH

Head, Earthquake Engineering Division, Earthquake Disaster Prevention Research Center, Public Works Research Institute, Ministry of Construction
Tsukuba, Japan 305

ABSTRACT

Yama-age Bridge in Tochigi Prefecture, Japan, which is the first Menshin design (seismically isolated) bridge using high damping rubber bearing (HDR). Strong motion observation has been made at the bridge since the completion of the construction in May 1993. The strong motion data was obtained during the Hokkaido-toho-oki Earthquake on October 4, 1994. Since there are a few strong motion data during earthquakes for the Menshin bridges, analyses of the data were made to study the effectiveness of the Menshin design. This paper presents the seismic response characteristics of the Menshin design bridge through the analyses of the observed strong motion data.

1. INTRODUCTION

There are over 80 Menshin design (seismically isolated) bridges in Japan including the bridges under construction and on planning stage. Since the Menshin design bridges have recently begun to be constructed, there are only a few data on the dynamic response characteristics of the Menshin design bridges during earthquakes. The strong motion data was obtained at the Miyagawa bridge in Shizuoka Prefecture, Japan, which was the first Menshin bridge in Japan constructed in March 1991 [1]. Although the observed acceleration response was not strong, the effectiveness of the Menshin design to reduce the acceleration response of deck was shown [2].

Yama-age bridge is located at Karasuyama, Tochigi Prefecture, on National Highway Route No.294. The Yama-age bridge is the first Menshin design bridge using High Damping Rubber (HDR) Bearings and was completed in May 1993 [3,4].

The strong motion observation has been made for the Yama-age Bridge to study the dynamic characteristics of Menshin design bridge. The strong motion data was obtained during the Hokkaido-toho-oki Earthquake on October 4, 1994. Since the bridge is located far from the earthquake epicenter, the observed response is not strong. However, since there are a few strong motion data for the Menshin bridges, analyses of the data were made to study the effectiveness of the Menshin design. This paper presents the seismic response characteristics of the Menshin design bridge through analyses of the observed strong motion data.

2. OUTLINE OF THE YAMA-AGE BRIDGE

Fig.1 and **Photo 1** show the Yama-age bridge. The superstructure is of 6-span continuous prestressed concrete two-cell box girder with deck length of 246.3m. The effective width of the deck ranging from 10.5m (standard section) to 13.5m (wide section). The gradient of the deck in the longitudinal direction is from 1% to 5%. The ground condition of the Yama-age bridge consists of sand-gravel layers and slate layer. N-value by the standard penetration test for the sand-gravel layers is ranging from 30 to 50, and that of the slate layer is greater than 50. The ground condition is classified as Class I.

The abutment is of a inverted T-type reinforced concrete substructure and the piers are of reinforced concrete wall type with rectangular section. The foundations of all substructures are of spread type foundation. High damping rubber (HDR) bearing is adopted for the bridge. Two bearings are installed on the abutments and the piers. Since Menshin design is applied only in the longitudinal direction, the displacement in the transverse direction is restrained by stoppers.

To study dynamic response characteristics of the bridge, forced excitation test using an eccentric-mass shaker and quick-release jacks was also made for the bridge in December 1992[5].

The Yama-age Bridge was designed in accordance with the regulations of the "Design Specifications for Highway Bridges [6]". "Guidelines for Design of Menshin Highway Bridges [7]" and "Manual for Menshin Design of Highway Bridges [8,9]" were also referred for the Menshin design issues. In the Manual, the design lateral force may be reduced by 30% maximum according to the damping ratio of a bridge. It should be noted that since the bridge was designed based on the Design Specifications for Highway Bridges, the design lateral force was not reduced in consideration of the damping effect of the isolation bearings.

In the Menshin design of highway bridges, the Menshin devices are designed by the "Lateral Force Coefficient Method" and the "Bearing Capacity Method". In both methods, the lateral force is statically applied to the bridge, and the seismic safety is checked based on the allowable stress design approach in the Lateral Force Coefficient Method and bearing capacity basis considering ductility in the Bearing Capacity Method. Bridges are designed by the Lateral Force Coefficient Method, and then the ductility is checked for reinforced concrete piers by the Bearing Capacity Method. Natural periods of the bridge in the longitudinal direction are 1.56 sec for Lateral Force Coefficient Method and 1.77 sec for the Bearing Capacity Method.

3. STRONG MOTION OBSERVATION

The strong motion observation has been made for the Yama-age Bridge to study the dynamic characteristics of the Menshin design bridge. Three accelerometers in total are arranged as shown in **Fig.1**. One with three components as longitudinal, transverse and up-down is in the ground (under the ground : -5.17m) between Pier 5 and Abutment 2. Two with two components as longitudinal and transverse are on the top of Pier 5 and the deck on Pier 5. Digital type recorder is used for the strong motion observation system.

4. EFFECTIVENESS OF MENSHIN DESIGN BASED ON THE STRONG MOTION OBSERVATION DATA

Strong motion data was obtained during the Hokkaido-toho-oki Earthquake on October 4, 1994. The epicenter of the Hokkaido-toho-oki earthquake with magnitude of 8.1 was located in the east of 200km from Nemuro city. The depth is 20km. The maximum intensity by Japan Meteorological Agency (JMA Intensity) was recorded as VI in Kushiro and Akkeshi as shown in **Fig.2**. The ground vibration was observed from Hokkaido to Kanto and Chubu areas. The JMA Intensity around the Yama-age bridge was estimated as II.

Fig. 3 shows the recorded acceleration data on the ground, pier top and deck. It is shown from the data in the longitudinal direction in which the Menshin design was made that the deck response is smaller than that of the pier top. On the other hand, the deck response is larger than that of the pier top in the transverse direction in which the Menshin design was not made. It is found from the observed acceleration waveform that the deck response contains longer period components comparing with the pier response. Thus, the Menshin effects to elongate natural period and to cut the response with short period components were found.

Table 1 shows the measured peak acceleration response. The peak acceleration of 9.1gal and 8.3gal was observed in the longitudinal and transverse directions under the ground. These ground motion was amplified at the pier top to 36.9gal and 14.2gal, respectively. The amplification factor is 4.1 and 1.7 in the longitudinal and transverse directions, respectively. On the other hand, although the deck response in the transverse direction in which the Menshin design was not made was amplified to 1.3 times the response of the pier top, the deck response in the longitudinal direction in which the Menshin design was made was decreased to 1/3 the response of the pier top.

Fig.4 shows the acceleration response spectrum of the observed data to analyse the frequency response characteristics. It is found from Fig.4(a) that there are two peaks around the natural periods of 0.1 sec and 0.7 sec in the response of the pier top. In the deck, response around natural period of 0.1 sec is not remarkable, but the response around the natural period of 0.7 sec is predominant.

Fig.5 shows the acceleration response spectrum ratio of observed data. The acceleration response spectrum ratio is defined as the ratio of the response spectrum of deck and pier top to that of ground. Therefore, it indicates a kind of the amplification factor in various natural periods.

The following characteristics are found from **Fig.5(a)** in the longitudinal direction in which the Menshin design was made.

1) The amplification of the response of the pier top from ground was remarkable around the natural period of 0.1 sec and 0.7 sec. The amplification with natural period around 0.1 sec is larger than that with natural period of 0.7 sec. In consideration that the amplification from ground to the deck is predominant at the natural period of around 0.7 sec, the natural period of 0.1 sec is estimated as the 1st mode of the pier itself and the natural period of 0.7 sec is estimated as the 1st mode of the total bridge.
2) The amplification of the response of the deck from the pier top in the short period range less than 0.4 sec is smaller than 1, in particular in the period less than 0.2 sec the amplification is smaller than about 0.5. Since the amplification at the natural period 0.1 sec which is the natural period of the pier itself is about 0.1, the response predominant in the pier is not transferred to the deck. It means that the short period response of the pier is not transferred to the deck because of the elongation of natural period by seismic isolation bearing, therefore, the isolation design to elongate the natural period is verified to be effectively functioned.

In the transverse direction in which the displacement was restrained by stoppers as shown in **Fig.5(b)**, the amplification from the pier top to the deck is similar to that in the longitudinal direction. The deck response in the short period range with the natural period of 0.2 sec is less than 1. This is because there is a gap space with about 1cm for

the stopper to restrict the displacement in the transverse direction. Since the relative displacement developed in the isolation bearings is about 1mm which will be discuss later, the isolation bearing absorb some of the short period response in the transverse direction.

5. ANALYTICAL SIMULATION OF THE STRONG MOTION OBSERVATION DATA

Dynamic analyses were made for the Yama-age bridge in the design stage to check the static design results. The same model used in the design was used to simulate the earthquake response. The analyses in the longitudinal direction was made and the acceleration data recorded under the ground was used as an input acceleration to the model. **Fig.6** shows the model with linear beam-mass members. The foundation and surrounding soils were modeled as spring members. For the comparison, the foundation was also modeled as rigid.

Since the isolation bearings have the nonlinear force-displacement relation, in order to know the stiffness and damping of the isolation bearings, it is required to precisely estimated the relative displacement developed in the isolation bearings. Therefore, the relative displacement was computed from the observed acceleration data. **Fig.7** shows the relative displacement developed in the isolation bearings. Relative displacement was computed as the difference between the displacement response of the deck and the pier top. The acceleration data were integrated in the frequency range.

The computed peak relative displacement was 0.8mm in the longitudinal direction and 1.0mm in the transverse direction. Since the yield displacement is about 10mm based on the loading tests of isolation bearings used for the Yama-age Bridge, the isolation bearing is in the elastic range. Stiffness of the isolation bearings used for the analyses was assumed as that with the displacement of 0.8mm for the bearings on the piers. For the stiffness of isolation bearings on the abutment is assumed as that with the deck displacement of 2.0mm. **Table 2** shows the equivalent stiffness of the isolation bearings used for the simulation analyses. The equivalent stiffness used for the design using lateral force coefficient methods is also shown for the comparison.

Table 3 shows the damping ratio assumed in the analyses. The equivalent damping used for the design in the lateral force coefficient methods is also shown for the comparison. Since the relative displacement was about 0.8mm and the isolation bearing was within the elastic range, the equivalent damping of isolation bearings was estimated as 0. The damping ratio was assumed as 5, 10, 15% for the comparison.

The computed natural period of 1st mode in the longitudinal direction was 0.86 sec

when the soil spring was considered, and 0.66 sec when the foundation was assumed rigid. Since measured natural period of 1st mode is about 0.7 sec, the computed natural period when the foundation is assumed to be rigid is closer to the measured one.

Table 4 shows the measured and computed peak acceleration response of the deck and the pier top. Good agreement was found in the deck response when the damping of the isolation bearing was assumed as 0. On the other hand, the computed peak response of the pier top is about half the measured. This may be because of the damping ratio assumed for the 1st mode of the pier itself. **Fig.8** shows the comparison between measured and computed acceleration response when the foundation is assumed as rigid and the damping ratio of the isolation bearings is assumed as 0. Good agreement between the measured and computed deck response. Since the measured acceleration response was not large, the yield was not developed in the isolation bearings and the damping effect was small.

6. CONCLUDING REMARKS

The effectiveness of the Menshin design was studied through the analyses of the strong motion data obtained at the Yama–age bridge during the Hokkaido–toho–oki earthquake. The following contusions are obtained.

(1) The peak acceleration response of the deck during Hokkaido–toho–oki earthquake was 11.8gal and 18.9gal in the longitudinal and transverse directions, respectively. The Menshin effect was found in the peak acceleration of the deck in the longitudinal direction in which the Menshin design was made. The peak acceleration of the deck was decreased to 1/3 that at pier top.

(2) The amplification of the response of the deck from the pier top in the short period range less than 0.4 sec is less than 1, in particular in the period less than 0.2 sec the amplification is less than about 0.5. Since the amplification at natural period 0.1 sec which is tha natural period of the pier itself is about 0.1, the response predominant in the pier is not transferred to the deck. It means that the short period response of the pier is not transferred to the deck because of the elongation of the natural period by seismic isolation bearings, therefore, isolation design to elongate natural period is verified to be effectively functioned.

(3) Simulation analyses was made using the same model used in the design and assuming that the acceleration of ground is as input acceleration to bridge. Good agreement between the measured and computed deck response was found.

ACKNOWLEDGEMENTS

Design data and strong motion acceleration data were provided by the road construction section of Tochigi Prefectural Government, Japan. Kind cooperation provided by them is greatly acknowledged. Appreciation is to Mr. Fumikazu NISHIHARA, bridge engineer of ARATANI Consulting Co., who performed the dynamic analyses of the Yama-age Bridge.

REFERENCES

1) Matsuo, Y., O-ishi, A., Hara, K. and Yamashita, M. : Design and Construction of Miyagawa Bridge, -First Menshin Bridge in Japan-, Bridge and Foundation Engineering, 91-2, 1991.2
2) Kawashima, K., Nagashima, H., Masumoto, H. and Hara, K. : Dynamic Response Characteristics of Miyagawa Bridge (Menshin Brigade) , Bridge and Foundation Engineering, 92-11, 1992.11
3) Ikeda, T., Ozeki, k., Kumakura, K. and Abe, N. : Design of the Karasuyama No.1 Bridge (Base Isolated Bridge), Bridge and Foundation Engineering, 91-6, 1991.6
4) Uzuka, T., Kawakami, K., Kumakura, K. and Tani, H. : Menshin Design and Construction of Multi-span Continuous Prestressed Concrete Bridge, Proc. the 2nd U.S.-Japan Workshop on Earthquake Protective Systems for Bridges, December, 1992, Technical Memorandum of PWRI, No.3196
5) Kakinuma, T., Kawakami, K., Kumakura, K., Tani, H. and Abe, N. : Vibration Test of A Menshin Designed Multi-span Continuous Prestressed Concrete Bridge, Proc. the 3rd U.S.-Japan Workshop on Earthquake Protective Systems for Bridges, January, 1994, San Francisco
6) Japan Road Association : Design Specifications for Highway Bridges, Part I - V, February 1990
7) Technology Research Center for National Land Development : Guidelines for Base Isolation of Highway Bridges (Draft), March 1989 (in Japanese)
8) Public Works Research Institute : Development of Menshin Design of Highway Bridges, October, 1992, Technical Note of PWRI, Vol.60
9) Kawashima, K. : Manual for Menshin Design of Highway Bridges, Proc. the 2nd U.S.-Japan Workshop on Earthquake Protective Systems for Bridges, December, 1992, Technical Memorandum of PWRI, No.3196

Table 1 Measured Peak Acceleration Response (gal)

	Longitudinal	Transverse	Up–down
Deck on Pier 5	11.8	18.9	–
Top of Pier 5	36.9	14.2	–
Underground (–5m)	9.1	8.3	4.6

Table 2 Equivalent Stiffness of Isolation Bearings (tf/m)

	Designed Value	Assumed in Analyses
Abutment A1	1,428	5,114
Pier 1	4,720	30,068
Pier 2	7,364	24,880
Pier 3	5,632	24,926
Pier 4	5,080	26,324
Pier 5	4,756	26,570
Abutment A2	1,300	5,618

Table 3 Damping Ratio Assumed in the Analyses

	Designed Value	Assumed in Analyses
Superstructure	0.03	0.03
Substructure	0.05	0.05
Foundation	0.10	0.10
Isolation Bearing	0.17	0−0.15

Table 4 Comparison between the Measured and Computed for Peak acceleration response (gal)

	Measured	Computed (h:Damping Ratio)			
		h=0%	h=5%	h=10%	h=15%
Deck	11.8	11.2	10.4	9.3	8.5
Pier Top	36.9	15.1	13.4	12.8	12.4

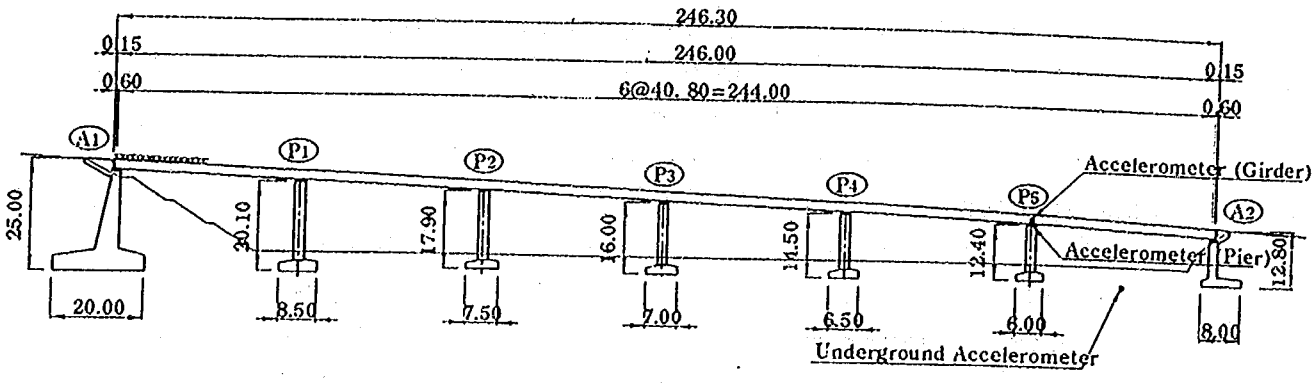


Fig.1 View of Yama-age Bridge and Strong Motion Observation

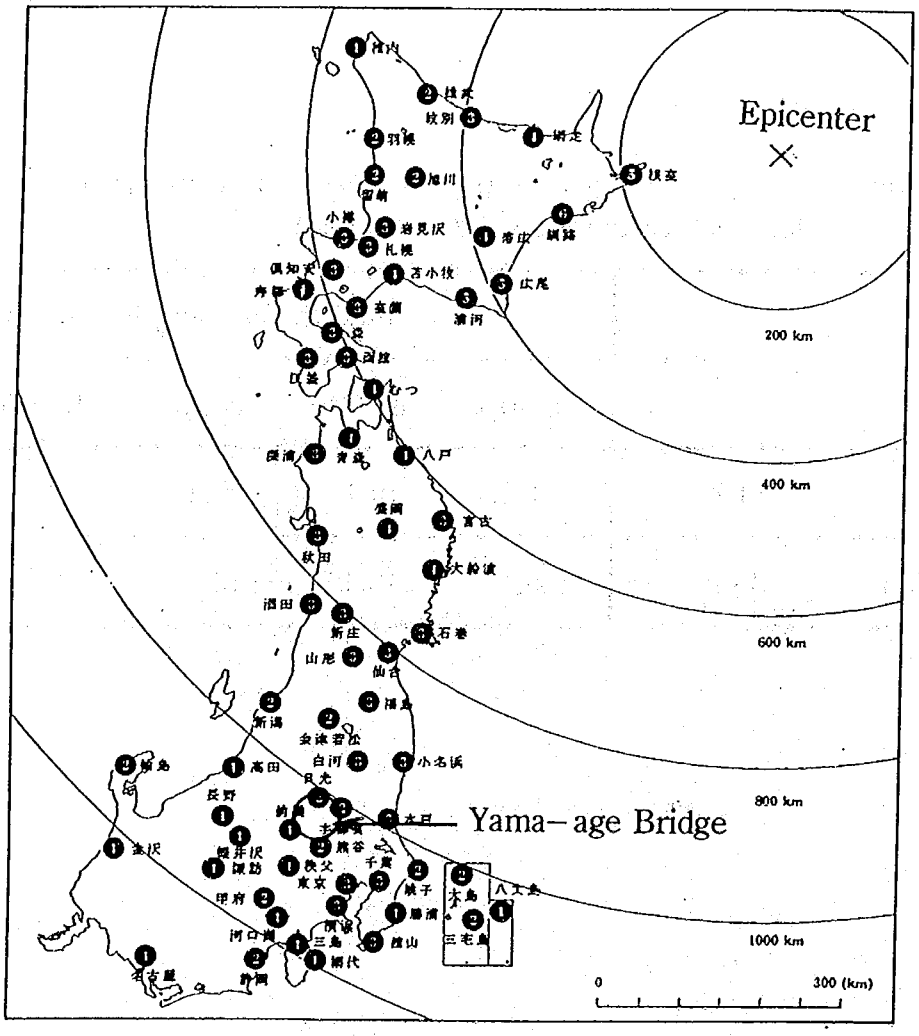
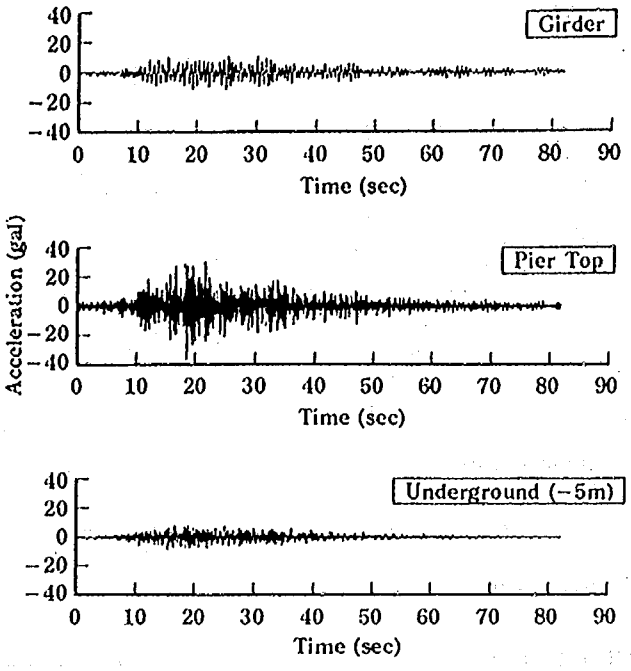
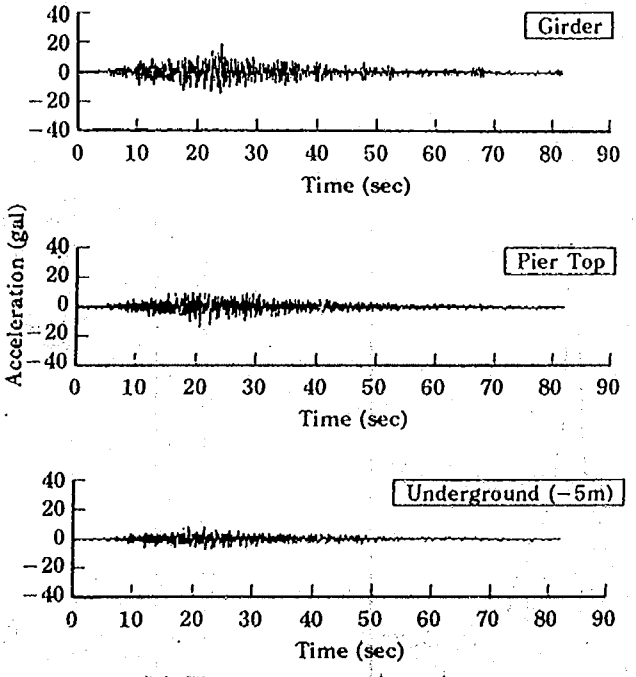


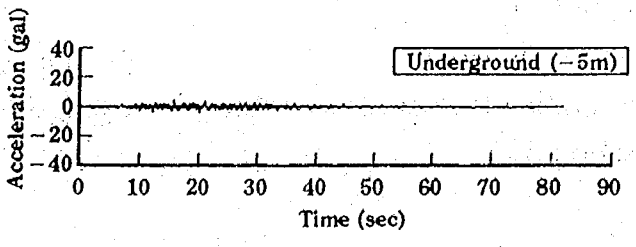
Fig. 2 JMA Intensity by Hokkaido-toho-oki Earthquake



(a) Longitudinal Direction

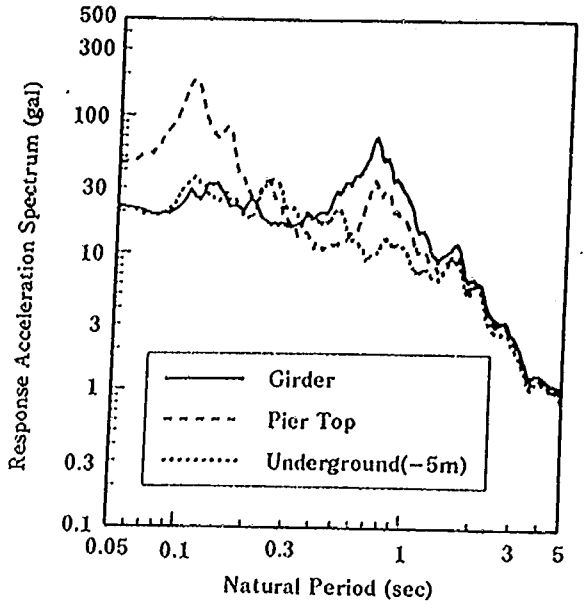


(b) Transverse Direction

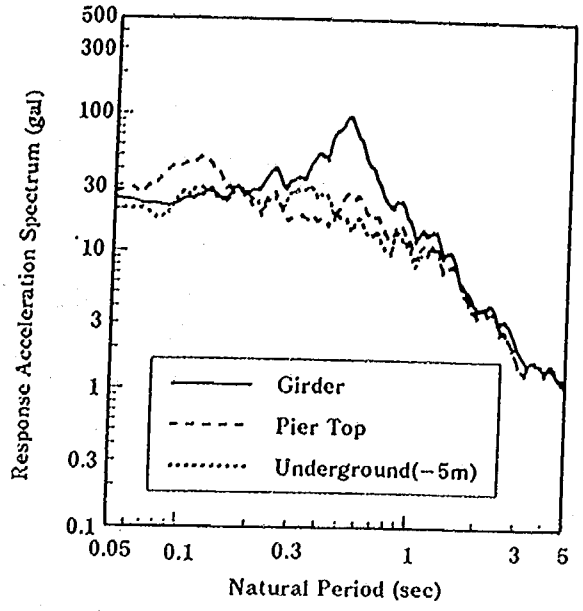


(c) Up−Down

Fig.3 Measured Acceleration Response

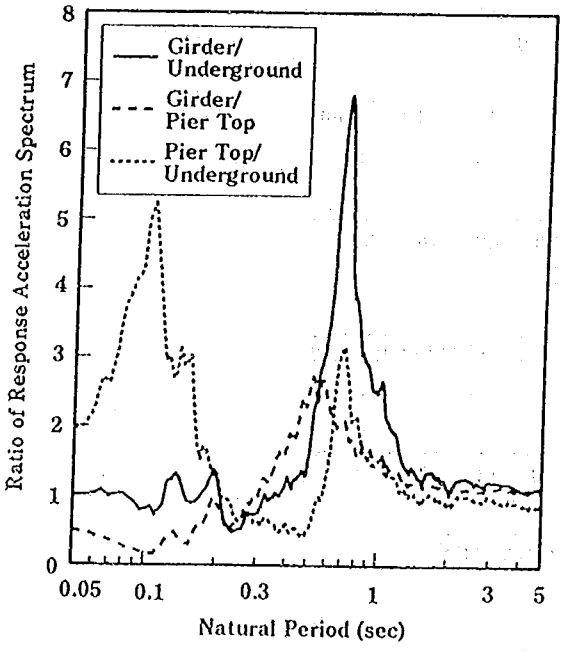


(a) Longitudinal Direction

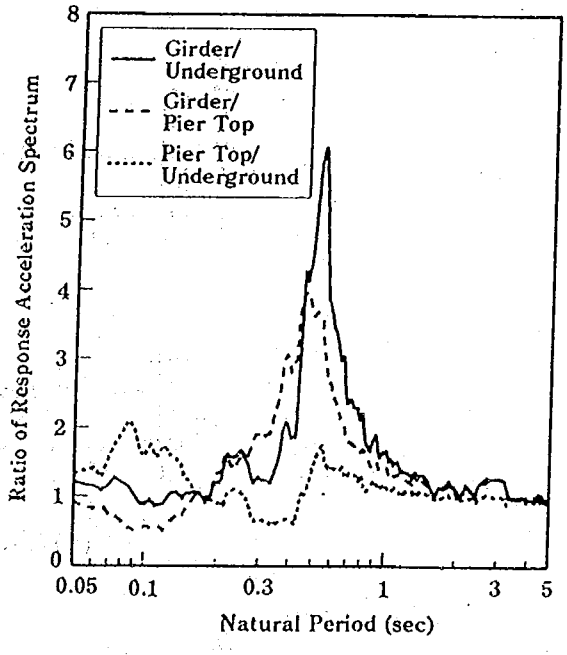


(b) Transverse Direction

Fig.4 Acceleration Response Spectrum of Measured Acceleration Data (Damping Ratio : 5%)



(a) Longitudinal Direction



(b) Transverse Direction

Fig.5 Ratio of Acceleration Response Spectrum of Measured Acceleration Data (Damping Ratio : 5%)

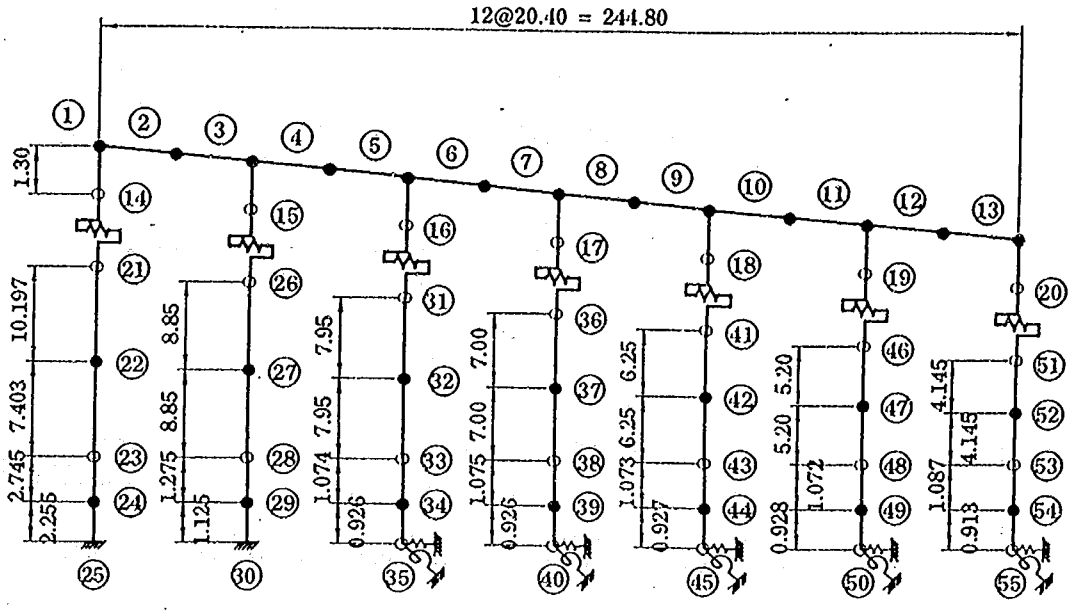
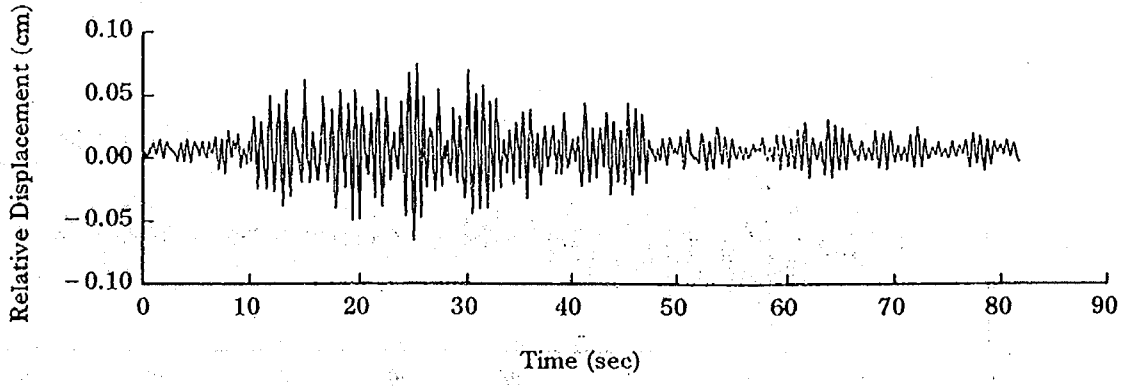
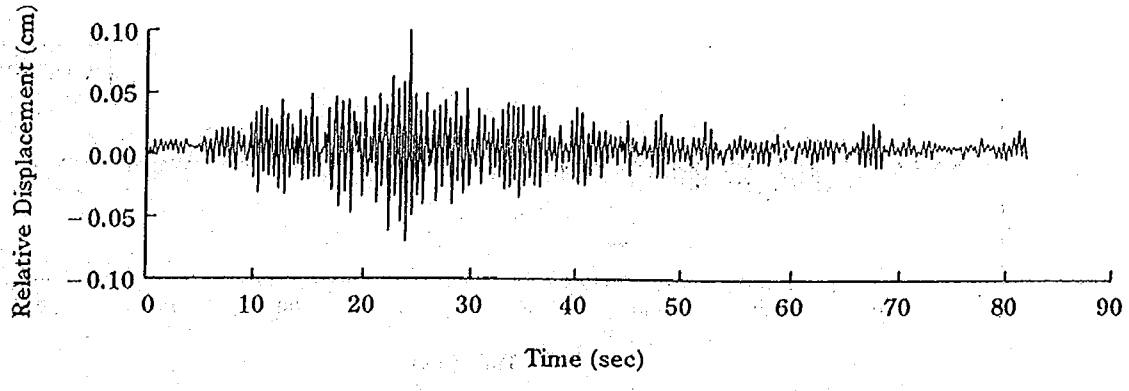


Fig.6 Analytical Idealization

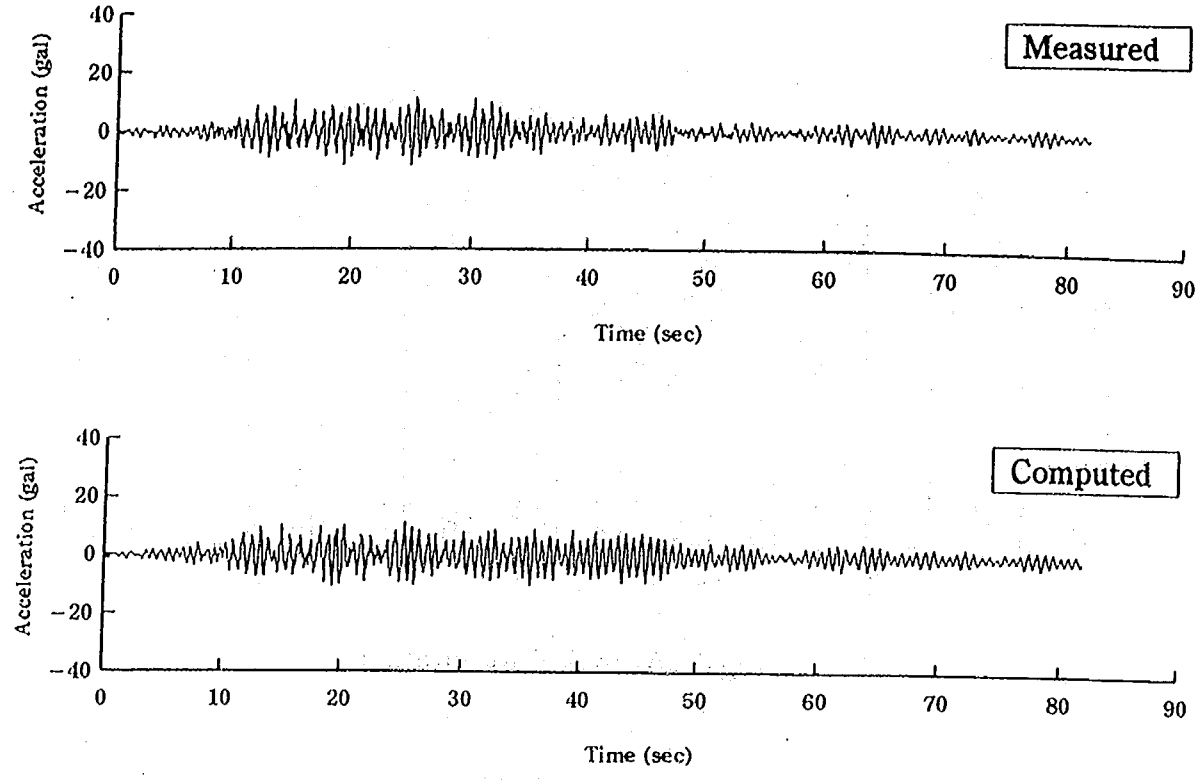


(a) Longitudinal Direction

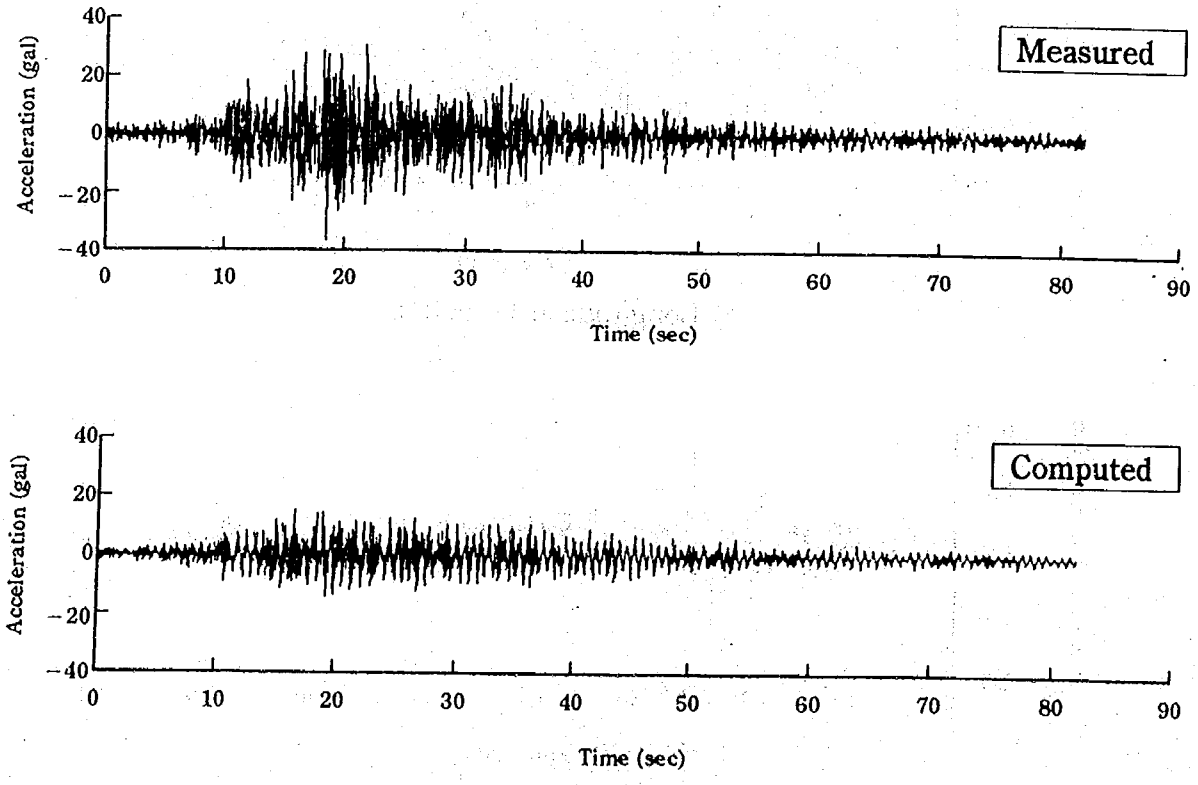


(b) Transverse Direction

Fig.7 Relative Displacement developed in the Isolation Bearings



(a) Deck Response



(b) Pier Top Response

Fig. 8 Comparison between the Measured and Computed Acceleration Response

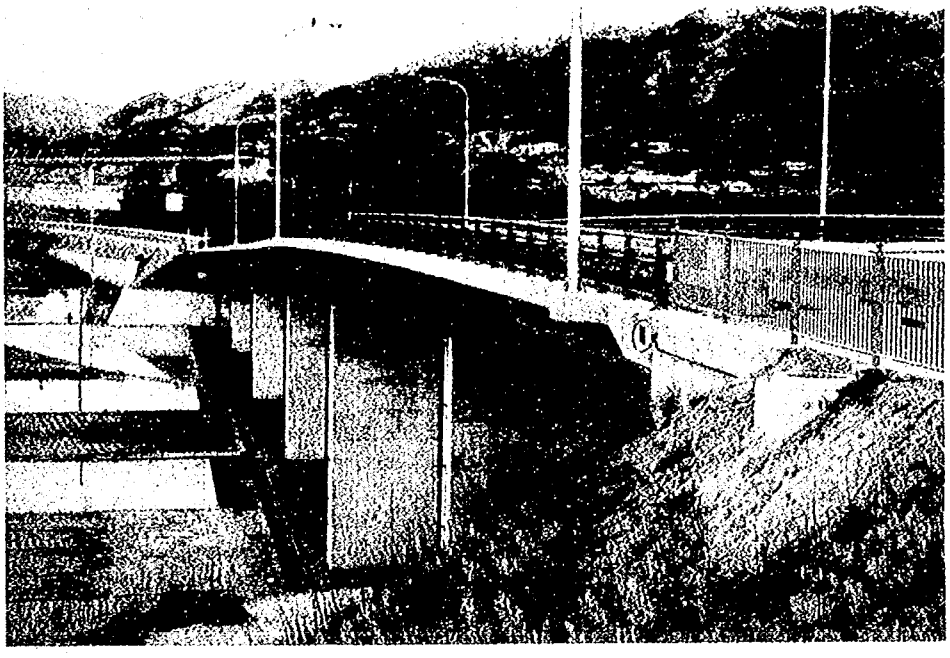


Photo 1 View of Yama－age Bridge

SEISMIC ISOLATION AND ENERGY DISSIPATION TECHNOLOGIES : A TEST AND EVALUATION PROGRAM FOR HIGHWAY BRIDGE APPLICATIONS

Kathleen H. Almand, P.E.
Director, Research Applications
Civil Engineering Research Foundation
Washington, D.C.

ABSTRACT

This paper describes the HITEC Evaluation Program for seismic isolation and energy dissipating systems. The program is designed to characterize the fundamental properties and performance characteristics of devices produced by eleven U.S. and global manufacturers. The program of full scale dynamic tests, is described, along with some preliminary test results. When complete, program findings should provide guidance to the highway community regarding the selection, design and use of seismic isolation and energy dissipating devices for different levels of performance.

THE NEED FOR AN EVALUATION PROGRAM FOR SEISMIC ISOLATION AND ENERGY DISSIPATION[1] TECHNOLOGIES

The concept of using seismic isolation bearings to reduce earthquake excitation and improve performance has been under development in the United States since the 1970's. Beginning with research in 1978 at UC Berkeley, the knowledge of isolator performance on bridges had developed in the U.S. to the point where guide specifications for seismic isolation design were developed and published by the American Association of State Highway and Transportation Officials (AASHTO).

However, since the publication of this specification in 1991, several new types of isolation devices have entered the U.S. marketplace and performance history has indicated that a better understanding of their effectiveness is required. In addition, there are several technologies which have been applied in different countries but have not yet been accepted in the United States. As a result AASHTO's Highway Subcommittee on Bridges and Structures has appointed an *ad hoc* panel to review the current specification for isolation.

The California Department of Transportation (Caltrans) was the first U.S. transportation agency to use seismic isolation on a bridge at the Sierra Point Overlook in 1985. Since then, isolation bearings have been installed on more than 90 bridges in the United States.

Despite a growing number of installations on U.S. bridges, questions remain about the real-world performance of seismic isolation devices. Bridge isolators are significantly larger in scale than the more common building isolator which has a longer performance history, the typical spans between bridge isolators are much larger, and the routine live load and environmental conditions are much more severe.

In response to these concerns, in 1994, HITEC, Caltrans and the Federal Highway Administration began a collaborative process to formulate plans to test and evaluate a range of seismic isolation and energy dissipation systems for highway bridges.

THE HITEC MISSION

The introduction of new or innovative technology to the U. S. highway community usually requires that a new product be demonstrated to many, if not all, state highway agencies. This practice is inefficient, time consuming, and often costly, particularly to small companies and entrepreneurs. To overcome these barriers, the Highway Innovative Technology Evaluation Center (HITEC) was established in 1994, in cooperation with the U.S. Federal Highway Administration, the American Association of State Highway and Transportation Officials

[1] The term "energy dissipator" used herein refers to hydraulic and friction devices used primarily for energy dissipation.

(AASHTO), and the Transportation Research Board (TRB). HITEC's mission is to accelerate the process of introducing technological advances to the highway community.

HITEC is structured to facilitate the conduct of consensus-based, nationally accepted performance evaluations of new or innovative technologies for the highway community. While the term "new or innovative technologies" connotes the "high tech" products often associated with the computer industry, HITEC is available to evaluate almost any product, system, service, material, equipment or other technology which the owner believes can be used on the nation's highways.

THE HITEC PROCESS

HITEC incorporates a consensus-based approach to its performance-based evaluation process. In general, HITEC follows a number of steps, including the development of an evaluation plan. In the case of the seismic evaluation program, a specially-modified version of the HITEC process designed for group evaluations, illustrated in Figure 1, was used.

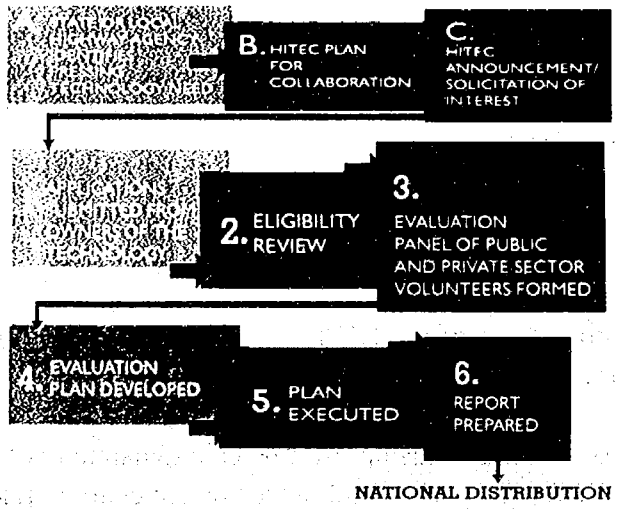


Figure 1. The HITEC Process

An important step in any HITEC evaluation program is the formation of a Technical Evaluation Panel composed of representatives from the user community, academia and the private sector. The Technical Evaluation Panel for the seismic program, Table 1, includes state transportation department personnel from each of the AASHTO regions and technical experts from the private sector knowledgeable in area of seismic design of bridge structures.

Table 1. Technical Evaluation Panel

Mohsen Sultan, P.E., Caltrans, **Chair**
Steve Bradford, P.E., Alaska DOT
Maria Feng, University of California, Irvine
Mr. Stewart Gloyd, Parsons Brinckerhoff, Quade & Douglas
Roy Imbsen, Imbsen & Associates
Salah Khayyat, Illinois DOT
Myint Lwin, Washington DOT
Rolando Nimis, Federal Highway Administration
Walt Podolny, Federal Highway Administration
Charles Seim, T.Y. Lin International
Li-Hong Sheng, Caltrans
Ayaz Malik, New York DOT
Edward Wassermann, Tennessee DOT

The HITEC Technical Evaluation Panel oversees the implementation of the evaluation plan, including preparation of the evaluation reports, as well as participating directly in technology transfer activities. HITEC staff "facilitates and coordinates" the program in close coordination with key Caltrans and FHWA officials.

EVALUATION OBJECTIVES

In accordance with deliberations of the HITEC Technical Evaluation Panel, this evaluation program has the following three major objectives:

1. Implement a program of testing, focusing on full scale dynamic tests, sufficient to characterize the fundamental properties and performance characteristics of the seismic isolation and energy dissipating devices evaluated.

2. Provide guidance regarding the selection, design and use of seismic isolation and energy dissipating devices for different levels of performance.

3. Develop suggested guide specifications for the use of isolation and energy dissipating devices in new bridge construction projects and retrofit applications.

The principal focus of the evaluation plan, which is designed to achieve objectives 1 and 2, is a program of laboratory testing currently being carried out by the Energy Technology Engineering Center (ETEC), a Department of Energy test and development center managed by the Rocketdyne Division of Rockwell International Inc., which has over 30 years of experience in testing of large scale components, including isolator and energy dissipating systems.

The Technical Evaluation Panel recommended a comprehensive test program to evaluate the important properties and performance characteristics of isolators and energy dissipators. The test program examines characteristics such as: stability, range, capacity, resilience,4 resistance to service loads, E nergy dissipation, survivability in extreme environment, resistance to aging and creep, predictability of response, fatigue and wear, and size effects.

These properties provide the bridge designer with critical information on the suitability of these devices for specific design applications and also provide insight into the reliability, longevity, and predictability of response. Furthermore, the program addresses the ability of the vendor or manufacturer to provide a quality product, understand and predict product response, and provide hardware in a timely manner.

TEST ARTICLES

HITEC, in collaboration with Caltrans, sought participation from all known manufacturers and suppliers of isolation and energy dissipating devices marketed in the U.S. Ten manufacturers, are participating in the program, representing four different categories of devices:

1. elastomeric devices
2. slider and roller devices
3. spherical slider devices
4. energy dissipators

Table 2 outlines the category of each technology participating in the program.

Table 2. Manufacturers and Technologies Participating in Evaluation Program

Manufacturer	Technology	Category
Dynamic Isolation Systems, Inc.	Force Control Bearing	elastomeric device
Enidine, Inc.	Hydraulic Damper	energy dissipator
FIP Energy Absorption Sys., L.L.C.	Seismic Device with Custom Response	slider and roller device
Oiles Corporation	Oiles MS-Stopper	energy dissipator
R.J. Watson, Inc.	Eradiquake	slider and roller device
Scougal Rubber Corporation	Seismic Bearing	elastomeric device
Skellerup Industries, Inc.	Elastomeric Bearing	elastomeric device
Taylor Devices, Inc.	Hydraulic Damper	energy dissipator
Tekton Manufacturing, Inc.	Steel Rubber Bearing	elastomeric device
Tekton Manufacturing, Inc.	Ball-in-Cone	spherical slider device
VSL Corporation	Friction Pendulum Bearing	spherical slider device

Each system met the following HITEC eligibility criteria:

- the product is owned by the applicant;
- the product is market ready, and
- the product is a unique technology for which there are no existing standards.

Each manufacturer submitted five test articles (70,000kg, 3@.225,000kg and 350,000kg) representative of the production device that the manufacturer intends to market. Each manufacturer was required to submit working drawings, material specifications, manufacturer's quality control program, analytical methods used to predict test article behavior for displacement or velocity load response, stiffness, and damping, and any test data generated prior to submitting the test article.

Acceptable ranges or limits have not been established for isolator or energy dissipator test performance since these requirements are typically specified on a project-by-project basis. However, for the purpose of the test program, target values were defined for selected parameters so that the manufacturer could provide the appropriate device for testing. The definition of design loads, design displacements, movement ratings, and operational temperature limits is critical since these values reflect on the suitability of these devices for specific applications that may vary from state to state.

DEVICE CHARACTERIZATION

Device characterization testing quantifies performance data and provides useful information to the bridge design engineer. Since a wide variety of designs have been submitted for evaluation, several test scenarios have been developed to satisfy individual test needs. There are three device groups that are assigned to one of four performance test categories:

(1) Weight-Bearing Parallel Shear Devices

Category 1: A flexible vertical load supporting device with energy dissipating capabilities that lengthens the period of lateral vibration of the system sufficiently to reduce the force response and then tends to return the system to its original position when the load is removed.

Category 2: A vertical load supporting device that utilizes rolling or sliding elements and that may require an auxiliary device to satisfy minimum damping requirements. The device lengthens the period of vibration of the system sufficiently to reduce the force response and has energy dissipating capabilities. The device may or may not be self-centering and therefore may or may not return to its original position when the load is removed.

(2) Weight-Bearing Spherical Devices

Category 3: A vertical load supporting device utilizing rollers or sliding elements that relies on gravity to assist in returning it to its original position when the lateral load is removed. The device lengthens the period of vibration of the system sufficiently to reduce the force response, and may or may not have energy dissipating capabilities.

(3) Non-Weight-Bearing Axial Devices

Category 4: A device that uses either mechanical friction or hydraulic fluid to dissipate energy. The device may or may not be self-centering and therefore may or may not return to its original position when the load is removed.

Table 3 is provided to assist in selecting the appropriate test category.

Table 3. Category Selection Criteria

Properties	Category 1 Elastomeric Isolators	Category 2 Rollers and Sliders	Category 3 Spherical Devices	Category 4 Damping Devices
Frequency Decoupling	Yes	Yes	Yes	No
Energy Dissipation	Yes	Yes/No	Yes/No	Yes
Restoring Capability	Yes	Yes/No	Yes/No	Yes/No
Vertical Movement	Yes	No	Yes	No

TEST APPARATUS

The isolator and energy dissipator device characterization tests are being conducted in the bearing test rig illustrated in Figures 1 and 2. This is a special test fixture that was specifically developed for dynamic testing of seismic bearings for nuclear power plants. The test fixture is currently configured to apply up to 360,000kg of steady vertical loading in combination with 110,000kg of dynamic horizontal load. The fully reversing horizontal cyclic displacements can be as high as ± 380mm within actuator velocity and load limits. An offset single stroke amplitude limit of 560mm is available for restoring force and stability tests.

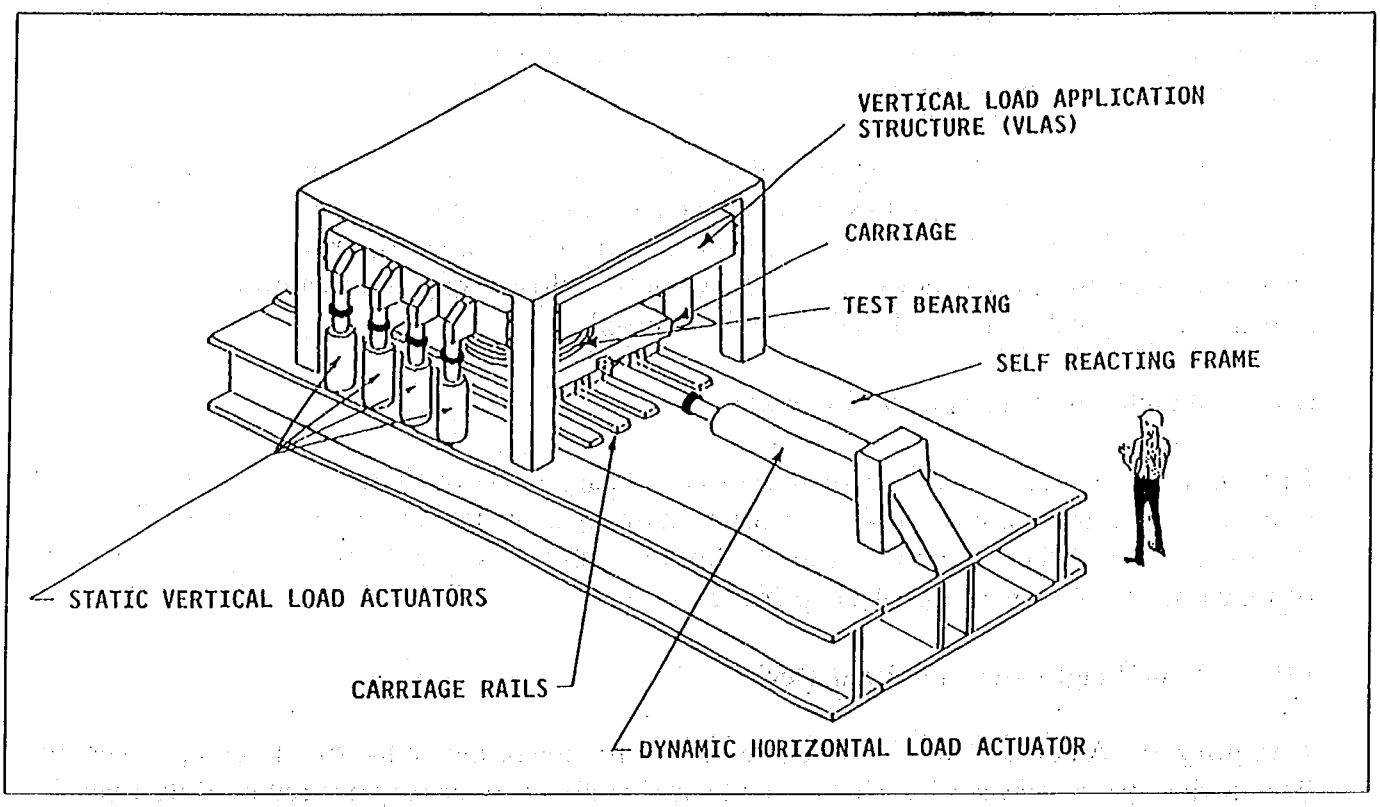


Figure 2. ETEC Bearing Test Rig Structural Elements

The horizontal displacements are applied to the test articles by a servo - controlled hydraulic actuator via a carriage assembly. The vertical loads are applied to the test articles by eight hydraulic actuators through the Vertical Load Application Structure (VLAS).

The carriage assembly is supported by ten low friction Tychoway roller bearings divided into two rows spaced sixty inches apart. The roller bearings travel on hardened steel tracks. The assembly is guided laterally by four Camrol bearings engaging guide rails. Three non-hardened steel tracks extend beyond the test zone to allow the carriage assembly to be moved to an open area for the installation and removal of test articles.

COMPONENT TEST DESCRIPTIONS

Test 1 Performance Benchmark (All Categories)

Purpose: To experimentally verify the initial stiffness and damping/friction of the device, and the number of cycles of loading required to stabilize response.

Procedure:

For Category 1, 2 and Category 3 devices 10 fully-reversed loading cycles at the design displacement (DD) are applied to the test device at 0.5 Hz (corresponding to a 2.0 second period). The design compressive load (DCL) is also applied.

For Category 4 devices 10 fully-reversed loading cycles at the design displacement (DD) are applied at 0.5 Hz (corresponding to a 2.0 second period). However, if the design velocity is exceeded, the displacement shall be reduced so that the maximum velocity does not exceed the design velocity (DV).

The intercept and peak values will be reported for each cycle.
Shake-down occurs if $.7 < F(2)/F(10) < 1.3$

The data will be used to determine shake down characteristics of the test article and confirm that minimum damping requirements are satisfied for the devices or combination of devices tested.

Test 2 Load-Deflection Characterization (Categories 1, 2, and 3)

Purpose: To determine load-deflection performance characteristics.

Procedure: Load-deflection and damping/friction characteristics are determined as follows. Circular devices are tested in one arbitrarily selected primary direction of operation and at 90 degrees to this direction. Bi-symmetric devices (square or rectangular) will be tested in the primary direction of operation, at 90 degrees to the primary direction, and in a diagonal direction through a point of the bearing surface that is farthest from its centroid (e.g., @ 45° to the primary loading direction for a square cross-section.). The tests consist of three cycles of fully-reversed design displacement (DD) applied at 0.5 Hz (corresponding to 2.0 second period) for all devices. Three tests are performed in the primary direction of operation; one at 40% DCL, one at 70% DCL, and one at 100% DCL. Tests in the other directions, when required, are performed with DCL. If the device is uni-directional it is tested only in that direction.

The data will be used to quantify performance characteristics (stiffness and damping) of weight-bearing devices under load.

Test 3 Frequency Dependant Characteristics (Categories 1, 2, & 3)

Purpose: To determine static and dynamic performance characteristics in the primary direction of operation.

Procedure: With the design compressive load (DCL) applied, three fully-reversed cycles of the design displacement (DD) are applied at 0.05 Hz, 0.2 Hz, and 1.0 Hz, and 50% of DD at 2.0 Hz (corresponding to 20.0 sec., 5.0 sec., 2.0 sec., 1.0 sec., and 0.5 sec. periods).

The data will be used to quantify performance characteristics (stiffness and damping) of weight-bearing devices under dynamic loading conditions.

Test 4 Frequency Dependent Characteristics (Category 4)

Purpose: To determine dynamic performance characteristics and verify the constitutive laws.

Procedure: Three fully-reversed cycles of the maximum displacement, are applied at each of the following harmonic frequencies; 0.05 Hz, 0.2 Hz, 0.5 Hz, 1.0 Hz, and 2.0 Hz (corresponding to 20.0 sec., 5.0 sec., 2.0 sec., 1.0 sec., and 0.5 sec. periods). Displacement ranges may have to be limited to ensure the maximum velocity of the device or test equipment is not exceeded.

The data will be used to quantify the performance of energy dissipating devices at various frequencies and velocities, confirm analytical predictions of the form F=CVn, and verify manufacturer's drop test data (if performed).

Test 5 Fatigue and Wear (All Categories)

Purpose: To simulate many small displacements due to temperature and live load fluctuations other than earthquake for evaluating possible deterioration in earthquake performance due to resulting debonding, wear, or fatigue.

Procedure: The device is subjected to a minimum of 10,000 cycles of simulated displacement representing the "movement rating" (MR) of the device specified by the manufacturer and applied at 0.1 Hz (corresponding to a 10. second period) or other frequency deemed acceptable to the manufacturer. However, the speed of application shall not be less than 115mm/minute. If the component is designed to be used as a isolation device and provides vertical support (i.e., a load bearing isolator), the full design compressive load DCL is applied.

The data will be used to quantify damage or degradation arising from the application of high-frequency, small-displacement loadings.

Test 6 Environmental Aging (All Categories)

Purpose: To verify performance of the device in a salt spray environment such as may be encountered over a long period of time under an open bridge deck joint which is subject to salting.

Procedure: The device shall be exposed in a salt spray chamber for 1000 hours in accordance with the requirements of ASTM B 117.

The accelerated aging will examine the degradation of the device resulting from key environmental factors.

Test 7 Dynamic Performance Characteristics at Temperature Extremes (All Categories)

Purpose: To assess the effects of temperature on component performance.

Procedure: With the full design compressive load DCL applied (for load bearing isolators), three fully-reversed cycles of the design displacement DD are applied at 0.5 Hz (corresponding to a 2.0 second period) at the upper and lower temperature extremes specified by the manufacturer. The temperature range of interest for this National Program is from -40° C to 50° C. [However, if specific devices cannot perform at these temperature extremes, manufacturer specified temperature limits will be used.]

The data will quantify changes in performance (stiffness, damping, friction, etc.) that occur from changes in ambient temperature conditions.

Test 8 Durability Test (All Categories)

Purpose: To assess component durability resulting from a moderate number of strong motion cycles.

Procedure: Twenty (20) fully-reversed cycles at 100% maximum design displacement DD or 100% maximum design velocity DV (for Category IV devices) are applied at 0.5 Hz (corresponding to a 2.0 second period). The full design compressive load DCL is simultaneously applied to the weight-bearing isolators.

The data will be used to assess performance degradation, quantify useable margins, and provide insight into the suitability of the device for applications where a large number of high-level aftershocks can be expected.

Test 9 Displacement Stability Test to Failure (All Categories)

Purpose: To determine failure loads and margins of safety.

Procedure: With the DCL applied, the component is loaded laterally at 0.5 Hz (corresponding to a 2.0 second period) with increasing displacement amplitude until "failure" occurs. Each cycle will increase the displacement amplitude by 1.1 times the preceding cycle, e.g, $(1.1)^0$xDD, $(1.1)^1$xDD, $(1.1)^2$xDD, $(1.1)^3$xDD ..... $(1.1)^n$xDD for the n^{th} cycle. For some devices this may be actual failure whereas for other devices it may be a programmed physical stop or ultimate restraint beyond which the device cannot operate. If failure does not occur before the cyclic limits of the test machine (±380mm) are reached, the device will be subjected to a slow rate monotonic loading to 560mm (the test machine limit).

The data will be used to quantify safety margins and provide insight into the stability of the device under high loading states. Failure of an elastomeric device is defined as when 1) the elastomeric material visually/audibly tears or delaminates, or a damping feature cracks or breaks and the lateral shear stiffness degrades significantly, or 2) additional lateral deflection reduces the lateral shear load. Failure of a spherical sliding or pure sliding device occurs when 1) gross structural damage is visible, 2) the rolling or sliding element does not function properly, 3) the rolling/sliding element reaches a physical stop, or 4) a significant change in performance is observed. Failure of a hydraulic energy dissipator occurs when 1) a major hydraulic leak is observed, 2) the piston assembly hits a physical stop, or 3) a significant change in performance is observed. Failure of a friction energy dissipator occurs when 1) there is a sudden unexpected increase/decrease in stiffness or 2) a significant change in performance occurs.

PRELIMINARY RESULTS - CHARACTERISTIC LOAD/DEFLECTION CURVES

As of November, 1996, approximately two thirds of the test program is complete. Figures 3 and 4 illustrate characteristic dynamic load/ displacement hysteritic behavior and the variation in behavior of seven different isolators tested to date. The program is scheduled for completion in the spring of 1997.

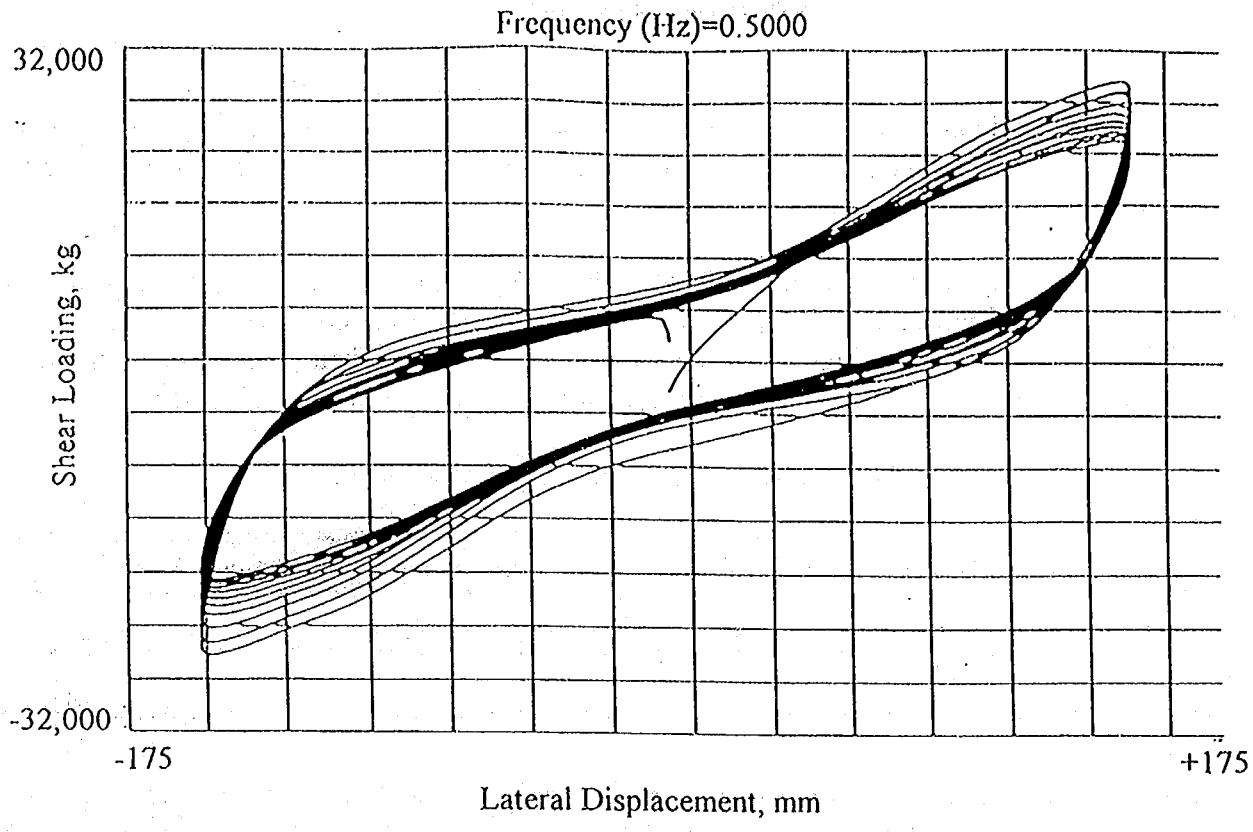


Figure 3. Characteristic Load/Displacement Behavior

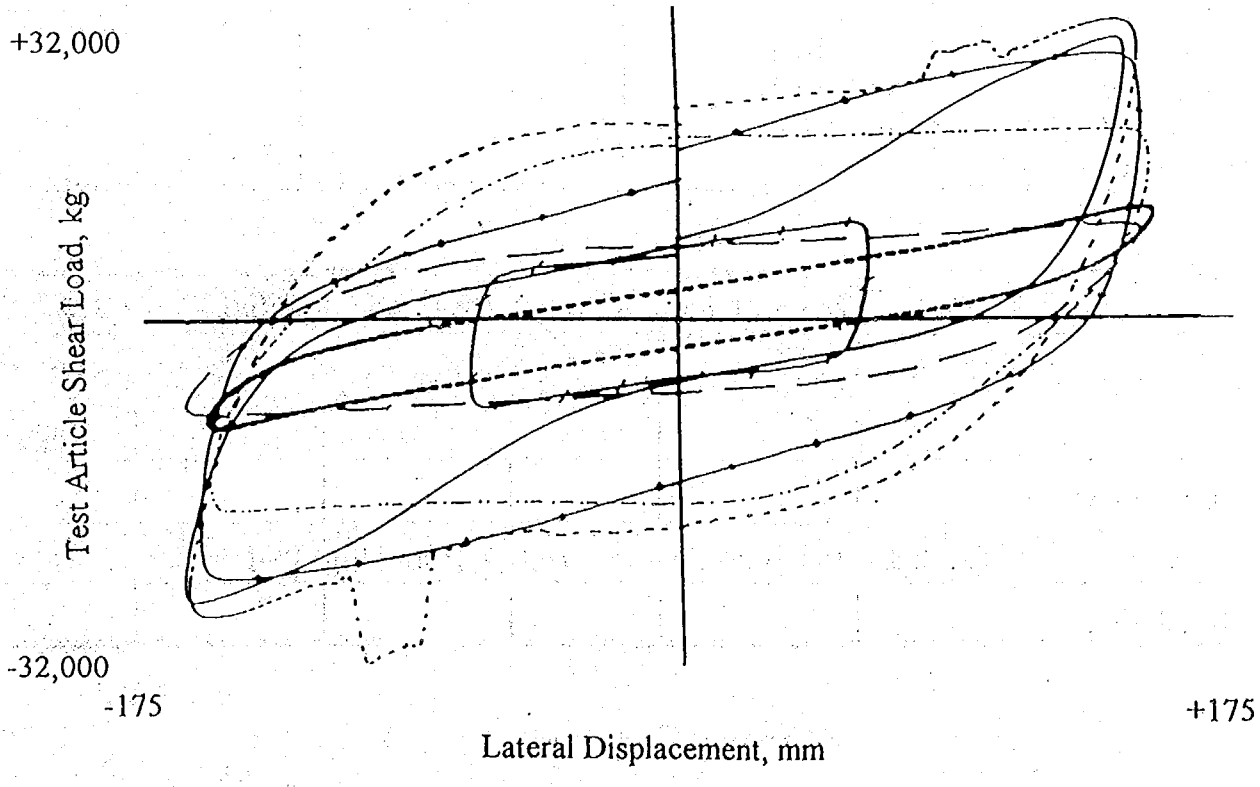


Figure 4. Variation in Load/Displacement Behavior

DISSEMINATION OF FINDINGS

The results of the test program will be summarized in a series of HITEC reports: a summary report of findings from all manufacturers and a detailed test report on each technology. Table 4 illustrates the format in which the test data will be summarized. In addition all testing has been documented in videotape and slide format.

Subsequently, Caltrans and the HITEC evaluation panel will utilize the information obtained from this program to make appropriate recommendations in code changes to the AASHTO Highway Subcommittee on Bridges and Structures, Technical Committee on Loads and Load Distribution, and Technical Committee on Bearings and Expansion Devices.

Table 4. Test Data Summary Presentation

Test 2.1 -- Test Article Stability - Peak Load at Design Displacement	
Test Article Identification	$F_{cycle.2}/F_{cycle.10}$
5 Test Articles	

Test 2.2 -- Compressive Load Effects @ DD & 0.5 Hz			
(T/A ID) -- DCL	Compressive Load	Stiffness(kg/mm)	Damping (%)
5 Test Articles Design Compressive Loads of 70,000kg, 225,000kg, 350,000kg	100% DCL 70% DCL 40% DCL		

Test 2.3 -- Dynamic Characterization (Stiffness) [kg/mm]					
Test Article Identification	Frequency [Hz]				
	.05	0.2	0.5	1	2.0*
5 test articles					
Test 2.3 -- Dynamic Characterization (Damping) [%]					
5 test articles					

Test 2.4 --Frequency Dependent characteristics				
Test Article ID	**C**	**n**	**F**	**V**
5 test articles				

Test 2.5 -- 10,000 Fatigue Cycles Service Degradation				
Test Condition	**Stiffness (kg/mm)**		**Damping (%)**	
	Before	**After**	**Before**	**After**
0.1 Hz at Design Movement Rating				

Test 2.6 -- Salt Spray Service Degradation, 1000 hours				
Test Condition	**Stiffness (kg/mm)**		**Damping (%)**	
	Before	**After**	**Before**	**After**
0.1 Hz at Design Movement Rating				

Test 2.7 -- Temperature Effects on Performance						
Test Article ID	**Temperature Range**		**Stiffness (kg/mm)**		**Damping (%)**	
	T_h (eg 50oC)	**T_L (eg 5oC)**	**T_H**	**T_L**	**T_H**	**T_L**
225,000kg Test Article						

Test 2.8 - Performance Stability After 20 Cycles of Strong Motion Input		
Test Article ID	**$Stiffness_{20}/Stiffness_2$**	**$Damping_{20}/Damping_2$**
Test Article		

Test 2.9 – Test to Failure				
Test Article ID	Design Disp. (mm)	Failure Disp. (mm)	FailureMargin	Failure Mode
5 Test Articles				

CONCLUSION

The HITEC test and evaluation program for seismic isolation and energy dissipation technologies has been designed to provide sufficient information to state bridge engineers, engineering and design firms, and others in the bridge engineering community so that they can develop a list of pre-approved suppliers and systems, and to assist them in incorporating seismic isolation technologies into plans to retrofit existing or build new bridges.

THE RESTORING FORCE CHARACTERISTICS OF LRB UNDER THE INFLUENCE OF VARIABLE AXIAL LOADS AND ROTATIONAL DEFORMATION

H. Iemura[1], A. Igarashi[1], Y. Chen[2] and H. Nakajima[3]

[1] Dept. of Civil Engineering Systems, Kyoto University

[2] Dept. of Civil Engineering, Kyoto University

[3] Hanshin Expressway Public Corporation

Abstract

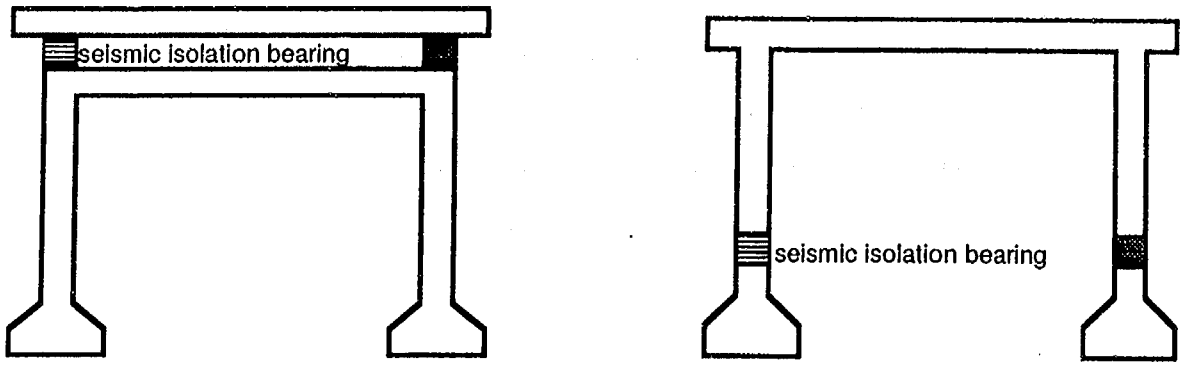
In the application of base isolation devices to bridge structures, in most cases the base isolation bearings are installed between the girders and the piers' top where conventional bearings have been installed. However, in the restoration of the Hanshin Expressway No.3 in Benten District, base isolation bearings (LRB) are installed at the bottom of the columns of the framed bridge structure because of space limitation for conventional type of bridge. For this type of bridge structure, not only the horizontal deformation, but also the variable axial load and rotaional deformation of the LRB take place in the event of strong earthquakes. It is of great importance to experimentally assess the influence of these effects to ensure the safety of the seismic isolator implementation of this type. The horizontal restoring force characteristics of LRB-type isolator were investigated by means of triaxial loading tests. It is shown that the effect of variable axial load is more significant than that of the rotational deformation.

1 INTRODUCTION

Recently, especially after the Hyogoken-Nanbu Earthquake, base isolated structures are becoming popular. The principle of the base isolation is "the elongation of the natural period of structures to reduce the inertia force acting on structures and the enhancement of energy dissipation capacity to reduce large displacements".

In the application of base isolation bearings to bridge structures, the bearings are mostly installed between the girders and the piers' top as shown in Fig. 1 (a), where conventional bearings have been installed.

However, in the restoration of the Hanshin Expressway No.3 in Benten District, base isolation bearings are installed at the bottom of the columns of the framed bridge structure as shown in Fig. 1 (b). This type of configuration is employed since the size of the space for the construction of the viaduct in a densely populated urban area is tightly limited, and excessive seismic loading to the foundation needs to be avoided.



(a) Typical Seismic Isolation for Bridge Structures

(b) Hanshin Expressway No.3 in Benten District

Figure 1 Implementation of Seismic Isolation Bearings

The base isolation bearings implemented as shown in Fig. 1 (b) is expected to undergo not only horizontal deformation, but also variable axial load and rotational deformation, due to the dynamic response of the framed structure. Effects of variable axial load and rotational deformation on the performance of the base isolation bearings have to be experimentally examined in order to use this unconventional implementation in practice.

In this paper, the verification test results conducted at the earthquake engineering laboratory of Kyoto University, using the newly developed test equipment for the triaxial loading of seismic isolatiors are presented.

2 EXPERIMENTAL SYSTEM

The schematic of the experimental system used in this study is shown in Fig. 2. Three actuators are digitally controlled to apply the specified horizonatial, rotational deformation and axial force. The digital controller allows a high accuracy of loading through the actuators.

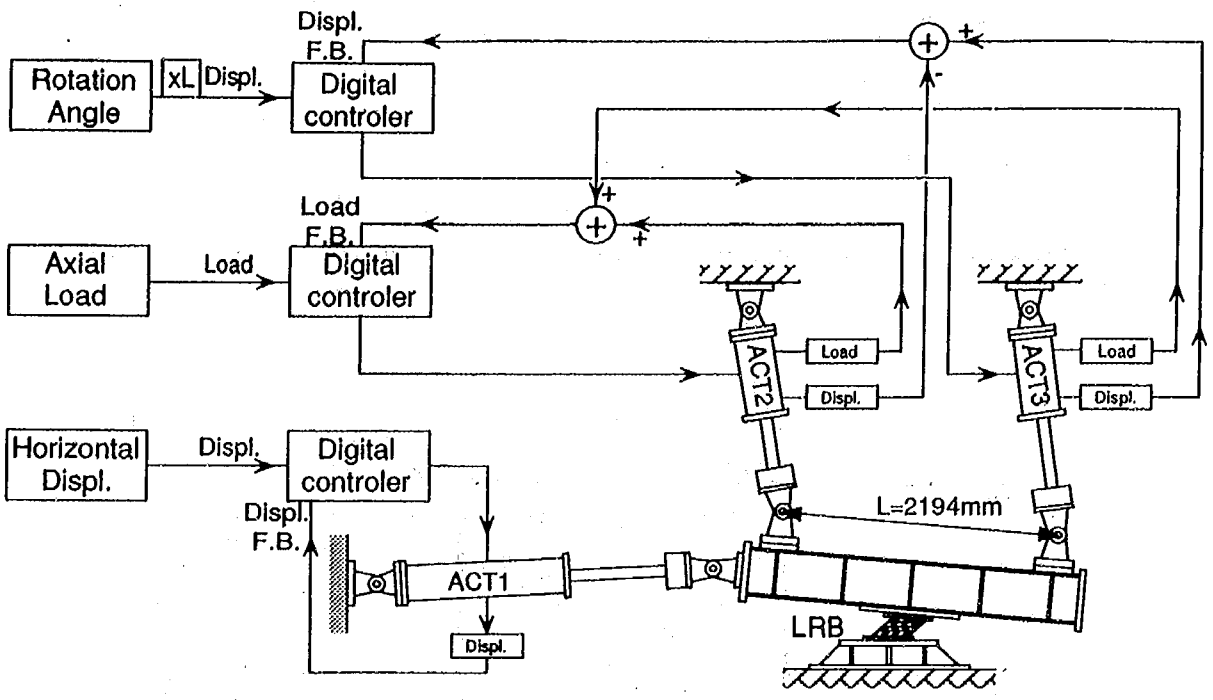


Figure 2 The Test System

2.1 Loading System

As shown in Fig. 2, the actuator No.1 (ACT1, hereafter) imposes the horizontal displacement on the loading beam and the specimen. The vertically hunged ACT2 and ACT3 apply the axial force and rotational deformation through the horizontal rigid beam.

2.2 Control System

ACT1 is operated in the displacement control mode. ACT2 is operated in the force control mode to apply the axial load, which is the sum of reaction forces of ACT2 and ACT3. ACT3 is operated in the displacement control mode to impose the angle of rotation on the loading beam, see Fig. 2.

2.3 Instrumentation

In addition to displacement and load transducers installed in ACT1, 2 and 3, external displacement transducers and sensors are set to the beam for the more accurate measurement. All the measured data are recorded on the hard disk of the computer.

3 LOADING EXPERIMENTS

In this study, Lead Rubber Bearing(LRB) are tested. There are four specimens(A1, A2, B1, B2) with two types(A, B). Both types of the specimens are one third models of the actual bearings used in the Hanshin Expressway restoration. The difference between the types A and B is the thickness of the steel plates. Dimensions of the bearings are shown in Fig. 3.

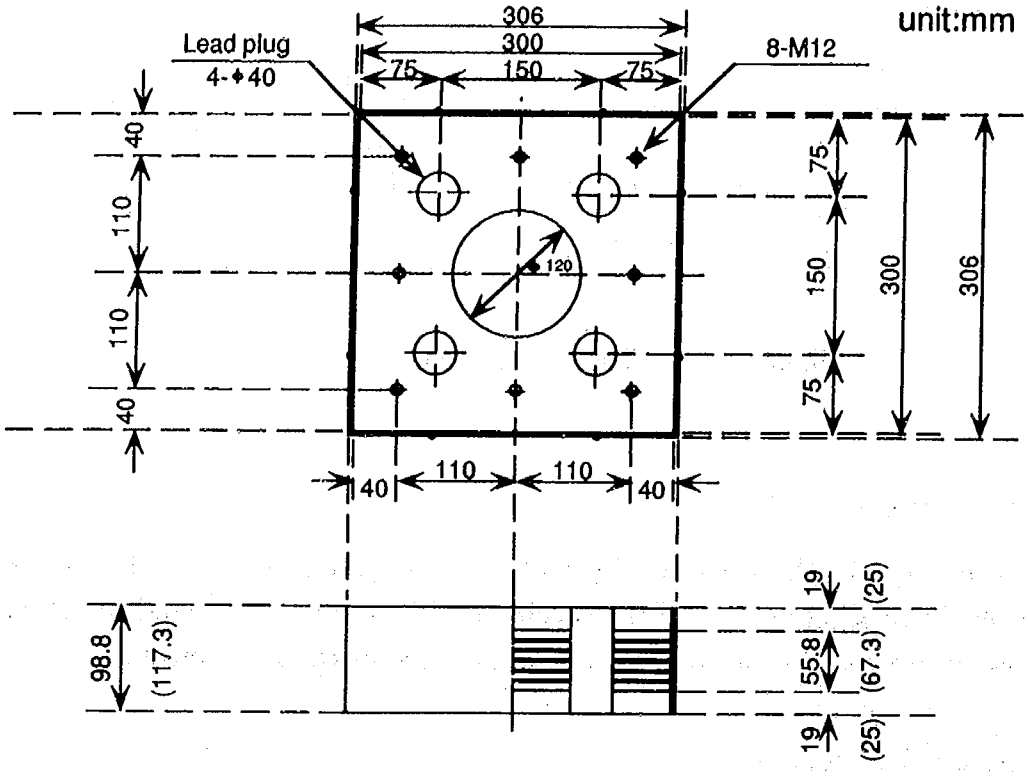


Figure 3 Dimensions of Specimens (Inside parenthesis: type B)

Since the purpose of the experiments is to verify the performance of the bearing under the triaxial loading for the application of Benten District reconstruction, the test scheme is devised to subject the seicmic isolator specimen to simulated horizontal displacements, variable axial loads, and rotation. The loading condition is first calculated by a dynamic response analysis of the framed bridge of the Benten section, modelled as in Fig. 4, in which the NS component of the acceleration record of the Hyogoken-Nanbu Earthquake at JR Takatori Station is used as the input.

Calculated horizontal displacement, axial load and rotational angle working on the bearing are shown in Figs. 6, 7 and 8. All of the three time histories have a similar shape, since the first mode is predominant in the response of the structure.

The following four types of tests were conducted.

Test 1: Under the constant axial load, forced rotation of which time history is shown in Fig. 5 is applied to examine rotational restoring force characteristics of the bearing.

Test 2: Under the constant axial force and without rotational deformation, a series of horizontal displacements shown in Fig. 6 is imposed on the specimen.

Test 3: Without rotational deformation, a series of horizontal displacements shown in Fig. 6 and the variable axial force shown in Fig. 7 are applied

Test 4: Horizontal displacement(Fig. 6) and variable axial force (Fig. 7) are applied while the rotational deformation shown in Fig. 8 is imposed on the specimen.

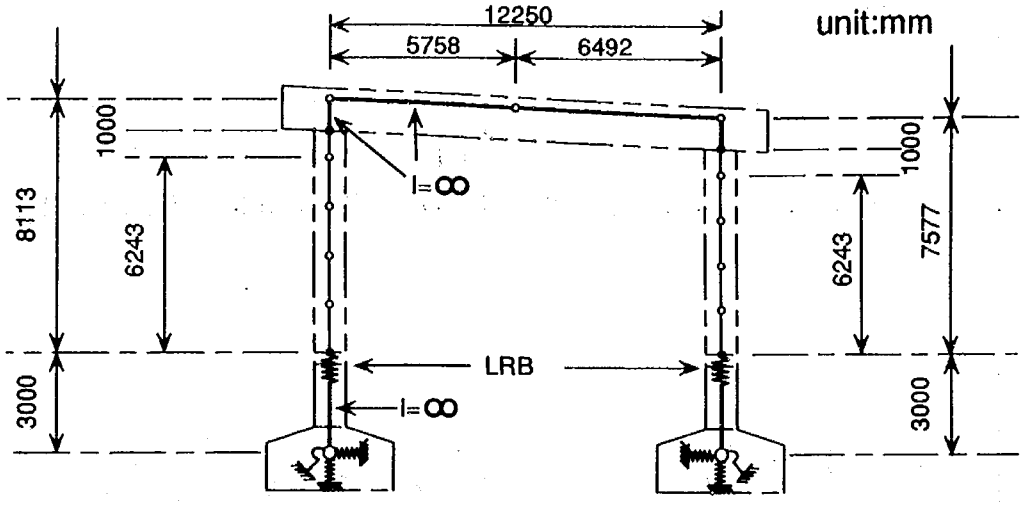


Figure 4 Transverse Model of The Viaduct

In Tests 2, 3 and 4, the horizontal displacement, axial load and rotational deformation as shown in Figs. 6, 7 and 8 are scaled down to 1/3, 1/9, 1, respectively, to fit the reduced scale of the specimen, and futhermore, scaled down to 80%, due to the loading capacity of the test equipment. The time history of 16 second as shown in Figs. 6, 7, 8 are divided into a series of 800 target values for the loading steps. The initial axial load for each test is $27.3tonf(267.3kN)$, which is equivalent to the weight of the upper part (the upper structure including the bent columns) of the viaduct.

Left direction, upper direction and counterclockwise rotation in the Fig. 2 are defined as the positive direction for horizontal displacement, axial load and rotational angle, respectively.

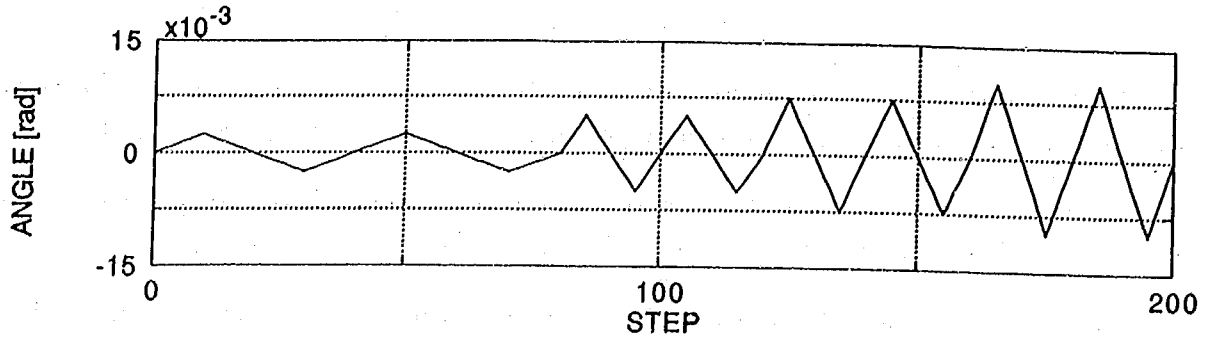


Figure 5 Rotational Angle Sequence for Test 1

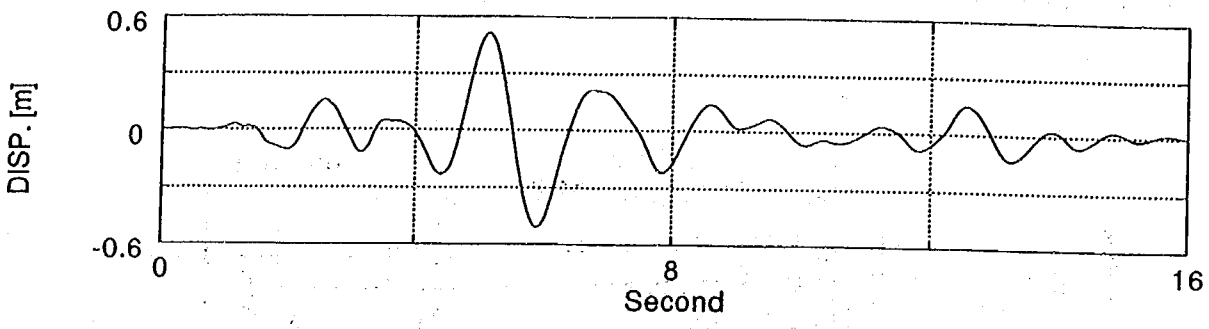


Figure 6 Horizontal Displacement Time Hisitory Obtained from Numerical Calculation

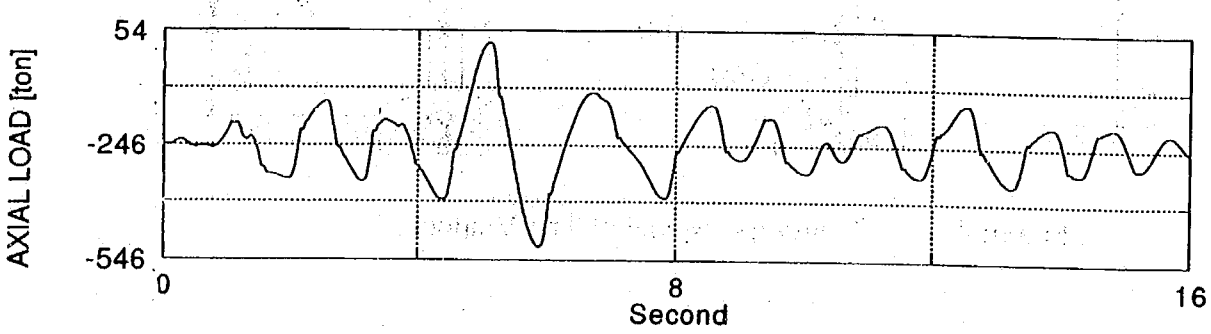


Figure 7 Variable Axial Load Hisitory Obtained from Numerical Calculation

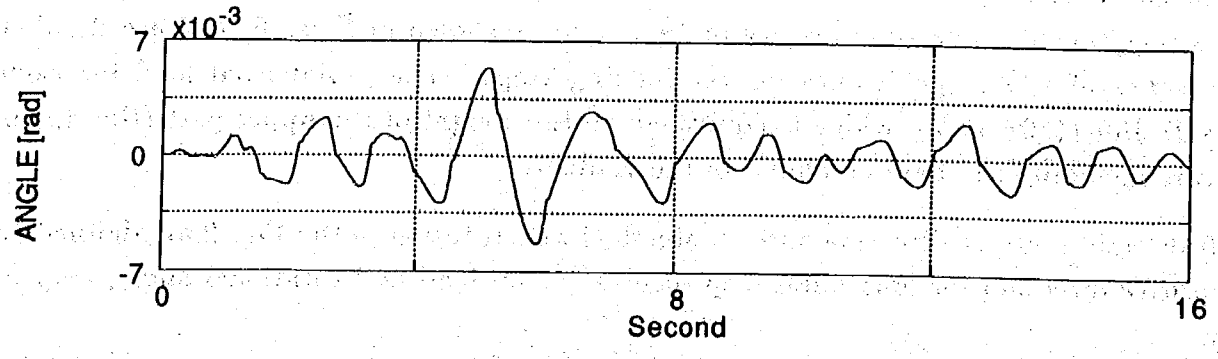


Figure 8 Rotational Angle Time Hisitory Obtained from Numerical Calculation

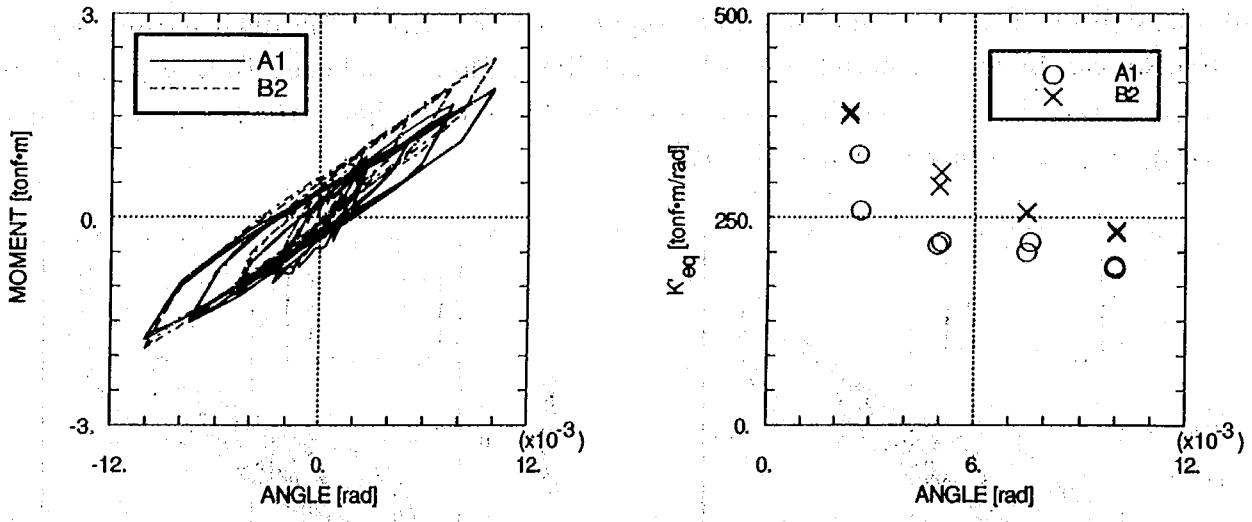
4 TEST RESULTS

In this section, the test results, namely the angle of rotation-resistance moment hysteretic response and equivalent rotational stiffness versus rotation angles obtained from Test 1, horizontal displacement-horizontal restoring force hysteresis loops, equivalent stiffness versus shear strain, equivalent damping ratio versus shear strain, and horizontal displacement-resistance moment hysteresis loops obtained from Tests 2, 3, and 4 are shown to verify the influence of the effects of variable axial load and rotational deformation.

Control errors of ACT 1, 2, and 3 throughout all the experiments were approximately $0.5mm$, $0.2tonf(2kN)$, and $0.1mm$, respectively.

4.1 Angle of Rotation and Resistance Moment

Rotational angle-resistance moment hysteresis loop obtained from Test 1 shows bilinear behavior as shown in Fig. 9 (a). Within the angle range of this experiments, so called hardening and deteriorarion of elastomer were not obserbed.



(a) Rotational Angle-Resistace Moment Hysteretic Response

(b) Angle of Rotation-Equivalent Rotational Stiffness

Figure 9 Test Result Obtaind from Test 1

The resistance moments at $10 \times 10^{-3}rad$ (the maximum angle of rotation for Test 1) were approximately $1.6tonf \cdot m$ (type A) and $1.8tonf \cdot m$ (type B), and at $5 \times 10^{-3}rad$ (the maximum angle of rotation for Test 4) the moments were about $1.3tonf \cdot m$ (type A) and $1.5tonf \cdot m$ (type B).

4.2 Equivalent Rotational Stiffness

As shown in Fig. 9 (a), rotational angle-resistance moment hysteresis loops obtained from Test 1 of all specimens show that the maximum angle of rotation and maximum resistance moment are achieved at the same loading steps. Hence the equivalent bending stiffness(K'_{eq}) can be defined by the following expression.

$$K'_{eq} = \frac{M_{max}}{\theta_{max}} \tag{1}$$

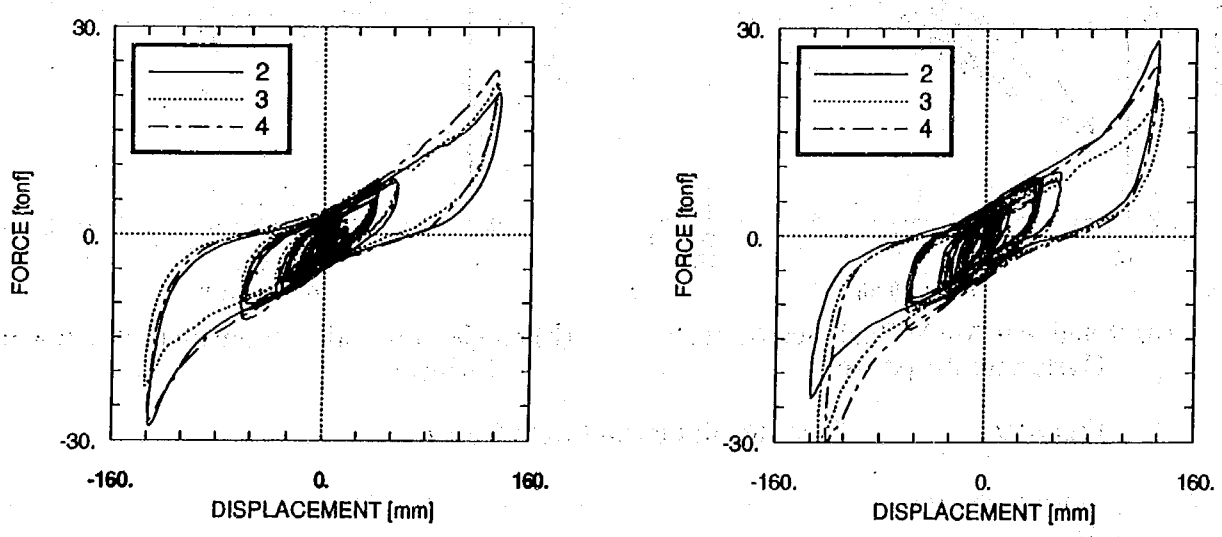
M_{max} : maximum resistance moment for each cycle
θ_{max} : maximum angle rotation for each cycle

Figure 9 (b) shows a plot of the equivalent rotational stiffness versus the angle of rotation. It shows that K'_{eq} decreases as the rotational angle becomes larger.

The value of K'_{eq} of specimen type B is slightly larger than that of type A.

4.3 Horizontal Displacement and Horizontal Restoring Force

Figure 10 shows the horizontal displacement-horizontal restoring force hysteresis response obtained from Tests 2, 3 and 4. The response curves within the deformation range of $\pm 100mm$ can be approximately described as bilinear hysteresis loops. However, hardening can be obserbed outside the displacement range of $\pm 100mm$, hence the hysteretic response develops the loops of a reverse S shape.



(a) Specimen A1 (b) Specimen B1

Figure 10 Horizontal Displacement-Restoring Force Hysteresis Loop

It should be noted that, at most of the loading steps, positeve horizontal displacement in Fig. 6 and the increase of axial load toward the positive direction take place simultaneously,

and vice versa. This implies that axial load vary to tension in the positive deformation range, and it to compression in the negative deformation range in the hysteresis loop shown in Fig. 10

The results of Tests 2 and 3 indicate that the variable axial loads cause an increase in the horizontal restoring force of the type A bearings in the positive deformation range and reduce the restoring force in the negative deformation range. However, specimen type B has the opposite tendency.

The horizontal restoring force of both specimens types takes approximetely similar or slightly larger value with the rotational loading, according to the results of Tests 3 and 4.

4.4 Equivalent Stiffness

The equivalent stifness is defined by the following expression.

$$K_{eq+} = \frac{F_{max}}{D_{max}} \tag{2}$$

$$K_{eq-} = \frac{F_{min}}{D_{min}} \tag{3}$$

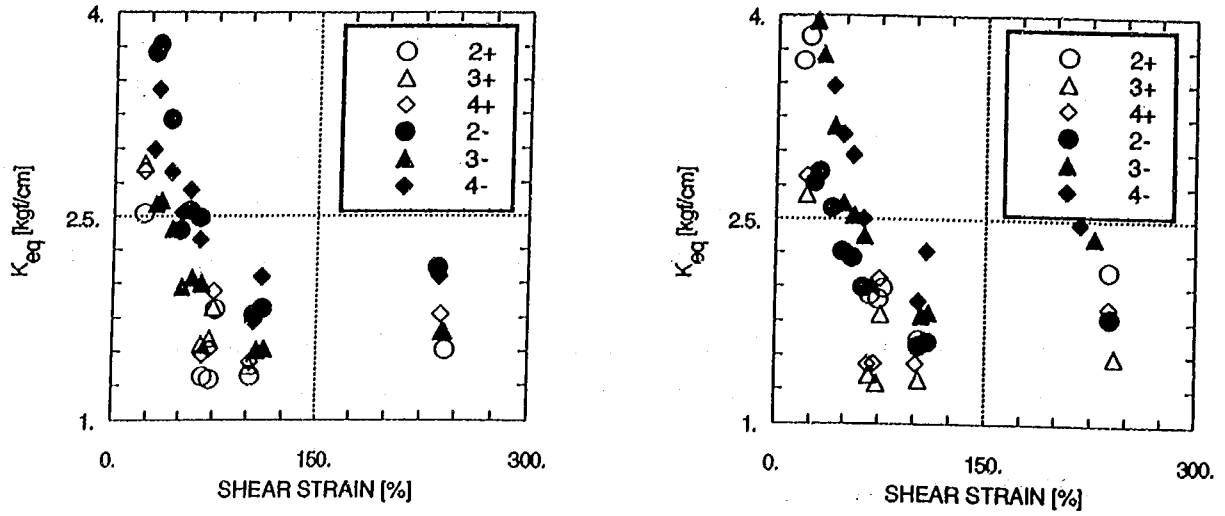
F_{max}, F_{min} : maximum and minimum restoring forces for each cycle
D_{max}, D_{min} : maximum and minimum horizontal displacements

The two types of equivalent stiffnesses are defined in order to evaluate the influence of the effect of variable axial load. K_{eq+} is the equivalent stiffness of the positive deformation range, where axial loads vary to tension. K_{eq-} is the equivalent stiffness of the negative deformation range, where axial loads vary to compression. The shear strain γ is defined as follows.

$$\gamma = \frac{Horizontal\ Displacement}{Total\ Rubber\ Thickness} \tag{4}$$

Figure 11 shows the equivalent stiffness versus shear strain plot obtained from Tests 2, 3, and 4. In the figure, test numbers with symbols '+' and '−' correspond to K_{eq+} and K_{eq-}, respectively.

Within a shear strain range up to 120%, a steep reduction of the equivalent stiffness with the development of shear strain can be seen. The eqivalent stiffness at 240% strain is slightly larger than the values at 120% strain. Although there are no data where the shear strain range between 120% and 240% (the deformation at the cycle reaching the peak amplitude is remarkably larger than that of the other cycles, see Fig. 6), it is possible to infer that the minimum value of the equivalent stiffness exists within this shear strain range. This tendency is common in all specimens and all Test types, and little difference can be seen in terms of the rate of increase and decrease among the test types.



(a) Specimen A1 (b) Specimen B1

Figure 11 Shear Strain-Equivalent Stiffness

Comparison of Test 2 with Test 3 reveals that the equivalent stiffness of type A is larger in the positive deformation range(K_{eq+}), and shows the smaller value in the negative deformation range(K_{eq-}) under variable axial loads. However, specimen of type B shows the opposite tendency.

From the results of Tests 3 and 4, no significant difference is induced by the rotational deformation in the equivalent stiffness, K_{eq+} and K_{eq-}, with the exception of the 240% shear strain case.

4.5 Equivalent Damping Ratio

The equivalent damping ratio is defined by the following expression.

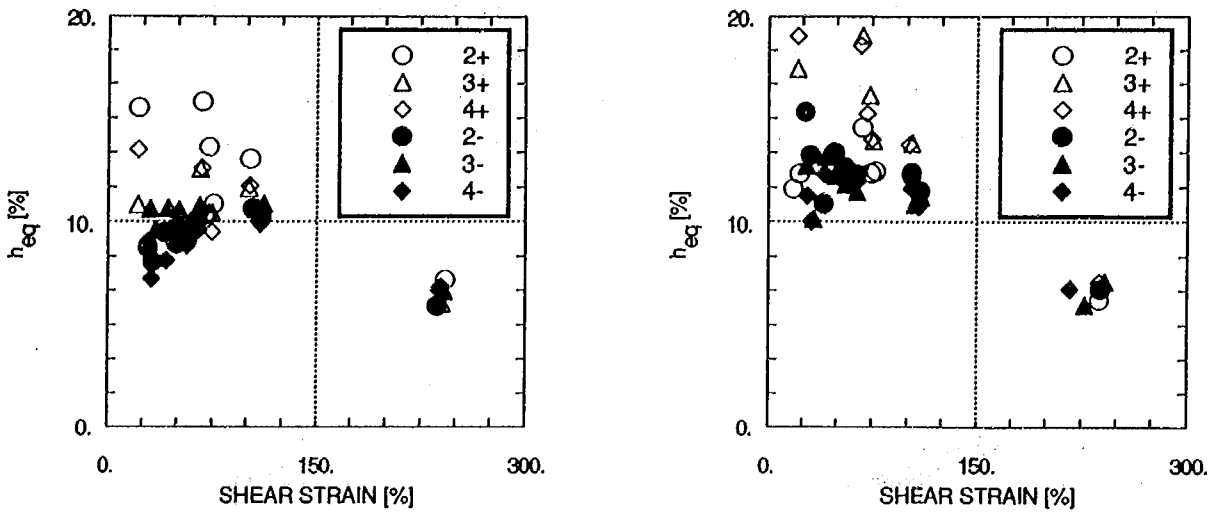
$$h_{eq+} = \frac{1}{4\pi} \cdot \frac{\Delta W_+}{W_+} \tag{5}$$

$$h_{eq-} = \frac{1}{4\pi} \cdot \frac{\Delta W_-}{W_-} \tag{6}$$

ΔW_+ : hysteretic enegy absorbed in the positive deformation range
ΔW_- : hysteretic enegy absorbed in the negative deformation range
W_+ : elastic strain enegy in the positive deformation range
W_- : elastic strain enegy in the positive deformaiton range

The two types of equivalent damping ratio, h_{eq+} and h_{eq-}, are defined in order to assess the influence of the effect of variable axial load.

Figure 12 shows the equivalent damping ratio versus shear strain obtained from Tests 2, 3, and 4. In the figures, test numbers with symbols '+' and '−' correspond to h_{eq-} and h_{eq-}, respectively.



(a) Specimen A1 (b) Specimen B1

Figure 12 Shear Strain-Equivalent Damping Ratio

In general, it is found that the equivalent damping ratio increases as shear strain becomes larger within 50%, and decreases in the shear strains exceeding 50%. The reduction of damping for type B is greater than that for type A.

Comparison of Test 2 with Test 3 in Fig. 12 indecates that the equivalent damping ratio is smaller under variable axial loads, while that of type B takes a larger value. The difference of both types of specimens between Test 2 and Test 3 reduces as the shear strain increases, and there exists little difference at the maximum deformation points. The equivalent damping h_{eq-} of type A takes larger values in almost all the shear strain range and type B takes smallr values. The magnitude of the difference of h_{eq-} between Test 2 and Test 3 is relatively small, hence h_{eq-} is less affected by the variable axial loads than h_{eq+}.

The test results of Test 3 with Test 4 indicate that the equivalent damping is smaller when the rotational deformaiton is induced for both specimens. However, at a number of points, the difference is rather negligible.

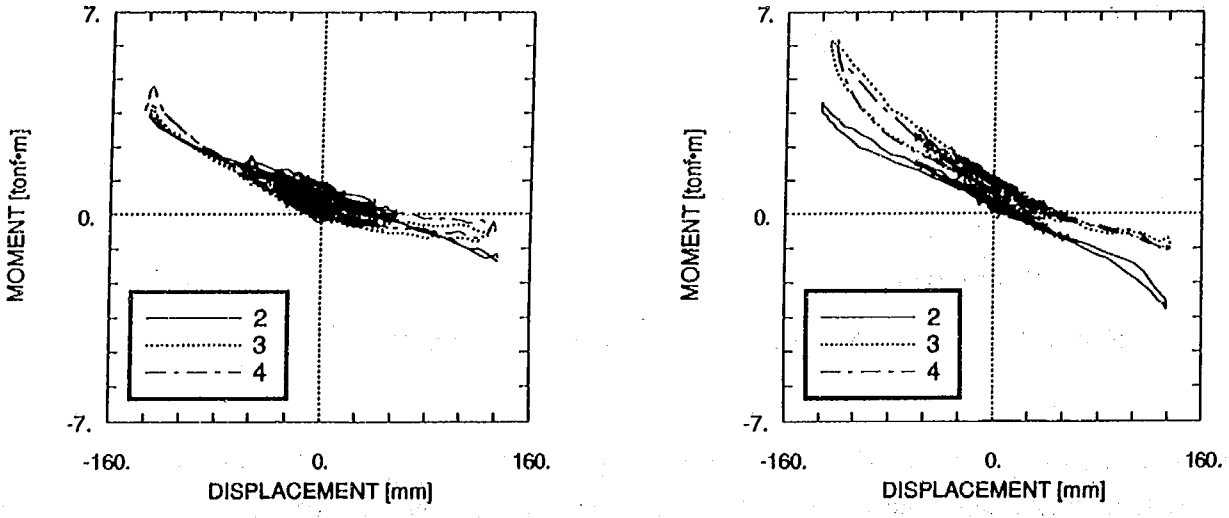
4.6 Horizontal Displacement-Resistance Moment Hysteresis Loop

Figure 13 shows the horizontal displacement-resistance moment hysteretic response obtaind from Tests 2, 3 and 4.

Comparing Test 2 with Test 3, the shape of the hysteresis loop obtained from Test 2 is alomost a straight line, and no residual horizontal displacement is observed. Whereas the

hysteresis loop of Test 3 deviates toward the positive direction of the resistance moment as the greater horizontal displacements. The resistance moment tends to decrease in the positive deformation range and increases in the negative deformation range under the variable axial loading. The resistance moments with variable axial loads decrease by 70% at the maximum positive deformation points and increase by 20% to 40% at the maximum negative deformation points with constant axial loads.

The hysteresis loops of both specimens in Tests 3 and 4 follow an almost similar pattern, indicating that the influence of the rotational deformation is smaller than that of the variable axial loads.



(a) Specimen A1 (b) Specimen B1

Figure 13 Horizontal Displacement-Resistance Moment Hysteresis Loop

Considering the angle of rotation-resistance moment hysteresis loop shown earlier, it is expected that the resistance moment under rotational deformation will vary to the negative direction in the negative deformation range. The for the opposite result of the tests may be explained by the larger magnitude of resistance moment by horizontal deformation than that by the rotational deformation, or greater influence of the effect on the loading history.

5 CONCLUSION

A series of tests of Lead Rubber Bearings (LRB) using a triaxial loading system is conducted in order to validate the preformance of LRB used in a section of Hanshin Expressway where variable axial loads and rotational deformation of the bearings are expected in the event of strong earthquakes. The hysteretic restoring force characteristics of scaled models under the simulated variable axial loads and the rotational deformation are experimentally investigated.

Based on the test results, the following conclusions have been reached.

1. In the cyclic rotational loading tests of LRB, the angle of rotation-resistance moment hysteresis loop shows the typical bileanear behavior, and equivalent rotational stiffness decreases as the rotational angle becomes larger.

2. The influence of the variable axial loads on the horizontal restoring force, equivalent stiffness, and equivalent damping ratio differs depending on the specimen type. Resistance moment increases when the axial load increases in compression. The influence of axial loads is considerably more significant than that of the rotational deformation.

3. The tests, which modelled Hanshin Expressway No.3 in Benten District, did not indicate any significant influence nor negarive influence of variable axial load and rotational deformation on the effectiveness of seismic base isolation.

ACKNOWLEDGMENTS

The authors wish to thank the engineers of Yokokawa Technology Information, Inc., Yokokawa Bridge, Inc., and OILES Industrial, Inc. for their supports and cooperation in conducting the experiments.

REFERENCES

[1] M.Hakuno, T.Okada, K.Takanashi, K.Toki, S.Ikeda, H.Iemura and T.Kitada, *Application Manual for Hybrid Experiments*, 1990 (in Japanease).

[2] Technology Center for National Land Development and Hanshin Expressway Public Corp., *Guidelines for Seismic Isolation Design of Highway Bridges*, 1989 (in Japanese).

[3] Public Works Research Institute Ministry of Construction, *Manuals for Seismic Isolation Design of Highway Bridges*, 1992 (in Japanese).

[4] Japan Road Association, *Specification for Highway Bridges (Part V Seismic Design)*, 1990 (in Japanese).

[5] Disaster Prevention Research Association, *Review of Seismic Isolation Design of Highway Bridges*, 1992 (in Japanese).

[6] Japan Construction Society, *Guidelines for Seismic Isolation Structure Design*, 1989 (in Japanese).

FIELD TESTING OF A FOUR-SPAN SEISMICALLY ISOLATED BRIDGE

by

Amir Gilani, Stephen Mahin, Gregory Fenves, Juan Chavez, and Ian Aiken

Earthquake Engineering Research Center

University of California at Berkeley

ABSTRACT

The opportunity for the field testing of an isolated bridge arose out of activities at the Interstate 680 / Route 24 interchange in Walnut Creek, California. The southern section of the temporary separator bridge is seismically isolated. The primary objective of this investigation was to collect field data for the determination of the dynamic properties of the bridge and to conduct analytical studies to verify the experimentally computed dynamic properties of the structure.

This paper provides a summary of the field testing program, subsequent data interpretation leading to the determination of the bridge dynamic properties, and the analytical studies conducted to interpret the experimental results.

INTRODUCTION

Bridge structures are often designed employing numerous assumptions regarding the bridge's response. In many cases, these assumptions have been validated on the basis of satisfactory performance of the structures under service conditions and observed bridge behavior during earthquakes. In addition, laboratory testing of components and assemblages and refined dynamic analysis have verified the viability of these assumptions. Field testing of full-scale structures, especially in the case of new construction, provides a reliable means to assess the validity of the design assumptions and the analytical models. An example of prior successful Caltrans sponsored field investigation is the testing of a segment of the I-880 Cypress bridge in Oakland, California, following the Loma Prieta earthquake in 1989 [Bollo, Mahin, Moehle, and Stephen, 1990].

Seismic isolation is being considered for the construction of bridges in California, but numerous modeling uncertainties exist in the analysis of bridges in general. Uncertainties in analysis and questions about performance may cause designers to hesitate in utilizing these new concepts. Full-scale filed tests and related analyses can help reduce these uncertainties, to address issues related to the integrity of new types of structures, and to improve design and analysis methods.

DESCRIPTION OF THE BRIDGE AND THE ISOLATION SYSTEM

The new temporary bridge carries the southbound I-680 traffic through the I-680/R-24 interchange. It is a temporary diversion for I-680 traffic while the new permanent interchange connectors are constructed below the temporary bridge. The southern end of the temporary bridge consists of a seismically isolated, four-span, 700 ft long, composite steel girder-concrete deck structure. The steel structure consists of three girders continuous over the four spans. The three bents are each a single circular column hammer head design with the three isolator bearings on the top. The circular column extends below grade in a cast-in-place drilled hole (CIDH) footing. This bridge segment is the first new bridge in California to be seismically isolated. Figure 1 shows a schematic view of the temporary viaduct, and Figure 2 and Figure 3 show the view and plan of the isolated portion of the bridge.

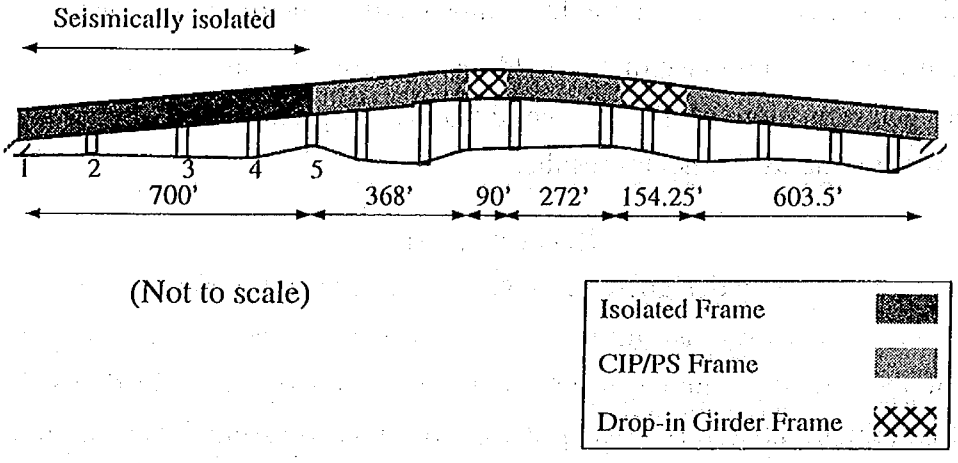


Figure1: Schematic view of the temporary viaduct

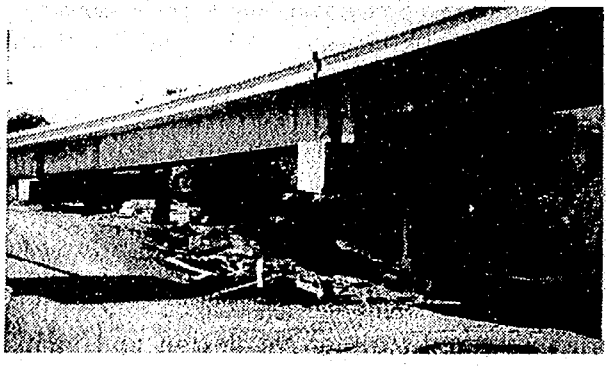


Figure 2: View of the isolated bridge

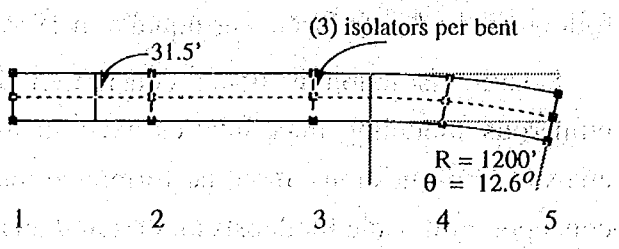


Figure 3: Plan of the isolated bridge

Assumptions and criteria used in the design of the bridge, methods employed to specify the required isolation bearing characteristics for the contract bidding process, and the typical details utilized in the construction have been previously presented [Thorkildsen, E., 1993]. The bridge was designed as if it were a permanent structure and thus it complies with all Caltrans design requirements in effect at the time of the design.

The isolation system for the bridge was designed by Caltrans, and the general performance requirements (maximum displacements, stiffness, and energy dissipation capacity) for the system were included in the plans and specifications for the structure. A peak ground acceleration of 0.60 g was assumed in the bridge design. The design spectrum is based on 10 to 80 ft of soil underlying the bridge. The isolation system, supplied by Dynamic Isolation Systems, Inc., of Lafayette, California, consists of 15 lead-rubber bearings, three per bent. The isolators were 23 inches square at bent 5 and abutment 1, and 27 inches square at the other bents. All isolators were 10-3/8 inches tall, with a 5-3/4 inches diameter lead core and a rubber thickness of 6 inches. The design displacement for the isolation system was 9.0 inches. Prototype bearings were tested to a displacement of 1.5 times the design displacement (13.5 inches). Figure 4 shows a typical hysteresis loop obtained from the test of a prototype isolator, and Figure 5 shows a view of a typical isolator.

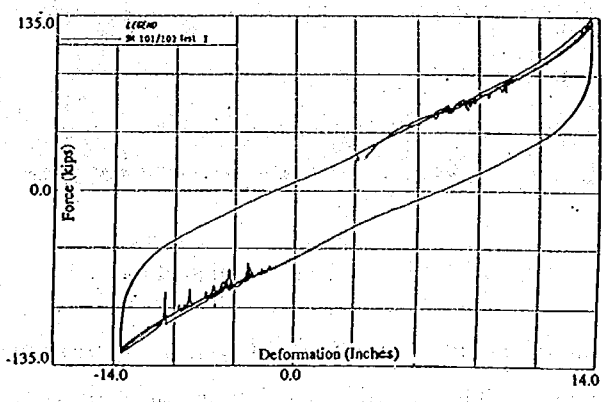


Figure 4: Typical isolator hysteresis loop

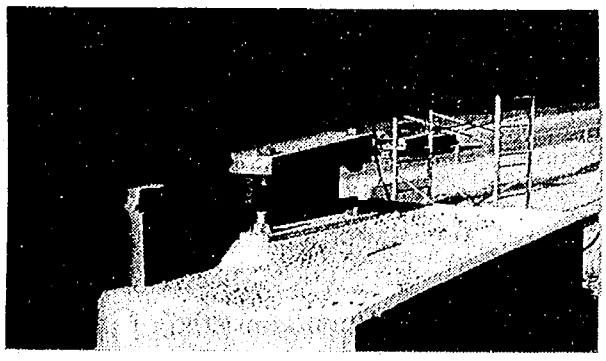


Figure 5: View of an isolation bearing

RESEARCH PROGRAM

The research program consisted of three phases. For each phase, field testing was conducted, post-test data analyses were carried out to interpret the test results, and computer analyses were performed. *Phase I* involved dynamic quick-release testing of individual bents. *Phase II* involved the forced vibration and ambient testing of the completed bridge. *Phase III* involved the snap-back free vibration testing of the completed four-span bridge.

Phase I - Bent Tests

In order to obtain the dynamic properties of individual bents, field testing of individual columns was undertaken prior to the placement of the superstructure. These tests allowed the determination of stiffness and damping characteristics of each of the four columns in the longitudinal direction. The test program for each column consisted of pullover and quick-release testing between pairs of bents.

A pair of adjacent columns were connected by means of wire cables. A hydraulic jack was used to load the wire cables slowly. Several levels of loading up to 50 kips were applied in this manner. In order to obtain good free vibration data, the applied load was released very rapidly. The quick-release was achieved by the detonation of an explosive bolt installed in the main loading cable. Figure 6 shows the test setup near bent 5, and Figure 7 shows a view of the loading system at bent 3.

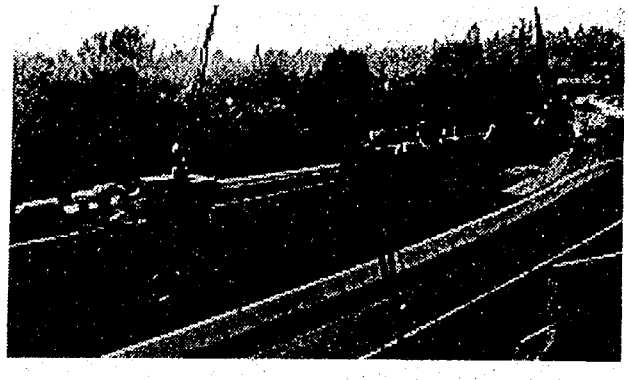


Figure 6: Quick release test setup

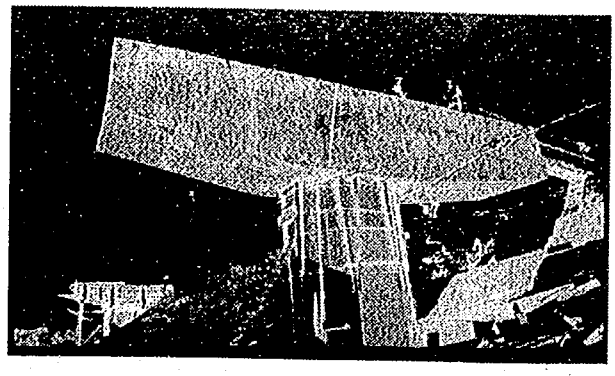


Figure 7: View of bent 3 with loading cable

The instrumentation consisted of two force balance accelerometers and range seismometers placed on top of the bent caps and at the ground level. The applied load was monitored by a digital pressure gage. Data were monitored and recorded by a portable data acquisition system and a spectrum analyzer. The typical test duration was nearly 41 seconds and data was collected at a sampling rate of 200 Hz. Peak accelerations of up to 0.25 g were induced at the top of the column bents, while accelerations at the ground level were about 25 to 40 percent of accelerations at the top.

The dynamic properties (natural frequency and damping ratio) of the columns were obtained

by calibrating a viscously damped single degree of freedom response to the measured accelerations. Figure 8 shows an accelerometer time history response and Figure 9 shows the resulting frequency domain response of bent 4 obtained from a typical test. For the three taller bents (3-5), the measured periods ranged approximately from 0.15 to 0.20 second, and the damping ratio was between 5 to 6 percent of critical. For the shorter bent 2, the measured period was about 0.11 second and damping was approximately 15 percent of critical. The column mode shapes were computed from the ratio of accelerations measured at top of the bents and at the ground level.

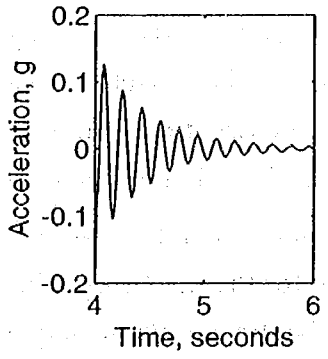


Figure 8: Time history response

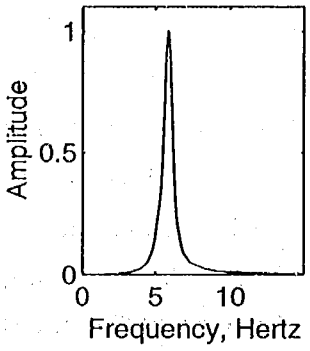


Figure 9: Fourier response

The moment-curvature and axial force-bending moment relationships were computed for the columns. For each column the maximum column bending moment due to the application of the 50 kips lateral load was smaller than the column cracking moment. Therefore, the analytical response of the columns were obtained using linear elastic modeling and the program SADSAP [Wilson, E., 1994]. The columns were modeled as cantilever elements assumed fixed at some point below the ground. The mass of each column was lumped at the top of the bent. The results of the analytical studies closely predicted the experimentally computed column properties. In addition, the experimental data compared favorably with the Caltrans assumed design values for this bridge. For example, the Caltrans calculated column vibration period of 0.19 second for a 40 ft column is very close to the measured period of column 3. The embedment depth of the CIDH shaft to the point of effective fixity of two to three column diameters, specified by Caltrans guidelines, is consistent with the values computed from the experimental results.

Table 1 provides a summery of the computed individual bent properties.

Table 1 Computed bent dynamic properties

Bent	Experimental			Analytical		No. of column diameters to point of fixity
	frequency (Hz)	damping ratio (% critical)	bent cap to ground acceleration	frequency (Hz)	bent cap to ground acceleration	
2	8.9	15.4	-----	9.0	2.1	2.4
3	5.0	5.3	3.9	5.0	4.2	2.3
4	5.8	5.9	3.9	5.8	3.4	2.4
5	5.3	7.4	2.4	5.3	2.5	3.1

Phase II - Forced Vibration Tests

The second phase of field testing involved using two rotating mass vibrating machines to apply harmonic excitations to the bridge at discrete frequencies. The dynamic properties of the bridge were determined from the measured steady state forced vibration response and from the ambient measurements taken prior and at the conclusion of the forced vibration tests.

Steel supporting frames for the mounting of the vibration generators were fabricated and placed on the bridge deck, providing a flat mounting surface for the machines. The shakers were placed approximately 20 ft north of bent 2 and 20 ft south of bent 4, approximately 340 ft apart, at about the quarter points along the length of the bridge. By altering the direction of loading, the phase between the two machines, and the rotational speed of the vibrators, a broad spectra of frequencies in the transverse in-phase, transverse out-of phase (torsional), and longitudinal directions were scanned. Figure 10 shows a vibration generator placed on the bridge deck.

Instrumentation consisted of 54 data channels with 44 force balance accelerometers and 10 wire pot displacement transducers. Pairs of accelerometers, aligned with the bridge longitudinal and transverse directions, were placed at four different levels of each bent: at the bridge deck, just above the isolators on the bottom flange of the girders, just below the isolators on top of the bent caps, and the ground. Six accelerometers were placed on the bridge deck, halfway between bents 3 and 4, close to the bridge center line, and close to the side barriers, oriented in the transverse, longitudinal, and vertical directions. A set of two wire pots at each bent cap measured the deformation of the isolators in the transverse and longitudinal directions. A portable data acquisition system was used to record the data.

The test program consisted of selecting a desired vibration input frequency and locking the vibrators at the corresponding rotational speed. The steady-state response of the bridge at the

given frequency was obtained. Some tests at a given frequency were repeated, especially close to structural resonance, to ensure the reliability of test results. Typically, successive frequencies were increment by 0.1 Hz. Close to resonance, tests were performed at finer frequency interval, producing a better definition of the modal peaks.

The experimental data were processed by fitting a sinusoidal function to each data record. Using the least squares method, the amplitude, frequency, and phase angle of the fitted curves were determined, and normalized to obtain constant-force spectrum for each record. A typical constant-force acceleration spectrum is shown in Figure 11.

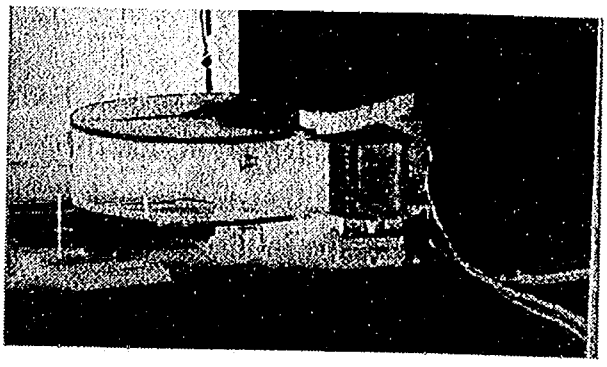


Figure 10: Vibration generator on the deck

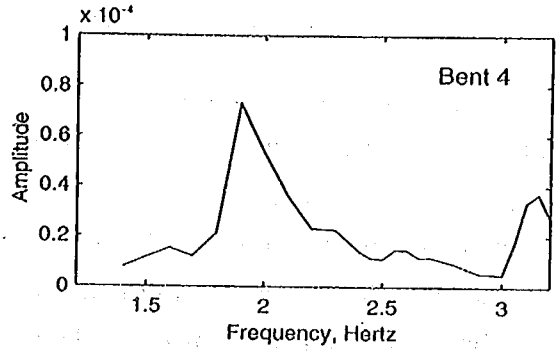


Figure 11: Typical constant-force spectrum showing the second transverse mode

Modal frequencies were obtained from the peaks of the response spectra. The peaks were generally well defined, and coincided for different data channels. The half-power technique was employed to calculate modal damping, and mode shapes were evaluated by identifying the steady-state time history amplitudes and phases.

Isolator deformations of the order of 0.01 in., a deformation level much smaller than the isolator yield deformation, were obtained during the tests. Therefore, it was expected that linear elastic analysis would predict the dynamic properties of the bridge adequately. The analytical studies were carried out using the SADSAP computer program. The superstructure was modeled as line elements and the properties of these elements were selected according to the design specifications. The superstructure weight was computed at approximately 3800 kips, and this weight was distributed among the nodes along the deck on a tributary length basis. The isolator properties were selected from the data available from the prototype tests, and the columns were modeled according to the results of Phase I tests. Equivalent axial and lateral stiffness for each bent were computed to represent the stiffness of the three isolators and the column stiffness at each bent. A summary of the experimental and analytical modal properties are presented in Table

2, and experimental and analytical mode shapes are shown in Figures 12 and 13, respectively.

Table 2 Bridge modal properties

Mode number	Principal direction	Modal frequency (Hz)			Damping ratio (% critical)
		ambient	forced vibration	analytical	
T-1	*transverse*	1.4	1.4	1.4	3
T-2	*transverse*	2.0	1.9	1.8	4
T-3	*transverse*	2.3	-------	2.2	------
T-4	*transverse*	3.4	3.1	3.3	6
L-1	*longitudinal*	2.7	2.5	2.4	5
V-1	*vertical*	1.6	1.6	1.6	

An important observation can be made from considering the various mode shapes. For the longitudinal mode shape the deformations primarily were concentrated in the isolators, corresponding to the nearly rigid, "isolated" mode shape. For the transverse modes, large deformations were observed in the superstructure corresponding to the in-plane bending of the superstructure. The difference in the behavior of the longitudinal and transverse mode shapes is due to the relative stiffness of the isolators and the superstructure. During the forced vibration tests, isolator deformations were very small, on the order of 0.01 in., in both principal directions. At this deformation level, the isolation bearings stiffness was still less than the longitudinal stiffness of the superstructure, resulting in mainly rigid body motion of the superstructure above the isolators. In the transverse direction, the isolator stiffness was on the order of the transverse flexural stiffness of the superstructure, resulting in large superstructure deformations in this direction.

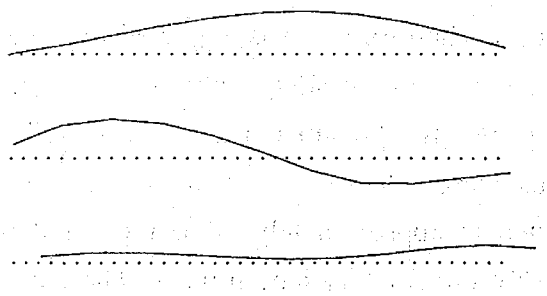


Figure 12: Experimental mode shapes

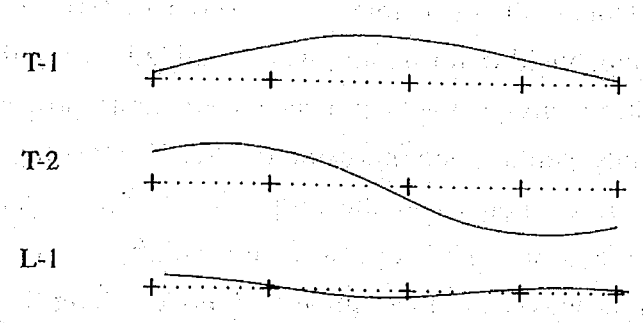


Figure 13: Analytical mode shapes

Phase III - Snap-Back Tests

The third phase of the field testing involved slowly loading of the bridge deck in the longitudinal direction. The imposed displacement was then suddenly released. From the ensuing nonlinear free vibration response, dynamic properties of the complete bridge were determined.

The isolated bridge segment was loaded by pushing off against the adjacent CIP/PS portion of the bridge. This section has a cast-in-place box girder design, and was sufficiently strong and stiff to resist the required loads. Loading was applied by four 200 ton hydraulic jacks placed in parallel. To obtain good free vibration response, quick release of the imposed displacements was essential. The success of the Phase I testing using explosive bolts led to selection of a special collapsible quick-release device as the displacement release method.

The device used, developed by ISMES in Italy, carries load in compression along its primary axis. The equilibrium of forces is maintained by the tensile force in the bolt in the direction orthogonal to the compression load. Since the device is statically determinate, release of tensile force in the bolt would eliminate its capacity to resist compression load and cause the collapse of the device. The collapse of the device was facilitated by the detonation of explosive bolts placed as the tensile member, as verified by the laboratory tests conducted prior to field tests. Figure 14 shows a view of hydraulic rams and quick release devices at bent 5 seismic gap.

A total of three snap-back tests were conducted. The low level test at a displacement of about 0.3 in. corresponded to the "yield" displacement of the isolators. The subsequent high-level tests were conducted at displacements of nearly 5.5 in., approximately two-third of the isolation design displacement. Figure 15 shows a typical isolator at bent 5 during the high-level tests.

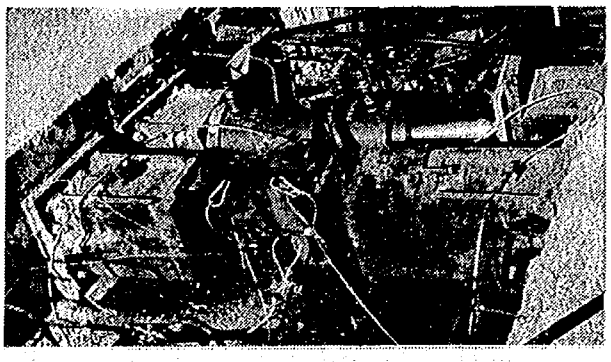


Figure 14: Hydraulic ram and collapsible device



Figure 15: Imposed isolator deformation

The applied load during the high-level tests was nearly 1200 kips. For each test, hydraulic rams were placed in position, and were loaded to the specified value. Next, the quick-release

devices were placed in position. The explosive bolts were then placed and wired to the firing unit. The hydraulic jacks were then retracted and removed. The retraction of the jacks placed the devices under compression, maintaining the imposed displacements. Free vibration was initiated by setting off the detonators from the firing unit.

Experimental data was monitored by a total of 57 channels. In addition to the instrumentation used in Phase II, global displacement transducers monitored the bridge response at several locations. These transducers measured the absolute motion of both the isolated and the adjacent CIP/PS portions of the bridge. The relative motion between the two parts was also monitored. An electronic pressure gage was used to measure the hydraulic load. Data was sampled at 200 Hz.

In the longitudinal direction, two distinct response components were identified. The first component was the wave propagation, or "superstructure" response due to the longitudinal in-plane flexibility of the superstructure. The second contribution was due to the "isolated" mode of response.The time history response across the isolators, shown in Figure 16, indicates the sequential release of imposed deformations, starting from bent 5. The time interval between release of deformations may be closely computed using the wave propagation velocity of the bridge. In addition, it is noted that shortly after the release of imposed deformations, the velocity at bent 3 is much less than the bridge ends, as is expected from the half-cosine superstructure in-phase mode shape with maxima at the ends, and a node (zero displacement) at the center. Figure 17 shows two distinct peaks in the Fourier response of the bent 5 deck acceleration for a window of time history response. The first peak at close to 1.7 Hz corresponds to the isolated vibration mode, the other peak at approximately 8.6 Hz is due to the superstructure response mode. The superstructure mode, more dominant at the initial phase of response having a much shorter period, decays out more quickly than the isolated mode, and therefore, nearly 1.5 seconds after the release of the imposed deformations the isolated mode dominates the response.

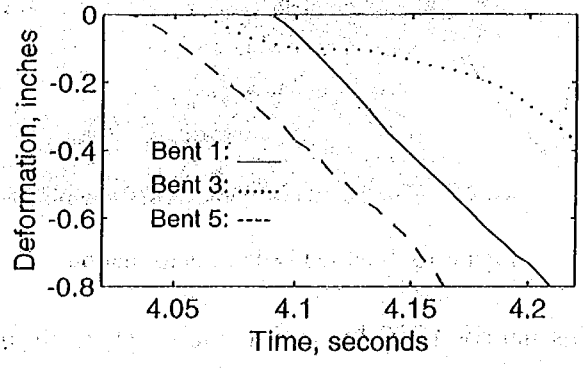


Figure 16: Release of imposed deformations

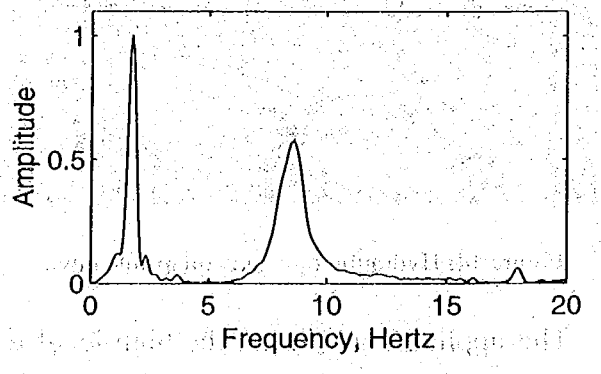


Figure 17: Longitudinal frequency response

From the decomposition of the total longitudinal response into the two distinct components, the following modal properties are obtained.

Table 3 Bridge longitudinal response modes

Mode identification	Frequency (Hz)	Damping ratio (% critical)	Mode shape description
isolated	1.7	9	rigid
superstructure	8.6	7	half cosine

In the transverse direction, the response was dominated by the in-plane bending of the superstructure, with a dominant frequency of close to 1.2 Hz and a damping ratio of 3% critical. The transverse modal properties were similar to those obtained during the Phase II tests.

The design criteria for the isolation system specified an isolator design displacement of 9.0 inches, an effective isolator stiffness of 12 kips/in., and an Energy Dissipation Capacity (EDC) (area of hysteresis loop) of 60 kip-in per isolator. At the design displacement, these specifications result in an isolated vibration period of 2.0 seconds and an equivalent viscous damping ratio of about 14% critical. The discrepancy between the design values and the experimentally computed ones can be explained by Figure 18, which is a qualitative representation of obtained experimental data. During the high-level tests, maximum isolator deformations of about two-thirds of isolator design value were attained. Shown with dashed lines in Figure 18 is the qualitative hysteresis envelope for this level of deformation. The area enclosed by this loop corresponds to the energy dissipated if the amplitude of the oscillations were about two-thirds the design displacements. The solid lines in the figure correspond qualitatively to the actual path followed by the isolation system. It is seen that the due to the small amplitude of oscillations, energy dissipation is much less than the design values. Therefore, smaller vibration periods and smaller equivalent viscous damping ratios were obtained for the "isolated" component of response.

The effectiveness of the isolation system may be estimated by considering the acceleration response just above and just below the isolators. Figure 19 shows these records for bent 4 for a two second time window. The accelerations were low-pass filtered to highlight the "isolated" mode response. It is seen that the bridge accelerations are attenuated by the isolation system, and the isolated vibration frequency is 1.7 Hz.

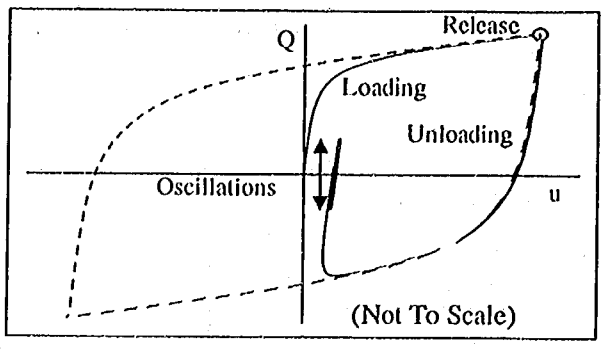


Figure 18: Qualitative isolation system response

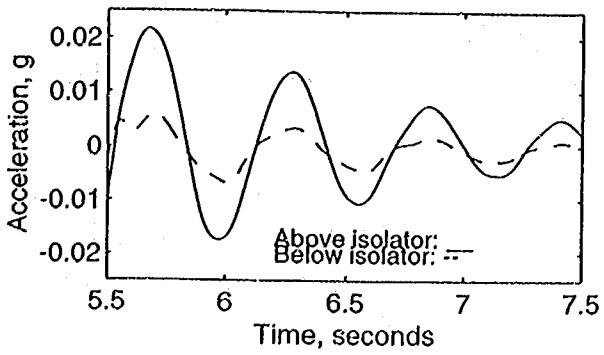


Figure 19: Acceleration records at bent 4

Nonlinear dynamic analysis were conducted to estimate the longitudinal free vibration response of the bridge during the Phase III high-level tests. The superstructure was modeled as a one dimensional elastic continuum, the column properties were selected from Phase I results, and the isolators at each bent were modeled as bilinear elements and their properties were based on the prototype test results. Figure 20 shows the plots of total longitudinal deck force versus deck displacement. The bilinear model closely predicted the force and displacement values. Due to the limitation of the model, the complete experimental response is only approximated.

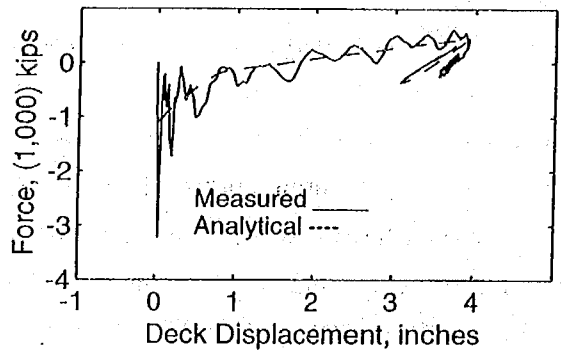


Figure 20: Bridge force-deformation response

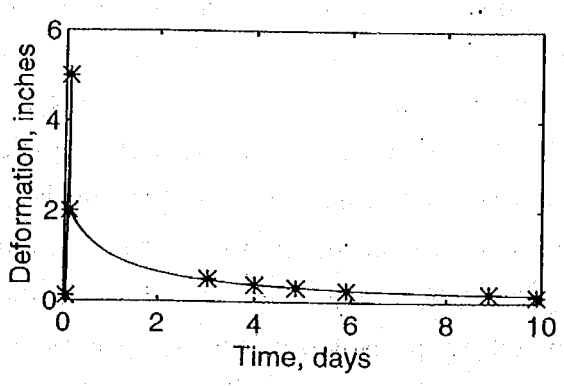


Figure 21: Recovery of a typical isolator

To monitor the response of isolators accurately, the pre-test deformation of the isolators, their deformation during the tests, and their behavior subsequent to the test completion were compiled. After the completion of both high-level tests, some residual deformations were present in the longitudinal direction of the isolators. It was anticipated that this residual displacement would

diminish quickly in time and would also be temperature dependent, as indicated in Figure 21 for a typical isolator (east isolator at bent 3).

SUMMARY

The field testing program provided a reliable mean of determining the dynamic properties of the bridge and its components. For typical taller bents, modal frequencies of close to 5 Hz and damping ratios of near 6% critical were obtained. The bridge transverse response was dominated by in-plane modes with the fundamental mode having a frequency of close to 1.4 Hz In the longitudinal direction, the modal properties were highly dependent on the amplitude of imposed vibrations. The frequency of the longitudinal "isolated" mode was 2.5 Hz during the forced vibration tests and 1.7 Hz during the snap-back tests. During the latter tests, longitudinal superstructure modes were observed. The fundamental frequency for this mode of response was 8.6 Hz, closely predicted from wave propagation frequency of the superstructure. The available analytical models were able to predict reasonably the linear and nonlinear response of the bridge. The experimental and analytical values were in agreement with the design analysis results, at the imposed level of isolator deformation.

ACKNOWLEDGMENTS

The work described in this paper was funded by the California Department of Transportation, under contract RTA-59A018. This support is gratefully acknowledged. Guidance and motivation provided by the Caltrans project monitor, Eric Thorkildsen, is greatly appreciated. The assistance of Fadal Allamadine, George Amaro, John Hicks, Pete Seigenthaler, and Michael Traffalis, all of Caltrans, is also acknowledged.

The authors would like to extend their appreciation to Drs. Changrui Yin, Juan C. De la Llera, Jose Inaudi, Marcial Blondet, and Jerry Dimsdale of U.C. Berkeley and EERC for their significant contributions to this project.

The authors wish to acknowledge the assistance of Dr. G. Bonacina of ISMES s.p.a., Bergamo, Italy, in generously making the collapsible devices available for this test program. Ron Varosh and Bert McDonald of RISI provided invaluable assistance in the development of the explosive bolts.

REFERENCES

- Bollo, M., Mahin, S.A., Moehle, J., and Stephen, R., "Observations and Implications of Tests on the Cypress Street Viaduct Test Structure," *Report No. UCB/EERC-90/21,* Earthquake Engineering Research Center, University of California at Berkeley, Berkeley, California, December 1990.
- Gilani, A.S., Mahin, S.A., Fenves, G.L., Aiken, I.D., and Chavez, J.W., "Field Testing of Bridge Design and Retrofit Concepts, Part 1 of 2: Field Testing and Dynamic Analysis of a Four-Span Seismically Isolated Bridge in Walnut Creek, California," *Report No. UCB/EERC-95/14,* Earthquake Engineering Research Center, University of California at Berkeley, December 1995.
- Jones, D.M. and Choudhury, D., "Isolation System Design and Specification for the Olympic Boulevard Off-Ramp," *Proceedings of the 3rd U.S.-Japan Workshop on Earthquake Protective Systems for Bridges*, Berkeley, California, January 1994.
- Thorkildsen, E., "Caltrans Seismic Design and Future Concepts," *Proceedings of the 1st U.S.-Japan Workshop on Earthquake Protective Systems for Bridges,* Technical Report NCEER-92-0004, National Center for Earthquake Engineering Research, State University of New York at Buffalo, 1992.
- Wilson, E.L., "SADSAP User Manual" Structural Engineering Mechanics and Materials, Department of Civil Engineering, University of California at Berkeley, 1992.

ENHANCEMENT OF LATERAL SEISMIC LOAD DISTRIBUTION IN CONTINUOUS GIRDER BRIDGES: TEST OF STIFFENING AND DAMPING COMPONENTS OF A NEW DEVICE

William TANZO
Assoc. Professor, Dept. of Civil and Environmental Engg.
Saitama University, Japan

Jaime HERNANDEZ Jr.
Masteral Student, Graduate School of Science and Engg.
Saitama University, Japan

Hiroshi MUTSUYOSHI
Professor, Dept. of Civil and Environmental Engg.
Saitama University, Japan

Akio TSUZUKI
Engineer-in-Charge, Technology Dept.
Kawaguchi Metal Industries Co., Japan

ABSTRACT

The safety of continuous span bridges during strong earthquake can be enhanced by distributing the large inertial forces on all substructure components. A new device is being developed which enables lateral loads to be transmitted to piers supporting movable bearings of a bridge during earthquakes but will not interfere with the behavior of the bridge under normal operating conditions. This device not only effectively distributes the lateral load but also dissipates a portion of the earthquake input energy through damping. Tests were made on the stiffening and damping component of the device separately. The stiffening component uses silicone putty compound while the damping component uses high-damping rubber.

To establish the properties of the stiffening component, a simple cylinder-piston assembly packed with silicone putty was first tested for its cyclic mechanical behavior with different piston sizes and different silicone compounds. In addition, the effect of imperfect packing was also investigated experimentally. Test results have shown that the stiffening component can provide for various design amenabilities with desired load-transmitting frequency and desired load-distribution ratios among the piers. A simple-span bridge model fitted with the stiffening component was then tested, and the effectiveness of the device in distributing seismic lateral loads to the piers has been shown.

In establishing the properties of the damping component, a cylindrical bushing of high-damping rubber material was vulcanized in-between two hollow metal cylinders which was then connected to a shaft. From the test results, it has been shown the rubber materials used possess sufficient damping capacity and has very stable hysteretic behavior.

1. INTRODUCTION

Bridge failures and damages during the 1994 Northridge and 1995 Hyogoken-Nanbu Earthquakes can be characterized by span fall-off and severe damage on just a few lateral load-resisting elements, i.e. piers and substructures supporting fixed bearing supports;

while piers supporting movable supports remained undamaged. Even bridges which were retrofitted with joint and hinge restrainers experienced fall-of-span because restrainers are not designed to improve the seismic resistance of the entire bridge but simply to hold on the girders which are about to be displaced off the supports.

Restrainers used at present are typically passive within the gap distance designed to accomodate allowable movement of the bearing supports. For displacement beyond this distance, added stiffness is provided by the restrainers to prevent fall of span due to excessive relative displacement. However, no satisfactory methods have been developed for designing the strength and stiffness of restrainers [Priestley et al, 1996]. Also, a study by Saiidi et al [1996] concluded that the current design procedure used in the United States (California 1990, 1991) needs to be modified to better represent the dynamic behavior of bridges.

In order to enhance the behavior of bridges under earthquake loading, the solution generally accepted is to distribute the lateral forces among all the supporting piers. This can be done by placing a device which utilizes the frequency-dependent properties of silicone putty - a compound which easily deforms under slow loads but will stiffen under shock and impulsive loads. The addition of a damping component to the device will greatly improve the performance of bridges during strong earthquakes as energy can be effectively dissipated lessening the demand on the device and the supporting piers.

The stiffening component using silicone putty, has been tested for its cyclic mechanical behavior as well as its effectiveness in a simple span bridge model. Results are presented in this paper. Test results of the damping component using high-damping rubber are also presented. Load deformation characteristics and frequency dependence of the equivalent damping and stiffness of the damping component were investigated.

2. A NEW DEVICE WITH DAMPING FOR SEISMIC LOAD DISTRIBUTION AND DISSIPATION

A few devices (e.g., rubber bearings, oil dampers, viscous shear dampers, ...) have been developed for seismic lateral load distribution with each offering several advantages and disadvantages in various aspects of performance, maintenance, reliability, and simplicity in construction as well as in design. The main objective of this research is to develop a device with similar functions, but possessing robustness that can better withstand adverse conditions and requiring minimum maintenance.

A device known as shock transmission unit (STU) has been developed using a special silicone compound, which upon receipt of a sudden impact load locks up and transmits the load through the structure [Stephen Brown, 1996]. This device has been placed at the expansion piers of the London Docklands Light Railway in order to distribute the braking forces between all piers of the supporting structure.

Offering several advantages primarily in performance and maintenance, a new device is being developed combining the favorable properties of silicone putty and high-damping rubber. The device is designed to be attached to the underside of the girder near a movable support and the top of the pier. In such an arrangement, it allows movement of the movable support during ambient temperature gradients, but will fix the girder-pier connection during shock or earthquake loadings and thereby transmitting a share of the lateral load to the piers with movable supports (Fig. 1). With the presence of the damping component, the device not only effectively distributes the lateral forces on all the supporting piers but also dissipates part of the energy which would otherwise be transmitted to the supporting piers.

During normal operating conditions, the silicone putty will flow slowly allowing an in-

ner shaft in the device to move freely thereby causing no interference on slow structure movements, e.g. temperature change, shrinkage, etc. However, once the device recieves a sudden impact load, the silicone putty will react as a solid restraining the inner shaft. This results in the activation of the damping component via the high-damping rubber which dissipates a part of the energy input, resulting in lesser energy transmitted to the pier.

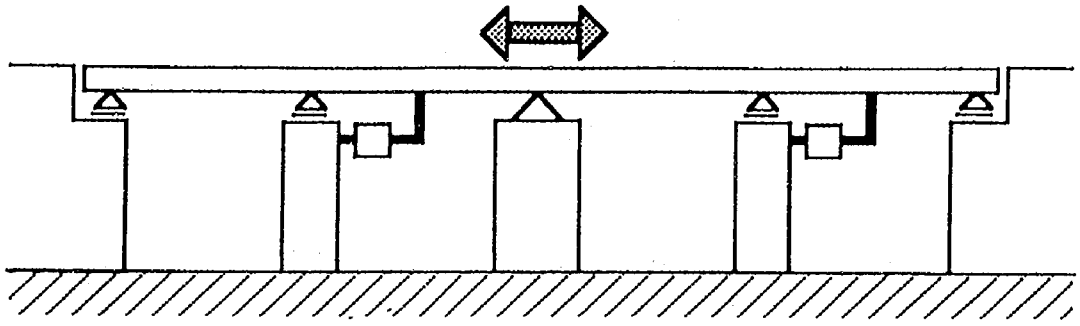


Fig. 1 A Continuous Girder Bridge with Load Transmission Devices

3. CYCLIC MECHANICAL BEHAVIOR OF THE STIFFENING COMPONENT

Preliminary objective is to investigate the basic mechanical behavior of a device with the stiffening component under cyclic loads. From these results, suitable putty compounds and device configurations are evaluated and improvements are made to obtain the desired device performance. A device has been developed consisting of a piston inside a cylinder housing filled with silicone putty compound to test its stiffening properties (shown in Fig. 2). A 10-tonf capacity has been fabricated and subjected to repeated cycles of force-controlled and displacement-controlled loadings with different amplitudes and frequencies.

The device was first tested under force-controlled loading under different frequencies (0.001 Hz to about 5. Hz). Load-deformation characteristics are shown in Fig. 3.

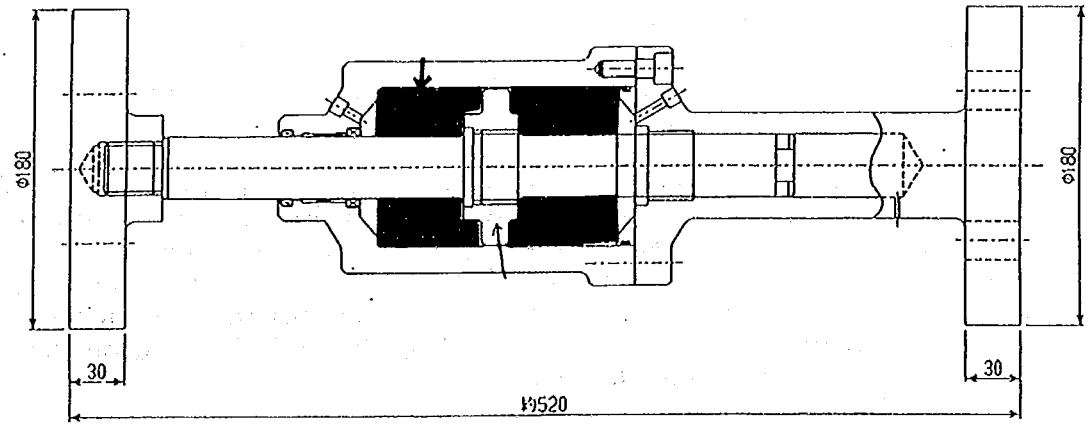


Fig. 2 Stiffening Component Device

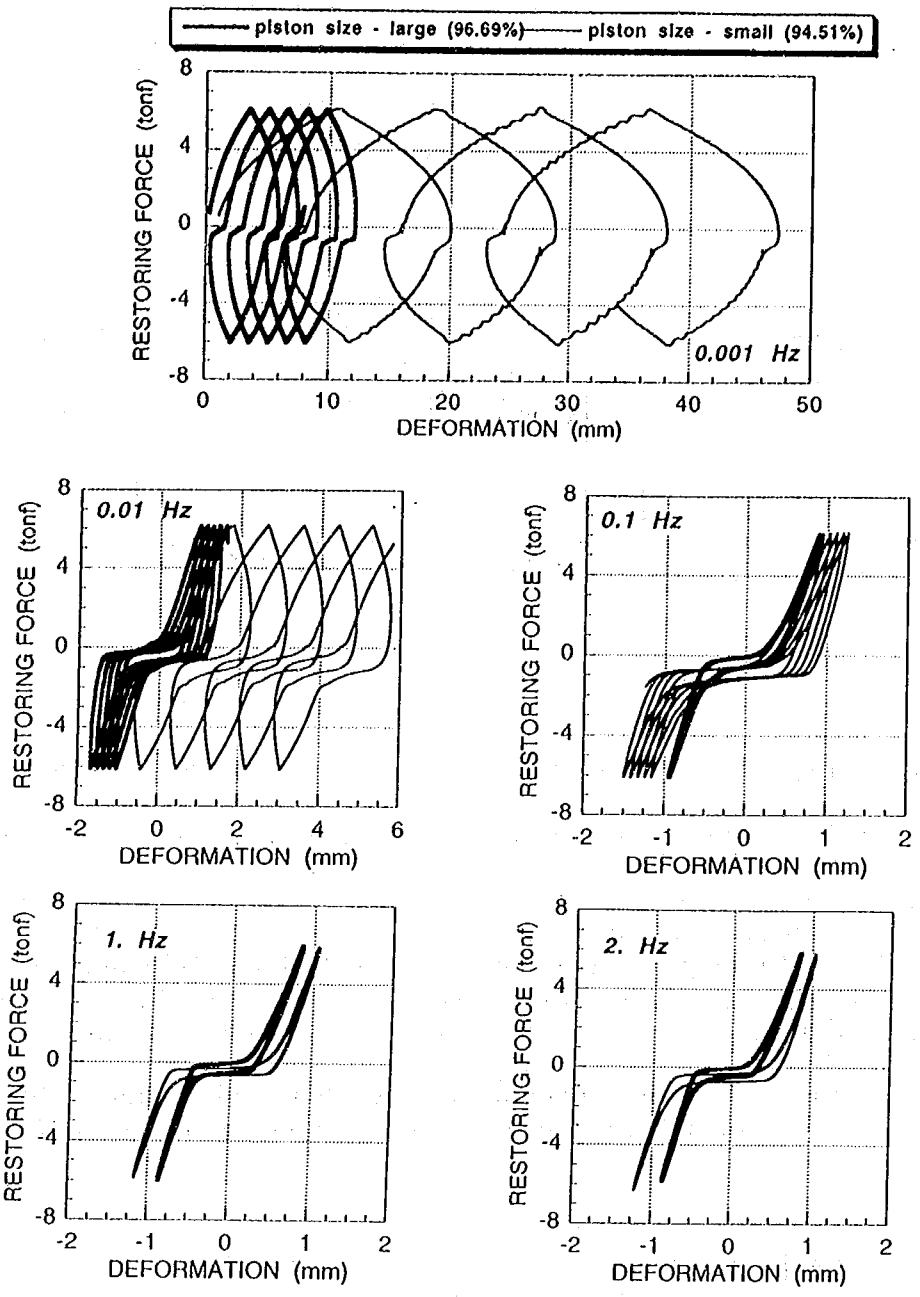


Fig. 3 Load-Deformation Behavior of Stiffening Device with Different Piston Sizes

It can be observed that the silicone putty readily allows deformation with significant hysteretic damping under low frequencies. Hystereses in Fig. 3 plotted with bold lines is for a device with a relatively bigger piston (smaller orifice) and relatively harder putty. Stiffening effect is exhibited at about 0.1 Hz. Beyond 0.1 Hz, no remarkable changes in the load-deformation behavior can be observed. That is above 0.1 Hz, the silicone putty acted almost like a rigid body and stiffness is provided by the load-deformation characteristics of the end rod of the cylinder and the piston.

The load-deformation curves under two cases of displacement-controlled loading are shown in the plots in Fig. 4. It can be observed that load induced (from about 5 tonf for 5 Hz case) is significantly reduced (to less than 0.7 tonf for 0.001 Hz case) when subjected to slowly applied loads. Under service loads due to temperature changes, a displacement-controlled cyclic loading with a period of 24 hours simulating daily temperature change or a period of one year for annual temperature change would have induced almost no load

resistance at all. In other words, the stiffening device does not interfere with the normal functioning of the movable bearings in relieving stresses due to elongation and contraction of the girders resulting from ambient temperature changes.

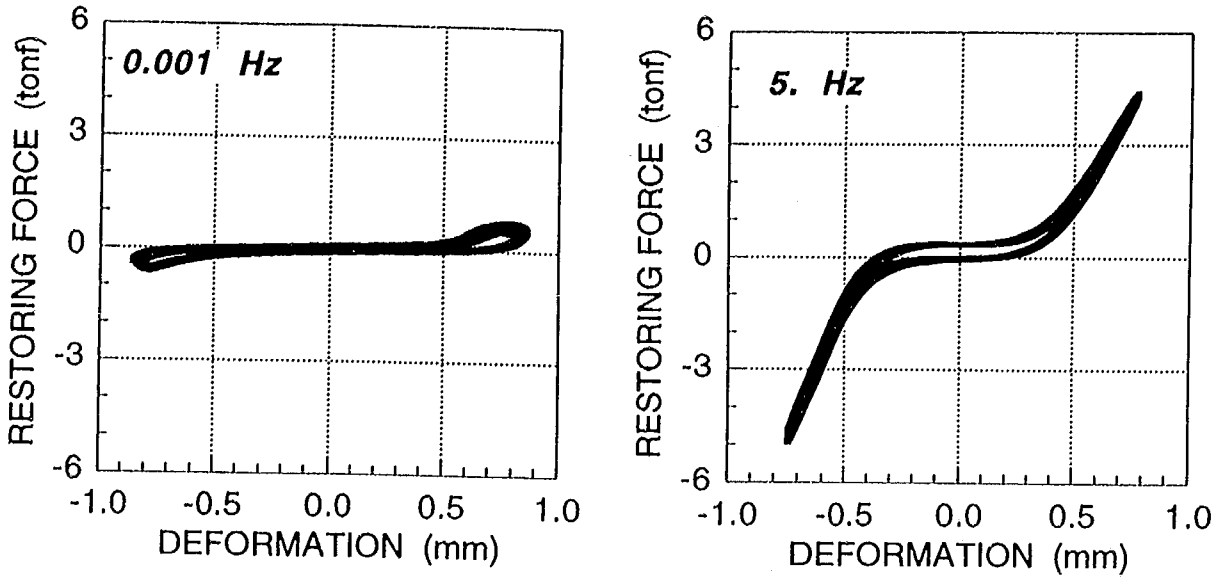


Fig. 4 Load-Deformation Behavior Under Displacement-Controlled Cyclic Loading

In order to investigate the effect of orifice sizes, the same stiffening device was then fitted with a smaller piston which would permit easier passage of the putty when squeezed. Results are shown in the hystereses plotted witth the thinner lines in Fig. 3. It can be observed that the piston was easier displaced inside the putty-filled cylinder and stiffening was initiated at a much higher frequency of about 1. Hz. Thus, the desired frequency at which stiffening is initiated to allow lateral load transmission may be set with the appropriate piston size.

Silicone putty compounds can be manufactured with different 'flow' properties. A 'softer' putty was packed into the device with the larger piston and its load-deformation hystereses (plotted with thinner lines in Fig. 5) are compared with the previous case of a 'harder' putty. It can be observed that the piston was easier displaced inside the putty-filled cylinder and stiffening was initiated at about 0.2 Hz. Thus, the desired frequency at which stiffening is initiated to allow lateral load transmission may be set with the appropriate rheological property of the silicone putty. In order to take advantage of this property, further investigation in rheological properties of putty compounds using appropriate tests [Ward and Hadley 1993] is needed to relate the material properties to the mechanical properties of the intended device.

It can be observed that slip-type behavior in the vicinity of the low load range in the load-deformation curves exists. This type of slip hysteresis is not desirable in that effective load transmission is not achieved within this interval. While it is not possible to ascertain at this stage all the exact causes of this slip, undoubtedly imperfect packing is one factor. This was investigated by testing the device filled with a proportion (90%) less than the maximum putty content to fill fully. Hystereses plotted with thinner lines in Fig. 6 shows the load-deformation behavior of a device with intentionally imperfect packing. A wide slip of constant width can be seen in all the hystereses.

The test results have shown that a device fitted with the stiffening component can provide

for various design amenabilities with desired load-transmitting frequency and desired load-distribution ratios among the piers. Proper characterization of the device configuration and the silicone putty properties should be the next important step in the investigation in order to better quantify the device performance.

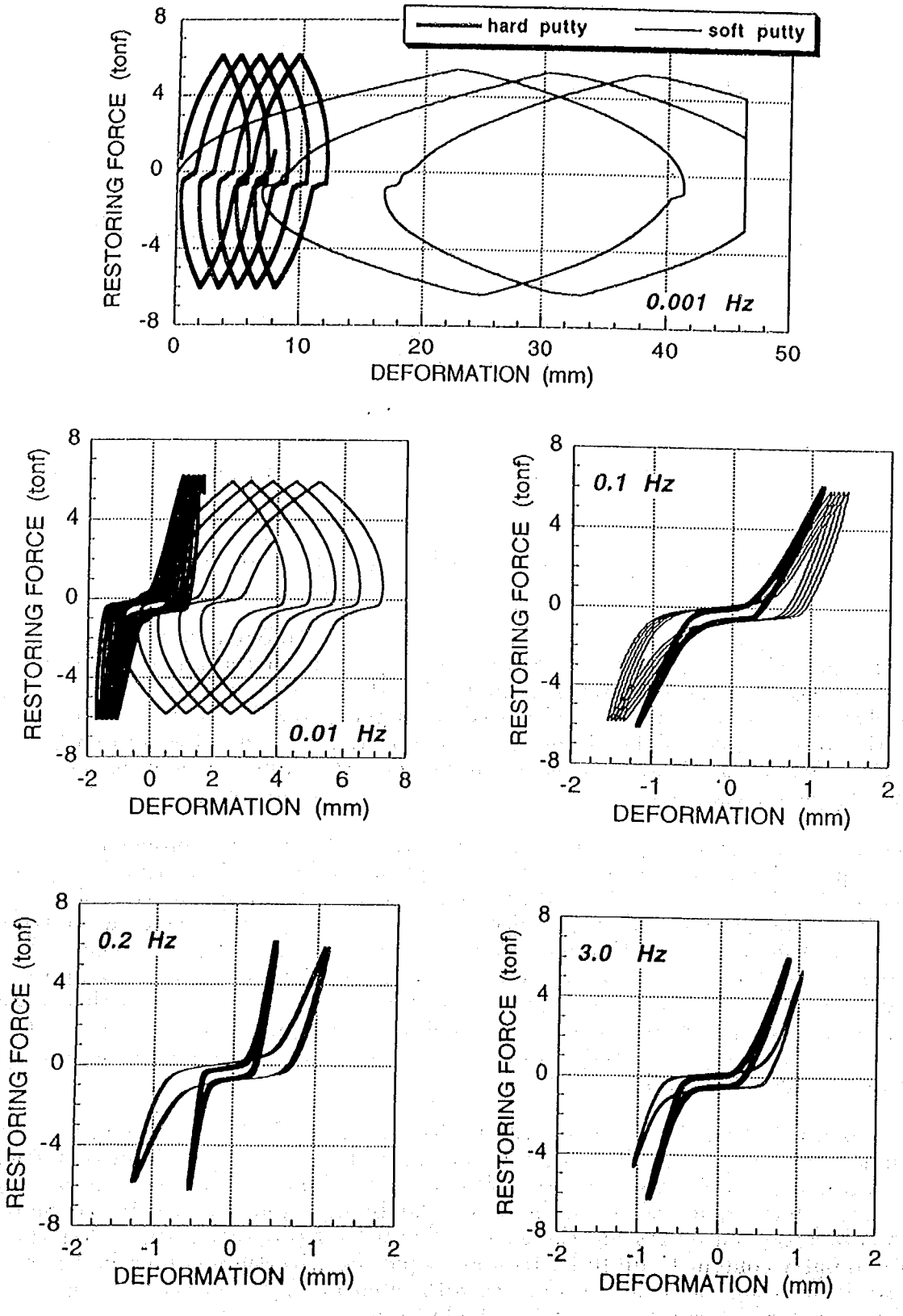


Fig. 5 Load-Deformation Behavior of Stiffening Device with Different Putty Properties

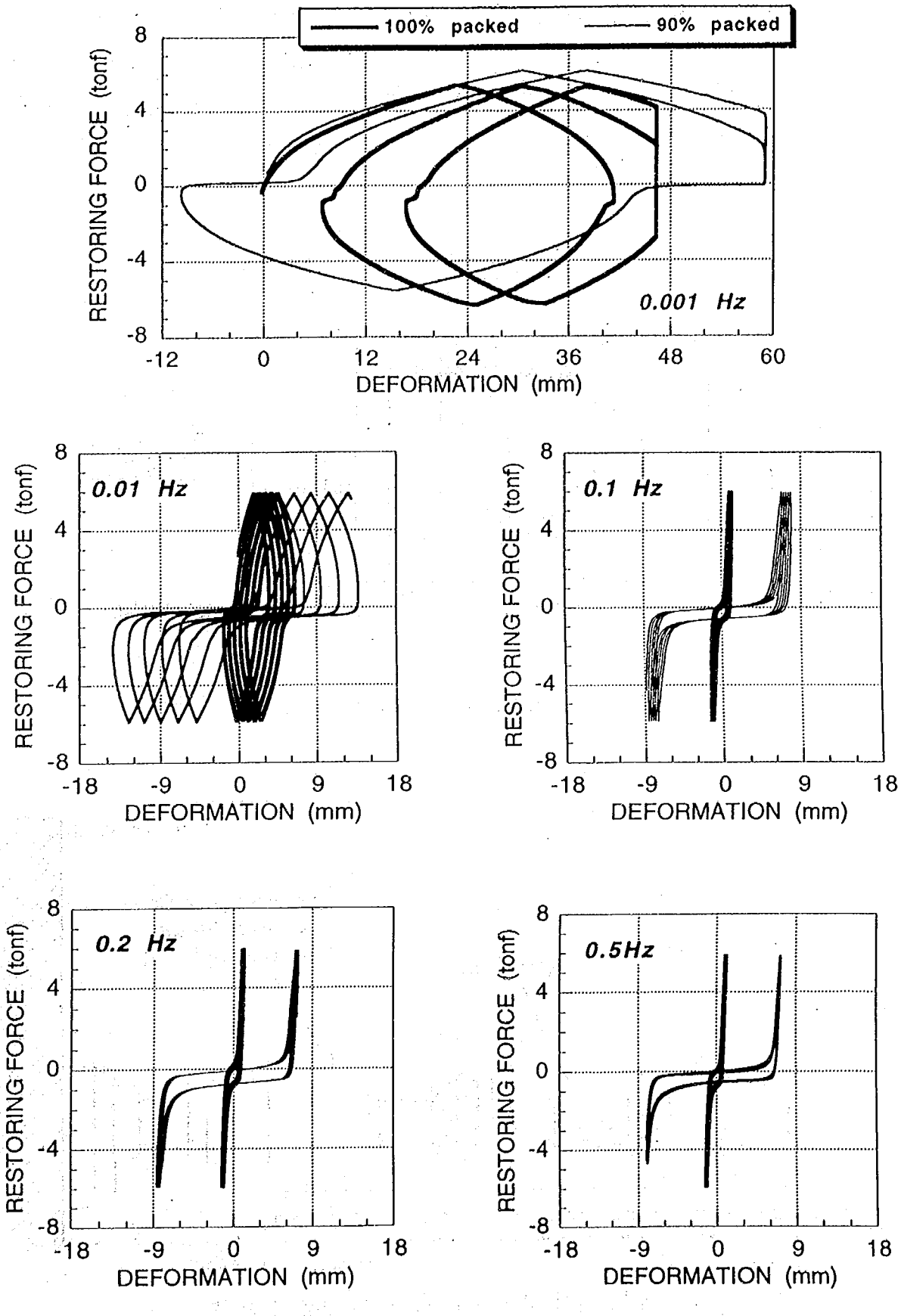


Fig. 6 Effect of Imperfect Packing of Putty Inside the Cylinder

4. CYCLIC MECHANICAL BEHAVIOR OF THE DAMPING COMPONENT

Testing of the damping component of the new device is made using a cylindrical bushing of high-damping rubber vulcanized in between two hollow metal cylinders which allows connection through a shaft in the assembly. Fig. 7 shows the assembly while Fig. 8 shows the schematic diagram of the testing system. The assembly was subjected to increasing amplitude displacement waves at varying frequencies and number of cycles.

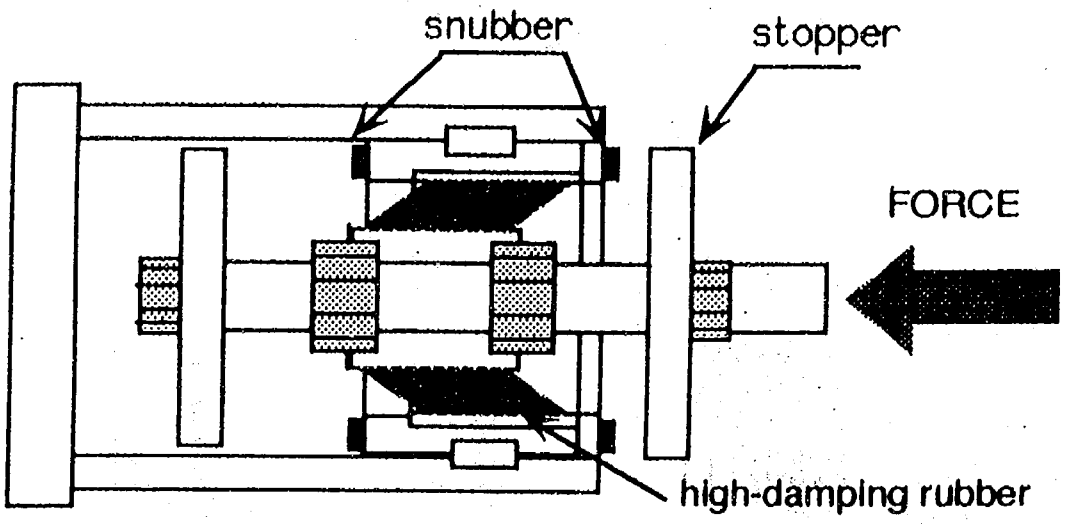


Fig. 7 Damping Component Assembly

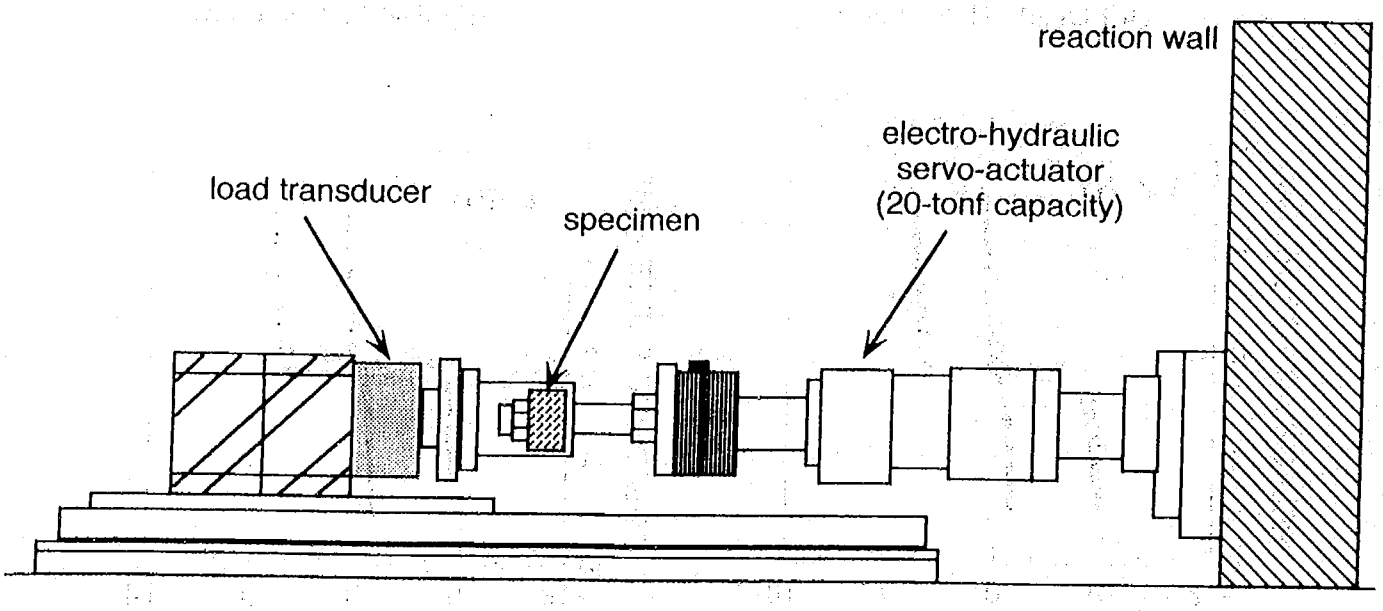


Fig. 8 Schematic diagram of the testing system

The force-deformation plots are shown in Figs. 9–12 for the 0.01 Hz, 0.1 Hz, 0.5 Hz, and 1.0 Hz tests, respectively.

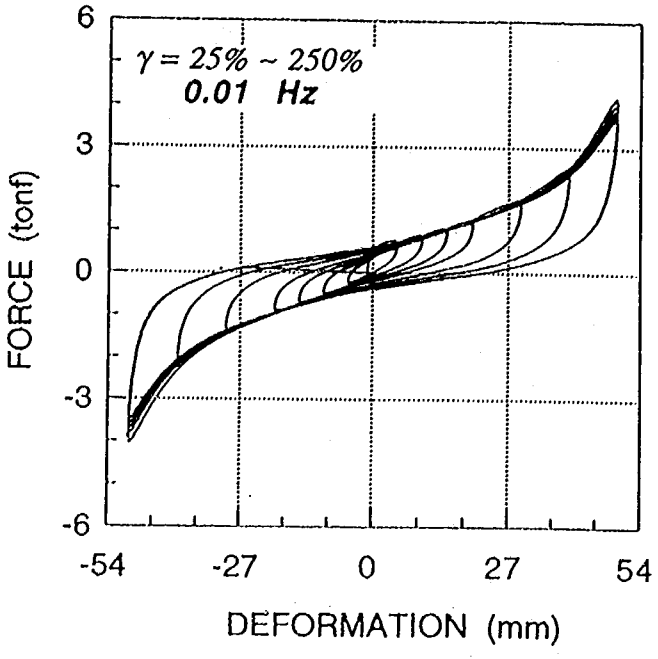


Fig. 9 Hysteresis for 0.01 Hz

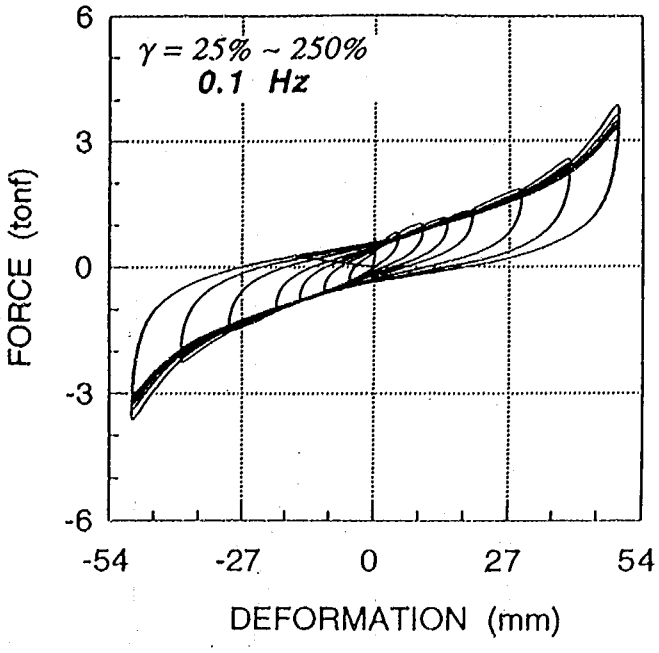


Fig. 10 Hysteresis for 0.1 Hz

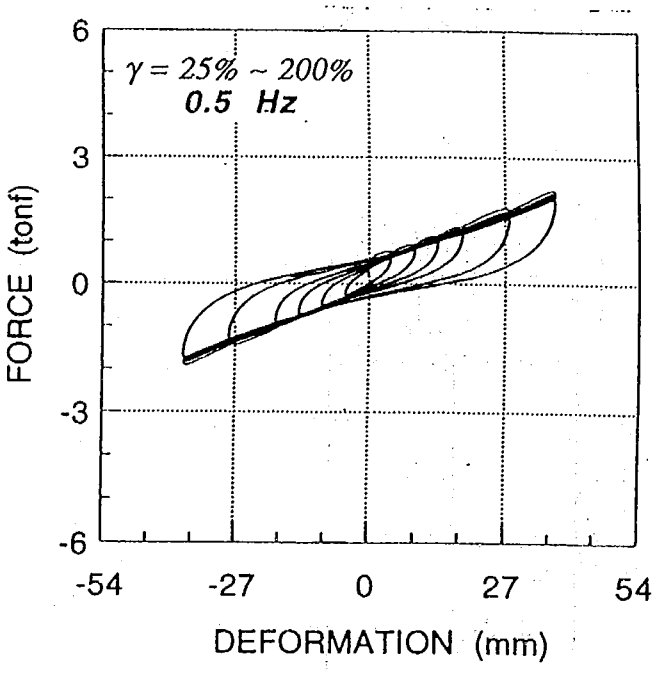


Fig. 11 Hysteresis for 0.5 Hz

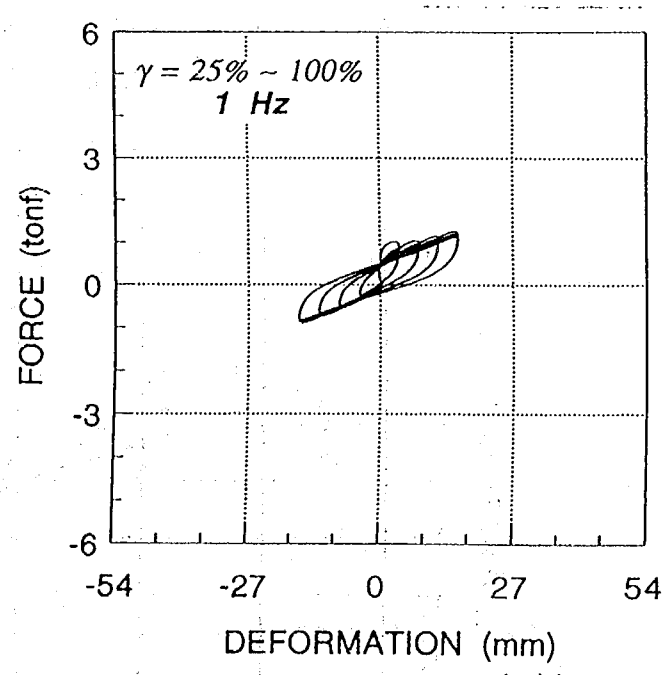


Fig. 12 Hysteresis for 1.0 Hz

The assembly shows very stable hysteresis loops in all frequencies and strain levels; as can be noted, there is almost perfect coincidence of the number of repetitions of cyclic loading except for some minor capacity deterioration in the final stages of the cyclic loading. Strain hardening is initiated at about 150% shear strain. In the high frequency range, due to the limitation of the actuator, loading up to 250% shear strain was not attained. But still, good hysteresis loops were drawn from the early stages of the cyclic loading.

The equivalent stiffness and viscous damping ratio were plotted on Figs. 13 and 14 for all the different frequencies used in the experiment. Fig. 13 shows an increasing equivalent

stiffness beyond the 150% shear strain which is the inherent hardening of rubber material at high strain. Fig. 14 shows the high level of damping of the restrainer device, having more than 15% value at the 200% shear strain level. From these plots, we may conclude that the stiffness and damping properties are not strongly influenced by the loading frequencies. In other words, the damping behavior is of hysteretic nature.

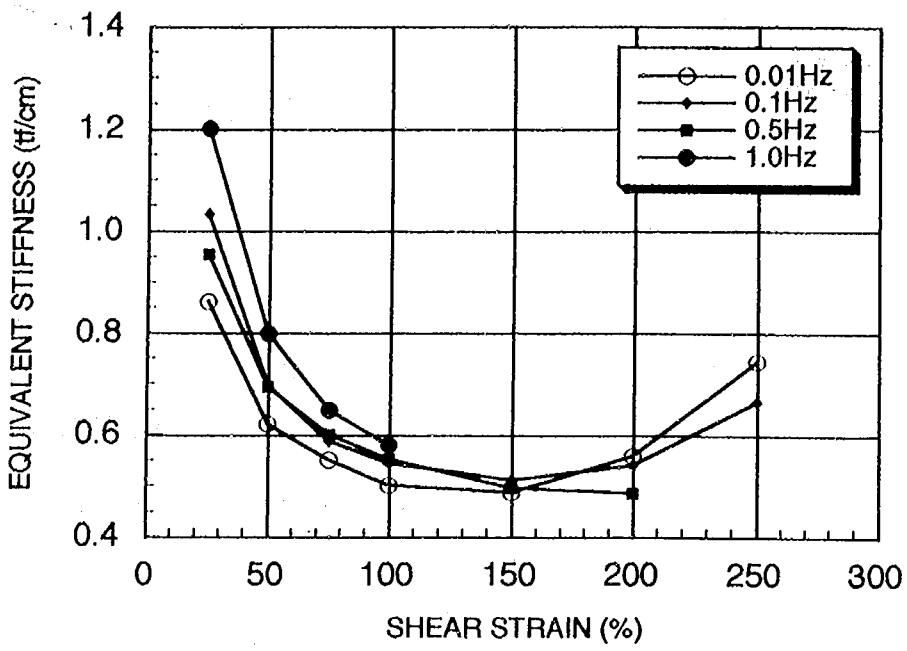


Fig. 13 Equivalent Stiffness vs Shear Strain

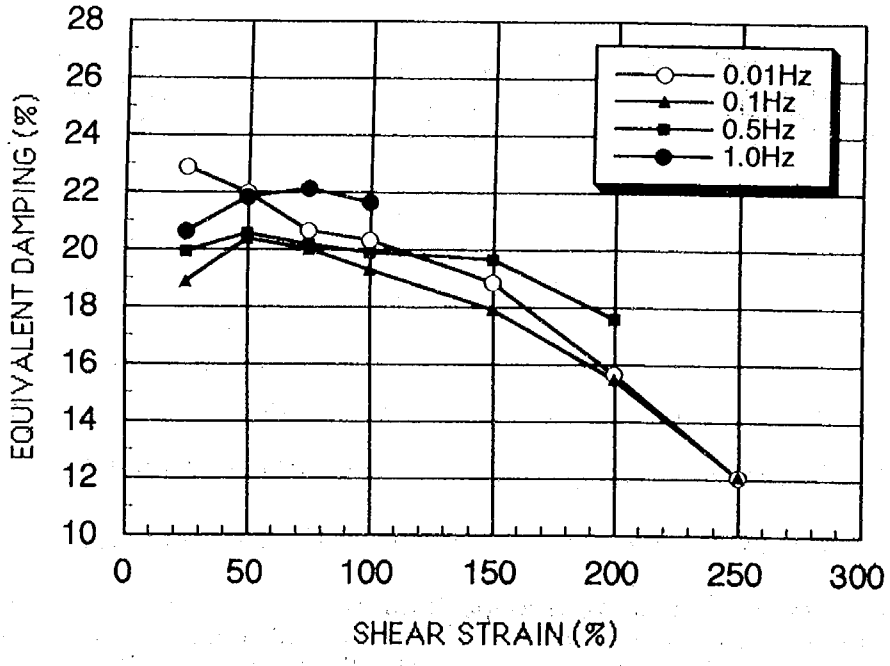


Fig. 14 Equivalent Viscous Damping vs Shear Strain

5. TEST OF BRIDGE MODEL TESTED WITH STIFFENING COMPONENT

A simple-span bridge model fitted with the stiffening component of the new device was next tested. The test setup is shown in Fig. 15. The piers are of identical steel section, and part of the lateral load applied through the girder can be transmitted to the pier

supporting the movable bearing through the device and thereby effecting load distribution between the two piers. Without the stiffening device, only a small amount of lateral load could be transmitted to the pier with movable bearing through friction of the roller support. The pier supporting the fixed bearing would take almost all of the lateral load.

In the tests, displacements of the piers were measured with displacement transducers. Likewise, the piston movement of the device was monitored through a displacement transducer attached to the shaft. In addition, a load cell was attached to the end of the device connected to the pier supporting the movable bearing to measure the amount of load transmitted. With the device having the stiffening component attached, the bridge model was subjected to cyclic loadings with increasing loading frequencies. Test results for loading frequencies of 0.001 Hz and 1. Hz are shown in Figs. 16 and 17.

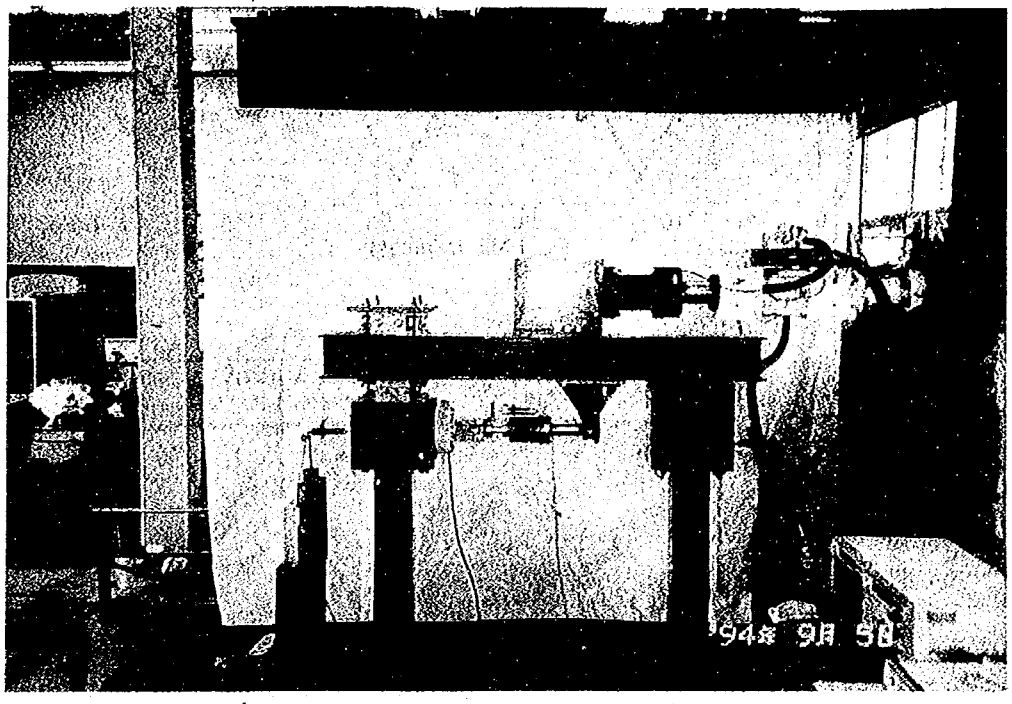


Fig. 15 Bridge Model Test Setup

For slowly applied loads, the device barely offered any resistance and moved along with the girder and the pier with the fixed bearing as can be seen in the displacement time history in Fig. 16, whereas it can also be observed that the pier supporting the movable bearing was only displaced slightly except for a small amount transferred through friction and also due to rotational restraint of the device joints. For loads due to daily and annual temperature changes, it can be considered that the device does not interfere with the normal functioning of the movable bearing in relieving stresses due to temperature effects.

When the bridge model is subjected to higher-frequency loads (the case of 1. Hz shown in Fig. 17) or earthquake-like loads, the device would act to transmit loads to the pier with the movable bearing. It can be observed from the displacement time history in Fig. 17 that both piers are displaced equally and thereby shared in resisting the total lateral load from the girder. The device had acted to transfer about half of the load acting on the pier with the rest transferred through friction of the roller bearing.

In considering load distribution, it is necessary first to evaluate the seismic capacity of the piers. The appropriate shares of loads to be taken by the piers are related to the relative stiffnesses of the piers and the devices. Tests and analyses on the total response with the

relative stiffnesses taken as parameter of investigation are needed. In addition, thorough study of the effectiveness of the device would also require an extensive study of the performance of the device under realistic earthquake excitations since the behavior of the device is very much frequency-dependent. Only performance under harmonic excitation had been conducted and presented in this study.

Lastly, it should be noted that a load-transmitting device would demand a stricter tolerance in the fabrication of the joints than a damper device. Even a slight slip or deformation in the hinges would negate the effectiveness of the device.

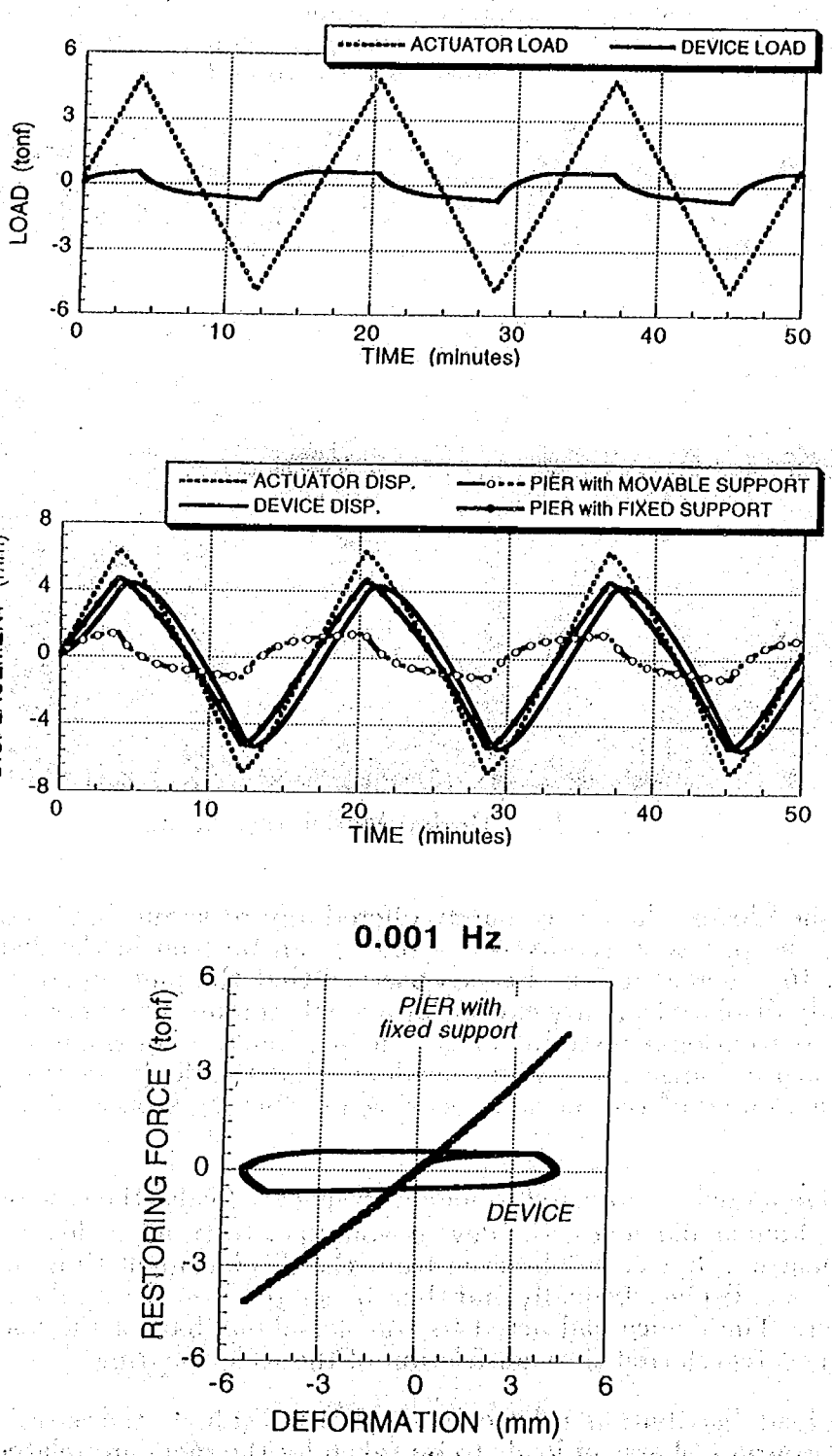
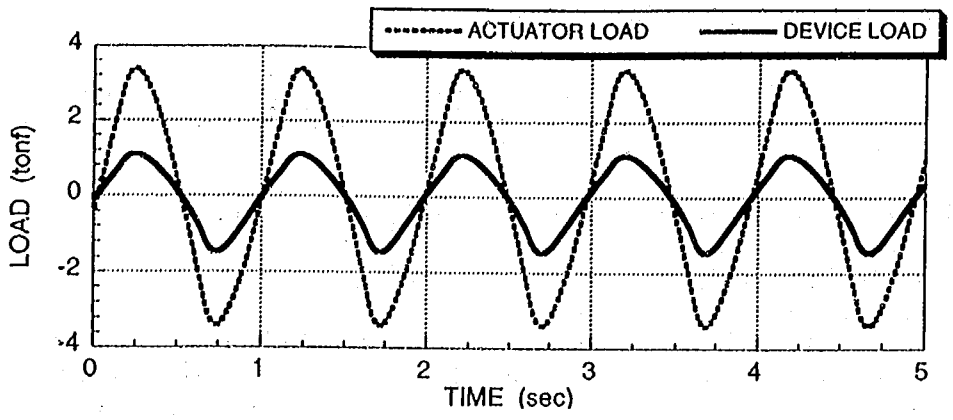
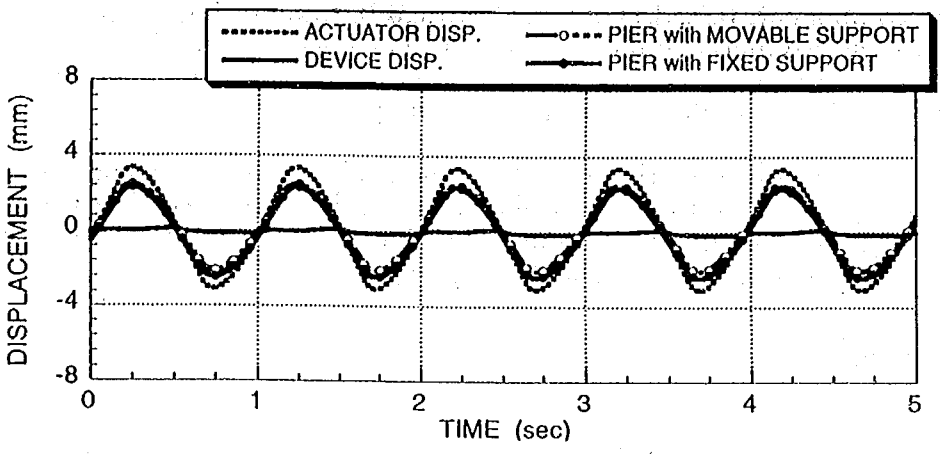


Fig. 16 Simple Span Bridge Prototype Subjected to Slowly Applied Loads (0.001 Hz)





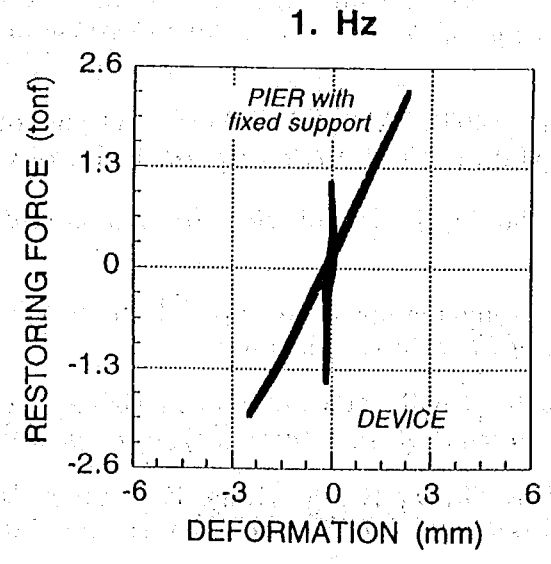


Fig. 17 Simple Span Bridge Prototype Subjected to Higher-frequency Loads (1. Hz)

6. SUMMARY AND CONCLUDING REMARKS

A new device is being developed to enable transmission of loads to piers with movable bearings during an earthquake with the added feature of dissipating energy through damping.

The stiffening component, tested using a simple piston-cylinder assembly packed with stable silicone putty proved to be effective in distributing lateral loads among the piers. Test results to obtain basic load-deformation behavior of the assembly under cyclic loadings were conducted in which the effect of packing, piston sizes, putty flow properties were investigated. While it had been shown experimentally that the device has excellent performance and can accomodate different design amenabilities, analytical modeling of the material behavior in rheologically quantifiable terms agreeable to both structural engineers and material scientists need to be done.

The damping component, tested using a cylindrical bushing of high-damping rubber vulcanized in-between two metal cylinders proved to be effective in dissipating energy. Thus, this additional feature greatly improves the behavior of the bridge under earthquake loading and decreases the possibility of damage or collapse.

The silicone putty used in the stiffening component allows an inner shaft to move freely under normal operating conditions but will react as a solid upon receiving a sudden impact load. This activates the damping component which uses high-damping rubber, dissipating a part of the energy being transmitted to the pier.

5. REFERENCES

D. Stephen Brown [1996]: "Bridge Strengthening with Shock Transmission Units," *Eleventh World Conference on Earthquake Engineering,* Paper No. 1849.

Kawashima [1990]: "Seismic Design, Seismic Strengthening and Repair of Highway Bridges in Japan," *Proceedings of the First U.S.-Japan workshop on Seismic Retrofit of Bridges,* pp. 3–61.

Ministry of Construction, Japan, [1994]: "Manual for Meshin Design of Highway Bridges", translated by Sugita and Mahin, *UCB/EERC-94/10,* Univ. of California, Berkeley.

Priestley M.J.N., Seible F. and Calvi G.M. [1996]: *Seismic Design and Retrofit of Bridges, Wiley Interscience.*

B. Pritchard [1989]: "Bridge Strengthening Using Load Relieving Techniques," *IABSE Symposium on Durability of Structures,* Lisbon.

Saiidi M., Maragakis E., Feng S. [1996]: "Parameters in Bridge Restrainer Design for Seismic Retrofit," *ASCE Journal of Structural Engineering,* Vol.122, pp. 61–68.

L. Selna, L. Malvar [1984]: "Box Girder Bridge Hinge Restrainer Test Program," *Proceedings, 8th World Conference on Earthquake Engineering,* San Francisco.

I. Ward, D. Hadley [1993]: *Mechanical Properties of Solid Polymers,* John Wiley & Sons.

Session 5

Experimental and Field Observations 2

(Co-Chairs: M. Abe, A. Elgamal)

"Design of the 19-Span Continuous Rigid Frame Bridge with Seismic Isolator"
by H. Hayashi, S. Kawakita,
Presented by: Shiro Kawakita

"Testing of Protective Systems and Hardware for Bridge Applications"
by A. Whittaker, I. Aiken, P. Clark, G. Fenves, N. Makris, S. Mahim
Presented by: Andrew Whittaker

"The Analysis of Seismic Response of the Bridge with Menshin Bearings during the Hyogo-ken Nanbu Earthquake"
by T. Naganuma, Y. Horie, H. Kobayashi, N. Sasaki
Presented by: Toshihiko Naganuma

DESIGN OF THE 19-SPAN CONTINUOUS RIGID FRAME BRIDGE WITH SEISMIC ISOLATOR

Hidenao HAYASHI
Head, Research and Design Div.
Kobe Route Reconstruction Dept.
Hanshin Expressway Public Corp
Kobe, Japan

Shiro KAWAKITA
Chief Engineer ,
Specified Planning Office, Planning Dept.
Hanshin Expressway Public Corp.
Osaka, Japan

SUMMARY

The Hanshin Awaji Earthquake occurred on January 17,1995, caused tremendous damage on the Hanshin Expressway Kobe Route., especially at Benten section (referred in Figure 1). Three bridges out of 8 completely fell down, subjecting all bridge structures except foundations removed after the earthquake. This paper reports the outline of the seismic isolation design of 19-span continuous rigid frame bridge with seismic isolator, which was installed at the bottom of steel pier. Results of vibration experiment applied onto the structure are also reported.

1. PROLOGUE

After the scrutiny of suffered condition caused by the earthquake the new Benten bridge was determined to be the 19-span continuous rigid frame with steel deck along with the installation of seismic isolator underneath the steel piers. The general view of design is shown in Figure 2.

Such a bridge structure that provides seismic isolator underneath the bridge supporting piers had theoretically been studied in the past [1] , however, actual application is almost none in practical use and it was indeed the first example to be introduced on the highway bridge. The experiment of vibration was carried out with the use of Rapid Release Jack System and heavy vehicles to inspect and to ascertain various structural behaviors. This paper describes the outline of seismic isolation design on the 19-span continuous rigid frame with the seismic isolator and its experiment.

2. OUTLINE OF DESIGN

2.1 Design Scheme

Before the earthquake one of piers stood on the middle of separating zone and the other on the pedestrian lane, and they were of single RC pier (1.0mx 1.7m). These piers were connected with the upper structure by means of steel bearings that were placed on each top of the pier. The cause of bridge fall or girder buckling such as shearing failure of the RC pier during the earthquake and the breakage of steel bearing at the connecting points were all taken into considerations to determine the basic scheme of construction. These elements were settled as follows ;

1) It was found that there has been no damage on the piled foundation so that it could be utilized as they are.
2) Deck of the expressway could become light weighted by using steel deck and design to decrease seismic force by using isolation bearing.
3) In order to prevent bridges from falling down each bridge pier and the beam of upper structure

would be tied rigidly and to maintain continuous girder forms as much longer as can be.

Above basic conditions were studied and it was decided to adopt a continuous rigid frame. It was supposed that the additional piling reinforcement is needed for rigid connection or hinge connection and finally concluded to adopt the structure of installing seismic isolation bearing on the foundation. Since the Benten bridge is warped to the seaside and the overhang length of crossbeams differs slightly, analyses were made on the whole structural model of the two types shown on Figure 3.

In static analysis model (a) in the Figure 3 was used. The upper structure consists of main girders, beams, and piers in conjunction with springs in the model. In dynamic analysis model the number of lattice was decreased in a manner that main girders and deck plates were assembled together to a piece of beam so that they would make a whole simple.

2.2 Seismic Isolation Design of Bearing

A study was made regarding the seismic isolation characteristic on whether the structure as a whole can anticipate vibration isolate effect based on the "Manual of Seismic Isolation Design for Highway Bridge" [2] .

In seismic isolation design the characteristic of structure is expressed in the value of natural period (T) and the ratio of yield point load Qd/Wu (Denomination is taken from the "Manual of Seismic Isolation Design for Highway Bridge"). In order to work out an appropriate value, were designed the period and the ratio of yield point load by applying a representative bridge pier that support the upper structure that would satisfy the following 3 design objectives;

1) In the designed vibration from the horizontal bearing capacity piers would not excessively be plastic during the earthquake. (Khe$<$0.68)
2) In seismic coefficient method, a designed vibration can at least be decreased by the damping effect (Damping constant by the seismic coefficient at the vibration h$>$10%)
3) Seismic Isolator will not be deformed extremely (Horizontal bearing capacity during earthquake was investigated referring to the upper structure that deflects$<$250%).

Specific figure to satisfy the above condition, a combination of T=1.4 sec Qd/Wu=12.6% has been adopted. One of the model of bearings is shown in Figure 4.

2.3 Dynamic Analysis

In the dynamic analyses two types of plane model shown in the Figure 5 were introduced and following points were inspected by comparing two models and ascertained the adequacy of simplified model.

1) A degree of influence whether the non linear characteristic of seismic isolator and material characteristic of steel bridge pier reflects to the responding results.
2) In inspecting three dimensional model, adequacy of replacing girders to one piece beam.

The seismic wave taken at the JR Takatori Station [3] was applied for the input of seismic vibration. Seismic force of EW wave was put into in chord direction of warped bridge and SN wave to the

lateral direction simultaneously. In comparing the responding values of each model it became apparent that there was least influence due to the non-linear characteristic of bearing and that the deflection at most part of steel pier was within the elastic deformation.

A comparison of the test results of simplified model that treats bearing and steel pier in a linear form to that of actual structure model, is shown on Table 1. The values for a simplified model are larger but being within safe side it was judged to present no problem to carry out dynamic analysis by applying whole model shown in Figure 3 (b).

2.4 Result of Analysis

From the static analysis, deflections were calculated for each bearing and for the girders at both ends. Girder's deflection reached ±84mm maximum depending on the various temperature range. Expansion joints was designed based on this movements.

The results of natural vibration analysis on the whole model is shown in Figure 6 and all up to 5th modes shows inherent mode of horizontal direction. From the result of natural vibration analysis applied on a plane model, the mode for horizontal move at the bearing position is so remarkable that the similar tendency may be seen in a three dimensional model.

The time histories were exemplified in the Figure 7 for the response in the horizontal deflection of the seismic isolator and the bending moment at the beam joint at P470. Maximum deflections were 428mm in the longitudinal direction of bridge and 568mm in the lateral direction, which were observed after 6 seconds from the beginning of earthquake.

Also the response analysis on time history is confirmed in the rotating deflection of seismic isolator and axial force of pier, which led to carry the test confirming of the effectiveness of bearing by using the response value for the 1/3 scale model bearing.
Again the stresses of intersection at the beam and the pier were investigated as the members that receive axial compressive force and bi-axial bending moment by applying maximum response values.

3. VIBRATION TEST

3.1 Outline of Experiment

In order to ascertain dynamic characteristic of the bridge, it was planned to carry out experiment using the actual bridge. Since the bridge has 19-spans which is so long and heavy that the vibration experiment by applying vibration of constant cycle using vibrator equipment, a rapid force release test were brought and the free damping vibration was measured after the release of force. Jointly with this horizontal reaction force and deflection was measured in the static load condition. In grasping vibration of girders and vibrational transmission through seismic isolation four axles wrecker vehicle of gross weight 47tf (Maximum 4 vehicles simultaneously) was used to run on the bridge and response was measured..

Reaction force support was installed on the bridge foundation and horizontal force was loaded to the lateral direction of the bridge, as shown in Figure 8. Six units of rapid release system were applied for loading. After studying the effective loading points it was determined to place them at both mountain and sea side piers between P462 and P464. Loaded positions and measured items as well as positions of measurement are also shown on Figure 9.

3.2 Static Loading Experiment

Static loading experiment was carried out for the piers of both mountain and sea side individually, or altogether between P462 to P464 and further carried simultaneous load test onto 3 bridge piers. The load was gradually incremented in the order of 50,100,150, and 180tf. As an example of experimental result of static loading, deformation of pier P463 is shown in Figure 10(a) and 10(b) when piers between P462 to P464 were loaded on only mountain side and simultaneously on both sea and mountain sides.

As has been studied from this drawing, the loading on one pier represents bigger deflection of loaded pier while the other members shows practically less deflection. Also the case of simultaneous loading from sea and mountain side piers confirms the move to lateral direction but even in this case the deflection value of upper part is smaller than the lower one. Deflection form of whole bridge in lateral direction at this time is shown in Figure 11.

The maximum deflection is 110mm at the pier P463 with the load of 180tf while there was little deflection on the piers with no loads. Figure 12 shows relationship in the horizontal spring rigidity to deflection figure obtained in the laboratory test as well as actual test on bridges. There is a slight difference in a small deflection but the actual data of the horizontal spring rigidity remains as same as those done in the laboratory in the range above 80mm.

3.3 Rapid Release Test

Rapid release test was carried out in the loaded condition to reach up to 180tf when the load was abruptly released. Deflection and acceleration were exemplified in Figure 13 as an example of mountain side P463. Deflection went back near to the original position when load was discharged and the vibration component is damped to die. Thereafter the deflection had slowly decreased and in a few minutes after the release went back to the original position completely.

In a response of acceleration, while the free damping vibration is confirmed to remain as in the case of deflection, its vibrated element shows high spectrum at the point of 2Hz. By measuring rotating deflection of bearing and pursuing the vibrating mode of gate bridge pier it became apparent that horizontal vibration at the pier foundation had been damped immediately after the release and thereafter rocking vibration was seen at the center of each bearing. From such observation in the response to the acceleration, higher frequency of vibration is considered to be due to the rocking effect and it corresponds with the result of inherent value analysis of hinge reaction which substitute bearing applied to the plane model.

In the response analysis on the time history applied on the three dimensional model that evaluates the rigidity, it is confirmed that vibration modes of 1st through 3rd are all located under the 0.7Hz, while all present experiments under partial vibrating condition shows a different vibrating element from the designed vibrating characteristics.

Secondly, vibration mode on the whole bridge at the release of load is like Figure 14 and ballooned vibration mode in the vicinity of bridge pier having two nodes prevails immediately after the release of load, However, the position of node moves near around the center of pier P466 and the ballooned mode had been changed to show different vibrating character. Also while the horizontal vibration of whole gate bridge pier has shown the damping effect at the first wave, it was the result to show the case that the vibration at the bearing showed over damping and the deformation figure at the

experiment is greater than the designed figure.

In the design of upper part, 2% damping was anticipated, however, calculated damping coefficient from the logarithmic decrement of actual damping wave in a vertical direction had dispersed in the 4 ~5% area.

At the time of rapid release the representing vibration mode of main girder and its vibrating frequency varies between 5.3Hz and 6.3Hz in torsional mode, and between 9.0Hz and 10.0Hz in bending mode, shown in Figure 15.

3.4 Test Vehicle Running Experiment

Vehicle Load running experiment had been carried out at the speed of 20,40,60 km/hr with one vehicle and parallel drive of 2 or 4 vehicles at 20km/hr speed and the effect of each running pattern was studied. As an example of the result, the pattern for the damping effect taken from the longitudinal direction of bridge with one vehicle at the speed of 60km/hr is shown in Figure 16.

Both underneath and upper bridge pier vibration had prevailed to show 2.32, 2.47, and 2.66, however, the above frequency zone did not prevail at the foundation. Similar tendency was observed in the lateral direction.

4. EPILOGUE

Here it was reported of the new trial of 19-span continuous rigid frame bridge with seismic isolator at the bridge piers and outline of design as well as contents of vibration experiment carried on actual bridge. Although the loading condition is limited to a partial, the vibration character of seismic isolator, bridge pier and upper structure was confirmed. However, the present experiment could not verify the vibration obtained in the dynamic analysis. This is due to the fact that the loading was done only 3 sets of bridge pier out of 18 and that the rigidity of bearing had a bigger value than what was presumed to be.

5.ACKNOWLEDGEMENTS

We are greatly indebted to the courtesy of Technical Committee for the Restoration from the Earthquake(Chairman, Dr.Yoshikazu YAMADA) and especially to the Benten Bridge Structure Study Sub-committee (Chairman Dr.Yuhshi FUKUMOTO) for their valued suggestions and comments. Our appreciation also goes to the courtesy of the Institute Of Laboratory, in The Japan Highway Public Corp. for providing equipment for Rapid Release Jack System.

6.REFERENCES

[1] Japan Institute of Construction Engineering : Report on the Anti-seismic Design for Highway Bridge with Seismic Isolator

[2] Public works Research Center : Manual of Seismic Isolation Design for Highway Bridge (draft) 1992

[3] Railway Technical Research Institute, Mr.Yutaka NAKAMURA : Seismic Vibration Report on The Hanshin Awaji Earthquake,1995 and Its analysis, JRVI,I Earthquake Report No.23c,1995

Table 1. Comparison Between Virtual Model and Simplified Model

			Virtual Structural Model	Simplified Model	Ratio
Position of main girder	Accelerated speed (gal)		1280	1313	1.03
	Horizontal defomation (cm)		660	70.1	1.06
Position of Bearing	Horizontal deformation	seaside (cm)	59.6	67.0	1.12
		mountain side (cm)	60.5	67.2	1.11

Table 2. Detail and Purpose of Experiment

Detail of Experiment	Purpose
Static load experiment	Confirmation of horizontal spring force equivalent damping constant value
Rapid force release Experiment	Confirmation of vibration mode in the rapid force release. No. of Cycle and damping constant value
Running Experiment of test vehicle	Confirmation of vibrating character of main girders and beams, and rigidity of upper structure Vibration transmittance mechanism to the sorrounding soil

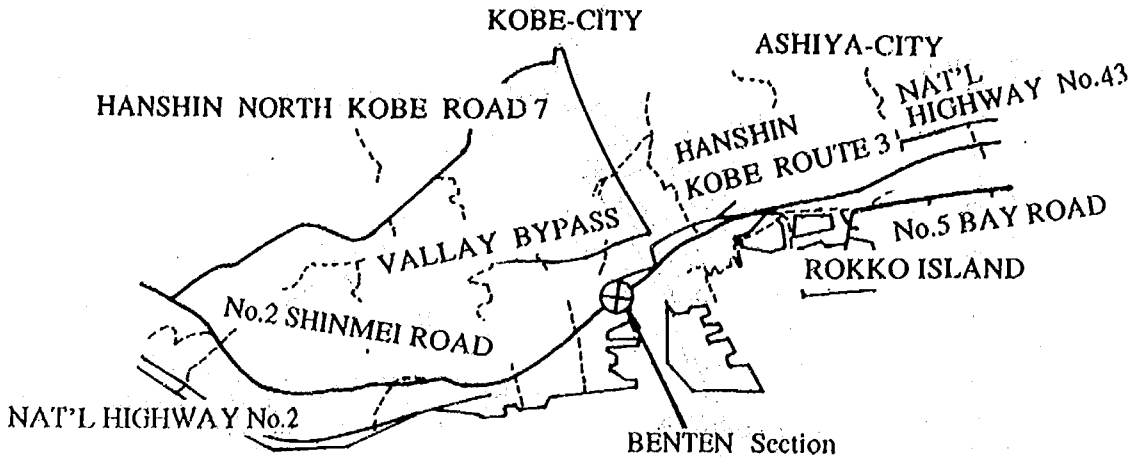


Figure 1. Location

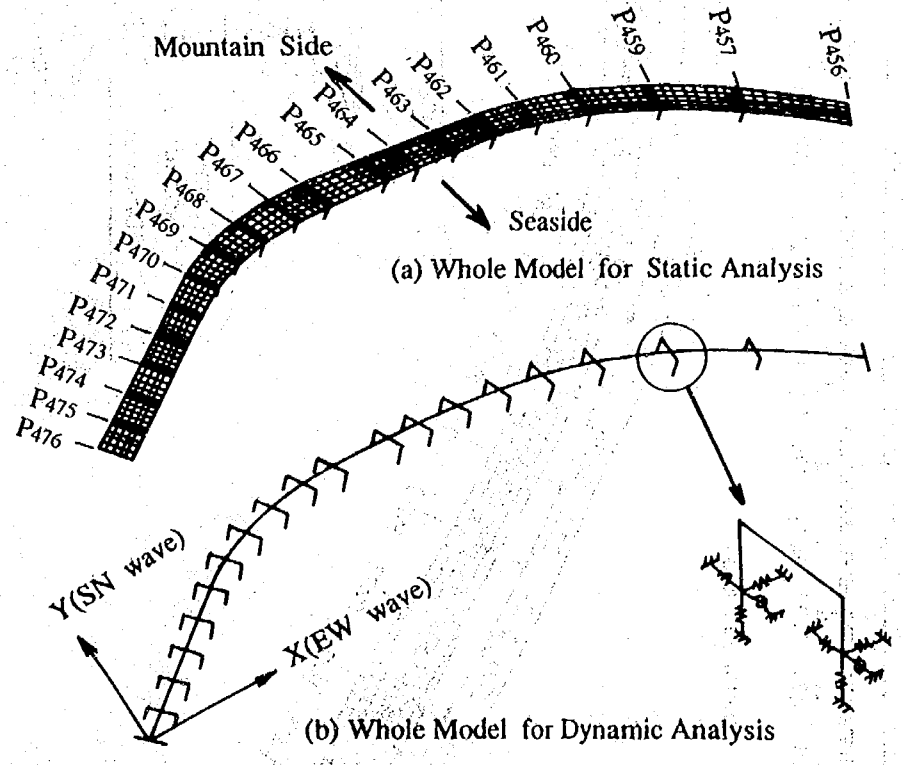


Figure 3. Whole Model for Analysis

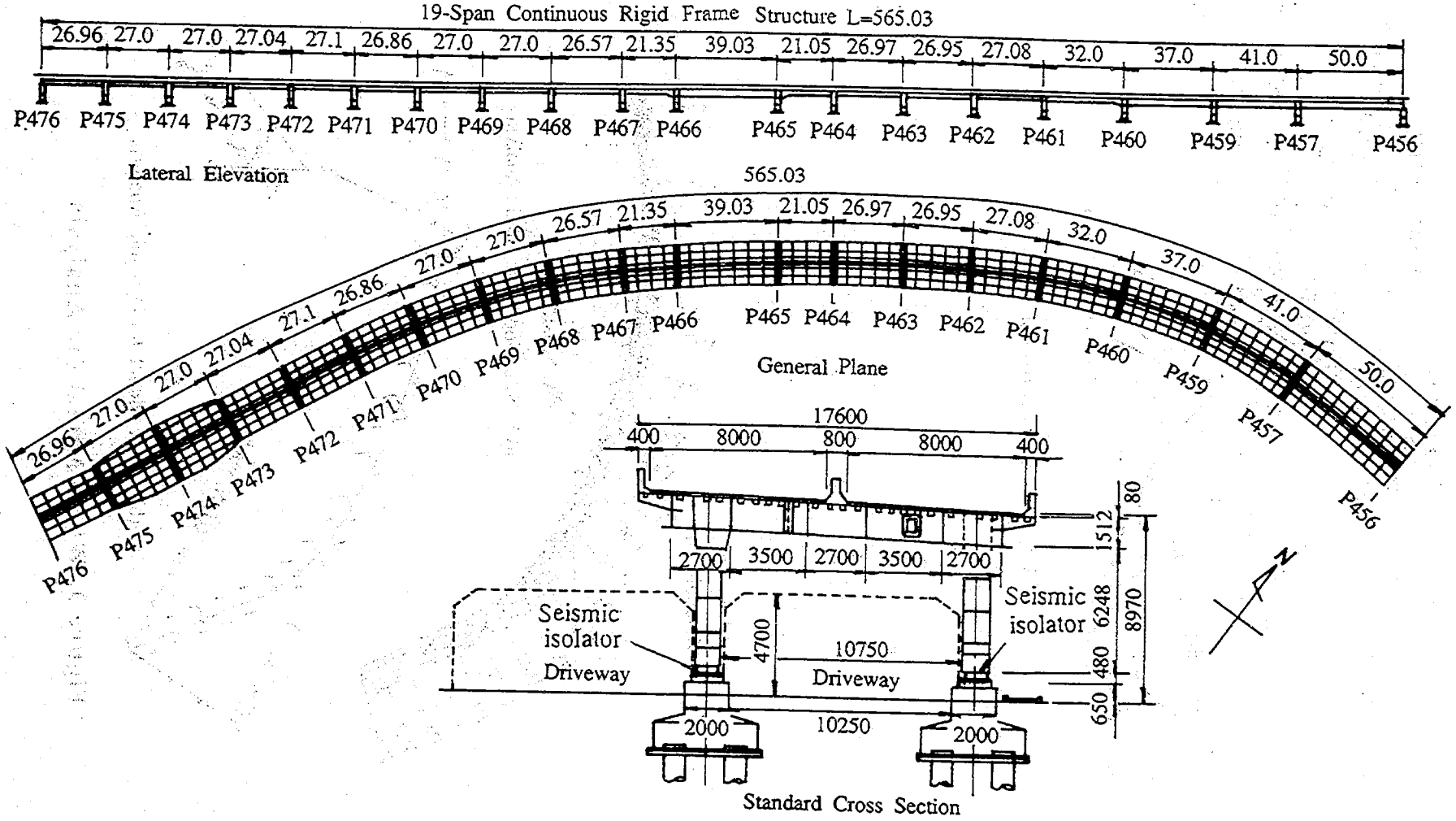
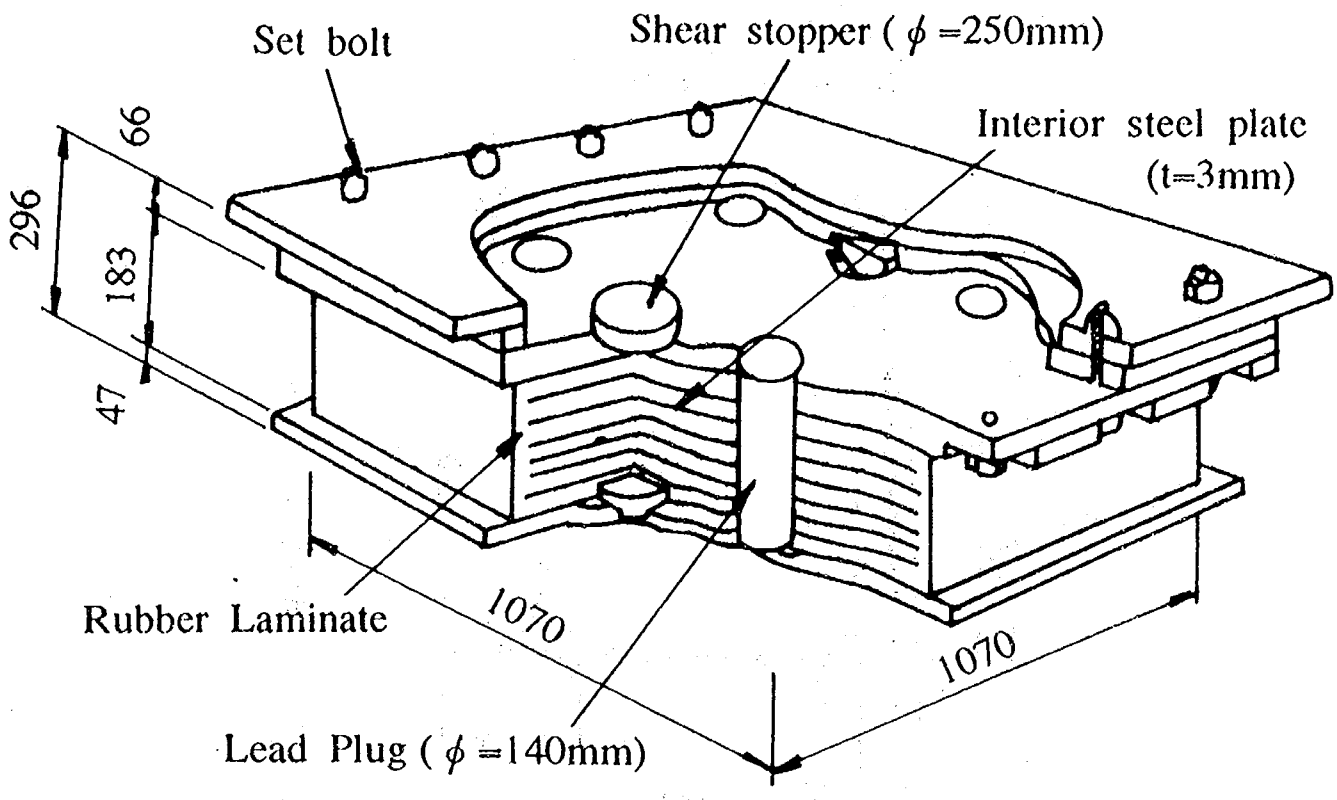


Figure 2. General View of Benten Bridge



Specification for Seismic Isolator (P457-P461)

Applied Reaction Force		R	987.6tf
Dead Lord Reaction Force		Rd	627.3tf
Vibration At dedign	Design Horizontal Vibration	Kh	0.23
	Allowable Shear deflection	γ_1	150%
Retained horizontal force durig Earthquake at design point	Design Horizontal Vibration	Khc	0.68
	allowable shear deflection	γ_2	250%
Reaction force by Wind load		F	85.5tf
Bearing height (Rubber thickness)		297(168)mm	
Lead plug : pieces×diameter		4pcs×140mm	

Figure 4. General View of Seismic Isolator

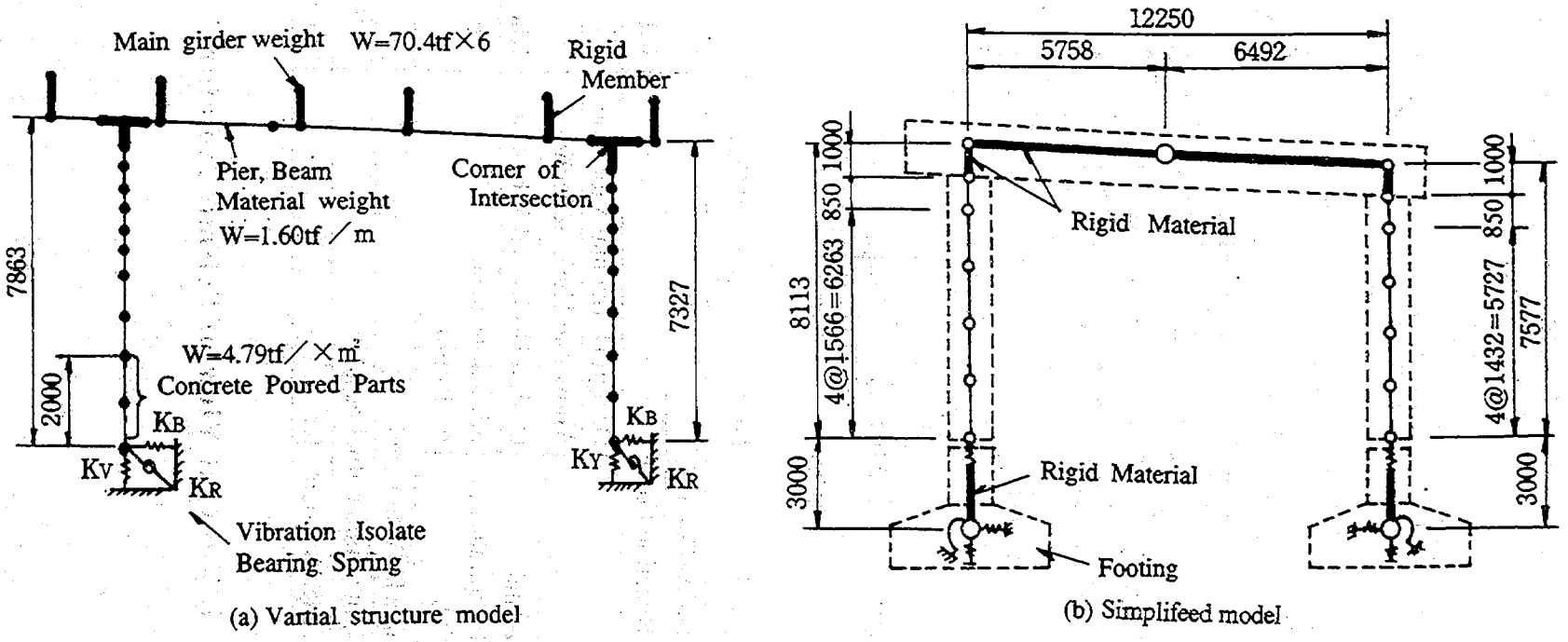


Figure 5. Plane Model for Earthquake Responding Analysis

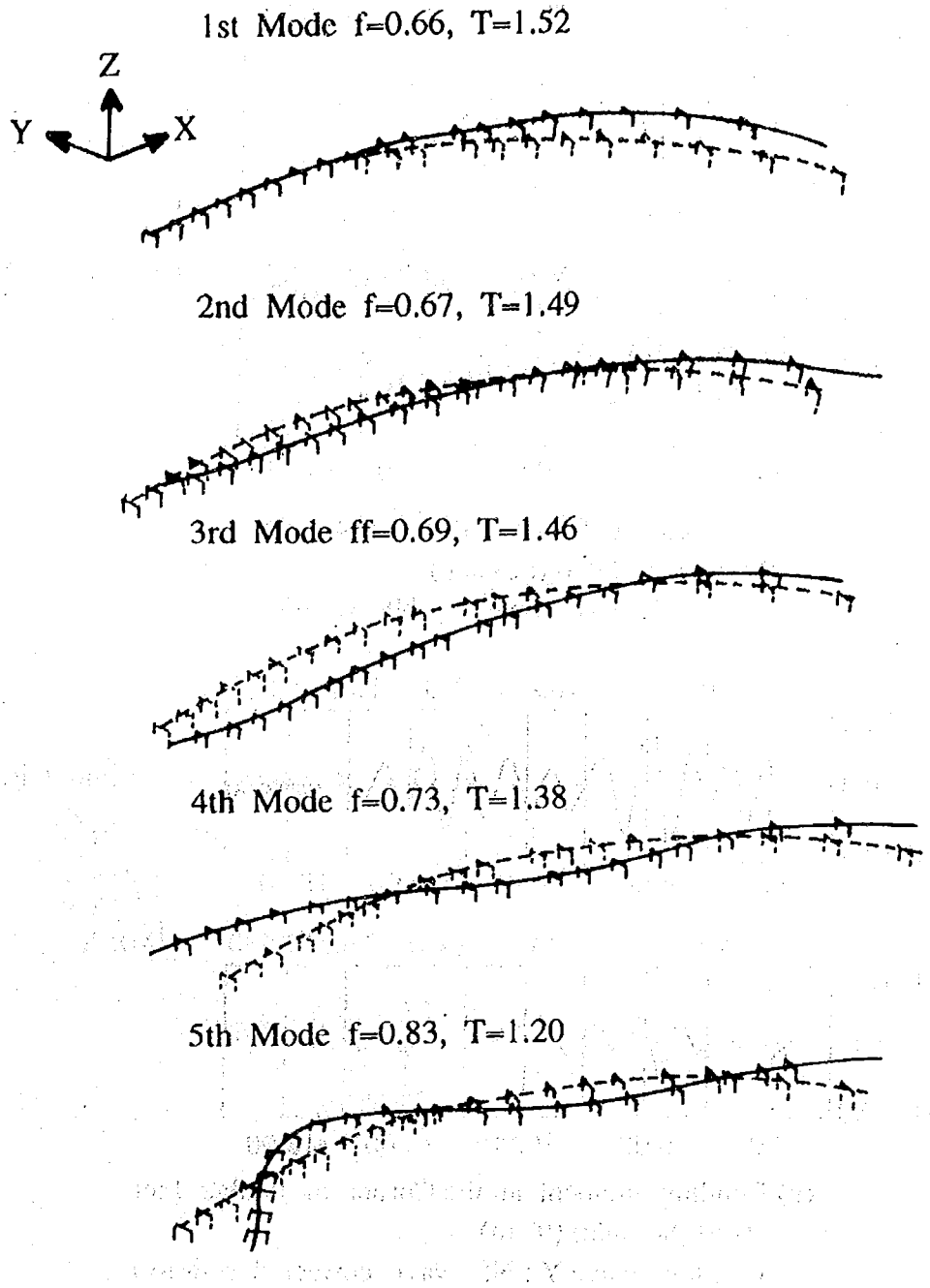
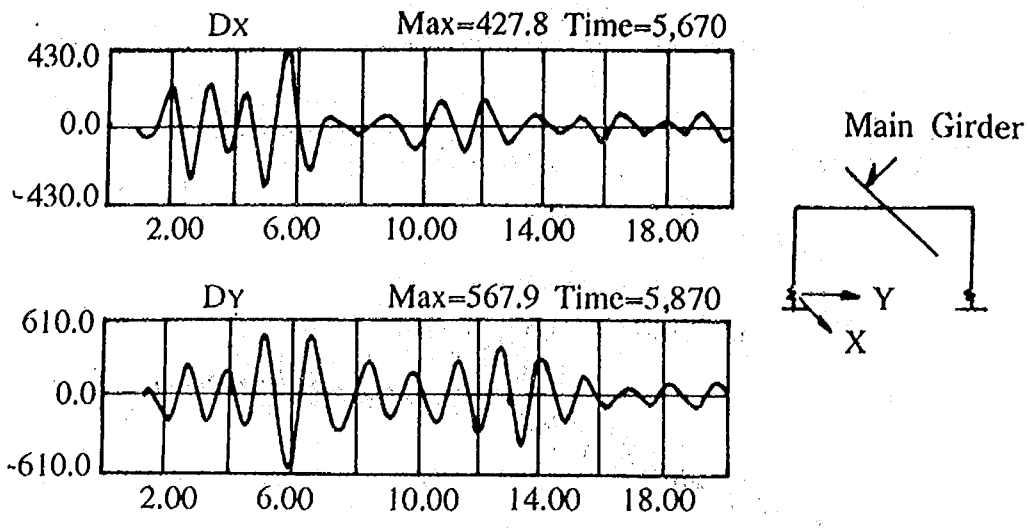
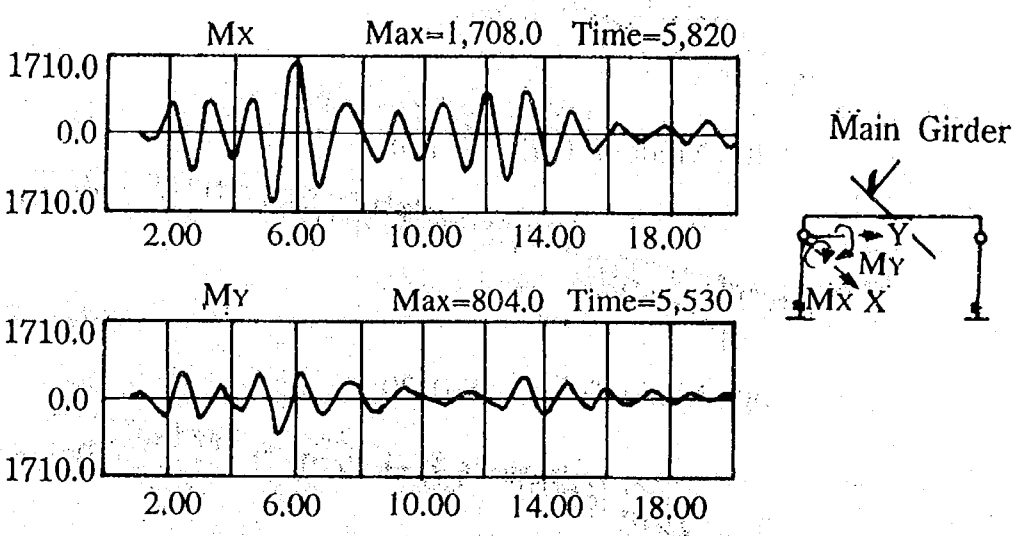


Figure 6. Result of Natural Vibration Analysis



(a) Horizontal deflection of Lead Rubber Bearing at P470 (Seaside)
(X, EW wave Y, NS wave)



(b) Bending moment at the Corner of Bridge Pier P470 (Seaside) (tf -m)
(X : EW wave Y : NS wave corrected rigidity)

Figure 7. An Example of Response Analysis on Time History

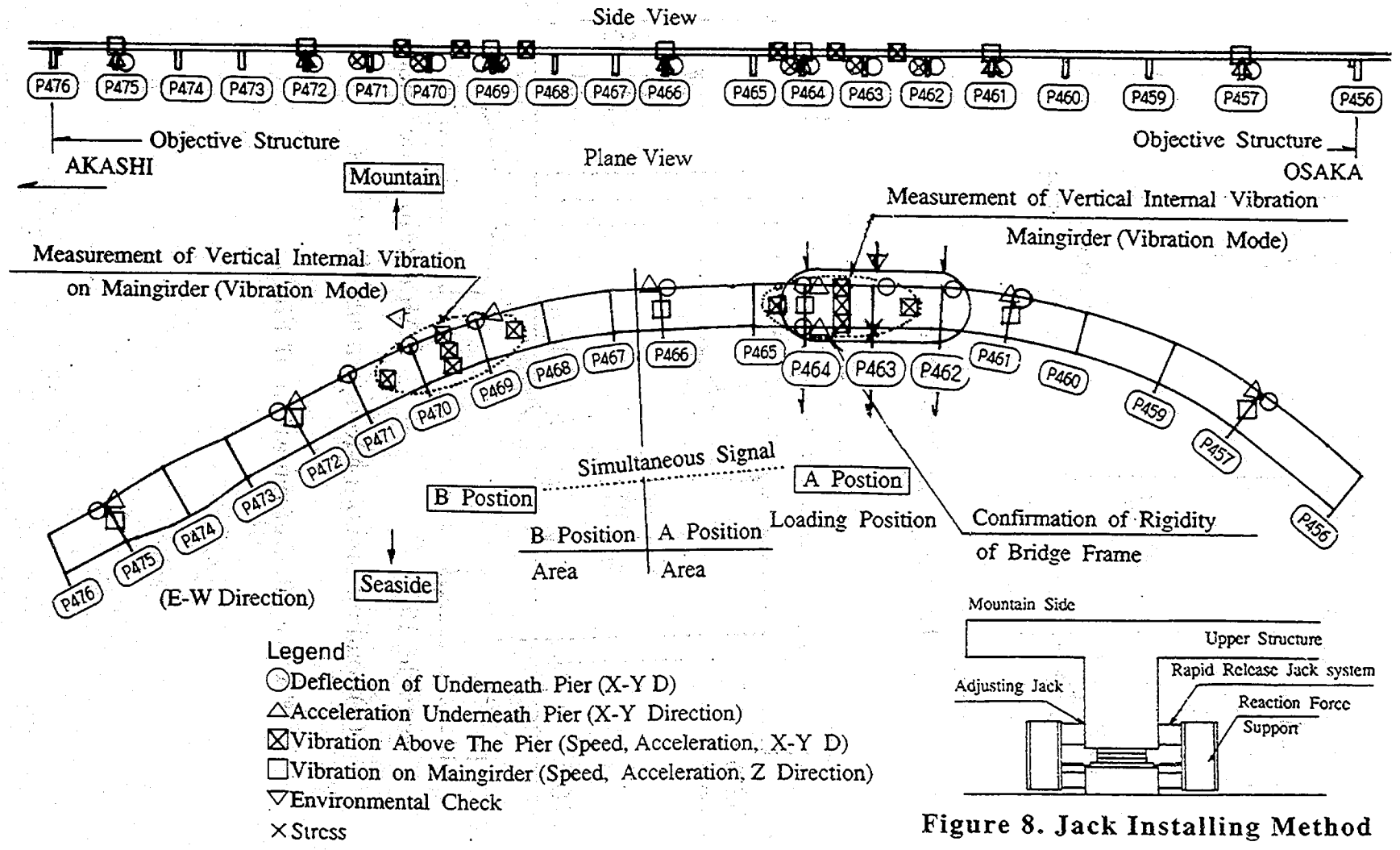
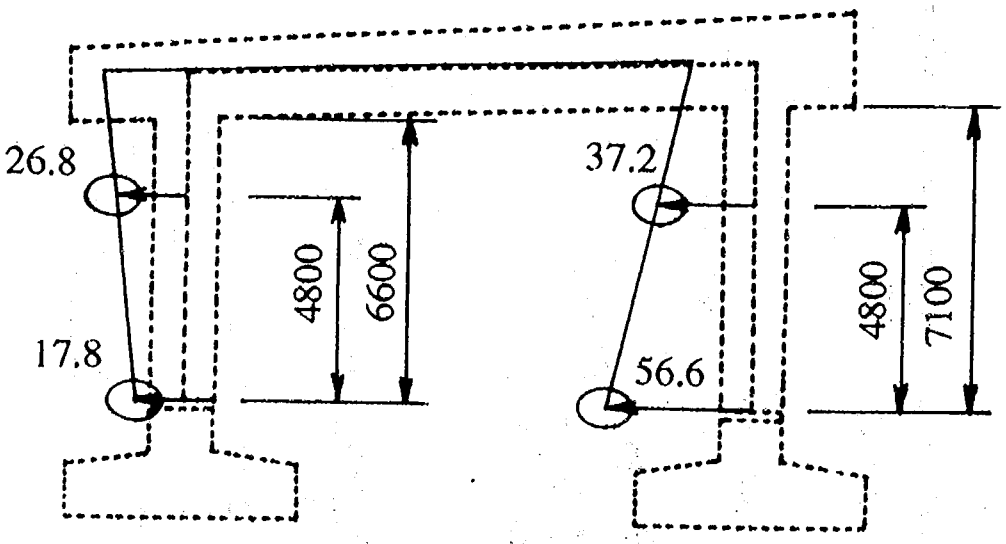
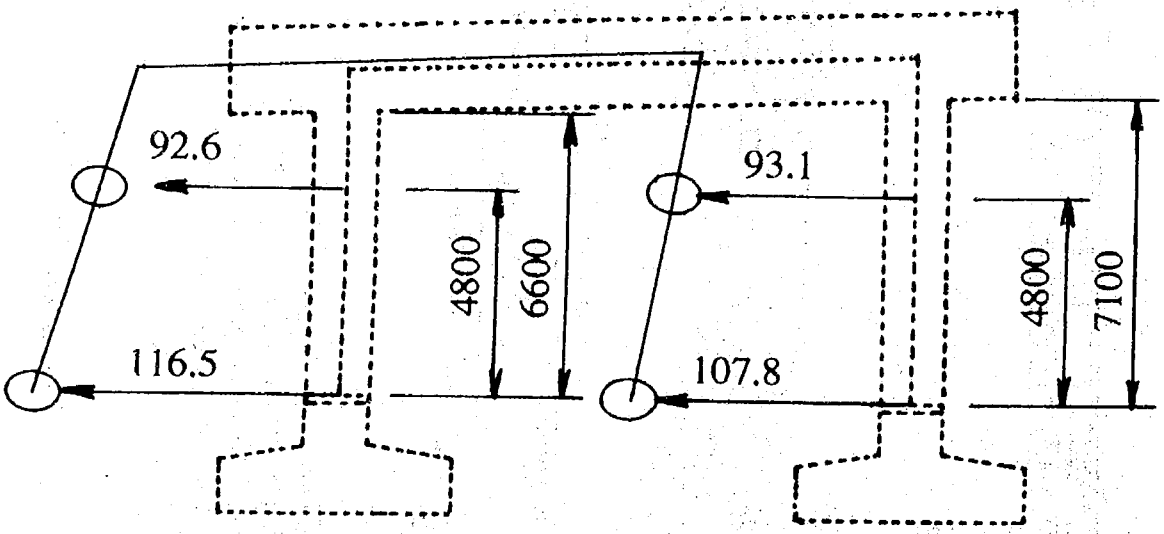


Figure 8. Jack Installing Method

Figure 9. Loading Position and Measured Position



(a) Loading on Mountain Side



Seaside Pier Mountain Side Pier

(b)Loading on both Mountain and Sea Sides

Figure 10. Deformation of Piers

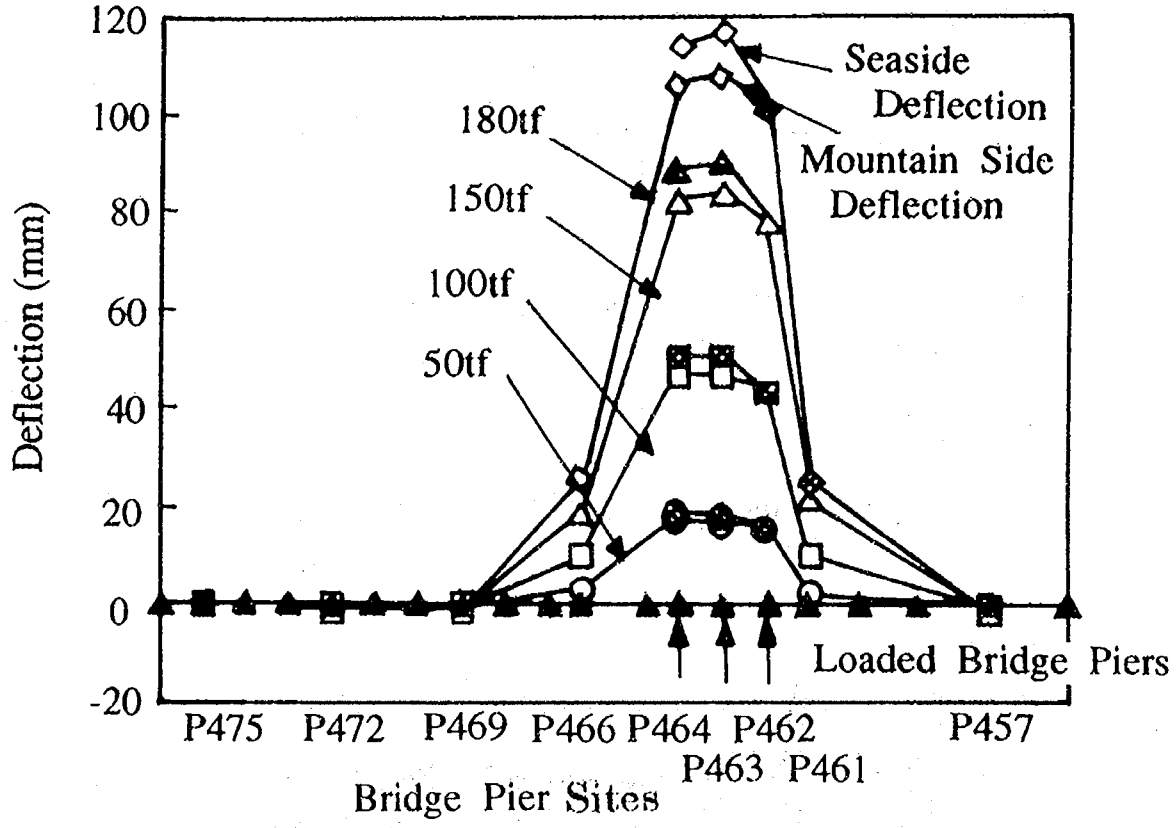


Figure 11. Deflection of Pier Loaded on Downside

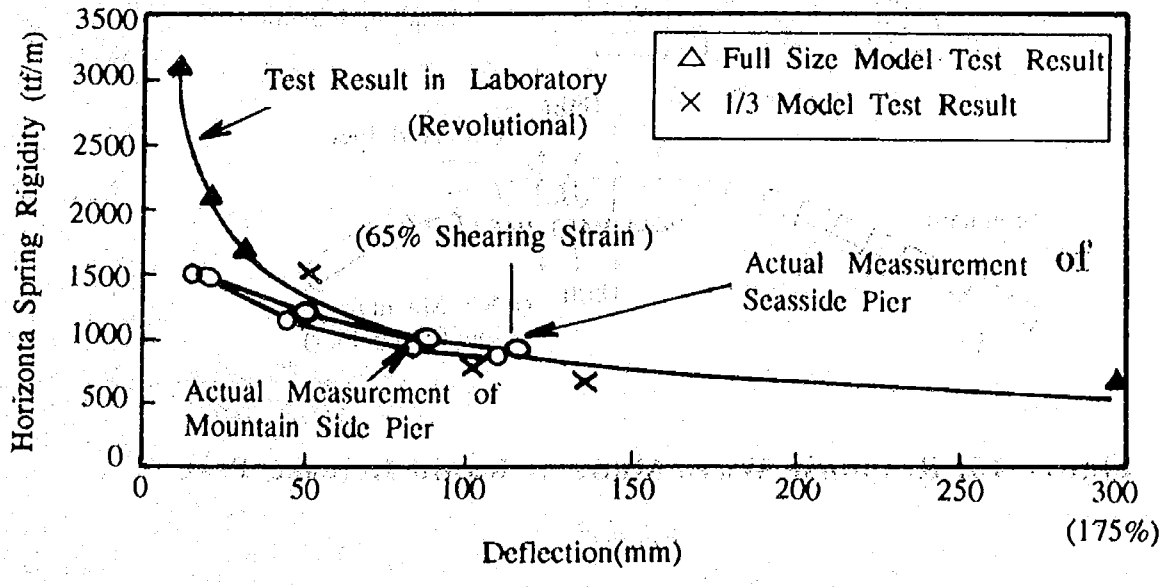


Figure 12. Design and Measurement of Spring Rigidity

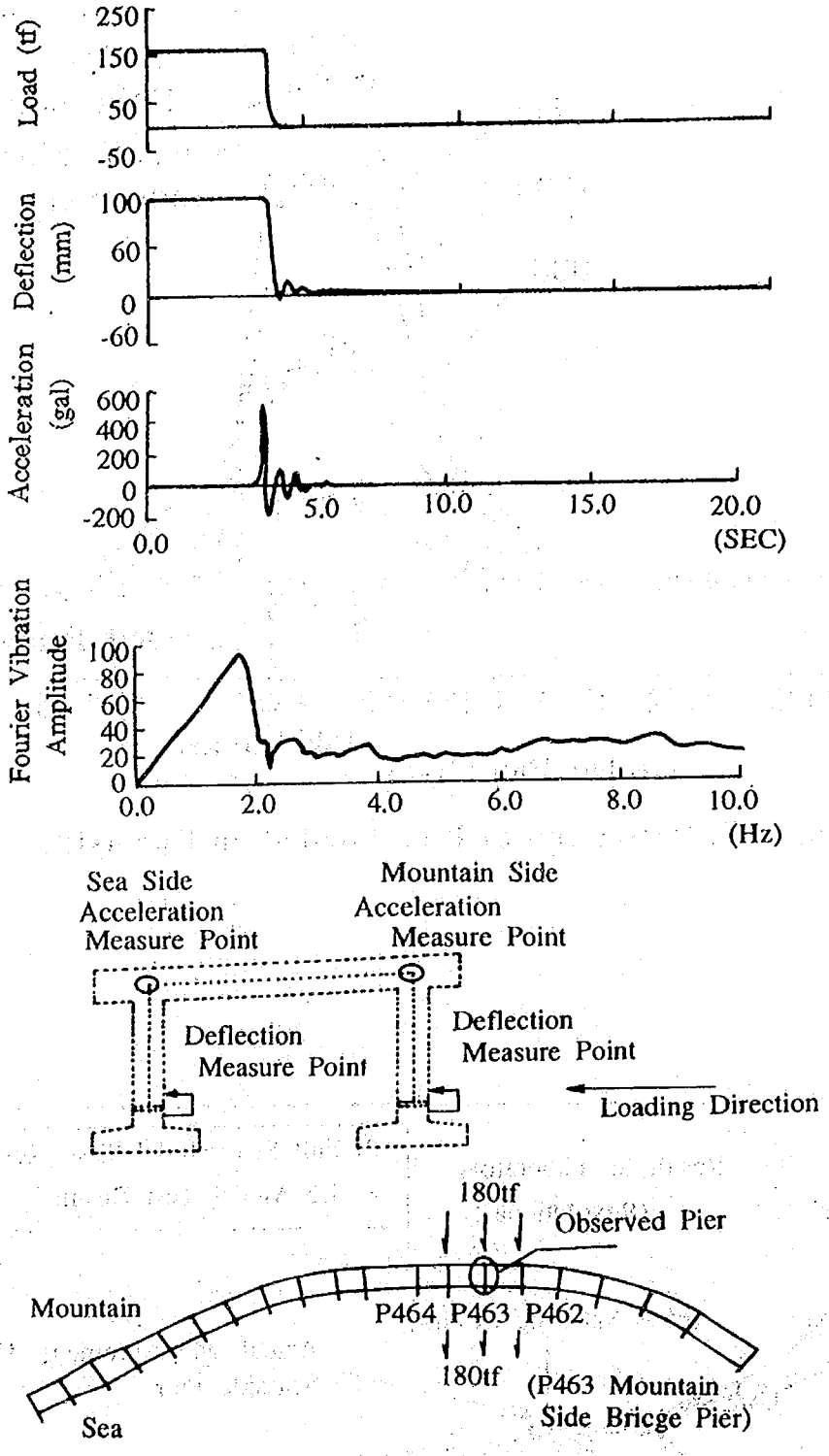


Figure 13: Response Wave Mode at Rapid Release Test

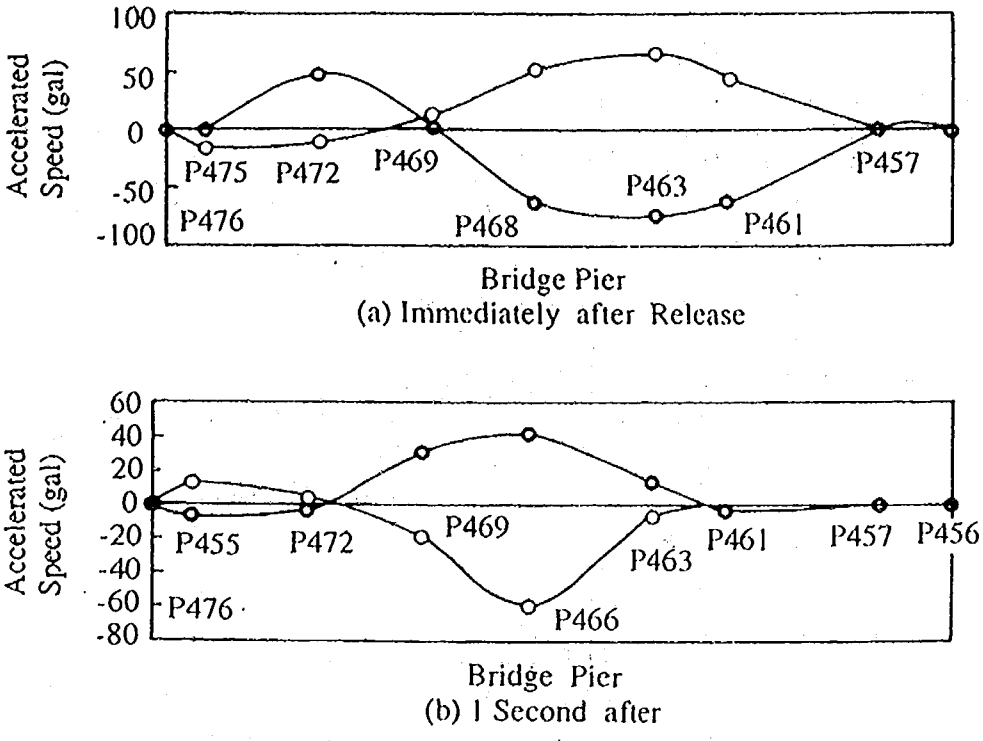


Figure 14. Vibration Mode after Release of Force

Vibration Mode	Vibration Frequency	Vibration Mode Figure
Tortional Mode	5.3~6.3 Hz	
Bend Mode	9.0~10.0 Hz	

Figure 15. Vibration Mode and Frequency on Main Girder

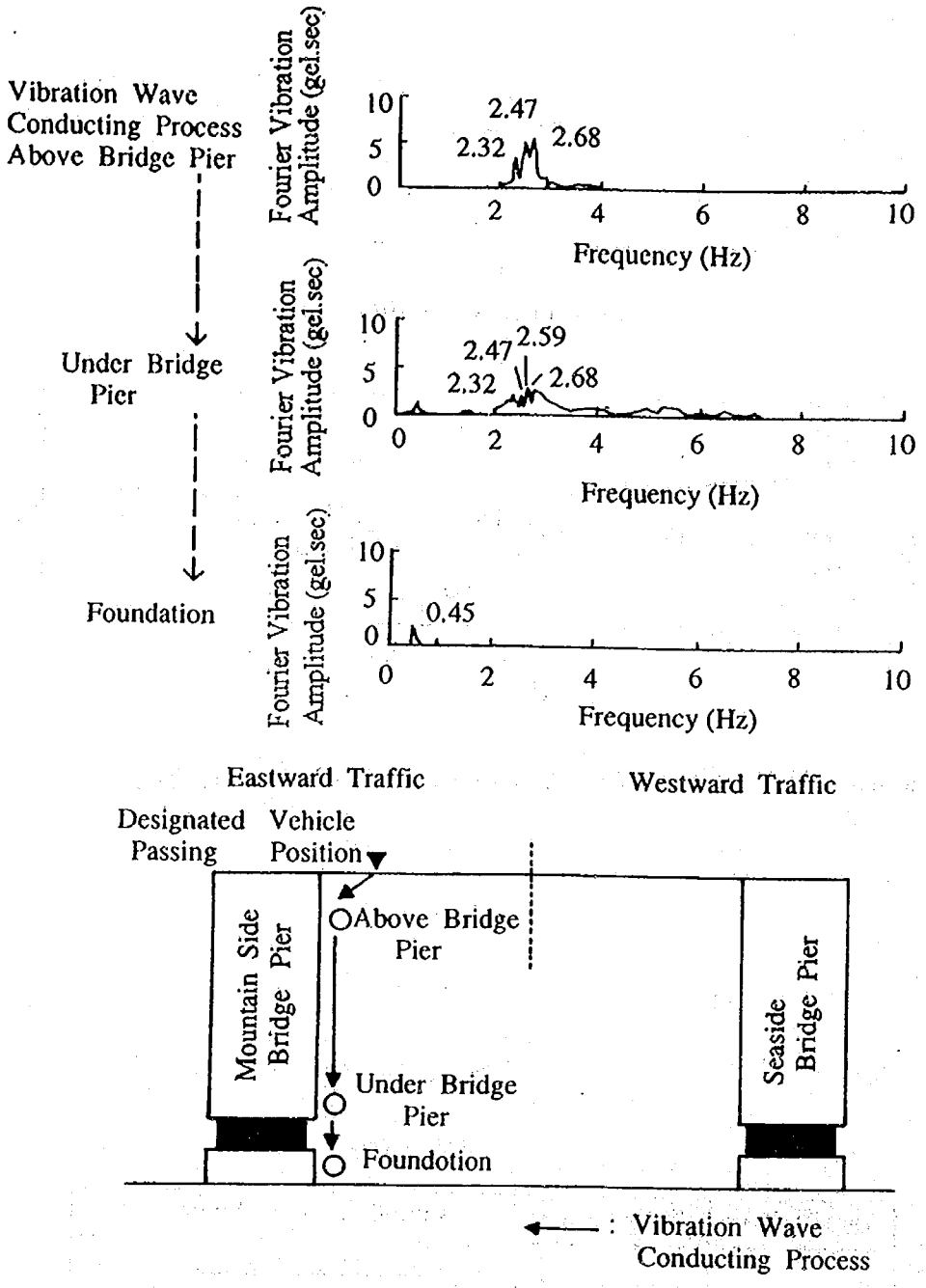


Figure 16. Damping Effect of Wave Frequency Zone at the Time of Test Vehicle Running Experiment (Bridge Axial Direction)

TESTING OF PROTECTIVE SYSTEMS AND HARDWARE FOR BRIDGE APPLICATIONS

Andrew Whittaker, Ian Aiken, Peter Clark, Gregory Fenves, Nikos Makris, Stephen Mahin
Earthquake Engineering Research Center
University of California at Berkeley

ABSTRACT

New technologies for protecting bridges from the effects of earthquakes are being implemented for new and retrofit construction. Two of these technologies are seismic (base) isolation and energy dissipation (supplemental damping). Knowledge has increased recently regarding the response of components of seismic isolation and supplemental damping systems as a result of comprehensive testing in university and corporate laboratories in the United States, Japan and elsewhere. Less knowledge is available on the response of systems of components, especially in bridges. The response of systems of isolation and damping components is the subject of much research at the University of California at Berkeley. This paper summarizes work under way at Berkeley studying the response of the seismically-isolated San Francisco-Oakland Bay Bridge. The studies of component response at Berkeley, SUNY Buffalo, and other universities in the United States have led to the development of draft standards for prototype testing of seismic isolators and supplemental dampers. This paper also presents and examines recently developed specifications for testing supplemental damping devices.

INTRODUCTION

Protective systems (seismic isolation and/or energy dissipation systems) and hardware (seismic isolators and/or energy dissipation hardware) are being used to mitigate the effects of earthquakes in bridges, buildings, and other structural systems in the built environment. Of the two technologies, seismic isolation is the more mature with numerous applications in Italy, Japan, New Zealand, and the United States. U.S. experimental data supporting the use of seismic isolation include component testing of elastomeric and sliding isolators, and systems testing of model buildings (e.g., Clark et al. [1996b]) and bridges (e.g., Constantinou et al. [1993]). Less experimental data are available on the behavior of energy dissipation components and systems incorporating such components.

There is much less information available on the use of seismic isolators and/or energy dissipators for bridges than buildings. This motivated Caltrans and researchers at the University of California at Berkeley to develop a coordinated analytical and experimental research program with the objective of improving the state-of-knowledge of the use of protective systems for bridge applications. This project is well under way, with some information from this program being presented at this meeting in Clark et al. [1996a].

The San Francisco-Oakland Bay Bridge (SFOBB) is a 4.3 mile (7 km) long viaduct linking San Francisco and Oakland in northern California. The bridge is the primary transportation link between these cities with a total of 10 lanes of traffic carrying upwards of 250,000 vehicles per day. The 1989 Loma Prieta earthquake caused significant damage to the East Bay Crossing (between Yerba Buena Island and Oakland) of the bridge, including the loss of one upper and one lower deck section. The multi-hundred million dollar retrofit of the East Bay Crossing will include the introduction of seismic isolators between the horizontal superstructure and the vertical substructure. The isolators are mission-critical hardware; acceptable performance of the Crossing in the maximum earthquake is dependent on high performance from the isolators. Given the importance of the bridge to Caltrans and the State of California, the lack of redundancy in the Crossing's seismic framing system, the critical mission of the isolation hardware, and the lack of information on the tri-directional behavior of seismic isolation components and systems, Caltrans has embarked on a fast-track research project to provide the requisite information with the specific focus being the seismic isolation system adopted for the retrofit of the Crossing. The proposed work is described in Systems Testing below.

Energy dissipation devices (also termed supplemental dampers) are being used in new and retrofit bridge construction in California. High profile projects incorporating dampers include the retrofits of the Golden Gate Bridge and the Richmond-San Rafael Bridge. Damper hardware being considered for these projects includes fluid viscous, friction, lead-extrusion devices. Most specifications for the supply of damper hardware include requirements for prototype and production testing. Although standards for testing energy dissipation devices for building applications are available [ATC, in preparation], similar standards for bridge applications have not yet been developed. The damper prequalification program [Aiken and Kelly, 1996] for the retrofit of the Golden Gate Bridge includes the most rigorous testing program developed to the time of this writing. The salient features of this testing program, and comments on issues not addressed in the program are presented in Damper Hardware Testing below.

SYSTEMS TESTING

The East Bay Crossing of the SFOBB is composed of multiple double-deck truss spans: 288' (88 m) deck trusses, 504' (154 m) through-trusses, and one 2420' (738 m) cantilever span. The column elements supporting these trusses include steel concentrically braced frames, reinforced concrete pier walls, and two column reinforced concrete frames. An elevation of the San Francisco-Oakland Bay Bridge (SFOBB), reproduced from Sundstrom [1996] is presented in Figure 1; the East Bay Crossing is to the right of Yerba Buena Island in this figure.

The retrofit strategy adopted by Caltrans for the 288' (88 m) and 504' (154 m) spans is seismic isolation. Additional strengthening of the substructures will be undertaken. Seismic isolation was selected for the purpose of reducing the average acceleration of the spans in the maximum earthquake to approximately 0.15g [Sundstrom, 1996]. Recognizing that the bridge was designed at the working stress level for a lateral seismic coefficient of 0.10 ($\geq$ 0.15 at the *strength* level), the choice of seismic isolation in lieu of conventional strengthening schemes has eliminated the need for extensive retrofit of the superstructure.

The friction-pendulum system (FPS) was selected by Caltrans for the seismic isolation of the truss spans. This sliding isolation system was chosen [Sundstrom, 1996] because the FPS isolators could (1) be installed without major modification to the pier caps, (2) accommodate the large displacements associated with a six-plus second isolation period, and (3) limit the shear forces transmitted to the piers to acceptable values. Two types of sliding isolators are to be used for the retrofit: spherical isolators, and cylindrical isolators. The Type 1 FPS spherical isolator for the retrofit of the East Bay Crossing is 120 in. (305 cm) by 120 in. (305 cm) in plan, 15 in. (38 cm) tall, has a radius of curvature equal to 352 in. (894 cm), and is designed for this application for a friction coefficient of 0.06 [Mellon, 1996]. See Figure 2 for sample details. The minimum lateral displacement capacity of this isolator is 38 in. (97 cm.). The target period of free vibration associated with this isolator is 6.0 seconds.

The seismic isolators will be mission-critical hardware in the retrofitted East Bay Crossing. Detailed knowledge of isolation system and isolator component responses is thus needed to verify the assumptions made for the analysis of the retrofitted spans. To provide the requisite information on system and component responses, the Earthquake Engineering Research Center has proposed the following work to Caltrans:

1. Detailed characterization of the response of individual scale-model isolators to service and seismic loads and displacements.

2. Earthquake simulator testing of a "rigid" model supported on combinations of cylindrical and spherical FPS isolators.

3. Earthquake simulator testing of a scale model of a 288 ft (88 m) prototype truss span supported by combinations of cylindrical and spherical FPS isolators on top of idealized piers.

A brief description of each of these tasks follows.

FPS Isolator Characterization

Elastomeric and sliding seismic isolation bearings have been the subject of significant study in the last 15 years. Key studies on the response of FPS sliding isolators include Al-Hussaini et al. [1994], Constantinou et al. [1993], Mohka et al. [1990], and Zayas et al. [1987, 1989]. These studies have focused on the isolator behavior under constant axial load and uni-directional, horizontally imposed displacements. More realistic dynamic, and especially tri-directional dynamic tests have not been carried out in general due to the lack of a dynamic test machine capable of subjecting seismic isolators to three-dimensional dynamic load and displacement inputs. (Limited data are available on the behavior of teflon bearings under tri-axial excitation [Mohka et al., 1993], but these data are likely not applicable to the FPS isolators due to differences in construction materials.)

The isolators in the SFOBB will be subjected to three-dimensional dynamic inputs during earthquake shaking. It is important therefore to understand the *three-dimensional* behavior of the isolators; merely inferring the three-dimensional behavior from analysis of two-dimensional response data cannot be justified given the mission-critical nature of the isolators. The knowledge

gained from the three-dimensional characterization of the isolators will be used to support the earthquake simulator studies described below and will allow Caltrans engineers to validate the constitutive models of the isolators used for the analysis of the retrofit strategy and assess the effects of various environmental factors such as thermal cycle-induced wear and salt water contamination.

We propose to study the three-dimensional response of scale models of the prototype FPS isolators using a dynamic test machine. A schematic design of the test machine is presented in Figure 3. This machine will allow EERC researchers and Caltrans engineers to thoroughly characterize the response of specific FPS isolators to uni- and bi-directional horizontal dynamic excitations under both constant and varying axial loads. A minimum of four isolators (two cylindrical and two spherical) will be subjected to detailed testing. The data obtained from these tests will be used to support similar tests on full-size prototype FPS isolators being planned by Caltrans.

The behavior of any type of isolator (elastomeric or sliding) is affected by service load wear and contamination. To study the effects of wear on the sliding surface due to thermally induced movement of the truss spans, we propose to subject one spherical and one cylindrical FPS isolator to 20,000+ {+0.5 in. (1.3 cm), -0.5 in. (1.3 cm)} displacement cycles to simulate the likely thermal and service load movement over the life span of the isolators. The issues of contamination will be addressed by individually evaluating the effects of condensation and salt water spray on the sliding surface. The protocol for the contamination tests will be determined by EERC and Caltrans engineers, using wherever possible the protocol developed for the Caltrans HiTEC testing program.

Earthquake Simulator Testing of a Rigid Model

Sophisticated analytical tools have been used by Caltrans to evaluate the seismic response of the seismically-isolated East Bay Crossing of the SFOBB. Key mathematical assumptions regarding the global behavior of the isolators have been made. The objective of this task is to verify some of those assumptions by testing simple, relatively *rigid* models that do not include the dynamic characteristics of the trusses.

A small "rigid" model supported on (a) four spherical FPS isolators, and (b) two spherical and two cylindrical FPS isolators will be tested. The FPS isolators used in this task may be re-used for the earthquake simulator testing of the truss model. The models will be subjected to prescribed earthquake inputs, and the responses of the models will be measured using acceleration and displacement transducers and load cells beneath each of the four isolators.

The earthquake inputs will include site-specific motions (used for the evaluation of the retrofitted bridge), near-field earthquake records adjusted for the distance between the bridge and the causative faults, and recorded and synthetic earthquake motions. Earthquake motions will include simultaneous horizontal and vertical components.

The small "rigid" models will be analyzed using both (a) the computer programs used for the analysis of the East Bay Crossing, and (b) state-of-the-art research-oriented mathematical

tools. The goal of these analytical studies is to predict the *global* behavior of these simple isolated models using the measured ground motion histories input to the models on the earthquake simulator. The *measured* responses from the earthquake simulator testing can then be compared with the *predicted* responses to validate the analytical models used for computing the dynamic behavior of the FPS isolators.

Good correlation between the *measured* and *predicted* responses of these two models will indicate that the modeling assumptions are reasonable, and that existing mathematical tools can be used with confidence to capture the response of the truss model. Poor correlation may indicate that the basic modeling assumptions used for the analysis of the bridge need to be improved.

Earthquake Simulator Testing of a Model Truss Span

A scale model of a retrofitted 288-foot (88 m) long truss span will be designed and fabricated for the purpose of earthquake simulator testing. The scale model will be tested in two configurations (A and B). In each configuration, the truss model will be supported on two sets of four bearings: four spherical FPS isolators (A); and two spherical and two cylindrical FPS isolators (B). Configuration A will correspond to the truss span at Piers E13 and E14, and Configuration B will represent the truss span at Piers E16 and E17. The isolators will in turn be supported on load cells and column elements designed to model the lateral stiffness, but not the mass of the piers.

Detailed analysis of the 288-foot (88 m) long truss span will be undertaken to establish the key dynamic characteristics of the truss spans and to provide bounding values for these characteristics. These data will then be used as the basis for designing the scale model using the appropriate similitude laws. The model of the retrofitted span will be designed and fabricated at approximately one-twelfth scale. The framing for the model will not necessarily replicate the retrofitted truss span, but will provide a reasonable representation of both the dynamic characteristics of the 288-foot long span and the mechanism of load transfer to the isolators. Prior to earthquake simulator testing, forced vibration testing of the scale model will be undertaken to establish (and correct, if necessary) its dynamic characteristics.

Each configuration of the truss models will be subjected to prescribed earthquake inputs, and the responses of the models measured using acceleration, velocity, and displacement transducers, and the load cells beneath each of the four isolators. Specific earthquake simulations will be repeated following modifications to the column elements representing the piers so as to investigate the effects of pier flexibility on the response of the isolated bridge.

The earthquake inputs will include site-specific motions (used for the evaluation of the retrofitted bridge), near-field earthquake records adjusted for the distance between the bridge and the causative faults, and other recorded earthquake motions. Earthquake motions will include simultaneous horizontal and vertical components. The effects of foundation rocking will be captured by rotational excitation of the simulator platform.

Prior to testing, the scaled earthquake input motions will be used to predict the response of the isolated truss models. Such analyses are performed prior to simulator testing so that (1) the

response transducers are correctly located on the models, (2) the response transducers are not over-ranged during testing, (3) damage to the scale model is avoided, and (4) analytical data are available for the purpose of response correlation following testing.

Specific objectives of the testing program include the evaluation of (1) the performance of the retrofitted truss span to different earthquake ground motions, (2) the effects of torsion and twisting on the response of the isolated bridge, (3) isolator and bridge response due to uplift effects caused by vertical accelerations and overturning, (4) the effects of high frequency vertical input on bridge response, (5) the influence of pier flexibility on bridge response, (6) the effects of superstructure flexibility on bridge response, (7) the effects of the wind-restraint devices, and (8) the likelihood of permanent and cumulative displacements following earthquake shaking.

Upon completion of the earthquake simulator testing program, one spherical and one cylindrical FPS isolator will be re-tested in the dynamic test machine using the protocol developed to test individual FPS isolators to characterize the change (if any) in the key dynamic properties of the isolators as a result of the earthquake simulator testing program.

DAMPER HARDWARE TESTING

The recent surge of interest in the use of supplemental damping hardware for new and retrofit bridge construction has highlighted the need for prototype and production damper testing standards and guidelines for in-service inspection and periodic testing of dampers. Recent developments in these areas, primarily resulting from studies by researchers at the University of California at Berkeley and the State University of New York at Buffalo are presented below.

Testing Standards

Testing standards for mechanical components such as seismic damping devices are unfamiliar to most bridge (and building) engineers. Such engineers rarely design components for bridges and buildings that incorporate moving parts, and as such have little to no experience with testing structural components with internal (often proprietary) moving components that are perhaps subject to failure by thermal cycling, seal damage, or corrosion. Nonetheless, component testing standards have been developed for, and used by the aerospace, defense, and nuclear power industries, among others, for more than 30 years. The information gleaned from testing of dampers for different types of loading environments, and recent knowledge gained from testing dampers using earthquake-type loading histories have been used in the development of guidelines for testing dampers for building applications [ATC, in preparation; BSSC, 1994]. Although project-specific testing programs have been developed for testing dampers for new and retrofit bridge construction (e.g., Aiken and Kelly [1995]), no national damper testing standard has yet been established. This paper does not attempt to develop such a standard, but rather identifies key issues that must be addressed in such a development effort. Further, there are no guidelines for production testing and in-service inspection and testing of supplemental damping hardware, although such testing and inspection may be crucial to the successful performance of the hardware during earthquake shaking.

Prototype Testing

The goals of a testing program for prototype dampers are two-fold: (1) to define the mechanical characteristics of the damper, and (2) to demonstrate the robustness (i.e., the degree of stiffness and strength degradation with repeated cycling) of the damper response. Typical mechanical characteristics to be evaluated include effective stiffness; hysteresis loop area; amplitude, frequency, velocity, and temperature dependence; and constitutive law.

Testing standards for prototype dampers for building applications are relatively mature. The most current of such standards, those presented in the ATC-33 *Guidelines* [ATC, in preparation], includes a minimum sequence of tests that address:

1. Damper response at displacements and velocities consistent with those anticipated at the maximum earthquake displacement.

2. Damper performance for levels of seismic hazard other than the maximum earthquake.

3. Damper response at displacements and velocities consistent with those anticipated in the design wind storm.

4. The likely duration of strong motion shaking — by linking the number of cycles of testing to the fundamental period of the structure.

5. Damper response as a function of ambient (operating) temperature, frequency, and bilateral load.

Specifically, the minimum testing program for prototype hardware for building applications [ATC, in preparation] is:

1. A complete sequence of production tests (to benchmark the response of the production dampers).

2. Testing for environmental effects (principally wind).

3. Twenty (20) displacement cycles consistent with maximum earthquake displacements and velocities. Static testing is permitted for displacement-dependent hardware; dynamic tests are required for velocity-dependent hardware.

4. If the response of the damper being tested is dependent on frequency or bi-lateral load, the tests of 3. are repeated at specified increments of frequency and bi-lateral displacement.

Acceptance criteria have been developed for use with the above prototype testing program. First, the response of the prototype damper, measured using effective stiffness, hysteresis loop area, and force-output at zero displacement, for any one cycle of loading, must not differ by more than 15 percent from the average values calculated from all cycles in that test. This criterion is a check on the robustness of the damper. The 15-percent limit may be increased or decreased by the engineer-of-record. Second, the average response of the prototype damper,

calculated from all cycles in a test, must fall within the limits set by the engineer-of-record in the specification.

For prototype testing of dampers for bridge applications, the above minimum sequence of tests should be augmented to include testing for endurance and environmental effects and contamination. The endurance tests should seek to replicate the effects of thermal cycling, traffic-induced vibration, and wind-induced vibration. Environmental effects to be considered include corrosion and ozone attack.

A detailed prototype testing program for the prequalification of vendors for the supply of dampers for the retrofit of the Golden Gate Bridge was developed by T.Y. Lin International and executed at the Earthquake Engineering Research Center in 1995. Details of the testing program and the response of each of the four dampers tested at Berkeley can be found in Aiken and Kelly [1995]. Salient features of the testing program are presented below. The program was developed to test fluid viscous dampers with the following constitutive law:

$$F(t) = C|\dot{u}(t)|^{05}\,\mathrm{sgn}(\dot{u}(t))$$

where F is the force output of the damper, C is the damping coefficient (= 75 kip.sec$^{0.5}$/in.$^{0.5}$), $\dot{u}(t)$ is the relative velocity between the ends of the damper, and sgn is the signum function. The design parameters for the full-scale dampers were: maximum force output = 650 kips (2.9 MN), total stroke = 48 inches (122 cm), maximum relative velocity = 75 in./sec. (190 cm/sec.), average maximum power = 350 HP (0.26 MW), and peak power = 5400 HP (7.25 MW). The frequency range of interest was 0.1 to 5.0 Hz, and the specified range for operating temperature was 40°F (4°C) to 100°F (38°C). Testing of full-scale dampers was not possible. Reduced-scale dampers, designed to suit the EERC damper test machine, were tested. The design parameters for the reduced-scale dampers were: maximum force output = 100 kips (444 KN), maximum relative velocity = 20 in./sec. (51 cm./sec), and total stroke = 12 inches (30 cm).

The prototype testing program developed for the reduced-scale dampers [Aiken and Kelly, 1995] consisted of the following tests. The acceptance criteria adopted for each test sequence are also presented. Such a program could be modified for use in other bridge projects.

1. Cyclic testing to provide benchmark data on damper response prior to prolonged cyclic testing (test sequence 2.)

2. Testing for seal longevity under wind excitation: 1800 cycles, displacement = ± 6 inches (15 cm), frequency = 0.02 Hz, peak velocity = ± 0.5 in./sec (1.3 cm/sec.). The dampers were considered to have passed this test if there was no significant fluid loss and no evidence of seal damage.

3. Cyclic testing to characterize the damper response: 5 to 10 cycles, constant velocity and sinusoidal test histories, peak force = 0 to 100 kips (444 KN); peak velocity = 0 to 20 in./sec (51 cm/sec.); displacement = ± 0 to ± 6 inches (15 cm), frequency = 0.1 to 5.0 Hz, temperature = 40°F (4°C), 70°F (21°C), 100°F (38°C). The acceptance criteria required that: (1) the force-velocity relation for the damper fall within ± 15 percent of specified constitutive

law, (2) the static friction force be no greater than 2.5 percent of the maximum force output of 100 kips, and (3) the damper loop area be at least 82 percent of the area of the idealized elasto-perfectly plastic loop.

4. Earthquake testing using the scaled maximum earthquake displacement history calculated by analysis.

It is often not physically possible to dynamically test full-scale dampers, and reduced-scale dampers must be used for prototype testing. A key step in the testing program is the design of the reduced-scale dampers. For metallic-yielding hardware, the design of reduced-scale dampers is generally relatively straightforward. For friction dampers, the general configuration, interface materials, and contact pressures should be identical in the full-scale and reduced-scale dampers. Reduced-scale viscoelastic dampers should use the same VE materials and bonding agents as those used in the full-scale dampers. For viscous damping hardware, the scaling procedures are more complicated and the design of the reduced-scale dampers is not trivial. For the design of the 100-kip viscous dampers for the Golden Gate Bridge testing program, five key parameters were identified: overall configuration, fluid, seals, orifices, and pressure. The general configuration and function of the reduced-scale damper was required to be *similar* to that of the full-scale damper. The type and grade of fluid in the reduced- and full-scale dampers was required to be identical. The general design and operation of the orifices (including flow velocity through the orifice) and seals, and the ambient and operating pressures in the reduced- and full-scale dampers were required to be identical. Different, or additional parameters may be key for the design of reduced-scale viscous dampers for other projects.

Production Testing

The goal of production testing is quality control. The scope of a production testing program should be dependent on the type of damper under consideration, and ought be developed by the engineer-of-record to suit the specific needs of the project. Acceptance criteria for the production dampers should be linked to the benchmark test data collected during the first sequence of tests on the prototype dampers.

Simple material tests and displacement cycling to 0.5 times the damper yield displacement may be sufficient for metallic-yielding dampers. Materials tests and displacement cycling to the displacement in the design (not maximum) earthquake may be sufficient for viscoelastic dampers. Production testing of viscous dampers should include cyclic dynamic or drop testing, proof pressure testing, and limited, low-velocity cyclic testing to check seal wear.

In-Service Testing and Inspection

Mission-critical hardware such as seismic isolators and energy dissipators (dampers) warrant regular inspection, and periodic testing as necessary. The precedent for in-service testing and inspection of damper hardware was set more than 30 years ago in the nuclear power industry.

Dampers composed of internal moving components, or of materials subject to aging and environmental effects (e.g., fluid viscous, viscoelastic, and friction dampers) should be regularly

inspected and periodically tested. Given that the current generation of such hardware has not been in service for more than approximately 10 years, there is no proven track record upon which engineers could base a decision to eliminate inspection and testing.

CONCLUSIONS

Seismic isolation and supplemental damping are two new technologies that are being used in new and retrofit bridge construction. Although there is much information in the literature on the bi-directional (1 vertical, 1 horizontal) behavior of elastomeric and sliding seismic isolators, there is scant data on the tri-directional (1 vertical, 2 horizontal) behavior of sliding isolators, and even less information on the response of isolation systems to tri-directional earthquake excitation.

To augment existing knowledge on the tri-directional response of seismically-isolated bridges, and specifically to validate the analysis and design procedures used for the seismic isolation retrofit of the East Bay Crossing of the San Francisco-Oakland Bay Bridge, Caltrans is supporting a fast-track research project at the Earthquake Engineering Research Center. The scope of this project includes: (1) detailed characterization of the tri-directional response of individual scale-model isolators to service and seismic loads and displacements, (2) earthquake simulator testing of a "rigid" scale model supported on combinations of cylindrical and spherical FPS isolators, and (3) earthquake simulator testing of a scale model of a 288 ft (88 m) prototype truss span supported by combinations of cylindrical and spherical FPS isolators on top of idealized piers. Results of this testing program will be presented at the next U.S-Japan Workshop on Earthquake Protective Systems for Bridges.

Recent interest in the use of supplemental damping hardware for new and retrofit bridge construction has highlighted the need for prototype and production damper testing standards, and guidelines for in-service inspection and periodic testing of dampers. In the last two years there has been unprecedented guidelines-development activity in the United States, with much of this work being based on experimental and analytical studies by researchers at the University of California at Berkeley and the State University of New York at Buffalo. State-of-the-knowledge guidelines and testing procedures were summarized, with the foci being prototype testing, production testing, and in-service inspection and periodic testing.

ACKNOWLEDGMENTS

The assistance and support of California Department of Transportation's George Amaro, Tim Leahy, Dorie Mellon, Jim Roberts, Li-Hong Sheng, and Mohsen Sultan in the development of the bridge systems testing programs are greatly appreciated. Mr. Don Clyde of EERC was responsible for much of the development work on the dynamic test machine; his contributions to the work described in this paper are gratefully acknowledged. The contributions of Professor Michael Constantinou (SUNY Buffalo) and Dr. Charles Kircher (Charles Kircher and Associates) to the development of the damper testing standards presented in ATC-33 [ATC, in preparation] is gratefully acknowledged.

The findings and conclusions summarized in this paper are those of the authors alone.

REFERENCES

Aiken, I.D. and J.M. Kelly, 1995, "Prequalification Testing of Viscous Dampers for the Golden Gate Bridge Seismic Rehabilitation Project," *Report No. EERC-STI/95-01*, Earthquake Engineering Research Center, University of California, December

Al-Hussaini, T.M., V.A. Zayas, and M.C. Constantinou, 1994, "Seismic Isolation of Multi-Story Frame Structures Using Spherical Sliding Isolation Systems," *Report No. NCEER-94-0007*, National Center for Earthquake Engineering Research, State University of New York, Buffalo, N.Y.

ATC, in preparation, "NEHRP Guidelines for the Seismic Rehabilitation of Buildings," *Reports FEMA 273 and 274*, Applied Technology Council, Redwood City, CA

BSSC, 1994, "NEHRP Recommended Provisions for Seismic Regulations for New Buildings," Report FEMA 222A, Building Seismic Safety Council, Washington, D.C.

Clark, P.W., J.M. Kelly, and I.D. Aiken, 1996a, "Aging studies of high-damping rubber and lead-rubber seismic isolators," *Proceedings of the Fourth US-Japan Workshop on Earthquake Protective Systems for Bridges*, Osaka, Japan, December

Clark, P.W., I.D. Aiken, and J.M. Kelly, 1996b, "Experimental Studies of the Ultimate Behavior of Seismically-Isolated Structures, *UCB/EERC report in preparation*, Earthquake Engineering Research Center, University of California, Berkeley, CA

Constantinou, M.C., P. Tsopelas, Y-S. Kim, and S. Okamoto, 1993, "NCEER-Tasei Corporation Research Program on Sliding Isolation Systems for Bridges: Experimental and Analytical Study of a Friction Pendulum System (FPS)," *Report No. NCEER-93-0020*, National Center for Earthquake Engineering Research, State University of New York, Buffalo, N.Y.

Mellon, D., 1996, Private Communication

Mohka, A.S., M.C. Constantinou, and A.M. Reinhorn, 1990, "Experimental Study and Analytical Prediction of Earthquake Response of a Sliding Isolation System with a Spherical Surface," *Report No. NCEER-90-0020*, National Center for Earthquake Engineering Research, State University of New York, Buffalo, N.Y.

Mohka, A.S., M.C. Constantinou, and A.M. Reinhorn, 1993, "Verification of friction model of teflon bearings under triaxial load," *Journal of the Structural Division*, Vol. 119, No. 1, ASCE, January

Sundstrom, J., 1996, "Seismic retrofit of the east spans of the San Francisco-Oakland Bay Bridge," *Proceedings of the 12th U.S.-Japan Bridge Engineering Workshop*, Buffalo, New York, October

Zayas, V.A., S.S. Low, and S.A. Mahin, 1987, "The FPS Earthquake Resisting System," *Report No. UCB/EERC-87/01*, Earthquake Engineering Research Center, University of California, Berkeley, CA., June

Zayas, V.A., S.S. Low, S.A. Mahin, L. Bozzo, 1989, "Feasibility and Performance Studies on Improving the Earthquake Resistance of New and Existing Buildings Using the Friction Pendulum System," *Report No. UCB/EERC-89/09*, Earthquake Engineering Research Center, University of California, Berkeley, CA., July.

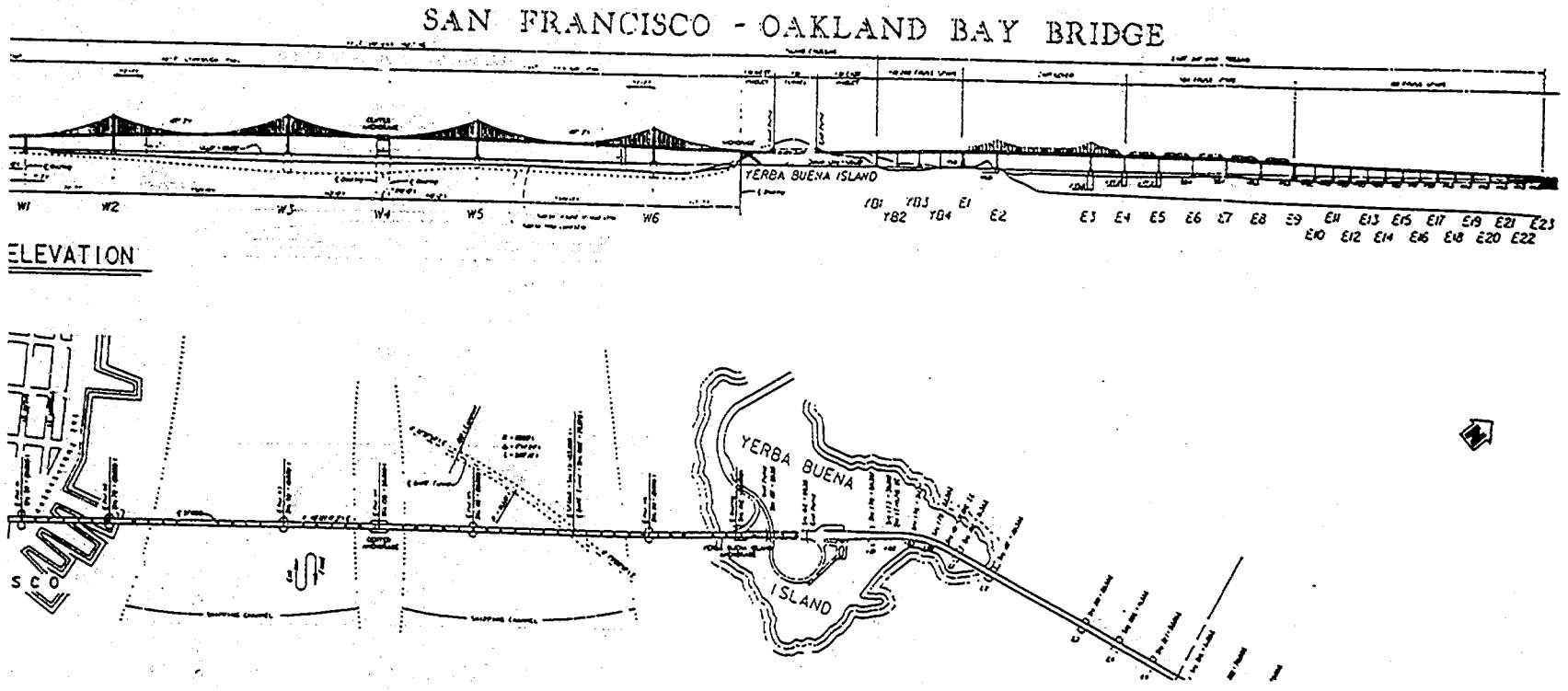
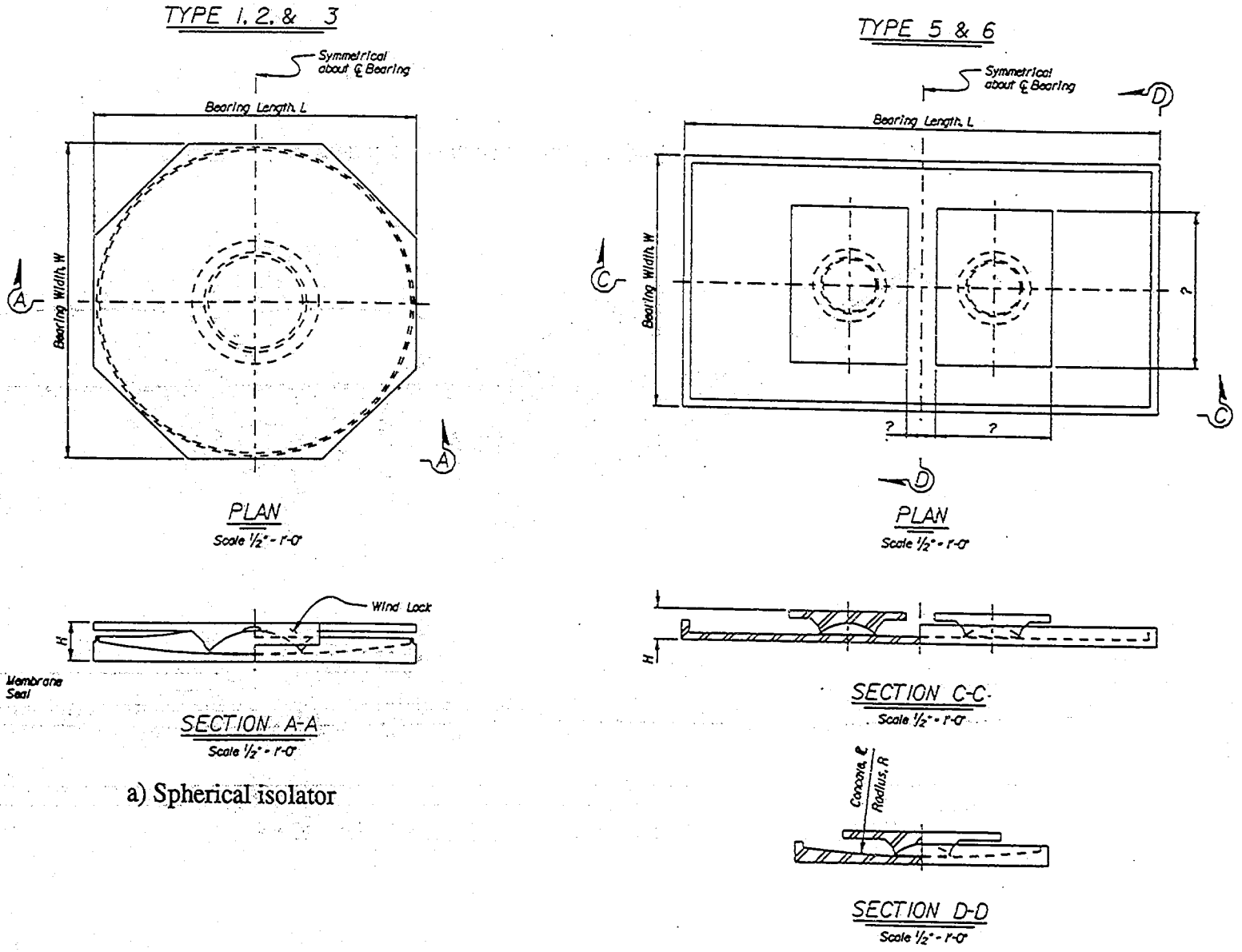


Figure 1. San Francisco - Oakland Bay Bridge (from Sundstrom [1996])



a) Spherical isolator

b) Cylindrical isolator

Figure 2. Preliminary FPS isolator details.

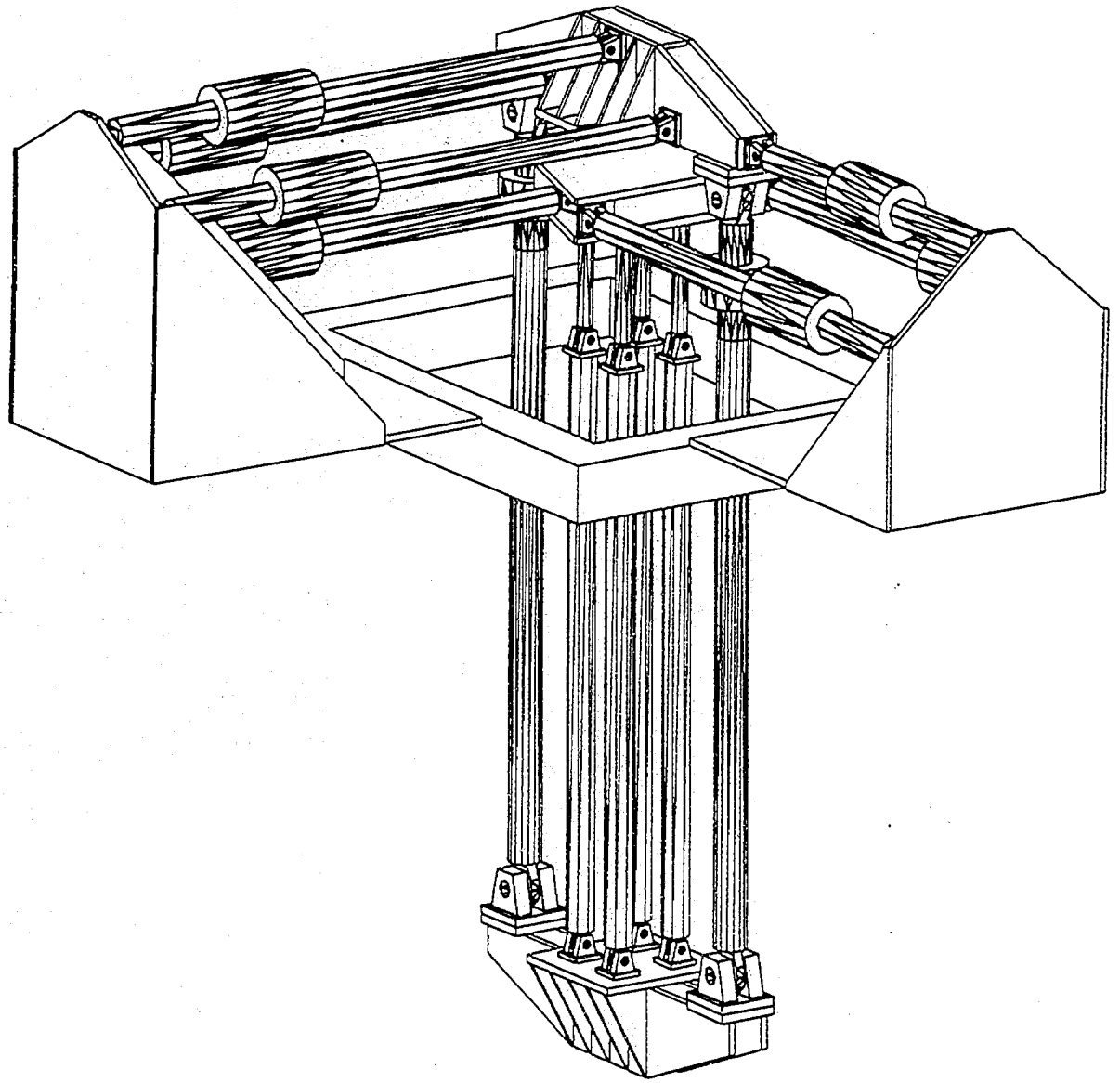


Figure 3. Isometric view of the tri-directional isolator test machine

The Analysis of Seismic Response of the Bridge with Menshin Bearings during the Hyogo-ken Nanbu Earthquake

Toshihiko NAGANUMA Dr. Eng. Sci.
Research and Development Division, Hanshin Expressway Management Technology Center

Yoshihei HORIE and Hiroshi KOBAYASHI
Design Section, Engineering Division, Hanshin Expressway Public Corporation

Nobuyuki SASAKI
Hiroshima Research & Development Center, Mitsubishi Heavy Industries, Ltd

Abstract

Matsunohama Viaduct on the Wangan Route of the Hanshin Expressway is a pioneer structure with a special consideration on earthquake resistant design: some of its continuous steel girders are supported by menshin bearings (base isolators with the energy absorbing function), and the functions of lateral force dispersion and energy dissipation are expected in case of earthquakes. On January 17th, 1995, a strong ground motion of the Hyogo-ken Nanbu Earthquake, whose epicenter was just across the bay, actually worked on the viaduct, and important data were obtained from seismometers installed on the several locations of the bridges. In this paper, the features of the recorded data are carefully investigated in different approaches. First, the recorded data of the bridge with menshin bearings are compared with the data from the adjacent bridge which has the similar conditions except that it has conventional rubber bearings without the dampening function. As a result of comparison, the clear effectiveness of the menshin device can be confirmed under the strong ground motion. Secondly, the model simulation of the bridge is carried out, and its numerically calculated seismic responses are compared with the observed records to verify its rationality. Lastly, the performance of the bridge under the strong motion of the Hyogo-ken Nanbu Earthquake is simulated with the consideration of nonlinear property of concrete piers and menshin bearings, and its safety is reconfirmed.

1. Introduction

The Hanshin Expressway is an intra-city highway network in Osaka and Kobe area, and the Wangan (bay shore in English) Route is one of its trunk routes linking the new international airport in the south to the center of Osaka and Kobe. Menshin bearings (base isolators with the energy absorbing function) are adopted to a 4-spanned continuous non-composite steel box-girder bridge in the Matsunohama Viaduct located at the southern part of the route (see *Figure-1*).

This is the first application of menshin bearings for bridge structures in the Hanshin Expressway, and therefore, the field vibration test and model analysis were conducted to

confirm its presumed performance under the earthquake. Furthermore, for data collection and follow-up study in the future, seismometers are installed on various locations on both this bridge and the adjacent similar bridge with non-menshin bearings.

On January 17th, 1995, the seismometers caught the strong ground motion known as the Hyogo-ken Nanbu Earthquake transmitted across the Bay of Osaka from the epicenter near Kobe. The recorded data are unique and worth being analyzed as to how the bridge actually responded and especially how effectively the menshin device functioned.

This paper comprises three sections: it starts with the introduction of the recorded data and its basic analysis, where the comparison between bridges with menshin and non-menshin bearings is the main approach to measure the performance of the menshin device during the earthquake. Secondly, a model simulation of the bridge is conducted, and its presumed seismic responses are compared with the actual data to evaluate the model's reproductivity. Lastly, by the same model simulation with the input of the earthquake records at Kobe, the response of the bridge is predicted assuming that the stronger tremor hits directly the Matsunohama Viaduct.

2. Outlines of the Matsunohama Viaduct

The Matsunohama Viaduct is located about 35 km east-south-east from the epicenter of the Hyogo-ken Nanbu Earthquake, as shown in *Figure-1*. Among the bridges in the viaduct, the one with menshin bearings has a bridge length of 211.5m and a total width of 21.94m with a radius of curvature of 560m, as illustrated in *Figure-2* and *3*. The substructure which supports the superstructure is T-shaped concrete piers with pile foundations.

Menshin bearings are mounted on three middle piers (B, C and D), and bearings for both end piers are conventional roller bearings. The type of menshin bearings are lead rubber bearings (LRB) which incorporates lead plugs within stratified rubber plates. Bearings are movable only to the longitudinal direction, and two side stoppers installed with a clearance of 5mm prevent the excessive movement to the transverse direction. (The structural details of the bridge and menshin bearings can be referred to the other references.[1])

The bridge with similar configuration but with non-menshin rubber bearings is located just 200m north of the menshin bridge. Non-menshin bearings can disperse seismic lateral force evenly to every column, but the bearing itself has no damping function. This bridge is a 4-spanned continuous non-composite steel I-girder bridge with the total length of 180m. Its width varies from 25.5m to 36.6m (see *Figure-2*). The superstructure of steel I-girders is supported by rigid-frame concrete piers on pile foundations. The bearings are also movable only to the longitudinal direction.

In the following, the bridge where menshin bearings are installed is referred to as the menshin bridge, while the one with non-menshin bearings is referred to as the non-menshin bridge.

3. Outlines of seismometer layout

Both menshin and non-menshin bridge have four servo-type acceleration gauges (ten components in total) around pier D (see *Figure-3*), which are installed on the ground (three components), on the footing (three components), on the pier-top (three components) and on the steel girder (one longitudinal component).

4. Results of survey and data analysis

(1) Survey results

Though both bridges did not undergo any damages by this earthquake, a substantial level of acceleration worked on them, and measurable records could be obtained at all points.

Figure-4 shows a typical acceleration seismograms recorded at each measurement point, and the horizontal distribution of the maximum acceleration is illustrated in *Figure-5*. The maximum horizontal acceleration on the ground level is in the range of 100gals to 140gals. Recorded response acceleration on the upper portion of the bridge (girder and pier-top) is doubled to be a range of 190gals and 240gals in the longitudinal direction. In contrast, in the transverse direction, it is amplified as three or four times as the ground value, to the range from 350gals to 450gals. This difference in the level of amplification is caused by sharp peaks appeared in the wave on the transverse direction. The sharp peaks are supposed to be the impact caused by the collision of girders and side stoppers.

(2) The analysis of menshin effects

a) Estimation from the response acceleration

In this paper, the analysis and comparison of the recorded data are focused only on the longitudinal direction where bearings are movable and a clear menshin effect is expected.

Figure-6 shows Fourier spectra of the original acceleration records at some points of the bridges. The spectrum on the footing level, where the ground motion is transmitted into the bridge, constitutes mainly of lower frequency compoents which are less than 3Hz on both bridges. As the frequency goes higher, the spectrum tapers down and it contains almost no component higher than 10Hz. In general, the configuration of the spectrum is similar in both bridges although it shows minor difference in part.

The first mode vibration component around 1.0Hz is rather surpassed in both girder level spectra. They also have higher frequency components over 10Hz, especially in the menshin bridge. However, since there are few such components on the footing and pier-top level, it can be said that they mainly consist of a noise factor caused by contact of the girder witth the bearing stopper.

Regarding the pier-top spectra, their predominant frequencies are between 2Hz and 7Hz which are slightly higher than the fundamental mode of the whole bridge although there exists the fundamental mode component. It can be estimated that the main vibration mode of the pier is within this frequency range.

In order to clarify the natural frequency of the superstructure, the ratio of the girder or the pier-top spectrum to the footing spectrum is calculated as shown in *Figure-7*. It shows that the fundamental mode frequency of the superstructure is estimated as 1.16Hz for the menshin bridge and 0.94Hz for the non-menshin bridge, and that of the pier is 6.34Hz and 3.65Hz respectively.

The features of spectra described above implies that the method of comparing the girder acceleration directly is not appropriate to evaluate the menshin effect, and the following should be reconsidered for more accurate analysis:

1) The ground motions acted on both bridges during the earthquake are not always identical.
2) The difference of seismic input into the superstructure due to the difference of the natural period also arises between the two bridges.
3) The girder acceleration responses include a high frequency component to some extent which is supposed to be noise.

Taking the above points into consideration, the first mode vibration portion which is the main element of the girder response is focused on, and the next method is taken to evaluate the menshin effect.

First of all, girder acceleration responses of the two bridges are processed by low-pass filtering, and higher frequecy compoents over 2.5Hz are cut off. The comonent uuder 2.5Hz can be regarded as the effective acceleration which corresponds to the seismic force working on the girders. Its maximum value is 110.9gals for the menshin bridge, and 212gals for the non-menshin bridge as shown in *Table-1*. The filtering lowers the acceleration value of the menshin bridge considerably. This decrease might be due to the noise factor caused by contact between girders and side stoppers since the alignment of this bridge is slightly curved.

Secondly, acceleration response spectra are calculated by taking the footing's acceleration response filtered also to the 2.5Hz level as an input wave from the ground, where a damping ratio and a natural period of one-degree-of-freedom system are given as structural parameters. Then the maximum value of girder's effective acceleration calculated above is plotted on the spectra at each point of the natural period of the girders. The result of this process is illustrated in *Figure-8*. The effective acceleration value of the girders is equivalent for the response value when the damping ratio is equal to 20% for the menshin bridge and 7% to 8% for the non-menshin bridge. This damping ratio for the menshin bridge is also found to be adequate for menshin design from *Figure-12* mentioned later, and the one for the non-menshin bridge seems to be reasonable value when taking account of damping effects of both rubber bearings and foundations.

This substantial difference of the damping factor between two bridges clarifies that the menshin device has actually been activated and substantially lowered the girder movement in this earthquake.

b) Estimation from the displacement of bearings

Another approach of examining the menshin effect focuses on the displacement response of bearings. As a displacement response of bearings, its wave form is drawn by integrating the relative acceleration which is deducting the pier-top value from girder value. The calculated maximum displacement is 2.2cm for menshin bridge and 3.9cm for non-menshin bridge.

The lateral force acting on the each bearing which corresponds to this bearing displacement is estimated by referring to the loading test data of bearings at the factory. Each acting force of all bearings in the bridge are then summed up to the total lateral force working on the entire bridge, which is further divided by the total girder weight to estimate the seismic coefficient. *Table-2* shows that the seismic coefficient for the menshin bridge is 0.13 and the one for the non-menshin is 0.18, both of which are different from the effective acceleration of girder plotted in *Figure-8* by 10% to 20%. Since this difference is insignificant, the effectiveness of the menshin device can still be explaind.

5. Model Simulation Analysis

(1) The outline of analysis

A simulative seismic response analysis using a simplified bridge model is carried out as a comparative approach with observed data. Here, the simulation uses the acceleration response at the footing as base input so that it can be evaluated to what degree the performance of the menshin bridge under this earthquake can be reproduced. *Figure-10* illustrates the three-dimensional frame model of the entire bridge used in this simulation. And the shear stiffness of menshin bearings is estimated by the three different method, as shown in *Figure-11*, and the results are compared each other; case 1 is a linear type represented by equivalent stiffness and equivalent damping ratio which correspond to the designed displacement of 10cm; case 2 is a non-linear type having the designed bi-linear property, and case 3 is another non-linear type which is formulated to approximate the results of the factory test. Of three cases, case 1 and 2 are generally applied to the design of bearings, and on the contrary, case 3 is employed in order to represent the complicated features of the menshin bearing in the small range of deformation.

Figure-12 shows the relation between equivalent stiffness (*Keq*), equivalent damping ratio (*heq*) and displacement of menshin devices. This diagram also include *Keq* and *heq* values directly obtained from the factory test. Also the recorded acceleration response used here has been processed by the noise-cut adjustment over 10Hz by reason described in **4.(2)**.

(2) Results of analysis

Examples of the model simulation are shown in *Figure-13* along with the observed data for comparison. The bridge with menshin bearings responds differently according to each modeling case, and case 3 agrees with the survey result well in terms of the wave shape and the maximum value of response acceleration. The reason why such a clear difference appears according to the modeling is that actual displacement of the menshin bearings by this earthquake is relatively small compared with the design displacement, and that the stiffness and damping are dependant of displacement.

Figure-14 shows the ratio of the Fourier spectrum of the acceleration response at the girder or the pier-top to that at the footing for case 3. This figure also shows a good agreement with the case of data analysis, which implies the adequacy of this analysis.

6. Seismic Response Analysis for a Large Scale Earthquake

Based on the results of two analyses mentioned above, the level of ground motion working on the Matsunohama Viaduct in this earthquake was near to the level of design seismic force, and the seismic response of the column stayed within a elastic range. In this chapter, assuming that the menshin bridge is closer to the epicenter and faced with stronger ground motion, its overall response is investigated by seismic response analysis including the column's non-linear performance.

The model used here, as illustrated in *Figure-15*, is a single column model in the longitudinal direction. The non-linear properties of the column are represented by Takeda model[3], and the shear stiffness of menshin bearings is the bi-linear type mentioned in **5.(1)**. One of acceleration records obtained in Kobe during the Hyogo-ken Nannbu Earthquake is used in this analysis, and the record of JR Takatori Station in the north-south component[4], which is assumed to induce a unfavorable response in this menshin bridge, is selected among available data.

Figure-16 shows the time histories of the response and energy accumulation of each part of the bridge. In terms of the maximum response value, the girder acceleration is 828gals, and its displacement is 69cm. And also, the menshin bearing deforms by 38cm, and its shear strain becomes about 300%.

The moment at the bottom of the column is 19,549tfm. This is slightly lower than the allowable value of 20,735tfm, which corresponds to the moment when the column's ductility factor is 8, and therefore the bridge stays in safety range.

The results prove that the main response of this bridge is in safety range against such a large scale earthquake due to the menshin effects of the overall bridge system, that is to say, the energy absorption effect of the menshin bearings and the column itself. Incidentally, it should be reminded that only the performance of the whole bridge system in case of the utmost ground motion is examined in this analysis, and the more precise safety check-up of each part of the bridge is not considerd.

In terms of the energy accumulation shift, the maximum value of input energy from the ground is 2,941tfm, whereas the energy absorbed in the menshin bearings and the column is 871 tfm and 1,061tfm respectively. Therefore, the rest of energy, which is about 1,000tfm, is assumed to be consumed in the bridge's damping function.

Even under a large scale earthquake where the column goes deeply into the nonlinear range, the amount of energy absorption by the menshin bearings is almost the same as that by the column, and therefore it can be concluded that a large proportion of energy absorption of this bridge is depending on the existence of the menshin bearings, and that the menshin effect can be expected even in a large scale earthquake.

7. Conclusions

The results from three different analytical approaches for investigating the menshin effect of the Matsunohama Viaduct which have been introduced in this paper can be summarized as follows:

(1) Damping ratios of two different bearing types, namely, menshin and non-menshin rubber bearings, can be estimated by use of the effective acceleration and response spectrum obtained from the observed records at the site. As a result, the effectiveness of the menshin device can be identified through the comparison of the obtained damping ratios.
(2) From the results of model simulation analysis which corresponds to the recorded data, it can be said that the modeling of the menshin bearings based on the factory test is more suitable than the linear or bi-linear model which is generally used in design if the displacement of bearings stays within a small range.
(3) Based on the nonlinear response analysis under a larger scale earthquake, the amount of energy absorption by the menshin bearings is the same level as that by the column's plastic deformation evevn in the case that the column shows nonlinear behavior in a large extent. It can be concluded that menshin bearings can contribute to the seismic safety of the whole bridge system even in this case.

References

1) Horimatsu, M. et al.: Vibration experiments and dynamic response analysis using the actual highway bridge with base isolators, Jour. of Bridge and Foundation Engineering, Vol. 28, No.4, April 1994, pp. 25-32 (in Japanese).
2) Horie, Y. et al.: The seismic response of a menshin bridge during the Great Hanshin Earthquake, Proc. of the 21st Japan Road Conference, General Issues(B), Oct. 1995, pp.868-869 (in Japanese).
3) Takeda, T. et al.: Reinforced concrete response to simulated earthquakes, Jour. of Structural Division, ASCE, Vol.96, No. ST 12, 1970, pp2557-2573.
4) Department of Yuredasu Development and Promotion: JR Earthquake Information No.23c, Railroad Research Institute, February 15th, 1995 (in Japanese).

Session 6

Methods/Issues and Applications

(Co-Chairs: H. Otsuka, A. Taylor)

"Use of Visco-Elastic Dampers to Suppress Seismic Vibration of Bridges"
by M. Shinozuka, J-M Kim, R. Purasinghe
Presented by: Masanobu Shinozuka

"Effectiveness of Unseating Prevention Devices with Energy Dissipation"
by K. Kawashima, M. Yabe,
Presented by: Masaaki Yabe

"Seismic Protection of Bridges with Fluid Dampers and the Issue of Viscous Heating"
by N. Makris, S. McMahon
Presented by: Nicos Makris

USE OF VISCO-ELASTIC DAMPERS TO SUPPRESS SEISMIC VIBRATION OF BRIDGES

Masanobu Shinozuka
Department of Civil Engineering
University of Southern California, Los Angeles, California

Jae-Min Kim
Department of Civil and Environmental Engineering
University of California at Irvine

Rupa Purasinghe
Department of Civil Engineering
California State University at Los Angeles

ABSTRACT

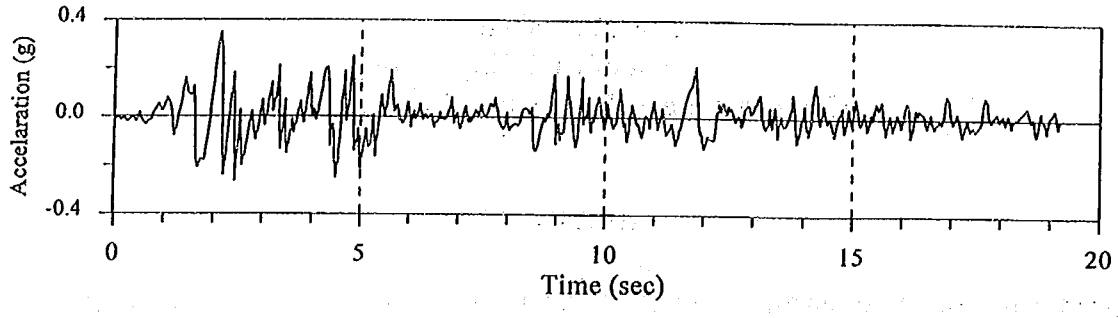
Retrofit use of visco-elastic dampers at expansion joints of bridges with hinges is studied for the purpose of demonstrating that they can prevent the girders from falling off the seat and/or colliding each other in the event of a severe earthquake. At this time, the Kelvin model, consisting of an elastic spring and a linear viscous dash pot combined in parallel, is considered for analysis. The two-dimensional finite element analysis performed on five example bridges with one or two hinges showed that the damper is effective in suppressing the relative displacement at the expense of some increase in the shear force and bending moment in the piers. It also showed that the spring component of the Kelvin model had little effect on the performance of the damper. In addition to the finite element analysis, an approximate method of evaluating the relative displacement was derived on the basis of two-degree-of-freedom models developed for two adjacent segments of bridges. The result obtained from the approximation agreed very well with the finite element results.

INTRODUCTION

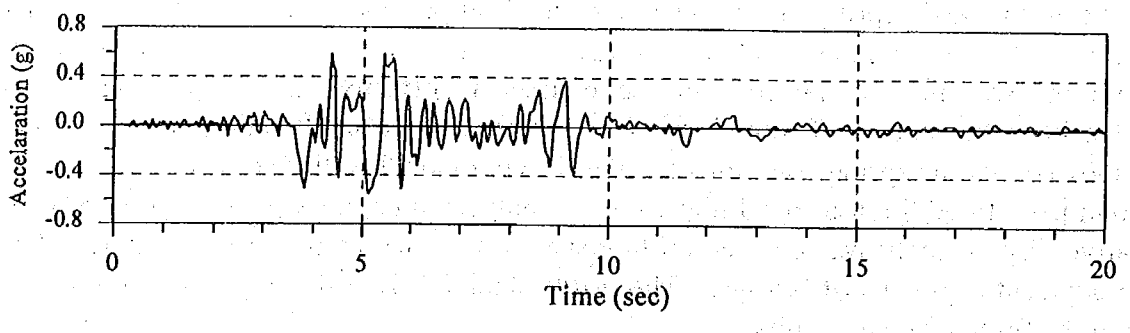
Past earthquakes, particularly the Northridge earthquake, suggested that there is a room for improvement with respect to the seismic restraining devices at expansion joints of existing 1960 vintage and other bridges particularly in California [1,2]. The objective of this study is to evaluate and improve the current state of technology for energy dissipation system appropriate for bridge seismic design and retrofitting applications. This study clearly indicates that the use of linear visco-elastic dampers offers a practical solution to the problem that often arises from the bridges with joints and thus provides them with a viable retrofitting technique.

Dealing with typical California bridges, this study investigates the effect of using visco-elastic dampers to suppress seismic vibration. It specifically recommends the use of spring-damper systems to suppress the relative motion of the bridge decks at joint locations. In the

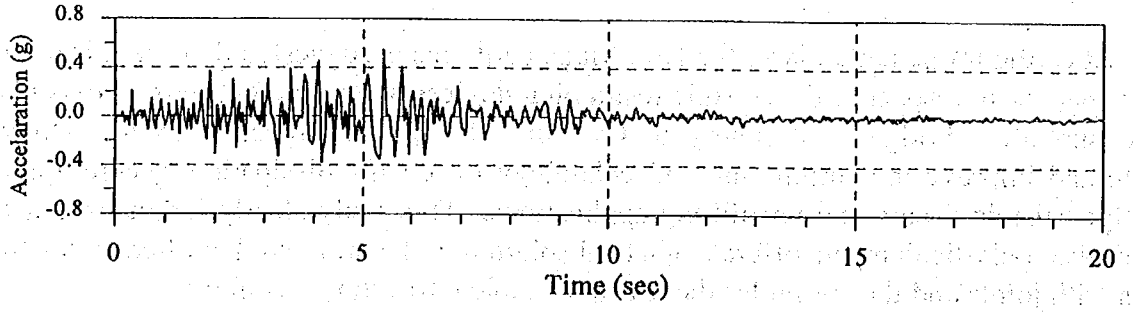
previous study [3,4], effort was made to demonstrate that spring-damper systems are in principle useful, and for the demonstration, Gavin Canyon Undercrossing that was damaged by the Northridge earthquake was analyzed. Because of the severe skewness this structure exhibited, the ANSYS finite element computer code was utilized to evaluate its dynamic response to a set of artificially generated ground motion [3]. This study deals with linear seismic response of typical Caltrans type bridges without skewness. For this reason, the SAP90 finite element computer code [5] is used for structural dynamic analysis under the seismic ground motion input given by the El Centro earthquake (NS-component, May 1940 with PGA=0.348g) and the Northridge earthquake (NS- and UD-components, New Hall Site, 1994 with PGA=0.589g and =0.548g respectively), which are shown in Fig. 1.



(a) El Centro earthquake (1940, NS-component)



(b) Northridge earthquake (New Hall Site, 1994, NS-component)



(c) Northridge earthquake (New Hall Site, 1994, UD-component)

Fig. 1 Time histories of earthquake ground motions used as input of SAP90

California highway bridges typically consist of a moment resisting frame system. It is typical of California overpasses/underpasses with more than four spans to have joints located on spans to connect girders which would be separated otherwise. They are located nearly at inflection points (i.e., 1/4 to 1/5th of spans). The bridge decks consist of box type girders with either reinforced or prestressed concrete. The bridges considered for this study are assumed to have straight alignment. The results of the analysis showed beneficial effect of the visco-elastic damper in reducing the relative displacement between girders at joint locations. The normalized relative displacement (as a function of spring constant k and the coefficient c of linear viscous damping) showed the same trend as observed in the result of the previous study [3] for the skewed Gavin Canyon Undercrossing. The normalized relative displacement is defined as the ratio of the reduced relative displacement to the relative displacement without the visco-elastic damper. It was found that the values of k and c, particularly of the latter, for which the visco-elastic dampers become effective are in the range that is obtainable from the devices available in the market.

SEISMIC RESPONSE ANALYSIS OF BRIDGES WITH VISCO-ELASTIC DAMPERS

Example Bridges

The bridge models considered in this study are as follows:

I) Model A: five span, one expansion joint bridge with variable pier heights of 9.15 m and 15.25 m
II) Model B: five span, one expansion joint bridge with equal pier height of 15.25 m
III) Gavin Canyon Undercrossing (but with no skewness) having five spans, two expansion joints, with variable pier height
IV) Model TY1H: five span, one expansion joint bridge with equal pier height of 19.83 m
V) Model TY2H: five span, two expansion joint bridge with equal pier height of 19.83 m

The geometry and boundary conditions of bridge models are shown in Fig. 2. The material and cross-sectional properties of the models are listed in Table 1. These bridges have periods of dominant horizontal free vibration modes of 0.5 to 1.0 second in each isolated segment separated by joints.

The bridges were modeled with beta version of SAP90 finite element computer program. A simplified two-dimensional model was used. The bridge deck was modeled by a series of frame elements of SAP90 along the center line of the superstructure. The piers were modeled using frame elements as well. The expansion joints were assumed to be constrained in relative

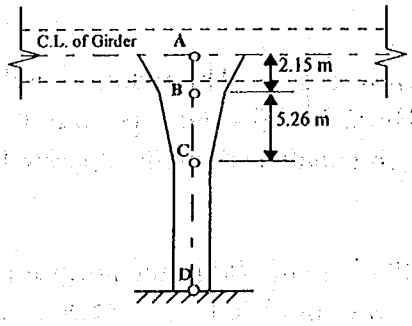
vertical movement at joints, while allowing horizontal relative movement and rotation. The pier bases were assumed fixed while the two abutments were modeled as roller supports. In the SAP90 model, at joint locations, the vertical relative displacement between the two nodes joining the joints were constrained while horizontal relative displacement and rotation were not. The simulation studies were performed on these bridge models with and without visco-elastic dampers at joints.

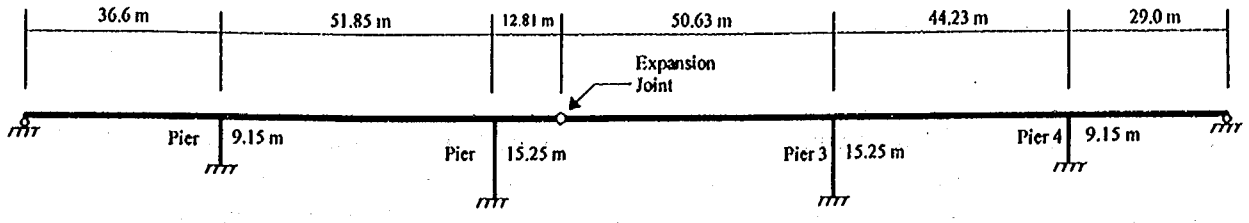
The dampers selected for this study are the Kelvin type linear visco-elastic dampers. They can be represented in an equivalent spring and a viscous damper in parallel. The locations for these dampers are at expansion joints between the adjacent bridge segments. The equivalent spring and stiffness were assumed linear.

Table 1 Material and cross-sectional properties of analysis models for SAP90

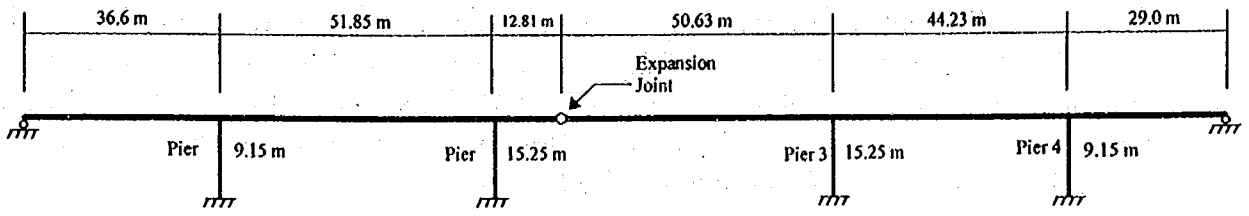
Example Bridge	Structural Component	Moment of Inertia (m^4)	Cross-Section Area (m^2)	Mass Density (Mg/m^3)	Young's Modulus (KPa)
A	Girders	9.382	11.058	2.40	$2.483x10^7$
	Piers	9.103	0.5806	2.40	$2.483x10^7$
B	Girders	9.382	11.058	2.40	$2.483x10^7$
	Piers	9.103	0.5806	2.40	$2.483x10^7$
Gavin Canyon	RC Girders	11.525	11.058	2.32	$2.621x10^7$
	PC Girders	12.395	11.852	2.32	$4.10 x10^3$
	Piers (AB*)	103.933	26.161	2.32	$2.621x10^7$
	Piers (BC*)	15.367	13.729	2.32	$2.621x10^7$
	Piers (CD*)	6.735	10.368	2.32	$2.621x10^7$
TY1H & TY2H	Girders	4.787	6.936	2.32	$2.621x10^7$
	Piers	1.735	4.670	2.32	$2.621x10^7$

Note: *

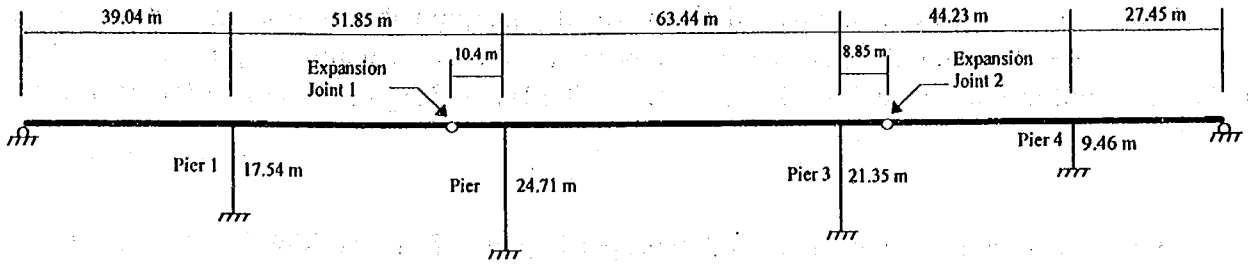




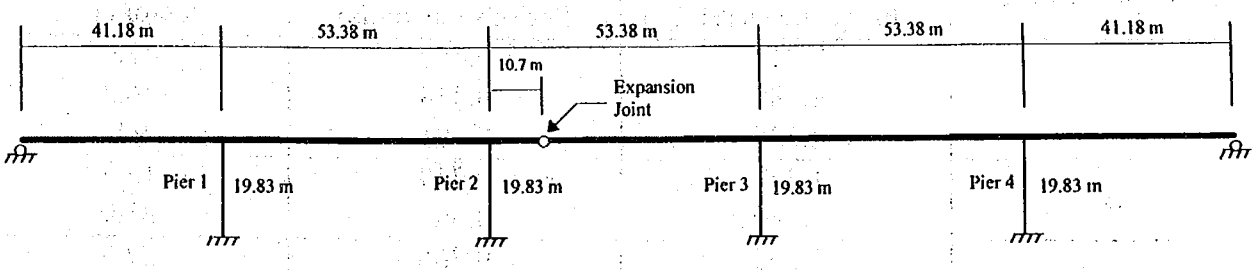
(a) Bridge A



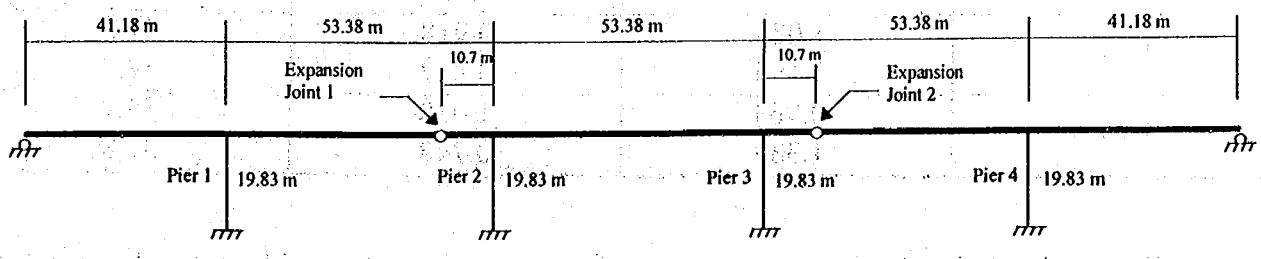
(b) Bridge B



(c) 2D Gavin Canyon Undercrossing



(d) Bridge TY1H



(e) Bridge TY2H

Fig. 2 Elevations of five example bridges

Numerical Results by SAP90

The effectiveness of the visco-elastic dampers in reducing the relative displacement at joint locations between bridge decks is a primary interest of this study. It is also necessary to know whether the relative motion is a closure or opening of the joints. Furthermore, there is a concern whether dampers installed at the expansion joints might produce additional shear forces and bending moments of significance on the bridge substructures when subjected to seismic excitations. Eleven different values of spring constant k and damping coefficient c were used in the ranges $0 \le k \le 35.72$ *tonf/cm* ($0 \le k \le 200$ *kips/in*) and $0 \le c \le 35.72$ *tonf-sec/cm* ($0 \le c \le 200$ *kips-sec/in*) for bridge models A and B, and $0 \le k \le 53.58$ *tonf/cm* ($0 \le k \le 300$ *kips/in*) and $0 \le c \le 53.58$ *tonf-sec/cm* ($0 \le c \le 300$ *kips-sec/in*) for the other models with a total of 121 different analysis runs performed for each model bridge.

Table 2 shows that the natural frequencies and mass participation factors of dominant modes for horizontal motion of five analysis models considered. Each of these bridge models is excited as a single structure because of the vertical constraint imposed at the joint. Table 3, however, shows the natural frequencies and periods of each structural segment separated by joints (right and left segments for bridges A, B and TY1H, and right, center and left segments for others).

Table 2 The natural frequencies and mass participation factors of dominant modes for horizontal motion of analysis models without visco-elastic dampers

Example Bridge	Natural Frequencies and Periods		Mass Participation Factors (%)
	Frequencies (Hz)	Periods (seconds)	
A	2.213	0.452	47.3
	2.286	0.438	36.3
	2.625	0.381	9.9
B	1.352	0.739	13.7
	1.440	0.694	81.9
2D Gavin Canyon Bridge	1.305	0.766	27.8
	1.537	0.651	38.9
	3.545	0.282	20.5
TY1H	1.089	0.918	41.2
	1.194	0.837	52.7
TY2H	0.963	1.038	55.7
	1.337	0.748	37.8

Table 4 lists peak relative displacement at expansion joints of structure without the damper. Figs. 3 and 4 show normalized plots of how spring stiffness k and damping coefficient c affect the reduction of relative displacements for bridges A and TY2H. As evident from the figure, for both opening and closure, higher damping consistently reduces the relative displacements, while

the variation of stiffness has little effect. Also note that the relative insensitivity of the results to the type of input ground motion.

Table 3 The natural frequencies and mass participation factors of horizontal dominant modes for bridge segments of analysis models

Example Bridge	Segment	Natural Frequencies and Periods		Mass Participation Factor* (%)
		Frequencies (Hz)	Periods (seconds)	
A	Left	2.270	0.441	20.4
		2.500	0.400	21.2
	Right	2.209	0.453	52.6
B	Left	1.476	0.678	43.4
	Right	1.397	0.716	53.9
2D Gavin Canyon Bridge	Left	0.747	1.339	4.3
		1.716	0.583	24.5
	Center	1.316	0.760	40.2
	Right	3.908	0.256	19.5
		8.300	0.120	2.1
TY1H	Left	1.200	0.833	41.2
	Right	0.614	1.628	2.4
		1.118	0.894	50.4
TY2H	Left	0.558	1.791	4.5
		1.046	0.956	26.7
	Center	1.354	0.738	31.1
	Right	0.558	1.791	4.5
		1.046	0.956	26.7

Note: * The values are ratio to whole bridge structure.

Table 4 Peak relative displacements at expansion joints of structure without dampers (unit: cm)

Example Bridge		El Centro (1940) NS Input	Northridge (1994) NS-UD Input
A		2.11 (1.93)	4.09 (4.01)
B		2.82 (2.44)	9.96 (9.93)
2D Gavin Canyon Bridge	Left Joint	7.59 (8.15)	28.27 (29.21)
	Right Joint	8.15 (8.18)	24.13 (20.73)
TY1H		10.49 (10.59)	13.97 (13.77)
TY2H	Left Joint	15.70 (14.58)	46.28 (44.5)

Note: Values in parentheses are max. closure and others are max. opening.

The results given in Table 4 and Fig. 3 are combined to suggest a set of minimum values of k and c that must be used for the damper to prevent the bridge A girders from falling off the seat as well as from colliding each other. For example, if bridge A has the seat width equal to 4 cm and clearance equal to 2 cm at the joint, then the damper should have the values of k and c corresponding to max. normalized closure less than 2/4.01=0.498 not to collide, while k and c should have the values corresponding to max. opening less than 4/4.09=0.977 not to fall off under the Northridge earthquake. The normalized base shear forces and bending moments of Fig. 5 show that at piers of left segment structure (piers 1 and 2) of bridge A these values are increased by as much as 30 %. Similar results can be shown in Fig. 6 for center segment structure (piers 2 and 3) of bridge TY2H.

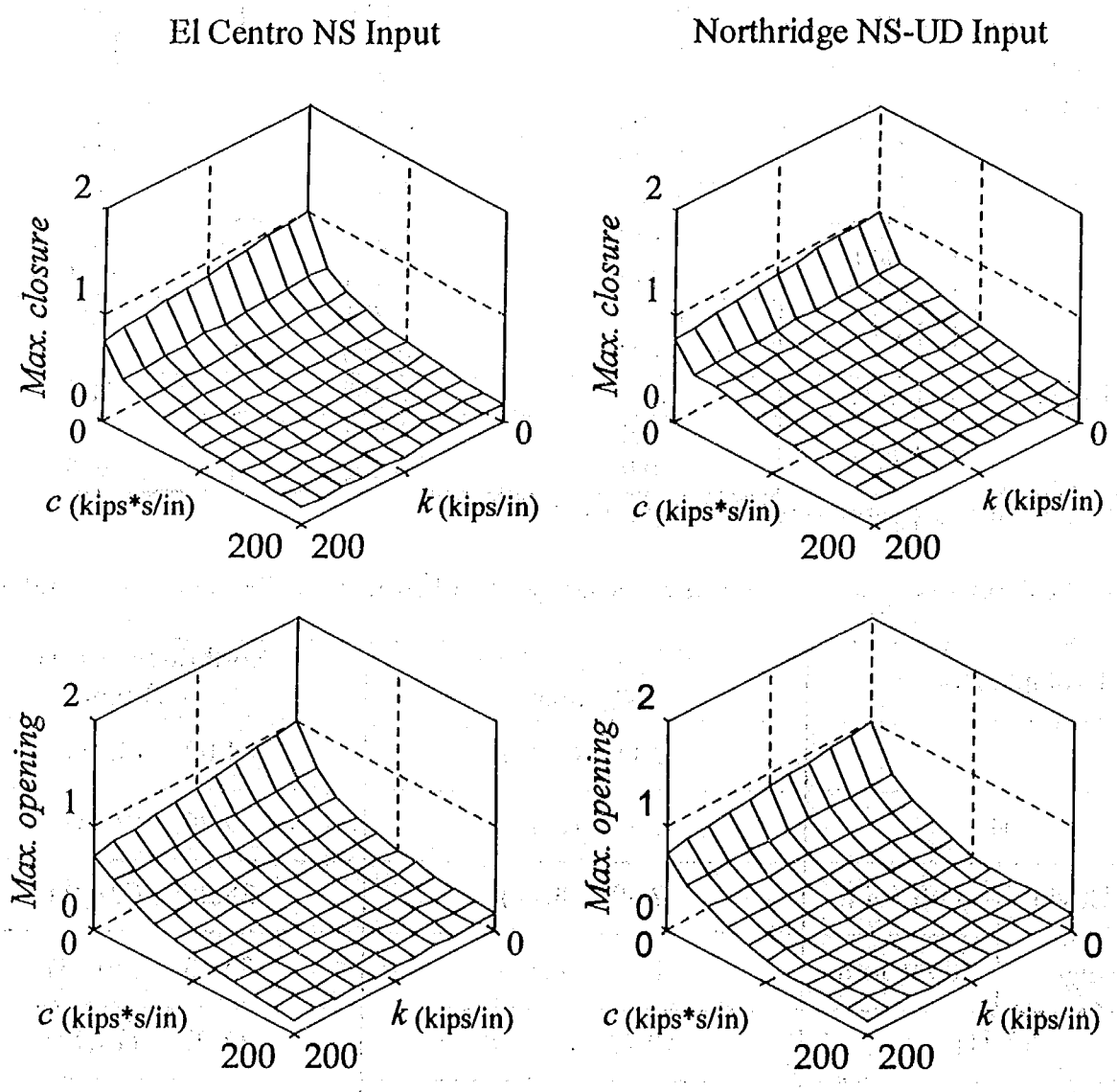


Fig. 3 Normalized peak relative displacements at expansion joint of bridge A by SAP90 (100 *kips/in* = 17.86 *tonf/cm* = 17.52 *MN/m*)

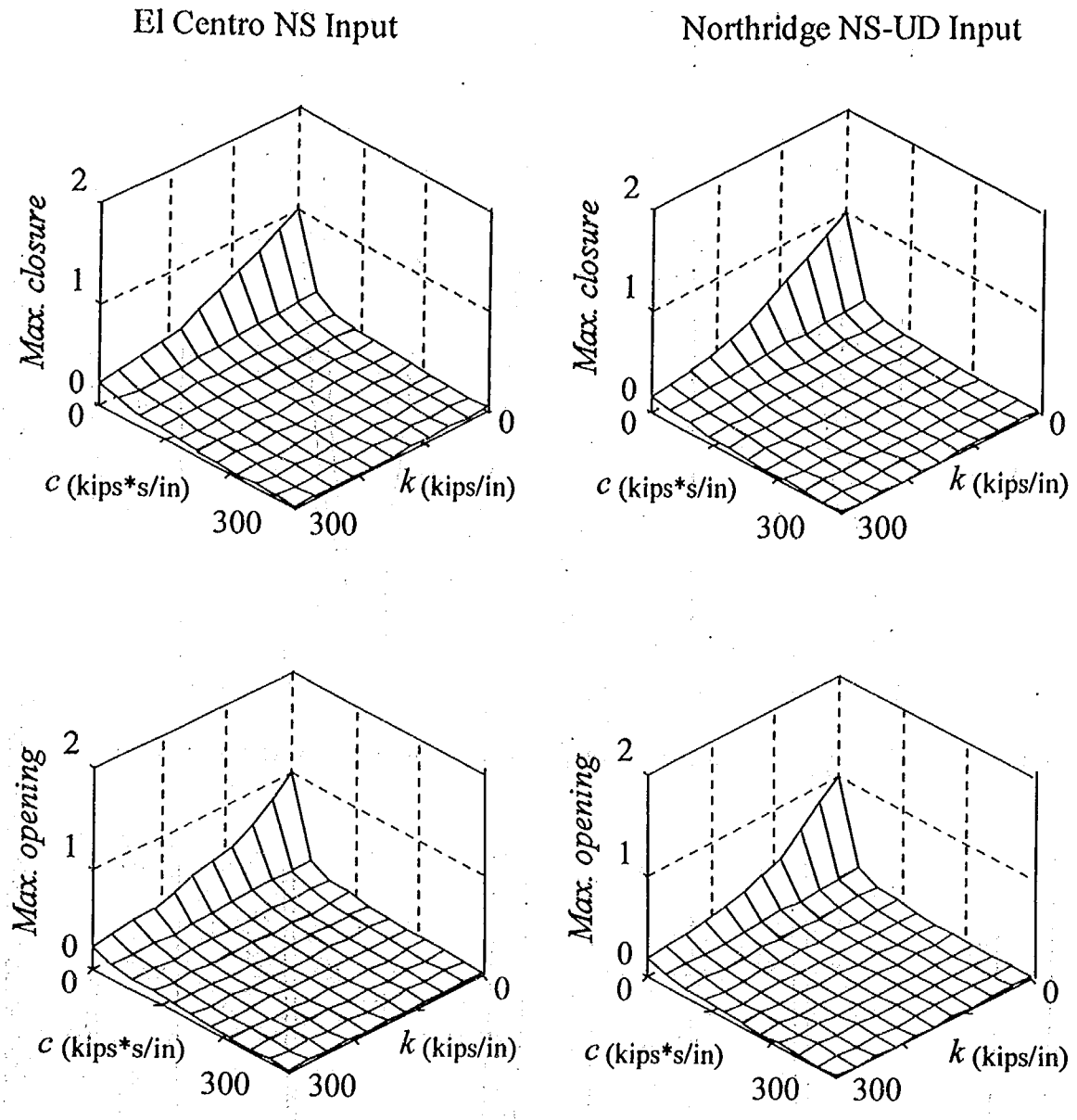


Fig. 4 Normalized peak relative displacements at expansion joint of bridge TY2H by SAP90 (100 *kips/in* = 17.86 *tonf/cm* = 17.52 *MN/m*)

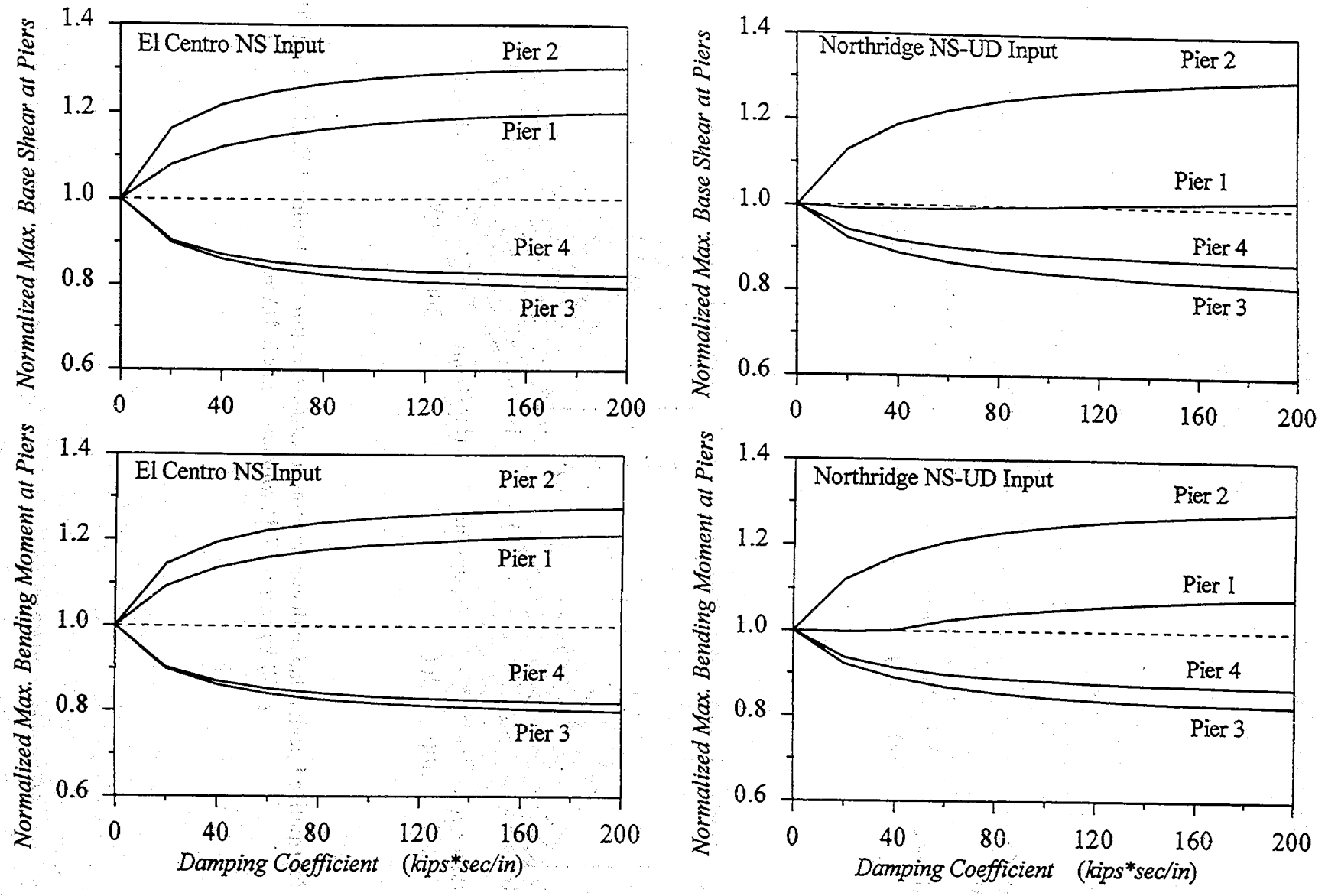


Fig. 5 Normalized base shear forces and bending moments at piers of bridge A by SAP90
(100 *kips/in* = 17.86 *tonf/cm* = 17.52 *MN/m*)

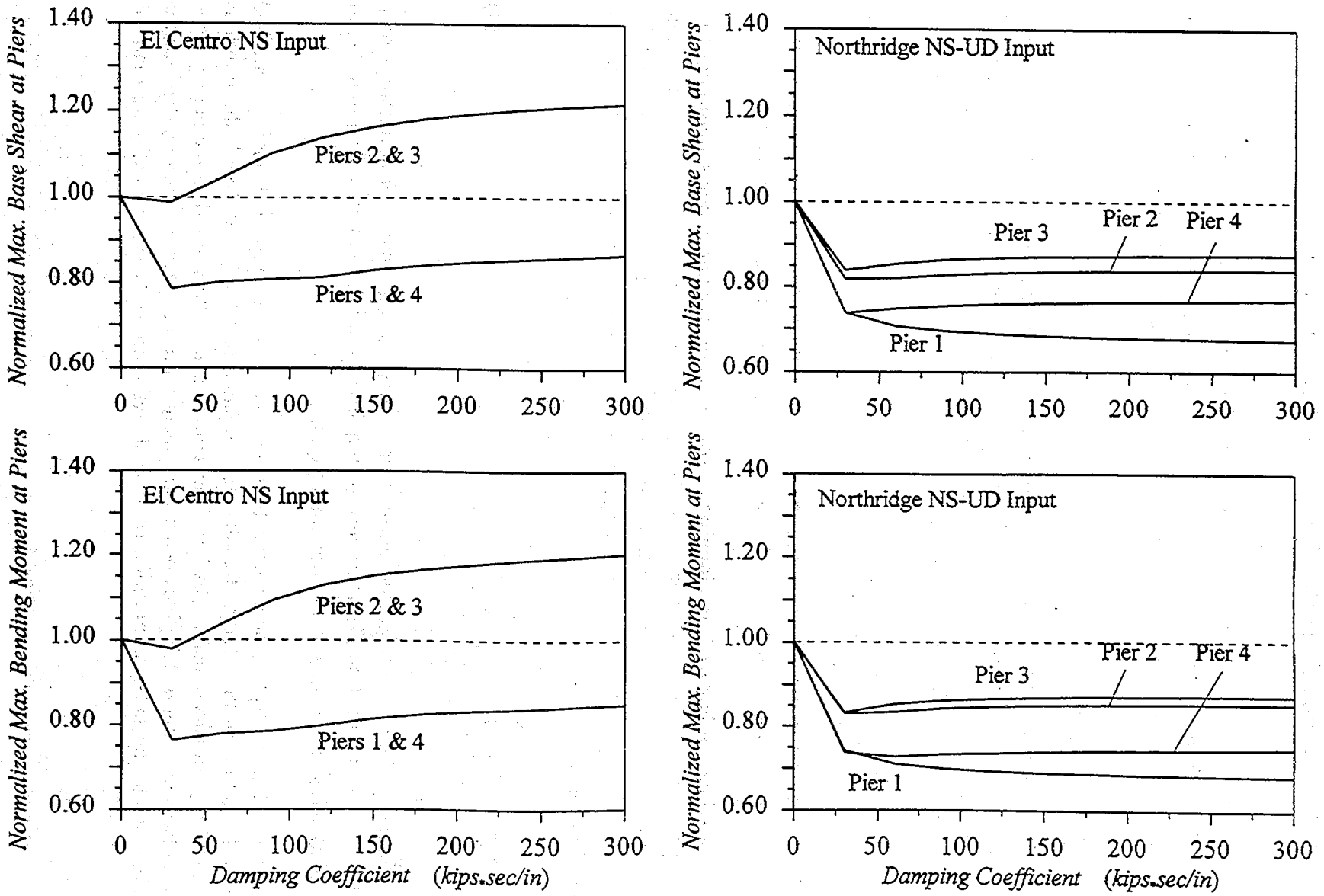


Fig. 6 Normalized base shear forces and bending moments at piers of bridge TY2H by SAP90
(100 *kips/in* = 17.86 *tonf/cm* = 17.52 *MN/m*)

Simplified Relationship of Peak Relative Displacement with Damping Coefficient

In addition to the analytical simulation performed above, the relationship between damping coefficient c_j and corresponding peak displacement $\hat{x}_j$ of a single-degree-of-freedom system subjected to a white noise was developed as below based on random vibration theory:

$$\hat{x}_j \propto \frac{1}{(\xi_{str}+\xi_d)^a} \tag{1}$$

where ξ_{str} and ξ_d are respectively critical damping ratio of structure itself and viscous dampers, and a is 0.5. However, a=1.0 if the peak response at resonant frequency is considered. Assuming conservatively that the stiffness is zero, the normalized relative displacement curve for zero spring constant is given in approximation:

$$\hat{x}_j = \hat{x}_0 \Big/ \left[1+\frac{c_j}{c_1}\left\{\left(\frac{\hat{x}_0}{\hat{x}_1}\right)^{\frac{1}{a}}-1\right\}\right]^a \tag{2}$$

where $\hat{x}_0$ is the peak relative displacement of structure without dampers, and $\hat{x}_1$ is peak relative displacement of the structure with damping value of c_1 and zero stiffness for the dampers.

This approximation is based on simplified two-degree-of-freedom models involving two adjacent segments of bridges (left-right segments for one hinge bridges, and left-center and center-right for two hinges bridges as shown in Table 3. Equation (2) can be rewritten for determining the value of damping coefficient c_{req} required to suppress the relative displacement within allowable value $\hat{x}_{all}$ as:

$$c_{req} = c_1 \left\{\left(\frac{\hat{x}_0}{\hat{x}_{all}}\right)^{\frac{1}{a}}-1\right\} \Big/ \left\{\left(\frac{\hat{x}_0}{\hat{x}_1}\right)^{\frac{1}{a}}-1\right\} \tag{3}$$

Therefore, equation (2) shows the normalized relative displacement as a function of c ($=c_{req}$) when k=0, while equation (3) represents the required damping coefficient as a function of allowable relative displacement at expansion joint ($\hat{x}_{all}$).

The peak relative displacements have been estimated by a simplified analysis method developed in the course of this study. Results are compared in Figs. 7 and 8 with the previous numerical solutions obtained using SAP90. The comparisons show good agreements. The comparisons also show that a=1.0 gives better agreement with the SAP90 solutions than for the case of a=0.5, while the latter assumption (a=0.5) shows more conservative estimate than the former.

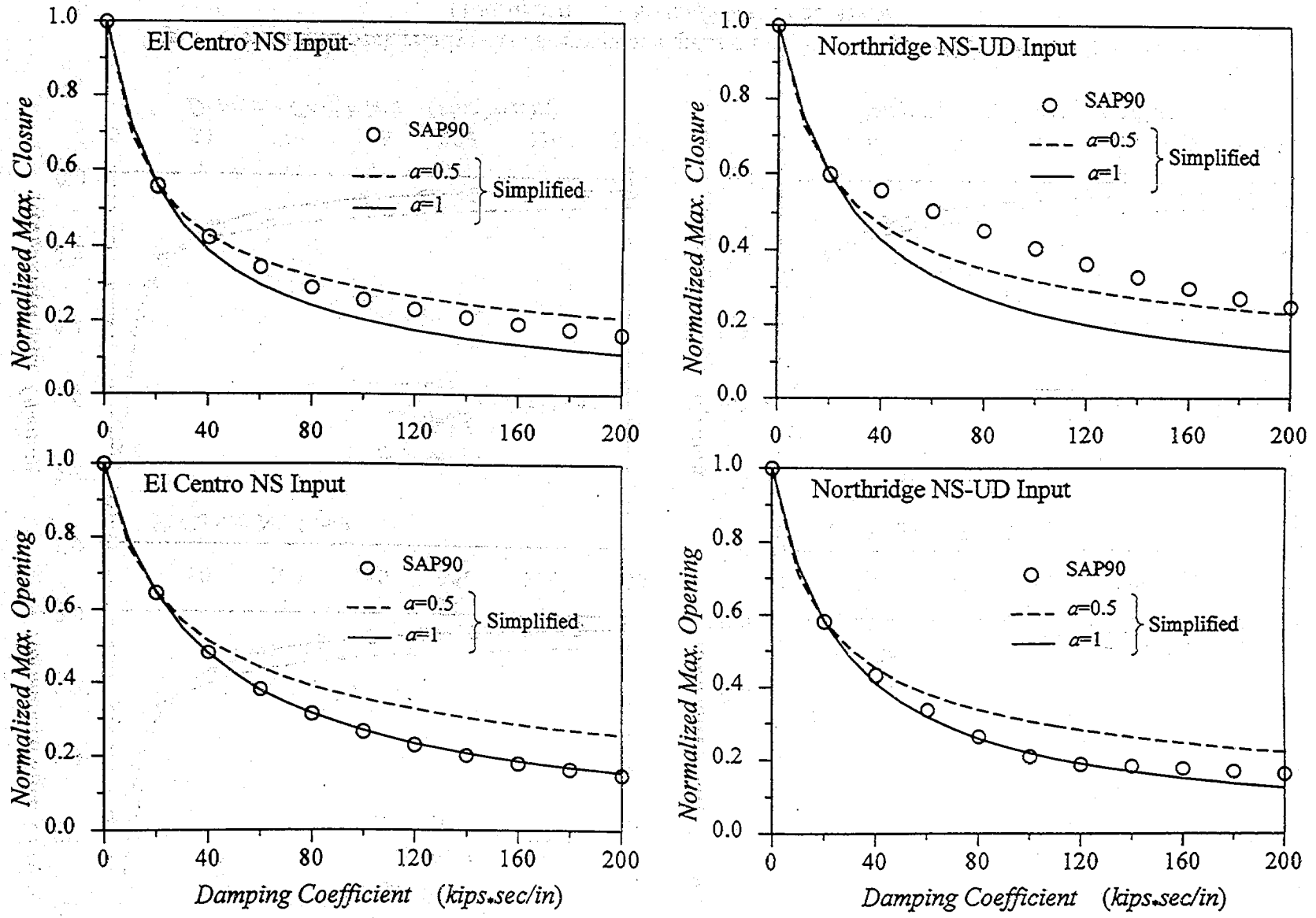


Fig. 7 Normalized peak relative displacement at expansion joint of bridge A by simplified method
(100 *kips/in* = 17.86 *tonf/cm* = 17.52 *MN/m*)

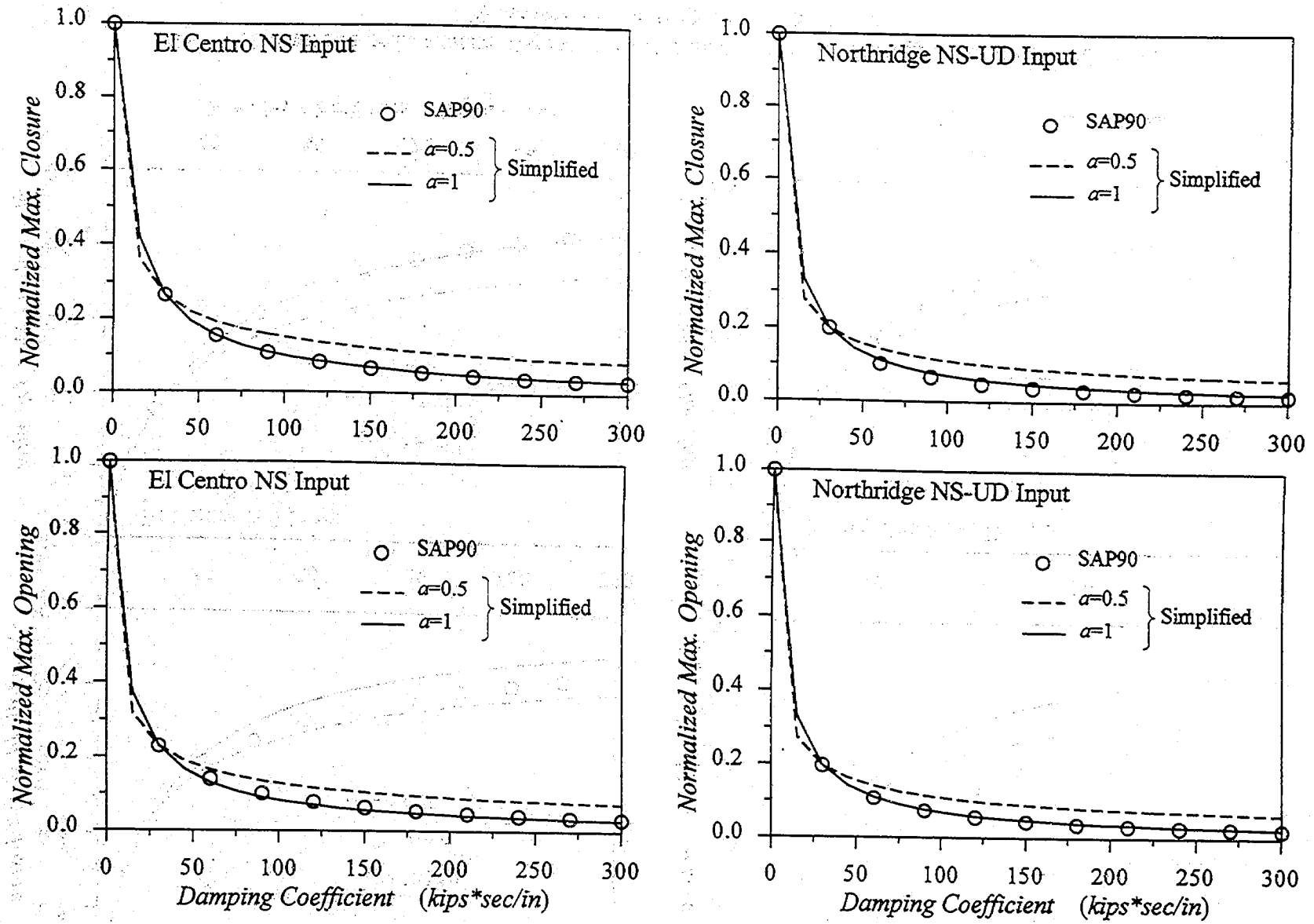


Fig. 8 Normalized peak relative displacement at expansion joint of bridge TY2H by simplified method
(100 *kips/in* = 17.86 *tonf/cm* = 17.52 *MN/m*)

FUTURE STUDIES

Following future studies are recommended to be performed.

- Effects of nonlinearity in viscous dampers
- Maxwell-type visco-elastic dampers
- Performance of the dampers on bridges with more than 3 expansion joints
- Other types of dampers such as friction or yielding devices as restrainers at expansion joints
- Details for damper installation
- Effects of differential ground motion at piers of bridge on relative displacement at expansion joints and effectiveness of the dampers

SUMMARY

This study presents a simple analysis technique using two-dimensional finite element model of bridges for displacement control. The numerical results of five different typical California bridge examples demonstrate effectiveness of visco-elastic dampers for relative displacement control at expansion joints. It is shown that, while damping in visco-elastic damper effectively control relative displacements, the stiffness in Kelvin-type visco-elastic damper has little effect. Also the simplified analysis method presented for design of dampers is very useful. The comparison of results of this method to those of SAP90 shows a good agreement. In summary, the visco-elastic dampers appear to be effective in controlling relative displacement at expansion joints of bridges thereby preventing failure in the event of an earthquake.

ACKNOWLEDGMENTS

This study is funded by Federal Highway Administration (Contract No. DTFH61-92-C-00106). The authors wish to thank the support.

REFERENCES

1. "Northridge Post Earthquake Investigation Report", *California Department of Transportation - Division of Structures*, 1994
2. "Northridge Earthquake Reconnaissance Report", *National Center for Earthquake Engineering Research*, 1994.
3. Klosek, J. T., Deodatis, G., and Shinozuka, M., "The Gavin Canyon Undercrossing: Failure Analysis Under Seismic Loading and a Retrofitting Proposal Using Spring-Damper Systems", ***Proceedings***, The National Science Conference on Bridges and Highways, San Diego, CA, Dec. 10-13, 1995.
4. Feng, M. Q. and Chen, W., "Dampers as Bridge Hinge Restrainers", ***Proceedings***, The National Science Conference on Bridges and Highways, San Diego, CA, Dec. 10-13, 1995.
5. *Computers and Structures, SAP90 v6.0 Beta Release Users Manual*, Berkeley, CA, 1994.

EFFECTIVENESS OF UNSEATING PREVENTION DEVICE WITH ENERGY DISSIPATION

Kazuhiko Kawashima[1] and Masaaki Yabe[2]

1) Professor, Department of Civil Engineering, Tokyo Institute of Technology, O-okayama, Meguroku, Tokyo, 152, Japan
2) Graduate Student, Department of Civil Engineering, Tokyo Institute of Technology, O-okayama, Meguroku, Tokyo, 152, Japan

ABSTRACT

This paper presents an effectiveness of unseating prevention devices with shock absorbing mechanism and energy dissipation to reduce response of a menshin bridge. Longitudinal response of a five-span continuous bridge supported by the lead rubber bearings was analyzed. It was found from the analysis that collisions occur between a deck and abutments at both ends to develop a large bending moment at the abutments, and that the collisions are effective to suppress the deck response displacement. It was also found that unseating prevention devices with shock absorbing mechanism and energy dissipation significantly reduce such response of the bridge.

Key Words: Menshin Design, Seismic Isolation, Bridge, Seismic Design, Dynamic Behavior, Dynamic Response Analysis

INTRODUCTION

Since the Hyogo-ken Nanbua earthquake of January 1995, the menshin design has been extensively adopted in highway bridges. It has been recognized effective to dissipate energy and transfer the lateral force of a superstructure to as many substructures as possible to prevent concentration of the lateral force to a certain substructure and to decrease bridge response during an earthquake. It has been recommended in the menshin design that the natural period of a bridge should be about 2 times or longer than the fundamental natural period of the same bridge supported by the conventional bearings, and that it should not be forcibly elongated aiming to decrease the lateral force[1)2)]. This is because the increase of natural period of a bridge causes an increase of deck response displacement. This tends to develop vibration and noise pollution due to an adoption of a large expansion joint. Furthermore, impacting either between a deck and an abutment or between two adjacent decks develops a large lateral force at bearings and abutments.

It has been required to provide an unseating prevention system at both ends of a bridge[1]. In the systems, it is required to provide a falling-down prevention device as well as proving a seat length in the menshin bridges. The falling-down prevention device has to be designed to a lateral force equivalent to 1.5 times reaction force. Because the design force is very large, it must have sufficiently high stiffness and strength. A concrete block installed at an abutment seat has been used as the device to prevent an excessive deck movement in longitudinal direction. However it makes large impacting force to occur at an abutment with a deck movement over a clearance between the deck and the concrete block. Similar collisions occur between two adjacent decks when relative deck movement reaches the clearance between the decks.

There are two evaluations on the clearance; one is to provide a normal gap of 100 - 150 mm, and the other is to provide enough clearance to avoid the collisions. Because the collisions either between a deck and an abutment or between two adjacent decks could transfer large lateral force from a girder to the other[3], it is worthwhile to study what is the most appropriate clearance. Because it is obvious that shock absorbers and energy dissipators are effective to mitigate such collisions, their effect must be studied.

This paper presents a first result of a series of studies conducted for the effect of collisions and the effectiveness of shock absorbers and energy dissipators.

A BRIDGE ANALYZED

A menshin bridge, as shown in Fig. 1, consisting of five-span continuous deck with a total length of 5 x 40m = 200m and a total weight of 30,772 kN was analyzed. The superstructure is of a plate girder with a width of 12 m. It is supported by four reinforced concrete piers and two abutments. The piers are 10 m high, 2.2 m long and 5 m wide. The abutments are 5.6 m high, 2.7 m long and 12 m wide. Pile foundations are used to support the piers and the abutments. Soil condition at the site is the group II (moderate ground) based on the Design Specifications of Highway Bridges[1].

The bridge was designed by the Seismic Coefficient Method and the Lateral Capacity Method based on the 1996 Design Specifications of Highway Bridges[1]. In the Lateral Capacity Method, the equivalent lateral force coefficient k_{hem} for a menshin bridge is evaluated as

$$k_{hem} = \frac{k_{hcm}}{\sqrt{2\mu_m - 1}} \tag{1}$$

$$k_{hcm} = c_E \cdot k_{hc} \tag{2}$$

in which k_{hcm} = lateral force coefficient in menshin design, μ_m = allowable displacement ductility factor of a pier, c_E = modification coefficient for energy dissipating capability (refer to Table 1), and k_{hc} = lateral force coefficient evaluated by Eq.(3). The modification coefficient c_E depends on the damping ratio of a bridge for the fundamental mode. The lateral force coefficient k_{hc} was evaluated as

$$k_{hc} = c_Z \cdot k_{hc0} \tag{3}$$

in which c_Z = modification coefficient for zone, and is 0.7, 0.85 and 1.0 depending on zone, and k_{hc0} = standard modification coefficient.

Fig. 2 shows the standard lateral force coefficients k_{hc0}, where the Type-I ground motions represent ground motions induced by the plate-boundary type earthquakes with magnitude of the order of 8, while the Type II ground motions represent ground motions induced by inland earthquakes with magnitude of about 7 such as the 1995 Hyogo-ken Nanbu earthquake.

Table 1 Modification Coefficient for Energy Dissipation Capability

Damping Ratio for 1st Mode h	Coefficient c_E
$h<0.1$	1.0
$0.1 \leqq h<0.12$	0.9
$0.12 \leqq h<0.15$	0.8
$h \geqq 0.15$	0.7

The lead rubber bearings were assumed in the bridge. The design displacement u_B of the devices was evaluated as

$$u_B = \frac{k_{hem} \cdot W_u}{K_B} \tag{4}$$

in which k_{hem} = equivalent lateral force coefficient by Eq. (1), K_B = equivalent stiffness, and W_u = dead weight of a superstructure.

Because the natural period, the displacement ductility factor of piers, and the design displacement, equivalent stiffness and the equivalent damping ratio of the device are interrelated, some iteration consisting of the equivalent static analysis and dynamic response analysis is required to get a final design value. Square-shaped lead rubber bearings were assumed with a design displacement of 420 mm. The LRBs at the abutments are 465 mm high, 550 long and 550 mm wide, while those at the piers are 405 mm high, 650 long and 650 wide. The LRBs on the abutment consist of 31 layers of natural rubber with a thickness of 15 mm while the LRBs on the piers consist of 27 layers

with a thickness of 15 mm. Four lead plugs with a diameter of 60 mm were used in all the LRBs. Five LRBs are used per substructure to support the deck. Thus a total of 30 LRBs are used in the bridge.

Based on the Design Specifications, the following clearance S_B must be provided at both ends of a superstructure.

$$S_B = \begin{cases} u_B + L_A & \text{between a deck and an abutment} \\ c_B \cdot u_B + L_A & \text{between two adjacent decks} \end{cases} \quad (5)$$

in which u_B = design displacement of a menshin device (mm) by Eq. (4), L_A = redundancy of a clearance (generally $\pm$ 15 mm), and c_B = modification coefficient for clearance (refer to Table 2).

Because the design displacement is 420 mm in the LRBs assumed in this study, the clearance S_B of 440 mm is required between the superstructure and the abutment at both ends.

Table 2 Modification Coefficient for Clearance c_B

$\Delta T / T_1$	c_B
$0 \leqq \Delta T / T_1 < 0.1$	1
$0.1 \leqq \Delta T / T_1 < 0.8$	$\sqrt{2}$
$0.8 \leqq \Delta T / T_1 \leqq 1.0$	1

UNSEATING PREVENTION DEVICE WITH ENERGY DISSIPATION

As well as in the conventional bridges, the unseating prevention systems are required in the menshin bridges. Because the LRBs are the "Type-B" bearings[1], a falling-down prevention device is required in the menshin bridge as well as proving a seat length at both ends of the superstructure. It is also recommended in the Design Specifications that a joint protector be provided, if required, to prevent damage at expansion joints during a moderate earthquake with a high probability to occur. The joint protector should be easily replaceable after a moderate earthquake.

Three types of falling-down prevention devices are assumed in the bridge as shown in Figs. 3, 4 and 5. The first is a device consisting of a concrete wall at an abutment seat. This provides no shock absorbing mechanism and energy dissipation. Strong collisions occur between the concrete wall and the deck. This device is called in this paper as Type-A device.

The second is a device consisting of four laminated rubber bearings with a diameter of 500 mm. This is called in this paper as Type-B device. Because 10 layers of natural rubber with a thickness of 10 mm are laminated with steel plates, it has a high initial stiffness of 1,480 MN/m per two devices and a high bearing capacity in compression. An energy dissipation equivalent to a damping ratio of about 14 % can be made as shown in Fig. 4(b). They are placed on a parapet wall of an abutment and on a concrete wall on an abutment seat so that an inertia force of the superstructure in longitudinal direction be supported by the device in compression. The number of devices were determined so that a compression stress of the devices subjected to a lateral force equivalent to the total deck weight (30,772 kN) be less that a credible bearing capacity of about 88 MPa. The force vs. displacement hysteresis was idealized as shown in Fig. 4 (b). Because of the strain hardening and deformation of rubber, the stiffness sharply increases as a displacement increasses. Because an experimental data was not available on the hysteresis loop over the displacement of 22 mm, it was assumed that the restoring force increases linearly with an increase of displacement over this displacement. As will be presented later, the restoring force reached as large as 55 MN. Four devices were provided at each end of the deck.

The third is a device consisting of 40 shock absorbing rubber pads. This is called as Type-C device. They are of a pad of a thickness of 50 mm and a section of 250 x 150 mm. Because it is not laminated with steel plates, the initial stiffness is only 390 MN/m per 40 rubber pads. The number of rubber pads was determined so that a compression stress of the rubber pads subjected to a lateral force equivalent to the total deck weight be less than a credible bearing capacity of 19.6 MPa. Similar to the Type-C device, they were placed on the parapet wall and a concrete wall on the abutment seat. The force vs. displacement hysteresis was idealized as shown in Fig. 5 (b). Because of the strain hardening and deformation of rubber, the stiffness sharply increases as a displacementi increases. Because the force vs. displacement in compression over 25mm was not available, it was assumed that the resoring force increases linearly with displacement over this displacement. As will be presented later, the restoring force increased as large as 77 MN.

For the simplicity of analysis, a clearance between the surface of concrete wall and the deck was assumed to be equal to a clearance between the surface of parapet and the deck as shown in Fig. 6. The clearance was varied as a parameter in the following analysis.

ANALYTICAL MODEL

The bridge was idealized by a discrete analytical model as shown in Fig. 7. The LRBs were idealized as a set of bilinear hysteretic springs. The first and the second stiffnesses of LRBs were

evaluated based on the standard procedure[2]. The piers were idealized by beam elements with the Takeda type hysteretic behavior[4]. The falling-down prevention devices and the joint protectors were idealized by hysteretic models as shown in Fig. 7.

To represent the impacting effect, an impact spring element[5][6] with the following stiffness was used

$$k_I = \begin{cases} \tilde{k}_I & \Delta u \le -u_G \\ 0 & \Delta u > -u_G \end{cases} \tag{6}$$

in which $\tilde{k}_I$ = stiffness of impact spring, u_G = clearance between the deck and the abutment, and Δu = relative displacement between the deck and the abutment defined as

$$\Delta u = u_j - u_i \tag{7}$$

in which u_i and u_j represent a response displacement of the deck and the abutment, respectively. The stiffness of impact spring $\tilde{k}_I$ should be large enough to realistically represent collisions between the deck and the abutment. It was assumed here that $\tilde{k}_I$ is about ten times larger than the longitudinal stiffness of a beam element representing the deck[7].

The Rayleigh-type damping force was assumed in the analysis as

$$[C] = \alpha[M] + \beta[K] \tag{8}$$

in which $[M]$, $[K]$ and $[C]$ are mass, stiffness and damping matrices, and α and β are coefficients to be determined from damping ratios for any two modes. The damping ratio for i-th mode may be obtained as

$$h_i = \frac{1}{2}\left(\alpha\omega_i + \frac{\beta}{\omega_i}\right) \tag{9}$$

in which ω_i is a angular natural frequency for i-th mode. Damping ratio for i-th mode was evaluated based on the energy proportional damping method as[8]

$$h_i = \frac{\sum \phi_{ij}^T \cdot h_{ij} \cdot k_j \cdot \phi_{ij}}{\Phi_i^T \cdot K \cdot \Phi_i} \tag{10}$$

in which h_{ij} = damping ratio of j-th substructure in i-th mode, ϕ_{ij} =mode vector of j-th substructure in i-th mode, k_j = stiffness matrix of j-th substructure, K = stiffness matrix of a bridge, and Φ_i = mode vector of a bridge in i-th mode.

Damping ratios were assumed in each substructure as shown in Table 3. It should be noted here that in addition to the damping ratios in Table 3, the hysteretic energy dissipation of the piers, the LRBs and the unseating prevention devices is included in the analysis by their nonlinear idealization. The abutments were assumed to behave elastically, because they have back-fill. The first and seventh modes were considered in determining α and β in Eq. (9). They are the first and

the second translational modes of the deck and the substructures. The damping ratio for the first and seventh modes was 0.025 and 0.111, respectively.

Table 3 Damping Ratios Assumed in Eq. (10)

Structural Components	Damping Ratio
Deck	0.03
Piers	0.02
Abutments	0.1
Footings/Soil Springs	0.2

The bridge was subjected to a Type II ground motion as shown in Fig. 8 in longitudinal direction. It is a spectral fitted ground motion to the Type-II design acceleration response spectrum at moderate soft site. The peak acceleration is 0.7g.

SEISMIC RESPONSE OF A BRIDGE WITH A FALLING-DOWN PREVENTION DEVICE WITHOUT ENERGY DISSIPATION

Fig. 9 shows a response of velocity at top and bending moment at bottom of the right abutment of the bridge with Type-A device. The responses for assumed clearance between the deck and the abutment u_G of 50 mm, 200 mm and 450 mm are presented here. It is seen from high spikes of both velocity and bending moment responses that several collisions developed between the deck and the abutments. Because the maximum relative displacement between the deck and the abutment is 470 mm, collisions occurs at the clearance smaller than this displacement.

The bending moment is higher in positive direction (right direction) than negative direction direction (left (back-fill side movement)). This clearly shows that an impacting force from the deck to the abutment increased the bending moment in the right direction. Peak bending moment developed at the bottom of the left abutment is the largest (174MNm) at the clearance of 200 mm among the three cases presented in Fig. 9. At this time, the peak lateral force transfered from the deck to the left abutment was 115.3 MN, which is 3.7 times larger than the deck weight of 30.772 MN. It should be noted that the design bending moment of the abutment based on the Seismic Coefficient Method (allowable stress design method) is 20.3 MNm. Although the capacity of the abutment in an inelastic range is much larger, it is inevitable to develop damage at the abutment and the deck under such large impact force.

Fig. 10 shows a shear strain induced in the LRBs on the 2nd pier from left. Because the LRBs on

other piers show the similar responses, only the response of the LRBs at the second pier from right is presented here. The shear strain increases as the clearance increases. This means that the deck displacement relative to the piers increases as the clearance increases. This shows that the abutments contribute to suppress the deck displacement.

Fig. 11 shows how the bending moment of an abutment and a pier and a shear strain of the LRBs depend on the clearance. Response at the second pier from right and at the left abutment are presented here as a typical example. The response for the bridge with the Type-B and Type-C devices , which will be describe later, are also presented in Fig. 11 for comparison. It is interesting to note that the bending moment at the left abutment increases as the clearance increases with a peak value of 174 MNm at a clearance of 200 mm, and then it decreases to 13 MNm at a clearance of 470 mm. As described previously, no collisions occur over the clearance of 470 mm. This clearly shows how predominant the collision effect is on the bending moment at the abutment.

On the other hand, as shown in Fig. 11 (c), the shear strain of the LRBs at the second pier from right increases almost linearly as the clearance increases until the clearance reaches 470 mm. Because the shear strain of the LRBs is linearly proportional to the deck displacement, this again shows that the multiple collisions are effective to reduce the deck displacement although they increase the bending moment at the abutment.However, as shown in Fig. 11(b), the bending moment at the pier does show a significant change depending on the clearance. Restoring force of LRBs at the second (plastic) stiffness does not significantly increase as the lateral displacement increases.

EFFECT OF TYPE-B AND TYPE-C DEVICES WITH ENERGY DISSIPATION

Figs. 12 and 13 show the velocity at top and the bending moment at bottom of the left abutment. Comparing those responses to the responses in Fig. 9, it is seen that the velocity response of the abutment with the Type-B and the Type-C devices are much smaller than that of the abutment with the Type-A device. Being diferent from the bending moment response of the abutment with the Type-A device, the bending moment of the abutment with the Type-B and C device is almost symetric in positive and negative direction, because the deck collides with the parapet wall and the concrete wall.

Fig. 11 compares the response with the Type-B and Type-C devices in comparison with the response of the bridge with the Type-A device. The bending moment at the abutment is almost the same between the Type-B and Type-C device, and it is about 70% of the Type-A value. The

clearance where the bending moment becomes the maximum is also almost the same between the Type-B and Type-C device; 350 mm in the Type-B device and 300 mm in the Type C device. The peak lateral force transferred from the deck to the left abutment was 53.3 MN and 77.3 MN in the Type-B and Type-C device, respectively. They are about 1.8-2.2 times as large as the total deck weight. Because a lateral force equivalent to the deck weight was the design value of the devices in this analysis, the actual force applied to the devices was much lager than the design values. As shown in Figs. 4 and 5, energy dissipation was not considered at the displacement in compression over 22-25 mm, more reduction of the bending moment could be made if a device with larger design force was used.

The shear strain of the LRBs at the second pier from left and the left abutment also decreases in the bridge with the Type-B and Type-C devices than the bridge with the Type-A device. Because the Type-B device is thicker than the Type-C device, the shear strain of LRBs is 30% smaller in the bridge with the Type-B device than the bridge with the Type-C device at a clearance less than 470 mm.

CONCLUDING REMARKS

An effectiveness of shock absorbing mechanism and energy dissipation of the falling-down prevention devices was studied through a series of analysis of a menshin bridge with 5 span continuous deck subjected to a Type-II ground motion. From the analysis presented herein, the following conclusions may be deduced:

(1) The Type-A device produces a large impacting force due to collisions between the deck and the concrete wall on the abutment seat, and the collisions develop a large bending moment at the abutment. The bending moment takes a peak value at a certain clearance between the concrete wall and the deck. The collisions are effective to suppress the displacement of deck relative to the piers. The relative displacement of the deck decreases as the clearance decreases. More analysis is required to study what is the most appropriate clearance.
(2) The Type-B and Type-C devices with shock absorbing mechanism and the energy dissipation are effective to reduce the impacting effect. They decrease the bending moment at both the abutment and piers, and the deck displacement.
(3) A lateral force applied from the deck to the left abutment was 115.3 MN, 77.3 MN and 53.3 MN in the bridge with the Type-A, B and C devices, respectively. It is 3.7, 2.2 and 1.8 times as large as the design value of the devices.

REFERENCES

1) Japan Road Association: Design Specifications of Highway Bridges, Part V Seismic Design, 1996

2) Public Works Research Institute: Menshin Manual of Highway Bridges, English version is available by Sugita, H. and Mahin, S.: Manual for Menshin Design of Highway Bridges: Ministry of Construction, Japan, Report No. UCB/EERC 94-10, Earthquake Engineering Research Center, University of California, Berkeley, 1994

3) Ministry of Construction: Report on the Damage of Highway Bridges by the Hyogo-ken Nanbu Earthquake, 1995

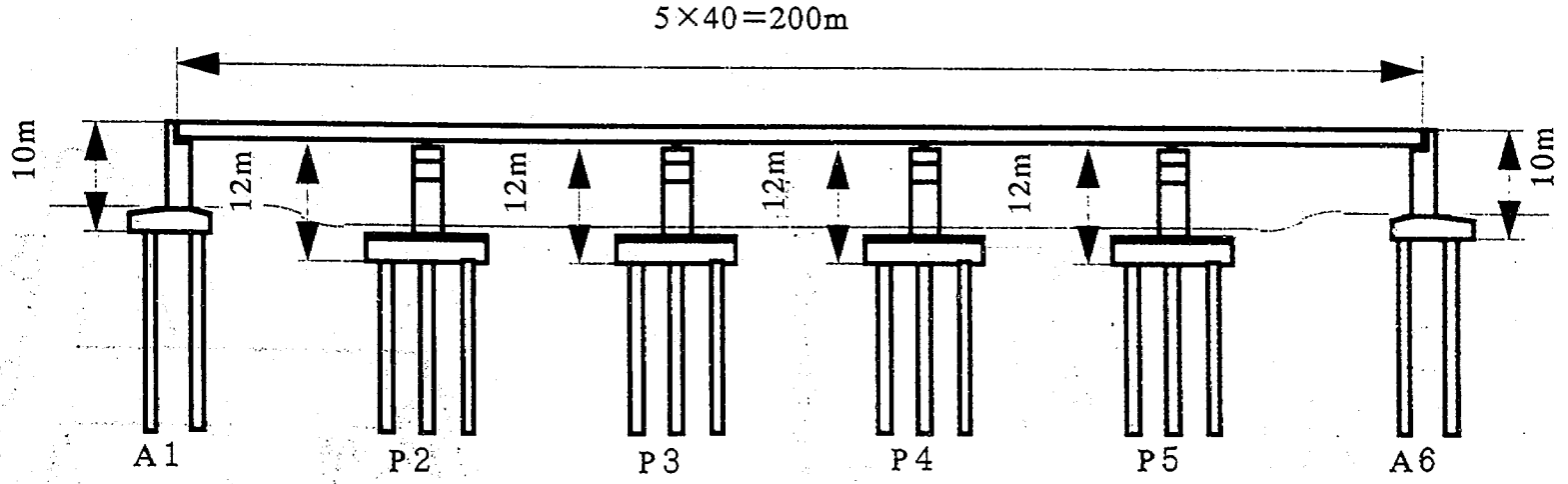
4) Takeda, T., Sozen, M. A., and Nielsen, N. N.: Reinforced Concrete Response to Simulated Earthquakes , Journal of Structural Engineering, ASCE, 96-12, 1970

5) Tseng, W. S. and Penzien, J.: Analytical Investigations of the Seismic Response of Long Multiple Span Highway Bridges, Report No. EERC 73-12, Earthquake Engineering Research Center, University of California, Berkeley, USA, 1973

6) Kawashima, K., and Penzien, J.: Correlative Investigation on Theoretical and Experimental Dynamic Behavior of A Model Bridge Structure, Report No. EERC 76-26, Earthquake Engineering Research Center, University of California, Berkeley, 1976

7) Kawashima, K.: An Analytical Model of Contact and Impact in Dynamic Response Analysis, Proc. Japan Society of Civil Engineers, No. 308, pp. 123-126, 1981

8) Kawashima, K., Nagashima, H. and Iwasaki, H.: Evaluation of Modal Damping Ratio of Bridges Based on Strain Energy Proportional Method, Proc. 9th Bridge Workshop, Technical Memorandum, Public Works Research Institute, Tsukuba, Japan, 1993



Superstructure Section

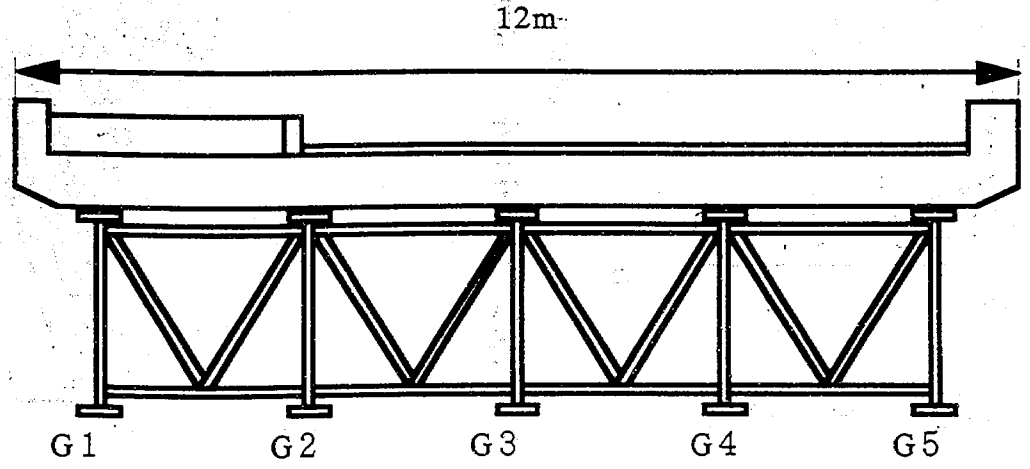


Fig.1 A Bridge Analyzed

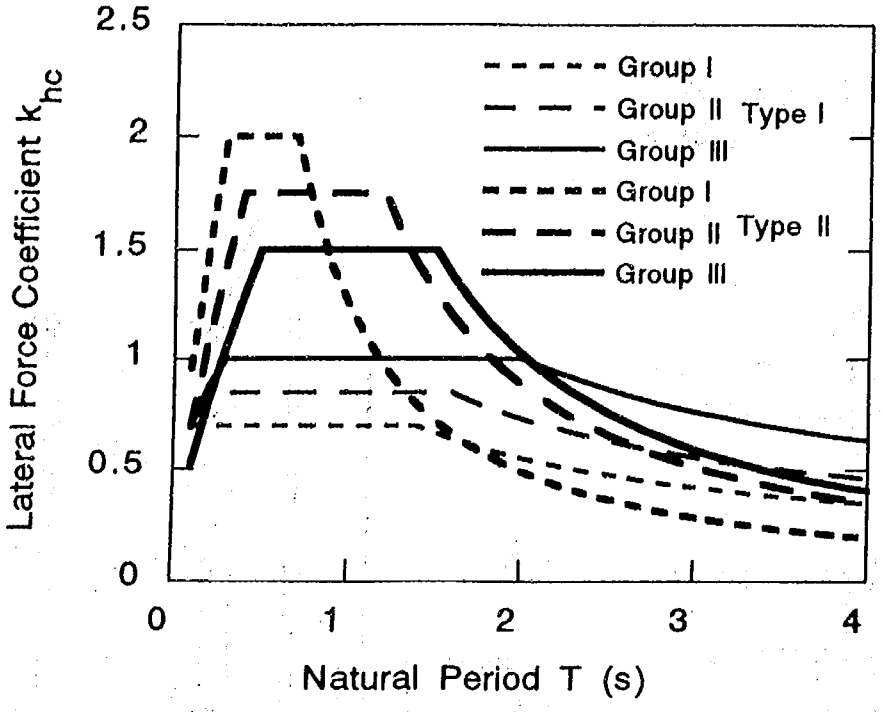


Fig.2 Standard Lateral Force Coefficients k_{hc0}

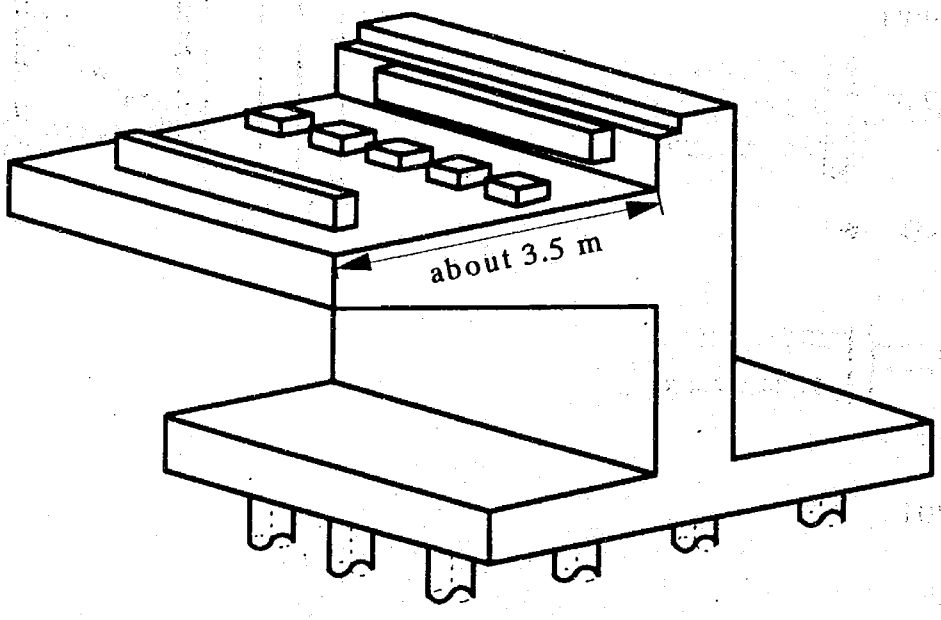
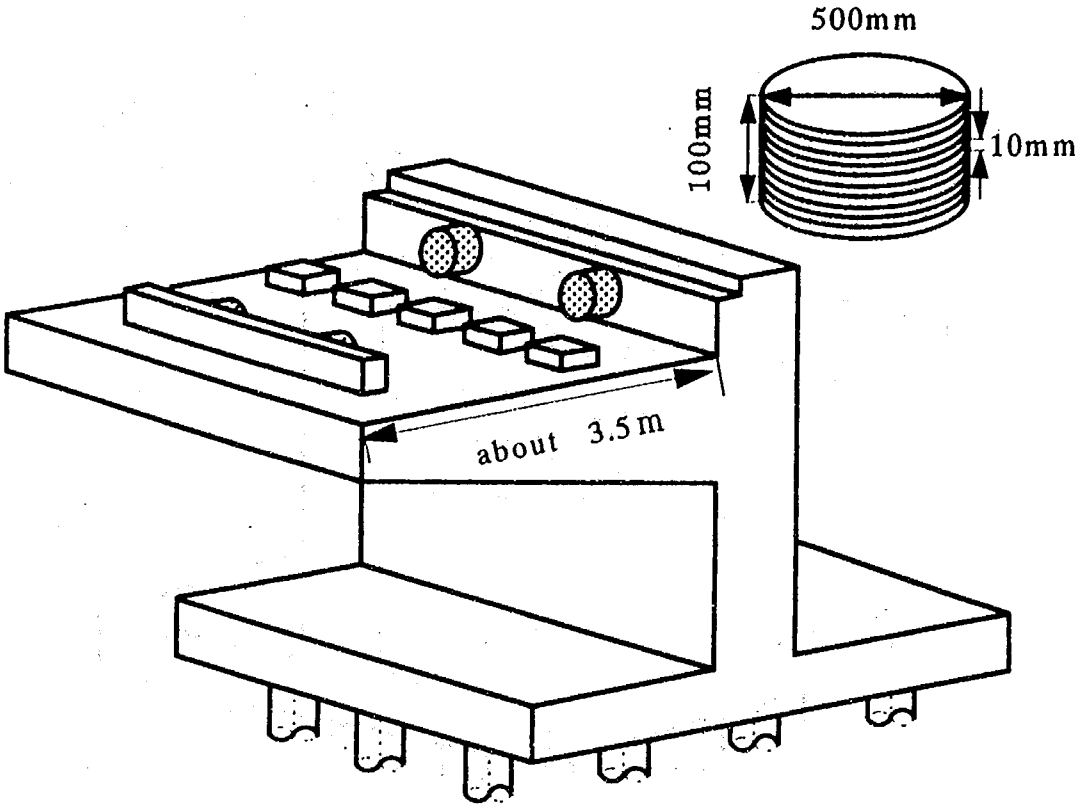
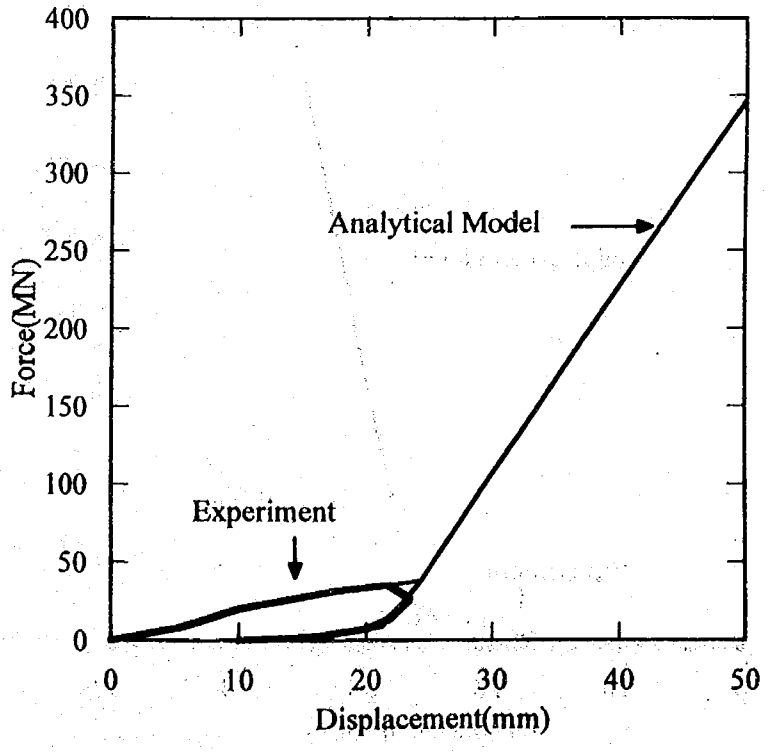


Fig.3 Type-A Device

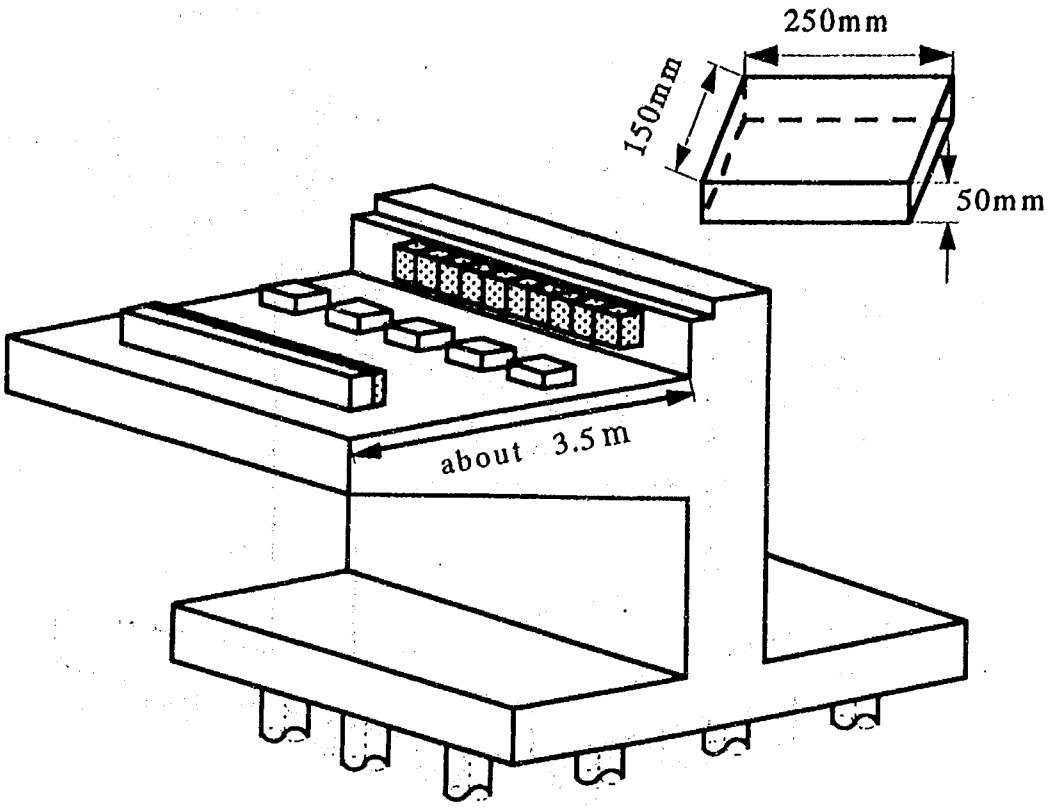


(a) Device

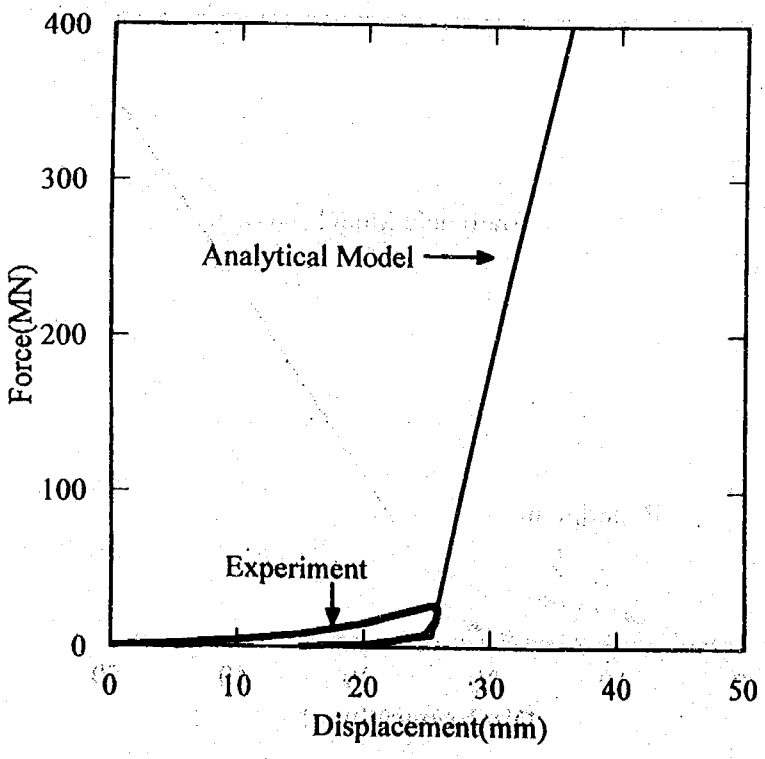


(b)Compression Force vs. Displacement Hysteresis

Fig.4 Type-B Device



(a) Device



(b)Compression Force vs. Displacement Hysteresis

Fig.5 Type-C Device

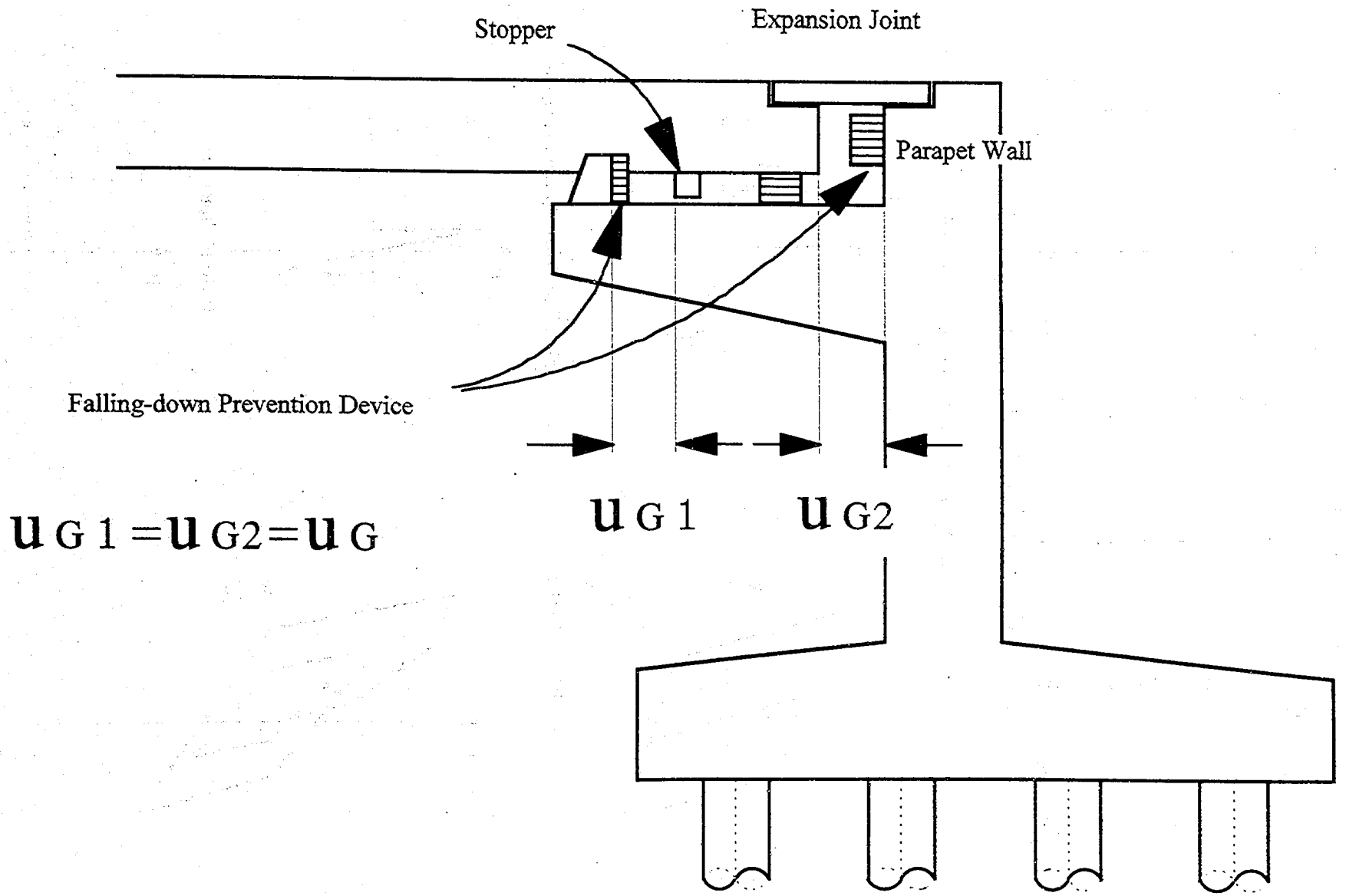
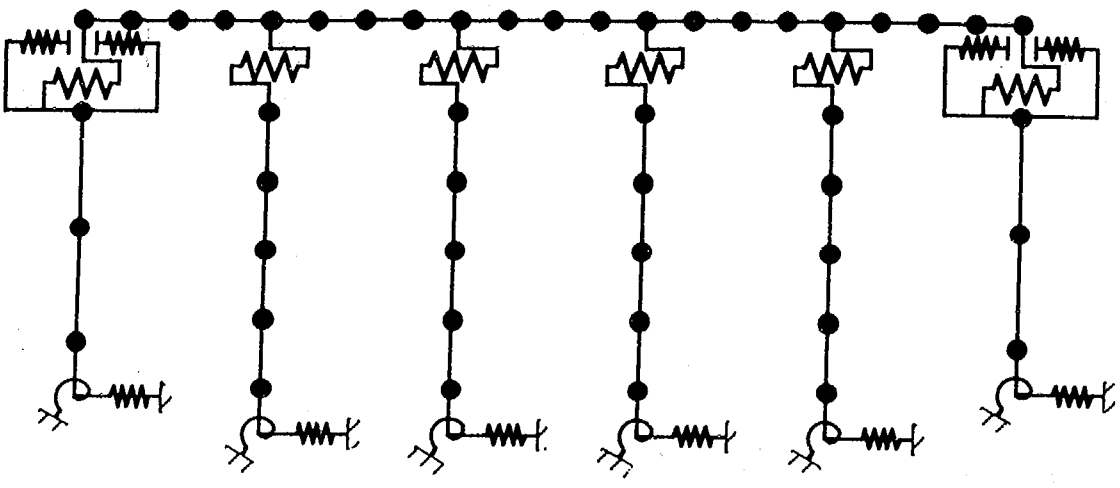
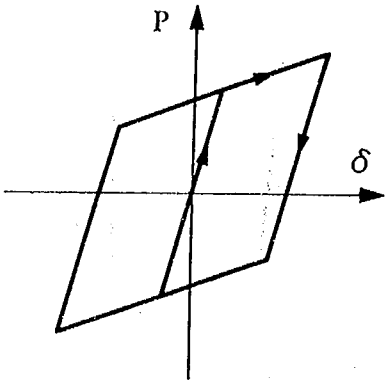


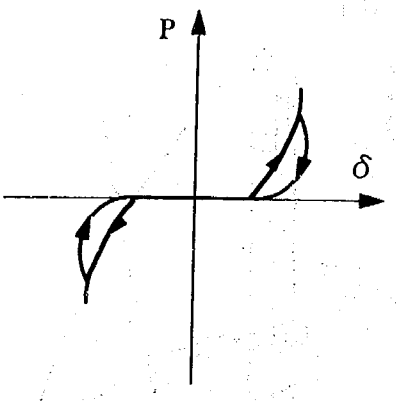
Fig.6 Clearance between a Deck and a Concrete Wall and between a Deck and a Parapet Wall



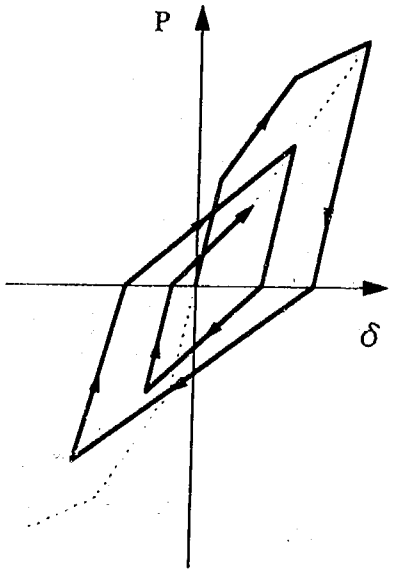
(a) Multidegree of Freedom Bridge Model



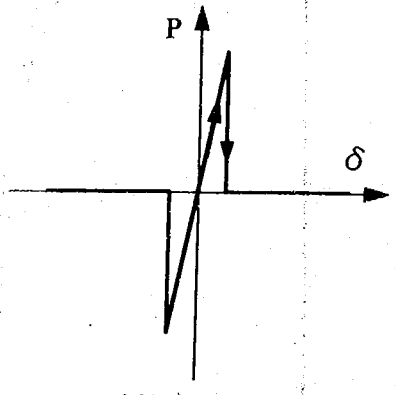
(b)Lead Rubber Bearing



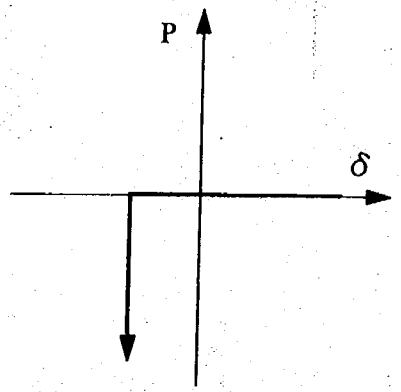
(d)Falling-down Prevention Device



(c)RC Pier (Takeda Model)

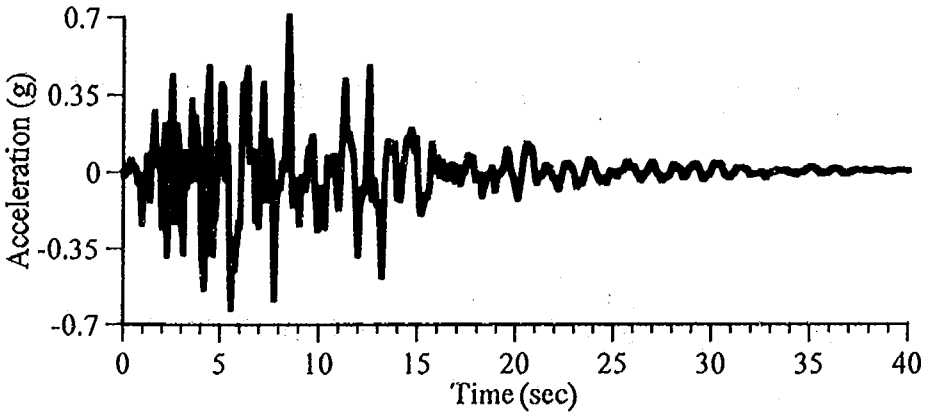


(e)Joint Protector

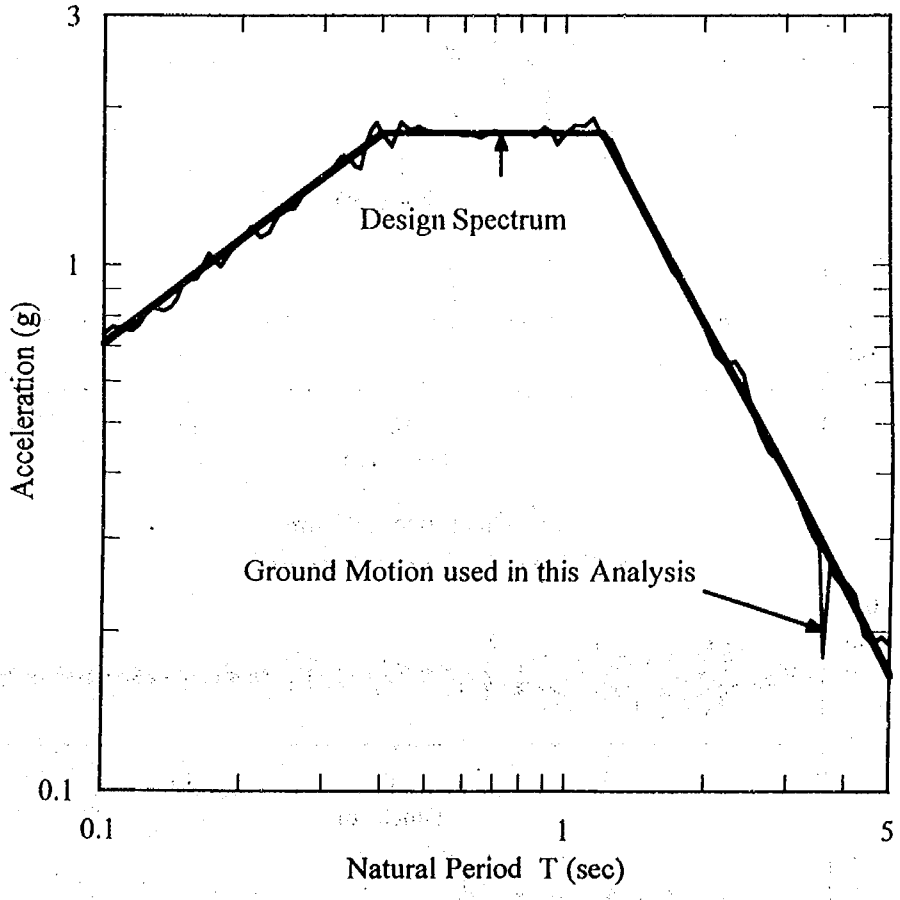


(f)Impact Spring

Fig.7 Analytical Model

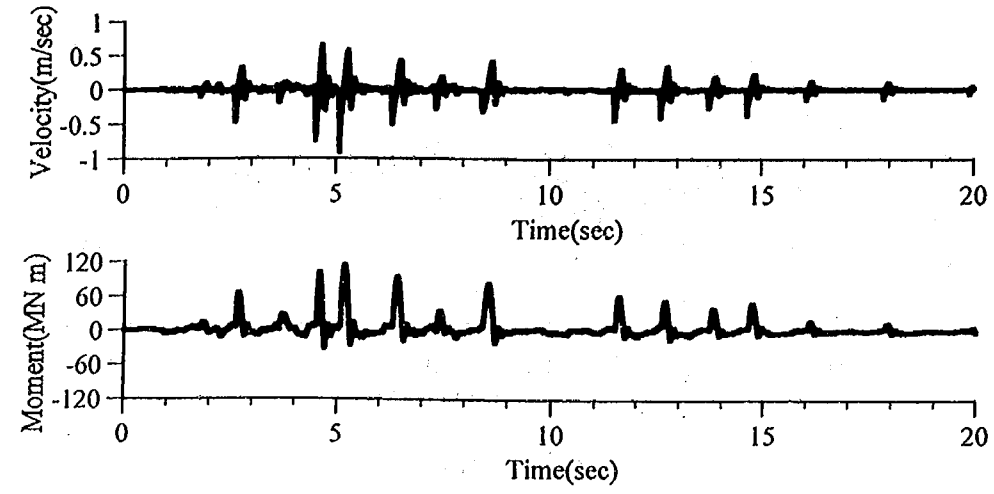


(a) Acceleration

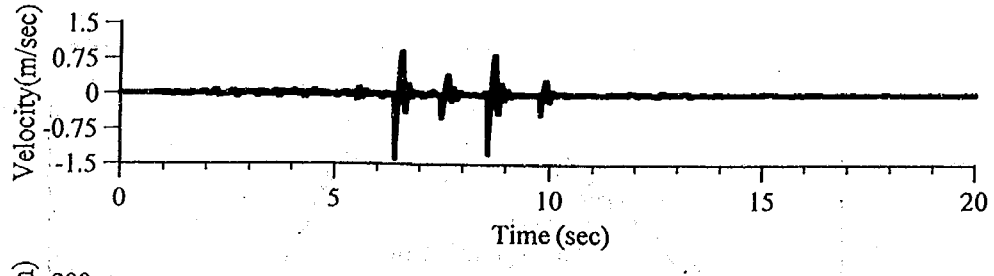


(b) Acceleration Response Spectrum of the Ground Motion in Comparison with the Type-II Design Acceleration Response Spectrum

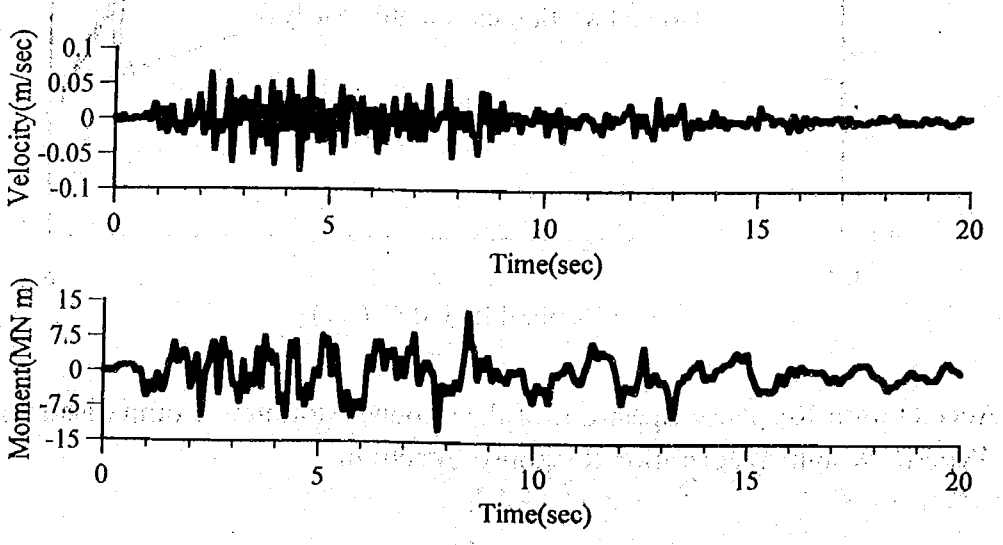
Fig.8 Type-II Ground Motion



(a)Clearance=50mm

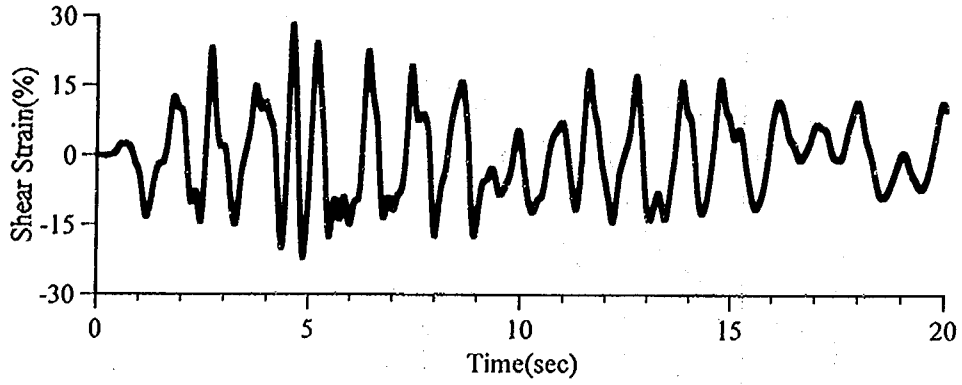


(b)Clearance=200mm

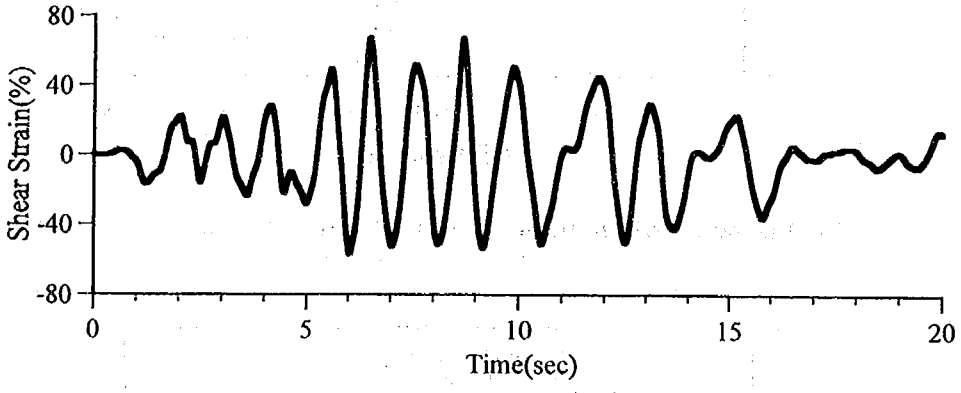


(c)Clearance=450mm

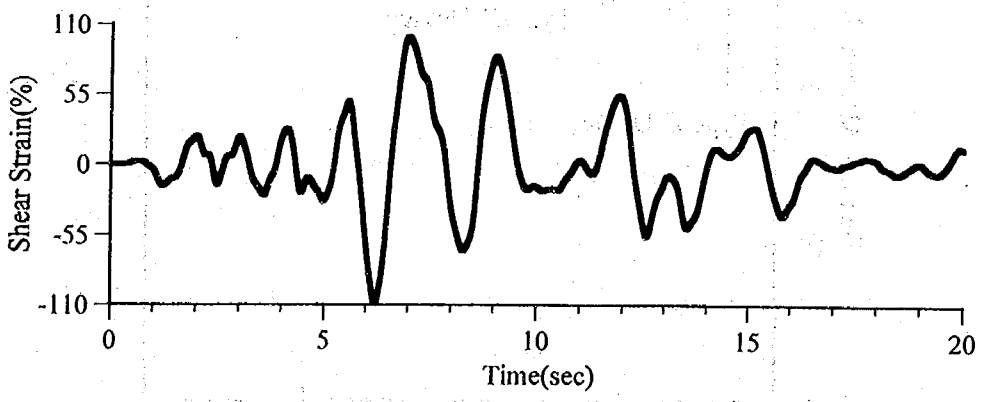
Fig.9 Velocity at Top and Bending Moment at Bottom of the Left Abutment (Type-A Device)



(a)Clearance=50mm

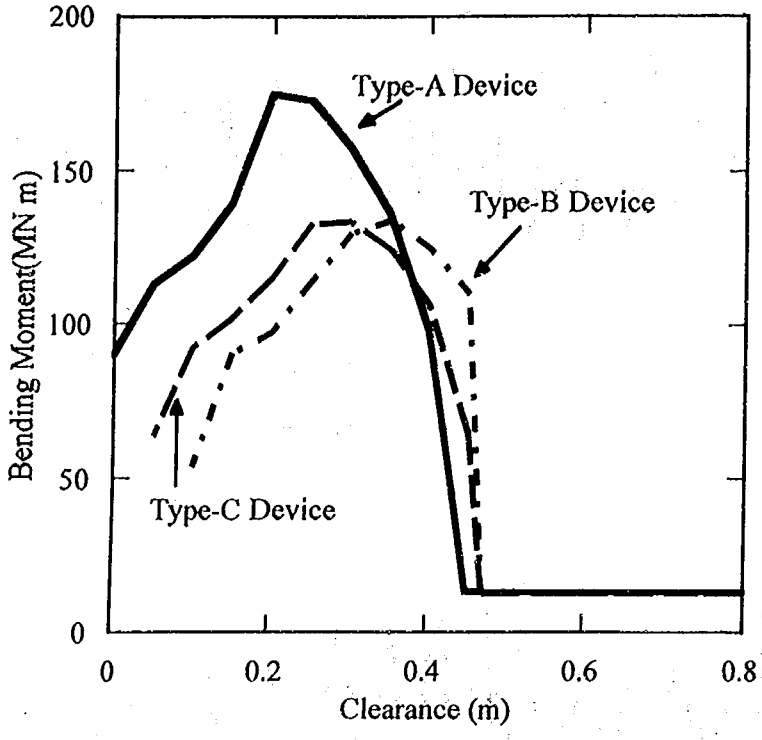


(b)Clearance=200mm

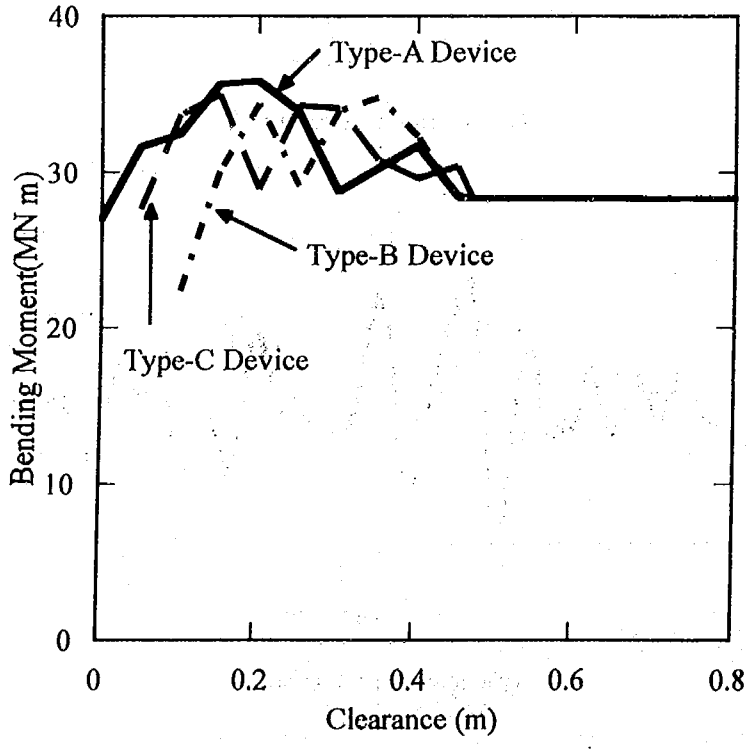


(c)Clearance=450mm

Fig.10 Shear Strain of Lead Rubber Bearings at Second Pier from Left

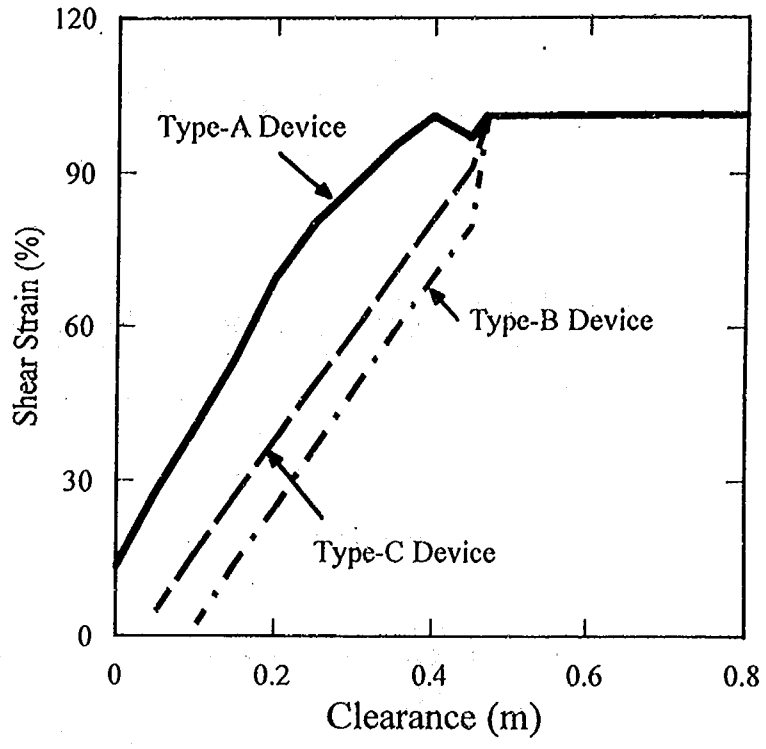


(a) Bending Moment at Bottom of Left Abutment

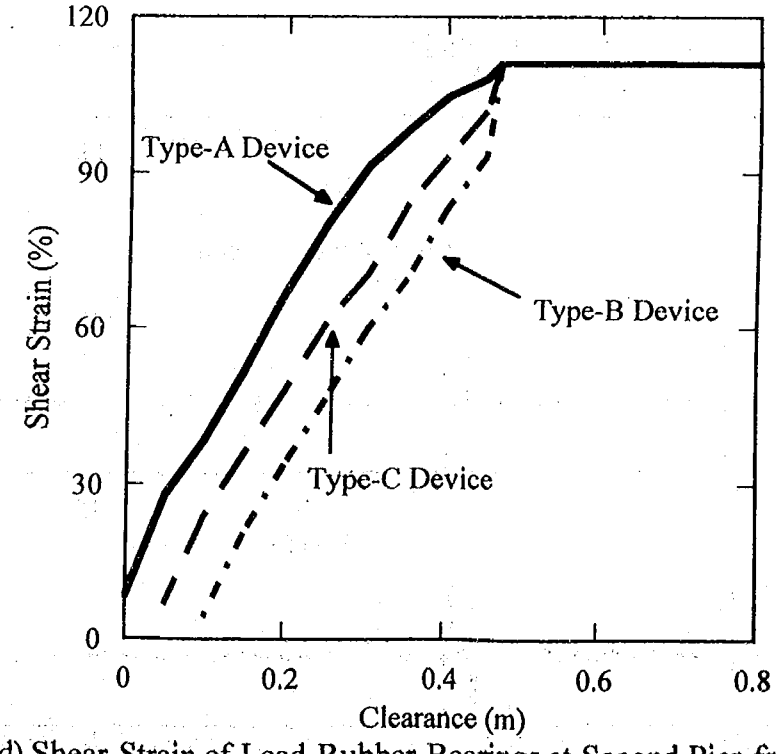


(b) Bending Moment at Second Pier from Left

Fig.11 Effect of Clearance on the Response of Bending Moment and Shear Strain of Lead Rubber Bearings

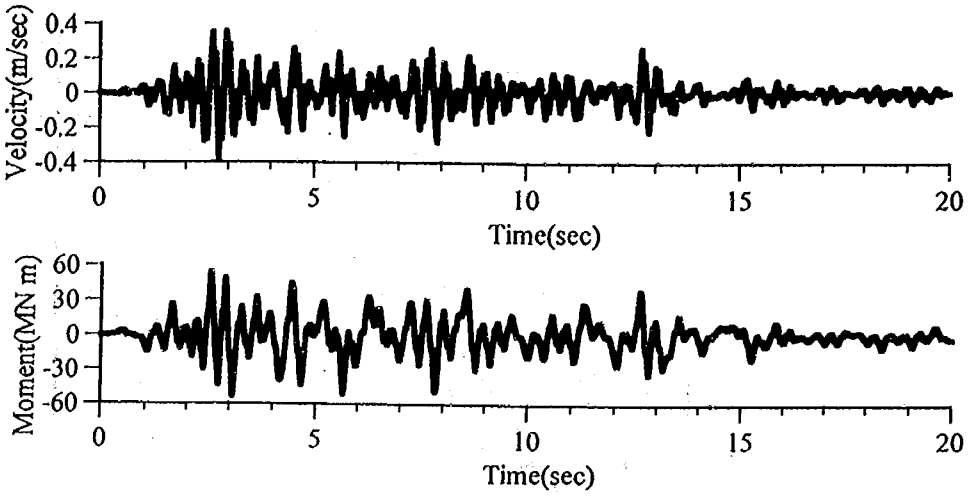


(c) Shear Strain of Lead Rubber Bearings at Left Abutment

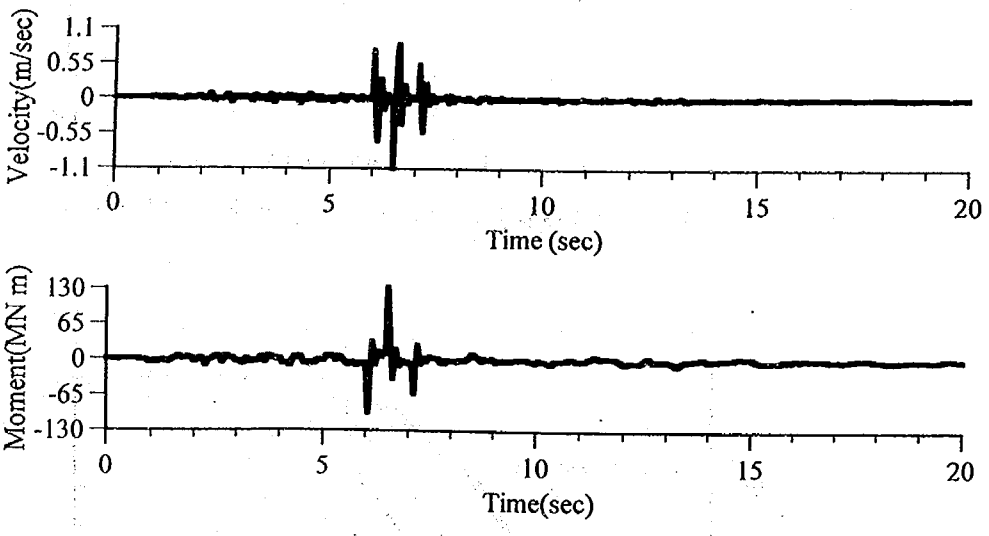


(d) Shear Strain of Lead Rubber Bearings at Second Pier from Left

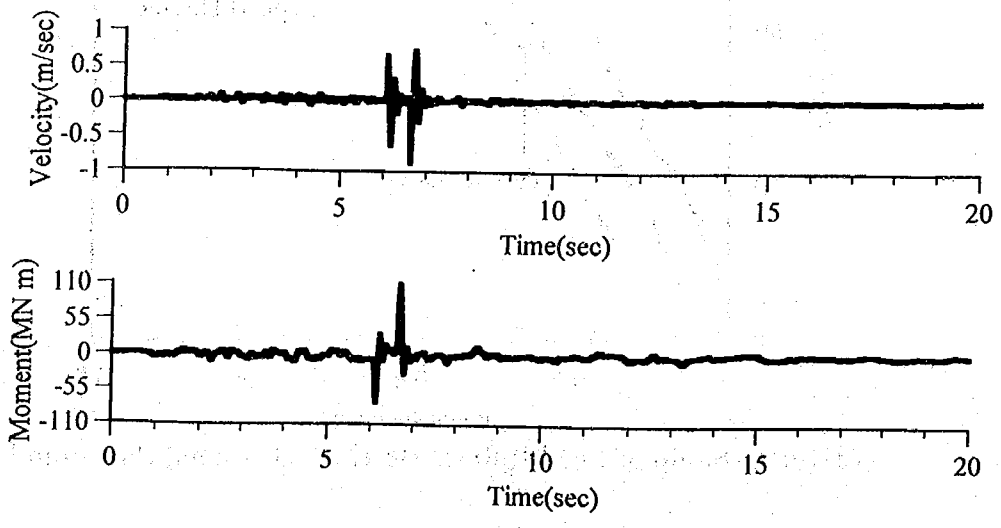
Fig.11 Effect of Clearance on the Response of Bending Moment and Shear Strain of Lead Rubber Bearings



(a)Clearance=50mm

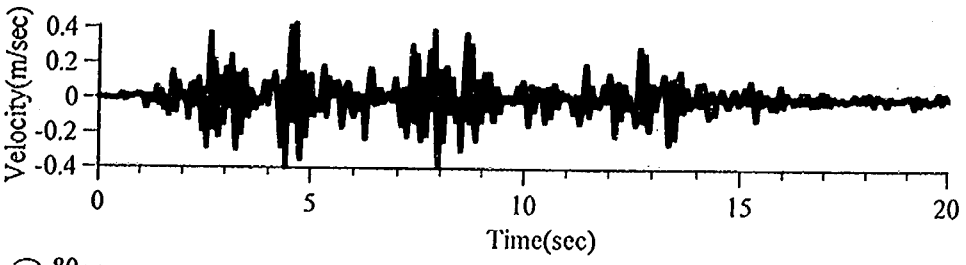


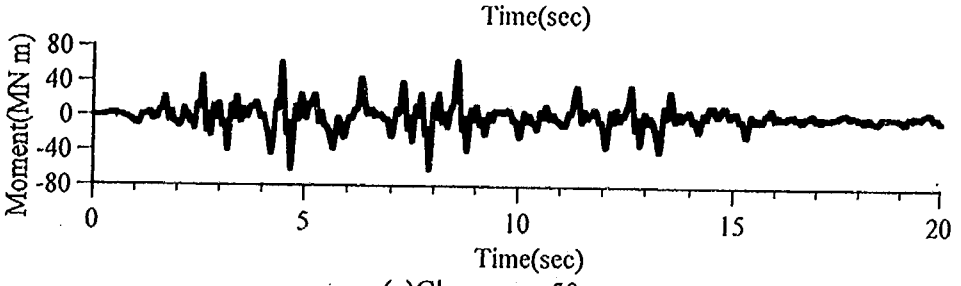
(b)Clearance=350mm



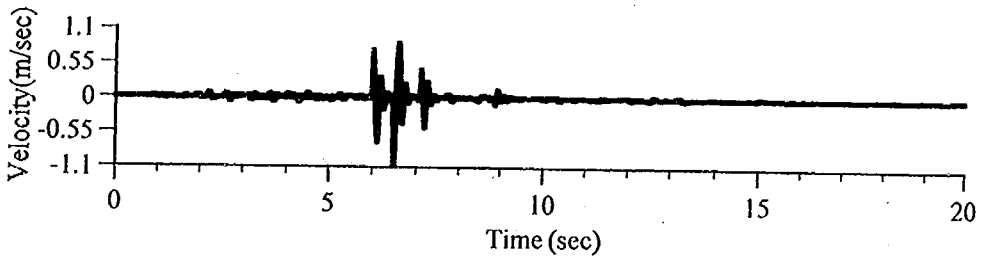
(c)Clearance=450mm

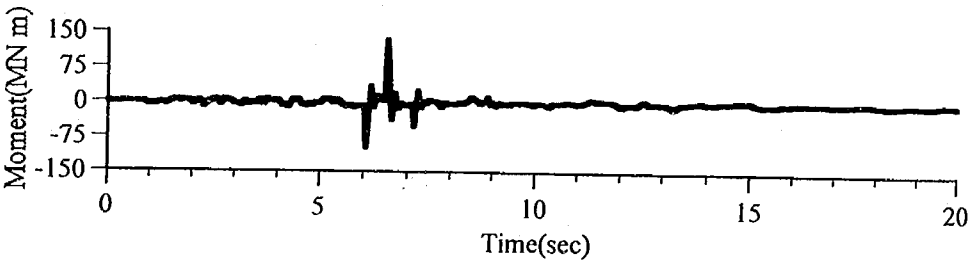
Fig.12 Velocity at Top and Bending Moment at Bottom of Left Abutment (Type-B Device)



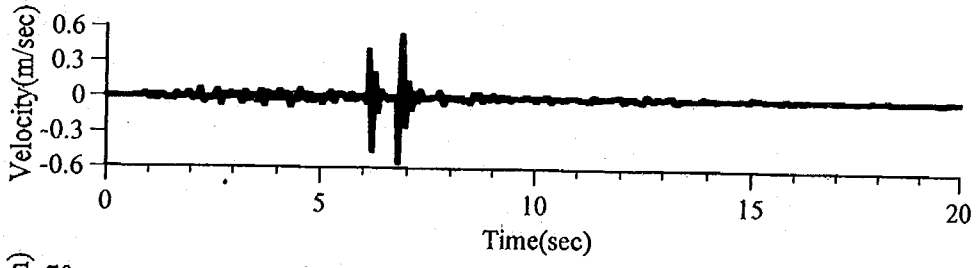


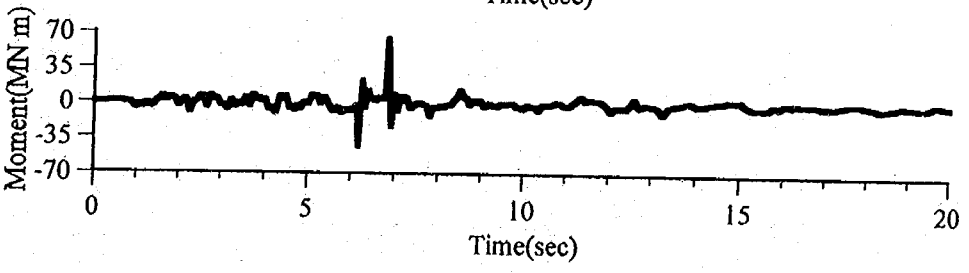
(a)Clearance=50mm





(b)Clearance=300mm





(c)Clearance=450mm

Fig.13 Velocity at Top and Bending Moment at Bottom of Left Abutment (Type-C Device)

SEISMIC PROTECTION OF BRIDGES WITH FLUID DAMPERS AND THE ISSUE OF VISCOUS HEATING

Nicos Makris
Department of Civil and Environmental Engineering, SEMM, University of California, Berkeley
Scott McMahon
Department of Civil Engineering and Geological Sciences, University of Notre Dame, Indiana

ABSTRACT

In this paper a closed form solution for the temperature increase within fluid dampers operating under harmonic motion is presented. The cases of a viscous behavior and of a rigid-plastic (hysteretic) behavior are considered. Results are presented in a dimensionless form accounting for heat convection in the environment. It is found that in most seismic applications temperature increases under nearly adiabatic conditions; which implies that the temperature increase per cycle is proportional to the maximum force developed by the damper during that cycle. Estimates for the temperature increase in prototype passive and semiactive dampers are presented.

INTRODUCTION

Fluid dampers have been accepted as a promising alternative to dissipate the induced energy in structures from earthquakes and other dynamic excitations. Typical fluid dampers utilize cylindrical shaped orifice (known as "square law" or Bernoullian orifices). Such orifices produce damping forces proportional to the square of the piston-velocity, a usually unacceptable performance in shock and vibration isolation. Dampers designed for seismic protection applications have specially shaped orifices which result forces proportional to $|\dot{u}|^{\alpha}$ where α is a predetermined coefficient, usually in the range $0 \le \alpha \le 1.5$ [4].

A combined experimental and analytical study on the response of structures equipped with fluid dampers with $\alpha \approx 1$ has been conducted by Constantinou and Symans[4]. Shake table tests were conducted on one- and three-story model structures with various configurations of damper placement. Fluid dampers have been implemented in several buildings in North America[2]. The most ambitious implementation of hydraulic fluid dampers in the U.S., is probably the under construction new San Bernandino County Medical Center[8].

Studies on the implementability of hydraulic fluid dampers in Bridges are under progress. Delis et al.[5] presented an analytical study on the response of the 91/5 HOV Connector separation bridge in Orange County California, while Aiken and Kelly[1] presented

experimental results from a pre-qualification testing program on fluid dampers as part of the seismic rehabilitation of the Golden Gate Bridge.

Recently, passive fluid dampers have been extended to controllable fluid dampers. Controllable fluid dampers such as electrorheological (ER)[6] or magnetorheological (MR)[3,15] fluids have the distinct property of exhibiting a finite yield stress when an electric or magnetic field is applied. Because of the presence of this yield stress, ER- and MR-fluid dampers can deliver a friction type force in addition to the viscous type force generated from the inherent viscosity of the controllable fluid[10,11,12]. Component testing on a large-scale ER damper developed for seismic protection of bridges has been also recently conducted.[13]

In building applications where the dampers are installed within the skeleton of the structure the stroke and maximum piston velocity are relative small, so that viscous heating is not a concern. In bridge applications; however, the stroke and velocity requirements on the damper are significant (displacements of the order of 1/2 m and velocities of the order of 1 m/sec or more). These severe requirements motivated this study on the issue of viscous heating. In this paper an approximate analytical study is presented to estimate the temperature increase within the fluid of passive and controllable fluid dampers.

MACROSCOPIC CONSTITUTIVE LAW

The proposed constitutive law for fluid dampers designed for seismic protection of bridges is of the form

$$P(t) = C|\dot{u}(t)|^{\alpha}\,\mathrm{sgn}\,[\dot{u}(t)] \tag{1}$$

where P(t)=piston force, u(t)=piston velocity, α=fractional exponent, $0 \le \alpha \le 1$, C=a damping constant with units (force)x(time)$^{\alpha}$ and sgn is the signum function. When α=1, equation (1) reduces to the viscous case,

$$P(t) = C\dot{u}(t)\,. \tag{2}$$

When α=0, equation (1) represents a rigid-plastic behavior

$$P(t) = P_y\,\mathrm{sgn}\,[\dot{u}(t)]\,, \tag{3}$$

where now $C=P_y$= a yield force. The constitutive laws given by (2) and (3) are the two limiting cases of (1) for $0 \le \alpha \le 1$. For the case of controllable fluid dampers, ER and MR fluids exhibit a viscous behavior in the absence of field; whereas, under the presence of field the behavior is viscoplastic. In particular, MR fluids manifest a larger yield stress than ER fluids and their behavior is nearly rigid-plastic. Accordingly, the laws given by (2) and (3) also describe the two extreme situations in the case of controllable fluid dampers without and with applied field.

VISCOUS HEATING

When the damper piston is in motion, macroscopic energy balance of the portion of the fluid that travels through the piston head gives

$$m\hat{C}_p \frac{d\theta(t)}{dt} + \frac{dQ(t)}{dt} = P(t)\frac{du(t)}{dt} \tag{4}$$

where $\hat{C}_p$ is the heat capacity at constant pressure, m, is the mass of the fluid that migrates, P(t) and u(t) are force and displacement at the piston rod and $Q = Q_{conv} + Q_{cond}$ is the net energy loss due to: (a) convection via the solid surfaces of the bypasses and (b) conduction in the remaining fluid within the damper. The convected term can be expressed as[7]

$$\dot{Q}_{conv} = \frac{k}{z}A_s(\theta(t) - \theta_0), \tag{5}$$

where, k, is the coefficient of thermal conductivity, A_s is the heat transfer surface (outer surface of the damper), z is the thickness of the damper housing and θ_0, is the ambient temperature. During the long stroke motions of interest, most of the fluid within the damper travels through the piston head and the energy loss due to conduction can be neglected. Accordingly, equation (4) takes the form

$$m\hat{C}_p \frac{d\theta(t)}{dt} + \frac{k}{z}A(\theta(t) - \theta_0) = P(t)\frac{du(t)}{dt}, \tag{6}$$

which is a linear first order differential equation that can be integrated using an integration factor. The solution of (6) is

$$\theta(t) = e^{-\lambda t}\int_{-\infty}^{t} Q(\xi)\, e^{\lambda\xi} d\xi + \Gamma e^{-\lambda t}, \tag{7}$$

where

$$Q(\xi) = \frac{1}{m\hat{C}_p}P(\xi)\,\dot{u}(\xi) + \lambda\theta_0 \tag{8}$$

and

$$\lambda = \frac{kA_s}{zm\hat{C}_p}, \tag{9}$$

which is a quantity with units in rad/sec. Γ is an integration constant that depends on the initial conditions. For a cylindrical damper with piston diameter, d_p, and length L,

$A_s = \pi d_p L$, and by neglecting the volume of the piston rod, $m = \rho \pi d_p^2 L/4$, where ρ is the mass density of the fluid (for silicone oil, $\rho \approx 970 kg/m^3$). In this case,

$$\lambda = \frac{4k}{z d_p \rho \hat{C}_p}. \tag{10}$$

For a steel damper housing, k=25 J/(m sec ^oC), and an average value for the heat capacity coefficient of the damper fluid is $\hat{C}_p \approx 2000$J/(kg ^oC)[16]. Using the value of the diameter of the damper tested by Aiken and Kelly[1], $d_p = 0.2m$, and assuming a thickness of the housing, z=0.005m, the resulting value for $\lambda \approx 0.05$ rad/sec.

For the general nonlinear constitutive law given by (1) a closed form solution of (4) is not known to the author. Nevertheless, equation (4) can be integrated in closed form for the two limiting cases given by (2) and (3).

For the viscous case (α=1), the force history in (8) is given by (2), and the resulting temperature history from (7) is

$$\theta(t) = \theta_0 + \frac{C\omega U_0^2}{m\hat{C}_p} \frac{1}{4 + (\frac{\lambda}{\omega})^2} \left[\cos\omega t \left(\frac{\lambda}{\omega} \cos\omega t + 2\sin\omega t \right) + 2\frac{\omega}{\lambda} - \left(\frac{\lambda}{\omega} + 2\frac{\omega}{\lambda} \right) e^{-\lambda t} \right]. \tag{11}$$

Figure 1 (left) plots the temperature increase as a function of time during one cycle of piston motion for different values of the ratio λ/ω. The curve for $\lambda = 0$ is the adiabatic solution. Figure 1 (left) shows that for the damper tested by Aiken and Kelly[1], even for an angular frequency as low as 5 rad/sec (f=0.8 Hz) the behavior is nearly adiabatic (λ/ω=0.01).

The temperature increase after one cycle is given by

$$\Delta\theta\left(\frac{2\pi}{\omega}\right) = \frac{C\omega^2 U_0^2}{m\hat{C}_p} \frac{\lambda^2 + 2\omega^2}{\lambda^2 + 4\omega^2} \frac{1}{\lambda} \left(1 - e^{-\frac{2\pi\lambda}{\omega}} \right). \tag{12}$$

At the limit where $2\pi\lambda \ll \omega$, $e^{-\frac{2\pi\lambda}{\omega}} \approx 1 - \frac{2\pi\lambda}{\omega}$ and equation (12) reduces to

$$\Delta\theta\left(\frac{2\pi}{\omega}\right) = \frac{\pi C\omega U_0^2}{m\hat{C}_p} \tag{13}$$

which is the expression for the temperature increase per cycle under adiabatic conditions. By approximating the mass of the fluid that travels with $2U_o A_p \rho$, and replacing $C\omega U_0$ with P_0, equation (13) simplifies to:

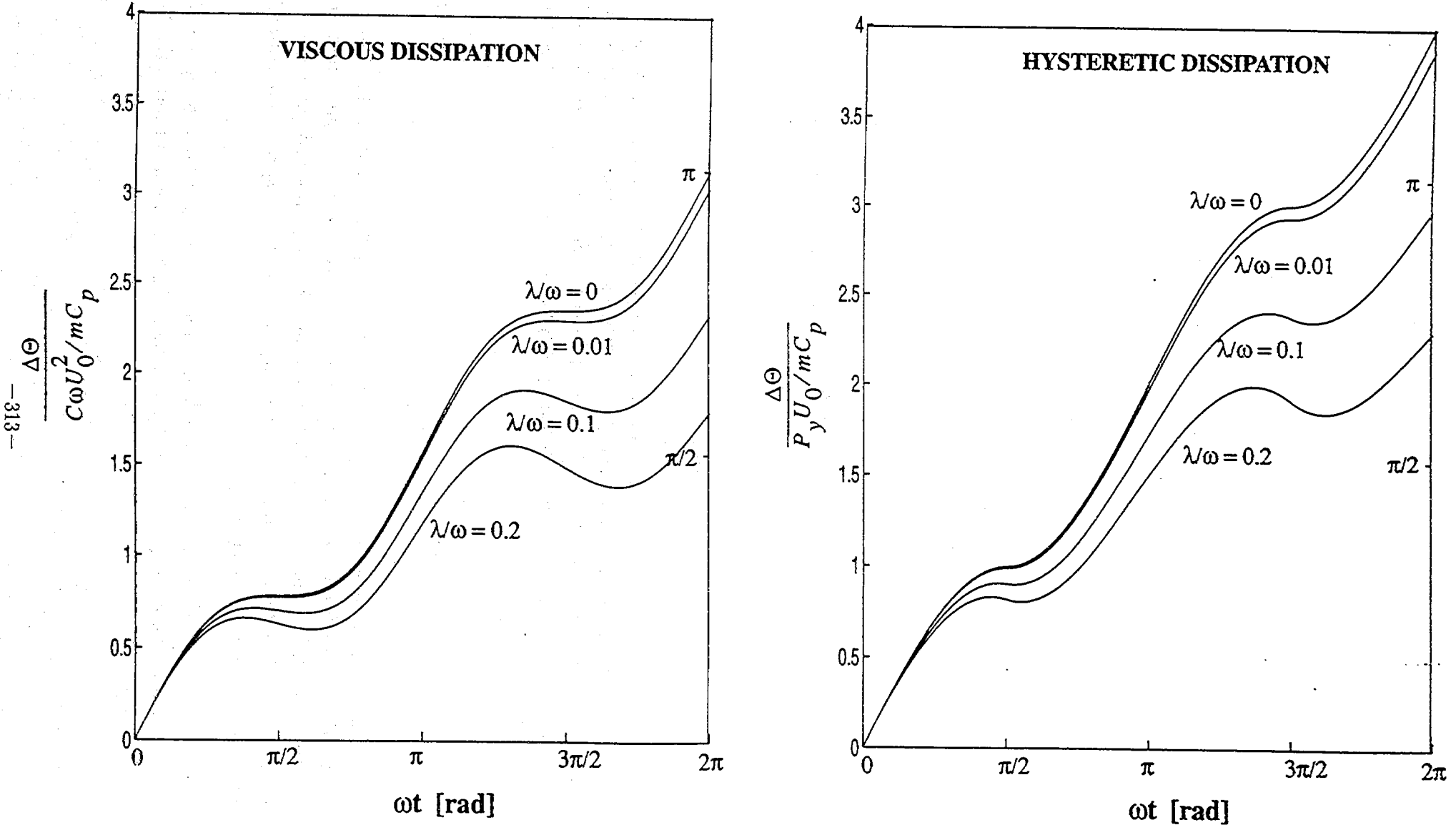


Figure 1. Temperature rise within the damper during a one-cycle motion.

$$\Delta\theta\left(\frac{2\pi}{\omega}\right) = \frac{\pi}{2}\frac{C\omega U_0}{\rho \hat{C}_p A_p} = \frac{2P_0}{\rho \hat{C}_p d^2{}_p}. \tag{14}$$

Using a maximum force of P_0=100 kips (445kN) and d_p = 0.19m, the conservative adiabatic solution for the viscous case gives an approximate temperature increase per cycle, $\Delta\theta\left(\frac{2\pi}{\omega}\right) \approx 12^0 C$.

For the rigid-plastic case (hysteretic case), α=0, the force history in (8) is now given by (2). Because of the signum function in the constitutive law of the force, the temperature history is given by:

$$\theta(t) = \theta_0 + \frac{P_y U_0}{m\hat{C}_p}\frac{\frac{\lambda}{\omega}\cos\omega t + \sin\omega t - \frac{\lambda}{\omega}exp(-\lambda t)}{1+\left(\frac{\lambda}{\omega}\right)^2}, \qquad 0 \le t \le \frac{\pi}{2}, \tag{15}$$

$$\theta(t) = \theta_0 + \frac{P_y U_0}{m\hat{C}_p}\frac{2exp(-\lambda t)\,exp\left(\frac{\pi\lambda}{2\omega}\right) - \frac{\lambda}{\omega}exp(-\lambda t) - \left(\frac{\lambda}{\omega}\cos\omega t + \sin\omega t\right)}{1+\left(\frac{\lambda}{\omega}\right)^2}, \qquad \frac{\pi}{2} \le t \le \frac{3\pi}{2}, \tag{16}$$

$$\theta(t) = \theta_0 + \frac{P_y U_0}{m\hat{C}_p}\frac{2exp(-\lambda t)\left(exp\left(\frac{\pi\lambda}{2\omega}\right) + exp\left(\frac{3\pi\lambda}{2\omega}\right)\right) - \frac{\lambda}{\omega}exp(-\lambda t) + \frac{\lambda}{\omega}\cos\omega t + \sin\omega t}{1+\left(\frac{\lambda}{\omega}\right)^2}. \tag{17}$$

$$\frac{3\pi}{2} \le t \le 2\pi$$

Figure 1 (right) plots the temperature increase as a function of time during one cycle of piston motion for hysteretic dissipation and different values of the ratio λ/ω. The curve for $\lambda = 0$ is the adiabatic solution. Using the same approximation for the mass of the fluid that travels, m= $2U_o A_p \rho$, the temperature increase per cycle under adiabatic conditions for the hysteretic case is

$$\Delta\theta\left(\frac{2\pi}{\omega}\right) = \frac{8}{\pi}\frac{P_y}{\rho \hat{C}_p d^2{}_p}. \tag{18}$$

For instance, with a maximum force of P_y=100 kips (445kN) and d_p = 0.19m, the conservative adiabatic solution for the hysteretic case gives an approximate temperature increase per cycle, $\Delta\theta\left(\frac{2\pi}{\omega}\right) \approx 16^0 C$, which is the upper bound value. With equation (18) one can estimate an upper bound for the temperature increase in any damper for a specified maximum force and a given piston diameter.

With the analytical solution presented herein one can compute the temperature increase in the damper after several cycles. Figure 2 plots the temperature histories for the

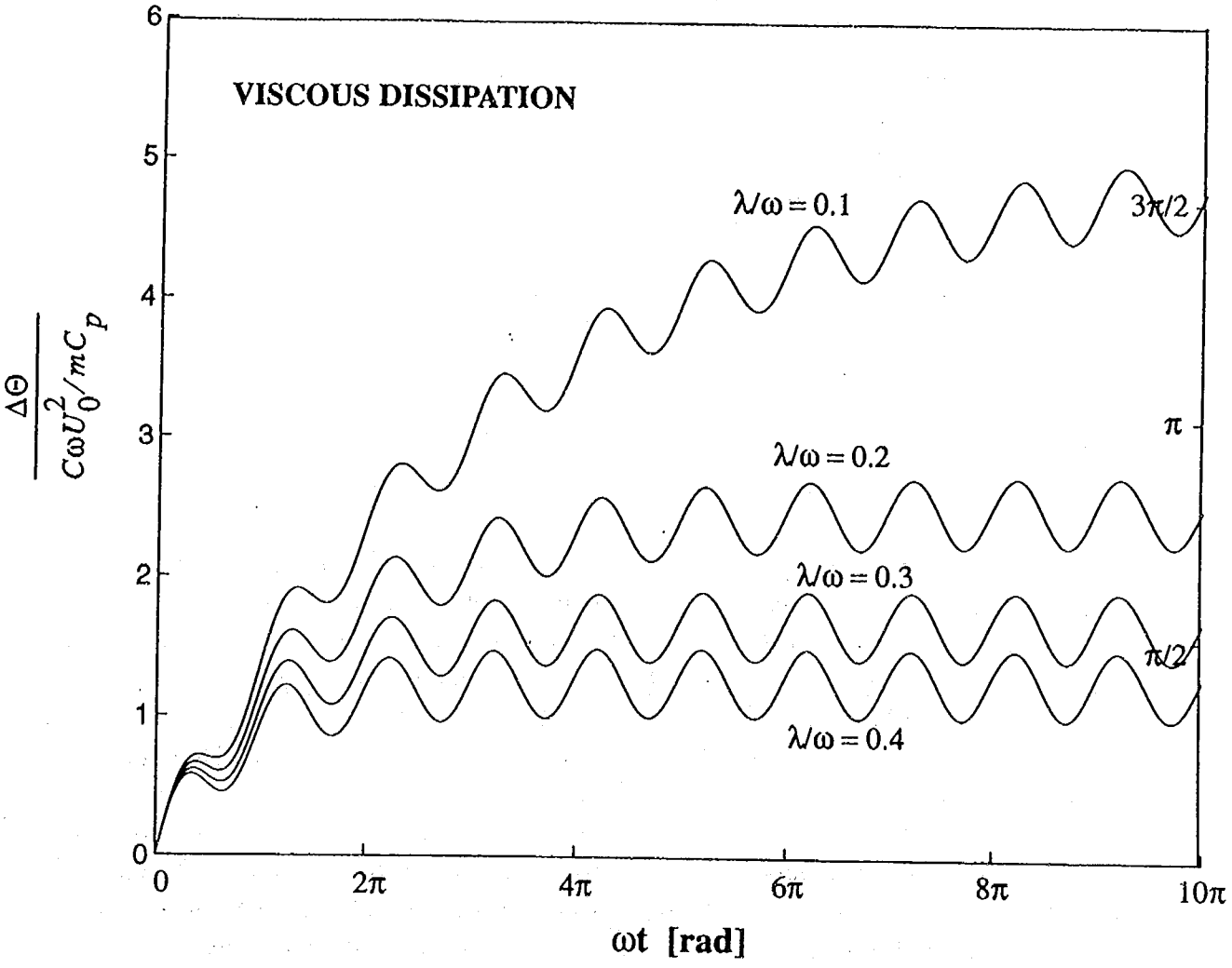


Figure 2. Temperature histories during a five-cycle motion.

viscous case during a five cycle motion. As the ratio λ/ω increases the temperature histories reach sooner steady-state conditions. Nevertheless, even after five cycles and with $\lambda/\omega = 0.1$, the temperature keeps increasing.

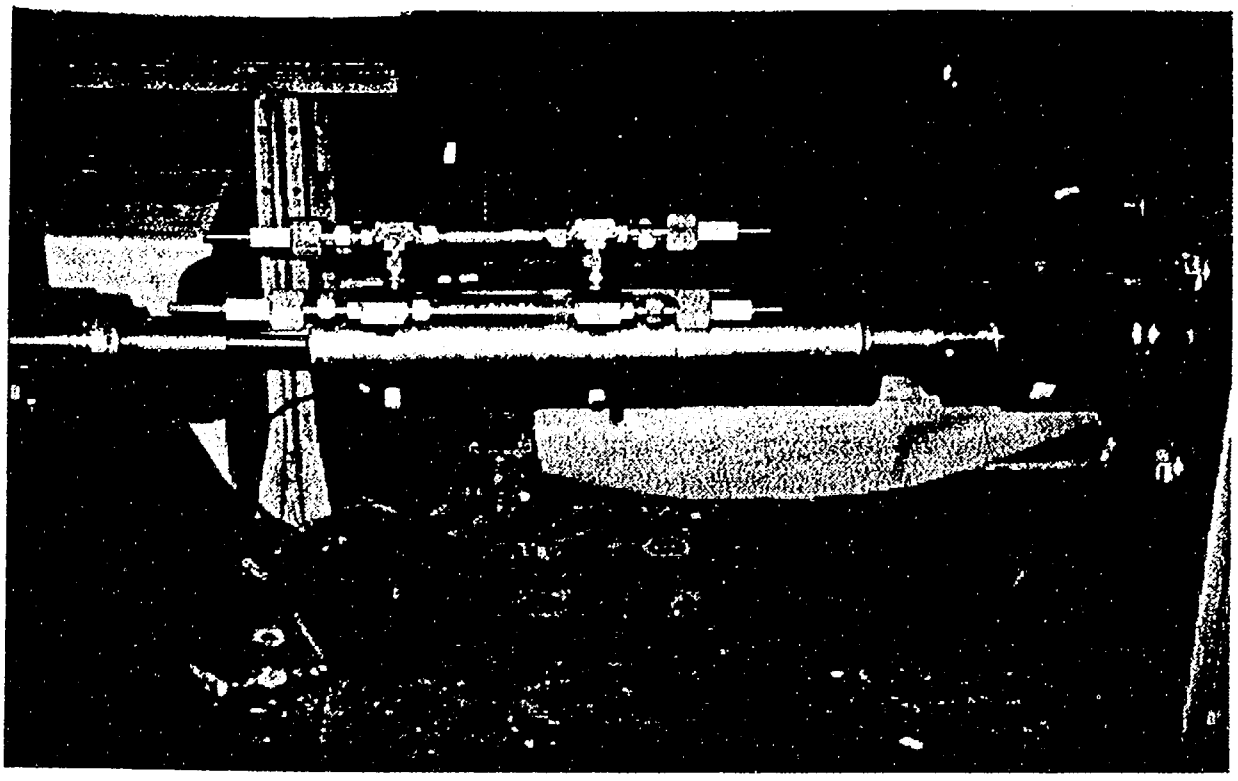
In the case of an arbitrary force-output history with length, T, in which the force maxima, $P_{max,j}$, at every cycle j are known, the temperature increase at the end of the motion after N cycles is bounded by

$$\Delta\theta(T) < \frac{8}{\pi\rho\hat{C}_p d^2 p} \sum_{j=1}^{N} P_{max,j}. \tag{19}$$

CONTROLLABLE FLUID DAMPERS

Electrorheological dampers have attracted considerable attention in the last decade for vibration control of mechanical and structural systems. Early studies by Stevens et *al.*[17], showed how a simple ER-damper is capable of reducing displacement amplitudes when electric field is applied; while Duclos[6] has reported on various applications that ER-dampers have found in the automotive industry. Recently, ER-dampers received considerable attention for vibration control of civil structures. The attraction of ER-dampers is that they are relatively inexpensive compared to hydraulic dampers with mechanically controlled orificing. Ehrgott and Masri[9], presented identification techniques to model the behavior of a small ER-damper that operates under shear flow. Gavin and Hanson[10] designed and tested an ER-damper that consists of a rectangular container and a moving plunger comprised of nine flat parallel plates which are rigidly interconnected.

Most of the ER-dampers proposed in the past involve shear flow. Figure 3 (top) is a photograph of an ER-damper designed by the authors and their coworkers[13]. It is a scaled up version of a prototype ER-damper which has been extensively studied previously[11,12]. A schematic of the ER-damper is shown on Figure 3 (bottom). The damper consists of an outer cylinder and a double ended piston rod that pushes the ER-fluid through a stationary annular duct. The electric field is created perpendicular to the fluid flow across the bypass. Some of the advantages of the developed ER-damper shown on Figure 1 are: 1) There are no moving parts within the damper besides the piston. 2) It is a compact device that can produce relatively large forces. 3) Because of the yield forces that ER-dampers can develop, they can provide significant rigidity and when the yield forces are exceeded they can dissipate substantial energy. 4) Once the power fails the damper operates as a passive device that provides a reasonable amount of damping. 5) The damper can operate in a passive state during many seismic events where viscous damping alone is sufficient to mitigate the response. 6) The proposed damper can be positioned in any direction as opposed to other dampers which have to be positioned horizontally due to the presence of a free surface. 7) Settling of the ER-fluid was never a problem in the response of our damper. Even when the damper has been inactive for more than 10 weeks, it responded in a consis-



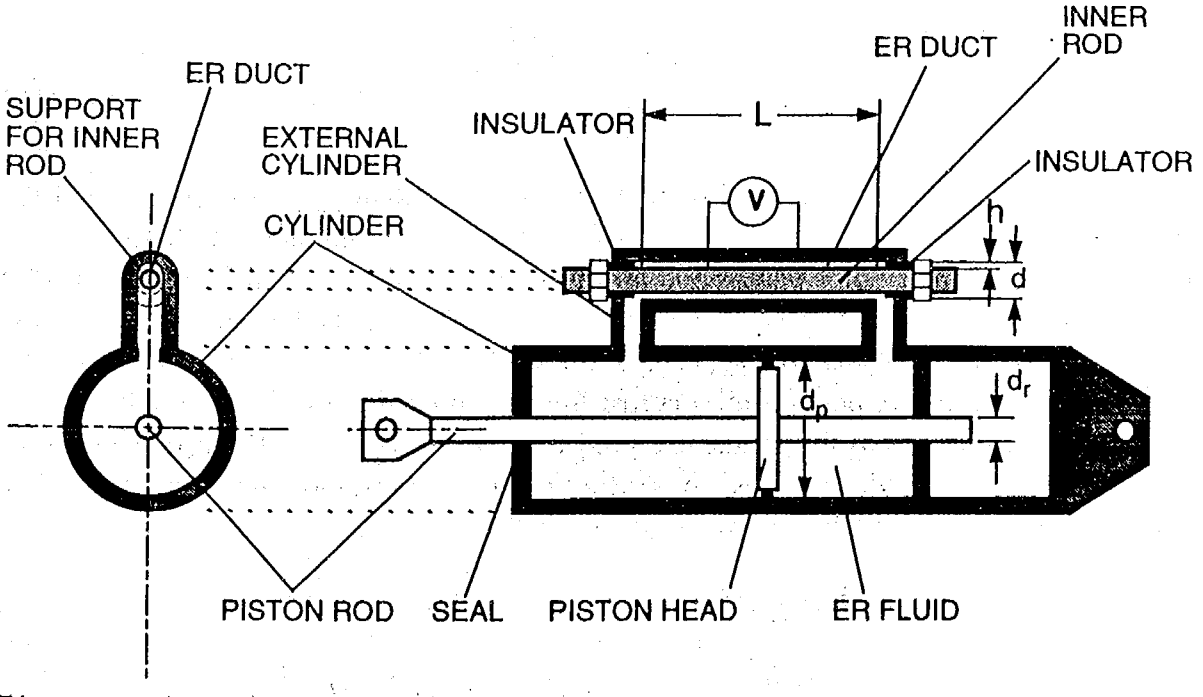


Figure 3. Top: View of constructed large-scale ER-damper. Bottom: Scematic of the ER-damper.

tent manner as in previous tests. Possible reason for this good performance is that the ER-material is nested within a very thin ring, and apparently the surface tension that develops on the fluid eliminated the settling problem.

Using one dimensional flow theory, the shear stress that develops across the bypass can be approximated by[11]

$$\tau_{xr}(r) = \Delta p \frac{r}{L}, \tag{20}$$

where Δp is the pressure drop across the piston head, r is the radial distance from the center line of the ER-duct, and L is the length of the duct (see Figure 1-bottom). The stress distribution given by (20) is independent of the material that flows. In the case where $h \ll d$, the solution for the Poisseuille flow between concentric cylinders collapses to that for flow between parallel plates. For instance, if the fluid that flows through is newtonian, with zero-shear-rate viscosity, η_0, the pressure drop due to viscous stresses under steady flow is given by

$$\Delta p_v = \frac{1}{n} \frac{12\eta_0 LQ}{\pi d h^3}, \tag{21}$$

where Q is the flow rate through the ER-duct, d is the diameter of the ER-duct, h is the width of the gap and n is the number of bypasses. Equation (21) approximates the pressure drop in the case of no field (E=0). In this case the damper behaves like a viscous dashpot, $P(t) = C\dot{u}(t)$, where the damping constant, C, is given by

$$C = \frac{1}{n} \frac{12\eta_0 L A_p^2}{\pi d h^3}. \tag{22}$$

When electric field is applied the behavior of the ER-fluid is viscoplastic and the shear stress $\tau_{xr}(r)$ has to exceed the finite "yield" stress, τ_y, to initiate flow. This value of the "yield" stress can be also understood as the *capacity* of the material to exist in a solid state. If the stress demand, $\tau_{xr}(r)$, given by Equation (20) exceeds the capacity of the ER-material, τ_y, then the ER-material adjacent to the walls will yield and flow. For a rigid-viscoplastic material the velocity profiles across these "fluidized" rings is parabolic whereas the velocity profile across the remaining solid core-ring is constant. From equation (20) one immediately recognizes that as the pressure drop increases, more material yields. The pressure drop under viscoplastic flow is given by[11,14]

$$\Delta p = \frac{1}{n} \frac{12\eta_0 LQ}{\pi d h^3} \frac{1}{1 - 3\frac{\tau_y}{\Delta p}\frac{L}{h} + 4\left(\frac{\tau_y}{\Delta p}\right)^3 \left(\frac{L}{h}\right)^3}. \tag{23}$$

As flow rate increases equation (23) reaches asymptotically the expression:

$$\Delta p\,(t) \;=\; \frac{P\,(t)}{A_p} \;=\; \frac{1}{n}\frac{12\eta_0 L A_p}{\pi d h^3}\dot{u}\,(t) + \frac{3L\tau_y}{h}\,\mathrm{sgn}\,[\dot{u}\,(t)]\,, \qquad (24)$$

where A_p is the area of the piston head and the flow rate, $Q = A_p\dot{u}\,(t)$. Equation (24) is valid everywhere but the zero-velocity limit where the factor, three, in the second term reduces to two.

Figure 4 shows recorded (left) and predicted (right) force-displacement loops from the large scale ER-damper without electric field (E=0) and with E=3kV/mm. As the piston velocity increases, viscous effects dominate over plastic effects and the fraction of the force that can be controlled reduces. The predicted response shown on the right of Figure 4 is computed with

$$P\,(t) \;=\; \Delta p\,(t)\,A_p + P_y\,\mathrm{sgn}\,[\dot{u}\,(t)]\,, \qquad (25)$$

where P_y is a permanent friction force acting on the damper seals and A_p is the area of the piston head. Δp is the pressure drop across the piston head given by (24). Substitution of (24) into (25) gives

$$P\,(t) \;=\; \frac{1}{n}\frac{12\eta_0 L A_p}{\pi d h^3}A_p\dot{u}\,(t) + \left[\frac{3L\tau_y}{h}A_p + P_y\right]\mathrm{sgn}\,[\dot{u}\,(t)] \qquad (26)$$

Equation (26) is the resulting piston force as a function of the piston velocity, the mechanical properties of the controllable fluid and the geometric characteristics of the damper. The predicted loops on Figure 4 were obtained with $\tau_y = 1.7kPa$ and $\eta_0 = 6Pa-s$. Figure 2 shows that equation (26) predicts satisfactorily the damper response at small piston velocities. At higher piston velocities, leakage through the piston head increases, thereby reducing the pressure drop. This is a desirable behavior since a reduced pressure drop will result in smaller forces and a less intense viscous heating. Equation (26) can be used to approximate the force output from other controllable fluid dampers with similar geometry, such as a recently developed magnetorheological damper.[3]

In order to have an effective ER-damper the viscous forces that develop have to be comparable with the friction-like forces. When ER-dampers are incorporated within the frame of a flexible structure the design piston velocities are relatively low ($\dot{u}$=3 to 10 in/sec), and the design of the damper shown on Figure 3 is appropriate[11]. As the piston velocity increases the number of bypasses has to increase to keep the flow rate at low values. The ER-damper shown on Figure 3 has been designed to accommodate up to four bypasses. When a substantial controllable force is needed at higher piston velocities a different design is needed. A new ER damper which can accommodate large piston velocities is under construction.

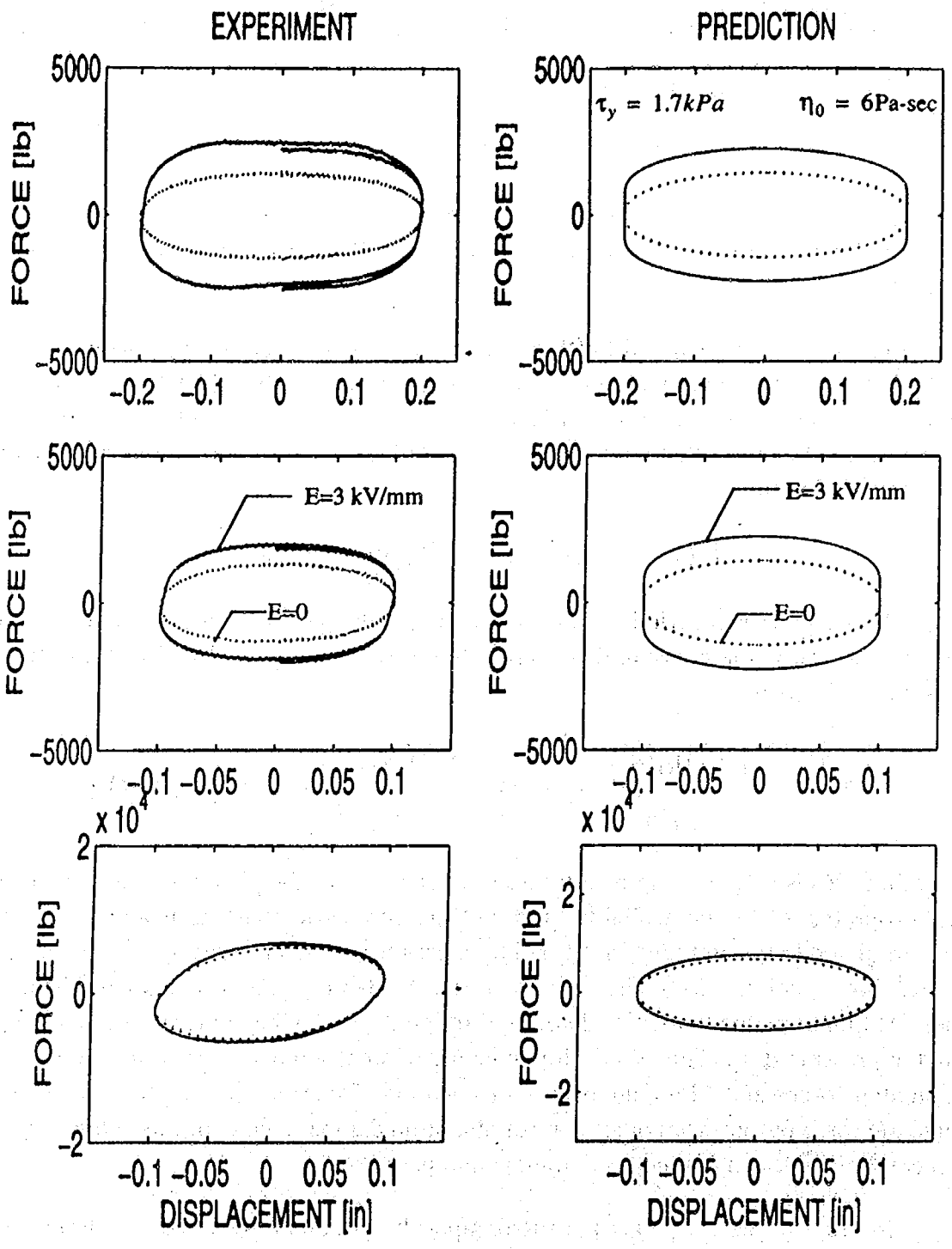


Figure 4. Comparison of Experimental Results to Predicted Response for E=0 kV/mm and E=3 kV/mm with Three Bypasses. From Top to Bottom (frequency/amplitude): 0.1 Hz/0.2 in; 0.2 Hz/0.1 in; 1.0 Hz/0.1 in.

Returning to the issue of viscous heating, the damper coefficient, C, in equation (14) is given by (22), and the temperature increase per cycle can be expressed directly as a function of the geometric characteristic of the damper and the physical properties of the fluid,

$$\Delta\theta\left(\frac{2\pi}{\omega}\right) = \frac{1}{n}\frac{6\eta_0 L\omega U_0 A_p}{\rho\hat{C}_p dh^3}. \tag{27}$$

Equation (28) is useful to estimate the temperature increase per cycle for a given damper. For instance using the parameters associated with the ER-damper shown on Figure 1 (η=6 Pa-sec, L=0.15m, A_p=0.004888m^2, ρ=1400kg/m^3, $\hat{C}_p \approx$ 2kJ/(kg ^{o}C), d=0.0145m, h=0.001m), the temperature increase during the bottom cycle shown on Figure 4 is less than 3 ^{o}C. Nevertheless during this cycle the velocity amplitude is small (~0.015 m/sec). In the case where the velocity amplitude is 0.5m/sec equation (28) yields a temperature increase of approximately 100 ^{o}C. This large value of temperature increase is because the damper shown on Figure 3 has a damping coefficient, C=1900kN-sec/m, which is more than two times the damping coefficient of the damper tested by Aiken and Kelly[1]. This shows that a couple of rapid cycles are enough to produce a temperature increase of several hundreds ^{o}C; therefore, the alternative approach of cooling the damper is worth investigating.

Equation (28) dictates that the temperature increase per cycle is inverse proportional to the diameter of the bypass, d. The proposed new ER damper has a bypass that its diameter can be 20 to 30 times larger of the diameter of the bypass shown on Figure 1. According to equation (28), the temperature increase per cycle can be also reduced by selecting a fluid with smaller viscosity. The viscosity of other ER-fluids[2] can be as low as 10 times the viscosity of the ER-fluid used herein (0.5 Pa-sec). Nevertheless; a smaller viscosity will reduce the energy dissipation capabilities of the damper in its passive state; and therefore, the total number of dampers installed in a building should be increased. Accordingly, when viscous heating is a concern, it is recommended that a larger number of dampers, each one having a reduced damping coefficient, should be installed.

Another effective way in reducing the temperature increase per cycle is to increase the width of the bypass, h. Nevertheless, after comprehensive testing we concluded that a gap, h=0.001m (1mm) seems to be an optimal value, since larger values of h resulted in a fluctuating electric field across the bypass.

CONCLUSIONS

In this paper a closed form solution for the temperature increase within fluid dampers operating under harmonic motion has been presented. The cases of a viscous behavior and of a rigid-plastic (hysteretic) behavior were considered separately. Results are presented in a dimensionless form accounting for heat convection in the environment. It is found that in most seismic applications temperature increases under nearly adiabatic con-

ditions; which implies that the temperature increase per cycle is proportional to the maximum force developed by the damper dyring that cycle. Estimates for the temperature increase in prototype pasive and semiactive dampers have been presented. For rapid motions it is recommended that a larger number of dampers, each one having a reduced damping coefficient, should be used. This design will reduce viscous heating.

ACKNOWLEDGEMENTS

This work is supported by the National Science Foundation Grant BCS-9300827, Dr. S. C. Liu, Program Director. The main cylinder of the damper was manufactured and donated by Taylor Devices, Inc., N. Tonawanda, NY. The constructive comments and suggestions offered by Mr. Douglas Taylor are appreciated.

REFERENCES

1. I. D. Aiken and J. M. Kelly, "Pre-qualification testing of viscous dampers for the Golden Gate Bridge seismic rehabilitation project," *Report No. EERC-STI/95-02*, Richmond, CA (1995).

2. ATC-17-1. *Proceedings of Seminar on Seismic Isolation, Passive Energy Dissipation, and Active Control*, Vol. 1&2, Applied Technology Council (1993).

3. J. D. Carlson and K. D. Weiss, "A growing attraction to magnetic fluids," *Machine Design*, 8, 61-64, (1994)

4. M. C. Constantinou and M. D. Symans, "Experimental and analytical investigation of seismic response of structures with supplemental fluid viscous dampers," *Technical Report NCEER-92-0032*, Buffalo, NY (1992).

5. E. A. Delis, R. B. Malla, M. Madani and K. J. Thompson, "Energy dissipation devices in Bridges using hydraulic dampers," *Proc. Structures Congress XIV*, Chicago, Ill (1996).

6. T. G. Duclos, "Design of devices using electrorheological fluids," *Society of Automotive Engineering*, paper 881134, 2.532-2.536 (1989).

7. I. M. Dulay, F. Furesz, G. Harkay and J. Lukacs, Fundamentals of Hydraulic Power Transmission. Elsevier, New York, NY (1988).

8. ENR, "Hospital girds for quake," Engrg News Record, Vol. 11, 24-26 (1995).

9. R. C. Ehrgott and S. F. Masri, "Modeling the oscillatory dynamic behavior of electrorheological materials in shear," *Smart Materials and Structures*, Vol. 1, 275-285 (1992).

10. H. P. Gavin and R. D. Hanson, "Electrorheologcal dampers for structural vibration suppression," Report No. UMCEE 94-35, Dept. Civil and Envir. Engrg, University of Michigan, Ann Arbor, MI, (1994).

11. N. Makris, S. A. Burton, D. Hill, and M. Jordan, "Analysis and design of an electrorheological damper for seismic protection of structures," *J. Engineering Mechanics, ASCE*, Vol. 122, 1003-1011, (1996).

12. N. Makris, D. Hill, S. A. Burton and M. Jordan, "Electrorheological fluid damper for seismic protection of structures," *Proc., SPIE, Smart Structures and Mat.*, I. Chopra, ed., The Int. Soc. of Optical Engirg., Bellingham, wash., 2443, 184-194.

13. S. McMahon and N. Makris, "Large scale ER-damper for seismic protection of brodges," Proc. XV Structures Congress, Portland (1997).

14. R. W. Phillips, "Engineering Applications of Fluids with Variable Yield Stress, "Ph.D Dissertation, University of California, Berkeley, CA, (1969).

15. A. Pinkos, E. Shtarkman and T. Fitzgerald, "Active damping using ERM fluids," *Automotive Engineering*, 6, 19-23, (1993).

16. J. F. Shackelford, W. Alexander and J. S. Park. *Materials Science and Engineering Handbook.* CRC Press, Boca Raton, FL, (1994).

17. N. G. Stevens, J. L. Sproston, and R. Stanway,"Experimental evaluation of a simple electroviscous damper," *J. Electrostatics*, Vol. 15, 275-283, (1984).

Resolutions

Fourth US-Japan Workshop on Earthquake Protective Systems for Bridges

Resolutions

General

The Fourth U.S.-Japan Workshop on Earthquake Protective Systems for Bridges was held at Osaka, Japan on December 9 and 10, 1996, under the auspices of Task Committee G on "Structural Control and Intelligent Materials Systems" in cooperation with Task Committee J on "Wind and Earthquake Engineering for Transportation Systems" of the UJNR Panel on Wind and Seismic Effects. The workshop was attended by 20 U.S. and 66 Japanese participants. The workshop was organized and sponsored by the Public Works Research Institute, Ministry of Construction from the Japan side. The U.S. sponsorship for the meeting was provided by the National Science Foundation and the Federal Highway Administration. Participation of the U.S. delegates was coordinated by the National Center for Earthquake Engineering Research.

The workshop comprised the presentation and discussion of 8 U.S. and 12 Japanese papers, which covered a wide range of topics including passive, active and hybrid control systems, experimental and field observation for isolated bridges, design issues and applications for new construction such as multi-span bridges and long-span bridges. Fruitful discussions on many issues of common concern took place. Participants also showed great interest in hybrid and active systems for bridges, as well as design method for seismic isolated/menshin bridges.

Resolutions

1. There are many topics of common interest related to the development and implementation of earthquake protective systems to bridges. It is therefore resolved that continued cooperation between researchers and bridge engineers in both countries be actively encouraged. The free exchange of research and design experien
ce, in both the laboratory and field, will facilitate the advancement of this technology and its practical implementation in both countries.

2. In view of the success of this workshop, the importance of this technology, and the rapidly advancing state-of-the-art, it is resolved that the Fifth U.S.
-Japan Workshop on Earthquake Protective Systems for Bridges be held in two years in the U.S.

3. It is resolved that in the intermediate year, specialist group meetings may be arranged to focus on single topics, such as design details, practical implementation issues related to hybrid control, comparative performance of different hardware, and so on. As a consequence, the meetings are expected to adopt a working format in order to facilitate the exchange of design details and philosophies. The meeting will be coordinated through the Task Committee G of the Panel on Wind and Seismic Effects, UJNR.

4. It is further resolved that the fifth workshop be oriented towards research and application rather than state-of-the-art reviews. Topics to be covered should include: (1) innovative protective systems; (2) design methods for seismic isolated/menshin bridges, for example, estimating clearances and allowance for pier ductilities; (3) full-scale verification of performance including recorded motions during earthquakes; and (4) design applications to new construction. As passive protective systems have begun to be implemented in both countries, increased emphasis on active and hybrid systems and on the use of smart and high-performance structural materials and systems will be made in this workshop.

Appendices

"The 4th WS on Earthquake Protective Systems for Bridges"

December 9, Monday

8:30-9:00 **Registration**

9:00-9:30 **Opening Session (Co-Chairs: T. Terayama, I. Friedland)**

Opening Remarks (Japan) Dr. Koichi Yokoyama
Opening Remarks (Japan) Dr. Shigeki Unjoh
Opening Remarks (U.S.A.) Dr. Ian G. Buckle

9:30-10:10 **Session 1: State of the Art**

(Co-Chairs: S. Unjoh, G. Fenves)

"Menshin Design of Highway Bridges"
by K. Kawashima, S. Unjoh
Presented by: Kazuhiko Kawashima

"Update on the Proposed AASHTO Guide Specification for Seismic Isolation Design"
by R. Lacalle
Presented by: Roberto Lacalle

10:10-10:30 Break

10:30-11:50 **Session 2: Passive/Hybrid Protective Systems**

(Co-Chairs: H. Iemura, A. Kiremidjian)

"Development of High Damping Systems for Long Span Bridges"
by S. Unjoh, H. Otsuka, Y. Goto, I. Shimoda, Y. Machara, T. Takeda
Presented by: Shigeki Unjoh

"Development of High Damping Devices for Long Span Bridges and the Design Method"
by S. Unjoh, Y. Goto, I. Shimoda, Y. Machara
Presented by: Yozo Goto

"Aging Studies of High-Damping Rubber and Lead-Rubber Seismic Isolators"
by P. Clark, J. Kelly, I. Aiken
Presented by: Peter Clark

"Development of Super High Damping Rubber Damper for the Seismic Response Control of Long Span Bridges"
by K. Goda, S. Suzuki, Y. Suitsu, S. Unjoh, H.Otsuka, K. Nagaya
Presented by: Kengo Goda

11:50-13:30 Lunch

13:30-14:30 **Session 3: Hybrid/Semi-active Systems and Smart Materials**

(Co-Chairs: A. Igarashi, A. Itani)

"Modeling of a Variable Damper and its Application"
by T. Sato, M. Sato, S. Tanaka, K. Toki
Presented by: Tadanobu Sato

"Seismic Response Control of PC Cable-Stayed Bridge under Construction by Active Mass Damper"
by M. Tsunomoto, H. Otsuka, S. Unjoh, K. Nagaya
Presented by: Meguru Tsunomoto

"Thermo-visco-elasto-plastic Modeling of Elastomeric and Lead-Rubber Bridge Bearings"
by J. Mander, D-K Kim, S. Chen
Presented by: John Mander

14:30-14:50 Break

14:50-16:30 **Session 4: Experimental and Field Observations 1**

(Co-Chairs: T. Sato, S. Arzoumanidis)

"Analysis of Seismic Response of Yamaage-Bridge"
by S. Unjoh
Presented by: Shigeki Unjoh

"Seismic Isolation and Energy Dissipation Technologies: a Test and Evaluation Program for Highway Bridge Applications"
by K. Almand
Presented by: Kathleen Almand

"The Restoring Force Characteristics of LRB under the Influence of Variable Axial Loads and Rotational deformation
by H. Iemura, A. Igarashi, Y. Chen, H. Nakajima
Presented by: Akira Igarashi

"Field Testing of a Four-span Seismically Isolated Bridge"
by A. Gilani, S. Mahin, G. Fenves, J. Chavez, I. Aiken
Presented by: Gregory Fenves

"Enhancement of Lateral Seismic Load Distribution in Continuous Girder Bridges : Test of Stiffening and Damping Components of a New Device"
by W. Tanzo, J. Hernandez Jr., H. Mutsuyoshi, A. Tsuzuki
Presented by: J. Hernandez Jr.

18:00 **Reception Hosted by Japan Side**

December 10, Tuesday

8:30-9:30 **Session 5: Experimental and Field Observations 2**
(Co-Chairs: M. Abe, A. Elgamal)

"Design of the 19-Span Continuous Rigid Frame Bridge with Seismic Isolator"
by H. Hayashi, S. Kawakita,
Presented by: Shiro Kawakita

"Testing of Protective Systems and Hardware for Bridge Applications"
by A. Whittaker, I. Aiken, P. Clark, G. Fenves, N. Makris, S. Mahin
Presented by: Andrew Whittaker

"The Analysis of Seismic Response of the Bridge with Menshin Bearings during the Hyogo-ken Nanbu Earthquake"
by T. Naganuma, Y. Horie, H. Kobayashi, N. Sasaki
Presented by: Toshihiko Naganuma

9:30-9:50 Break

9:50-10:50 **Session 6: Methods/Issues and Applications**
(Co-Chairs: H. Otsuka, A. Taylor)

"Use of Visco-Elastic Dampers to Suppress Seismic Vibration of Bridges"
by M. Shinozuka, J-M Kim, R. Purasinghe
Presented by: Masanobu Shinozuka

"Effectiveness of Unseating Prevention Devices with Energy Dissipation"
by K. Kawashima, M. Yabe,
Presented by: Masaaki Yabe

"Seismic Protection of Bridges with Fluid Dampers and the Issue of Viscous Heating"
by N. Makris, S. McMahon
Presented by: Nicos Makris

10:50-11:10 Break

11:10-11:40 **Resolutions and Closure**
(Co-Chairs: S. Unjoh, I. Buckle)

11:40-11:50 Group Photo

11:50-13:20 Lunch

18:00 **Reception Hosted by Japan Side**

December 10, Tuesday

8:30-9:30 **Session 5: Experimental and Field Observations 2**

(Co-Chairs: M. Abe, A. Elgamal)

"Design of the 19-Span Continuous Rigid Frame Bridge with Seismic Isolator"

by S. Kawakita, H. Hayashi

Presented by: Shiro Kawakita

"Testing of Protective Systems and Hardware for Bridge Applications"

by A. Whittaker

Presented by: Andrew Whittaker

"The Analysis of Seismic Response of the Bridge with Menshin Bearings during the Hyogo-ken Nanbu Earthquake"

by T. Naganuma, Y. Horie, H. Kobayashi, N. Sasaki

Presented by: Toshihiko Naganuma

9:30-9:50 Break

9:50-10:50 **Session 6: Methods/Issues and Applications**

(Co-Chairs: H. Otsuka, A. Taylor)

"Use of Visco-Elastic Dampers to Suppress Seismic Vibration of Bridges"

by M. Shinozuka

Presented by: Masanobu Shinozuka

"Effectiveness of Unseating Prevention Devices with Energy Dissipation"

by M. Yabe, K. Kawashima

Presented by: Masaaki Yabe

"Seismic Protection of Bridges with Fluid Dampers and the Issue of Viscous Heating"

by N. Makris

Presented by: Nicos Makris

10:50-11:10 Break

11:10-11:40 **Resolutions and Closure**

(Co-Chairs: S. Unjoh, I. Buckle)

11:40-11:50 Group Photo

11:50-13:20 Lunch

"The 3rd WS on Seismic Retrofit of Bridges"

13:20-13:50 **Opening Session**

(Co-Chairs: T. Terayama, I. Friedland)

Opening Remarks (Japan) Mr. Yasuyuki Fujishiro

Opening Remarks (U.S.A.) Dr. H. S. Lew

13:50-14:30 **Session 1: State of the Art**

(Co-Chairs: S. Unjoh, M. Shinozuka)

"Damage to Highway Bridges by the 1995 Hyogoken Nanbu Earthquake And the Retrofit of Highway Bridges in Japan"
by H. Otsuka, T. Terayama, J. Hoshikuma, K. Kosa
Presented by: Hisanori Otsuka

"Innovative Seismic Retrofit of California Highway Structures"
by S. El-Azazy
Presented by: Saad El-Azazy

14:30-14:50 Break

14:50-15:30 **Session 2: Screening and Prioritization of Bridges for Retrofitting**

(Co-Chairs: H. Mutsuyoshi, J. Mander)

"Seismic Retrofitting Manuals for Highway Systems: System Assessment, Screening, Evaluation, and Retrofitting"
by I. Buckle, I. Friedland
Presented by: Ian Friedland

"Use of Transportation Network Systems for Bridge Retrofit Prioritization and Emergency Response"
by A. Kiremidjian, N. Basöz
Presented by: Anne Kiremidjian

15:30-15:50 Break

15:50-16:50 **Session 3: Evaluation of Existing Bridges**

(Co-Chairs: J. Hoshikuma, N. Makris)

"Analytical Methods for the Seismic Evaluation of Existing Bridges"
by R. Imbsen, F. Nobari
Presented by: Roy Imbsen

"Seismic Evaluation and Retrofit of Existing Multi-column Bents"
by T. Terayama, H. Otsuka
Presented by: Toru Terayama

"Queensboro Bridge: Seismic Condition Assessment and Retrofit of a Landmark Bridge"
by S. Arzoumanidis, R. Gajer, A. Malik
Presented by: Serafim Arzoumanidis

16:50-17:10 Break

17:10-18:10 **Session 4: Retrofit Methods for RC Columns 1**

(Co-Chairs: Y. Kimura, R. Imbsen)

"Seismic Retrofit of Square RC Columns by Steel Jacketing"
by J. Hoshikuma, H. Otsuka, K. Nagaya
Presented by: Jun-ichi Hoshikuma

"An Experimental Study on Seismic Retrofit of Reinforced Concrete Bridge Piers"
by H. Ikeda, N. Wada, K. Osada, Y. Igase, Y. Tamura
Presented by: Yoshinori Igase

"Retrofits of Reinforced Concrete Bridge Columns with Prestressing Steel Ties"

by T. Yoshioka
Presented by: Tamio Yoshioka

December 11, Wednesday

8:40-10:20 **Session 5: Retrofit Methods for RC Columns 2**
(Co-Chairs: Y. Adachi, P. Clark)

"Development of Base Isolation System of Existing Bridges"
by Y. Hishiki, T. Takeda, H. Nagumo, T. Ichinomiya, Y. Okimi
Presented by: Hiroyuki Nagumo

"An Experimental Study on Ductility of RC Pier Models Winded with FRP Tape"
by H. Mikami, M. Sato, H. Konno, N. Kishi
Presented by: Hiroshi Mikami

"Seismic Retrofit of Bridge Columnsing Prefabricated Composite Jackets"
by Y. Xiao
Presented by: Yan Xiao

"Seismic Retrofit of Reinforced Concrete Bridge Piers by Carbon Fiber Sheet"
by M. Hosotani, K. Kawashima, J. Hoshikuma
Presented by: Manabu Hosotani

"Experimental Study Concerning Retrofit of RC Column by CFRP Sheet"
by F. Hakamada, Y. Maekawa, J. Hoshikuma
Presented by: Fumio Hakamada

10:20-10:40 Break

10:40-12:00 **Session 6: Retrofit Methods for Steel Columns, Superstructure and Restrainers**
(Co-Chairs: K. Tamura, Y. Xiao)

"Cyclic Behavior of Shear Links in Retrofitted Richmond-San Rafael Bridge Towers"
by A. Itani
Presented by: Ahmad Itani

"An Experimental Study on Seismic Retrofit of Steel Bridge Piers"
by K. Nishikawa, J. Murakoshi, Y. Josen, M. Takahashi
Presented by: Jun Murakoshi

"Intermediate Hinge Restrainers for Bridges: Performance, Design, and Retrofit"
by R.DesRoches, G. Fenves
Presented by: Gregory Fenves

"Seismic Vulnerability Analysis of Steel Bridge Bearings"
by J. Mander, D-K Kim, I. Buckle
Presented by: John Mander

12:00-13:30 Lunch

13:30-15:10 **Session 7: Retrofit Methods for Foundations and Geotechnical Considerations**
(Co-Chairs: J. Murakoshi, K. Almand)

"Inspection and Restoration of Damaged Foundations due to the Great Hanshin Earthquake 1995"
by H. Ishizaki, A. Nanjoh, J. Kawakami,N. Egawa, Y. Adachi,
Presented by: Yukio Adachi

"Seismic Design of Pile Foundations"
by M. Nakano, Y. Kimura,
Presented by: Yoshitomi Kimura

"Site Remediation and Seismis Response Meshanisns"
by K. Adalier, A. Elgamal
Presented by: Ahmed Elgamal

"Seismic Design Treatment of Liquefaction-Induced Ground Flow"

by M. Hosotani, K. Kawashima, J. Hoshikuma

Presented by: Manabu Hosotani

"Experimental Study Concerning Retrofit of RC Column by CFRP Sheet"

by F. Hakamada, J. Maekawa, J. Hoshikuma

Presented by: Fumio Hakamada

10:20-10:40 Break

10:40-12:00 **Session 6: Retrofit Methods for Steel Columns, Superstructure and Restrainers**

(Co-Chairs: K. Tamura, Y. Xiao)

"Cyclic Behavior of Shear Links in Retrofitted Richmond-San Rafael Bridge Towers"

by A. Itani

Presented by: Ahmad Itani

"An Experimental Study on Seismic Retrofit of Steel Bridge Piers"

by K. Nishikawa, J. Murakoshi, Y. Josen

Presented by: Jun Murakoshi

"Intermediate Hinge Restrainers for Bridges: Performance, Design, and Retrofit"

by G. Fenves

Presented by: Gregory Fenves

"Seismic Vulnerability Analysis of Steel Bridge Bearings"

by J. Mander

Presented by: John Mander

12:00-13:30 Lunch

13:30-15:10 **Session 7: Retrofit Methods for Foundations and Geotechnical Considerations**

(Co-Chairs: J. Murakoshi, K. Almand)

"Inspection and Restoration of Damaged Foundations due to the Great Hanshin Earthquake 1995"

by Y. Adachi, H. Ishizaki, A. Nanjo, J. Kawakami, N. Egawa

Presented by: Yukio Adachi

"Seismic Behavior of Piles of Bridge Foundation"

by Y. Kimura, M. Nakano

Presented by: Yoshitomi Kimura

"Site Remediation and Seismic Response Mechanisms"

by A. Elgamal

Presented by: Ahmed Elgamal

"Seismic Design Treatment of Liquefaction-Induced Ground Flow"

by K. Tamura, T. Hamada, T. Azuma
Presented by: Kei-ichi Tamura

"A Study on Measures against Ground Flow Using The Finite Element Method"
by M. Ogasawara, H. Tsunoda, T. Makita, S. Gose
Presented by: Hiroshi Tsunoda

15:10-15:30 Break

15:30-16:10 **Special Session: Effects of Loading History**
(Co-Chairs: K. Kawashima, A. Whittaker)

"Effect of Loading Hysteresis on Ductility of Reinforced Concrete Columns"
by J. Hoshikuma, S. Unjoh, K. Nagaya
Presented by: Jun-ichi Hoshikuma

"Testing Methodologies for the Seismic Performance of Reinforced Concrete Bridge Piers"
by A. Taylor
Presented by: Andrew Taylor

16:10-16:30 Break

16:30-17:00 **Resolutions and Closure**
(Co-Chairs: S. Unjoh, H. S. Lew)

Participants

Participants from The U.S. Side

Kathleen Almand
HITEC
1015 15th Street, NW, Suite 600
Washington, D.C. 20005-2605
Tel. 202-842-0555
Fax. 202-789-5345
E-mail kalmand@cerf.asce.org

Serafim G. Arzoumanidis
Steinman, Boyton, Gronquist &Birdsall
110 William Street
New York, NY 10038
Tel. 212-266-8370
Fax. 212-266-8540

Ian G. Buckle
National Center for Earthquake Engineering Research
State University of NY at Buffalo
105 Red Jacket Quadrangle
Buffalo, NY 14261
Tel. 716-645-3391
Fax. 716-645-3399
E-mail igb@acsu.buffalo.edu

Peter Clark
Earthquake Engineering Research Center
University of California, Berkeley
1301 South 46th Street
Richmond, CA 94804-4698
Tel. 510-231-9556
Fax. 510-231-5696
E-mail sacsteel@eerc.berkeley.edu

Saad El-Azazy
Senior Bridge Engineer
California Dept. of Transportation
Division of Structures
1801 30th Street, West Bldg. P.O. Box 942874
Sacramento, CA 94274-0001
Tel. 916-227-8124
Fax. 916-227-8898

Ahmed-W. Elgamal
Columbia University
Department of Civil Engineering
610 Mudd Building
New York, NY 10027
Tel. 212-854-1203
Fax. 212-854-6267

Gregory Fenves
Professor
University of California, Berkeley
Department of Civil Engineering
729 Davis Hall
Berkeley, CA 94720-1710
Tel. 510-643-8543
Fax. 510-643-8928
E-mail fenves@ce.berkeley.edu

Ian Friedland
National Center for Earthquake Engineering Research
State University of NY at Buffalo
102 Red Jacket Quadrangle
Buffalo, NY 15261-0025
Tel. 716-645-3391
Fax. 716-645-3399
E-mail imf@acsu.buffalo.edu

Roy A. Imbsen
Imbsen&Associates, Inc.
9912 Business Park Drive, Suite 130
Sacramento, CA 95827
Tel. 916-366-0632
Fax. 916-366-1501
E-mail raimbsen@imbsen.com

Ahmad M. Itani
Assistant Professor
University of Nevada, Reno
Department of Civil Engineering
258 Reno, NV 89557-0152
Tel. 702-784-4379
Fax. 702-784-4466
E-mail itani@scs.unr.edu

Anne S. Kiremidjian
Professor and Direstor
Stanford University
Department of Civil Engineering
Terman 238
Stanford, CA 94305-4042
Tel. 415-723-4164
Fax. 415-725-9755
E-mail ask@ce.stanford.edu

Roberto Lacalle
California Dept. of Transportation
Division of Structures, MS-9
P.O. Box 942874
Sacramento, CA 94274-0001
Tel. 916-227-8070
Fax. 916-227-8245

H.S. Lew
Chief
Structural Division
National Institute of Standards and Technology
Building 226, Rm. 168
Gaithersburg, MD 20899
Tel. 301-975-6060
Fax. 301-869-6275

Nicos Makris
University of California, Berkeley
Department of Civil and Environmental Engineering
711 Davis Hall
Berkeley, CA 94702-1710
Tel. 510-643-2682
Fax. 510-643-8928
E-mail makris@ce.berkeley.edu

John B. Mander
State University of New York at Buffalo
Department of Civil Engineering
230 Ketter Hall
Buffalo, NY 14260
Tel. 716-645-2114
Fax. 716-645-3733
E-mail jmander@ubvms.cc.buffalo.edu

Masanobu Shinozuka
Profrssor
University of Southern California
Department of Civil Engineering
3620 South Vermont Avenue, KAP254
Los Angeles, CA 90089-2531
Tel. 213-740-9528
Fax. 213-740-9529

Andrew W. Taylor
Research Structural Engineer
National Institute of Standards and Technology
Structures Division
Bldg. 226, Room B158
Gaithersburg, MD 20899
Tel. 301-975-6078
Fax. 301-869-6275
E-mail ataylor@nist.gov

Andrew S. Whittaker
Associate Director
Earthquake Engineering Research Center
University of California, Berkeley
1301 South 46th Street
Richmond, CA 94804-4698
Tel. 510-231-9554
Fax. 510-231-9471

Yan Xiao
Assistant Professeor
University of Southern California
Dept. of Civil Engineering
Kaprielian Hall, 224B
Los Angeles, CA-90089-2531
Tel. 213-740-6130
Fax. 213-744-1426
E-mail yanxiao@ref.usc.edu

Lalliana Mualchin
California Dept. of Transportation
Division of Structures, MS-9
(Carrently Visiting Kyoto Univ.)
P.O. Box 942874
Sacramento, CA 94274-0001
Tel. 916-227-8735
Fax. 916-227-8898
E-mail tslmual@ts1.dot.ca.gov

Participants from The Japan Side

Masato Abe
Assistant Professor
Department of Civil Engineering
University of Tokyo
Hongo 7-3-1, Bunkyo-ku,
Tokyo, 113
Tel. 03-5802-3312
Fax. 03-5689-7292
E-mail masato@kyouryou.t.u-tokyo.ac.jp

Yukio Adachi
Senior Research Engineer
Earthquake Engineering Division,
Earthquake Disaster Prevention Research Center
Public Works Research Institute,
Ministry of Construction
1, Asahi, Tsukuba-shi,
Ibaraki, 305
Tel. 0298-64-4966
Fax. 0298-64-4424
E-mail y-adachi@pwri.go.jp

Yoshihiko Akao
Chief Engineer
Isolation Design Section,
MB Development Department
Yokohama Rubber Co., Ltd.
Tel. 0463-35-9703
Fax. 0463-35-9765

Haruki Akiyama
Manager
First Design Division,
Design Department
Honshu Shikoku Bridge Authority
5-1-5, Toranomon, Minato-ku,
Tokyo, 105
Tel. 03-3434-7281
Fax. 03-3578-9298

Noriaki Egawa
Engineer
Second Kobe Construction Department
Hanshin Expressway Public Corp.
1-3-3, Higashikawasaki-cho, Chuo-ku, Kobe-shi,
Hyogo, 650
Tel. 078-360-8144
Fax. 078-360-8158

Yasuyuki Fujishiro
Director
Structure and Bridge Department
Public Works Research Institute,
Ministry of Construction
1, Asahi, Tsukuba-shi,
Ibaraki, 305
Tel. 0298-64-2835
Fax. 0298-64-0565
E-mail fujisiro@pwri.go.jp

Kengo Goda
Seismic Isolation Technology Development Department
Bridgestone Co., Ltd.
1, Kashio-cho, Tozuka-ku, Yokohama-shi,
Kanagawa, 244
Tel. 045-825-7589
Fax. 045-825-7676

Shingo Gose
Deputy Manager
Traffic Structure Division,
Road and Traffic Department
CTI Engineering Co., Ltd.
9th Chuo Bldg., 4-9-11, Honcho Nihonbashi, Chuo-ku,
Tokyo, 103
Tel. 03-3668-0451
Fax. 03-5695-1847

Yozo Goto
General Manager
Civil Engineering Department No.5
Obayashi Corp.,
Technical Research Institute
640, Shimokiyoto 4-chome, Kiyose-shi,
Tokyo, 204
Tel. 0424-95-0951
Fax. 0424-95-0903

Fumio Hakamada
Senior Engineer
Maintenance Department
Hanshin Expressway Public Corp.
4-1-3, Kyutaro-machi, Chuo-ku,
Osaka, 541
Tel. 06-252-8121
Fax. 06-252-4583

Masahiro Hayashi
Third Design Division,
Design Department
Honshu-Shikoku Bridge Authority
45 Mori Bldg., 5-1-5, Toranomon, Minato-ku,
Tokyo, 105
Tel. 03-3434-7281
Fax. 03-3578-9298

Hidenao Hayashi
Manager
Kobe Maintenance Department
Hanshin Expressway Public Corp.
16-1, Shinko-cho, Chuo-ku, Kobe-shi,
Hyogo, 650

Mituhiro Hayashida
Engineer
Maintenance and Facility Section
Hanshin Expressway Public Corp.
2-3 D2-105 Shin-senri-Nisimachi, Toyonaka-shi,
Osaka, 565

Jaime Y. Hemandez Jr.
Master of Engineering Student
Graduate School of Science and Engineering
Saitama University
Rm. 3209, 645 Shimo-Okubo, Urawa-shi,
Saitama, 338
Tel. 048-859-4218

Yasuhisa Hishijima
Director
General Manager of Technical Department
Kawaguchi Metal Industries Co,. Ltd.
3-6-107, Sakurada Washinomiya-machi,
Kitakatsushika-gun,
Saitama, 340-02
Tel. 048-259-1118
Fax. 048-259-1139

Yoshihiro Hishiki
Chief
Structural Engineering Section,
Civil Engineering Department 1
Kajima Corp.,
Kajima Technical Research Institute
19-1, Tobitakyu 2-chome, Chofu-shi,
Tokyo, 182
Tel. 0424-89-7076
Fax. 0424-89-7078

Riki Honda
Research Engineer
Ground Vibration Division,
Earthquake Disaster Prevention Research Center
Public Works Research Institute,
Ministry of Construction
Tel. 0298-64-2211
Fax. 0298-64-0598
E-mail rhonda@pwri.go.jp

Yoshihei Horie
Senior Engineer
Engineering Department
Hanshin Expressway Public Corp.
Tel. 06-252-8121
Fax. 06-252-4583

Jun-ichi Hoshikuma
Research Engineer
Earthquake Engineering Division,
Earthquake Disaster Prevention Research Center
Public Works Research Institute,
Ministry of Construction
Tel. 0298-64-4966
Fax. 0298-64-4424
E-mail hosikuma@pwri.go.jp

Manabu Hosotani
Research Student
Department of Civil Engineering
Tokyo Institute of Technology
2-12-1, O-okayama, Meguro-ku,
Tokyo, 152
Tel. 03-5734-2922
Fax. 03-3729-0728

Hirokazu Iemura
Professor
Life Line Engineering Lab,
Graduate School of Civil Engineering,
Kyoto University
Yoshida Honmachi, Sakyo-ku,
Kyoto, 606-01
Tel. 075-753-5087
Fax. 075-753-5926

Akira Igarashi
Associate Professor
Department of Civil Engineering Systems
Kyoto University
Yoshida Honmachi, Sakyo-ku,
Kyoto, 606-01
Tel. 075-753-5088
Fax. 075-753-5926
E-mail igarashi@catfish.kuciv.kyoto-u.ac.jp

Yoshinori Igase
Deputy Head
Bridge Section
Japan highway Public Corp.,
Research Institute
4-1, 1Chome, Tadao, Machida-Shi,
Tokyo, 194
Tel. 0427-91-1621
Fax. 0427-92-8650

Hiroshi Ishizaki
Manager
Second Kobe Construction Department
Hanshin Expressway Public Corp.
1-3-1, Higashi Kawasaki-cho, Chuo-ku, Kobe-shi,
Hyougo 650

Touta Katsukawa
Technical Research & Development Institute,
Kumagai Gumi Co., Ltd.
1043 Onigakubo, Tsukuba-shi,
Ibaraki, 300-22
Tel. 0298-47-7501
Fax. 0298-47-7480

Yoriko Kawakami
Engineer
First Kobe Construction Department
Hanshin Expressway Public Corp.
17-1 Aza-Higashimukai, Shimotanigaami,
Yamada-cho, Kita-ku, Kobe-shi,
Hyogo, 651-12
Tel. 078-582-0345
Fax. 078-582-0348

Shiro Kawakita
Chief Engineer
Specified Planning Office
Planning Division
Hanshin Expressway Public Corp.
4-1-3, Kyutaro-machi, Chuo-ku,
Osaka, 541
Tel. 06-252-8121
Fax. 06-252-4583

Kazuhiko Kawashima
Professor
Department of Civil Engineering
Tokyo Institute of Technology
2-12-1, O-okayama, Meguro-ku,
Tokyo, 152
Tel. 03-5734-2922
Fax. 03-3729-0728
E-mail kawasima@cv.titech.ac.jp

Masaharu Kawashima
Deputy Director-General
Road Department
Kyushu Regional Construction Bureau,
Ministry of Construction
2chome 10-7, Hakataeki higashi, Hakata-ku,
Fukuoka-shi,
Fukuoka, 812
Tel. 092-471-6331
Fax. 092-476-3494

Yoshitomi Kimura
Senior Research Engineer
Foundation Engineering Division,
Structure and Bridge Department
Public Works Research Institute,
Ministry of Construction
1, Asahi, Tsukuba-Shi
Ibaraki, 305
Tel. 0298-64-4916
Fax. 0298-64-0565

Kenji Kohsa
Senior Engineer
Kobe Reconstruction Division
Hanshin Expressway Public Corp.
Tel. 078-331-9801
Fax. 078-331-9733
E-mail GCH06310@niftyserve.or.jp

Hisashi Kon-no
Head
Structures Section,
Structures Division
Civil Engineering Research Institute,
Hokkaido Development Agency
1-3, Hiragishi, Toyohira, Sapporo,
Hokkaido, 062
Tel. 011-841-1111
Fax. 011-824-1226

Shin-ichiro Kumagai
Deputy General Manager
Construction & Engineering Division,
Civil Engineering Department,
Civil Engineering Operations
Sumitomo Construction Co., Ltd.
13-4, Araki-Cho, Shinjuku-ku,
Tokyo, 160
Tel. 03-3225-5132
Fax. 03-3353-6656

Hiroshi Mikami
Senior Research Engineer
Technical Research Institute
Mitsui Construction Co., Ltd.
518-1, Komaki, Nagareyama-shi,
Chiba, 270-01
Tel. 0471-40-5202
Fax. 0471-40-5216

Yoshihiro Morioka
Development Section
Engineering Development Department,
Civil Engineering Design Division
Kajima Corp.
Tel. 03-5561-2111
Fax. 03-5561-2152

Kazuhiko Murai
Visiting Researcher
Earthquake Engineering Division,
Earthquake Disaster Prevention Research Center
Public Works Research Institute,
Ministry of Construction
1, Asahi, Tsukuba-shi,
Ibaraki, 305
Tel. 0298-64-4966
Fax. 0298-64-4424
E-mail murai@pwri.go.jp

Jun Murakoshi
Senior Research Engineer
Bridge Division,
Structure and Bridge Department
Public Works Research Institute,
Ministry of Construction
1, Asahi, Tsukuba-shi,
Ibaraki, 305
Tel. 0298-64-4919
Fax. 0298-64-0565
E-mail murakosi@pwri.go.jp

Hiroshi Mutsuyoshi
Professor and Head of Foreign Student Office in Graduate
Program Department of Civil and Environmental Engineering
Saitama University
225 Shimo-okubo Urawa-shi,
Saitama, 338
Tel. 048-858-3553
Fax. 048-855-9361

Toshihiko Naganuma
Chief
First Research and Development Section,
Research and Development Division
Hanshin Expressway Management Technology Center
Toa Bldg., 4-5-7, Minami-Honmachi, Chuo-ku,
Osaka, 541
Tel. 06-244-6043
Fax. 06-244-9612

Kazuhiro Nagaya
Research Engineer
Earthquake Engineering Division,
Earthquake Disaster Prevention Research Center
Public Works Research Institute,
Ministry of Construction
1, Asahi, Tsukuba-shi,
Ibaraki, 305
Tel. 0298-64-4966
Fax. 0298-64-4424
E-mail nagaya@pwri.go.jp

Hiroyuki Nagumo
Engineer
Civil Engineering Design Division,
2nd Design Department
Kajima Corp.
5-30, Akasaka 6-chome, Minato-ku,
Tokyo, 107
Tel. 03-5561-2111
Fax. 03-5561-2156

Yuji Nakai
Sumitomo Construction Co., Ltd.
13-4, Araki-Cho, Shinjuku-ku,
Tokyo, 160
Tel. 03-3225-5132
Fax. 03-3353-6656

Sachio Nakamura
Chief Research Engineer
Computational Analysis Lab.,
R&D Department
Yokohama Rubber Co., Ltd.
2-1 Oiwake, Hiratsuka-shi,
Kanagawa, 254
Tel. 0463-35-9588
Fax. 0463-35-9758

Atsushi Nanjo
Senior Engineer
Engineering Department,
Design Division
Hanshin Expressway Public Corp.
4-3-1, Kyutaro-machi, Chuo-ku,
Osaka, 541
Tel. 06-252-8121
Fax. 06-252-4583

Hajime Ohuchi
Chief Research Engineer
Structural Engineer Department
Obayashi Corp.,
Technical Research Institute
640, Shimokiyoto 4-chome, Kiyose-shi,
Tokyo, 204
Tel. 0424-95-0995
Fax. 0424-95-0904

Hiroaki Okamoto
Senior Engineer
Civil Engineering Design Division,
2nd Design Department
Kajima Corp.
5-30, Akasaka 6-chome, Minato-ku,
Tokyo, 107
Tel. 03-5561-2111
Fax. 03-5561-2156

Koji Osada
Engineer
Tokyo 1st Operation Bureau
Japan Highway Public Corp.
1-1, Nanpeidai, Miyamae-ku, Kawasaki-shi,
Kanagawa, 216
Tel. 044-865-8247
Fax. 044-866-3521

Hisanori Otsuka
Professor
Department of Civil Engineering
Kyushu University
6-10-1, Hakozaki, Higashi-ku,
Fukuoka, 812
Tel. 092-642-3266
Fax. 092-642-3266
E-mail otsuka@civil.doc.kyushu-u.ac.jp

Kai Qi
Researcher
Division of Earthquake Disaster
Kyoto University,
Disaster Prevention research Institute
Gokasho, Uji,
Kyoto, 611
Tel. 0774-38-4070
Fax. 0774-38-4070

Haruyuki Sakoda
Senior Manager
Steel Structure Division,
Bridge Engineering Department
Kawasaki Heavy Industries, Ltd.
8, Niijima, Harima-cho, Kako-gun,
Hyogo, 675-01
Tel. 0794-35-8413
Fax. 0794-35-0249

Tadanobu Sato
Professor
Section of Dynamics of foundation Structures,
Division of Earthquake Disaster Prevention
Kyoto University,
Disaster Prevention research Institute
Gokasho, Uji,
Kyoto, 611
Tel. 0774-38-4065
Fax. 0774-38-4070
E-mail sato@catfish.dpri.kyoto-u.ac.jp

Chiaki Sudo
Section Manager Seismic Isolation,
Technology Development Department
Bridgestone Co., Ltd.
1, Kashio-cho, Tozuka-ku, Yokohama-shi,
Kanagawa, 244
Tel. 045-825-7589
Fax. 045-825-7676

Shigenobu Suzuki
Seismic Isolation Technology Development Department
Bridgestone Co., Ltd.
1, Kashio-cho, Totsuka-ku, Yokohama-shi,
Kanagawa, 244
Tel. 045-825-7589
Fax. 045-825-7676

Yoshinori Tachibana
Manager
Infrastructure Engineering Department
Oriental Consultants Co., Ltd.
3-5-7, Hisamoto, Takatsu-ku, Kawasaki-shi,
Kanagawa, 213
Tel. 044-812-8815
Fax. 044-812-8825

Mitsunori Takahashi
Visiting Researcher
Earthquake Engineering Division,
Earthquake Disaster Prevention Research Center
Public Works Research Institute,
Ministry of Construction
1, Asahi, Tsukuba-shi,
Ibaraki, 305
Tel. 0298-64-4966
Fax. 0298-64-4424
E-mail m-takahs@pwri.go.jp

Isao Takatori
General Manager
Planing Division
Public Works Research Center
Takara Bldg., 1-6-4, Taito, Taito-ku,
Tokyo, 110
Tel. 03-3835-3609
Fax. 03-3832-7397

Keiichi Tamura
Head
Ground Vibration Division,
Earthquake Disaster Prevention Research Center
Public Works Research Institute,
Ministry of Construction
1, Asahi, Tsukuba-shi,
Ibaraki, 305
Tel. 0298-64-2926
Fax. 0298-64-0598
E-mail tamura@pwri.go.jp

Yoji Tamura
Bridge Section
Japan highway Public Corp.,
Research Institute
4-1, 1-Chome, Tadao, Machida-Shi,
Tokyo, 194
Tel. 0427-91-1621
Fax. 0427-92-8650

William Tanzo
Associate Professor
Civil and Environmental Engineering Department,
Faculty of Engineering
Saitama University
225 Shimo-okubo Urawa-shi,
Saitama, 338
Tel. 048-858-3556
Fax. 048-858-3556

Kenji Tasaki
Visiting Researcher
Earthquake Engineering Division,
Earthquake Disaster Prevention Research Center
Public Works Research Institute,
Ministry of Construction
1, Asahi, Tsukuba-shi,
Ibaraki, 305
Tel. 0298-64-4966
Fax. 0298-64-4424
E-mail k-tasaki@pwri.go.jp

Toru Terayama
Senior Research Engineer
Earthquake Engineering Division,
Earthquake Disaster Prevention Research Center
Public Works Research Institute,
Ministry of Construction
1, Asahi, Tsukuba-shi,
Ibaraki, 305
Tel. 0298-64-4966
Fax. 0298-64-4424
E-mail terayama@pwri.go.jp

Hiroshi Tsunoda
Engineer
Design and Research Division,
Engineering Department
Metropolitan Expressway Public Corp.
1-4-1, Kasumigaseki, Chiyoda-ku,
Tokyo, 100
Tel. 03-3502-7311
Fax. 03-3502-2411

Meguru Tsunomoto
Senior Research Engineer
Technical Division
Oriental Construction Co., Ltd.
1-2, 2-Chome Hirakawa-cho, Chiyoda-ku,
Tokyo, 102
Tel. 03-3261-1176
Fax. 03-3261-1139
E-mail LDX04457@niftyserve.or.jp

Shigeki Unjoh
Head
Earthquake Engineering Division,
Earthquake Disaster Prevention Research Center
Public Works Research Institute,
Ministry of Construction
1, Asahi, Tsukuba-shi,
Ibaraki, 305
Tel. 0298-64-2932
Fax. 0298-64-4424
E-mail unjoh@pwri.go.jp

Sadafumi Uno
Chief Manager
Technical Development Room
Kawaguchi Metal Industries Co,. Ltd.
2-25-1, Kizawa, Toda-shi,
Saitama, 335
Tel. 048-259-1118
Fax. 048-259-1139

Masaaki Yabe
Graduate Student
Department of Civil Engineering
Tokyo Institute of Technology
2-12-1, O-okayama, Meguro-ku,
Tokyo, 152
Tel. 03-5734-2922
Fax. 03-3729-0728

Furitsu Yasuda
Chief Engineer
Engineering Division, Design Section
Hanshin Expressway Public Corp.
1-3, 4-chome, Kyutaro-machi, Chuo-ku,
Osaka, 541
Tel. 06-252-8121
Fax. 06-252-4583

Koichi Yokoyama
Director
Earthquake Disaster Prevention Research Center
Public Works Research Institute,
Ministry of Construction
1, Asahi, Tsukuba-shi,
Ibaraki, 305
Tel. 0298-64-2829
Fax. 0298-64-0598
E-mail yokoyama@pwri.go.jp

Tamio Yoshioka
Director
Research Laboratory
Oriental Construction Co., Ltd.
5, Kinugaoka, Moka-shi,
Tochigi, 321-43
Tel. 0285-83-7921
Fax. 0285-83-0021
E-mail KYL06022@niffyserve.or.jp

Copyright © (1997) by P.W.R.I.

All rights researved. No part of this book may be reproduced by any means, nor transmitted, nor translated into a machine language without the written permission of the Director General of P.W.R.I.

この報告書は、土木研究所長の承認を得て刊行したものである。したがって、本報告書の全部又は一部の転載、複製は、土木研究所長の文書による承認を得ずしてこれを行ってはならない。